# Silencing and counter-silencing of the Lsr2-like protein CgpS in *Corynebacterium glutamicum*

Inaugural Dissertation

for the attainment of the title of doctor
in the Faculty of Mathematics and Natural Sciences
at the Heinrich-Heine-University Düsseldorf

presented by

**Johanna Wiechert**
born in Mettingen

Jülich, February 2020

The thesis has been conducted at the Institute of Bio- and Geosciences, IBG-1: Biotechnology, Forschungszentrum Jülich, from September 2016 until February 2020 under the supervision of Prof. Dr. Julia Frunzke.

Published by permission of the Faculty of Mathematics and Natural Sciences at Heinrich-Heine-University Düsseldorf.

**Supervisor:** Prof. Dr. Julia Frunzke
Institute of Bio- and Geosciences, IBG-1: Biotechnology,
Forschungszentrum Jülich, Jülich

**Co-supervisor:** Prof. Dr. Matias Zurbriggen
Institute of Synthetic Biology,
Heinrich-Heine-University Düsseldorf, Düsseldorf

Date of oral examination: 15.07.2020

***„Der Weg zu allem Großen geht durch die Stille.“***

*Paul Keller, Das letzte Märchen – Ein Idyll (1905)*

The studies presented in this dissertation have been published or submitted for publication in the following articles and manuscripts:

Wiechert, J., Filipchyk, A., Hünnefeld, M., Gätgens, C., Brehm, J., Heermann, R. and Frunzke, J. (2020). Deciphering the rules underlying xenogeneic silencing and counter-silencing of Lsr2-like proteins using CgpS of *Corynebacterium glutamicum* as a model. *mBio. 11*, e02273-02219, doi: 10.1128/mBio.02273-19

Wiechert, J., Gätgens, C., Wirtz, A. and Frunzke, J. (2020). Inducible expression systems based on xenogeneic silencing and counter-silencing and the design of a metabolic toggle switch. *Submitted*.

Krüger, A.*, Wiechert, J.*, Gätgens, C., Polen, T., Mahr, R. and Frunzke, J. (2019). Impact of $CO_2$/$HCO_3^-$ availability on anaplerotic flux in pyruvate dehydrogenase complex-deficient *Corynebacterium glutamicum* strains. *J. Bacteriol. 201*, e00387-00319, doi: *10.1128/JB.00387-19.*

Further publications not discussed in this thesis:

Stella, R. G., Wiechert, J., Noack, S. and Frunzke, J. (2019). Evolutionary engineering of *Corynebacterium glutamicum*. *Biotechnol. J. 14*, e1800444, doi: *10.1002/biot.201800444.*

Wiechert, J. and Frunzke, J. (2018). Lichtblicke in der mikrobiellen Stammentwicklung. *Nachr. Chem. 66*, 589-592, doi: *10.1002/nadc.20184067195.*

**These authors contributed equally to this work.*

# Abbreviations

| | | | |
|---|---|---|---|
| Abi | Abortive infection | MTase | Methyltransferase |
| ALE | Adaptive laboratory evolution | NAP | Nucleoid-associated protein |
| ATc | Anhydrotetracycline | NMR spectroscopy | Nuclear magnetic resonance spectroscopy |
| a.u. | arbitrary unit | NTP | Nucleoside triphosphate |
| BREX | Bacteriophage exclusion | PALM | Photoactivated localization microscopy |
| BS | Binding site | PAM | Protospacer adjacent motif |
| CBASS | Cyclic oligonucleotide-based anti-phage signalling system | PBM | Protein binding microarray |
| cGAMP | Cyclic GMP-AMP | PCx | Pyruvate carboxylase |
| cGAS | Cyclic GMP–AMP synthase | PDHC | Pyruvate dehydrogenase complex |
| CRISPR-Cas | Clustered regularly interspaced short palindromic repeats and CRISPR-associated proteins | PEPCx | Phosphoenolpyruvate carboxylase |
| crRNA | CRISPR RNA | REase | Restriction endonuclease |
| CgpS | *C. glutamicum* prophage silencer | R-M system | Restriction modification system |
| ChAP-seq | Chromatin affinity purification and sequencing | RNA | Ribonucleic acid |
| ChIP | Chromatin immunoprecipitation | RNA Pol | RNA polymerase |
| DDFA | Differential DNA footprint analysis | SFM | Scanning force microscopy |
| DISARM | Defence islands system associated with restriction modification | STORM | Stochastic optical reconstruction microscopy |
| DNA | Deoxyribonucleic acid | SPI | *Salmonella* pathogenicity island |
| DNA BD | DNA binding domain | SPR analysis | Surface plasmon resonance analysis |
| Dnd defence system | DNA degradation defence system | sptPALM | Single-particle tracking PALM |
| DRE | Downstream regulatory element | TCA cycle | Tricarboxylic acid cycle |
| e.g. | *exempli gratia* | TF | Transcription factor |
| EHEC | Enterohemorrhagic *E. coli* | TSS | Transcriptional start site |
| EPEC | Enteropathogenic *E. coli* | T3SS | Type III secretion system |
| et al. | *et alii* | UPEC | Uropathogenic *E. coli* |
| HGT | Horizontal gene transfer | URE | Upstream regulatory element |
| Ler | Locus of enterocyte effacement (LEE)-encoded regulator | WT | Wild-type |
| LLPS | Liquid-liquid phase separation | XS | Xenogeneic silencer |
| MGE | Mobile genetic element | | |

Further abbreviations not included in this section are according to international standards, as, for example, listed in the author guidelines of the Journal of Cell Biology (https://rupress.org/jcb/pages/standard-abbreviations).

# Table of contents

# 1. Abstracts

## 1.1. Summary

Horizontal gene transfer (HGT) is a major driving force of microbial evolution as it allows the rapid acquisition of new genetic traits. However, foreign DNA is likely to decrease the fitness of recipient cells by causing detrimental effects and therefore requires stringent control of gene expression. Hence, bacteria evolved a number of mechanisms allowing them to discriminate between self and non-self. Xenogeneic silencer (XS) proteins are nucleoid-associated proteins that preferentially bind to horizontally acquired DNA based on differences in nucleotide composition, in particular a higher AT content. XS proteins are widely distributed in bacteria and belong to one of the four classes comprising the H-NS-like XS, Rok, MvaT/U-like proteins, and Lsr2-like XS proteins. They play a predominant role in the acquisition of novel genetic material and oligomerization of XS proteins to higher-order nucleoprotein complexes tightly inhibits transcription. Binding of a transcription factor (TF) within a silenced region may interfere with the XS-DNA complex leading to counter-silencing and activation of gene expression. Consequently, XS and counter-silencing facilitate the integration of novel genetic material into host regulatory circuits enabling the appropriate expression in response to physiological and environmental stimuli.

The aim of this thesis was to investigate the rules underlying silencing and counter-silencing of the medically and biotechnologically relevant Lsr2-like proteins conserved in actinobacteria by using CgpS from *Corynebacterium glutamicum* as a model. CgpS has previously been identified as an Lsr2-like XS, which is crucial for maintaining the lysogenic state of an AT-rich, cryptic prophage element.

In this thesis, genome-wide bioinformatic analyses showed that CgpS preferentially binds to long and consecutive AT-rich stretches and that CgpS targets typically feature a distinct drop in GC-profile close to the transcriptional start site (TSS). Furthermore, a sequence-specific binding motif containing multiple A/T steps was overrepresented in CgpS bound regions. The importance of the drop in GC-profile and the putative binding motif for CgpS silencing was verified by performing in vivo reporter studies with synthetic variants of native CgpS target promoters, demonstrating that both DNA features cooperatively support CgpS-mediated silencing.

Following a synthetic counter-silencer approach, the operator sequence of the gluconate-responsive TF GntR was inserted within diverse CgpS silenced promoters at different positions. Binding of GntR led to disruptive counter-silencing at various CgpS target promoters demonstrating flexibility in promoter architecture of these horizontally acquired targets. Almost all binding site positions resulted in differential gene expression, but counter-silencing efficiency strongly depended on the binding site position. The most prominent effect was observed at the position of maximal CgpS binding close to the TSS.

Counter-silencer constructs usually showed only low background activity. To verify their potential as expression systems for synthetic biology applications demanding stringent control of gene expression, activities were compared to established expression systems ($P_{tac}$ and $P_{tet}$). It was demonstrated that counter-silencer constructs have a significantly reduced background activity while showing strong inducibility with temporal tunability.

By combining all synthetic constructs showing differential gene expression, a gluconate-responsive synthetic promoter library was generated (28 activated and 16 repressed promoters). Finally, this overall principle of xenogeneic silencing and counter-silencing was harnessed for the design of a GntR-controlled synthetic toggle switch featuring robust and reversible output in response to gluconate availability. This regulatory circuit was successfully implemented as metabolic toggle in a *C. glutamicum* L-valine production strain and enabled the dynamic redirection of carbon flux between biomass and product formation.

In conclusion, this thesis provides comprehensive insights into the CgpS target recognition mechanism during silencing and shows the first systematic analysis of mechanisms allowing counter-silencing of Lsr2-like XS proteins in actinobacteria. Furthermore, the potential of silencing and counter-silencing for synthetic and biotechnological applications was demonstrated.

## 1.2. Zusammenfassung

Der horizontale Gentransfer (HGT) stellt eine wichtige treibende Kraft der mikrobiellen Evolution dar, da er die schnelle Gewinnung neuer genetischer Merkmale ermöglicht. Fremd-DNA verringert jedoch aufgrund schädlicher Auswirkungen mit hoher Wahrscheinlichkeit die Fitness der Empfängerzellen und erfordert daher eine stringente Kontrolle der Genexpression. Daher entwickelten Bakterien eine Reihe von Mechanismen, die ihnen die Unterscheidung zwischen Selbst und Nicht-Selbst ermöglichen. Xenogene *silencer* (XS) Proteine sind Nukleoid-assoziierte Proteine, die auf Basis von Unterschieden in der Nukleotid-Zusammensetzung, insbesondere einem höheren AT-Gehalt, bevorzugt an horizontal erworbene DNA binden. XS-Proteine sind in Bakterien weit verbreitet und gehören zu einer von vier Klassen. Diese umfassen die H-NS- und MvaT/U-artigen XS, Rok und Lsr2-ähnliche XS-Proteine. XS spielen eine entscheidende Rolle bei dem Gewinn von neuem genetischen Material und durch Oligomerisierung zu Nukleoprotein-Komplexen höherer Ordnung inhibieren sie stark die Transkription. Die Bindung eines Transkriptionsfaktors (TF) innerhalb einer stillgelegten Region kann mit dem XS-DNA-Komplex interferieren. Dies führt zu einer Aufhebung des *silencing* und zur Aktivierung der Genexpression (*counter-silencing*). Demnach erleichtern XS und *counter-silencing* die Integration von neuem genetischen Material in das regulatorische Netzwerk des Wirts und ermöglichen dessen angemessene Expression in Reaktion auf physiologische und umgebungsbedingte Stimuli.

Das Ziel dieser Dissertation war die Untersuchung der Regeln, die dem *silencing* und *counter-silencing* der medizinisch und biotechnologisch relevanten, in Aktinobakterien konservierten Lsr2-ähnlichen Proteinen zugrunde liegen, unter Verwendung von CgpS von *Corynebacterium glutamicum* als Modell. CgpS war zuvor als ein Lsr2-ähnliches XS-Protein identifiziert worden und ist für die Aufrechterhaltung des lysogenen Zustands eines AT-reichen, kryptischen Prophagen-Elements von entscheidender Bedeutung.

In dieser Arbeit zeigten genomweite bioinformatische Analysen, dass CgpS bevorzugt lange und konsekutive AT-reiche Sequenzen bindet und dass CgpS-Ziele typischerweise einen deutlichen Abfall des GC-Profils in der Nähe des Transkriptionsstarts (TSS) aufweisen. Zusätzlich war ein sequenzspezifisches DNA-Motiv mit mehreren A/T-Schritten in CgpS-gebundenen Regionen überrepräsentiert. Dessen Bedeutung und die des mutmaßlichen DNA-Bindungsmotivs für das CgpS-*silencing* wurde durch in vivo Reporterstudien mit synthetischen Varianten von nativen CgpS-Zielpromotoren verifiziert. Diese zeigten, dass beide DNA-Merkmale kooperativ zum CgpS-vermittelten *silencing* beitragen.

In einem synthetischen *counter-silencing* Ansatz wurde die Operatorsequenz des Glukonat-abhängigen TF GntR in verschiedene CgpS-gebundene Promotoren an unterschiedlichen Positionen eingefügt. Die Bindung von GntR führte zu disruptivem *counter-silencing* von mehreren CgpS-Zielpromotoren, wodurch die Flexibilität in der Promotorenarchitektur dieser horizontal erworbenen Ziele demonstriert wurde. Fast alle Bindestellenpositionen führten zu einer differentiellen Genexpression, jedoch war die *counter-silencing* Effizienz stark von der Positionierung abhängig. Der auffälligste Effekt wurde an der Stelle der maximalen CgpS-Bindung in der Nähe des TSS beobachtet.

Üblicherweise wiesen die *counter-silencing*-Konstrukte nur eine geringe Basalaktivität auf. Zur Verifizierung ihres Potenzials als Expressionssysteme für Anwendungen der Synthetischen Biologie, die eine stringente Kontrolle der Genexpression erfordern, wurden ihre Aktivitäten mit denen von etablierten Expressionssystemen ($P_{tac}$ und $P_{tet}$) verglichen. Dabei konnte gezeigt werden, dass *counter-silencing*-Konstrukte eine signifikant reduzierte Basalaktivität und gleichzeitig eine starke Induzierbarkeit mit zeitlicher Abstimmbarkeit aufweisen.

Durch die Kombination aller synthetischen Konstrukte, die eine differentielle Genexpression zeigten, wurde eine Glukonat abhängige, synthetische Promotorbibliothek generiert (28 aktivierte und 16 reprimierte Promotoren). Die *silencing* und *counter-silencing* Prinzipien wurden schließlich für die Konstruktion eines synthetischen, GntR-gesteuerten genetischen Schalters genutzt, der robust und reversibel auf die Verfügbarkeit von Glukonat reagierte. Dieser Regelkreis wurde erfolgreich als metabolischer Schalter in einem *C. glutamicum* L-Valin Produktionsstamm implementiert, wo er die dynamische Umlenkung des Kohlenstoffflusses zwischen Biomasse- und Produktbildung ermöglichte.

Zusammenfassend bietet diese Arbeit umfassende Einblicke in den CgpS-Zielerkennungsmechanismus während des *silencing* und zeigt die erste systematische Analyse von Mechanismen, die das *counter-silencing* von Lsr2-ähnlichen XS-Proteinen in Aktinobakterien ermöglichen. Darüber hinaus wurde das Potenzial von *silencing* und *counter-silencing* für synthetische und biotechnologische Anwendungen demonstriert.

# 2. Scientific context and key results of this thesis

## 2.1. Horizontal gene transfer – a major driving force of microbial evolution

Horizontal gene transfer (HGT), the lateral transfer of DNA between unicellular or multicellular organisms, represents an important evolutionary driving force and strongly increases genetic diversity (Will et al., 2015). Evidences for horizontally transferred DNA are widespread and detectable in all free-living bacteria (Navarre, 2016). Such events were identified among prokaryotes (Jain et al., 1999) and even between members of different kingdoms, e.g. from animals to bacteria (Wolf et al., 1999), from bacteria to archaea (Nelson et al., 1999), and from bacteria to eukaryotes (Doolittle, 1998; White et al., 1983). In contrast to point mutations and genome rearrangements, horizontally transferred mobile genetic elements (MGEs) like plasmids, gene cassettes, transposons, and bacteriophages allow the dynamic acquisition and deletion of large parts of DNA, thereby contributing to rapid adaptations of bacteria to fluctuating and challenging environments (de la Cruz and Davies, 2000; Ochman et al., 2000). For instance, such beneficial traits may provide new metabolic abilities like the utilization of alternative carbon sources (Chu et al., 2018), provide tolerance towards different stresses (Wang et al., 2010) and mainly contribute to the rapid spread of antibiotic drug resistance within microbial communities (Raz and Tannenbaum, 2010; Walsh, 2000). Furthermore, most bacterial virulence genes were acquired via HGT (Navarre, 2016).

The high evolutionary impact of HGT becomes especially remarkable in the light of bacterial speciation and pathogenicity. One example is the contribution of HGT to the divergent evolution of *Salmonella* and *Escherichia coli* from their last common ancestor during the last 140 million years. While housekeeping genes of both species are still very similar (90% identity) (de la Cruz and Davies, 2000), horizontally transferred DNA contributed to evolution of *Salmonella´*s unique pathogenic lifestyle comprising the utilization of various carbon sources, the use of alternative electron acceptors in the absence of oxygen and the induction of inflammation (Desai et al., 2013; Navarre, 2016).

HGT can occur via three different mechanisms: Natural transformation, conjugation, and transduction (Figure 1). While transformation describes the active import of free naked DNA fragments (ssDNA or dsDNA) by a natively competent cell from its surrounding environment (e.g. after cell lysis of a neighbouring cell) (Sun, 2018; Vogan and Higgs, 2011) (Figure 1A), plasmids are typically transferred via conjugation. Conjugation depends on direct cell-cell contacts which are formed by a pilus bridge allowing conjugative plasmids and transposons to autonomously transport one copy of the MGE into another cell (Villa et al., 2019; Vogan and Higgs, 2011) (Figure 1B). Viruses that prey on bacteria, so-called bacteriophages, are present in all ecological niches and represent the most abundant biological entity on earth with an estimated number of $10^{31}$ – which is ten-times higher than the estimated sum of all bacteria cells (Hendrix et al., 1999). By mediating the transfer of bacterial DNA between a donor

and a recipient cell, bacteriophages represent the key players of the generalized and specialized transduction mechanisms (Touchon et al., 2017; Villa et al., 2019) (Figure 1C).

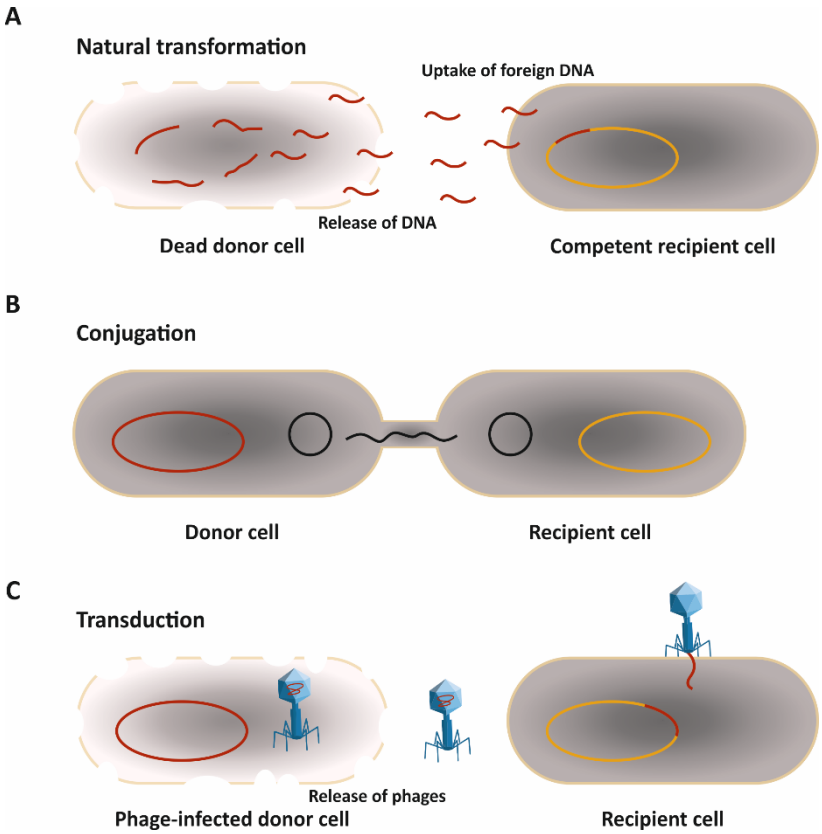


**Figure 1: Mechanisms of horizontal gene transfer. A)** Natural transformation: Uptake, integration, and expression of extracellular DNA, which has been released upon lysis of the donor cell. **B)** Conjugation: DNA is transferred from the donor to the recipient cell via adhesins or pili by direct cell-cell contact. **C)** Transduction: Bacteriophage-mediated DNA transfer from a previously infected donor cell to a recipient cell. Two transduction processes are known. Shown is the generalized transduction mechanism. Instead of phage DNA, random fragments of bacterial DNA (red) are accidentally loaded into the phage head. The second variant, described as specialized transduction, means that fragments of genomic DNA neighbouring the integrated phage DNA are co-excised and additionally loaded into the phage head (not shown). Adapted from Furuya and Lowy (2006).

Depending on their lifestyles, phages are grouped into lytic and temperate phages. The infection with a lytic phage is indispensably connected with the reprogramming of the bacterial host towards the synthesis of new virions, followed by cell lysis and the release of infectious particles. In contrast, temperate phages have two options: the lytic cycle or the stable maintenance as a prophage (lysogenic cycle). During the lysogenic cycle, the viral DNA is replicated in concert with the bacterial DNA, e.g. upon integration into the host genome or by existing as extrachromosomal elements (Casjens, 2003). Functional temperate phages can be induced either SOS-independently, e.g. as response to quorum-sensing signalling molecules, or by the cellular SOS response. DNA damage as a result of antibiotics or physiological stresses can trigger the SOS response which subsequently induces the lytic-lysogenic switch (Ghosh et al., 2009; Janion, 2008; Melechen and Go, 1980). Since the induction of functional prophages usually results in lysis of the host, these viral elements represent a ubiquitous threat for the

cellular fitness. However, whole-genome sequencing approaches revealed that DNA of viral origin is highly abundant in bacterial chromosomes. In some extreme cases, up to 20% of the bacterial genome is comprised by viral DNA (Casjens, 2003). Most of this DNA is not expressed in the prophage state. However, several temperate phage genes can be expressed in the lysogenic state, which may have effects on the host phenotype, causing the lysogenic conversion of the bacterial cell. For instance, prophages often provide pathogenicity determinants such as toxin encoding genes, as reported for the cholera toxin of *Vibrio cholerae*, the diphtheria toxin of *Corynebacterium diphtheriae* as well as for different toxins of *Pseudomonas aeruginosa* and *E. coli* (Hacker et al., 1997). Interestingly, temperate phages can confer resistance to secondary phage infections by different mechanisms, e.g. by surface modifications to block phage binding or DNA injection as well as by repressing the replication of phage DNA (Bondy-Denomy et al., 2016; van Houte et al., 2016).

The high amounts of cryptic, degenerated phage DNA within bacterial genomes reveal the gradual decay which prophage DNA may undergo during the course of evolution. The results are phage elements with defects in specific functions related to cell lysis, viral replication, the formation of phage particles or infectivity (Bobay et al., 2014). These cryptic, grounded prophages have a lower probability to kill the cell, while beneficial traits such as immunity to secondary phage attack may be maintained. Furthermore, they represent hotspots for HGT and are important drivers of bacterial evolution (Ramisetty and Sudhakari, 2019).

## 2.2. How to discriminate between self and foreign?

Although HGT and phage-host interactions strongly shaped bacterial evolution and provided countless beneficial traits, invading foreign DNA still represents a constant threat for the recipient cell forcing microbes to develop defence and control mechanisms. HGT mediated by phages is a double-edged sword for the microbial cell (Faure et al., 2019). It allows the acquisition of beneficial DNA elements. On the other hand, the probability that invading DNA results in harmful effects on the fitness of the recipient cell is high. Foreign DNA elements can interfere with the host regulatory network, disturb the structural integrity of the host chromosome, cause high transcriptional and translational costs or may lead to the production of cytotoxic gene products and sequestration of cellular machineries (Baltrus, 2013; Navarre, 2016; Park and Zhang, 2012; Pfeifer et al., 2016; Vogan and Higgs, 2011). Even the acquisition of potentially useful genes can be a disadvantage if they are not properly controlled in terms of expression timing and strength (Navarre, 2016). Consequently, bacteria evolved various defence mechanisms allowing them to deal with foreign DNA, e.g. DNA of viral origin (Doron et al., 2018). Phage-specific immune systems target different stages of the phage lifecycle. Early systems aim at blocking phage binding and DNA injection, e.g. by surface modification leading to masking, mutating

or loss of host receptor proteins (van Houte et al., 2016). Later mechanisms are based on the recognition of phage nucleic acids or proteins leading to targeted cleavage of the phage genome, to inhibition of phage replication or to the programmed cell death of the host cell (Figure 2). While some defence mechanisms mainly provide immunity for a single cell, others can be considered as multicellular strategy acting at population level. It is important to note that the targeted recognition and degradation of xenogeneic DNA is not limited to phages and can be considered as general mechanisms allowing cells to deal with foreign DNA elements. One important prerequisite of suitable defence systems are mechanisms allowing the recognition and discrimination between self (host) and non-self (horizontally acquired) DNA elements (Goldberg and Marraffini, 2015). Known mechanisms and their molecular basis to meet this challenge will be discussed in the following sections.

### 2.2.1. Destructive defence systems

Destructive defence mechanisms targeting nucleic acids allow the specific recognition and degradation of foreign genetic elements and thereby limit the risk of HGT and phage infection. During evolution, microorganisms developed two general strategies of cellular immunity: the innate immunity comprising genetically encoded mechanisms that recognize general features of foreign nucleic acids and the adaptive immune system that can be considered as cellular memory to previous infections (Amitai and Sorek, 2016).

In the 1950s, Bertani and Luria firstly described the phenomenon of restriction modification after observing that bacteriophage production in newly infected bacterial strains differs depending on the original host strain (Bertani and Weigle, 1953; Luria and Human, 1952). Restriction modification (R-M) systems are considered as innate immune systems providing resistance against foreign DNA independently of previous adaptation steps (Vasu and Nagaraja, 2013). Nowadays, R-M systems summarize widespread defence mechanisms (present in about 74% of prokaryotic genomes (Oliveira et al., 2014)) which cleave and degrade foreign DNA (Figure 2AI). R-M systems were found in a variety of organisms including bacteria and archaea (Pingoud et al., 2005) and often several different systems co-exist in one genome (Oliveira et al., 2014).

The classical R-M systems combine two enzymatic mechanisms, either separated or combined in one protein complex: a restriction endonuclease (REase, restriction enzyme) recognizing and cleaving specific DNA sequences and a methyltransferase (MTase) which epigenetically methylates these sequences in the host chromosome to protect the own genome from self-cleavage (Vasu and Nagaraja, 2013). Even if the invading DNA is methylated, based on the high diversity of systems (almost 4,000 identified restriction enzymes with more than 300 different specificities), in most cases, the methylation pattern will differ from the one of the host cell (Roberts et al., 2010; Vasu and Nagaraja, 2013). R-M systems are currently categorized into four types (I-IV), differing in the mechanisms of

target recognition and cleavage, subunit compositions, required cofactors and substrate specificity (Roberts et al., 2003; Vasu and Nagaraja, 2013).

Interestingly, host-specific DNA modifications allowing to distinguish DNA in terms of self and non-self are not restricted to methylation. The innate Dnd (DNA degradation) defence system is based on phosphorothioate modification at the sugar phosphate backbone of the DNA. It confers nuclease resistance in bacteria (Wang et al., 2007) and prevents replication of viral DNA in archaea (Xiong et al., 2019). Dpd, a further mechanism of DNA modification with the potential to discriminate between self and non-self was previously identified by Thiaville and colleagues. The authors reported the occurrence of inserted 7-deazaguanine derivatives within the DNA which influenced restriction efficiencies during plasmid transformation (Thiaville et al., 2016). Remarkably, a system derivate was identified in different phages, e.g. *in E. coli* phage 9g, and the authors suggested that this modification might act as anti-restriction system by conferring resistance to restriction enzymes of the host (Thiaville et al., 2016).

Further R-M related anti-phage mechanisms are the BREX (Bacteriophage Exclusion) and the DISARM (Defence Islands System Associated with Restriction Modification) system, both using methylation as basis for self/non-self-discrimination (Goldfarb et al., 2015; Ofir et al., 2018). While DISARM results in restriction of phage DNA and act as a multi-gene restriction-modification module (Ofir et al., 2018), the BREX system leads to a blockage of phage DNA replication (Goldfarb et al., 2015).

In contrast to the abovementioned innate R-M systems, the highly diverse and complex CRISPR-Cas (Clustered Regularly Interspaced Short Palindromic Repeats and CRISPR-associated proteins) systems represent the adaptive bacterial and archaeal immunity with a memory function (Figure 2AII) (Amitai and Sorek, 2016; Faure et al., 2019). CRISPR-Cas systems were identified in almost all archaeal genomes and in about one third of all bacteria (Faure et al., 2019; Koonin et al., 2017). The CRISPR-Cas immune response can be divided into three stages: adaptation, processing, and interference. During adaptation, a complex of different Cas proteins recognizes and binds a two to four base pair short protospacer adjacent motif (PAM) within the foreign DNA, followed by the excision of a short DNA fragment (protospacer), which is inserted as spacer into the host CRISPR array. Upon transcription of the CRISPR array, the precursor CRISPR RNA (crRNA) is processed into small maturated, one spacer crRNAs by Cas proteins or non-Cas ribonucleases. During interference, crRNAs function as guide for Cas nucleases by specifically recognizing sequence complementarities to protospacers in an invading plasmid or viral genome. Finally, Cas nucleases cleave and inactivate the complementary foreign DNA, thereby protecting the cell against potentially detrimental fitness effects (Amitai and Sorek, 2016; Faure et al., 2019). Remarkably, the authors of a recent review summarized observations hinting that CRISPR-Cas might have functions going beyond immunity, e.g. inhibiting or stimulating regulatory

effects on HGT, signal transduction, programmed cell death, DNA repair systems, plasmid maintenance and transposon integration (Faure et al., 2019).

R-M and CRIPSR-Cas systems were intensively studied in the past and were demonstrated to efficiently provide resistance against incoming foreign DNA. However, recent studies revealed that we have still underestimated the degree of complexity of bacterial defence systems. While the above described mechanisms mainly act at the cellular level, the secretion of small secondary molecules were recently described by Kronheim and colleagues as putative innate chemical anti-phage defence strategy at population level (Figure 2B) (Kronheim et al., 2018). By systematically screening secondary molecules naturally produced by *Streptomyces*, they could show that sub-inhibitory concentrations of several DNA-intercalating molecules (e.g. daunorubicin and doxorubicin) inhibit replication of phage dsDNA but not bacterial cell growth. The authors suggested that the self/non-self-discrimination was based on differences in the DNA states of the host and the phage genome: the invading phage genome is linear, non-supercoiled and unbound by protecting DNA-binding proteins (Kronheim et al., 2018).

Further anti-phage defence strategies are collectively referred to as abortive infection (Abi) systems (Bernheim and Sorek, 2020) (Figure 2C). In general, these post infection resistance mechanisms are part of the bacterial innate immunity and act at population level (Dy et al., 2014). In cases when earlier immune responses failed to prevent phage infection (e.g. R-M systems), Abi systems prevent the spreading of phages by enabling the host cell to kill itself (programmed cell death) or to arrest in a dormant state before functional phage particles are formed (Bernheim and Sorek, 2020). These strategies are diverse and found in a variety of microorganism, e.g. *E. coli* (Bingham et al., 2000), *Lactococcus spp.* (Durmaz and Klaenhammer, 2007), and *Staphylococcus spp.* (Depardieu et al., 2016). Their common objective is the protection of the bacterial community from a viral epidemic by sacrificing the infected host cell. Therefore, Abi systems are considered as altruistic cell death systems (Bernheim and Sorek, 2020; Dy et al., 2014; van Houte et al., 2016). Typical triggers of these mechanisms are phage proteins, phage nucleic acids or the state of a cell after phage infection (Bernheim and Sorek, 2020).

In addition to the discussed strategies, a variety of further systems exist which are suggested to provide defence against foreign DNA elements (reviewed in (Bernheim and Sorek, 2020; van Houte et al., 2016)), highlighting the multiplicity of defence mechanisms. At present, we are only just beginning to understand the complexity of prokaryotic immune systems, including their molecular mechanisms, not to mention the far-reaching interplay of these mechanisms in living cells.

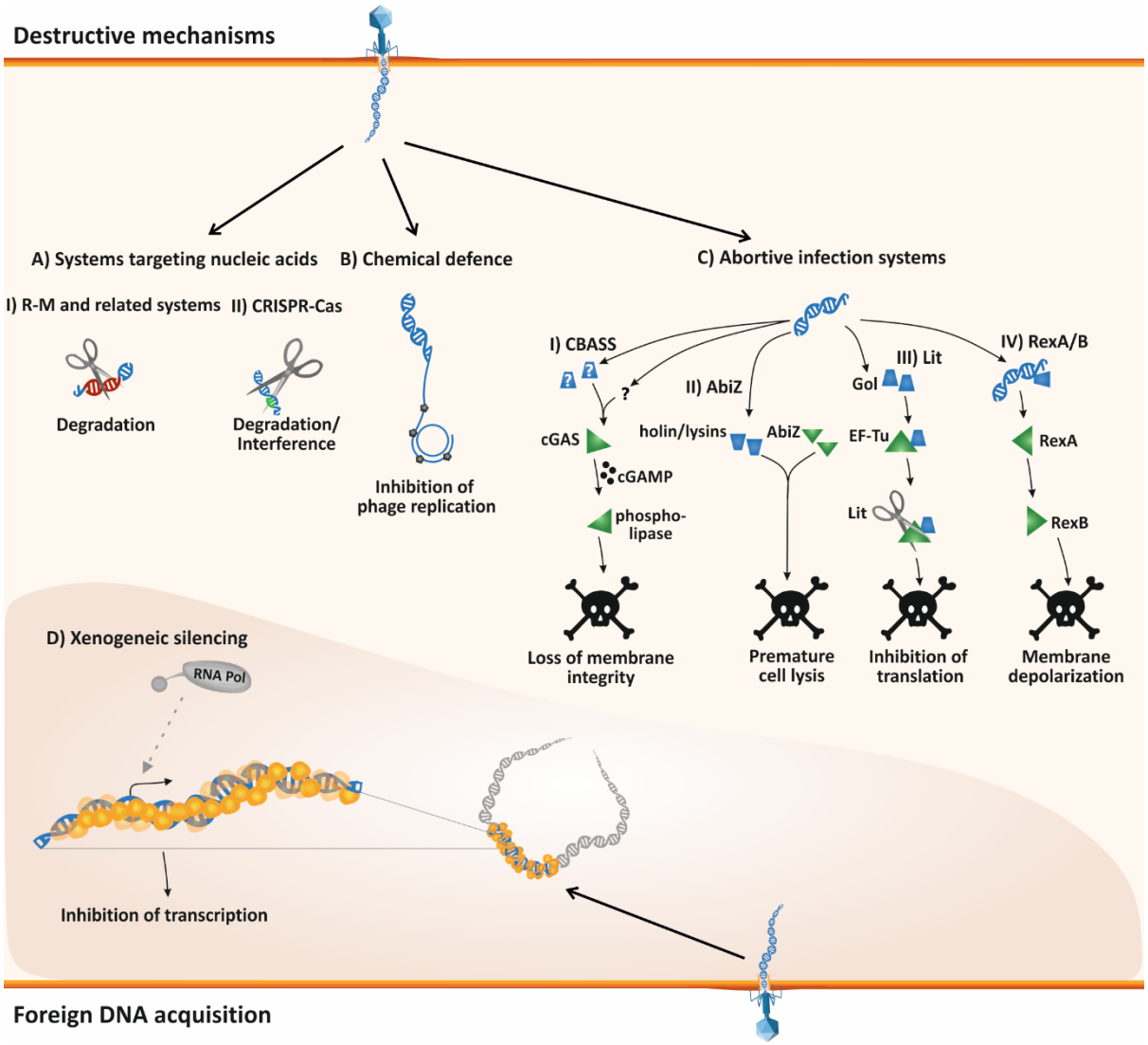


**Figure 2: Defence systems protecting cells against invading foreign DNA. A)** Systems targeting nucleic acids. **I)** Restriction modification (R-M) and related systems. **II)** CRISPR-Cas systems. **B)** Chemical defence systems. **C)** Abortive infection (Abi) systems. Different examples for Abi systems are given. **I)** Cyclic oligonucleotide-based anti-phage signalling systems (CBASSs) of *E. coli* and *V. cholerae*. Cyclic GMP-AMP (cGAMP) is produced by cyclic GMP–AMP synthase (cGAS) as response to phage infection. The molecular mechanism has yet not been identified. cGAMP signalling activates downstream effector proteins, e.g. a phospholipase which degrades the inner cell membrane, which finally leads to cell death (Cohen et al., 2019). **II)** The AbiZ protein of *Lactococcus spp.* acts together with phage lysins and holins and triggers cell lysis before functional phage particles are formed (Durmaz and Klaenhammer, 2007). **III)** *E. coli* Lit protein senses a complex composed of the T4 phage peptide Gol and the ribosomal elongation factor EF-Tu. Consequently, Lit cleaves EF-Tu resulting in translation inhibition and cell death (Bingham et al., 2000). **IV)** The Rex system of lysogenic *E. coli strains* which is involved in maintaining the lysogenic state of phage λ. Upon sensing of phage protein-DNA complexes, RexA becomes active and activates the membrane-anchored ion channel protein RexB. RexB activation leads to membrane depolarization and dropping ATP levels. Consequently, ATP-dependent replication of phage DNA is aborted (Parma et al., 1992; van Houte et al., 2016) **D)** Foreign DNA acquisition mediated by xenogeneic silencing. Xenogeneic silencer proteins recognize AT-rich foreign DNA. DNA binding of these proteins leads to the formation of a higher-order nucleoprotein complex which inhibits transcription, thereby leading to silencing of the horizontally acquired DNA (Pfeifer et al., 2019). Although XS proteins preferentially bind to these foreign genetic elements and play an important role in maintaining the lysogenic state of prophages (Pfeifer et al., 2016), the function of XS proteins during phage infection is still unclear. Adapted from Bernheim and Sorek (2020), Pfeifer et al. (2019), van Houte et al. (2016).

Interestingly, different defence systems or derivates of the same mechanism often co-exist in one single genome with the potential to act synergistically (Bernheim and Sorek, 2020). In general, defence systems are often physically clustered in certain genome regions, so-called defence islands. These

regions are often enriched with genes encoding recombinases and transposases which might facilitate HGT by conferring mobility of the islands (Makarova et al., 2011). Furthermore, these islands can provide hotspots for the integration of horizontally transferred elements (Bernheim and Sorek, 2020). Recently, Doron and colleagues performed an elegant analysis based on the clustering of immune systems in defence islands (Doron et al., 2018). Following the idea that unknown defence systems might be located close to known systems in bacterial genomes and that gene orders could be conserved, they systematically mapped microbial genome regions to identify putative candidates. By performing comprehensive characterization, they were able to identify nine new anti-phage defence systems and one system involved in defence against plasmids (Doron et al., 2018), highlighting the abovementioned complexity of defence strategies.

### 2.2.2. Xenogeneic silencers

In contrast to destructive defence mechanisms, xenogeneic silencer (XS) proteins promote tolerance towards foreign (xenogeneic) DNA (Figure 2D) (Navarre et al., 2007; Pfeifer et al., 2019). XS proteins are specialized nucleoid-associated proteins (NAPs) and represent the molecular basis of the xenogeneic silencing mechanism. They recognize and bind AT-rich, horizontally acquired DNA and their subsequent oligomerization inhibits transcription of these genetic elements (Fang and Rimsky, 2008; Gordon et al., 2011; Navarre, 2016; Navarre et al., 2007). The discrimination between self and non-self is mainly based on differences in nucleotide composition of the DNA, in particular the proportion of adenines and thymines (AT content), between the foreign element and the genome of the recipient cell (Navarre et al., 2007). Since XS proteins prevent the uncontrolled expression of foreign DNA and consequently protect the cells from potential detrimental effects, they were recently considered as part of the bacterial immune system (Navarre, 2016; Pfeifer et al., 2019). Xenogeneic silencing prevents the production of putative toxic compounds. Furthermore, it also represents an important fitness trait to avoid sequestering of the RNA polymerase and spurious transcription of AT-rich DNA sequences from adventitious promoters, explaining XS binding sites in intragenic regions. In particular, XS prevents the titration of the RNA polymerase away from GC-rich promoters, antisense transcript expression as well as transcription of neighbouring genes (Lamberte et al., 2017; Singh et al., 2014). The importance of XS proteins is reflected in the consequences of their loss for bacterial fitness, ranging from subtle to extreme and even to cell death depending on the bacterial species (Castang and Dove, 2012; Navarre, 2016; Navarre et al., 2006; Pfeifer et al., 2016).

### 2.2.3. Base composition as discrimination factor between self and non-self

Bacterial genomes show strong variance in overall GC content and differ between less than 20% in bacterial endosymbionts to actinobacterial genomes of more than 70% (Hildebrand et al., 2010;

Zamenhof et al., 1952). Extreme examples are the genomes of the proteobacterial symbiont *Carsonella ruddii* strain Pv with a low GC content of about 16.5% (Nakabachi et al., 2006) and the actinobacterium *Frankia alni* strain ACN14a having a high GC content of 72.8% (Normand et al., 2007). Nevertheless, as mentioned before, all known XS preferentially target DNA which has a higher AT content than the host genome, meaning they use base composition as discrimination factor between self and non-self.

Theoretically, different molecular reasons would prefer the accumulation of adenines and thymines in bacterial genomes in the course of evolution (Figure 3). For instance, energetic costs for guanine and cytosine are higher compared to adenine and thymine and high amounts of adenosine triphosphate (ATP) are present in bacterial cells (Rocha and Danchin, 2002). Furthermore, reactive oxygen species can trigger the oxidative deamination of cytosine to uracil-like products, resulting in C-T transitions, or can induce the oxidation of guanine, leading to G-T transversions (Wang et al., 1998) (Figure 3). In theory, in the absence of appropriate DNA repair systems, these factors would favour the accumulation of A and T within a bacterial genome over time. Indeed, in bacterial endosymbionts lacking important DNA repair systems due to drastic genome reductions, mutation rates from G/C to A/T are three times higher than from A/T to G/C, resulting in highly AT-rich genomes of these host-restricted bacteria (Moran et al., 2009).

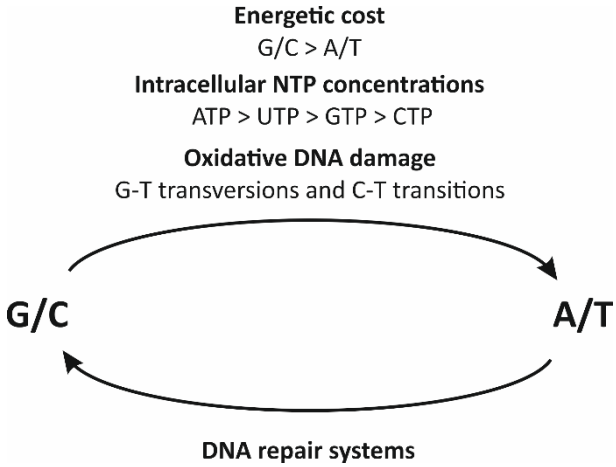


**Figure 3: Molecular reasons for the shift towards high AT content in the absence of appropriate DNA repair systems.** Different molecular reasons would favor the accumulation of A and T in DNA molecules, including the lower energetic costs of A and T in comparison to G and C, the intracellular ratios of nucleoside triphosphates (NTPs), as well as G-T transversions and C-T transitions caused by oxidative DNA damages. Appropriate DNA repair systems counteract this base shift allowing bacteria to keep a certain GC content (Moran et al., 2009; Rocha and Danchin, 2002; Wang et al., 1998). [Abbreviations: NTP, nucleoside triphosphate; ATP, adenosine triphosphate; UTP, uridine triphosphate; GTP, guanosine triphosphate; CTP, cytidine triphosphate].

These reasons might also explain why HGT elements such as plasmids and phages often tend to be AT-rich when they enter a host cell (Rocha and Danchin, 2002). Consistently, genes which are unique for single or few species and therefore considered as being horizontally acquired typically show lower, even decreasing GC contents over time. In contrast, many bacteria species strictly keep a certain GC

content in their core genome, e.g. by using efficient DNA repair mechanisms (Desai et al., 2013; Navarre, 2016). These stable differences in GC content between ancestral core genes and horizontally acquired DNA elements suggest an evolutionary selection pressure which prevents the adaptation of GC contents (Desai et al., 2013; Navarre, 2016). In the light of evolution, a potential reason for this phenomenon might be that XS proteins use base composition as discrimination factor between self and non-self (Navarre et al., 2007). XS proteins preferentially bind to AT-rich DNA and therefore enable silencing of previously acquired AT-rich foreign DNA elements as well as of those which prospectively enter the cell. In this way, they protect the cell from uncontrolled expression of potentially harmful genes. In contrast, GC-rich xenogeneic DNA cannot be silenced by most XS proteins due to their mechanism of target recognition (will be discussed in chapter 2.3.3. "How do xenogeneic silencers recognize their targets?"). Therefore, XS proteins cannot buffer against harmful effects of GC-rich elements. These fitness consequences might lead to cell death of the recipient cell and prevent the stable manifestation of GC-rich elements in bacterial genomes (Navarre, 2016). Consistently, XS do not target all DNA elements which are horizontally acquired. For instance, Smits and colleagues demonstrated that the XS protein Rok does not bind the defective prophage PBSX which has a nucleotide composition similar to that of the *Bacillus subtilis* host genome (Smits and Grossman, 2010).

## 2.3. Xenogeneic silencing

The following sections will provide an overview on the four currently known classes of XS proteins, their main targets, the molecular basis of target recognition and formation of the nucleoprotein complex as well as involved accessory factors.

### 2.3.1. Four classes of xenogeneic silencers

XS proteins are present in a variety of different bacterial species including Gram-positive and -negative bacteria (Suzuki-Minakuchi and Navarre, 2019). Currently known XS proteins are grouped into four previously described classes based on their amino acid sequence and structure: H-NS and its paralogs were found in different α-, β-, and λ-proteobacteria like *Salmonella*, *Yersinia* and *E. coli* (Heroven et al., 2004; Navarre et al., 2006; Oshima et al., 2006), MvaT/U-like XS proteins have been identified in λ-proteobacteria of the order Pseudomonodales, e.g. *P. aeruginosa* (Castang et al., 2008; Tendeng et al., 2003), while Lsr2-like proteins function as XS in Actinomycetes (Gordon et al., 2008; Gordon et al., 2010; Pfeifer et al., 2016). Finally, Smits and colleagues proposed in 2010 that Rok, found in different *bacilli* species such as *B. subtilis*, is a functional analogue of H-NS and Lsr2 and represents the fourth class of XS proteins (Smits and Grossman, 2010).

Members of the different XS families display no or very low sequence similarities (<20%) but share a similar overall domain architecture comprising an N-terminal oligomerization domain and a C-terminal DNA binding domain connected by a flexible linker (Duan et al., 2018; Gordon et al., 2010; Navarre, 2016; Smits and Grossman, 2010; Tendeng et al., 2003). Interestingly, recent studies reported that the linker of H-NS has multiple functions: it provides flexibility between both domains and contributes to filament formation as well as to DNA binding affinity (Gao et al., 2017; Gulvady et al., 2018). Although they differ in terms of their molecular binding mechanism, they all show a preference for DNA sequences which are AT-rich in comparison to their host genomes and these elements are often of horizontal origin (Navarre, 2016). Upon binding to the AT-rich DNA, XS proteins oligomerize to form a dense nucleoprotein complex which finally leads to gene silencing. These convergently evolved functional similarities allowed in several cross-complementation studies with unrelated XS the full or partial recovery of wild type-like phenotypes of XS-deficient strains (Gordon et al., 2008; Pfeifer et al., 2016; Tendeng et al., 2003). Interestingly, Gordon and colleagues demonstrated even an interchangeability of the single domains between H-NS and Lsr2 resulting in functional chimeric XS proteins (Gordon et al., 2010), highlighting the functional similarities of the single domains.

The best characterized XS, the histone-like nucleoid structuring protein H-NS, is with about 20,000 copies per cell highly abundant in exponentially growing proteobacterial cells and represents one of the major NAPs in these species (Amit et al., 2003). The family of H-NS-like XS is highly diverse and one main function of these proteins is the silencing of AT-rich, horizontally acquired foreign DNA elements (Lucchini et al., 2006; Navarre et al., 2006). However, disruption of H-NS affected over 5% of all genes in *E. coli* which appear to be unlinked (Amit et al., 2003; Arold et al., 2010; Hommais et al., 2001). Furthermore, H-NS mediates gene expression in response to changes in osmolarity, pH, and temperature (Amit et al., 2003; Arold et al., 2010), demonstrating its function as global regulator of gene expression. As a NAP, H-NS inherits also an important role in the organization of the chromosome structure (Noom et al., 2007; Ueguchi et al., 1996; Wang et al., 2011)

In 1998, MvaT was initially identified as regulator of mevalonate catabolism in *Pseudomonas mevalonii* (Rosenthal and Rodwell, 1998). Based on complementation assays with *hns* deficient *E. coli* mutants and sequence alignments, Tendeng and colleagues showed that MvaT from *Pseudomonas Y1000* is functionally related to H-NS (Tendeng et al., 2003). MvaT shares structurally similarity with H-NS (Ding et al., 2015). However, in comparison to H-NS from *E. coli*, MvaT displays an amino acid sequence similarity of less than 20% and has a different DNA binding mechanism (Tendeng et al., 2003). Remarkably, while MvaT was only found in λ-proteobacteria, all *Pseudomonas* species harbour at least one MvaT homologous; *Pseudomonas putida* has even five (Tendeng et al., 2003). By performing

chromatin immunoprecipitation (ChIP) coupled with DNA microarrays (ChIP-on-chip) experiments, Castang and colleagues demonstrated strongly overlapping binding patterns for MvaT and its homolog MvaU in the opportunistic pathogen *P. aeruginosa*, suggesting that both proteins function coordinately and even form heteromeric silencer complexes. Based on the binding preference of these proteins for AT-rich DNA regions which are often horizontally acquired, the authors confirmed that MvaT and MvaU function as XS in *Pseudomonas* (Castang et al., 2008).

Rok was initially identified as negative regulator of natural competence in *B. subtilis* since it represses the expression of the *comK* gene, coding for the master regulator of this pathway (Hoa et al., 2002). However, Rok controls the acquisition of horizontal gene elements on a second layer. ChIP-chip analyses revealed that Rok binds to DNA elements which are characterized to be AT-rich and many of its targets are thought to be horizontally acquired (Smits and Grossman, 2010). Comparably to H-NS and MvaT, the N-terminal domain of Rok mediates multimerization into a higher-order nucleoprotein complex leading to silencing of target genes (Duan et al., 2018; Smits and Grossman, 2010). Interestingly, Rok itself is suggested to be the result of a HGT event since it is only present in some *bacilli* species including *B. subtilis*, *B. licheniformis*, and *B. amyloliquefaciens* where it is inserted into an otherwise conserved chromosome region (Albano et al., 2005; Duan et al., 2018). Contrastingly, no Rok orthologs could be identified in other *Bacillus* species such as *B. anthracis*, *B. cereus*, and *B. halodurans* (Albano et al., 2005; Duan et al., 2018).

Lsr2 is a strongly conserved XS protein found in Gram-positive Actinomycetes, e.g. in mycobacterial and *Streptomyces* species (Gehrke et al., 2019; Gordon et al., 2008). Although it displays no significant sequence similarity with H-NS and both differ strongly in their secondary structure, complementation assays with *E. coli* H-NS-deficient mutants revealed that Lsr2 acts as a functional analogue of H-NS (Gordon et al., 2008). Comparably, its targets appear to have higher AT contents and are often horizontally acquired (Gordon et al., 2010).

Recently, Pfeifer and colleagues identified CgpS (*C. glutamicum* prophage silencer) as the first example of a prophage-encoded Lsr2-like XS protein in the actinobacterium *Corynebacterium glutamicum* (Pfeifer et al., 2016). It is homologous to mycobacterial Lsr2. While both proteins share considerable low amino acid sequence identity (~23%), they display striking similarities at the structural level. Genome-wide binding profiles of chromatin affinity purification and sequencing (ChAP-seq) experiments revealed an association of CgpS to AT-rich DNA elements, most of which are located within cryptic prophage regions (about 65% of the 90 targets). CgpS is not essential in the absence of the cryptic prophage CGP3, but interference with CgpS oligomerization resulted in prophage induction in wild-type cells. Altogether, these findings demonstrated that its major function is the silencing of

the prophage element CGP3 to control its lysogenic state (Pfeifer et al., 2016). Remarkably, CgpS was the first characterized example of a prophage-encoded XS and further bioinformatic analysis revealed that this feature is unique for Lsr2-like XS (Pfeifer et al., 2019). The rules underlying CgpS mediated xenogeneic silencing and mechanisms allowing the implementation of foreign DNA elements into host regulatory networks of *C. glutamicum* were the main topics of this thesis (Wiechert et al., 2020a).

### 2.3.2. Main targets of xenogeneic silencer proteins

A huge amount of transcriptome and binding assays revealed that the scopes of targets of individual XS proteins are highly diverse and most of them are thought to be horizontally acquired and significantly AT-rich (Castang et al., 2008; Gehrke et al., 2019; Gordon et al., 2010; Navarre et al., 2006; Pfeifer et al., 2016; Smits and Grossman, 2010). Remarkably, binding assays identified an association of XS-silencer proteins of all families with their own promoter region, indicating autoregulation as important point in controlling silencing activity (Castang et al., 2008; Gordon et al., 2010; Pfeifer et al., 2016; Smits and Grossman, 2010; Ueguchi et al., 1993).

Furthermore, proteins from all XS classes are involved in the repression of prophage-like elements (Castang and Dove, 2012; Gordon et al., 2010; Hong et al., 2010; Pfeifer et al., 2016; Smits and Grossman, 2010), highlighting their ancient function to protect the host cells from detrimental effects caused by viral gene expression. However, in contrast to the Lsr2-like XS protein CgpS from *C. glutamicum* which has a specialized function as regulator of prophage elements (Pfeifer et al., 2016), several other XS proteins act as central regulators of virulence, secondary metabolic pathways, and drug resistance. For instance, ChIP-on-chip experiments with H-NS from *Salmonella* revealed that H-NS binds to more than 17% of all chromosomal genes comprising several virulence elements such as *Salmonella* pathogenicity island (SPI) -1 and SPI-2, encoding two type III secretion systems (T3SSs) (Navarre et al., 2006). Comparably, H-NS is an important regulator of virulence in *Yersinia* (Heroven et al., 2004), in enterohemorrhagic and uropathogenic *E. coli* (Müller et al., 2006; Wan et al., 2016), in *Shigella flexneri* (Turner and Dorman, 2007) as well as in *V. cholerae* (Ghosh et al., 2006).

ChIP-on-chip experiments with MvaT and its homolog MvaU from *P. aeruginosa* PAO1 revealed a large set of targets (almost 400 genes) including genes coding for toxic secondary metabolites, regulators of virulence and quorum sensing, the filamentous prophage Pf4 as well as many putative and known virulence factors (Castang and Dove, 2012; Castang et al., 2008). ChIP-seq analysis with Rok from *B. subtilis* led to the identification of more than 250 target regions, which were often associated with cooperative DnaA binding, e.g. the *oriC* region (Seid et al., 2017). Targets of Rok are the conjugative transposon *ICEBs1* and prophage elements, demonstrating its function as XS. Further important targets of Rok are the aforementioned *comK* gene as well as genes encoding secreted antibiotics and signalling molecules or for proteins involved in transport and secretion (Albano et al., 2005; Smits and Grossman,

2010). By performing ChIP-chip analyses with Lsr2 from *Mycobacterium tuberculosis*, Gordon and colleagues identified binding to 21% of all coding genes. Lsr2 targets are involved in virulence, cell wall and cell processes as well as PE/PEE genes coding for surface-exposed antigens which are important for interactions with the host (Gordon et al., 2010). In contrast, Lsr2 from *Streptomyces venezuelae* has evolved as a central regulator of specialized metabolic clusters comprising horizontally acquired and well-conserved clusters (Gehrke et al., 2019).

These findings that Lsr2 is involved in the regulation of medically relevant mycobacterial virulence determinants (Gordon et al., 2010) and biotechnologically interesting cryptic metabolite clusters in *Streptomyces* (Gehrke et al., 2019) motivated us to understand Lsr2-mediated silencing as well as the mechanisms allowing the reactivation of silenced genes. In the here presented work we used CgpS of *C. glutamicum* as a model system to decipher the rules underlying silencing and counter-silencing of Lsr2-like XS proteins (Wiechert et al., 2020a).

Loss of the silencing mechanism, e.g. by deleting the encoding gene or by inducing interference effects, can, but do not need to cause lethality. This strongly depends on how increased expression of XS targets affect the bacterial fitness. As mentioned before, the presence of the prophage element CGP3 determines the essentiality of CgpS for *C. glutamicum* (Pfeifer et al., 2016). Castang and colleagues showed in a systematic transposon screen that *P. aeruginosa* cannot tolerate the double deletion of the genes encoding the XS paralogs MvaT and MvaU in the absence of suppressor mutations affecting the lifecycle of the Pf4 phage, indicating phage activity as detrimental fitness consequence (Castang and Dove, 2012). Interestingly, the essentiality of H-NS-like XS depends on the genetic background of the respective strain. While H-NS is essential in *Yersinia* species (Ellison and Miller, 2006; Heroven et al., 2004) and loss of H-NS results in severe growth defects in *Salmonella*, probably caused by increased expression of H-NS regulated pathogenic islands (Ali et al., 2014; Lucchini et al., 2006; Navarre et al., 2006), laboratory *E. coli* strains can tolerate H-NS deficiency to a certain extent (Barth et al., 1995; Navarre, 2016).

### 2.3.3. How do xenogeneic silencers recognize their targets?

As mentioned above, XS proteins show a clear preference for AT-rich DNA. These proteins interact with the DNA via their C-terminal DNA binding domain. Mutant variants of XS proteins which are able to oligomerize but lose their ability to bind the DNA, e.g. due to point mutations or the absence of the C-terminal domain, interfere with silencing, demonstrating that DNA binding is essential for silencing (Chen et al., 2008; Gehrke et al., 2019; Gordon et al., 2008; Pfeifer et al., 2016; Williamson and Free, 2005). High-resolution structures obtained with nuclear magnetic resonance (NMR) spectroscopy of the C-terminal DNA binding domains of H-NS (Gordon et al., 2011), Lsr2 (Gordon et al., 2010), MvaT

(Ding et al., 2015), and Rok (Duan et al., 2018) in complex with DNA revealed that they all insert with specific residues into the narrow, deep and electronegative minor groove of AT-rich DNA. The exocyclic 6-amino group present in GC-rich DNA sequences can sterically block the minor groove of the DNA. Thus, the absence of this group in AT-rich DNA can further facilitated the interaction of XS proteins with the DNA (Ali et al., 2012; Duan et al., 2018; Navarre, 2016; Pfeifer et al., 2019). However, the underlying molecular binding mechanisms are different (Figure 4). H-NS and Lsr2 binding is mediated via a convergently evolved Q/RGR motif: the prokaryotic AT-hook (Ali et al., 2012). Based on secondary structure predictions, Pfeifer and colleagues suggested that CgpS, the Lsr2-like XS of *C. glutamicum*, binds the DNA via a similar RGI motif (Pfeifer et al., 2016). In contrast, MvaT inserts into the DNA minor groove via a conserved lysine (R) and a downstream located GN motif (R-GN), the so-called AT-pincer, while additional conserved lysine residues interact with the DNA backbone (Ding et al., 2015; Duan et al., 2018). Rok has neither an AT-hook nor an AT-pincer motif. Instead, Rok uses a motif of three non-consecutive amino acids (N-T-R) to form hydrogen bonds with the DNA minor groove, while four lysine residues interact with the negatively charged phosphate backbone of the DNA (Duan et al., 2018) (Figure 4).

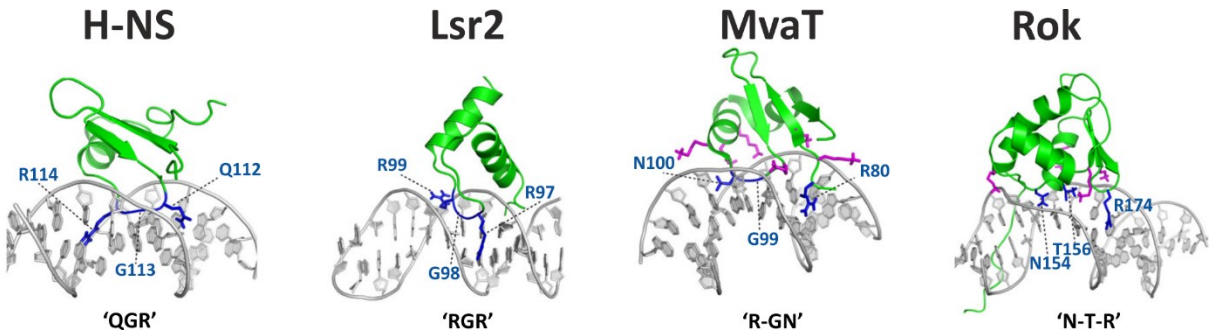


**Figure 4: The DNA recognition mechanisms of the four XS protein classes based on structure models.** H-NS and Lsr2: Amino acid residues forming the AT-hook motif of H-NS (´QGR´) and Lsr2 (´RGR´) are highlighted in blue. MvaT: Residues forming the AT-pincer of MvaT (´R-GN´) are coloured in blue, while the lysine residues interacting with the sugar-phosphate backbone are shown in magenta. Rok: The three non-consecutive amino acids (´N-T-R´) allowing Rok to form hydrogen bonds with the DNA minor groove are highlighted in blue. The four lysine residues interacting with the negative charged phosphate groups of the DNA are coloured magenta. Figure and information adapted from Duan et al. (2018).

Although all XS proteins are reported to bind specifically to AT-rich DNA and are able to silence in heterologous hosts (Gordon et al., 2008; Pfeifer et al., 2016; Tendeng et al., 2003), diversity in their recognition mechanisms leads to differences in target preferences. In vitro protein binding microarray (PBM) experiments with MvaT, H-NS, Lsr2 and Rok were previously performed (Ding et al., 2015; Duan et al., 2018; Gordon et al., 2011). For the analysis of their DNA binding affinities, microarray slides with short double stranded DNA oligonucleotides were used. These short DNA sequences differed in AT content, in the presence of TpA steps or A-tracts as well as in length of contiguous AT-stretches. Typically, these arrays were designed in such a way that all possible eight nucleotide long sequences

(8-mer) were present multiple times. To determine binding affinities and preferences of the XS proteins to the different DNA oligonucleotides, XS were N-terminally fused to a glutathione S-transferase (GST) tag allowing their detection on the microarray slide via GST-specific antibodies (Ding et al., 2015; Duan et al., 2018; Gordon et al., 2011). The screening for highly scored 8-mer sequences in DNA regions which were bound by the respective XS protein in ChIP-seq or ChIP-on-chip experiments revealed an overrepresentation of these 8-mers, suggesting that they are relevant for silencing in vivo (Duan et al., 2018; Gordon et al., 2011). These studies demonstrated that MvaT, H-NS and Rok prefer DNA stretches containing flexible TpA steps, which induce local widening of the DNA minor groove, while Lsr2 from *M. tuberculosis* prefers A-tracts instead of TpA steps (Ding et al., 2015; Duan et al., 2018; Gordon et al., 2011). Furthermore, these experiments showed that Lsr2, MvaT and H-NS uniformly favour contiguous AT-sequences without strict sequence specificity (Duan et al., 2018). In contrast, the unique binding mechanism of MvaT provides greater tolerance for G/C interruptions in comparison to H-NS and Lsr2, possibly due to the AT-pincer motif which leaves a cavity in the protein-DNA interface for exocyclic amino groups (Ding et al., 2015). Interestingly, Rok disfavours rigid A-tracts and even prefers single G/C interruptions within its target sequence. Additionally, a distinct number of sequence-specific Rok binding motifs containing flexible TpA steps were identified (AACTA, TACTA) (Duan et al., 2018). These motifs are highly underrepresented in the core genomes of *rok* encoding *bacilli* strains and even allow specific binding of Rok to targets that do not differ in GC content from the core genome, e.g. the promoter regions of *comK* and of its own gene (Duan et al., 2018; Smits and Grossman, 2010).

In our recent study, which is part of this thesis, we investigated the rules underlying target recognition of the Lsr2-like XS CgpS from *C. glutamicum*. Therefore, we performed bioinformatic analyses of recently obtained CgpS ChAP-seq data, in vitro binding studies as well as in vivo reporter assays (Wiechert et al., 2020a). Consistently with the previously mentioned in vitro binding studies for Lsr2, the genome-wide analysis of CgpS targets revealed a clear preference of CgpS towards consecutive AT-rich stretches. The fraction of CgpS targets increased with the length of the AT-rich stretch, while GC-interruptions tended to decrease binding, revealing similarities to the abovementioned results for Lsr2 from *M. tuberculosis* (Ding et al., 2015; Duan et al., 2018). However, in contrast to reports for Lsr2 which failed to identify a sequence-specific binding motif (Chen et al., 2008; Duan et al., 2018; Gehrke et al., 2019), our analysis revealed the overrepresentation of a 10 bp long AT-rich binding motif containing A/T steps (alteration of A to T and vice versa) (Figure 5A) within CgpS targets. The rather specialized function of CgpS as a silencer of prophage elements in *C. glutamicum* could be a possible explanation for this discrepancy. The identified motif was present in 51 of 54 bound promoters and often located close to the position of maximal CgpS binding (exemplarily shown in Figure 5B). Based

on the analysis of the GC-profiles of CgpS target promoters and their CgpS binding peaks, we grouped in our study the promoters into two different classes. Class 1 promoters, e.g. $P_{lys}$ and $P_{cg1999}$, were typically characterized by a distinct drop in GC content and a bell-shaped CgpS binding peak and were mainly focused in our analyses (Wiechert et al., 2020a) ($P_{cg1999}$ exemplarily shown in Figure 5B). In contrast, CgpS coverage peaks of class 2 promoters were wider and characterized by broader or multiple drops in GC content. We were able to confirm the importance of the identified motif for CgpS-mediated silencing by performing in vivo reporter studies with synthetic promoter variants based on the class 1 CgpS target promoter $P_{lys}$. To monitor promoter activities in vivo, we fused the $P_{lys}$ variants to the reporter gene *venus*. A construct containing the motif was efficiently bound by CgpS, while CgpS was not able to silence the control promoter lacking this motif (Wiechert et al., 2020a). However, in contrast to the binding motif of Rok which is underrepresented in the host genome (Duan et al., 2018), our genome wide analysis of CgpS motif occurrence revealed that about 85% of these sequences are not bound by CgpS in vivo under standard conditions, indicating that the motif alone does not efficiently mediate CgpS binding (Wiechert et al., 2020a).

A sophisticated model for the mechanism of silencing was proposed for *E. coli* H-NS. In vitro studies with H-NS demonstrated high affinity of H-NS towards DNA enabling scanning of the molecule until the XS protein reaches sequence-specific motifs (tCG(t/a)T(a/t)AATT) serving as nucleation sites. Subsequent cooperative binding of additional XS proteins to adjacent, lower affinity sites leads to their oligomerization and to the formation of the tight nucleoprotein complex allowing silencing (Gulvady et al., 2018; Lang et al., 2007; Navarre, 2016; Sette et al., 2009). Based on our findings, we therefore suggested that the identified motif serves as nucleation site - but the formation of a stable CgpS nucleoprotein complex is additionally determined by the adjacent DNA regions. Consistently, an overlay of the GC contents of CgpS target promoters revealed a high degree of similarity in GC-profiles with a distinct drop in the area of maximal CgpS binding (Wiechert et al., 2020a). Furthermore, the identified binding motif was often located within these regions of low GC content featuring highest CgpS coverage, as exemplarily shown in Figure 5B.

To test our hypothesis that the GC content of the DNA sequences flanking the putative nucleation site contributes to CgpS silencing, we constructed and analysed two synthetic promoter variants which were based on the native CgpS target promoter $P_{cg1999}$ (Wiechert et al., 2020a) (Figure 5B). While the sequence of the core promoter region which also contained the putative CgpS nucleation site was kept constant, the sequence of the adjacent flanks was changed. One variant ($P_{cg1999}$_A-T/G-C) was designed to mimic the native GC-profile by exchanging G to C and A to T and vice versa. This construct was efficiently silenced by CgpS. This demonstrated that, in contrast to the binding motif, sequence specificity does not play a role in the adjacent flanks. The second design ($P_{cg1999}$_rand) was based on a

randomized GC-profile in the adjacent flanks. This promoter was not silenced by CgpS, although the putative nucleation site was present, confirming that the GC-profile is important for silencing (Wiechert et al., 2020a).

These identified DNA features are consistent with previous observations of Pfeifer and colleagues (Pfeifer et al., 2016). By expressing *cgpS* of *C. glutamicum* in *E. coli* Δ*hns* mutants, the authors were able to complement a distinct mutant phenotype, indicating that CgpS can bind to H-NS targets. The applied assay was based on bromothymol blue salicin indicator plates allowing the colour-based visualization of the activity of enzymes encoded in the *bgl* operon (Pfeifer et al., 2016). This operon is suggested to be horizontally acquired and is natively silenced by H-NS (Sankar et al., 2009). Interestingly, the *bgl* promoter region also shows a distinct drop in GC content and at least two slightly truncated versions (8/10 and 9/10 bp) of CgpS motifs identified in native CgpS target sequences (Figure 5C). In conclusion, these findings support our hypothesis that the CgpS binding motif and a drop in GC content collectively mediate CgpS silencing.

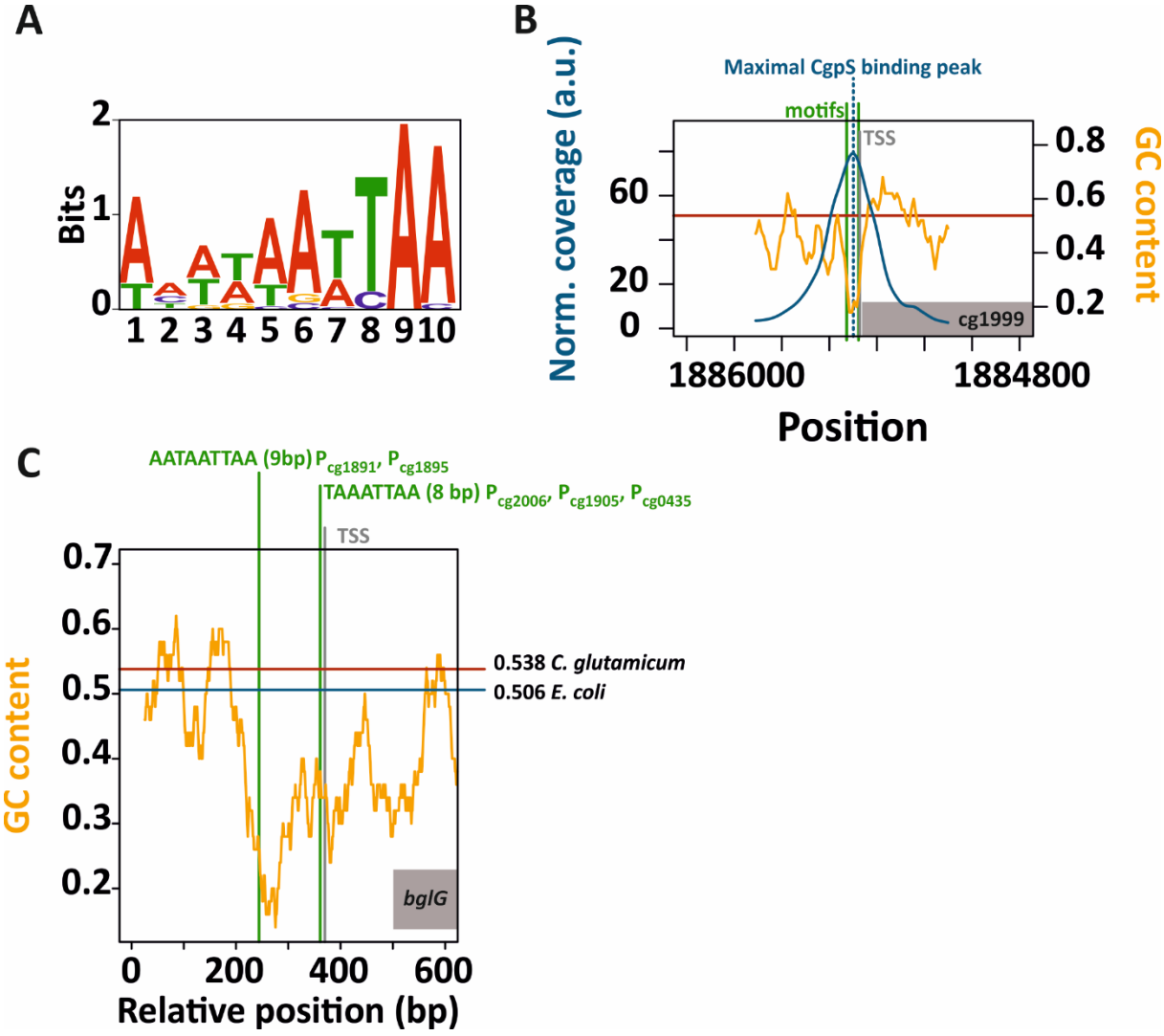


**Figure 5: The sequence specific binding motif and the drop in GC-profile cooperatively support CgpS silencing. A)** Identified binding motif which was present in 51 of 54 CgpS target promoters. Figure taken from Wiechert et al. (2020a). **B)** GC-profiles and CgpS binding peaks of the representative class 1 promoter $P_{cg1999}$. A rolling mean was applied to calculate the GC-profiles and CgpS coverage peaks based on previous ChAP-seq experiments (Pfeifer et al., 2016) as recently reported (Wiechert et al., 2020a). The position of TSS (Wiechert et al., 2020a) is given as vertical grey line and position of maximal CgpS binding (Pfeifer et al., 2016) as vertical blue dashed line. Positions of the putative binding motif (non-overlapping) from previous FIMO analyses (Wiechert et al., 2020a) are given as vertical green lines. The average GC content of the genome from *C. glutamicum* of 53.8% (Kalinowski et al., 2003) is shown as horizontal red dashed line. The corresponding genes are displayed as grey boxes. **C)** The *E. coli bgl* promoter features a drop in GC content and contains truncated variants of naturally occurring CgpS binding motifs (Wiechert et al., 2020a) located in areas of GC minimum and close to the TSS. The GC-profile of $P_{bglG}$ was calculated and plotted as described in B).The average GC contents of genomes of *C. glutamicum* (red (Kalinowski et al., 2003)) and *E. coli* (blue (Mann and Chen, 2010)) are displayed as coloured horizontal lines. The positions of reference motifs are given, all of them are located within CgpS binding peaks close to the maximal CgpS binding peak.

A model for CgpS binding and silencing based on our observations and inspired by the ideas for H-NS could be that CgpS initially binds to the putative sequence-specific nucleation sites. In the following, further CgpS molecules cooperatively bind to the adjacent flanks depending on the particular GC content in these regions, but apparently without strict sequence specificity. This might also explain the inverse correlation between CgpS binding and the GC-profile of its target regions (Figure 6). Another scenario could be that CgpS initially binds non-specifically to the DNA allowing the scanning of the DNA

for the sequence specific motif. In this case, the drop in GC content, meaning the stepwise increase in AT content, could direct CgpS towards these high affinity binding site allowing efficient binding and subsequent oligomerization.

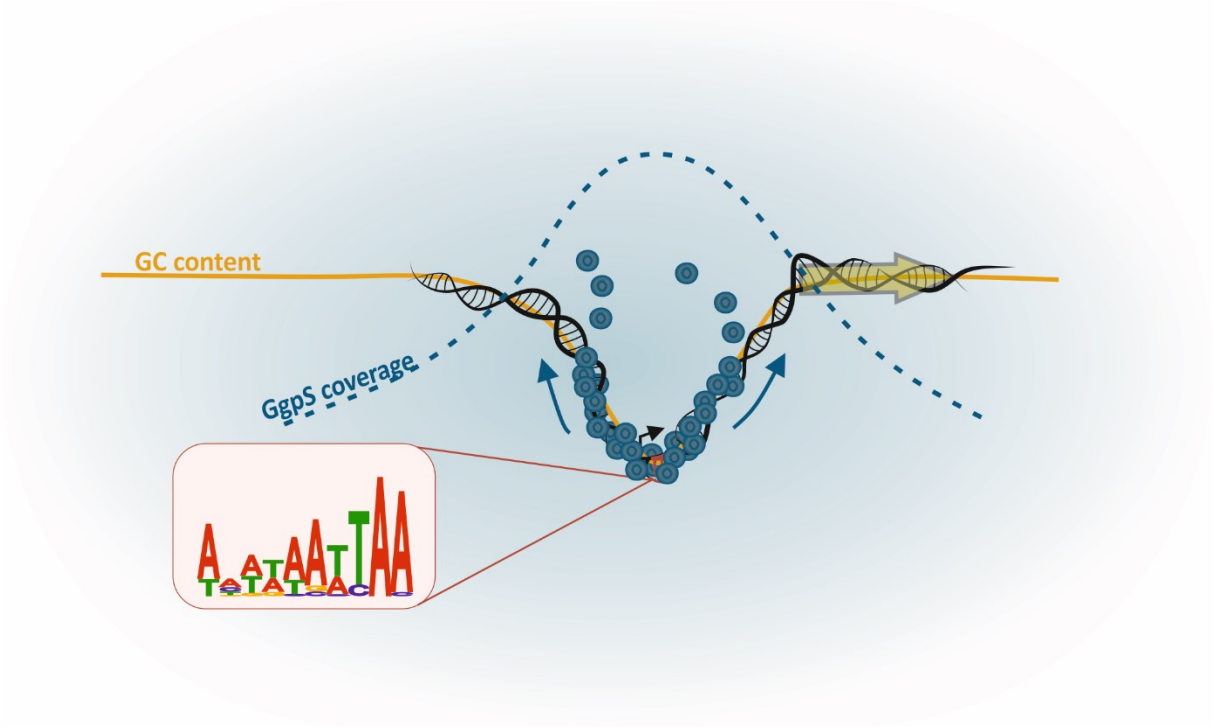


**Figure 6: The proposed model for the CgpS target recognition mechanism.** CgpS initially binds to its sequence-specific nucleation site containing multiple A/T steps, which is located in a region of low GC content (Wiechert et al., 2020a). In the following, further CgpS molecules cooperatively bind to the adjacent flanks depending on the particular GC content of these regions, but apparently without strict sequence specificity (Wiechert et al., 2020a).

As mentioned above, the synthetic promoter variant containing the correct motif but a randomized GC-profile ($P_{cg1999}$_rand) was not silenced by CgpS in vivo. However, this observation does not exclude partly CgpS binding, e.g. at the putative nucleation site. In vitro binding assays such as SPR analysis or electrophoretic mobility shift assays might demonstrate whether this variant is still bound by CgpS. Furthermore, protein binding microarray approaches as performed by Ding and colleagues (Ding et al., 2015) as well as by Duan and co-workers (Duan et al., 2018) could be used to study the in vitro affinity of CgpS for the identified motif in comparison to randomized sequences with same nucleotide composition. However, these in vitro approaches investigate binding of a XS protein in an isolated context, which does not necessarily lead to silencing. Our reporter-based analyses were applied to demonstrate CgpS-mediated silencing in vivo. It allows to investigate the result of the interplay of all parameters contributing to transcriptional repression of target genes in living cells and may therefore represent a promising approach for future investigations.

For instance, although we have confirmed the importance of the GC-profile based on one synthetic promoter variant and identified a certain degree of similarity in GC-profiles of different CgpS target

promoters (Wiechert et al., 2020a), the exact rules of how the shape of the GC-profile influences silencing remained unclear. What is the exact impact of the stepwise decreasing GC content and is CgpS able to silence a long promoter region containing only or at least mostly adenines and thymines? Based on these questions, an interesting experiment for future studies could be the expansion of our approach by constructing a library of synthetic promoters containing a functional core promoter region and the CgpS binding motif but differing in density and length of AT-rich stretches, which directly influence the GC-profile. By using flow cytometry, high-throughput screenings of this library might provide further insights into the importance of the surrounding GC-profile for in vivo CgpS silencing.

### 2.3.4. Formation of the nucleoprotein complex

Different studies demonstrated that DNA binding of XS proteins alone does not mediate efficient silencing and that oligomerization and the formation of the higher-order nucleoprotein complex are essential for repressing gene expression (Chen et al., 2008; Spurio et al., 1997; Winardhi et al., 2012). NMR analysis demonstrated that H-NS has a mainly α-helical N-terminal oligomerization domain and that H-NS molecules form dimers in solution. These dimers are capable of self-assembly resulting in the formation of large oligomers (Esposito et al., 2002; Smyth et al., 2000). Comparably, Lsr2, MvaT and Rok can form oligomers allowing the formation of higher-order nucleoprotein complexes (Chen et al., 2008; Duan et al., 2018; Winardhi et al., 2012).

The molecular mechanism of H-NS multimerization was studied in detail and is shown in Figure 7A. H-NS forms oligomers via two separated dimerization interfaces which are located within the N-terminal coiled-coil domain (Badaut et al., 2002; Ueguchi et al., 1996) (Figure 7A). The N-terminal dimerization interface consisting of three helices (H1, H2 and H3) is responsible for the formation of H-NS dimers in solution (Ali et al., 2012; Badaut et al., 2002; Ueguchi et al., 1996). High local H-NS concentrations, e.g. upon binding to the DNA, enables the interaction between different dimers via the central dimerization domain (helix-turn-helix motif between C-terminal end of helices H3 and H4), leading to elongation of the H-NS filament by head-to head/tail-to-tail multimerization (Ali et al., 2012; Arold et al., 2010) (Figure 7A). Oligomerization of XS proteins can result in silencing of the bound DNA regions by different mechanisms (Figure 7B): by binding in the core promoter region and consequently inhibiting binding of the RNA polymerase (I: occlusion), by preventing the RNA polymerase to escape the promoter (II: obstruction), by trapping the RNA polymerase in a formed DNA loop (III) or, putatively, by stimulating Rho-dependent termination (IV) (Landick et al., 2015; Lim et al., 2012).

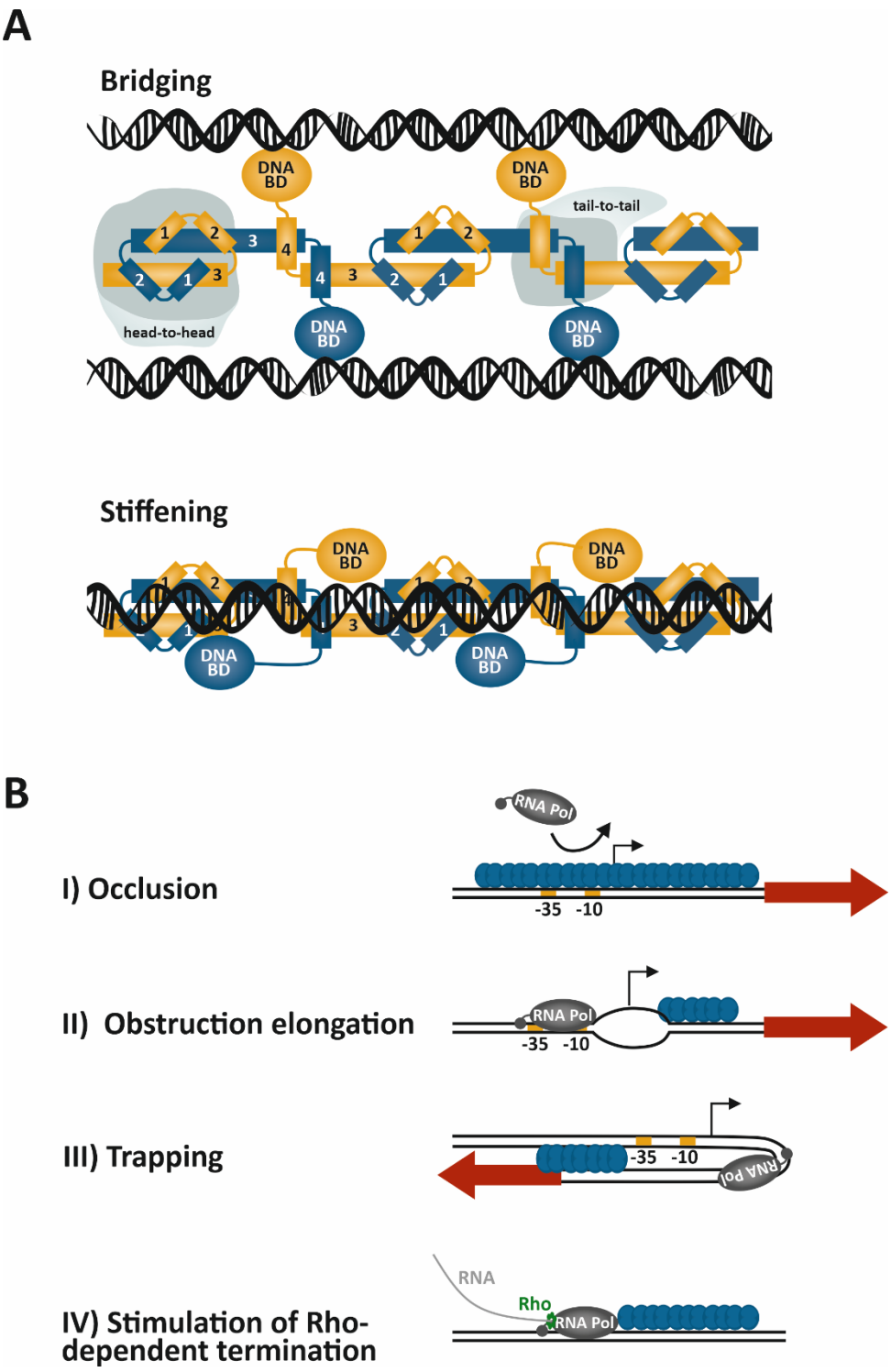


**Figure 7: Mechanisms underlying xenogeneic silencing. A)** Head-to head/tail-to-tail multimerization of H-NS is based on its two oligomerization interfaces: N-terminal dimerization interface formed by helices H1, H2 and H3 (head-to-head interaction) and the central dimerization domain (tail-to-tail interaction) formed as helix-turn-helix motif between the end of H3 and H4. H-NS molecules are alternatively coloured in blue and yellow and helices on the left filament site are labelled with helices numbers. Two binding modes for XS proteins were proposed: bridging and stiffening. DNA bridging is caused by DNA binding domains located on opposing faces of the helical XS protein filament which can interact with different sites of a DNA molecule. Rotations in the filament can result in DNA binding domains being located on the same face of the filament, allowing interaction with a single DNA molecule in the stiffening mode. Adapted from Ali et al. (2012), Singh et al. (2016). **B)** Mechanisms leading to xenogeneic silencing **I)** The XS nucleoprotein filament is formed along the RNA polymerase binding site leading to occlusion of the RNA polymerase. **II)** XS proteins bind and oligomerize downstream of the RNA polymerase binding site leading to obstruction of the elongation process. **III)** The bridging mode of XS proteins can induce a loop, which subsequently trap the RNA polymerase leading to silencing. **IV)** The XS nucleoprotein filament blocks the elongating RNA polymerase and putatively stimulates its susceptibility to Rho-dependent termination. Adapted from Landick et al. (2015),

Lim et al. (2012), Qin et al. (2019a). Models are mainly based on H-NS studies. [Abbreviations: RNA Pol, RNA polymerase; DNA BD, DNA binding domain].

Intensively applied in vitro assays such as electron microscopy, atomic force microscopy as well as magnetic tweezer and other single-molecule approaches revealed that the binding of XS proteins can lead to two distinct confirmations: the bridging mode and the stiffening mode (Ali et al., 2012). The bridging state describes XS-mediated crosslinking of two distantly located sites of the DNA molecule resulting in loop formation and DNA bending (Dame et al., 2005) (Figure 7A). Silencing of the gene loci *bgl* and *proU* in *E. coli* is putatively caused by H-NS binding to regions located upstream and downstream of the promoters. Interactions between distantly bound H-NS molecules might lead to DNA bridging and is suggested to allow trapping of the RNA-polymerase (Nagarajavel et al., 2007). In addition to controlling gene expression, bridging is suggested to be involved in structural compaction of the chromosome (Dame et al., 2005). Stiffening, the second binding mode, was previously described by Amit and colleagues. Stiffening means the end-to-end extension of the H-NS filament leading to the formation of a rigid nucleoprotein complex which might lead to occlusion of the RNA-polymerase or to obstruction of elongation (Amit et al., 2003) (Figure 7).

These modes of action shown in different in vitro assays are still topic of controversial discussions. However, Liu and colleagues were able to demonstrate that the experimental conditions, in particular the concentrations of divalent cations such as $Mg^{2+}$ and $Ca^{2+}$, were responsible for this observed discrepancy: high concentrations of $Mg^{2+}$ lead to bridging, while low concentrations result in stiffening of H-NS (Liu et al., 2010). Later biochemical and biophysical assays performed by Will and colleagues demonstrated that the bridging and stiffening modes depend on the local concentration of H-NS and its corresponding binding sites as well as the binding affinity of H-NS for these sites which is directly influenced by $Mg^{2+}$. The authors concluded that both modes can play a physiological role in a bacterial cells and that silenced genes are predominantly bound via the stiffening mode (Will et al., 2018). Comparably, MvaT and Lsr2 binding and oligomerization was reported to lead to stiffening and bridging (Qu et al., 2013; Winardhi et al., 2012), while Rok seems to act via bridging (Qin et al., 2019b).

The binding mode of CgpS in terms of stiffening and bridging has not been characterized so far. By using previously reported approaches like scanning force microscopy (SFM) (Dame et al., 2005), electron microscopy (Amit et al., 2003) or single-molecule magnetic tweezer experiments (Gulvady et al., 2018; Liu and Gordon, 2012), the CgpS binding mode could be further analysed. However, as mentioned above, these in vitro approaches can be challenging since they do not necessarily reflect the physiological conditions within a cell. Alternatively, live-cell imaging with high resolution microscopy methods such as stochastic optical reconstruction microscopy (STORM) or photoactivated localization microscopy (PALM) might be suitable techniques to analyse the subcellular distribution of

CgpS within the cell. For instance, these methods provided insights into the clustered distribution of photoactivatable fluorescent protein fusions of H-NS (H-NS-mEos2) in *E. coli* (Wang et al., 2011). The combination of this approach with staining of the DNA in living cells might allow the visualization of the DNA conformation in regions bound by CgpS. A suitable DNA dye could be SYTOX, which was demonstrated to perform well in living Gram-negative and Gram-positive bacteria (Bakshi et al., 2014). Alternatively, chromosome conformation capture coupled with deep sequencing (HI-C) experiments allow the detection of physical proximity between DNA loci in the three-dimensional (3D) space, which are distantly localized in the DNA molecule (Verma et al., 2019). This approach could represent a suitable method to detect putative DNA bridges formed by CgpS in vivo. In HI-C studies, the chromosome of a cell is cross-linked with formaldehyde to stabilise contacts between distant loci. In a next step, restriction enzymes are used to digest the genome into smaller fragments. Subsequently, fragments which have been cross-linked, due to their physical proximity in the 3D chromosome organisation, are ligated. Typically, the implementation of a biotinylated adaptor into these ligation junctions allows their enrichment in pull down assays (Verma et al., 2019). To identify DNA bridges or loops which are directly associated with CgpS binding, a Strep-tagged CgpS variant which was used in previous ChAP-seq analyses from Pfeifer and colleagues (Pfeifer et al., 2016) might be a promising alternative for this enrichment step. Finally, these fragments are sequenced, which allows for the detection of ligated DNA loci and therefore the identification of originally bridged DNA (Verma et al., 2019).

In our current study, we performed plasmid-based analysis of CgpS target promoters which were fused to reporter genes to monitor their activity (Wiechert et al., 2020a). These promoters were efficiently silenced, indicating that the native genomic context of this regulatory elements is not important for silencing which might favour the stiffening mode theory. We further determined the positions of transcriptional start sites (TSSs) of CgpS target promoters relative to the position of maximal CgpS binding. Remarkably, in most target promoters, the TSSs were located close to the position of maximal CgpS coverage and GC minimum (exemplarily shown in Figure 5B), indicating that binding close to the TSS is important for efficient CgpS mediated silencing (Wiechert et al., 2020a). In line with our findings, H-NS was also reported to bind within the core promoter region of some of its targets, thereby preventing the binding of the RNA polymerase (Dame et al., 2002). This might support the hypothesis that CgpS silences its targets by occlusion of the RNA polymerase which would match the stiffening binding mode.

In our study, we mainly focused on class 1 CgpS target promoters (one distinct drop in GC content and a bell-shaped CgpS binding peak) (Wiechert et al., 2020a). In contrast, class 2 promoters (e.g. $P_{cg1940}$ and $P_{cg1936}$) show broader or multiple drops in GC content and often putatively overlapping CgpS

binding peaks (Figure 8A). Remarkably, the identified CgpS binding motif was highly present in these promoters and often matched the different areas of low GC content. Hypothetically, the adjacent drops in GC-profile and the broad CgpS binding peaks could hint for bridging of these regions by CgpS. However, succeeding analysis with truncated variants of two class 2 promoters resulting in constructs featuring only one drop in GC content demonstrated that the upstream region is not essential for efficient CgpS silencing (Figure 8B). This indicates that bridging of adjacent regions with low GC content is not a prerequisite for this mechanism.

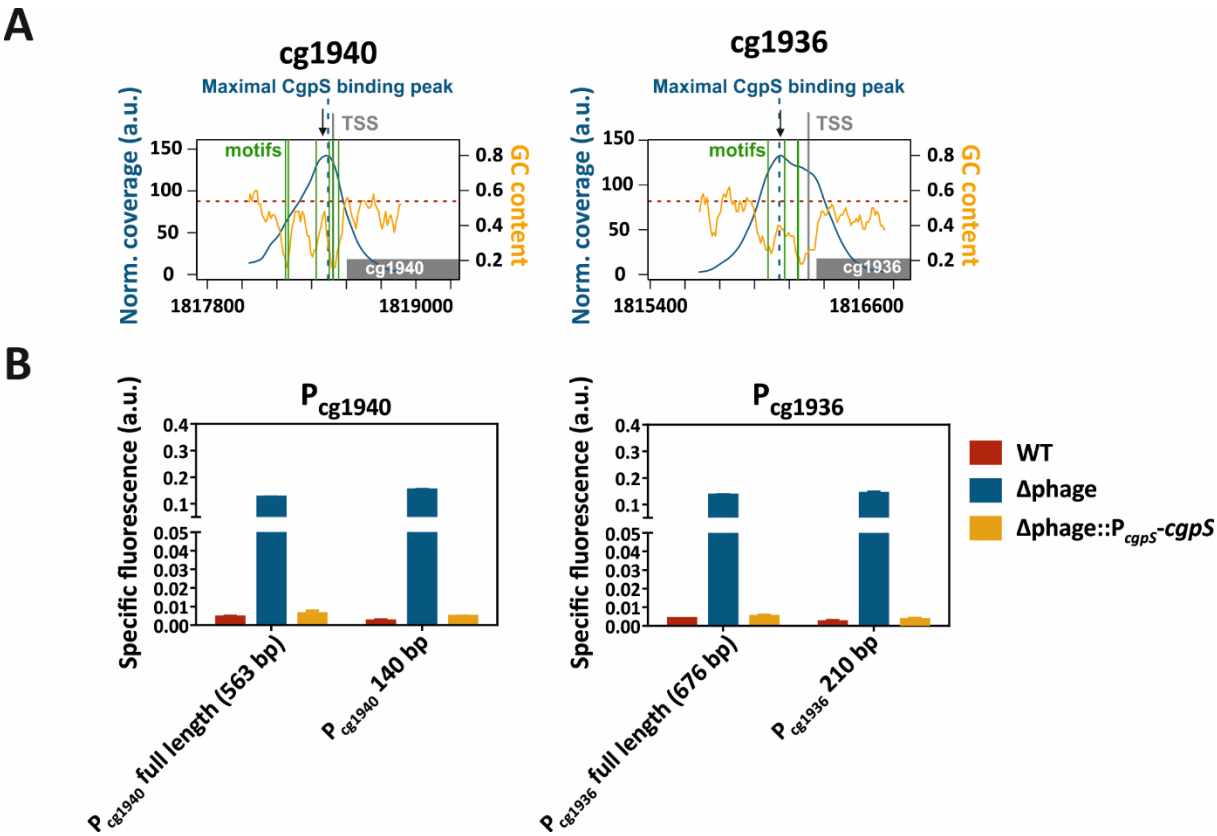


**Figure 8: The upstream drops are not essential for silencing of class 2 CgpS target promoters featuring multiple drops in GC-profile. A)** GC-profiles and CgpS binding peaks of class 2 promoter $P_{cg1940}$ and $P_{cg1936}$. A rolling mean was applied to calculate the GC-profiles and CgpS coverage peaks based on previous ChAP-seq experiments (Pfeifer et al., 2016) as recently reported (Wiechert et al., 2020a). Highest ranked TSS (Wiechert et al., 2020a) are given as vertical grey lines and position of maximal CgpS binding (Pfeifer et al., 2016) as vertical blue dashed lines. Positions of the putative binding motif (non-overlapping) from previous FIMO analyses (Wiechert et al., 2020a) are given as vertical green lines. The average GC content of the genome from *C. glutamicum* of 53.8% (Kalinowski et al., 2003) is shown as horizontal red dashed line. The corresponding genes are shown as grey boxes. Black vertical arrows indicate the removed upstream regions in the truncated promoter variants. **B)** Reporter outputs (specific Venus fluorescence) after five hours of cultivation driven by full length or truncated promoter variants. 5´-ends of full-length constructs coincided with the upstream end of the CgpS binding peak. Promoters were plasmid-based (pJC1) analysed in *C. glutamicum* wild-type cells, in the prophage free strain Δphage (MB001 (Baumgart et al., 2013)) as well as in the prophage-free strain with reintegrated *cgpS* under its native promoter (Δphage::$P_{cgpS}$-*cgpS* (Wiechert et al., 2020a)). Cultivations were performed in CGXII minimal medium containing 100 mM glucose in a microtiter cultivation system as recently described (Wiechert et al., 2020a). The results demonstrated that the upstream drops in GC content of both class 2 promoters are not essential for silencing. All constructs showed significant reporter outputs in the prophage-free strain Δphage confirming that all constructs are transcriptionally competent. Silencing was fully restored after reintegration of CgpS in the prophage-free strain (Δphage::$P_{cgpS}$-*cgpS*).

In a previous study, Kane and Dorman analysed H-NS mediated silencing of the *proU* promoter from *E. coli*. This promoter has two H-NS binding regions, the upstream (URE) and the downstream regulatory elements (DRE), flanking the core promoter which are suggested to allow the formation of H-NS bridges (*trans*-binding mode) leading to silencing (Kane and Dorman, 2011). Interestingly, removing the URE did not lead to promoter activation in wild-type cells, while the promoter showed high activity in a *hns* mutant strain, indicating that H-NS was still able to silence this promoter. The authors suggested a model in which the removal of the URE element leads to a reorganisation of the H-NS complex and to filament formation (*cis*-binding mode) within the DRE region. Subsequently, this *cis*-binding mode provides efficient silencing and inhibits transcription (Kane and Dorman, 2011). The comprehensive model of Kane and Dorman (Kane and Dorman, 2011) might also explain our results. At class 2 promoters, CgpS potentially binds to both drops and forms bridges between them leading to silencing. Removal of the upper region, which could represent the URE model, prevents bridging but triggers filament formation at the remaining high affinity binding site resulting in silencing.

### 2.3.5. The interplay of xenogeneic silencers and accessory factors

As mentioned above, oligomerization of XS proteins and their interaction with the DNA are critical steps for efficient silencing. In some cases, hetero-oligomer formation was reported. For instance, the paralogs MvaT and MvaU cooperatively regulate their target genes and have the ability to form hetero-oligomer complexes (Castang et al., 2008). The report of Castang and colleagues revealed that MvaT can influence binding of MvaU in specific DNA regions. However, MvaU was able to interact with other genomic regions independently of MvaT suggesting that heteromeric filaments are not essential for the silencing function of MvaU (Castang et al., 2008). Similar observations for H-NS and its paralog StpA propose that both proteins can form hetero-oligomer complexes, although a single *stpA* deletion had no detectable effect on gene expression (Müller et al., 2006).

In contrast, accessory factors of the Hha/YmoA family can strongly affect xenogeneic silencing efficiencies of H-NS-like proteins, e.g. by stabilizing the nucleoprotein complex over long areas of AT-rich DNA (Navarre, 2016). These proteins are characterized by molecular masses of about 8 kDa (half of the mass of H-NS) and structurally mimic the N-terminal oligomerization domain of H-NS (Banos et al., 2009). Hha-like proteins have a positively charged surface, which can contribute to silencing. Interactions of these accessory proteins with H-NS allow for cooperative regulation of gene expression. This interplay depends on the Hha binding motif within the N-terminal oligomerization domain of H-NS (Banos et al., 2009). Interestingly, all species of the *Enterobacteriaceae* family (e.g. *E. coli*, *Yersinia* sp. and *Salmonella* sp.) encode at least one member of the Hha/YmoA family of accessory factors, while

no homologs interact with other XS proteins or with H-NS from species outside of this family (Banos et al., 2009; Vivero et al., 2008).

Hha and its paralog YdgT preferentially influence H-NS mediated silencing of horizontally acquired DNA regions like virulence factors (e.g. SPIs from *Salmonella*), while ancestral H-NS target genes are often not influenced by these accessory proteins (Vivero et al., 2008). This indicates that these accessory proteins have a specialized regulatory function in silencing horizontally acquired DNA. Banos and colleagues suggested that these accessory proteins might enable H-NS to discriminate between self and non-self, thereby enabling stronger silencing of horizontally acquired DNA (Banos et al., 2009).

By analysing CgpS mediated silencing in a strain lacking all other phage genes (Δphage::$P_{cgpS}$-*cgpS*), we confirmed in our study that CgpS is the only prophage-encoded protein responsible for silencing of the phage promoter $P_{lys}$ (Wiechert et al., 2020a). We performed further comparable experiments with full length and truncated variants of the class 2 promoters $P_{cg1940}$ and $P_{cg1936}$ in the same strain (Figure 8). Silencing of all promoters was fully restored after reintegrating the *cgpS* gene, indicating that no further phage-encoded protein was involved in silencing of these promoters. Since we did not analyse all CgpS targets in this strain, we cannot exclude that some of them are silenced by a heteromeric nucleoprotein complex. Potentially, host-encoded accessory proteins could also be involved.

Previously, Pfeifer and colleagues performed transcriptome arrays with *C. glutamicum* cells expressing a truncated version of CgpS, which interferes with the CgpS nucleoprotein complex leading to prophage induction. While phage genes were strongly affected, only 2 of 32 targets outside of CGP3 region showed differential gene expression (Pfeifer et al., 2016). This observation might provide a first hint for differences in silencing and/or in the formation of the nucleoprotein complexes. Potentially, accessory proteins could stabilize the CgpS nucleoprotein complex outside of the prophage region. In this regard, further investigations would be necessary. However, it has to be kept in mind, that CgpS is a prophage-encoded XS protein that might play a rather specialized role in the control of the phage life cycle. Therefore, CgpS could possibly act independently of accessory factors. In contrast, H-NS from *E. coli* already evolved from a XS protein towards a global regulator of gene expression (Chib and Mahadevan, 2012), which is also fostered by its interaction with further accessory proteins.

## 2.4. Evolutionary network expansion by counter-silencing

Xenogeneic silencing globally sets the default state of AT-rich, foreign DNA to the off state - independent of potential effects on cellular fitness (Navarre, 2016; Navarre et al., 2007; Will et al., 2015). At first sight, silencing of beneficial xenogeneic genes seems to be counterintuitive but can be explained by different factors. One point is that a cell cannot differentiate whether invading DNA is

useful or harmful before it is expressed (Navarre, 2016). In general, foreign DNA has a greater chance to reduce the bacterial fitness and this global silencing strategy avoids potential fitness costs. Furthermore, since the value of a gene is defined by its time- and condition-dependent effect, even theoretically useful genes can result in fitness costs if their expression is not appropriately controlled (Sorek et al., 2007; Will et al., 2015). For instance, Ali and colleagues demonstrated that the strong growth defects observed in *Salmonella hns* mutant strains is caused by overexpression of the T3SS encoded in SPI-1. In contrast, an appropriately controlled T3SS mainly contributes to fitness and pathogenicity of this species by allowing invasion of the host and by triggering the inflammatory response (Ali et al., 2014). This example demonstrates the importance of evolving mechanisms, so-called counter-silencing strategies, to integrate foreign genes into existing regulatory networks of the host - thereby allowing their controlled expression at appropriate time points and environmental and physiological conditions (Will et al., 2014; Will et al., 2015). Evolutionary network expansion by counter-silencing allows cells to achieve control over silenced genes and to get access to novel beneficial traits (Will et al., 2014). Different counter-silencing strategies exist in bacteria which enable the transient alleviation of silencing in response to environmental conditions or physiological states (Navarre et al., 2007; Pfeifer et al., 2019; Stoebel et al., 2008). Remarkably, as result of the ongoing evolutionary arms race between bacteria and foreign DNA elements, pathogenicity islands, phages, and other MGEs also provide a variety of mechanisms enabling counteracting of host-mediated silencing (Ali et al., 2011; Navarre, 2016; Pfeifer et al., 2019). Mechanisms leading to counter-silencing can be grouped into different categories (Figure 9): I) Other NAPs or silencer-like proteins can interfere with the oligomerization of a XS protein preventing the formation of a stable silencer-DNA complex (e.g. H-NST (Williamson and Free, 2005)). Furthermore, DNA mimic proteins like the T4 phage protein Arn are suggested to be bound by H-NS leading to titration of the XS protein and to reduced H-NS binding to its genomic DNA targets (Ho et al., 2014). II) Sequence-specific DNA binding proteins such as transcription factors (TFs) compete with the silencer for binding to DNA regions (e.g. RovA (Heroven et al., 2004)). III) Alternative σ-factors not being affected by the silencer (e.g. by RpoS-mediated counter-silencing of *E. coli hdeAB* promoter (Shin et al., 2005)) can enable transcription. IV) Furthermore, protein-DNA interactions (e.g. SlyA (Corbett et al., 2007)) or environmental conditions (e.g. temperature (Falconi et al., 1998)) which induce alterations in promoter architecture can interfere with the silencer-DNA complex (Figure 9). For instance, Falconi and colleagues showed that H-NS represses the expression of the *virF* gene encoding an important regulator of virulence genes in *S. flexneri* only below 32°C. While under this conditions H-NS molecules bound at two distant sites in the *virF* promoter and cooperatively interact, higher temperatures induce conformational changes in the *virF* promoter structure, counteracting H-NS mediated silencing (Falconi et al., 1998). Remarkably, while the TF SlyA of *E. coli* appears to compete with H-NS for binding at certain DNA sequences (e.g.

at the *hlyE* gene (Lithgow et al., 2007)), SlyA is thought to antagonize H-NS silencing at other loci by remodelling the nucleoprotein complex without competing for binding (e.g. at the capsule gene cluster) (Corbett et al., 2007).

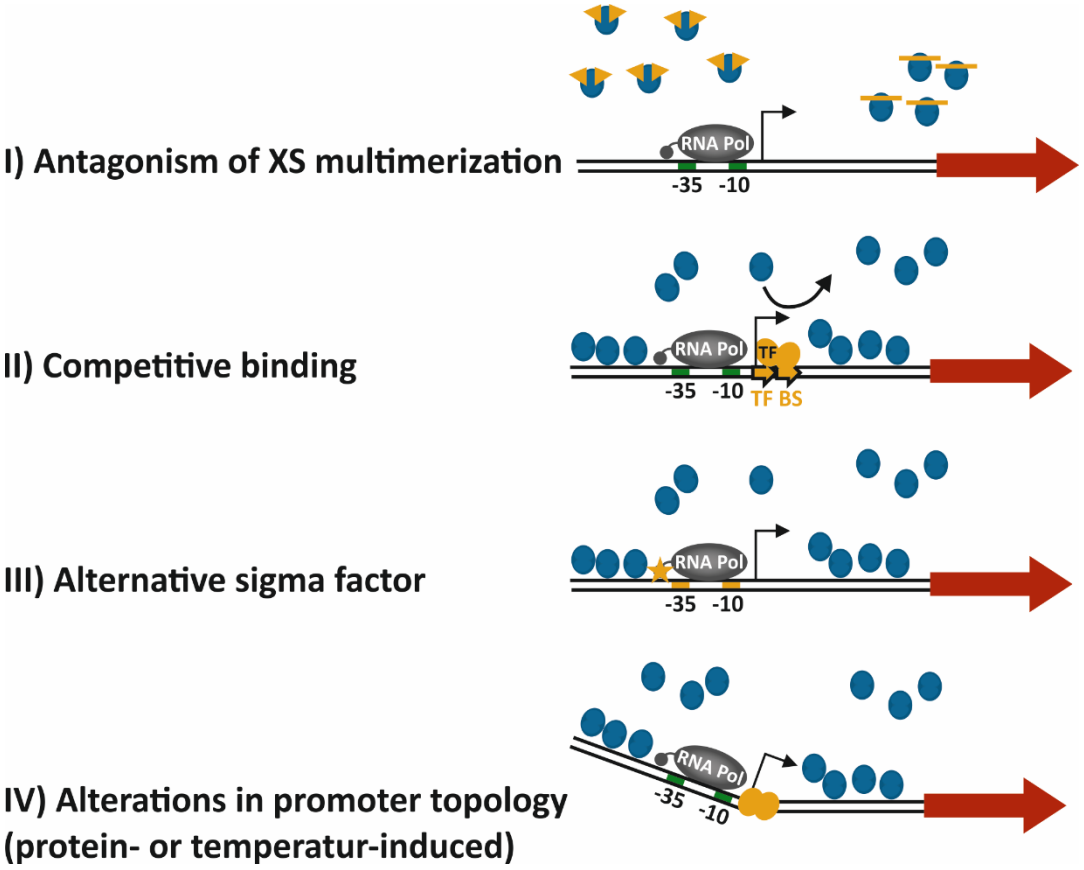


**Figure 9: Different mechanisms of XS counter-silencing leading to the activation of transcription**. **I)** Antagonists of XS multimerization can interfere with the oligomerization of the XS protein preventing the formation of a stable silencer-DNA complex (e.g. H-NST (Williamson and Free, 2005), 5.5 protein of phage T7 (Ali et al., 2011) orange triangles, left). Additionally, DNA mimic proteins (e.g. the T4 phage protein Arn; orange lines, right) are suggested to bind H-NS, leading to reduced H-NS binding at genomic targets (Ho et al., 2014). **II)** Sequence-specific DNA binding proteins such as TFs (e.g. RovA (Heroven et al., 2004); orange ovals) can compete with the silencer for DNA binding. **III)** Activation of transcription can be mediated by an alternative σ-factor (e.g. RpoS (Shin et al., 2005); orange star). **IV)** Alterations in the DNA topology caused by environmental changes (e.g. temperature-induced expression of *virF* (Falconi et al., 1998)) or DNA binding proteins (e.g. SlyA (Corbett et al., 2007); orange ovals) can disrupt the silencer-DNA complex. Adapted from Fang and Rimsky (2008). [Abbreviations: RNA Pol, RNA polymerase; TF, transcription factor; TF BS, TF binding site].

Furthermore, Brucoli and colleagues reported that small natural compounds like polyamides can bind into the minor groove of AT-rich DNA and interfere with DNA binding proteins, suggesting that these compounds might also antagonize binding of XS proteins (Brucoli et al., 2015). Remarkably, Rangarajan and Schnetz identified the transcribing RNA polymerase as further mechanism, which is able to relieve H-NS mediated repression. While poorly transcribed genes are repressed by H-NS, efficiently transcribed DNA regions escape silencing presumably by remodelling of the nucleoprotein complex (Rangarajan and Schnetz, 2018).

Examples of counter-silencing by interference between different NAPs as well as natively existing mechanisms of TF-mediated counter-silencing will be the topic of the following sections. In the here presented work, we performed a synthetic approach to decipher the rules underlying TF-mediated counter-silencing of Lsr2-like proteins using CgpS from *C. glutamicum* as a model (Wiechert et al., 2020a). I will discuss our results as well as findings from other synthetic counter-silencer approaches conducted previously for the XS protein H-NS in the following chapters.

### 2.4.1. Antagonism of XS multimerization

The oligomerization of XS proteins allowing the formation of higher-order nucleoprotein complexes is a prerequisite for their silencing function. Some NAPs cooperatively bind to their target regions leading to the formation of hetero-oligomer complexes with increased stability, as discussed for the H-NS/Hha complex (chapter 2.3.5. “The interplay of xenogeneic silencers and accessory factors.”). However, other proteins interfere with the multimerization mechanism or compete for XS binding sites leading to counter-silencing. Apparently, these strategies were evolved by horizontally acquired genomic islands to avoid silencing by the host XS protein. Examples are the H-NST and Ler proteins found in different *E. coli* strains (Williamson and Free, 2005; Winardhi et al., 2014).

H-NST is a horizontally acquired truncated version of H-NS lacking the C-terminal DNA binding domain and was identified in large genomic islands (ancestral MGE) of enteropathogenic (EPEC) and uropathogenic (UPEC) *E. coli* strains. By interfering with the N-terminal oligomerization domain of H-NS, H-NST has a dominant-negative effect on the formation of the nucleoprotein complex leading to reactivation of silenced genes (Williamson and Free, 2005). Surprisingly, H-NS encoded by the conjugative IncHI plasmid R27, where it is involved in the regulation of plasmid conjugation in response to temperature, exhibits a reduced sensitivity for H-NST interference allowing appropriate regulation of R27 conjugation (Baños et al., 2011).

The idea of counter-silencing by truncated variants of XS proteins was recently applied by different groups. Banos and colleagues heterologously expressed H-NST from EPEC in *Yersinia* allowing counter-silencing of the essential XS protein H-NS and the analysis of the regulatory network of H-NS (Baños et al., 2008). In another study, Pfeifer and co-workers overexpressed the N-terminal domain of the XS protein CgpS. Via interference with the formation of the CgpS nucleoprotein complex, this truncated variant led to prophage induction in *C. glutamicum* (Pfeifer et al., 2016). Remarkable, this effect was reproducible in a comparable experiment with N-terminal domains of Lsr2 variants from mycobacterial species (Pfeifer et al., 2016). Additionally, Gehrke and colleagues used a DNA binding deficient Lsr2 variant from *S. venezuelae* to activate expression of specialized metabolic clusters by counter-silencing Lsr2 in different *Streptomyces* species (Gehrke et al., 2019). Remarkably, strategies aiming at interfering with the formation of higher-order XS oligomers are also used by phages. For instance, the

5.5 protein of coliphage T7 interacts with the central oligomerization domain of H-NS and thereby inhibits H-NS repression, although H-NS is still bound to the DNA (Ali et al., 2011).

The horizontally acquired H-NS paralog Ler (locus of enterocyte effacement (LEE)-encoded regulator) of enterohemorrhagic *E. coli* (EHEC) and EPEC strains represents a further example of a NAP acting as an H-NS counter-silencer. Ler also binds to AT-rich DNA but has a highly different N-terminal oligomerization domain compared to H-NS (Winardhi et al., 2014). By performing magnetic tweezer experiments, Winardhi and colleagues showed that Ler binds to the DNA non-specifically and non-cooperatively and that the subsequent effects on DNA topology differ depending on the local concentration of Ler. DNA folding and wrapping was observed at low concentrations, while high amounts of bound Ler increased the rigidity of the DNA and replaced H-NS from the DNA, leading to counter-silencing (Winardhi et al., 2014). Interestingly, Levine and colleagues demonstrated that H-NST supports Ler binding in the presence of H-NS, thereby facilitating Ler-mediated counter-silencing (Levine et al., 2014).

HU is a conserved NAP which is highly abundant in eubacteria and has important functions in the regulation of cell growth, virulence, SOS response, and many other processes (Stojkova et al., 2019). Magnetic tweezer experiments and atomic force microscopy experiments hinted that HU and H-NS compete for the same DNA regions, putatively enabling HU to locally antagonize H-NS-mediated DNA condensations and silencing (van Noort et al., 2004). Fis, another highly abundant NAP is able to modulate the DNA topology (Ouafa et al., 2012) and was also proposed to counteract H-NS mediated gene silencing (Stoebel et al., 2008).

Bioinformatic analyses revealed that bacterial species frequently encode several XS proteins from the same class, while silencers from different classes do not co-exist in the same species (Perez-Rueda and Ibarra, 2015). In addition to the abovementioned results, Pfeifer and colleagues showed that the expression of *hns* from *E. coli* in wild-type *C. glutamicum* cells results in loss of CgpS mediated silencing and prophage induction (Pfeifer et al., 2016). These findings suggest that not related XS proteins compete for the binding at AT-rich genomic stretches, which hinders the formation of a silencing-competent nucleoprotein complex (Pfeifer et al., 2016).

### 2.4.2. Transcription factor-mediated counter-silencing in nature

The abovementioned NAP-based interfering mechanisms target the oligomerization process of XS proteins or compete with them for DNA binding. Thus, they often lead to global inhibition of the formation of higher-order nucleoprotein complexes. In contrast, TF-mediated counter-silencing can be considered as targeted process allowing the reactivation of single genes. TFs represent key players in the cellular regulatory network by activating or repressing gene expression in response to extra- and intracellular stimuli and their binding affinity for the DNA is determined by sequence-specific binding

motifs (von Hippel and Berg, 1986). As mentioned before, the control of beneficial, foreign gene expression is an important step for improving bacterial fitness (Will et al., 2015). Evolutionary network expansion by using existing regulatory circuits to control foreign gene expression, e.g. by developing TF-mediated counter-silencing mechanisms, is a common strategy found in bacteria (Navarre, 2016; Will et al., 2014; Will et al., 2015).

One of the best characterized system is the PhoPQ two-component system from *Salmonella*. This system is responsive to different environmental stimuli (low pH, antimicrobial peptides, low magnesium concentration) and represents a key player for virulence in *Salmonella* (Bader et al., 2003; Groisman et al., 1997; Miller et al., 1989). Upon stimulus perception, PhoQ phosphorylates PhoP leading to sequence-specific binding of the response regulator to the DNA. Will and colleagues systematically analysed the regulatory network of PhoP comprising ancestral core genes as well as horizontally acquired genes (Will et al., 2014). By analysing activities of promoters of both categories in different *Salmonella* mutant strains as well as in in vitro transcription assays, the authors demonstrated that ancestral promoters are controlled by classical PhoP-mediated activation. In contrast, transcription of horizontally acquired promoters depends on binding of PhoP and the TF SlyA, which cooperatively act as counter-silencing factors. Binding of SlyA and PhoP had no effect in the absence of H-NS, indicating that PhoP-mediated counter-silencing and classical activation are distinct mechanisms (Will et al., 2014).

Analyses of the promoter architectures of both categories revealed remarkable differences (Will et al., 2014; Zwir et al., 2012). Activated ancestral core genes typically exhibit a conserved promoter architecture with a PhoP binding site close to the -35 box and bound PhoP can recruit the RNA polymerase (Will et al., 2014; Zwir et al., 2012). In contrast, horizontally acquired targets typically show flexible promoter architectures regarding the number of operator sequences, the sequence of the binding site itself as well as the orientation of the binding motif and its distance to the TSS (Will et al., 2014; Zwir et al., 2012). This variability in promoter architectures indicates that, in contrast to classical activation, counter-silencing factors might not activate the promoter by recruiting the RNA polymerase. Instead, they enable transcription by interfering with the silencer-DNA complex (Will et al., 2014; Will et al., 2015). This flexibility in promoter architectures is assumed to facilitate evolutionary network expansion by counter-silencing in comparison to the de novo evolution of classical activator circuits (Will et al., 2014; Will et al., 2015).

In addition to the PhoPQ regulon, several diverse counter-silencing examples exist in nature highlighting the complexity of counter-silencing evolution. For instance, the important virulence regulator VirB from *S. flexneri* is suggested to counteract H-NS silencing by DNA binding, oligomerizing, and by DNA bending (Gao et al., 2013; Turner and Dorman, 2007). It is assumed that VirB is neither

involved in recruiting the RNA polymerase nor in promoting open complex formation, but that it antagonises H-NS mediated silencing (Turner and Dorman, 2007). In the absence of H-NS, VirB target promoters like $P_{icsB}$ are constitutively active (Porter and Dorman, 1994), showing that counter-silencing and classical activation are distinct mechanisms. LeuO, a LysR-type TF found in *Salmonella enterica* and *E. coli*, leads to counter-silencing of H-NS by acting as boundary element: it binds between the nucleation site of H-NS and the promoter region, oligomerizes and bends the DNA around itself, thereby blocking the H-NS polymerization process and enabling transcription (Chen et al., 2003; Shimada et al., 2011). Further examples of TFs, which have been co-opted to act as H-NS counter-silencer, are the MarR-type regulators SlyA and RovA of *S. enterica* and *Yersinia tuberculosis* (Heroven et al., 2004; Navarre et al., 2005; Perez et al., 2008). MarR-type regulators, which play an important role in multiple antibiotic resistance, belong to a widespread, ancient family of TFs and typically function as environmentally responsive repressors (Alekshun et al., 2001; Perera and Grove, 2010). However, the SlyA/RovA lineage in *Enterobacteriaceae* has evolved an additional function as pleiotropic counter-silencer leading to a strong extension of their regulons including many virulence genes (Will et al., 2019). In a current review, Will and Fang suggested that the evolution of MarR-type regulators towards counter-silencing factors could be facilitated by similarities between their target sequences and those of XS proteins (Will and Fang, 2020). Furthermore, binding of these TFs induces distorting effects on the DNA leading to bending of the H-NS-DNA complex (Will and Fang, 2020). Several other examples of TF-mediated H-NS counter-silencing have been described comprising a large set of AraC-like proteins including GadX and GadW, HilC and HilD as well as ToxT from *V. cholerae* (Olekhnovich and Kadner, 2007; Tramonti et al., 2006; Yu and DiRita, 2002). In contrast to abovementioned examples, ToxT is assumed to have a dual function during counter-silencing: interfering with H-NS silencing and transcription activation by interacting with the RNA polymerase (Hulbert and Taylor, 2002; Yu and DiRita, 2002). A comparable dual activity was observed for the TF SsrB of *Salmonella* (Walthers et al., 2007) suggesting that classical activation and counter-silencing are distinct regulatory mechanisms but can be combined in a single TF.

In conclusion, counter-silencing of H-NS plays an important role in several cellular processes including activation of virulence genes and antibiotic resistance. Furthermore, a connection between counter-silencing and quorum sensing was recently reported. Binding of LuxR, the master quorum sensing TF of *Vibrio harveyi*, displaces H-NS from gene loci involved in quorum sensing (Chaparian et al., 2020). These reports combined with several other examples highlight that xenogeneic silencing and TF-mediated counter-silencing provide access to horizontally acquired DNA and thereby foster evolutionary network expansion and bacterial evolution. This might explain why using existing regulatory circuits, e.g. by co-opting a TF from its original function to act as counter-silencer, is a common strategy of bacteria to control expression of horizontally acquired genes. Although counter-

silencing reports mainly focused on the reactivation of targets of H-NS-like XS proteins in different species, they provide insights into the complexity of regulatory network expansion and into the variability of counter-silencing mechanisms.

However, while TF-mediated counter-silencing of H-NS-like proteins has been studied in detail, little is known about mechanisms allowing the reactivation of genes silenced by XS proteins of the other classes. For instance, to the best of our knowledge, only one native example for an Lsr2 counter-silencer has been reported (Kurthkoti et al., 2015). IdeR, a central regulator of iron homeostasis in *M. tuberculosis*, counteracts Lsr2-mediated repression of the *bfrB* locus encoding a bacterioferritin (Kurthkoti et al., 2015). As mentioned before, Lsr2 is a master regulator of virulence genes and might be involved in multidrug tolerance in *M. tuberculosis* and was therefore highlighted as promising drug candidate (Colangeli et al., 2007; Gordon et al., 2010; Gordon et al., 2011). Additionally, in *Streptomyces*, Lsr2 acts as a silencer of specialized metabolic clusters (Gehrke et al., 2019). Both examples underline the importance that motivated our recent study to understand the mechanisms of xenogeneic silencing and counter-silencing of Lsr2-like proteins.

Binding of the TF is a critical step for efficient counter-silencing and this process directly depends on the presence of the corresponding TF binding site within the silenced promoter region. This was demonstrated in different mutant analyses lacking the respective TF and in studies with mutated binding sites preventing binding of the regulator (Caramel and Schnetz, 1998; Kane and Dorman, 2011; Wiechert et al., 2020a; Will et al., 2014). Regarding the evolution of counter-silencing, one could think of three different scenarios (partially reviewed by (Navarre, 2016; Will et al., 2015)): I) Accidentally, a foreign DNA element already contains a binding motif which is recognized by a host encoded TF. If the interplay of gene and stimulus-dependent TF binding increases the fitness of the host, this DNA element will be vertically transferred to the following bacterial generations. Otherwise, the resulting fitness costs will prevent its manifestation within the bacterial population. II) A second scenario would be that a foreign DNA element encodes an activating TF and contains the corresponding target promoter. Upon entering the bacterial cell, this target promoter might be silenced by host-encoded XS proteins leading to the addition of a repressive regulatory layer. Now, the TF might act in a dual fashion: original activity as activator and newly gained counter-silencing function. III) The third scenario is a try and error approach. The horizontally acquired DNA is initially repressed by a XS protein and resides as cryptic element within the bacterial genome. During evolution, random mutations within silenced promoter sequences can lead to the formation of TF binding sites. Binding of the corresponding TF interferes with the silencer DNA complex leading to counter-silencing and to the transcription of the following gene. Since binding of TFs can depend on a variety of stimuli (Seshasayee et al., 2011), those signals can be integrated into counter-silencing by co-opting corresponding host TFs. If the gene

product and its expression state fulfil the requirements of the bacterial cell, this mutation will provide a fitness advantage and will manifest within the bacterial population (Will et al., 2014; Will et al., 2015). In contrast, if the gene product reduces cellular fitness, this cell will die and mutations will be lost (Navarre, 2016; Will et al., 2015).

### 2.4.3. Synthetic disruptive counter-silencing

The flexibility in promoter architecture, which was reported by Will and colleagues for the PhoPQ regulon of *Salmonella* (Will et al., 2014), was reflected by our current study as well as in two other synthetic approaches aiming at counter-silencing H-NS target promoters (Caramel and Schnetz, 1998; Kane and Dorman, 2011; Wiechert et al., 2020a). In our study, we performed a comprehensive synthetic counter-silencer approach using the Lsr2-like XS protein CgpS of *C. glutamicum* as a model to decipher the rules underlying counter-silencing of Lsr2-like proteins (Wiechert et al., 2020a). In this plasmid-based approach, we used different phage promoters targeted by CgpS as platforms for our synthetic counter-silencer design. We artificially inserted the binding site of the TF GntR, the regulator of gluconate catabolism of *C. glutamicum*, within 12 different silenced phage promoters and analysed counter-silencing efficiencies by performing in vivo reporter assays. We could show that binding of GntR to various silenced promoters resulted in their activation, demonstrating that GntR can act as a counter-silencer in a set of different promoters (Wiechert et al., 2020a). We varied the position of the GntR binding site within two exemplary class 1 CgpS target promoters ($P_{lys}$ and $P_{cg1999}$, one single drop in GC-profile and a bell-shaped CgpS binding peak) to analyse the potential and constraints of CgpS counter-silencing. Counter-silencing was achieved at different positions within $P_{lys}$ in a range of 15 bp upstream and 10 bp downstream of the position of maximal CgpS coverage and highest efficiency was observed at this maximum position. The results for $P_{cg1999}$ were in a comparable range, highlighting a certain degree of flexibility in promoter architectures. Positions outside of this region were not activated by GntR binding and often tended to be repressed. Remarkably, several constructs showed only low reporter outputs under non-inducing conditions demonstrating that they are still tightly controlled by CgpS (Wiechert et al., 2020a). In conclusion, almost all binding positions resulted in differential gene expression, highlighting the potential of xenogeneic silencing and counter-silencing to facilitate regulatory network expansion by providing tuneable promoter systems with low background activity. In line with the promoter studies of Will and colleagues (Will et al., 2014), our design allowed a certain degree of flexibility in terms of binding site orientation and position. Interestingly, the distances between the closest PhoP binding site and the TSS vary by only 34 bp (Will et al., 2014; Zwir et al., 2012), indicating that the range of binding site positions allowing counter-silencing was comparable to our study.

Similar results were previously described by Caramel and Schnetz (Caramel and Schnetz, 1998). The authors inserted the binding sites of the Isopropyl-β-D-1-thiogalactopyranoside- (IPTG-) dependent TF LacI and of the temperature-sensitive λ-repressor into the well-characterized *bgl* promoter of *E. coli,* which is silenced by H-NS. Observed counter-silencing effects by TF binding at different positions, which were in a similar window as discussed before (Wiechert et al., 2020a; Will et al., 2014), confirmed the abovementioned constraints of counter-silencing (Caramel and Schnetz, 1998). Furthermore, comparable to our results, this study highlighted that counter-silencing allows the conversion of a repressor into an activating regulator (Caramel and Schnetz, 1998). Examples for such an evolutionary conversion can also be found in nature as shown for the MarR-type repressors RovA and SlyA (Will et al., 2019). Another synthetic approach was based on the VirB protein from *S. flexneri* (Kane and Dorman, 2011) which natively acts as a counter-silencer by wrapping the DNA around itself (Turner and Dorman, 2007). By implementing the corresponding binding site at different positions and orientations into the heterologous *E. coli proU* promoter, which is silenced by H-NS but natively not bound by VirB, counter-silencing was achieved (Kane and Dorman, 2011).

In conclusion, the extensive analysis of the PhoP regulon in *Salmonella* and the two synthetic studies which focused on H-NS counter-silencing revealed important insights into the potential and constraints of H-NS counter-silencing. In our recent study, we performed the first systematic analysis of counter-silencing of a Lsr2-like XS protein (Wiechert et al., 2020a). Remarkably, the obtained results from all approaches exhibit a high degree of agreement, e.g. the flexibility in promoter architectures. However, in some points, the transferability shows limitations. For instance, we tested a set of different binding sites of heterologous and homologous effector-responsive TFs for the design of counter-silencer constructs based on the CgpS target promoter $P_{lys}$ (Figure 10). Comparable to the *bgl* promoter-based study of Caramel and Schnetz (Caramel and Schnetz, 1998), we also tested constructs based on the LacI repressor. While the inserted LacI binding site only slightly influenced H-NS silencing and LacI binding efficiently reactivated the *bgl* promoter activity (Caramel and Schnetz, 1998), the introduction of this sequence into the $P_{lys}$ promoter led to drastically increased background activities. Furthermore, LacI binding did not significantly further alleviate CpgS silencing (Figure 10). This scenario was repetitively shown for different TFs including IpsA from *C. glutamicum* and TrpR from *E. coli* (Figure 10). We assumed that the binding site composition, especially its GC content and length, strongly influence CgpS silencing independent of TF binding. This hypothesis was confirmed by the high reporter outputs driven from the $P_{lys}$ promoter with the inserted LacI binding site in the absence of the corresponding TF (Figure 10). Obviously, the *bgl* promoter shows a higher degree of tolerance for the inserted LacI binding site (Caramel and Schnetz, 1998). In conclusion, the results of H-NS and our study revealed that differences between H-NS- and CgpS-mediated silencing exist.

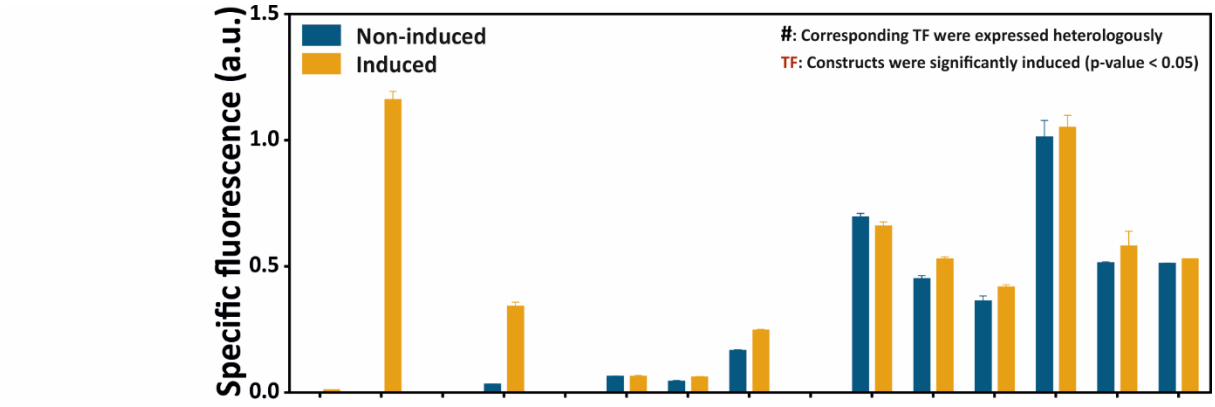


| Transcription factor binding site | WT Δphage no BS | GntR | TyrR# | VanR | RbsR | DtxR | MntR | IpsA | TrpR# | LacI# | LacI |
|---|---|---|---|---|---|---|---|---|---|---|---|
| Binding site length (bp) | | 15 | 18 | 24 | 18 | 19 | 18 | 30 | 26 | 23 | |
| Binding site GC content (%) | | 27 | 11 | 25 | 33 | 37 | 39 | 40 | 46 | 48 | |
| | | GC-low binding sites | | | | GC-rich binding sites | | | | | |

**Figure 10: Impact of effector-responsive TF binding and of inserted operator sequences on promoter activities of synthetic variants of the CgpS target promoter $P_{lys}$.** Different TF binding sites (BS) were inserted within the phage promoter $P_{lys}$ directly upstream of the position associated with maximal CgpS binding obtained in previous ChAP-seq experiments by Pfeifer and colleagues (Pfeifer et al., 2016). Reporter outputs (Venus expression) driven by plasmid-based (pJC1) promoter constructs were analysed regarding silencing and counter-silencing in *C. glutamicum* wild-type cells after five hours of cultivation. The native phage promoter $P_{lys}$ served as reference and was analysed in *C. glutamicum* wild-type cells as well as in the absence of CgpS in the prophage free strain Δphage (MB001 (Baumgart et al., 2013)). Cells were cultivated in a microtiter cultivation system under conditions that induced (yellow bars; +) or did not induce (blue bars; -) binding of the respective TF. In cases of constructs with binding sites of heterologous TFs, the corresponding TF encoding gene was inserted within the respective construct (#). For the LacI-based promoter variant, constructs with and without the *lacI* gene were tested. Cultivations were performed in CGXII minimal medium (Keilhauer et al., 1993). Used carbon sources and additives are listed in the following. For the ion-dependent TFs MntR and DtxR, the usually used concentrations of $MnSO_4$ (59 µM) and $FeSO_4$ (36 µM) were adjusted according to the TF, and amounts are given below. Effectors controlling TF binding are underlined, respectively. **No BS**: 100 mM gluconate; **GntR**: **-**: 100 mM gluconate, **+**: 111 mM glucose; **TyrR**: **-**: 111 mM glucose + 3 mM Ala-Ala, **+**: 111 mM glucose + 3 mM Ala-Ala + 0.3 mM Ala-Tyr; **VanR**: **-**: 111 mM glucose + 2 mM vanillate, **+**: 111 mM glucose; **RbsR**: **-**: 111 mM glucose + 66.6 mM ribose, **+**: 111 mM glucose + 66.6 mM gluconate; **DtxR**: **-**: 111 mM glucose + 5 µM $FeSO_4$, **+**: 111 mM glucose + 36 µM $FeSO_4$; **MntR**: **-**: 55 mM glucose + 0.059 µM $MnSO_4$, **+**: 55 mM glucose + 0.59 µM $MnSO_4$; **IpsA**: **-**: 111 mM glucose + 50 mM myo-inositol, **+**: 111 mM glucose; **TrpR**: **-**: 111 mM glucose, **+**: 111 mM glucose + 0.3 mM Ala-Trp; **LacI**: **-**: 111 mM glucose + 100 µM IPTG, **+**: 111 mM glucose. All cells were pre-cultivated in CGXII minimal medium under non-inducing conditions in microtiter plates. The lengths of the inserted binding sites as well their average GC contents are specified, and constructs were sorted based on the latter feature. Constructs which were significantly induced by binding of the TF (t-test, p-value < 0.05) are highlighted by red TF names. The figure demonstrates that CgpS mediated silencing is strongly affected by long and/or GC-rich inserted TF binding sites leading to high background expression levels. [Abbreviations: BS, binding site; a.u., arbitrary unit; WT, wild-type; TF, transcription factor].

In our study, we performed detailed plasmid-based counter-silencing analyses with class 1 promoters which were characterized by a single distinct drop in GC-profile and a bell-shaped CgpS binding peak resulting in a large set of counter-silencer constructs. However, most of the class 2 promoters showing broader or multiple drops in GC content and broad or even overlapping CgpS coverage peaks failed to be counter-silenced when GntR binds at the annotated position of maximal CgpS binding (Wiechert et al., 2020a). We speculated that the annotation of the maximal CgpS coverage position of $P_{cg1936}$ (Pfeifer et al., 2016), which was located between two areas of low GC content and distant to the TSS, might be incorrect (Figure 8A). In a following attempt, we inserted the GntR binding site at two different positions close to the TSS in a region of low GC content, but counter-silencing was not detectable

(Wiechert, Frunzke, unpublished). As discussed in chapter 2.3.4. ("Formation of the nucleoprotein complex."), we hypothesised that these broader peaks might stabilize silencing, e.g. by bridging the DNA between two CgpS high affinity sites, and thereby preventing GntR mediated remodelling of the nucleoprotein complex.

Although most class 1 promoters were efficiently counter-silenced in our plasmid-based approach, we must consider that we inspected the CgpS target promoters isolated from their native genomic context. For instance, CgpS coverage peaks located in high density and close distance in the CGP3 prophage region (Pfeifer et al., 2016) very likely influence each other, e.g. by forming bridges or determining the DNA topology together. Furthermore, high local concentrations of CgpS in the prophage region, a high density of CgpS binding sites as well as the surrounding GC-profile might influence CgpS target recognition and nucleoprotein complex stability, which could lead to higher silencing efficiencies. For instance, Will and colleagues demonstrated in biochemical and biophysical assays that the binding mode of H-NS strongly depend on the local concentration of H-NS and its corresponding binding sites as well as the binding affinity of H-NS (Will et al., 2018).

An important question therefore remains open: How well can our isolated plasmid system reflect the natively occurring mechanisms of silencing and counter-silencing? One promising approach for future studies could be the integration of the counter-silencer promoter into its native locus. Since native phage proteins have the risk to be toxic, e.g. the gene *lys* encodes a putative lysine, the native gene should either be translational inactivated (promoter activity measurements based on transcript level) or replaced by a reporter gene. This question will be further discussed in the outlook in chapter 2.6.

### 2.4.4. Counter-silencing and classical activation are distinct mechanisms

Previously, two mechanisms allowing counter-silencing were discussed: supportive and disruptive counter-silencing (Will et al., 2014). Some examples of supportive counter-silencing exist where the TF interferes with the silencer DNA complex but also directly interacts with the RNA polymerase to promote transcription, e.g. by recruiting the RNA polymerase (Hulbert and Taylor, 2002; Walthers et al., 2007; Will et al., 2014; Yu and DiRita, 2002). However, other studies characterized a disruptive counter-silencing mechanism which is assumed to be independent of direct interaction between the TF and the RNA polymerase (Caramel and Schnetz, 1998; Kane and Dorman, 2011; Wiechert et al., 2020a), indicating that counter-silencing and activation are distinct regulatory mechanisms showing the possibility to be combined in a single TF. These discrepancies of the abovementioned studies likely reflect the complexity of regulatory networks and the individual evolutionary relationships between promoter and counter-silencing factor.

In accordance with the previous findings, we suggested that GntR-mediated counter-silencing is rather a disruptive mechanism than a supportive (Wiechert et al., 2020a). This hypothesis is based on three different observations:

I) We observed highest counter-silencing efficiencies when GntR bound directly at the position of maximal CgpS coverage. These positions were often located in close distance to the TSSs (Wiechert et al., 2020a). Based on the scientific status quo, these positions would rather lead to the repression of gene expression by blocking transcription (Rojo, 1999; Rydenfelt et al., 2014). Indeed, GntR binding to different constructs led to counter-silencing in the wild type, but decreased promoter activities were observed in the absence of CgpS in the prophage-free strain Δphage, showing that the regulatory output is strongly affected by the interplay of different DNA binding proteins (Wiechert et al., 2020a).

II) In the native GntR target promoter $P_{gntK}$, the GntR binding site overlaps with the TSS (Frunzke et al., 2008) and GntR binding led to decreased promoter activities (Wiechert et al., 2020a), demonstrating that GntR binding close to the TSS acts as repressor. In accordance with the abovementioned examples RovA and SlyA (Will et al., 2019), our results nicely demonstrated that counter-silencing allows the conversion of a repressor to an activating counter-silencer (Wiechert et al., 2020a).

III) None of our constructs, which was tested in the absence of CgpS in the prophage-free strain, showed significantly increased activity under conditions which induced GntR binding, demonstrating that its activating effect depends on the interplay with CgpS and not on a classical activation mechanism. Furthermore, all tested native phage promoters were strongly upregulated in this strain, indicating that they are constitutively active in the absence of CgpS (Wiechert et al., 2020a).

In accordance, previous studies from Will and colleagues suggested that open complex formation at AT-rich promoters is often not the rate-limiting step for transcription in the absence of XS proteins (Will et al., 2014). By performing combined differential DNA footprint analysis (DDFA) like $KMnO_4$ footprint assays with the H-NS target promoter $P_{pagC}$, the authors obtained comprehensive insights into the molecular mechanisms of silencing and counter-silencing. By systematically analysing the importance of different proteins for this process, the authors demonstrated that RNA polymerase binding is sufficient for the formation of a stable open complex in the absence of H-NS. In contrast, H-NS strongly inhibits this structural DNA change, defining its silencing effect. The open complex formation was restored in the presence of the counter-silencing factors PhoP and SlyA, explaining the molecular mechanism of counter-silencing: PhoP induces bending of the silencer-DNA filament leading to recovery of the open complex conformation (Will et al., 2014).

## 2.5. The potential of counter-silencer promoters for biotechnological and synthetic biological applications

Inducible expression systems represent key modules in biotechnological and synthetic biological applications, since they allow the precise and rational modulation of gene expression (Patek et al., 2013). They are frequently used to accurately coordinate metabolic fluxes in a variety of production processes and typically form the first layer of synthetic regulatory circuits (Liu et al., 2016; Xu et al., 2019). Synthetic Biology aims to provide suitable libraries of modular genetic parts, including promoters and TFs which can be assembled in genetic circuits (García-Granados et al., 2019). Various intensive promoter engineering studies and designed promoter libraries from this research field highlight the demand of appropriate expression systems which meet the requirements of specific application, e.g. metabolic engineering strategies (Alper et al., 2005; Blazeck and Alper, 2013; Han et al., 2019). A stringent but flexible control of gene expression is of particular importance for applications which have to deal with toxic products and pathway intermediates or with disturbances of the central carbon flux (Baritugo et al., 2018). Furthermore, gene function studies often do not depend on high expression rates, but on strictly controlled gene expression to allow the conditional knockdown of essential genes (Fitz et al., 2018; Shang et al., 2002).

In various bacteria, for instance in *C. glutamicum*, the well-established heterologous expression systems $P_{tac}$ (Patek et al., 2013), $P_{tet}$ (Lausberg et al., 2012) and $P_{araBAD}$ (Ben-Samoun et al., 1999) are widely applied. However, they do not meet the requirements for all approaches due to inducer toxicity, high inducer costs, heterogeneous inducer uptake, high background expression levels and inappropriate induction levels (Baritugo et al., 2018; Patek et al., 2013; Yim et al., 2013; Zhang et al., 2012b).

Interestingly, the investigations of our synthetic promoter variants, which are controlled by xenogeneic silencing and counter-silencing, revealed that several of them have very low background expression levels and can be strongly induced by binding of the gluconate-dependent TF GntR (Wiechert et al., 2020a). Based on this observation, a further project of this PhD thesis was the detailed characterization of promising promoters to determine their potential as gene expression system in *C. glutamicum*. The results are summarized in our current manuscript: “Inducible expression systems based on xenogeneic silencing and counter-silencing and the design of a metabolic toggle switch” (Wiechert et al., 2020b). In contrast to inducers like IPTG, gluconate represents a non-toxic and cheap effector molecule (Wiechert et al., 2020b). The comparison of exemplarily chosen counter-silencer promoters with the heterologous expression systems LacI-$P_{tac}$ and TetR-$P_{tet}$ confirmed that our constructs have significantly lower background expression levels (Wiechert et al., 2020b). In the presence of the effector molecule gluconate which inhibits binding of GntR to the DNA, the counter-silencer promoters were in the OFF state. However, promoter activities increased after a certain period of time, probably

due to depletion of gluconate. Cultivation approaches with increasing amounts of gluconate revealed a gradual shift of the time point of promoter induction, highlighting the potential of counter-silencer constructs as expression systems with temporal tunability. By choosing defined amounts of gluconate, the increase in promoter activity could be correlated with the culture entry into stationary phase (Wiechert et al., 2020b), suggesting that counter-silencer promoters could be applied for approaches where a gene is supposed to be expressed after an initial growth phase.

The repertoire of homologous inducible promoters is comparatively small in *C. glutamicum* and includes the $P_{malE}$ promoter induced by maltose (Okibe et al., 2010), the gluconate responsive promoters $P_{git1}$ (Okibe et al., 2010), $P_{gntK}$ (Hentschel et al., 2013; Letek et al., 2006), and $P_{gntP}$ (Letek et al., 2006), the propionate inducible $P_{prpD2}$ promoter (Plassmeier et al., 2013) as well as amino acid responsive biosensors like Lrp-$P_{brnFE'}$ (Mustafi et al., 2012) and LysG-$P_{lysE'}$ (Binder et al., 2012). Therefore, our counter-silencer promoters might represent suitable candidates to expand this limited set of inducible promoter systems.

We combined our synthetic constructs in a GntR-dependent promoter library comprising 44 regulatory elements which were repressed (16) or activated (28) by GntR binding (Wiechert et al., 2020b) Our promoter sets were characterized by small increment steps and covered a wide range of expression levels (repressed: 70-fold, activated: 100-fold) (Wiechert et al., 2020b), emphasising that they show important features of high-quality promoter libraries (Fitz et al., 2018). Since only a few promoter libraries had been designed for *C. glutamicum* containing either synthetic, IPTG inducible regulatory elements (Rytter et al., 2014) or constitutive promoters (Rytter et al., 2014; Shang et al., 2018; Yim et al., 2013), we suggest that our synthetic, gluconate inducible library containing activated and repressed regulatory elements could be useful for different approaches in *C. glutamicum*.

Finally, it should be noted that it might also be worthwhile to investigate counter-silencing of naturally silenced genes in future research. For instance, Gehrke and colleagues showed that Lsr2 targets a variety of specialized metabolic clusters in *S. venezuelae* (Gehrke et al., 2019). If our findings about TF-mediated counter-silencing of the Lsr2-like XS protein CgpS are transferable to Lsr2 in *Streptomyces*, the specific and controlled reactivation of these clusters could be an interesting engineering target for the discovery of novel bioactive compounds. Furthermore, the implementation of TF binding sites within specific silenced promoters could be applied for studying the functions of one specific gene product within the cellular network. An interesting field of research could be the reactivation of phage genes, e.g. from *C. glutamicum*, which allows for their functional characterization within the native host.

### 2.5.1. Synthetic genetic toggle switches

Inspired by the genetic switch that governs the lysis-lysogeny decision of bacteriophage λ, Gardner and colleagues imitated this circuit design to construct a bistable synthetic toggle switch (Gardner et al., 2000). The regulatory network of bacteriophage λ combines the two repressors Cro and CI and their target promoters $P_R$ and $P_{RM}$, each being repressed by the gene product of the other (Khalil and Collins, 2010). Comparably, Gardner and colleagues combined the IPTG-inducible expression system LacI-$P_{trc}$ with the anhydrotetracycline- (ATc-) dependent TetR-$P_L$tetO-1 system, or with the temperature-sensitive λ repressor ($CI_{ts}$) and its corresponding promoter $P_L$slcon and arranged them such that both promoters were repressed by the gene product of the other (Gardner et al., 2000). The additional expression control of a reporter gene (e.g. *gfpmut3*) by one of the promoters allowed them to monitor the state of the toggle (fluorescence on versus fluorescence off) (Gardner et al., 2000).

The analysis of reporter outputs driven by the native GntR target promoter $P_{gntK}$ and the synthetic counter-silencer construct $P_{lys}$_CS_0 revealed a very similar, but inverted response to gluconate availability (Wiechert et al., 2020a). Based on this observation, we combined both promoters in a synthetic toggle switch and fused them to different reporter genes (*venus* and *e2-crimson*) to monitor the state of our toggle (Wiechert et al., 2020a) (Figure 11). Analysis of reporter outputs during long-term cultivations in the microfluidic cultivation system allowed us to characterize our toggle design in detail and demonstrated its robust and reversible functionality (Wiechert et al., 2020a; Wiechert et al., 2020b).

In contrast to the circuit architecture from Gardner and colleagues, which was based on the ratio of two repressors and two stimuli (Gardner et al., 2000), our design is controlled by only one specific TF, namely GntR, and one effector molecule, namely gluconate, allowing us to use native GntR levels (Wiechert et al., 2020a; Wiechert et al., 2020b). This simple design might be advantageous since it circumvents problems like inappropriate TF synthesis and degradation rates as well as insufficient repression efficiencies, which were discussed as major challenges for toggle functionality and stability in the previous publication (Gardner et al., 2000). Additionally, our modular circuit architecture is thought to allow the independent tuning of both toggle sides without affecting the response of the other side, demonstrating its potential for applications in Synthetic Biology. For instance, our GntR-dependent promoter library comprising 28 activated and 16 repressed synthetic regulatory elements provides a large set of potential building blocks allowing application-specific adjustments of the toggle (Wiechert et al., 2020b).

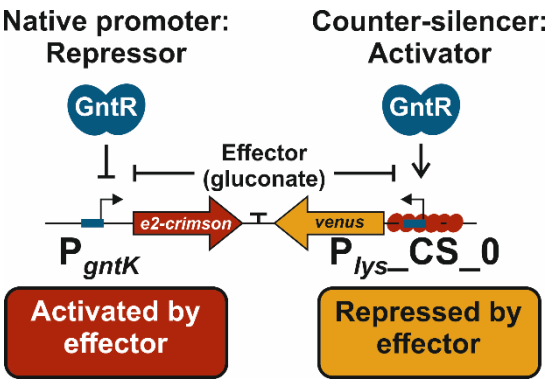


**Figure 11: Design scheme of the GntR-dependent fluorescence toggle switch.** The GntR-dependent toggle switch is based on the native GntR target promoter $P_{gntK}$ and the synthetic GntR-dependent $P_{lys}$ counter-silencer construct ($P_{lys}$_CS_0), both reacting inversely to gluconate availability. Both promoters were fused to different reporter genes ($P_{lys}$_CS_0-*venus* and $P_{gntK}$-*e2-crimson*) to monitor promoter activities. Figure taken from Wiechert et al. (2020a).

### 2.5.2. Metabolic toggle switches to optimize flux balances by dynamic pathway regulation

Rationally engineered microbial cells enable improved production of value-added compounds from renewable feedstocks and represent an ecological, economical and sustainable alternative to production processes depending on limited fossil resources and high energy supply (Lee et al., 2012; Prather and Martin, 2008). The majority of bio-based products including natural and non-natural compounds are derived from intermediates of the central carbon metabolism, e.g. from tricarboxylic acid (TCA) cycle or glycolysis. Consequently, production processes frequently compete with pathways essential for microbial physiology and cell growth (Doong et al., 2018; Gupta et al., 2017; Soma et al., 2014). Permanent knockouts or knockdowns of competing reactions from the central carbon metabolism combined with the overexpression of production pathways (heterologous or endogenous) are established engineering strategies to redirect carbon flux towards the desired product (Becker et al., 2011; Blombach et al., 2008; Blombach et al., 2007; Huser et al., 2005; Krause et al., 2010; Litsanov et al., 2012). However, the permanent knockout of competing pathways and highly expressed heterologous biosynthesis routes can result in strong metabolic imbalances leading to severe growth defects and reduced overall productivity (Brockman and Prather, 2015a).

In contrast, the implementation of metabolic toggle switches or other synthetic genetic circuits allows the dynamic redirection of metabolic fluxes towards cell growth or product biosynthesis in several engineered *E. coli* strains (Brockman and Prather, 2015b; Doong et al., 2018; Farmer and Liao, 2000; Gupta et al., 2017; Lo et al., 2016; Soma et al., 2014; Soma et al., 2017; Tsuruno et al., 2015; Zhang et al., 2012a). By controlling timing of strain performance, cell growth as well as the overall productivity were significantly improved. For instance, Soma and colleagues constructed a metabolic toggle switch for isopropanol production in *E. coli,* which was inspired by the aforementioned circuit design from Gardner and co-workers (Soma et al., 2014). The conditional knockout of the citrate synthase GltA and

the simultaneous upregulation of a synthetic isopropanol production pathway enabled the switch between growth and production and circumvented the challenge that both pathways would otherwise compete for acetyl-CoA (Soma et al., 2014). Tsuruno and colleagues used a comparable circuit architecture to overcome competition between growth and product formation by dynamically redirecting the central carbon flux from glycerol towards 3-hydroypropionic acid (Tsuruno et al., 2015). In *C. glutamicum*, the pyruvate dehydrogenase complex (PDHC) is an important target for metabolic engineering strategies aiming at increasing production of pyruvate-derived compounds like L-valine, isobutanol, ketoisovalerate and L-lysine (Blombach et al., 2007; Buchholz et al., 2013; Eikmanns and Blombach, 2014). Several of these successful approaches were based on the inactivation of PDHC, e.g. by deleting the *aceE* gene encoding the E1 subunit of this complex, to improve precursor supply. PDHC-deficiency results in strong growth defects on sugars like glucose, which can be complemented by the addition of acetyl-CoA replenishing carbon sources, such as acetate (Schreiner et al., 2005). The inactivation of the PDHC in Δ*aceE* deletion strains leads to decoupling of biomass and L-valine formation and cells mainly consume acetate during the initial growth phase (Blombach et al., 2007; Schreiner et al., 2005). However, acetate represents a costly and inefficient carbon source, which allows only low biomass yields (Blombach et al., 2007; Schreiner et al., 2005).

To overcome the challenges associated with the permanent knockout of the PDHC and to circumvent the competition of biomass and product formation, we implemented our GntR-dependent circuit design as metabolic toggle switch in a *C. glutamicum* L-valine production strain (Wiechert et al., 2020b) (Figure 12A, B). By replacing the native promoter of *aceE* with the gluconate-inducible $P_{gntK}$ promoter, we could control cell growth in dependency of gluconate availability (Figure 12B, C). Remarkably, our dynamically controlled $P_{gntK}$-*aceE* strain was able to co-utilize glucose in the presence of gluconate leading to significantly improved biomass yields in comparison to those obtained for the previously established static Δ*aceE* deletion strain in the presence of acetate and glucose (Figure 12C). In contrast, both strains were not able to grow in media containing solely glucose (Figure 12C) and produced comparable amounts of L-valine (Figure 12D), indicating that controlling PDHC allowed the redirection of carbon flux towards product formation (Wiechert et al., 2020b).

Engineering approaches of PDHC activity based on *aceE* promoter replacements to improve L-valine production were previously applied by two groups. Ma and colleagues applied a growth-phase dependent promoter of an industrial used L-leucine strain ($P_{CP\_2836}$; *C. glutamicum* CP) for phase-dependent control of the PDHC activity to overcome the competition between cell growth and L-valine production. While the PDHC was active and allowed the formation of biomass during exponential growth phase, the activity of the enzyme complex was strongly reduced during stationary phase resulting in accumulation of pyruvate (Ma et al., 2018). In the second study, the authors replaced the *aceE* promoter with mutated, constitutive promoter variants of *dapA* leading to decreased *aceE*

expression, acetate independent cell growth and increased L-valine productivity (Buchholz et al., 2013). However, in contrast to our effector-responsive system which is assumed to provide the opportunity to adjust PDHC activity during a production process, these strain designs are constrained with regard to fine-tuning.

The counter-part of our initial toggle design, the $P_{lys}$ counter-silencer promoter, was used to control the plasmid-based overexpression of L-valine biosynthesis genes (Wiechert et al., 2020b) (Figure 12B). However, this design lowered the productivity compared to previously established production strains, which were based on overexpression plasmids containing the L-valine biosynthesis operons controlled by their native promoters (Figure 12D). We hypothesized that this could be caused by lower expression rates driven by the counter-silencer promoter and suggested the implementation of stronger promoters in future toggle designs (Wiechert et al., 2020b).

Another optimization strategy of our toggle design could focus on protein stability and degradation rates. Since we have controlled PDHC activity at the transcription level, we cannot exclude that when gluconate is depleted and *aceE* expression is downregulated, PDHC remains active to a certain extend. In this regard, degradation tags, e.g. SsrA tags which make proteins susceptible for tail-specific proteases (Herman et al., 1998), could accelerate AceE depletion and thereby improve the response of the system to changes in gluconate availability. The functionality of these signal peptides in *C. glutamicum* was already confirmed in previous studies (Hentschel et al., 2013; Huber et al., 2017).

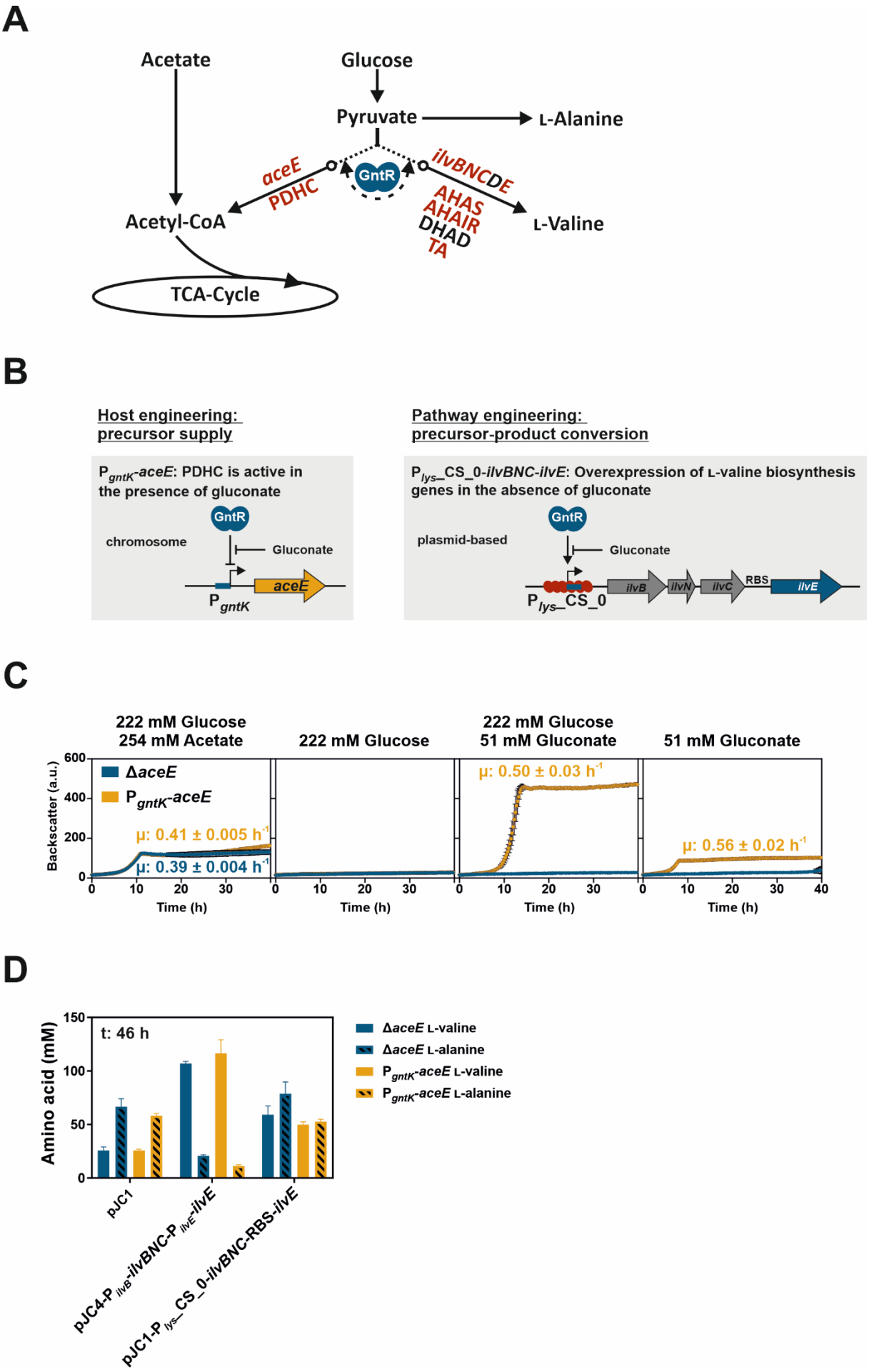
A
Acetate
Glucose
Pyruvate
L-Alanine
aceE
PDHC
GntR
ilvBNCDE
AHAS
AHAIR
DHAD
TA
Acetyl-CoA
L-Valine
TCA-Cycle
B
Host engineering:
precursor supply
Pathway engineering:
precursor-product conversion
PgntK-aceE: PDHC is active in the presence of gluconate
chromosome
GntR
Gluconate
aceE
PgntK
Plys_CS_0-ilvBNC-ilvE: Overexpression of L-valine biosynthesis genes in the absence of gluconate
plasmid-based
GntR
Gluconate
ilvB
ilvN
ilvC
RBS
ilvE
Plys_CS_0
C
222 mM Glucose
254 mM Acetate
222 mM Glucose
222 mM Glucose
51 mM Gluconate
51 mM Gluconate
Backscatter (a.u.)
ΔaceE
PgntK-aceE
μ: 0.41 ± 0.005 h-1
μ: 0.39 ± 0.004 h-1
μ: 0.50 ± 0.03 h-1
μ: 0.56 ± 0.02 h-1
Time (h)
D
Amino acid (mM)
t: 46 h
ΔaceE L-valine
ΔaceE L-alanine
PgntK-aceE L-valine
PgntK-aceE L-alanine
pJC1
pJC4-PilvB-ilvBNC-PilvE-ilvE
pJC1-Plys_CS_0-ilvBNC-RBS-ilvE

**Figure 12: Application of the GntR-dependent toggle for the dynamic switch between growth and L-valine production. A)** Schematic representation of relevant parts of the central carbon metabolism and the L-valine biosynthesis pathway of *C. glutamicum*. The GntR-dependent toggle controlled the redirection of the carbon flux allowing the conversion of pyruvate to either L-valine or acetyl-CoA entering the tricarboxylic acid cycle (TCA-Cycle). *aceE* encodes for the E1 subunit of the pyruvate dehydrogenase complex (PDHC), which converts pyruvate to acetyl-CoA. L-valine is formed from pyruvate in a four-step reaction pathway catalysed by acetohydroxyacid synthase (AHAS, *ilvBN*), acetohydroxyacid isomeroreductase (AHAIR, *ilvC*), dihydroxyacid dehydratase (DHAD, *ilvD*), and transaminase B (TA, *ilvE*). Dynamically controlled genes and their products are highlighted in red. **B)** Schematic overview of the genetic background of the dynamic L-valine production strain. The native promoter of the *aceE* gene was replaced by the GntR target promoter $P_{gntK}$ allowing control of PDHC activity. The L-valine biosynthesis genes were combined in a synthetic operon by fusing *ilvE* via a linker containing an RBS sequence to the end of the operon *ilvBNC*. Its expression was controlled by the synthetic GntR counter-silencer promoter $P_{lys}$_CS_0. **C)** Growth of the strain with dynamically controlled *aceE* expression ($P_{gntK}$-*aceE*) in comparison to the previously established Δ*aceE* strain (Blombach et al., 2007; Schreiner et al., 2005). Both strains had been pre-cultivated in CGXII containing 222 mM glucose and 254 mM acetate before they were cultivated in a microtiter cultivation system in medium with either 222 mM glucose and 254 mM acetate, 222 mM glucose, 222 mM glucose and 51 mM gluconate or 51 mM gluconate. Calculated growth rates (μ) are given (colour-coded) when significant growth had been observed. **D)** L-valine titers of the *aceE* toggle strain ($P_{gntK}$-*aceE*) and the Δ*aceE* L-valine production strain harbouring either the empty control plasmid pJC1 (pJC1-*venus*-term (Baumgart et al., 2013)), plasmid-based L-valine biosynthesis genes controlled by the counter-silencer (pJC1-$P_{lys}$_CS_0-*ilvBNC*-RBS-*ilvE*) or the natively regulated variant pJC4-$P_{ilvB}$-*ilvBNC*-$P_{ilvE}$-*ilvE* (pJC4-*ilvBNCE*; (Radmacher et al., 2002)). All strains were cultivated in CGXII supplemented with 222 mM glucose and 254 mM acetate. Bar plots represent the L-valine and L-alanine titers of biological triplicates and error bars the corresponding standard deviations after 46 h of cultivation. Figure and legend taken from Wiechert et al. (2020b).

### 2.5.3. Metabolic imbalances in static pathway engineering approaches

As previously mentioned, static downregulation of central metabolic reactions can lead to metabolic imbalances and to impaired cell growth, as well as to a reduced overall productivity of a fermentation process. One example of such a metabolic imbalance was recently described in our study "Impact of $CO_2$/$HCO_3^-$ availability in anaplerotic flux in pyruvate dehydrogenase complex deficient *Corynebacterium glutamicum* strains" (Krüger et al., 2019), which is part of this thesis. In this work, we systematically analysed the effect of imbalances of the intracellular $CO_2$/$HCO_3^-$ pool on cell growth of *C. glutamicum* strains lacking the PDHC. In addition to the formation of acetyl-CoA, this enzyme complex catalyses an important decarboxylation reaction that leads to the release of $CO_2$ (de Kok et al., 1998). The results of our study strongly emphasize that the absence of the central decarboxylation reaction impairs the intracellular $CO_2$/$HCO_3^-$ pool, resulting in elongated lag phases of PDHC-deficient strains in the presence of acetate and glucose (Krüger et al., 2019).

$HCO_3^-$ is an important substrate of the anaplerotic reactions catalysed by the pyruvate carboxylase (PCx, encoded by *pyc*) and by the phosphoenolpyruvate carboxylase (PEPCx, encoded by *ppc*). Anaplerotic reactions are essential during growth on glycolytic substrates since they allow the replenishment of TCA cycle intermediates, which are consumed in anabolic reactions (Peters-Wendisch et al., 1998; Sauer and Eikmanns, 2005). The additional inactivation of the dominating anaplerotic enzyme PCx in the strain Δ*aceE* Δ*pyc* was shown to further improve L-valine production by increasing pyruvate supply (Blombach et al., 2008). However, we observed an elongated lag phase of more than 15 hours for the strain Δ*aceE* Δ*pyc* during cultivation in the presence of glucose and acetate, which could be complemented by different approaches aiming at improving the intracellular $HCO_3^-$ availability. We assumed that higher $HCO_3^-$ levels increased PEPCx activity allowing to complement the

inactivation of PCx. Interestingly, this growth defect depends on glucose since it was not observed during cultivation on acetate or after inactivation of the main glucose uptake system PtsG (Krüger et al., 2019).

In *C. glutamicum* wild-type cells, the glyoxylate cycle enables the replenishment of the TCA cycle intermediates during growth of on acetate as well as on the combination of glucose and acetate, but is turned off during growth on glucose (Wendisch et al., 2000; Wendisch et al., 1997). We characterized the phenomenon of glucose sensitivity of Δ*aceE* Δ*pyc* cells in detail and suggested that the inactivation of PDHC and/or PCx led to metabolic imbalances of glycolytic intermediates resulting in inhibition of the glyoxylate cycle enzymes and to depletion of oxaloacetate, which caused the growth defect (Krüger et al., 2019).

In conclusion, our findings emphasised that static interruptions of central decarboxylation and carboxylation reactions aiming at improving productivity of microbial strains can result in severe metabolic imbalances with detrimental effects on cellular growth (Krüger et al., 2019), highlighting the demand for alternative engineering strategies, e.g. metabolic toggle switches.

## 2.6. Conclusion and outlook

Xenogeneic silencing and TF-mediated counter-silencing represent important drivers of bacterial evolution: they can provide access to new beneficial traits while buffering against putative detrimental fitness consequences of foreign DNA elements. Silencing and counter-silencing of H-NS-like XS proteins has been intensively addressed by previous studies, but up to now little was known about the medically and biotechnologically relevant Lsr2-like XS proteins of actinobacteria. This thesis contributes to the understanding of the underlying rules of xenogeneic silencing of the Lsr2-like XS protein CgpS from *C. glutamicum* and provides the first systematic analyses of TF-mediated counter-silencing of an Lsr2-like XS protein (Wiechert et al., 2020a). It shows that CgpS-mediated silencing is determined by a sequence-specific binding motif as well as a distinct drop in GC-profile and that binding of the TF GntR leads to counter-silencing at a variety of promoter architectures (Wiechert et al., 2020a). Furthermore, this work reveals for the first time the potential of synthetic counter-silencer promoters as tightly controlled expression systems and as modular part of genetic toggle switches for synthetic biological applications (Wiechert et al., 2020b). Finally, this thesis provides evidence that static interruptions of central catabolic pathway reactions aiming at improving product formation in biotechnological approaches can result in metabolic imbalances (Krüger et al., 2019) and that metabolic toggle switches allowing dynamic pathway regulation represent a promising alternative strategy (Wiechert et al., 2020b).

Nevertheless, the present work raises interesting questions, especially regarding the in vivo interference of XS and TFs during counter-silencing, the evolutionary process of regulatory network expansion by counter-silencing, and regarding putative mutual interactions of highly concentrated CgpS molecules in the prophage region.

An remaining question is the molecular effect on the nucleoprotein complex formed by the XS CgpS during binding of the TF GntR. Detailed biochemical footprint analysis performed by Will and colleagues revealed that counter-silencing does not depend on the complete relief of the XS protein H-NS and that structural changes of the nucleoprotein complex enable transcription (Will et al., 2014). Based on preliminary electrophoretic shift assays with GntR and CgpS, we got first hints that both proteins simultaneously bind to the DNA in vitro (Wiechert and Frunzke, unpublished). Additionally, none of our counter-silencing constructs reached the same level of promoter activity as it was observed in the absence of CgpS in the prophage-free strain, suggesting that GntR DNA binding does not fully displace CgpS from the DNA (Wiechert et al., 2020a). However, further studies are necessary to decipher the structural changes of the nucleoprotein complex during GntR-mediated counter-silencing. As an alternative to the previously performed in vitro footprint assays from Will and colleagues, in vivo ChIP- or ChAP-seq analyses with the synthetic constructs could provide comprehensive insights into the binding profile of both regulators during silencing (GntR DNA binding is inhibited) and counter-silencing (GntR is bound to the DNA). These approaches might show reduced and/or differentially shaped CgpS coverage peaks when CgpS and GntR compete for DNA binding.
Additionally, no native CgpS counter-silencing factor has yet been identified. Genome-wide binding profiles of GntR, could allow for the identification of new targets and might reveal putative overlaps with known CgpS targets, thereby giving first hints for native GntR-mediated counter-silencing. In general, the large amounts of available ChIP- and ChAP-seq data sets of various TFs and XS proteins from different organisms could provide a promising platform for the systematic search for overlapping binding regions of TFs and XSs. Although this phenomenon is not necessarily linked to counter-silencing, as recently shown by Hünnefeld and colleagues for the MarR-type regulator MalR and CgpS from *C. glutamicum* (Hünnefeld et al., 2019), it could give a first hint for native TF-mediated counter-silencing effects.

Another interesting question focuses on the evolutionary network expansion by counter-silencing. Previously, it was convincingly discussed that, in comparison to the de novo evolution of classical activation circuits, counter-silencing facilitates regulatory network expansion by tolerating a higher degree of flexibility in promoter architectures (Will et al., 2014). This hypothesis was based on the detailed comparison of natively occurring counter-silencer promoters with conservatively activated

regulatory elements belonging to the same regulon (Will et al., 2014). Three synthetic approaches, including our own study, demonstrated that the insertion of TF binding sites allow the large development leap from a silenced promoter to a controllable counter-silencer promoter (Caramel and Schnetz, 1998; Kane and Dorman, 2011; Wiechert et al., 2020a). But what are the steps in between, and can we simulate this evolutionary process? Regarding this, one approach for future studies could be an adaptive laboratory evolution (ALE) experiment with silenced promoters, which have to evolve the mechanism of counter-silencing, in comparison to promoters, which need to develop a classical activation circuit. Promoter fusions with antibiotic resistance genes or other growth-related selection markers could provide a suitable platform for the identification of clones with desired mutations. CgpS target promoters from *C. glutamicum* could be used as starting point for the counter-silencer evolution. The choice of promoters of the second category, which need to evolve an activating circuit, represents probably a greater challenge. Those promoters should have the ability to functionally drive transcription, but this process should be dependent on a TF that activates gene expression, e.g. by recruiting the RNA polymerase. By disturbing native activating regulatory circuits, e.g. by deleting an activating TF in the genome, these requirements could be fulfilled for the corresponding target promoters. A comparative ALE experiment with both promoter categories could answer the question which mechanism – classical activation or counter-silencing - is more likely to be evolved. Furthermore, this experiment could provide comprehensive insights into the evolutionary process of co-opting a TF as a counter-silencing factor during regulatory network expansion.

A third interesting point is the effect of the high number of CgpS binding peaks located in high density and close distances within the AT-rich prophage element CGP3 (Pfeifer et al., 2016), which is probably associated with high local concentrations of bound but also unbound CgpS molecules. But do CgpS molecules influence each other, and is there even an attractive molecular interaction similar as observed during liquid-liquid phase separation (LLPS)? LLPS describes the dynamic condensation of proteins and nucleic acids into macromolecular condensates based on attractive molecular interactions which counterbalance entropy-driven effects like protein diffusion (Monterroso et al., 2019). Thereby, LLPS allows the compartmentalisation of cellular components independent of membranes and mainly contributes to their sub-cellular spatial organisation (Guilhas et al., 2019). In eukaryotic cells, LLPS is involved in many processes including chromatin rearrangements and three-dimensional genome organisation as well as transcriptional regulation (Wang and Liu, 2019). Guilhas and colleagues recently identified nanometre-sized droplets formed by LLPS which consist of components of the bacterial ParABS DNA segregation system. These structures were able to inhibit ParB (DNA binding protein) diffusion leading to trapping of ParB close to defined DNA regions (Guilhas et al., 2019). For future studies, it would be interesting to investigate whether XS proteins play a role

in the subcellular organisation of prophage elements in bacterial nucleoids via LLPS. Recently used methods in LLPS research such as super-resolution PALM microscopy and single-particle tracking PALM (sptPALM) (Guilhas et al., 2019) combined with protein reporter fusions represent promising approaches to investigate local accumulations of CgpS proteins. Furthermore, they might allow the analysis of the localization and diffusion dynamics of single CgpS molecules and the identification of putative trapping effects caused by high-affinity interactions between CgpS molecules.

As discussed in chapter 2.4.3. ("Synthetic disruptive counter-silencing."), we inspected counter-silencing of CgpS target promoters plasmid-based and in vivo, but isolated from their native genomic context (Wiechert et al., 2020a). Therefore, another interesting point would be the effect of the TF GntR on these molecular interactions in the native genomic context. Here, super-resolution microscopy approaches could provide interesting insights into the CgpS-dependent organization of the prophage element when it is integrated into the bacterial genome as well as during the process of prophage induction.

## 2.7. References

Albano, M., Smits, W. K., Ho, L. T. Y., Kraigher, B., Mandic-Mulec, I., Kuipers, O. P. and Dubnau, D. (2005). The Rok protein of *Bacillus subtilis* represses genes for cell surface and extracellular functions. *J. Bacteriol. 187*, 2010-2019, doi: *10.1128/JB.187.6.2010-2019.2005.*

Alekshun, M. N., Levy, S. B., Mealy, T. R., Seaton, B. A. and Head, J. F. (2001). The crystal structure of MarR, a regulator of multiple antibiotic resistance, at 2.3 A resolution. *Nat. Struct. Biol. 8*, 710-714, doi: *10.1038/90429.*

Ali, S. S., Beckett, E., Bae, S. J. and Navarre, W. W. (2011). The 5.5 protein of phage T7 inhibits H-NS through interactions with the central oligomerization domain. *J. Bacteriol. 193*, 4881-4892, doi: *10.1128/JB.05198-11.*

Ali, S. S., Soo, J., Rao, C., Leung, A. S., Ngai, D. H.-M., Ensminger, A. W. and Navarre, W. W. (2014). Silencing by H-NS potentiated the evolution of *Salmonella*. *PLoS Pathog. 10*, e1004500, doi: *10.1371/journal.ppat.1004500.*

Ali, S. S., Xia, B., Liu, J. and Navarre, W. W. (2012). Silencing of foreign DNA in bacteria. *Curr. Opin. Microbiol. 15*, 175-181, doi: *10.1016/j.mib.2011.12.014.*

Alper, H., Fischer, C., Nevoigt, E. and Stephanopoulos, G. (2005). Tuning genetic control through promoter engineering. *Proc. Natl. Acad. Sci. U S A. 102*, 12678-12683, doi: *10.1073/pnas.0504604102.*

Amit, R., Oppenheim, A. B. and Stavans, J. (2003). Increased bending rigidity of single DNA molecules by H-NS, a temperature and osmolarity sensor. *Biophys. J. 84*, 2467-2473, doi: *10.1016/S0006-3495(03)75051-6.*

Amitai, G. and Sorek, R. (2016). CRISPR–Cas adaptation: insights into the mechanism of action. *Nat. Rev. Microbiol. 14*, 67-76, doi: *10.1038/nrmicro.2015.14.*

Arold, S. T., Leonard, P. G., Parkinson, G. N. and Ladbury, J. E. (2010). H-NS forms a superhelical protein scaffold for DNA condensation. *Proc. Natl. Acad. Sci. U S A. 107*, 15728-15732, doi: *10.1073/pnas.1006966107.*

Badaut, C., Williams, R., Arluison, V., Bouffartigues, E., Robert, B., Buc, H. and Rimsky, S. (2002). The degree of oligomerization of the H-NS nucleoid structuring protein is related to specific binding to DNA. *J. Biol. Chem. 277*, 41657-41666, doi: *10.1074/jbc.M206037200.*

Bader, M. W., Navarre, W. W., Shiau, W., Nikaido, H., Frye, J. G., McClelland, M., Fang, F. C. and Miller, S. I. (2003). Regulation of *Salmonella typhimurium* virulence gene expression by cationic antimicrobial peptides. *Mol. Microbiol. 50*, 219-230, doi: *10.1046/j.1365-2958.2003.03675.x.*

Bakshi, S., Choi, H., Rangarajan, N., Barns, K. J., Bratton, B. P. and Weisshaar, J. C. (2014). Nonperturbative imaging of nucleoid morphology in live bacterial cells during an antimicrobial peptide attack. *Appl. Environ. Microbiol. 80*, 4977-4986, doi: *10.1128/AEM.00989-14.*

Baltrus, D. A. (2013). Exploring the costs of horizontal gene transfer. *Trends Ecol. Evol. 28*, 489-495, doi: *10.1016/j.tree.2013.04.002.*

Baños, R. C., Aznar, S., Madrid, C. and Juárez, A. (2011). Differential functional properties of chromosomal- and plasmid-encoded H-NS proteins. *Res. Microbiol. 162*, 382-385, doi: *10.1016/j.resmic.2011.02.003.*

Baños, R. C., Pons, J. I., Madrid, C. and Juárez, A. (2008). A global modulatory role for the *Yersinia enterocolitica* H-NS protein. *Microbiology. 154*, 1281-1289, doi: *10.1099/mic.0.2007/015610-0.*

Banos, R. C., Vivero, A., Aznar, S., Garcia, J., Pons, M., Madrid, C. and Juarez, A. (2009). Differential regulation of horizontally acquired and core genome genes by the bacterial modulator H-NS. *PLoS Genet. 5*, e1000513, doi: *10.1371/journal.pgen.1000513.*

Baritugo, K. A., Kim, H. T., David, Y., Choi, J. I., Hong, S. H., Jeong, K. J., Choi, J. H., Joo, J. C. and Park, S. J. (2018). Metabolic engineering of *Corynebacterium glutamicum* for fermentative production of chemicals in biorefinery. *Appl. Microbiol. Biotechnol. 102*, 3915-3937, doi: *10.1007/s00253-018-8896-6.*

Barth, M., Marschall, C., Muffler, A., Fischer, D. and Hengge-Aronis, R. (1995). Role for the histone-like protein H-NS in growth phase-dependent and osmotic regulation of sigma S and many sigma S-dependent genes in *Escherichia coli*. *J. Bacteriol. 177*, 3455-3464, doi: *10.1128/jb.177.12.3455-3464.1995.*

Baumgart, M., Unthan, S., Rückert, C., Sivalingam, J., Grünberger, A., Kalinowski, J., Bott, M., Noack, S. and Frunzke, J. (2013). Construction of a prophage-free variant of *Corynebacterium glutamicum* ATCC 13032 for use as a platform strain for basic research and industrial biotechnology. *Appl. Environ. Microbiol. 79*, 6006-6015, doi: *10.1128/aem.01634-13.*

Becker, J., Zelder, O., Hafner, S., Schroder, H. and Wittmann, C. (2011). From zero to hero--design-based systems metabolic engineering of *Corynebacterium glutamicum* for L-lysine production. *Metab. Eng. 13*, 159-168, doi: *10.1016/j.ymben.2011.01.003.*

Ben-Samoun, K., Leblon, G. and Reyes, O. (1999). Positively regulated expression of the *Escherichia coli araBAD* promoter in *Corynebacterium glutamicum*. *FEMS Microbiol. Lett. 174*, 125-130, doi: *10.1111/j.1574-6968.1999.tb13558.x.*

Bernheim, A. and Sorek, R. (2020). The pan-immune system of bacteria: antiviral defence as a community resource. *Nat. Rev. Microbiol. 18*, 113-119, doi: *10.1038/s41579-019-0278-2.*

Bertani, G. and Weigle, J. J. (1953). Host controlled variation in bacterial viruses. *J. Bacteriol. 65*, 113-121,

Binder, S., Schendzielorz, G., Stäbler, N., Krumbach, K., Hoffmann, K., Bott, M. and Eggeling, L. (2012). A high-throughput approach to identify genomic variants of bacterial metabolite producers at the single-cell level. *Genome Biol. 13*, R40, doi: *10.1186/gb-2012-13-5-r40.*

Bingham, R., Ekunwe, S. I., Falk, S., Snyder, L. and Kleanthous, C. (2000). The major head protein of bacteriophage T4 binds specifically to elongation factor Tu. *J. Biol. Chem. 275*, 23219-23226, doi: *10.1074/jbc.M002546200.*

Blazeck, J. and Alper, H. S. (2013). Promoter engineering: recent advances in controlling transcription at the most fundamental level. *Biotechnol. J. 8*, 46-58, doi: *10.1002/biot.201200120.*

Blombach, B., Schreiner, M. E., Bartek, T., Oldiges, M. and Eikmanns, B. J. (2008). *Corynebacterium glutamicum* tailored for high-yield L-valine production. *Appl. Microbiol. Biotechnol. 79*, 471-479, doi: *10.1007/s00253-008-1444-z.*

Blombach, B., Schreiner, M. E., Holátko, J., Bartek, T., Oldiges, M. and Eikmanns, B. J. (2007). L-Valine production with pyruvate dehydrogenase complex-deficient *Corynebacterium glutamicum*. *Appl. Environ. Microbiol. 73*, 2079-2084, doi: *10.1128/AEM.02826-06.*

Bobay, L.-M., Touchon, M. and Rocha, E. P. C. (2014). Pervasive domestication of defective prophages by bacteria. *Proc. Natl. Acad. Sci. U S A. 111*, 12127-12132, doi: *10.1073/pnas.1405336111.*

Bondy-Denomy, J., Qian, J., Westra, E. R., Buckling, A., Guttman, D. S., Davidson, A. R. and Maxwell, K. L. (2016). Prophages mediate defense against phage infection through diverse mechanisms. *ISME J. 10*, 2854-2866, doi: *10.1038/ismej.2016.79.*

Brockman, I. M. and Prather, K. L. (2015a). Dynamic metabolic engineering: New strategies for developing responsive cell factories. *Biotechnol. J. 10*, 1360-1369, doi: *10.1002/biot.201400422.*

Brockman, I. M. and Prather, K. L. J. (2015b). Dynamic knockdown of *E. coli* central metabolism for redirecting fluxes of primary metabolites. *Metab. Eng. 28*, 104-113, doi: *10.1016/j.ymben.2014.12.005.*

Brucoli, F., Guzman, J. D., Maitra, A., James, C. H., Fox, K. R. and Bhakta, S. (2015). Synthesis, anti-mycobacterial activity and DNA sequence-selectivity of a library of biaryl-motifs containing polyamides. *Bioorg. Med. Chem. 23*, 3705-3711, doi: *10.1016/j.bmc.2015.04.001.*

Buchholz, J., Schwentner, A., Brunnenkan, B., Gabris, C., Grimm, S., Gerstmeir, R., Takors, R., Eikmanns, B. J. and Blombach, B. (2013). Platform engineering of *Corynebacterium glutamicum* with reduced pyruvate dehydrogenase complex activity for improved production of L-Lysine, L-Valine, and 2-Ketoisovalerate. *Appl. Environ. Microbiol. 79*, 5566-5575, doi: *10.1128/AEM.01741-13.*

Caramel, A. and Schnetz, K. (1998). Lac and lambda repressors relieve silencing of the *Escherichia coli bgl* promoter. Activation by alteration of a repressing nucleoprotein complex. *J. Mol. Biol. 284*, 875-883, doi: *10.1006/jmbi.1998.2191.*

Casjens, S. (2003). Prophages and bacterial genomics: what have we learned so far? *Mol. Microbiol. 49*, 277-300, doi: *10.1046/j.1365-2958.2003.03580.x.*

Castang, S. and Dove, S. L. (2012). Basis for the Essentiality of H-NS Family Members in *Pseudomonas aeruginosa*. *J. Bacteriol. 194*, 5101-5109, doi: *10.1128/JB.00932-12.*

Castang, S., McManus, H. R., Turner, K. H. and Dove, S. L. (2008). H-NS family members function coordinately in an opportunistic pathogen. *Proc. Natl. Acad. Sci. U S A. 105*, 18947-18952, doi: *10.1073/pnas.0808215105.*

Chaparian, R. R., Tran, M. L. N., Miller Conrad, L. C., Rusch, D. B. and van Kessel, J. C. (2020). Global H-NS counter-silencing by LuxR activates quorum sensing gene expression. *Nucleic Acids Res. 48*, 171-183, doi: *10.1093/nar/gkz1089.*

Chen, C. C., Ghole, M., Majumder, A., Wang, Z., Chandana, S. and Wu, H. Y. (2003). LeuO-mediated transcriptional derepression. *J. Biol. Chem. 278*, 38094-38103, doi: *10.1074/jbc.M300461200.*

Chen, J. M., Ren, H., Shaw, J. E., Wang, Y. J., Li, M., Leung, A. S., Tran, V., Berbenetz, N. M., Kocíncová, D., Yip, C. M., Reyrat, J.-M. and Liu, J. (2008). Lsr2 of *Mycobacterium tuberculosis* is a DNA-bridging protein. *Nucleic Acids Res. 36*, 2123-2135, doi: *10.1093/nar/gkm1162.*

Chib, S. and Mahadevan, S. (2012). Involvement of the global regulator H-NS in the survival of *Escherichia coli* in stationary phase. *J. Bacteriol. 194*, 5285-5293, doi: *10.1128/JB.00840-12*

Chu, H. Y., Sprouffske, K. and Wagner, A. (2018). Assessing the benefits of horizontal gene transfer by laboratory evolution and genome sequencing. *BMC Evol. Biol. 18*, 54, doi: *10.1186/s12862-018-1164-7.*

Cohen, D., Melamed, S., Millman, A., Shulman, G., Oppenheimer-Shaanan, Y., Kacen, A., Doron, S., Amitai, G. and Sorek, R. (2019). Cyclic GMP–AMP signalling protects bacteria against viral infection. *Nature. 574*, 691-695, doi: *10.1038/s41586-019-1605-5.*

Colangeli, R., Helb, D., Vilchèze, C., Hazbón, M. H., Lee, C.-G., Safi, H., Sayers, B., Sardone, I., Jones, M. B., Fleischmann, R. D., Peterson, S. N., Jacobs, W. R., Jr. and Alland, D. (2007). Transcriptional regulation of multi-drug tolerance and antibiotic-induced responses by the histone-like protein Lsr2 in *M. tuberculosis*. *PLoS Pathog. 3*, e87-e87, doi: *10.1371/journal.ppat.0030087.*

Corbett, D., Bennett, H. J., Askar, H., Green, J. and Roberts, I. S. (2007). SlyA and H-NS regulate transcription of the *Escherichia coli* K5 capsule gene cluster, and expression of *slyA* in *Escherichia coli* is temperature-dependent, positively autoregulated, and independent of H-NS. *J. Biol. Chem. 282*, 33326-33335, doi: *10.1074/jbc.M703465200.*

Dame, R. T., Luijsterburg, M. S., Krin, E., Bertin, P. N., Wagner, R. and Wuite, G. J. L. (2005). DNA bridging: a property shared among H-NS-like proteins. *J. Bacteriol. 187*, 1845-1848, doi: *10.1128/JB.187.5.1845-1848.2005.*

Dame, R. T., Wyman, C., Wurm, R., Wagner, R. and Goosen, N. (2002). Structural basis for H-NS-mediated trapping of RNA polymerase in the open initiation complex at the *rrnB* P1. *J. Biol. Chem. 277*, 2146-2150, doi: *10.1074/jbc.C100603200.*

de Kok, A., Hengeveld, A. F., Martin, A. and Westphal, A. H. (1998). The pyruvate dehydrogenase multi-enzyme complex from Gram-negative bacteria. *Biochim. Biophys. Acta, Protein Struct. Mol. Enzymol. 1385*, 353-366, doi: *10.1016/s0167-4838(98)00079-x.*

de la Cruz, F. and Davies, J. (2000). Horizontal gene transfer and the origin of species: lessons from bacteria. *Trends Microbiol. 8*, 128-133, doi: *10.1016/s0966-842x(00)01703-0.*

Depardieu, F., Didier, J. P., Bernheim, A., Sherlock, A., Molina, H., Duclos, B. and Bikard, D. (2016). A eukaryotic-like serine/threonine kinase protects *Staphylococci* against phages. *Cell Host Microbe. 20*, 471-481, doi: *10.1016/j.chom.2016.08.010.*

Desai, P. T., Porwollik, S., Long, F., Cheng, P., Wollam, A., Clifton, S. W., Weinstock, G. M. and McClelland, M. (2013). Evolutionary genomics of *Salmonella enterica* subspecies. *mBio. 4*, e00579-00512, doi: *10.1128/mBio.00579-12.*

Ding, P., McFarland, K. A., Jin, S., Tong, G., Duan, B., Yang, A., Hughes, T. R., Liu, J., Dove, S. L., Navarre, W. W. and Xia, B. (2015). A novel AT-Rich DNA recognition mechanism for bacterial xenogeneic silencer MvaT. *PLoS Pathog. 11*, e1004967, doi: *10.1371/journal.ppat.1004967.*

Doolittle, W. F. (1998). You are what you eat: a gene transfer ratchet could account for bacterial genes in eukaryotic nuclear genomes. *Trends Genet. 14*, 307-311, doi: *10.1016/s0168-9525(98)01494-2.*

Doong, S. J., Gupta, A. and Prather, K. L. J. (2018). Layered dynamic regulation for improving metabolic pathway productivity in *Escherichia coli*. *Proc. Natl. Acad. Sci. U S A. 115*, 2964-2969, doi: *10.1073/pnas.1716920115.*

Doron, S., Melamed, S., Ofir, G., Leavitt, A., Lopatina, A., Keren, M., Amitai, G. and Sorek, R. (2018). Systematic discovery of antiphage defense systems in the microbial pangenome. *Science. 359*, eaar4120, doi: *10.1126/science.aar4120.*

Duan, B., Ding, P., Hughes, T. R., Navarre, W. W., Liu, J. and Xia, B. (2018). How bacterial xenogeneic silencer rok distinguishes foreign from self DNA in its resident genome. *Nucleic Acids Res. 46*, 10514-10529, doi: *10.1093/nar/gky836.*

Durmaz, E. and Klaenhammer, T. R. (2007). Abortive phage resistance mechanism AbiZ speeds the lysis clock to cause premature lysis of phage-infected *Lactococcus lactis*. *J. Bacteriol. 189*, 1417-1425, doi: *10.1128/JB.00904-06.*

Dy, R. L., Przybilski, R., Semeijn, K., Salmond, G. P. C. and Fineran, P. C. (2014). A widespread bacteriophage abortive infection system functions through a Type IV toxin-antitoxin mechanism. *Nucleic Acids Res. 42*, 4590-4605, doi: *10.1093/nar/gkt1419.*

Eikmanns, B. J. and Blombach, B. (2014). The pyruvate dehydrogenase complex of *Corynebacterium glutamicum*: an attractive target for metabolic engineering. *J. Biotechnol. 192*, 339-345, doi: *10.1016/j.jbiotec.2013.12.019.*

Ellison, D. W. and Miller, V. L. (2006). H-NS represses transcription in *Yersinia enterocolitica* through competition with RovA and interaction with YmoA. *J. Bacteriol. 188*, 5101-5112, doi: *10.1128/JB.00862-05.*

Esposito, D., Petrovic, A., Harris, R., Ono, S., Eccleston, J. F., Mbabaali, A., Haq, I., Higgins, C. F., Hinton, J. C., Driscoll, P. C. and Ladbury, J. E. (2002). H-NS oligomerization domain structure reveals the mechanism for high order self-association of the intact protein. *J. Mol. Biol. 324*, 841-850, doi: *10.1016/s0022-2836(02)01141-5.*

Falconi, M., Colonna, B., Prosseda, G., Micheli, G. and Gualerzi, C. O. (1998). Thermoregulation of *Shigella* and *Escherichia coli* EIEC pathogenicity. A temperature-dependent structural transition of DNA modulates accessibility of *virF* promoter to transcriptional repressor H-NS. *EMBO J. 17*, 7033-7043, doi: *10.1093/emboj/17.23.7033.*

Fang, F. C. and Rimsky, S. (2008). New insights into transcriptional regulation by H-NS. *Curr. Opin. Microbiol. 11*, 113-120, doi: *10.1016/j.mib.2008.02.011.*

Farmer, W. R. and Liao, J. C. (2000). Improving lycopene production in *Escherichia coli* by engineering metabolic control. *Nat. Biotechnol. 18*, 533-537, doi: *10.1038/75398.*

Faure, G., Makarova, K. S. and Koonin, E. V. (2019). CRISPR-Cas: Complex functional networks and multiple roles beyond adaptive immunity. *J. Mol. Biol. 431*, 3-20, doi: *10.1016/j.jmb.2018.08.030.*

Fitz, E., Wanka, F. and Seiboth, B. (2018). The promoter toolbox for recombinant gene expression in *Trichoderma reesei*. *Front. Bioeng. Biotechnol. 6*, 135, doi: *10.3389/fbioe.2018.00135.*

Frunzke, J., Engels, V., Hasenbein, S., Gatgens, C. and Bott, M. (2008). Co-ordinated regulation of gluconate catabolism and glucose uptake in *Corynebacterium glutamicum* by two functionally equivalent transcriptional regulators, GntR1 and GntR2. *Mol. Microbiol. 67*, 305-322, doi: *10.1111/j.1365-2958.2007.06020.x.*

Furuya, E. Y. and Lowy, F. D. (2006). Antimicrobial-resistant bacteria in the community setting. *Nat. Rev. Microbiol. 4*, 36-45, doi: *10.1038/nrmicro1325.*

Gao, X., Zou, T., Mu, Z., Qin, B., Yang, J., Waltersperger, S., Wang, M., Cui, S. and Jin, Q. (2013). Structural insights into VirB-DNA complexes reveal mechanism of transcriptional activation of virulence genes. *Nucleic Acids Res. 41*, 10529-10541, doi: *10.1093/nar/gkt748.*

Gao, Y., Foo, Y. H., Winardhi, R. S., Tang, Q., Yan, J. and Kenney, L. J. (2017). Charged residues in the H-NS linker drive DNA binding and gene silencing in single cells. *Proc. Natl. Acad. Sci. U S A. 114*, 12560-12565, doi: *10.1073/pnas.1716721114.*

García-Granados, R., Lerma-Escalera, J. A. and Morones-Ramírez, J. R. (2019). Metabolic engineering and synthetic biology: synergies, future, and challenges. *Front. Bioeng. Biotechnol. 7*, 36-36, doi: *10.3389/fbioe.2019.00036.*

Gardner, T. S., Cantor, C. R. and Collins, J. J. (2000). Construction of a genetic toggle switch in *Escherichia coli*. *Nature. 403*, 339-342, doi: *10.1038/35002131.*

Gehrke, E. J., Zhang, X., Pimentel-Elardo, S. M., Johnson, A. R., Rees, C. A., Jones, S. E., Hindra, Gehrke, S. S., Turvey, S., Boursalie, S., Hill, J. E., Carlson, E. E., Nodwell, J. R. and Elliot, M. A. (2019). Silencing cryptic specialized metabolism in *Streptomyces* by the nucleoid-associated protein Lsr2. *Elife. 8*, doi: *10.7554/eLife.47691.*

Ghosh, A., Paul, K. and Chowdhury, R. (2006). Role of the histone-like nucleoid structuring protein in colonization, motility, and bile-dependent repression of virulence gene expression in *Vibrio cholerae*. *Infect. Immun. 74*, 3060-3064, doi: *10.1128/IAI.74.5.3060-3064.2006.*

Ghosh, D., Roy, K., Williamson, K. E., Srinivasiah, S., Wommack, K. E. and Radosevich, M. (2009). Acyl-homoserine lactones can induce virus production in lysogenic bacteria: an alternative paradigm for prophage induction. *Appl. Environ. Microbiol. 75*, 7142-7152, doi: *10.1128/AEM.00950-09.*

Goldberg, G. W. and Marraffini, L. A. (2015). Resistance and tolerance to foreign elements by prokaryotic immune systems - curating the genome. *Nat. Rev. Immunol. 15*, 717-724, doi: *10.1038/nri3910.*

Goldfarb, T., Sberro, H., Weinstock, E., Cohen, O., Doron, S., Charpak-Amikam, Y., Afik, S., Ofir, G. and Sorek, R. (2015). BREX is a novel phage resistance system widespread in microbial genomes. *EMBO J. 34*, 169-183, doi: *10.15252/embj.201489455.*

Gordon, B. R., Imperial, R., Wang, L., Navarre, W. W. and Liu, J. (2008). Lsr2 of *Mycobacterium* represents a novel class of H-NS-like proteins. *J. Bacteriol. 190*, 7052-7059, doi: *10.1128/JB.00733-08.*

Gordon, B. R., Li, Y., Wang, L., Sintsova, A., van Bakel, H., Tian, S., Navarre, W. W., Xia, B. and Liu, J. (2010). Lsr2 is a nucleoid-associated protein that targets AT-rich sequences and virulence genes in *Mycobacterium tuberculosis*. *Proc. Natl. Acad. Sci. U S A. 107*, 5154-5159, doi: *10.1073/pnas.0913551107.*

Gordon, B. R. G., Li, Y., Cote, A., Weirauch, M. T., Ding, P., Hughes, T. R., Navarre, W. W., Xia, B. and Liu, J. (2011). Structural basis for recognition of AT-rich DNA by unrelated xenogeneic silencing proteins. *Proc. Natl. Acad. Sci. U S A. 108*, 10690-10695, doi: *10.1073/pnas.1102544108.*

Groisman, E. A., Kayser, J. and Soncini, F. C. (1997). Regulation of polymyxin resistance and adaptation to low-$Mg^{2+}$ environments. *J. Bacteriol. 179*, 7040-7045, doi: *10.1128/jb.179.22.7040-7045.1997.*

Guilhas, B., Walter, J. C., Rech, J., David, G., Walliser, N.-O., Palmeri, J., Mathieu-Demaziere, C., Parmeggiani, A., Bouet, J. Y., Gall, A. L. and Nollmann, M. (2019). ATP-driven separation of liquid phase condensates in bacteria. *bioRxiv.* 791368, doi: *10.1101/791368*

Gulvady, R., Gao, Y., Kenney, L. J. and Yan, J. (2018). A single molecule analysis of H-NS uncouples DNA binding affinity from DNA specificity. *Nucleic Acids Res. 46*, 10216-10224, doi: *10.1093/nar/gky826.*

Gupta, A., Reizman, I. M., Reisch, C. R. and Prather, K. L. (2017). Dynamic regulation of metabolic flux in engineered bacteria using a pathway-independent quorum-sensing circuit. *Nat. Biotechnol. 35*, 273-279, doi: *10.1038/nbt.3796.*

Hacker, J., Blum-Oehler, G., Muhldorfer, I. and Tschape, H. (1997). Pathogenicity islands of virulent bacteria: structure, function and impact on microbial evolution. *Mol. Microbiol. 23*, 1089-1097, doi: *10.1046/j.1365-2958.1997.3101672.x.*

Han, L., Cui, W., Suo, F., Miao, S., Hao, W., Chen, Q., Guo, J., Liu, Z., Zhou, L. and Zhou, Z. (2019). Development of a novel strategy for robust synthetic bacterial promoters based on a stepwise evolution targeting the spacer region of the core promoter in *Bacillus subtilis*. *Microb. Cell Fact. 18*, 96-96, doi: *10.1186/s12934-019-1148-3.*

Hendrix, R. W., Smith, M. C., Burns, R. N., Ford, M. E. and Hatfull, G. F. (1999). Evolutionary relationships among diverse bacteriophages and prophages: all the world's a phage. *Proc. Natl. Acad. Sci. U S A. 96*, 2192-2197, doi: *10.1073/pnas.96.5.2192.*

Hentschel, E., Will, C., Mustafi, N., Burkovski, A., Rehm, N. and Frunzke, J. (2013). Destabilized eYFP variants for dynamic gene expression studies in *Corynebacterium glutamicum*. *Microb. Biotechnol. 6*, 196-201, doi: *10.1111/j.1751-7915.2012.00360.x.*

Herman, C., Thevenet, D., Bouloc, P., Walker, G. C. and D'Ari, R. (1998). Degradation of carboxy-terminal-tagged cytoplasmic proteins by the *Escherichia coli* protease HflB (FtsH). *Genes Dev. 12*, 1348-1355, doi: *10.1101/gad.12.9.1348.*

Heroven, A. K., Nagel, G., Tran, H. J., Parr, S. and Dersch, P. (2004). RovA is autoregulated and antagonizes H-NS-mediated silencing of invasin and *rovA* expression in *Yersinia pseudotuberculosis*. *Mol. Microbiol. 53*, 871-888, doi: *10.1111/j.1365-2958.2004.04162.x.*

Hildebrand, F., Meyer, A. and Eyre-Walker, A. (2010). Evidence of selection upon genomic GC-content in bacteria. *PLoS Genet. 6*, e1001107, doi: *10.1371/journal.pgen.1001107.*

Ho, C.-H., Wang, H.-C., Ko, T.-P., Chang, Y.-C. and Wang, A. H. J. (2014). The T4 phage DNA mimic protein Arn inhibits the DNA binding activity of the bacterial histone-like protein H-NS. *J. Biol. Chem. 289*, 27046-27054, doi: *10.1074/jbc.M114.590851.*

Hoa, T., Tortosa, P., Albano, M. and Dubnau, D. (2002). Rok (YkuW) regulates genetic competence in *Bacillus subtilis* by directly repressing *comK*. *Mol. Microbiol. 43*, 15-26, doi: *10.1046/j.1365-2958.2002.02727.x.*

Hommais, F., Krin, E., Laurent-Winter, C., Soutourina, O., Malpertuy, A., Le Caer, J.-P., Danchin, A. and Bertin, P. (2001). Large-scale monitoring of pleiotropic regulation of gene expression by the prokaryotic nucleoid-associated protein, H-NS. *Mol. Microbiol. 40*, 20-36, doi: *10.1046/j.1365-2958.2001.02358.x.*

Hong, S. H., Wang, X. and Wood, T. K. (2010). Controlling biofilm formation, prophage excision and cell death by rewiring global regulator H-NS of *Escherichia coli*. *Microb. Biotechnol. 3*, 344-356, doi: *10.1111/j.1751-7915.2010.00164.x.*

Huber, I., Palmer, D. J., Ludwig, K. N., Brown, I. R., Warren, M. J. and Frunzke, J. (2017). Construction of recombinant Pdu metabolosome shells for small molecule production in *Corynebacterium glutamicum*. *ACS Synth. Biol. 6*, 2145-2156, doi: *10.1021/acssynbio.7b00167.*

Hulbert, R. R. and Taylor, R. K. (2002). Mechanism of ToxT-dependent transcriptional activation at the *Vibrio cholerae tcpA* promoter. *J. Bacteriol. 184*, 5533-5544, doi: *10.1128/jb.184.20.5533-5544.2002.*

Hünnefeld, M., Persicke, M., Kalinowski, J. and Frunzke, J. (2019). The MarR-type regulator MalR is involved in stress-responsive cell envelope remodeling in *Corynebacterium glutamicum*. *Front. Microbiol. 10*, doi: *10.3389/fmicb.2019.01039.*

Huser, A. T., Chassagnole, C., Lindley, N. D., Merkamm, M., Guyonvarch, A., Elisakova, V., Patek, M., Kalinowski, J., Brune, I., Puhler, A. and Tauch, A. (2005). Rational design of a *Corynebacterium glutamicum* pantothenate production strain and its characterization by metabolic flux analysis and genome-wide transcriptional profiling. *Appl. Environ. Microbiol. 71*, 3255-3268, doi: *10.1128/aem.71.6.3255-3268.2005.*

Jain, R., Rivera, M. C. and Lake, J. A. (1999). Horizontal gene transfer among genomes: the complexity hypothesis. *Proc. Natl. Acad. Sci. U S A. 96*, 3801-3806, doi: *10.1073/pnas.96.7.3801.*

Janion, C. (2008). Inducible SOS response system of DNA repair and mutagenesis in *Escherichia coli*. *Int. J. Biol. Sci. 4*, 338-344, doi: *10.7150/ijbs.4.338.*

Kalinowski, J., Bathe, B., Bartels, D., Bischoff, N., Bott, M., Burkovski, A., Dusch, N., Eggeling, L., Eikmanns, B. J., Gaigalat, L., Goesmann, A., Hartmann, M., Huthmacher, K., Kramer, R., Linke, B., McHardy, A. C., Meyer, F., Mockel, B., Pfefferle, W., Puhler, A., Rey, D. A., Ruckert, C., Rupp, O., Sahm, H., Wendisch, V. F., Wiegrabe, I. and Tauch, A. (2003). The complete *Corynebacterium glutamicum* ATCC 13032 genome sequence and its impact on the production of L-aspartate-derived amino acids and vitamins. *J. Biotechnol. 104*, 5-25, doi: *10.1016/s0168-1656(03)00154-8.*

Kane, K. A. and Dorman, C. J. (2011). Rational design of an artificial genetic switch: Co-option of the H-NS-repressed *proU* operon by the VirB virulence master regulator. *J. Bacteriol. 193*, 5950-5960, doi: *10.1128/jb.05557-11.*

Keilhauer, C., Eggeling, L. and Sahm, H. (1993). Isoleucine synthesis in *Corynebacterium glutamicum*: molecular analysis of the *ilvB-ilvN-ilvC* operon. *J. Bacteriol. 175*, 5595-5603, doi: *10.1128/jb.175.17.5595-5603.1993.*

Khalil, A. S. and Collins, J. J. (2010). Synthetic biology: applications come of age. *Nat. Rev. Genet. 11*, 367-379, doi: *10.1038/nrg2775.*

Koonin, E. V., Makarova, K. S. and Zhang, F. (2017). Diversity, classification and evolution of CRISPR-Cas systems. *Curr. Opin. Microbiol. 37*, 67-78, doi: *10.1016/j.mib.2017.05.008.*

Krause, F. S., Blombach, B. and Eikmanns, B. J. (2010). Metabolic engineering of *Corynebacterium glutamicum* for 2-ketoisovalerate production. *Appl. Environ. Microbiol. 76*, 8053-8061, doi: *10.1128/aem.01710-10.*

Kronheim, S., Daniel-Ivad, M., Duan, Z., Hwang, S., Wong, A. I., Mantel, I., Nodwell, J. R. and Maxwell, K. L. (2018). A chemical defence against phage infection. *Nature. 564*, 283-286, doi: *10.1038/s41586-018-0767-x.*

Krüger, A., Wiechert, J., Gätgens, C., Polen, T., Mahr, R. and Frunzke, J. (2019). Impact of $CO_2$/$HCO_3^-$ availability on anaplerotic flux in pyruvate dehydrogenase complex-deficient *Corynebacterium glutamicum* strains. *J. Bacteriol. 201*, e00387-00319, doi: *10.1128/JB.00387-19.*

Kurthkoti, K., Tare, P., Paitchowdhury, R., Gowthami, V. N., Garcia, M. J., Colangeli, R., Chatterji, D., Nagaraja, V. and Rodriguez, G. M. (2015). The mycobacterial iron-dependent regulator IdeR induces ferritin (*bfrB*) by alleviating Lsr2 repression. *Mol. Microbiol. 98*, 864-877, doi: *10.1111/mmi.13166.*

Lamberte, L. E., Baniulyte, G., Singh, S. S., Stringer, A. M., Bonocora, R. P., Stracy, M., Kapanidis, A. N., Wade, J. T. and Grainger, D. C. (2017). Horizontally acquired AT-rich genes in *Escherichia coli* cause toxicity by sequestering RNA polymerase. *Nat. Microbiol. 2*, 16249, doi: *10.1038/nmicrobiol.2016.249.*

Landick, R., Wade, J. T. and Grainger, D. C. (2015). H-NS and RNA polymerase: a love-hate relationship? *Curr. Opin. Microbiol. 24*, 53-59, doi: *10.1016/j.mib.2015.01.009.*

Lang, B., Blot, N., Bouffartigues, E., Buckle, M., Geertz, M., Gualerzi, C. O., Mavathur, R., Muskhelishvili, G., Pon, C. L., Rimsky, S., Stella, S., Babu, M. M. and Travers, A. (2007). High-affinity DNA binding sites for H-NS provide a molecular basis for selective silencing within proteobacterial genomes. *Nucleic Acids Res. 35*, 6330-6337, doi: *10.1093/nar/gkm712.*

Lausberg, F., Chattopadhyay, A. R., Heyer, A., Eggeling, L. and Freudl, R. (2012). A tetracycline inducible expression vector for *Corynebacterium glutamicum* allowing tightly regulable gene expression. *Plasmid. 68*, 142-147, doi: *10.1016/j.plasmid.2012.05.001.*

Lee, J. W., Na, D., Park, J. M., Lee, J., Choi, S. and Lee, S. Y. (2012). Systems metabolic engineering of microorganisms for natural and non-natural chemicals. *Nat. Chem. Biol. 8*, 536-546, doi: *10.1038/nchembio.970.*

Letek, M., Valbuena, N., Ramos, A., Ordonez, E., Gil, J. A. and Mateos, L. M. (2006). Characterization and use of catabolite-repressed promoters from gluconate genes in *Corynebacterium glutamicum*. *J. Bacteriol. 188*, 409-423, doi: *10.1128/jb.188.2.409-423.2006.*

Levine, J. A., Hansen, A. M., Michalski, J. M., Hazen, T. H., Rasko, D. A. and Kaper, J. B. (2014). H-NST induces LEE expression and the formation of attaching and effacing lesions in enterohemorrhagic *Escherichia coli*. *PLoS One. 9*, e86618, doi: *10.1371/journal.pone.0086618.*

Lim, C. J., Lee, S. Y., Kenney, L. J. and Yan, J. (2012). Nucleoprotein filament formation is the structural basis for bacterial protein H-NS gene silencing. *Sci. Rep. 2*, 509, doi: *10.1038/srep00509.*

Lithgow, J. K., Haider, F., Roberts, I. S. and Green, J. (2007). Alternate SlyA and H-NS nucleoprotein complexes control *hlyE* expression in *Escherichia coli* K-12. *Mol. Microbiol. 66*, 685-698, doi: *10.1111/j.1365-2958.2007.05950.x.*

Litsanov, B., Kabus, A., Brocker, M. and Bott, M. (2012). Efficient aerobic succinate production from glucose in minimal medium with *Corynebacterium glutamicum*. *Microb. Biotechnol. 5*, 116-128, doi: *10.1111/j.1751-7915.2011.00310.x.*

Liu, J. and Gordon, B. R. G. (2012). Targeting the global regulator Lsr2 as a novel approach for anti-tuberculosis drug development. *Expert Rev. Anti-Infect. Ther. 10*, 1049-1053, doi: *10.1586/eri.12.86.*

Liu, X., Yang, Y., Zhang, W., Sun, Y., Peng, F., Jeffrey, L., Harvey, L., McNeil, B. and Bai, Z. (2016). Expression of recombinant protein using *Corynebacterium glutamicum*: progress, challenges and applications. *Crit. Rev. Biotechnol. 36*, 652-664, doi: *10.3109/07388551.2015.1004519.*

Liu, Y., Chen, H., Kenney, L. J. and Yan, J. (2010). A divalent switch drives H-NS/DNA-binding conformations between stiffening and bridging modes. *Genes Dev. 24*, 339-344, doi: *10.1101/gad.1883510.*

Lo, T. M., Chng, S. H., Teo, W. S., Cho, H. S. and Chang, M. W. (2016). A two-layer gene circuit for decoupling cell growth from metabolite production. *Cell Syst. 3*, 133-143, doi: *10.1016/j.cels.2016.07.012.*

Lucchini, S., Rowley, G., Goldberg, M. D., Hurd, D., Harrison, M. and Hinton, J. C. (2006). H-NS mediates the silencing of laterally acquired genes in bacteria. *PLoS Pathog. 2*, e81, doi: *10.1371/journal.ppat.0020081.*

Luria, S. E. and Human, M. L. (1952). A nonhereditary, host-induced variation of bacterial viruses. *J. Bacteriol. 64*, 557-569,

Ma, Y., Cui, Y., Du, L., Liu, X., Xie, X. and Chen, N. (2018). Identification and application of a growth-regulated promoter for improving L-valine production in *Corynebacterium glutamicum*. *Microb. Cell Fact. 17*, 185, doi: *10.1186/s12934-018-1031-7.*

Makarova, K. S., Wolf, Y. I., Snir, S. and Koonin, E. V. (2011). Defense islands in bacterial and archaeal genomes and prediction of novel defense systems. *J. Bacteriol. 193*, 6039-6056, doi: *10.1128/JB.05535-11.*

Mann, S. and Chen, Y.-P. P. (2010). Bacterial genomic G+C composition-eliciting environmental adaptation. *Genomics. 95*, 7-15, doi: *10.1016/j.ygeno.2009.09.002.*

McNutt, M. K., Bradford, M., Drazen, J. M., Hanson, B., Howard, B., Jamieson, K. H., Kiermer, V., Marcus, E., Pope, B. K., Schekman, R., Swaminathan, S., Stang, P. J. and Verma, I. M. (2018). Transparency in authors' contributions and responsibilities to promote integrity in scientific publication. *Proc. Natl. Acad. Sci. U S A. 115*, 2557-2560, doi: *10.1073/pnas.1715374115.*

Melechen, N. E. and Go, G. (1980). Induction of lambdoid prophages by amino acid deprivation: differential inducibility; role of *recA*. *Mol. Gen. Genet. 180*, 147-155, doi: *10.1007/bf00267364.*

Miller, S. I., Kukral, A. M. and Mekalanos, J. J. (1989). A two-component regulatory system (*phoP phoQ*) controls *Salmonella typhimurium* virulence. *Proc. Natl. Acad. Sci. U S A. 86*, 5054-5058, doi: *10.1073/pnas.86.13.5054*

Monterroso, B., Zorrilla, S., Sobrinos-Sanguino, M., Robles-Ramos, M. A., Lopez-Alvarez, M., Margolin, W., Keating, C. D. and Rivas, G. (2019). Bacterial FtsZ protein forms phase-separated condensates with its nucleoid-associated inhibitor SlmA. *EMBO Rep. 20*, doi: *10.15252/embr.201845946.*

Moran, N. A., McLaughlin, H. J. and Sorek, R. (2009). The dynamics and time scale of ongoing genomic erosion in symbiotic bacteria. *Science. 323*, 379-382, doi: *10.1126/science.1167140.*

Müller, C. M., Dobrindt, U., Nagy, G., Emödy, L., Uhlin, B. E. and Hacker, J. (2006). Role of histone-like proteins H-NS and StpA in expression of virulence determinants of uropathogenic *Escherichia coli*. *J. Bacteriol. 188*, 5428-5438, doi: *10.1128/JB.01956-05.*

Mustafi, N., Grünberger, A., Kohlheyer, D., Bott, M. and Frunzke, J. (2012). The development and application of a single-cell biosensor for the detection of L-methionine and branched-chain amino acids. *Metab. Eng. 14*, 449-457, doi: *10.1016/j.ymben.2012.02.002.*

Nagarajavel, V., Madhusudan, S., Dole, S., Rahmouni, A. R. and Schnetz, K. (2007). Repression by binding of H-NS within the transcription unit. *J. Biol. Chem. 282*, 23622-23630, doi: *10.1074/jbc.M702753200.*

Nakabachi, A., Yamashita, A., Toh, H., Ishikawa, H., Dunbar, H. E., Moran, N. A. and Hattori, M. (2006). The 160-kilobase genome of the bacterial endosymbiont *Carsonella*. *Science. 314*, 267, doi: *10.1126/science.1134196.*

Navarre, W. W. (2016). The impact of gene silencing on horizontal gene transfer and bacterial evolution. *Adv. Microb. Physiol. 69*, 157-186, doi: *10.1016/bs.ampbs.2016.07.004.*

Navarre, W. W., Halsey, T. A., Walthers, D., Frye, J., McClelland, M., Potter, J. L., Kenney, L. J., Gunn, J. S., Fang, F. C. and Libby, S. J. (2005). Co-regulation of *Salmonella enterica* genes required for virulence and resistance to antimicrobial peptides by SlyA and PhoP/PhoQ. *Mol. Microbiol. 56*, 492-508, doi: *10.1111/j.1365-2958.2005.04553.x.*

Navarre, W. W., McClelland, M., Libby, S. J. and Fang, F. C. (2007). Silencing of xenogeneic DNA by H-NS-facilitation of lateral gene transfer in bacteria by a defense system that recognizes foreign DNA. *Genes Dev. 21*, 1456-1471, doi: *10.1101/gad.1543107.*

Navarre, W. W., Porwollik, S., Wang, Y., McClelland, M., Rosen, H., Libby, S. J. and Fang, F. C. (2006). Selective silencing of foreign DNA with low GC content by the H-NS protein in *Salmonella*. *Science. 313*, 236-238, doi: *10.1126/science.1128794.*

Nelson, K. E., Clayton, R. A., Gill, S. R., Gwinn, M. L., Dodson, R. J., Haft, D. H., Hickey, E. K., Peterson, J. D., Nelson, W. C., Ketchum, K. A., McDonald, L., Utterback, T. R., Malek, J. A., Linher, K. D., Garrett, M. M., Stewart, A. M., Cotton, M. D., Pratt, M. S., Phillips, C. A., Richardson, D., Heidelberg, J., Sutton, G. G., Fleischmann, R. D., Eisen, J. A., White, O., Salzberg, S. L., Smith, H. O., Venter, J. C. and Fraser, C. M. (1999). Evidence for lateral gene transfer between Archaea and bacteria from genome sequence of *Thermotoga maritima*. *Nature. 399*, 323-329, doi: *10.1038/20601.*

Noom, M. C., Navarre, W. W., Oshima, T., Wuite, G. J. and Dame, R. T. (2007). H-NS promotes looped domain formation in the bacterial chromosome. *Curr. Biol. 17*, R913-914, doi: *10.1016/j.cub.2007.09.005.*

Normand, P., Lapierre, P., Tisa, L. S., Gogarten, J. P., Alloisio, N., Bagnarol, E., Bassi, C. A., Berry, A. M., Bickhart, D. M., Choisne, N., Couloux, A., Cournoyer, B., Cruveiller, S., Daubin, V., Demange, N., Francino, M. P., Goltsman, E., Huang, Y., Kopp, O. R., Labarre, L., Lapidus, A., Lavire, C., Marechal, J., Martinez, M., Mastronunzio, J. E., Mullin, B. C., Niemann, J., Pujic, P., Rawnsley, T., Rouy, Z., Schenowitz, C., Sellstedt, A., Tavares, F., Tomkins, J. P., Vallenet, D., Valverde, C., Wall, L. G., Wang, Y., Medigue, C. and Benson, D. R. (2007). Genome characteristics of facultatively symbiotic *Frankia* sp. strains reflect host range and host plant biogeography. *Genome Res. 17*, 7-15, doi: *10.1101/gr.5798407.*

Ochman, H., Lawrence, J. G. and Groisman, E. A. (2000). Lateral gene transfer and the nature of bacterial innovation. *Nature. 405*, 299-304, doi: *10.1038/35012500.*

Ofir, G., Melamed, S., Sberro, H., Mukamel, Z., Silverman, S., Yaakov, G., Doron, S. and Sorek, R. (2018). DISARM is a widespread bacterial defence system with broad anti-phage activities. *Nat. Microbiol. 3*, 90-98, doi: *10.1038/s41564-017-0051-0.*

Okibe, N., Suzuki, N., Inui, M. and Yukawa, H. (2010). Isolation, evaluation and use of two strong, carbon source-inducible promoters from *Corynebacterium glutamicum*. *Lett. Appl. Microbiol. 50*, 173-180, doi: *10.1111/j.1472-765X.2009.02776.x.*

Olekhnovich, I. N. and Kadner, R. J. (2007). Role of nucleoid-associated proteins Hha and H-NS in expression of *Salmonella enterica* activators HilD, HilC, and RtsA required for cell invasion. *J. Bacteriol. 189*, 6882-6890, doi: *10.1128/JB.00905-07*

Oliveira, P. H., Touchon, M. and Rocha, E. P. C. (2014). The interplay of restriction-modification systems with mobile genetic elements and their prokaryotic hosts. *Nucleic Acids Res. 42*, 10618-10631, doi: *10.1093/nar/gku734.*

Oshima, T., Ishikawa, S., Kurokawa, K., Aiba, H. and Ogasawara, N. (2006). *Escherichia coli* histone-like protein H-NS preferentially binds to horizontally acquired DNA in association with RNA polymerase. *DNA Res. 13*, 141-153, doi: *10.1093/dnares/dsl009.*

Ouafa, Z.-A., Reverchon, S., Lautier, T., Muskhelishvili, G. and Nasser, W. (2012). The nucleoid-associated proteins H-NS and FIS modulate the DNA supercoiling response of the *pel* genes, the major virulence factors in the plant pathogen bacterium *Dickeya dadantii*. *Nucleic Acids Res. 40*, 4306-4319, doi: *10.1093/nar/gks014.*

Park, C. and Zhang, J. (2012). High expression hampers horizontal gene transfer. *Genome Biol. Evol. 4*, 523-532, doi: *10.1093/gbe/evs030.*

Parma, D. H., Snyder, M., Sobolevski, S., Nawroz, M., Brody, E. and Gold, L. (1992). The Rex system of bacteriophage lambda: tolerance and altruistic cell death. *Genes Dev. 6*, 497-510, doi: *10.1101/gad.6.3.497.*

Patek, M., Holatko, J., Busche, T., Kalinowski, J. and Nesvera, J. (2013). *Corynebacterium glutamicum* promoters: a practical approach. *Microb. Biotechnol. 6*, 103-117, doi: *10.1111/1751-7915.12019.*

Perera, I. C. and Grove, A. (2010). Molecular mechanisms of ligand-mediated attenuation of DNA binding by MarR family transcriptional regulators. *J. Mol. Cell. Biol. 2*, 243-254, doi: *10.1093/jmcb/mjq021.*

Perez-Rueda, E. and Ibarra, J. A. (2015). Distribution of putative xenogeneic silencers in prokaryote genomes. *Comput. Biol. Chem. 58*, 167-172, doi: *10.1016/j.compbiolchem.2015.06.007.*

Perez, J. C., Latifi, T. and Groisman, E. A. (2008). Overcoming H-NS-mediated transcriptional silencing of horizontally acquired genes by the PhoP and SlyA proteins in *Salmonella enterica*. *J. Biol. Chem. 283*, 10773-10783, doi: *10.1074/jbc.M709843200.*

Peters-Wendisch, P. G., Kreutzer, C., Kalinowski, J., Pátek, M., Sahm, H. and Eikmanns, B. J. (1998). Pyruvate carboxylase from *Corynebacterium glutamicum*: characterization, expression and inactivation of the *pyc* gene. *Microbiology. 144*, 915-927, doi: *10.1099/00221287-144-4-915.*

Pfeifer, E., Hünnefeld, M., Popa, O. and Frunzke, J. (2019). Impact of xenogeneic silencing on phage-host interactions. *J. Mol. Biol. 431*, 4670-4683, doi: *10.1016/j.jmb.2019.02.011.*

Pfeifer, E., Hünnefeld, M., Popa, O., Polen, T., Kohlheyer, D., Baumgart, M. and Frunzke, J. (2016). Silencing of cryptic prophages in *Corynebacterium glutamicum*. *Nucleic Acids Res. 44*, 10117-10131, doi: *10.1093/nar/gkw692.*

Pingoud, A., Fuxreiter, M., Pingoud, V. and Wende, W. (2005). Type II restriction endonucleases: structure and mechanism. *Cell Mol. Life. Sci. 62*, 685-707, doi: *10.1007/s00018-004-4513-1.*

Plassmeier, J. K., Busche, T., Molck, S., Persicke, M., Puhler, A., Ruckert, C. and Kalinowski, J. (2013). A propionate-inducible expression system based on the *Corynebacterium glutamicum prpD2* promoter and PrpR activator and its application for the redirection of amino acid biosynthesis pathways. *J. Biotechnol. 163*, 225-232, doi: *10.1016/j.jbiotec.2012.08.009.*

Porter, M. E. and Dorman, C. J. (1994). A role for H-NS in the thermo-osmotic regulation of virulence gene expression in *Shigella flexneri*. *J. Bacteriol. 176*, 4187-4191, doi: *10.1128/jb.176.13.4187-4191.1994.*

Prather, K. L. and Martin, C. H. (2008). De novo biosynthetic pathways: rational design of microbial chemical factories. *Curr. Opin. Biotechnol. 19*, 468-474, doi: *10.1016/j.copbio.2008.07.009.*

Qin, L., Erkelens, A. M., Ben Bdira, F. and Dame, R. T. (2019a). The architects of bacterial DNA bridges: a structurally and functionally conserved family of proteins. *Open Biol. 9*, 190223, doi: *10.1098/rsob.190223.*

Qin, L., Erkelens, A. M., Markus, D. and Dame, R. T. (2019b). The *B. subtilis* Rok protein compacts and organizes DNA by bridging. *bioRxiv.* 769117, doi: *10.1101/769117.*

Qu, Y., Lim, C. J., Whang, Y. R., Liu, J. and Yan, J. (2013). Mechanism of DNA organization by *Mycobacterium tuberculosis* protein Lsr2. *Nucleic Acids Res. 41*, 5263-5272, doi: *10.1093/nar/gkt249.*

Radmacher, E., Vaitsikova, A., Burger, U., Krumbach, K., Sahm, H. and Eggeling, L. (2002). Linking central metabolism with increased pathway flux: L-valine accumulation by *Corynebacterium glutamicum*. *Appl. Environ. Microbiol. 68*, 2246-2250, doi: *10.1128/aem.68.5.2246-2250.2002.*

Ramisetty, B. C. M. and Sudhakari, P. A. (2019). Bacterial 'grounded' prophages: hotspots for genetic renovation and innovation. *Front. Genet. 10*, 65-65, doi: *10.3389/fgene.2019.00065.*

Rangarajan, A. A. and Schnetz, K. (2018). Interference of transcription across H-NS binding sites and repression by H-NS. *Mol. Microbiol. 108*, 226-239, doi: *10.1111/mmi.13926.*

Raz, Y. and Tannenbaum, E. (2010). The influence of horizontal gene transfer on the mean fitness of unicellular populations in static environments. *Genetics. 185*, 327-337, doi: *10.1534/genetics.109.113613.*

Roberts, R. J., Belfort, M., Bestor, T., Bhagwat, A. S., Bickle, T. A., Bitinaite, J., Blumenthal, R. M., Degtyarev, S. K., Dryden, D. T. F., Dybvig, K., Firman, K., Gromova, E. S., Gumport, R. I., Halford, S. E., Hattman, S., Heitman, J., Hornby, D. P., Janulaitis, A., Jeltsch, A., Josephsen, J., Kiss, A., Klaenhammer, T. R., Kobayashi, I., Kong, H., Krüger, D. H., Lacks, S., Marinus, M. G., Miyahara, M., Morgan, R. D., Murray, N. E., Nagaraja, V., Piekarowicz, A., Pingoud, A., Raleigh, E., Rao, D. N., Reich, N., Repin, V. E., Selker, E. U., Shaw, P.-C., Stein, D. C., Stoddard, B. L., Szybalski, W., Trautner, T. A., Van Etten, J. L., Vitor, J. M. B., Wilson, G. G. and Xu, S.-y. (2003). A nomenclature for restriction enzymes, DNA methyltransferases, homing endonucleases and their genes. *Nucleic Acids Res. 31*, 1805-1812, doi: *10.1093/nar/gkg274.*

Roberts, R. J., Vincze, T., Posfai, J. and Macelis, D. (2010). REBASE-a database for DNA restriction and modification: enzymes, genes and genomes. *Nucleic Acids Res. 38*, D234-D236, doi: *10.1093/nar/gkp874.*

Rocha, E. P. C. and Danchin, A. (2002). Base composition bias might result from competition for metabolic resources. *Trends Genet. 18*, 291-294, doi: *10.1016/S0168-9525(02)02690-2.*

Rojo, F. (1999). Repression of transcription initiation in bacteria. *J. Bacteriol. 181*, 2987-2991,

Rosenthal, R. S. and Rodwell, V. W. (1998). Purification and characterization of the heteromeric transcriptional activator MvaT of the *Pseudomonas mevalonii mvaAB* operon. *Protein Sci. 7*, 178-184, doi: *10.1002/pro.5560070118.*

Rydenfelt, M., Garcia, H. G., Cox, R. S., 3rd and Phillips, R. (2014). The influence of promoter architectures and regulatory motifs on gene expression in *Escherichia coli*. *PLoS One. 9*, e114347-e114347, doi: *10.1371/journal.pone.0114347.*

Rytter, J. V., Helmark, S., Chen, J., Lezyk, M. J., Solem, C. and Jensen, P. R. (2014). Synthetic promoter libraries for *Corynebacterium glutamicum*. *Appl. Microbiol. Biotechnol. 98*, 2617-2623, doi: *10.1007/s00253-013-5481-x.*

Sankar, T. S., Neelakanta, G., Sangal, V., Plum, G., Achtman, M. and Schnetz, K. (2009). Fate of the H-NS-repressed *bgl* operon in evolution of *Escherichia coli*. *PLoS Genet. 5*, e1000405-e1000405, doi: *10.1371/journal.pgen.1000405.*

Sauer, U. and Eikmanns, B. J. (2005). The PEP-pyruvate-oxaloacetate node as the switch point for carbon flux distribution in bacteria. *FEMS Microbiol. Rev. 29*, 765-794, doi: *10.1016/j.femsre.2004.11.002.*

Schreiner, M. E., Fiur, D., Holátko, J., Pátek, M. and Eikmanns, B. J. (2005). E1 enzyme of the pyruvate dehydrogenase complex in *Corynebacterium glutamicum*: molecular analysis of the gene and phylogenetic aspects. *J. Bacteriol. 187*, 6005-6018, doi: *10.1128/JB.187.17.6005-6018.2005.*

Seid, C. A., Smith, J. L. and Grossman, A. D. (2017). Genetic and biochemical interactions between the bacterial replication initiator DnaA and the nucleoid-associated protein Rok in *Bacillus subtilis*. *Mol. Microbiol. 103*, 798-817, doi: *10.1111/mmi.13590.*

Seshasayee, A. S., Sivaraman, K. and Luscombe, N. M. (2011). An overview of prokaryotic transcription factors : a summary of function and occurrence in bacterial genomes. *Subcell. Biochem. 52*, 7-23, doi: *10.1007/978-90-481-9069-0_2.*

Sette, M., Spurio, R., Trotta, E., Brandizi, C., Brandi, A., Pon, C. L., Barbato, G., Boelens, R. and Gualerzi, C. O. (2009). Sequence-specific recognition of DNA by the C-terminal domain of nucleoid-associated protein H-NS. *J. Biol. Chem. 284*, 30453-30462, doi: *10.1074/jbc.M109.044313.*

Shang, X., Chai, X., Lu, X., Li, Y., Zhang, Y., Wang, G., Zhang, C., Liu, S., Zhang, Y., Ma, J. and Wen, T. (2018). Native promoters of *Corynebacterium glutamicum* and its application in L-lysine production. *Biotechnol. Lett. 40*, 383-391, doi: *10.1007/s10529-017-2479-y.*

Shang, Y., Song, X., Bowen, J., Corstanje, R., Gao, Y., Gaertig, J. and Gorovsky, M. A. (2002). A robust inducible-repressible promoter greatly facilitates gene knockouts, conditional expression, and overexpression of homologous and heterologous genes in *Tetrahymena thermophila*. *Proc. Natl. Acad. Sci. U S A. 99*, 3734-3739, doi: *10.1073/pnas.052016199.*

Shimada, T., Bridier, A., Briandet, R. and Ishihama, A. (2011). Novel roles of LeuO in transcription regulation of *E. coli* genome: antagonistic interplay with the universal silencer H-NS. *Mol. Microbiol. 82*, 378-397, doi: *10.1111/j.1365-2958.2011.07818.x.*

Shin, M., Song, M., Rhee, J. H., Hong, Y., Kim, Y.-J., Seok, Y.-J., Ha, K.-S., Jung, S.-H. and Choy, H. E. (2005). DNA looping-mediated repression by histone-like protein H-NS: specific requirement of Esigma70 as a cofactor for looping. *Genes Dev. 19*, 2388-2398, doi: *10.1101/gad.1316305.*

Singh, K., Milstein, J. N. and Navarre, W. W. (2016). Xenogeneic silencing and its impact on bacterial genomes. *Annu. Rev. Microbiol. 70*, 199-213, doi: *10.1146/annurev-micro-102215-095301.*

Singh, S. S., Singh, N., Bonocora, R. P., Fitzgerald, D. M., Wade, J. T. and Grainger, D. C. (2014). Widespread suppression of intragenic transcription initiation by H-NS. *Genes Dev. 28*, 214-219, doi: *10.1101/gad.234336.113.*

Smits, W. K. and Grossman, A. D. (2010). The transcriptional regulator Rok binds A+T-rich DNA and is involved in repression of a mobile genetic element in *Bacillus subtilis*. *PLoS Genet. 6*, e1001207, doi: *10.1371/journal.pgen.1001207.*

Smyth, C. P., Lundbäck, T., Renzoni, D., Siligardi, G., Beavil, R., Layton, M., Sidebotham, J. M., Hinton, J. C. D., Driscoll, P. C., Higgins, C. F. and Ladbury, J. E. (2000). Oligomerization of the chromatin-structuring protein H-NS. *Mol. Microbiol. 36*, 962-972, doi: *10.1046/j.1365-2958.2000.01917.x.*

Soma, Y., Tsuruno, K., Wada, M., Yokota, A. and Hanai, T. (2014). Metabolic flux redirection from a central metabolic pathway toward a synthetic pathway using a metabolic toggle switch. *Metab. Eng. 23*, 175-184, doi: *10.1016/j.ymben.2014.02.008.*

Soma, Y., Yamaji, T., Matsuda, F. and Hanai, T. (2017). Synthetic metabolic bypass for a metabolic toggle switch enhances acetyl-CoA supply for isopropanol production by *Escherichia coli*. *J. Biosci. Bioeng. 123*, 625-633, doi: *10.1016/j.jbiosc.2016.12.009.*

Sorek, R., Zhu, Y., Creevey, C. J., Francino, M. P., Bork, P. and Rubin, E. M. (2007). Genome-wide experimental determination of barriers to horizontal gene transfer. *Science. 318*, 1449-1452, doi: *10.1126/science.1147112.*

Spurio, R., Falconi, M., Brandi, A., Pon, C. L. and Gualerzi, C. O. (1997). The oligomeric structure of nucleoid protein H-NS is necessary for recognition of intrinsically curved DNA and for DNA bending. *EMBO J. 16*, 1795-1805, doi: *10.1093/emboj/16.7.1795.*

Stoebel, D., Free, A. and Dorman, C. (2008). Anti-silencing: Overcoming H-NS-mediated repression of transcription in Gram-negative enteric bacteria. *Microbiology. 154*, 2533-2545, doi: *10.1099/mic.0.2008/020693-0.*

Stojkova, P., Spidlova, P. and Stulik, J. (2019). Nucleoid-associated protein HU: a lilliputian in gene regulation of bacterial virulence. *Front. Cell. Infect. Microbiol. 9*, doi: *10.3389/fcimb.2019.00159.*

Sun, D. (2018). Pull in and push out: mechanisms of horizontal gene transfer in bacteria. *Front. Microbiol. 9*, 2154-2154, doi: *10.3389/fmicb.2018.02154.*

Suzuki-Minakuchi, C. and Navarre, W., 2019. Xenogeneic silencing and horizontal gene transfer. In: Nishida, H., Oshima, T., DNA Traffic in the Environment. Springer, Singapore, pp. 1-27.

Tendeng, C., Soutourina, O. A., Danchin, A. and Bertin, P. N. (2003). MvaT proteins in *Pseudomonas spp.*: a novel class of H-NS-like proteins. *Microbiology. 149*, 3047-3050, doi: *10.1099/mic.0.C0125-0.*

Thiaville, J. J., Kellner, S. M., Yuan, Y., Hutinet, G., Thiaville, P. C., Jumpathong, W., Mohapatra, S., Brochier-Armanet, C., Letarov, A. V., Hillebrand, R., Malik, C. K., Rizzo, C. J., Dedon, P. C. and de Crécy-Lagard, V. (2016). Novel genomic island modifies DNA with 7-deazaguanine derivatives. *Proc. Natl. Acad. Sci. U S A. 113*, E1452-E1459, doi: *10.1073/pnas.1518570113.*

Touchon, M., Moura de Sousa, J. A. and Rocha, E. P. (2017). Embracing the enemy: the diversification of microbial gene repertoires by phage-mediated horizontal gene transfer. *Curr. Opin. Microbiol. 38*, 66-73, doi: *10.1016/j.mib.2017.04.010.*

Tramonti, A., De Canio, M., Delany, I., Scarlato, V. and De Biase, D. (2006). Mechanisms of transcription activation exerted by GadX and GadW at the *gadA* and *gadBC* gene promoters of the glutamate-based acid resistance system in *Escherichia coli*. *J. Bacteriol. 188*, 8118-8127, doi: *10.1128/JB.01044-06*

Tsuruno, K., Honjo, H. and Hanai, T. (2015). Enhancement of 3-hydroxypropionic acid production from glycerol by using a metabolic toggle switch. *Microb. Cell Fact. 14*, 155, doi: *10.1186/s12934-015-0342-1.*

Turner, E. C. and Dorman, C. J. (2007). H-NS antagonism in *Shigella flexneri* by VirB, a virulence gene transcription regulator that is closely related to plasmid partition factors. *J. Bacteriol. 189*, 3403-3413, doi: *10.1128/JB.01813-06*

Ueguchi, C., Kakeda, M. and Mizuno, T. (1993). Autoregulatory expression of the *Escherichia coli hns* gene encoding a nucleoid protein: H-NS functions as a repressor of its own transcription. *Mol. Gen. Genet. 236*, 171-178, doi: *10.1007/bf00277109.*

Ueguchi, C., Suzuki, T., Yoshida, T., Tanaka, K.-i. and Mizuno, T. (1996). Systematic mutational analysis revealing the functional domain organization of *Escherichia coli* nucleoid protein H-NS. *J. Mol. Biol. 263*, 149-162, doi: *10.1006/jmbi.1996.0566.*

van Houte, S., Buckling, A. and Westra, E. R. (2016). Evolutionary ecology of prokaryotic immune mechanisms. *Microbiol. Mol. Biol. Rev. 80*, 745-763, doi: *10.1128/mmbr.00011-16.*

van Noort, J., Verbrugge, S., Goosen, N., Dekker, C. and Dame, R. T. (2004). Dual architectural roles of HU: Formation of flexible hinges and rigid filaments. *Proc. Natl. Acad. Sci. U S A. 101*, 6969-6974, doi: *10.1073/pnas.0308230101.*

Vasu, K. and Nagaraja, V. (2013). Diverse functions of restriction-modification systems in addition to cellular defense. *Microbiol. Mol. Biol. Rev. 77*, 53-72, doi: *10.1128/MMBR.00044-12.*

Verma, S. C., Qian, Z. and Adhya, S. L. (2019). Architecture of the *Escherichia coli* nucleoid. *PLoS Genet. 15*, e1008456, doi: *10.1371/journal.pgen.1008456.*

Villa, T. G., Feijoo-Siota, L., Sánchez-Pérez, A., Rama, J. R. and Sieiro, C., 2019. Horizontal gene transfer in bacteria, an overview of the mechanisms involved. In: Villa, T. G., Viñas, M., Horizontal Gene Transfer: Breaking Borders Between Living Kingdoms. Springer International Publishing, Cham, pp. 3-76.

Vivero, A., Baños, R. C., Mariscotti, J. F., Oliveros, J. C., García-del Portillo, F., Juárez, A. and Madrid, C. (2008). Modulation of horizontally acquired genes by the Hha-YdgT proteins in *Salmonella enterica* Serovar Typhimurium. *J. Bacteriol. 190*, 1152-1156, doi: *10.1128/JB.01206-07*

Vogan, A. A. and Higgs, P. G. (2011). The advantages and disadvantages of horizontal gene transfer and the emergence of the first species. *Biol. Direct. 6*, 1, doi: *10.1186/1745-6150-6-1.*

von Hippel, P. H. and Berg, O. G. (1986). On the specificity of DNA-protein interactions. *Proc. Natl. Acad. Sci. U S A. 83*, 1608-1612, doi: *10.1073/pnas.83.6.1608.*

Walsh, C. (2000). Molecular mechanisms that confer antibacterial drug resistance. *Nature. 406*, 775-781, doi: *10.1038/35021219.*

Walthers, D., Carroll, R. K., Navarre, W. W., Libby, S. J., Fang, F. C. and Kenney, L. J. (2007). The response regulator SsrB activates expression of diverse *Salmonella* pathogenicity island 2 promoters and counters silencing by the nucleoid-associated protein H-NS. *Mol. Microbiol. 65*, 477-493, doi: *10.1111/j.1365-2958.2007.05800.x.*

Wan, B., Zhang, Q., Tao, J., Zhou, A., Yao, Y.-F. and Ni, J. (2016). Global transcriptional regulation by H-NS and its biological influence on the virulence of Enterohemorrhagic *Escherichia coli*. *Gene. 588*, 115-123, doi: *10.1016/j.gene.2016.05.007.*

Wang, D., Kreutzer, D. A. and Essigmann, J. M. (1998). Mutagenicity and repair of oxidative DNA damage: insights from studies using defined lesions. *Mutat. Res. 400*, 99-115, doi: *10.1016/s0027-5107(98)00066-9.*

Wang, L., Chen, S., Xu, T., Taghizadeh, K., Wishnok, J. S., Zhou, X., You, D., Deng, Z. and Dedon, P. C. (2007). Phosphorothioation of DNA in bacteria by *dnd* genes. *Nat. Chem. Biol. 3*, 709-710, doi: *10.1038/nchembio.2007.39.*

Wang, N. and Liu, C. (2019). Implications of liquid-liquid phase separation in plant chromatin organization and transcriptional control. *Curr. Opin. Genet. Dev. 55*, 59-65, doi: *10.1016/j.gde.2019.06.003.*

Wang, W., Li, G.-W., Chen, C., Xie, X. S. and Zhuang, X. (2011). Chromosome organization by a nucleoid-associated protein in live bacteria. *Science. 333*, 1445-1449, doi: *10.1126/science.1204697.*

Wang, X., Kim, Y., Ma, Q., Hong, S. H., Pokusaeva, K., Sturino, J. M. and Wood, T. K. (2010). Cryptic prophages help bacteria cope with adverse environments. *Nat. Commun. 1*, 147-147, doi: *10.1038/ncomms1146.*

Wendisch, V. F., de Graaf, A. A., Sahm, H. and Eikmanns, B. J. (2000). Quantitative determination of metabolic fluxes during coutilization of two carbon sources: comparative analyses with *Corynebacterium glutamicum* during growth on acetate and/or glucose. *J. Bacteriol. 182*, 3088-3096, doi: *10.1128/JB.182.11.3088-3096.2000.*

Wendisch, V. F., Spies, M., Reinscheid, D. J., Schnicke, S., Sahm, H. and Eikmanns, B. J. (1997). Regulation of acetate metabolism in *Corynebacterium glutamicum*: transcriptional control of the isocitrate lyase and malate synthase genes. *Arch. Microbiol. 168*, 262-269, doi: *10.1007/s002030050497.*

White, F. F., Garfinkel, D. J., Huffman, G. A., Gordon, M. P. and Nester, E. W. (1983). Sequences homologous to *Agrobacterium rhizogenes* T-DNA in the genomes of uninfected plants. *Nature. 301*, 348-350, doi: *10.1038/301348a0.*

Wiechert, J., Filipchyk, A., Hünnefeld, M., Gätgens, C., Brehm, J., Heermann, R. and Frunzke, J. (2020a). Deciphering the rules underlying xenogeneic silencing and counter-silencing of Lsr2-like proteins using CgpS of *Corynebacterium glutamicum* as a model. *mBio. 11*, e02273-02219, doi: *10.1128/mBio.02273-19*

Wiechert, J., Gätgens, C., Wirtz, A. and Frunzke, J. (2020b). Inducible expression systems based on xenogeneic silencing and counter-silencing and the design of a metabolic toggle switch. *Inside this Thesis. Submitted.*

Will, W. R., Bale, D. H., Reid, P. J., Libby, S. J. and Fang, F. C. (2014). Evolutionary expansion of a regulatory network by counter-silencing. *Nat. Commun. 5*, 5270, doi: *10.1038/ncomms6270.*

Will, W. R., Brzovic, P., Le Trong, I., Stenkamp, R. E., Lawrenz, M. B., Karlinsey, J. E., Navarre, W. W., Main-Hester, K., Miller, V. L., Libby, S. J. and Fang, F. C. (2019). The evolution of SlyA/RovA transcription factors from repressors to countersilencers in *Enterobacteriaceae*. *mBio. 10*, e00009-00019, doi: *10.1128/mBio.00009-19.*

Will, W. R. and Fang, F. C. (2020). The evolution of MarR family transcription factors as counter-silencers in regulatory networks. *Curr. Opin. Microbiol. 55*, 1-8, doi: *10.1016/j.mib.2020.01.002.*

Will, W. R., Navarre, W. W. and Fang, F. C. (2015). Integrated circuits: how transcriptional silencing and counter-silencing facilitate bacterial evolution. *Curr. Opin. Microbiol. 23*, 8-13, doi: *10.1016/j.mib.2014.10.005.*

Will, W. R., Whitham, P. J., Reid, P. J. and Fang, F. C. (2018). Modulation of H-NS transcriptional silencing by magnesium. *Nucleic Acids Res. 46*, 5717-5725, doi: *10.1093/nar/gky387.*

Williamson, H. S. and Free, A. (2005). A truncated H-NS-like protein from enteropathogenic *Escherichia coli* acts as an H-NS antagonist. *Mol. Microbiol. 55*, 808-827, doi: *10.1111/j.1365-2958.2004.04421.x.*

Winardhi, R. S., Fu, W., Castang, S., Li, Y., Dove, S. L. and Yan, J. (2012). Higher order oligomerization is required for H-NS family member MvaT to form gene-silencing nucleoprotein filament. *Nucleic Acids Res. 40*, 8942-8952, doi: *10.1093/nar/gks669.*

Winardhi, R. S., Gulvady, R., Mellies, J. L. and Yan, J. (2014). Locus of enterocyte effacement-encoded regulator (Ler) of pathogenic *Escherichia coli* competes off histone-like nucleoid-structuring protein (H-NS) through noncooperative DNA binding. *J. Biol. Chem. 289*, 13739-13750, doi: *10.1074/jbc.M113.545954.*

Wolf, Y. I., Aravind, L. and Koonin, E. V. (1999). *Rickettsiae* and *Chlamydiae*: evidence of horizontal gene transfer and gene exchange. *Trends Genet. 15*, 173-175, doi: *10.1016/s0168-9525(99)01704-7.*

Xiong, L., Liu, S., Chen, S., Xiao, Y., Zhu, B., Gao, Y., Zhang, Y., Chen, B., Luo, J., Deng, Z., Chen, X., Wang, L. and Chen, S. (2019). A new type of DNA phosphorothioation-based antiviral system in archaea. *Nat. Commun. 10*, 1688, doi: *10.1038/s41467-019-09390-9.*

Xu, N., Wei, L. and Liu, J. (2019). Recent advances in the applications of promoter engineering for the optimization of metabolite biosynthesis. *World J. Microbiol. Biotechnol. 35*, 33, doi: *10.1007/s11274-019-2606-0.*

Yim, S. S., An, S. J., Kang, M., Lee, J. and Jeong, K. J. (2013). Isolation of fully synthetic promoters for high-level gene expression in *Corynebacterium glutamicum*. *Biotechnol. Bioeng. 110*, 2959-2969, doi: *10.1002/bit.24954.*

Yu, R. R. and DiRita, V. J. (2002). Regulation of gene expression in *Vibrio cholerae* by ToxT involves both antirepression and RNA polymerase stimulation. *Mol. Microbiol. 43*, 119-134, doi: *10.1046/j.1365-2958.2002.02721.x.*

Zamenhof, S., Brawerman, G. and Chargaff, E. (1952). On the desoxypentose nucleic acids from several microorganisms. *Biochim. Biophys. Acta. 9*, 402-405,

Zhang, F., Carothers, J. M. and Keasling, J. D. (2012a). Design of a dynamic sensor-regulator system for production of chemicals and fuels derived from fatty acids. *Nat. Biotechnol. 30*, 354-359, doi: *10.1038/nbt.2149.*

Zhang, Y., Shang, X., Lai, S., Zhang, G., Liang, Y. and Wen, T. (2012b). Development and application of an arabinose-inducible expression system by facilitating inducer uptake in *Corynebacterium glutamicum*. *Appl. Environ. Microbiol. 78*, 5831-5838, doi: *10.1128/aem.01147-12.*

Zwir, I., Latifi, T., Perez, J. C., Huang, H. and Groisman, E. A. (2012). The promoter architectural landscape of the *Salmonella* PhoP regulon. *Mol. Microbiol. 84*, 463-485, doi: *10.1111/j.1365-2958.2012.08036.x.*

# 3. Publications and manuscripts

The "Contributor Roles Taxonomy" (CRediT) methodology describes a transparent standard for authorships of scientific publications and for defining author contributions roles (McNutt et al., 2018). The following table contains aspects of this taxonomy which were used to describe author contributions to publications and manuscripts presented in this thesis.

| **Contributor role** | **Role definition** |
|---|---|
| Conceptualization | Ideas; formulation or evolution of overarching research goals and aims. |
| Formal analysis | Application of statistical, mathematical, computational, or other formal techniques to analyse or synthesize study data. |
| Investigation/Experiments | Conducting a research and investigation process, specifically performing the experiments, or data/evidence collection. |
| Methodology | Development or design of methodology; creation of models. |
| Project administration | Management and coordination responsibility for the research activity planning and execution. |
| Software | Programming, software development; designing computer programs; implementation of the computer code and supporting algorithms; testing of existing code components. |
| Supervision | Oversight and leadership responsibility for the research activity planning and execution, including mentorship external to the core team. |
| Visualization | Preparation, creation and/or presentation of the published work, specifically visualization/data presentation. |
| Writing – original draft | Preparation, creation and/or presentation of the published work, specifically writing the initial draft (including substantive translation). |
| Writing – review & editing | Preparation, creation and/or presentation of the published work by those from the original research group, specifically critical review, commentary or revision – including pre- or post-publication stages. |

## 3.1. Deciphering the rules underlying xenogeneic silencing and counter-silencing of Lsr2-like proteins using CgpS of *Corynebacterium glutamicum* as a model

**Wiechert, J.**, Filipchyk, A., Hünnefeld, M., Gätgens, C., Brehm, J., Heermann, R. and Frunzke, J.

Published in *mBio*, 2020.

| Contributor Role | Contributor |
|---|---|
| Conceptualization | JW 60 %, JF 40 % |
| Formal analysis | JW 85 %, AF 10 %, RH 5 % |
| Investigation/Experiments | JW 65 %, MH 7.5 %, CG 20 %, JB 2.5 %, RH 5 % |
| Methodology | JW 55 %, AF 10 %, MH 2.5 %, CG 10 %, JB 2.5 %, RH 5 %, JF 15 % |
| Project administration | JW 50 %, JF 50 % |
| Software | JW 50 %, AF 50 % |
| Supervision | JW 40 %, JF 60 % |
| Visualization | JW 95 %, AF 5 % |
| Writing – original draft | JW 70 %, JF 30 % |
| Writing – review & editing | JW 50 %, AF 5 %, MH 5 %, JF 40 % |

Overall contribution JW: 70 %

This publication is the central work resulting from this doctoral thesis. All visualizations and data analyses were done by JW, except of the heat maps in Fig 1B and C which were done by AF and the analyses of the SPR measurements, done by RH. JW performed most of the experimental work and a large part of the bioinformatic analysis, comprising Fig. 1 A,D, and data evaluation of 1E (RNA samples were prepared by MH and TSS determination as well as first analyses steps of the raw sequencing data were done by the company Vertis Biotechnology AG (Freising, Germany)), Fig. 2A (Bar plot was based on data shown in the heat maps prepared by AH), sample preparation (protein and DNA fragments) for SPR analyses shown in Fig. 2C and 4D (SPR experiments were performed by RH and JB), Fig. 3, Fig. 4B and C, Fig. 5, Fig. 6, Fig S1, S2, S3, S4 and S6. CG performed experiments shown in Fig. 2B and D, Fig. 4A and Fig. S5.The original draft was mainly prepared by JW and JW took over a large part (50 %) of the revision and editing process.

AMERICAN SOCIETY FOR MICROBIOLOGY | mBio®

RESEARCH ARTICLE
Molecular Biology and Physiology

# Deciphering the Rules Underlying Xenogeneic Silencing and Counter-Silencing of Lsr2-like Proteins Using CgpS of *Corynebacterium glutamicum* as a Model

**Johanna Wiechert,[a] Andrei Filipchyk,[a] Max Hünnefeld,[a] Cornelia Gätgens,[a] Jannis Brehm,[b] Ralf Heermann,[b] Julia Frunzke[a]**

[a]Institut für Bio- und Geowissenschaften, IBG-1: Biotechnologie, Forschungszentrum Jülich, Jülich, Germany
[b]Institut für Molekulare Physiologie, Mikrobiologie und Weinforschung, Johannes-Gutenberg-Universität Mainz, Mainz, Germany

**ABSTRACT** Lsr2-like nucleoid-associated proteins play an important role as xenogeneic silencers (XS) of horizontally acquired genomic regions in actinobacteria. In this study, we systematically analyzed the *in vivo* constraints underlying silencing and counter-silencing of the Lsr2-like protein CgpS in *Corynebacterium glutamicum*. Genome-wide analysis revealed binding of CgpS to regions featuring a distinct drop in GC profile close to the transcription start site (TSS) but also identified an overrepresented motif with multiple A/T steps at the nucleation site of the nucleoprotein complex. Binding of specific transcription factors (TFs) may oppose XS activity, leading to counter-silencing. Following a synthetic counter-silencing approach, target gene activation was realized by inserting operator sites of an effector-responsive TF within various CgpS target promoters, resulting in increased promoter activity upon TF binding. Analysis of reporter constructs revealed maximal counter-silencing when the TF operator site was inserted at the position of maximal CgpS coverage. This principle was implemented in a synthetic toggle switch, which features a robust and reversible response to effector availability, highlighting the potential for biotechnological applications. Together, our results provide comprehensive insights into how Lsr2 silencing and counter-silencing shape evolutionary network expansion in this medically and biotechnologically relevant bacterial phylum.

**IMPORTANCE** In actinobacteria, Lsr2-like nucleoid-associated proteins function as xenogeneic silencers (XS) of horizontally acquired genomic regions, including viral elements, virulence gene clusters in *Mycobacterium tuberculosis*, and genes involved in cryptic specialized metabolism in *Streptomyces* species. Consequently, a detailed mechanistic understanding of Lsr2 binding *in vivo* is relevant as a potential drug target and for the identification of novel bioactive compounds. Here, we followed an *in vivo* approach to investigate the rules underlying xenogeneic silencing and counter-silencing of the Lsr2-like XS CgpS from *Corynebacterium glutamicum*. Our results demonstrated that CgpS distinguishes between self and foreign by recognizing a distinct drop in GC profile in combination with a short, sequence-specific motif at the nucleation site. Following a synthetic counter-silencer approach, we studied the potential and constraints of transcription factors to counteract CgpS silencing, thereby facilitating the integration of new genetic traits into host regulatory networks.

**KEYWORDS** AT-rich DNA, Lsr2, actinobacteria, counter-silencing, horizontal gene transfer, regulatory networks, xenogeneic silencing

Horizontal gene transfer (HGT) is a major driver of bacterial evolution and plays an important role in creating genetic diversity (1). The rapid acquisition of beneficial new traits can create a competitive advantage for the recipient cells (1, 2). However, the chance that foreign DNA decreases the fitness of the cell is high, since it may lead to

**Citation** Wiechert J, Filipchyk A, Hünnefeld M, Gätgens C, Brehm J, Heermann R, Frunzke J. 2020. Deciphering the rules underlying xenogeneic silencing and counter-silencing of Lsr2-like proteins using CgpS of *Corynebacterium glutamicum* as a model. mBio 11:e02273-19. https://doi.org/10.1128/mBio.02273-19.

**Invited Editor** William W. Navarre, University of Toronto

**Editor** Eduardo A. Groisman, Yale School of Medicine



Address correspondence to Julia Frunzke, j.frunzke@fz-juelich.de.

**Received** 27 August 2019
**Accepted** 18 December 2019
**Published** 4 February 2020

interference with regulatory networks, high transcriptional and translational costs, sequestration of cellular machineries, and cytotoxic gene products (3–8). Therefore, bacteria evolved a variety of immune systems allowing them to deal with foreign DNA (9). CRISPR-Cas and restriction modification systems are nuclease-based defense mechanisms enabling the recognition and targeted degradation of invading DNA (10–12). In contrast to these destructive immune systems, xenogeneic silencing enables the tolerance of foreign DNA and consequently fosters the acquisition of novel genetic material into the host chromosome (13). Xenogeneic silencing is based on specific nucleoid-associated proteins (NAPs), so-called xenogeneic silencers (XS) (3). Known XS proteins belong to one of four currently described classes: H-NS-like proteins of proteobacteria, like *Escherichia coli*, *Yersinia*, and *Salmonella* (14–16), MvaT/U-like proteins found in gammaproteobacteria of the *Pseudomonodales* order (17), Lsr2-like XS of *Actinomycetes* (18, 19), and Rok, present in different bacilli, including *Bacillus subtilis* (20, 21). Although XS were convergently evolved and show only low sequence similarity within the different classes, the domain properties of their N-terminal oligomerization domains and their C-terminal DNA-binding domains are similar (19, 20, 22, 23). Their binding mechanisms are diverse, but they all preferentially bind to horizontally acquired DNA, which typically has a higher AT content than the genome of the recipient cell (4, 24). The broad distribution of XS among prokaryotes emphasizes the strong need to discriminate between self and non-self across phylogenetic clades (13). Even so, the GC content of microbial genomes dramatically varies, from 75% (*Actinobacteria*) to less than 20% (bacterial endosymbionts) (25, 26), and horizontally acquired regions typically feature a lower GC content than their resident genome, emphasizing base composition as a major discrimination factor shaping microbial genome evolution (3).

Several studies based on variants defective in oligomer formation revealed that binding of XS proteins to the DNA alone is insufficient for silencing (27–29). The formation of higher-order nucleoprotein complexes instead mediates silencing of the target genes by occlusion or trapping of the RNA polymerase, by interference with the transcription elongation complex, or by enhancing termination (30, 31). To get access to potentially encoded beneficial traits, cells must integrate foreign genes into preexisting regulatory circuits, allowing their controlled expression at appropriate time points and physiological or environmental conditions (32, 33). In contrast to classical activation, counter-silencing is based on the interference of a DNA-binding protein, e.g., a transcription factor (TF), with the silencer-DNA complex leading to transcription initiation without depending on the direct interaction with the RNA polymerase (32, 33). Counter-silencing of H-NS was addressed by several studies either by following a synthetic approach at well-studied promoters (34, 35) or by the analysis of the promoter architectures in the PhoPQ regulatory network (33). The recent study by Will et al. emphasizes that the principle of H-NS xenogeneic silencing and counter-silencing provides a certain degree of flexibility, fostering evolutionary network expansion (33).

Compared to H-NS in proteobacteria, much less is known about Lsr2-like XS proteins conserved throughout the actinobacteria. In *Mycobacterium tuberculosis*, Lsr2 acts as a master regulator of multiple virulence-associated genes (19, 22) and was suggested to be involved in the manifestation of multidrug tolerance (36). The essentiality of Lsr2 for this human pathogen makes this XS protein a highly promising drug candidate (37). In *Corynebacterium glutamicum*, the Lsr2-like XS protein CgpS also was shown to play an essential role as a silencer of cryptic prophage elements whose entrance into the lytic cycle would otherwise cause cell death (4, 38). In contrast to mycobacteria and corynebacterial species, *Streptomyces* species typically encode two Lsr2-like proteins. Here, the prototypical *lsr2* gene, showing the highest sequence identity to mycobacterial Lsr2, was recently described to silence the expression of specialized metabolic clusters (39). Considering the important role of Lsr2 proteins in the medically and biotechnologically important phylum of *Actinobacteria*, a detailed mechanistic understanding of Lsr2 binding *in vivo* is relevant as a potential drug target and for the identification novel bioactive compounds.

In this study, we set out to systematically assess the rules underlying silencing and

counter-silencing of Lsr2-like XS by using the Lsr2-like protein CgpS of *Corynebacterium glutamicum* as a model (4). To the best of our knowledge, this is the first detailed analysis of the counter-silencing mechanism of an Lsr2-like XS protein. Bioinformatic analysis of CgpS ChAP-seq (chromatin affinity purification and sequencing) data revealed a clear preference of CgpS toward AT-rich stretches containing A/T steps (alternation of A to T and vice versa). *In vivo* reporter studies with synthetic promoter variants verified the importance of a distinct drop in GC profile and revealed the overrepresentation of a short, sequence-specific motif at CgpS target regions. Insertion of TF operator sites at different positions within various CgpS target promoters was shown to counteract CgpS silencing, showing the most prominent effect at the position of maximal CgpS binding. With this approach, we provide important insights into the *in vivo* constraints of Lsr2 counter-silencing and contribute to an understanding of how bacteria can evolve control over the expression of horizontally acquired genes.

## RESULTS

***In vivo* analysis of CgpS binding preferences.** Recent genome-wide profiling studies revealed that the Lsr2-like xenogeneic silencer CgpS preferentially binds to AT-rich DNA sequences in the genome of *C. glutamicum* ATCC 13032 (4). To determine the parameters affecting CgpS binding and silencing *in vivo*, we systematically analyzed the peak sequences obtained from CgpS ChAP-seq analysis (4) and subsequently verified our conclusion by testing the silencing of synthetic promoter variants. Remarkably, an overlay of the GC profiles of all 35 CgpS target promoters located within the prophage element CGP3 revealed a high degree of similarity with a distinct drop in GC content matching the position of maximal CgpS coverage (Fig. 1A). Genome-wide analysis of AT-rich genomic regions revealed that the fraction of CgpS-bound sequences increased with the length of the particular AT stretch. While increasing numbers of G/C interruptions (occurrence of G or C within an AT stretch) negatively influenced the proportion of CgpS-bound targets (Fig. 1B), a larger number of A/T steps (alternation of A to T and vice versa) increased the fraction of CgpS-bound sequences by trend (Fig. 1C). This trend became especially evident in the case of AT-rich stretches of medium length (14 to 30 bp).

Overall, this analysis suggested that long and consecutive AT stretches represent the main determinant of CgpS target binding. Individual inspection of CgpS-targeted phage promoters revealed a significant correlation between the CgpS peak maximum and the GC minimum in this area (Fig. 1D). Depending on the widths of the CgpS coverage peaks, promoters were grouped into two classes. Class 1 consists of promoters with peak widths between 500 and 850 bp, which typically show one distinct drop in GC profile, while CgpS coverage peaks of class 2 promoters are wider than 850 bp and the corresponding GC profiles often feature broader or multiple drops.

Due to efficient CgpS-mediated silencing of gene expression, most transcriptional start sites (TSS) of CgpS target promoters had not been identified in previous studies (40). It represents, however, an advantage of the chosen model system that expression of the majority of CgpS targets can be induced by triggering prophage induction using the DNA-damaging antibiotic mitomycin C. To provide comprehensive insights into the promoter architecture of CgpS targets, TSS were determined under conditions triggering phage gene expression (600 nM mitomycin C). For 46 out of all 54 CgpS target promoters, at least one TSS was identified (for 31 out of 35 prophage promoters) (see Table S1 in the supplemental material). Strikingly, the analysis of the relative distances between the positions of TSS and maximal CgpS binding revealed that in the majority of CgpS target promoters, TSS are located close to the position of maximal CgpS coverage and GC minimum (Fig. 1D and E; see Table S1 for the complete data set).

**Design, build, and test: relevance of a DNA motif for CgpS binding and silencing.** Bioinformatic analysis of CgpS target sequences confirmed the preference of CgpS for AT-rich DNA sequences. However, neither the distinct drop in GC content nor the occurrence of long and consecutive AT stretches were unique to CgpS targets (Fig. 1), indicating that additional parameters support CgpS to specifically recognize its

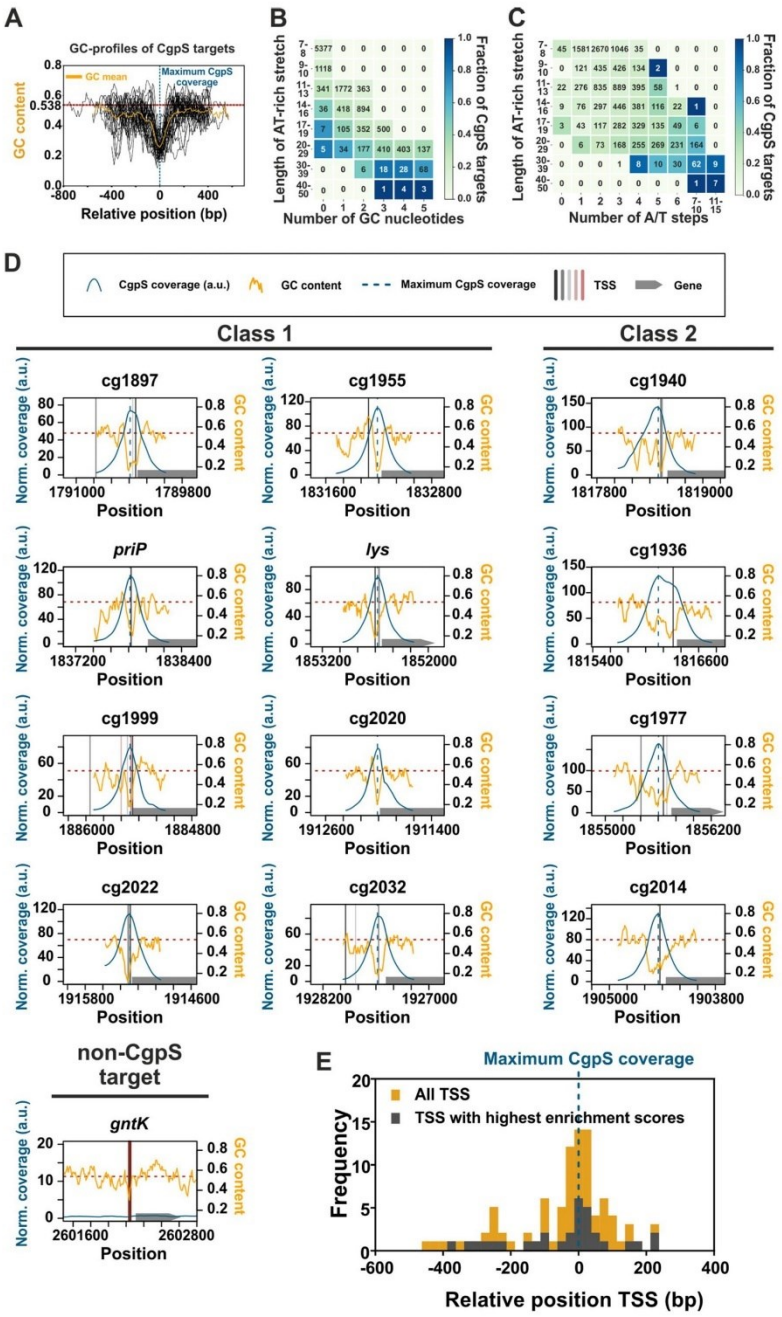


**FIG 1** CgpS preferentially binds to long and consecutive AT stretches. (A) Overlay and calculated mean (orange curve) of GC profiles of CgpS target promoters located within the CGP3 prophage ($n$ = 35) (4). Profiles were calculated by a

(Continued on next page)

targets. Interestingly, a MEME-ChIP analysis (41) on CgpS-bound promoter sequences revealed a 10-nucleotide-long AT-rich binding motif (E value, $5.2 \times 10^{-9}$) containing A/T steps (Fig. 2A), which was found in 51 of 54 bound promoter regions. Remarkably, the presence of this motif within AT-rich stretches of different lengths significantly increased the fraction of CgpS-bound sequences by a factor of up to 2.8-fold (Fig. 2A). However, the genome-wide search for motif occurrence using the online tool FIMO (Find Individual Motif Occurrences) (42) revealed that about 85% of the motifs (669/785) within the *C. glutamicum* genome were not bound by CgpS, indicating that the motif alone is not sufficient to permit CgpS binding.

In the following experiments, we used an *in vivo* approach to test whether the combination of the motif and the drop in GC profile are sufficient for CgpS-mediated silencing of gene expression. For this purpose, different synthetic promoter variants were designed based on the 50- to 70-bp core promoter regions of the phage genes $P_{cg1999}$ and $P_{lys}$. Both promoters were highly active in the absence of CgpS, indicating that the chosen core regions efficiently drive transcription. In the case of $P_{cg1999}$, the DNA sequence containing the core promoter elements (−10 and −35 box and TSS) and the predicted binding motif (shown in Fig. 2A) was kept constant (Fig. 2B). The adjacent sequence was either designed to mimic the native GC profile of $P_{cg1999}$ (exchange of A to T and G to C and vice versa, $P_{cg1999}$_A-T/G-C) or contained a randomized sequence varying in GC profile and sequence ($P_{cg1999}$_rand). The resulting promoter designs were fused to a gene encoding the yellow fluorescent protein Venus. In line with our hypothesis, the construct $P_{cg1999}$_A-T/G-C, featuring the native GC profile, was efficiently silenced by CgpS in the wild-type strain and displayed even lower reporter output than the native phage promoter $P_{cg1999}$ (Fig. 2B). Surface plasmon resonance (SPR) analysis revealed CgpS binding kinetics and affinities for this synthetic promoter (equilibrium dissociation constant [$K_D$], 42 nM) similar to those of the corresponding native CgpS target promoter $P_{cg1999}$ ($K_D$ = 58 nM). CgpS also interacted with the control promoter fragment $P_{cg3336}$ but with much lower affinity ($K_D$ = 381 nM) and very fast dissociation rates (Fig. 2C). In the prophage-free strain Δphage, which lacks the phage-encoded *cgpS* gene, the reporter output was significantly higher for all tested promoter fusions, confirming that all designs functionally drive transcription. Silencing of the promoter variant with randomized adjacent flanks was strongly impaired, demonstrating that the motif-containing 50-bp core promoter region alone did not mediate silencing. This highlights the importance of the overall drop in GC content observed at CgpS target promoters (Fig. 2B).

The relevance of the identified motif was verified using synthetic promoter designs of the phage promoter $P_{lys}$. Here, constructs carrying only parts of the predicted motif (70-bp core) did not permit silencing, while constructs covering the motif entirely enabled silencing (Fig. 2D). In all $P_{lys}$-based synthetic constructs, the native GC profile

**FIG 1** Legend (Continued)
rolling mean with a window size of 50 bp and a step size of 10 bp. The GC profiles of the promoters were normalized regarding the orientation and position of the maximal CgpS binding peak (blue line), which was defined for all sequences as position 0. The mean GC content of the *C. glutamicum* genome (69) is shown as a red line (53.8%). (B and C) Genome-wide analysis of CgpS binding to consecutive AT stretches of different lengths considering G/C interruptions (occurrence of G or C within an AT stretch) (B) or number of A/T steps (allowing up to five G/C interruptions) (C). A/T steps are defined as alterations of A to T and vice versa. The value in the array represents the number of stretches found in the *C. glutamicum* genome fitting the respective criteria, while the color indicates the fraction of CgpS targets per array. (D) Inverse correlation of GC profiles and CgpS coverage of CgpS target promoters. CgpS coverage obtained from previous ChAP-seq experiments (4) was calculated with a rolling mean with a window size of 50 and a step size of 10. All identified TSS (see Materials and Methods and Text S1) are shown in Table S1 and represented as vertical black, gray, and red lines (mapped according to their enrichment scores: black > shades of gray > red). Positions of maximal CgpS coverage and average GC content are shown as described for panel A. The corresponding genes are shown as gray arrows. Promoters were grouped into two classes based on the width of the region bound by CgpS (class 1 promoters, 500 to 850 bp, typically featuring one distinct drop in GC profile; class 2 promoters, >850 bp, often broader and containing multiple drops in GC content). As a negative control, the non-CgpS target promoter of the gene *gntK* is shown. a.u., arbitrary units. (E) Frequency distribution of relative positions of all new identified TSS (yellow) of CgpS target promoters referred to the position of maximal CgpS binding. TSS showing the highest enrichment scores per gene are highlighted in gray.

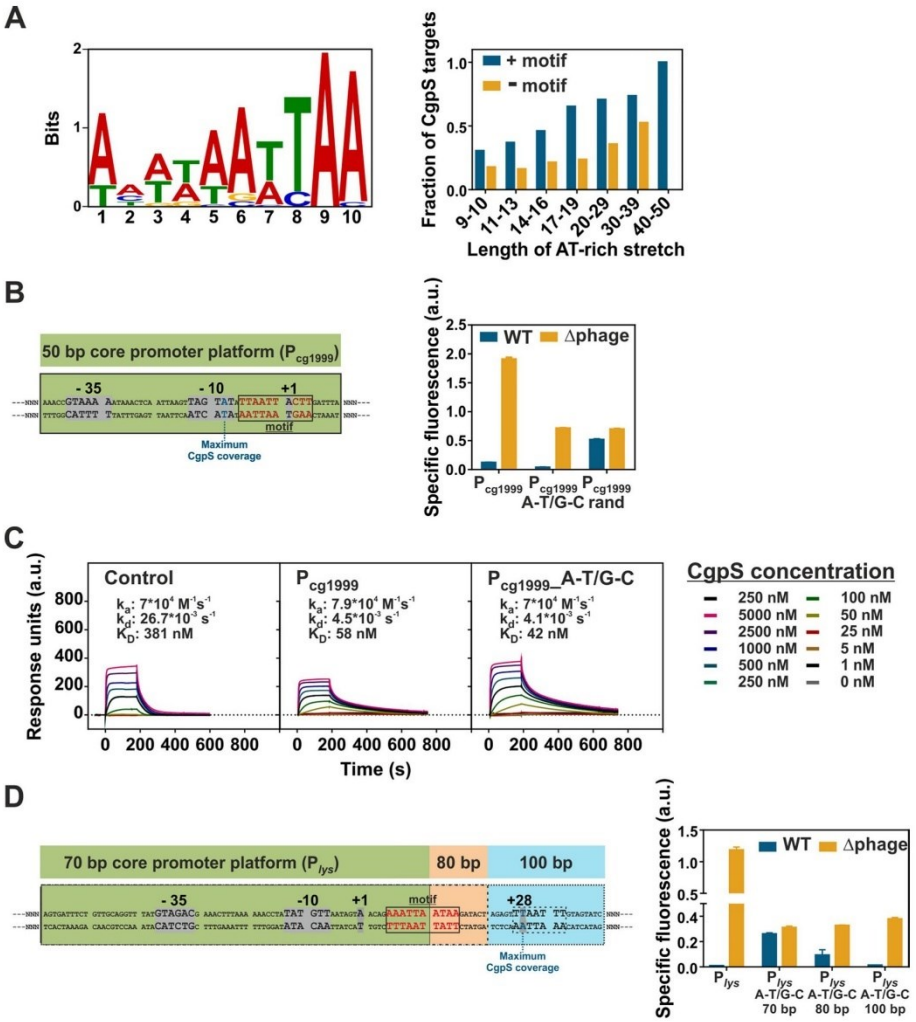


**FIG 2** Synthetic *in vivo* approach to dissect the relevance of the GC profile and a sequence-specific binding motif for CgpS silencing. (A) Identified 10-bp CgpS binding motif using MEME-ChIP (41) analysis found within 51 of 54 CgpS target promoters (4) (E value, $5.2 \times 10^{-9}$). The bar plot represents the genome-wide fraction of CgpS targets in AT stretches of different length, allowing up to 5 G/C interruptions with or without the identified motif. (B) CgpS silencing of synthetic constructs ($P_{cg1999}$_A-T/G-C and $P_{cg1999}$_rand), based on a 50-bp core promoter region (green box) of the phage gene cg1999. The fixed 50-bp DNA sequence covered the −10 and −35 box, positions of the TSS (40), and potential binding motif (gray box). The adjacent sequence (N upstream, 260 bp; N downstream, 48 bp) was either adjusted to maintain the native density of AT stretches ($P_{cg1999}$_A-T/G-C, exchange of A to T and G to C) or randomized ($P_{cg1999}$_rand). (C) Surface plasmon resonance analysis of CgpS binding to the synthetic promoter $P_{cg1999}$_A-T/G-C (423 bp) compared to that of the negative-control $P_{cg3336}$ (424 bp) and the corresponding native CgpS target $P_{cg1999}$ (423 bp). $k_a$, association constant; $k_d$, dissociation constant. (D) CgpS silencing of synthetic constructs based on fixed 70- to 100-bp promoter regions of the phage gene *lys*. The 70-bp sequence (green box) covered the −10 and −35 box and TSS but only half of the putative motif. The 80-bp region (green and orange boxes) covered the motif completely, and the 100-bp region (all boxes) additionally covered the position of maximal CgpS coverage. The adjacent sequences (N upstream, 304 bp; N downstream, 70 to 100 bp) were adjusted to maintain the native density of AT stretches (A-T/G-C). (B and D) Reporter outputs (Venus) of the native and corresponding synthetic variants (plasmid backbone pJC1) in wild-type and Δphage (Δ*cgpS*) strains after 5 h of cultivation in a microtiter cultivation system in CGXII medium containing 100 mM glucose. Shown are mean values and standard deviations from biological triplicates. All synthetic sequences are listed in Table S2I.

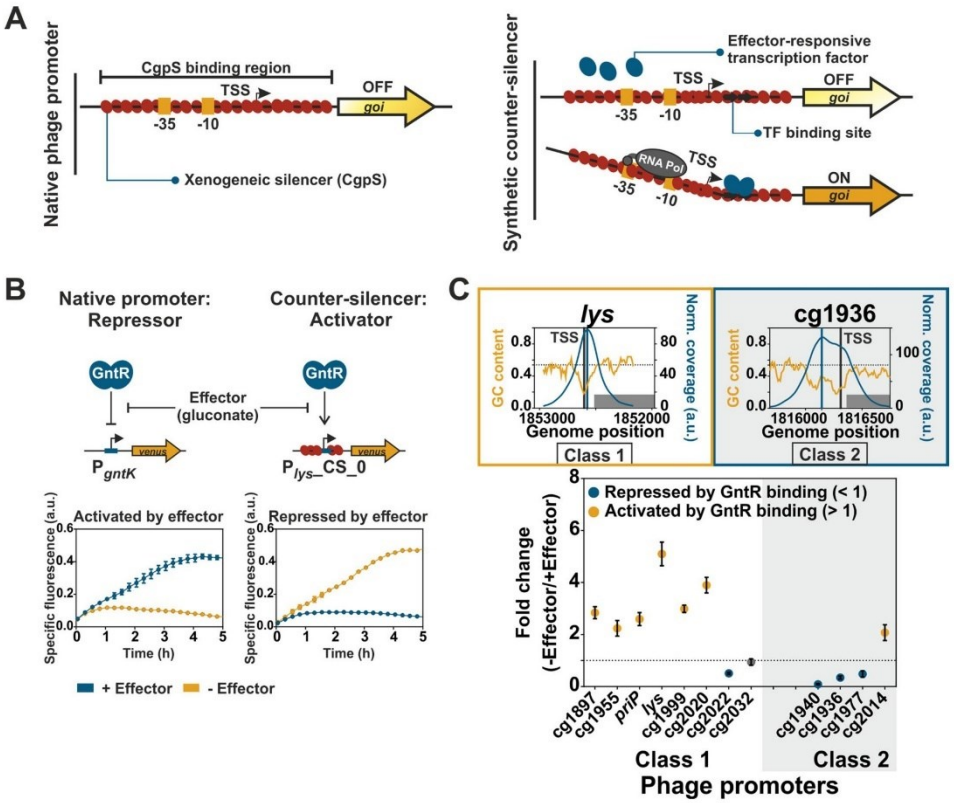


**FIG 3** Synthetic approach to study disruptive counter-silencing. (A) Schematic overview of a native CgpS target promoter (phage) and the corresponding synthetic counter-silencer construct. (B) Signal inversion by synthetic counter-silencing. Comparison of the reporter outputs of $P_{gntK}$, the native target promoter of the regulator of gluconate catabolism GntR (43), and the synthetic GntR-dependent counter-silencer promoter $P_{lys}$_CS_0. *C. glutamicum* wild-type strains harboring the plasmid-based constructs (pJC1) were cultivated in the absence of the effector (111 mM glucose) or in its presence (100 mM gluconate) in a microtiter cultivation system. Graphs represent the means and error bars the standard deviations from biological triplicates. Backscatter and fluorescence were measured at 15-min intervals. (C) Counter-silencing efficiency of different phage promoters with inserted GntR binding sites located directly upstream of the position of maximal CgpS binding. Promoters were grouped into two classes based on the width of the region bound by CgpS (class 1 promoters, 500 to 850 bp, often one distinct drop in GC profile; class 2 promoters, >850 bp, often broader or multiple drops in GC content). CgpS coverage and GC profiles of two representative promoters are shown. The highest-ranked TSS are marked as vertical gray lines and the position of maximal CgpS binding as vertical blue lines. GC profiles of all used phage promoters are shown in Fig. 1D. *C. glutamicum* wild-type cells harboring the plasmid-based (pJC1) counter-silencers were cultivated in the presence (100 mM gluconate) or absence (100 mM glucose) of the effector molecule gluconate in a microtiter cultivation system. Fold change ratios of Venus reporter outputs in the absence and in the presence of the effector were calculated based on the specific reporter outputs after 5 h of cultivation (Fig. S1A). Dots represent the means and error bars the standard deviations from at least biological triplicates. Yellow dots demonstrate counter-silencing (activated by GntR binding), while blue dots represent repression (repressed by GntR binding). Promoters, which did not show significant changes in reporter output, are shown as gray dots (*t* test; $P < 0.05$).

of the sequence flanking the core promoter region was mimicked but the DNA sequence was changed (A to T and G to C and vice versa). This *in vivo* analysis of synthetic phage promoter variants revealed that efficient CgpS silencing depended on both specific DNA sequences (binding motif) and the drop in GC profile.

**Synthetic disruptive counter-silencing.** Disruptive counter-silencing was previously described as a mechanism that may provide access to horizontally acquired genes silenced by nucleoid-associated proteins (32). To study the potential and constraints of evolutionary network expansion by counter-silencing of CgpS target promoters, a synthetic counter-silencer (CS) design was applied in this study (Fig. 3A). At native

target promoters (e.g., $P_{cg1999}$ or $P_{lys}$), oligomerization of the xenogeneic silencer CgpS leads to the formation of a nucleoprotein complex inhibiting transcription (4, 31). In the following experiments, we used a set of 12 different phage promoters as a basis for synthetic CS constructs and inserted the operator sequence of an effector-responsive transcription factor (TF) into the silenced promoter regions. We postulated that binding of the TF to its operator sequence would interfere with the silencer nucleoprotein complex and thereby mediate counter-silencing (Fig. 3A). To avoid interference of the inserted operator site with CgpS-mediated silencing, we chose the operator site of the functionally redundant TFs GntR1 (Cg2783) and GntR2 (Cg1935) (summarized as GntR in the following), which bind to a well-defined short (15 bp) and AT-rich (GC content, 27%) DNA motif (43). One of the native targets of GntR is the promoter of the *gntK* gene, which is repressed by binding of GntR. The $P_{gntK}$ promoter and the synthetic promoter constructs were fused via a consistent linker containing a ribosomal binding site (RBS) to the reporter gene *venus* and were inserted into the plasmid pJC1. The effector molecule gluconate was shown to act as an inducer triggering the dissociation of GntR from its operator site (43), consequently leading to derepression of $P_{gntK}$ (Fig. 3B).

Monitoring of fluorescent outputs driven by phage-based synthetic promoter constructs allows the *in vivo* analysis of silencing and counter-silencing efficiencies. GntR operator sites were indeed confirmed as suitable candidates for the construction of counter-silencers, since the insertion into different phage promoters led to only slightly increased background expression levels in the wild-type strain in the presence of the effector molecule (Fig. S1A). The insertion of a GntR binding site (BS) within the CgpS-silenced phage promoter $P_{lys}$ ($P_{lys}$_CS_0) led to effector-dependent reporter outputs. GntR binding resulted in an increased reporter output of the counter-silencer construct $P_{lys}$_CS_0 when glucose was added as a carbon source, while gluconate (effector addition) triggered the dissociation of GntR, leading to silencing of promoter activity by CgpS (Fig. 3B). This is especially remarkable considering that the binding site was inserted at the position of maximal CgpS coverage close to the annotated TSS (27 bp downstream [Table S1]). Based on textbook knowledge, this position would rather fit to a repressor function (44, 45). In the case of $P_{gntK}$, the GntR binding site overlaps the TSS, leading to repression of gene expression (43). In the context of xenogeneic silencing, however, GntR binding appeared to efficiently interfere with CgpS silencing. Thus, in contrast to the native GntR target $P_{gntK}$, the synthetic $P_{lys}$-counter-silencer promoter was activated in the absence of the effector molecule. Although both promoters ($P_{gntK}$ and $P_{lys}$_CS_0) were completely different and had only the 15-bp-long GntR binding site in common, they showed very similar but inverted responses to effector availability (Fig. 3B). This demonstrates the potential of the counter-silencing principle to convert a repressor to an activating, tunable counter-silencer, thereby facilitating the expansion of regulatory networks.

**Disruptive counter-silencing is most efficient at the CgpS nucleation site.** To systematically assess the constraints of counter-silencing, 12 representative phage promoters of both classes (eight class 1 and four class 2) were selected as targets to test the efficiency of synthetic counter-silencing. The GntR binding site was inserted directly upstream of the previously identified position of maximal CgpS binding obtained from ChAP-seq analysis (4). To study counter-silencing efficiency, all constructs were analyzed in *C. glutamicum* wild-type cells in the presence and absence of the effector molecule gluconate. The ratio of maximal (− effector; GntR binding) and minimal (+ effector; GntR dissociation) reporter outputs was used to compare the counter-silencing efficiency of the different constructs (Fig. 3C and Fig. S1). Overall, counter-silencing appeared to be more efficient in class 1 promoters typically featuring a bell-shaped CgpS peak and a distinct drop in GC profile. Here, six out of eight constructs showed an effector-responsive counter-silencing behavior. In contrast, only one of four class 2 promoters was activated by GntR binding. The broader regions bound by CgpS are probably stabilizing the silencer-DNA complex, compensating for the local interference

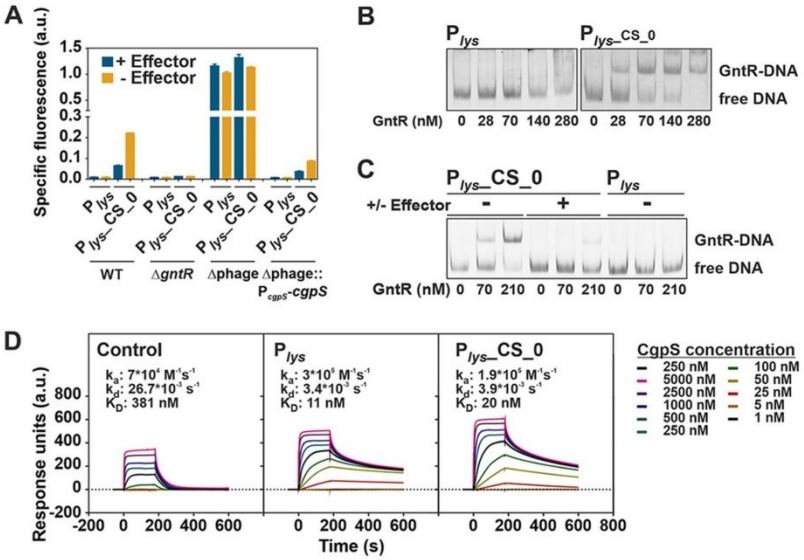


**FIG 4** Silencing is mediated by CgpS, while counter-silencing depends of GntR binding. (A) Reporter output (*venus* expression) of different *C. glutamicum* strains carrying the native $P_{lys}$ promoter or the counter-silencing design $P_{lys}$_CS_0 after 5 h of cultivation. Both constructs were analyzed in *C. glutamicum* wild-type cells, in a *gntR1-gntR2* double deletion strain, in the prophage-free strain Δphage (lacking the phage-encoded *cgpS*), and in its variant with reintegrated *cgpS* under the control of its native promoter (Δphage::$P_{cgpS}$-*cgpS*). Cells were cultivated in a microtiter cultivation system in CGXII medium supplemented with either 100 mM gluconate (+ effector) or 100 mM fructose (− effector). (B) EMSA of GntR binding to DNA fragments covering the synthetic counter-silencer promoter $P_{lys}$_CS_0 (533 bp, 14 nM) or the native phage promoter $P_{lys}$ (518 bp, 14 nM). (C) Impact of the effector molecule gluconate on binding of GntR to the synthetic counter-silencer construct. EMSA was performed as described for panel B, but GntR and the DNA fragments were incubated either in the presence of the effector (100 mM gluconate) or in its absence (100 mM glucose). (D) Surface plasmon resonance analysis of CgpS binding kinetics to biotinylated DNA fragments covering the negative-control $P_{cg3336}$ (424 bp), the native phage promoter $P_{lys}$ (424 bp), or the corresponding synthetic counter-silencer construct (439 bp) that were captured onto a streptavidin-coated sensor chip. Different concentrations of CgpS were passed over the chip using a contact (association) time of 180 s, followed by a 420-s dissociation phase. The increase in response units correlates with increasing CgpS concentrations.

effects caused by GntR binding. The general functionality of promoter variants (Fig. S1A) was confirmed in the strain Δphage, where all variants showed a significant fluorescent signal (Fig. S1B). Interestingly, GntR binding to $P_{cg2014}$ led to counter-silencing in the wild type but to slight repression in the Δphage strain, suggesting that only the destructive interference between CgpS and GntR facilitates efficient transcription of the downstream gene.

**Silencing is mediated by CgpS binding, and counter-silencing depends on GntR binding.** CgpS as silencer and GntR as counter-silencer are the two key components of the synthetic counter-silencer approach presented in this study. To confirm their presumed functions, mutant analysis and *in vitro* binding assays with both proteins were performed. The reporter outputs of the native phage promoter $P_{lys}$ as well as of the corresponding counter-silencer construct ($P_{lys}$_CS_0) were analyzed in *C. glutamicum* wild-type cells and different mutant strains. In the wild type, the counter-silencing construct showed the expected increase of reporter output upon GntR binding (− effector). In line with the assumed counter-silencing function of GntR, both constructs featured a low reporter output in the Δ*gntR* strain lacking both functionally redundant GntR1 and GntR2 regulators (Fig. 4A). To confirm the relevance of the inserted GntR operator sequence, different mutated variants were tested as well. Here, neither the insertion of a randomized operator sequence, identical in length and nucleotide

composition, nor a mutated operator site, where only one conserved base in the GntR motif was exchanged, led to counter-silencing of the $P_{lys}$ promoter (Fig. S2). These results confirmed that counter-silencing directly depends on GntR binding. However, the insertion of a reverse-oriented GntR binding site within the silenced promoter allowed counter-silencing, showing that this mechanism does not depend on the directionality of the binding site (Fig. S3). $P_{lys}$ and the corresponding counter-silencer construct showed strongly increased promoter activities in the Δphage strain in the absence of CgpS, suggesting that CgpS is responsible for silencing. Effector-dependent activation was abolished in the absence of CgpS, indicating that GntR acts as a counter-silencer rather than as a classical activator. Reintegration of the *cgpS* gene into the Δphage strain, resulting in Δphage::$P_{cgpS}$-*cgpS*, confirmed CgpS as the only factor responsible for silencing of the native phage promoter $P_{lys}$ and, thus, emphasized that CgpS function does not depend on further phage-encoded accessory proteins (Fig. 4A).

As a further piece of evidence, electrophoretic mobility shift assays (EMSA) were performed to confirm the specific binding of GntR to the synthetic counter-silencing construct ($P_{lys}$_CS_0) *in vitro*. In contrast to the native phage promoter, the $P_{lys}$ fragment containing the GntR operator site showed a significant shift at low GntR concentrations, confirming specific GntR binding to $P_{lys}$_CS_0 (Fig. 4B). Addition of the effector molecule gluconate led to dissociation of GntR (Fig. 4C), which is in agreement with previous reports (43). Surface plasmon resonance analysis of CgpS binding to DNA fragments covering either $P_{lys}$ or the synthetic counter-silencer construct $P_{lys}$_CS_0 showed comparable high-affinity binding of CgpS to both promoters ($K_D$, $P_{lys}$, 11 nM; $P_{lys}$_CS_0, 20 nM) (Fig. 4D).

**Impact of operator site position.** When analyzing the promoter architecture of horizontally acquired gene clusters, previous studies revealed a certain variability (33). To systematically assess the potential and constraints of the counter-silencing mechanism for evolutionary network expansion, we analyzed the impact of operator site position on counter-silencing efficiency. Therefore, the GntR binding site was inserted at different positions using the prophage promoter $P_{lys}$ as a test case (Fig. 5A). Position 0 is defined as the position located directly upstream of the nucleotide featuring maximal CgpS binding in ChAP-seq studies (4). The position of maximal CgpS binding was located 27 bp downstream of the TSS. *C. glutamicum* wild-type cells harboring the plasmid-based constructs [pJC1-$P_{lys}$::GntR BS_pos(variable)-*venus*] were cultivated in the presence or absence of the effector molecule gluconate. Induced and noninduced reporter outputs were strongly influenced by the binding site position. This demonstrated that the inserted binding site itself, depending on its position, already interferes with the silencer-DNA complex (Fig. 5B). Comparison of the fold change ratio of reporter outputs in the absence and presence of the effector gluconate revealed that the construct with the GntR binding site located directly upstream of the maximal CgpS binding peak (position 0) showed the highest dynamic range (~5-fold). This dynamic range decreased when the operator was inserted between 15 bp upstream (−15) and 10 bp downstream (+10) of the maximal CgpS binding peak, but constructs still showed counter-silencing in the absence of the effector (Fig. 5C). However, analyzing the −15 promoter variant in the absence of CgpS (Δphage) revealed repression caused by GntR binding, demonstrating again that the observed counter-silencing effect is a result of regulatory interference (Fig. S4). GntR binding sites located at greater distances led in most cases to relatively low reporter outputs. Here, the expression level tended to be higher when GntR binding was inhibited, suggesting GntR acts mainly as a repressor of gene expression at these positions (Fig. 5B and C). A similar trend was observed for the phage promoter $P_{cg1999}$ (Fig. S5). Altogether, these results demonstrated that the impact of GntR binding on promoter activity strongly depends on the context of xenogeneic silencing. While interference with CgpS binding triggered promoter activation by counter-silencing, GntR binding in the absence of CgpS often lowered the reporter output. Analysis of reporter outputs driven by 5′-truncated promoter variants of $P_{lys}$ and $P_{lys}$_CS_0 revealed that the region >89 bp upstream of

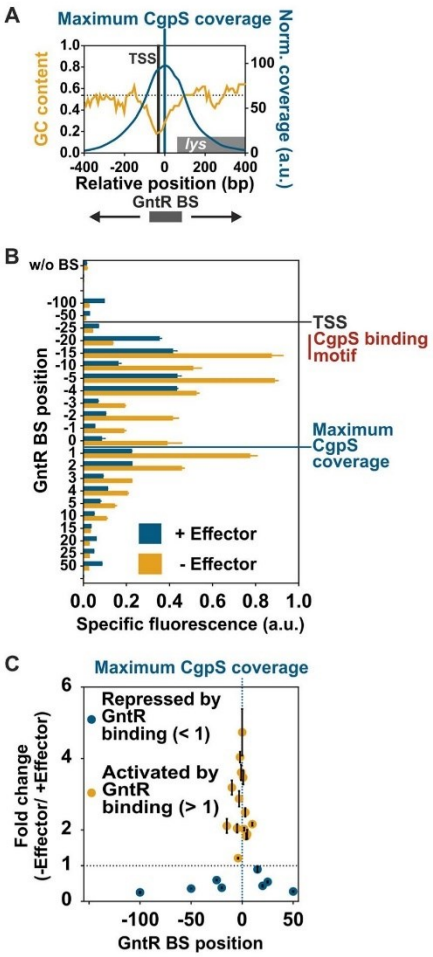


**FIG 5** Impact of GntR operator position on inducibility of $P_{lys}$-based promoter constructs. (A) Inverse correlation of GC profile and CgpS binding coverage (4) of the phage promoter $P_{lys}$. The transcriptional start site (TSS) and the position of maximal CgpS binding are shown as vertical lines. Binding site positions (also used in panels B and C) refer to the sequence base associated with maximal CgpS binding. The position directly upstream of this nucleotide was defined as position 0. (B) Impact of inserted GntR binding site position on specific reporter outputs in the presence (gluconate) and absence (glucose) of the effector molecule after 5 h of cultivation. Positions of TSS and maximal CgpS coverage are marked by horizontal lines, and the range of the putative CgpS binding motif is shown. (C) Impact of GntR binding site position on counter-silencing efficiency of $P_{lys}$-based promoter constructs. Ratio of specific reporter outputs, shown in panel B, were used for the calculation of their inducibility (fold change). Cells harboring the plasmid-based synthetic promoter constructs were grown in CGXII medium supplemented with either 111 mM glucose or 100 mM gluconate. Bars (B) and dots (C) represent the means and error bars the standard deviations from at least biological triplicates.

the maximal CgpS binding peak is not required for silencing or counter-silencing (Fig. S6).

**Implementation in a genetic toggle switch.** The $P_{lys}$ counter-silencing construct ($P_{lys}$_CS_0) and the native GntR target promoter $P_{gntK}$ showed a very similar promoter output but an inverted response to effector availability. While $P_{gntK}$ is repressed by

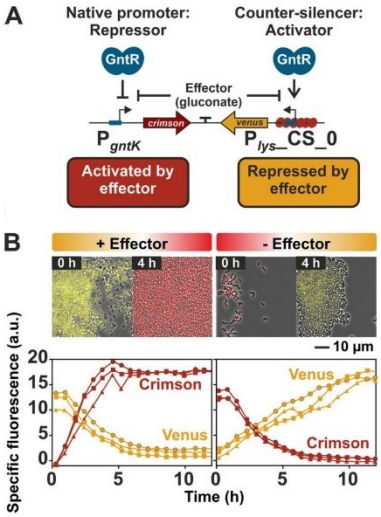


**FIG 6** Implementation of $P_{gntK}$ and $P_{lys}$_CS_0 in a genetic toggle switch. (A) Scheme of the designed toggle switch based on the native GntR target promoter $P_{gntK}$ and the synthetic GntR-dependent $P_{lys}$ counter-silencer construct. In order to monitor their activities, the promoters were fused to different reporter genes ($P_{lys}$_CS_0-*venus* and $P_{gntK}$-*e2-crimson*). The promoter reporter gene fusions were oriented in opposite directions and separated by a short terminator sequence. (B) Dynamic switch between both reporter outputs. *C. glutamicum* wild-type cells harboring the plasmid-based toggle were cultivated in a microfluidic cultivation system (46) with continuous supply of CGXII medium supplemented either 111 mM glucose or 100 mM gluconate and analyzed by time-lapse microscopy at 20-min intervals. Switch of carbon source supply was performed after the first 17 h. This time point was defined as $T_0$. The graphs show the specific fluorescence of three independent microcolonies (circles, squares, and triangles) over time, and images display one representative colony.

binding of GntR, the counter-silencer promoter is activated by GntR binding in the absence of the effector molecule gluconate (Fig. 3B). Both promoters were combined in a gluconate-dependent, GntR-controlled genetic toggle switch. To monitor the switching between different expression states, $P_{lys}$_CS_0 was fused to the reporter gene *venus*, while the native GntR target promoter $P_{gntK}$ was fused to the reporter gene *e2-crimson* (Fig. 6A). Since the toggle output is only regulated by GntR binding, native GntR levels could be used for toggle control, avoiding a negative impact of artificial TF levels on cellular growth. *C. glutamicum* wild-type cells harboring the plasmid-based toggle (pJC1-$P_{lys}$_CS_0-*venus*-T-$P_{gntK}$-*e2-crimson*) were cultivated in a microfluidic chip device (46) in minimal medium containing either gluconate (+ effector) or glucose (− effector) as carbon source. The carbon sources were switched after the first 17 h. The following time-lapse microscopy analysis revealed that the output of this synthetic toggle is reversible, as shown by the rapid changes in reporter outputs (Fig. 6B). This overall design principle allows the control of the toggle by only one specific effector-responsive TF and features a robust and reversible response to effector availability, highlighting the potential of this toggle for biotechnological applications, for example, to switch between biomass production and product formation.

## DISCUSSION

The nucleoid-associated protein Lsr2 is conserved throughout the phylum of *Actinobacteria*, where it plays an important role in the xenogeneic silencing of horizontally acquired genomic regions (4, 18, 19, 39). The Lsr2-like protein CgpS was recently described as a classical XS protein silencing the expression of cryptic prophage elements and further horizontally acquired elements in *C. glutamicum* (4).

**CgpS binds DNA with a distinct drop in GC content close to the TSS.** In this study, we systematically assessed the promoter architecture of CgpS targets as well as the constraints underlying silencing and counter-silencing of target gene expression. The genome-wide analysis of CgpS-bound regions obtained from ChAP-seq analysis revealed that CgpS targets share a distinct drop in GC content (Fig. 1). The binding to AT-rich DNA is a common feature of XS proteins (3) and was shown to represent an important fitness trait to avoid spurious transcription and the sequestering of the RNA polymerase (8). The importance of this drop in GC content was confirmed by measuring the CgpS-mediated silencing of $P_{cg1999}$-based synthetic variants, where changes in GC profile abolished silencing (Fig. 2B). The analysis of relative distance between the TSS and position of maximal CgpS binding emphasized that binding of CgpS close to the TSS is important for efficient silencing (Fig. 1E).

**CgpS recognizes a sequence-specific binding motif containing A/T steps.** *In vitro* protein binding microarray experiments revealed a clear preference of the xenogeneic silencers H-NS, MvaT, and Rok for DNA stretches containing flexible TpA (thymine-p-adenine) steps, while no positive effect of TpA steps was observed for Lsr2 from *Mycobacterium tuberculosis* (20, 47). Our design-test-build approach, where different synthetic promoter variants were tested *in vivo* concerning CgpS-mediated silencing, however, revealed a certain degree of sequence specificity of CgpS toward a binding motif containing A/T steps. While the GC content was kept constant, alteration of the proposed motif in the $P_{lys}$ promoter significantly affected *in vivo* silencing (Fig. 2). A scenario that has been proposed for H-NS features a high affinity toward DNA ($K_D$ of 60 nM), allowing the scanning of DNA until it reaches high-affinity sites, triggering the nucleation of the tight nucleoprotein complex required for silencing (3, 48, 49). Based on the systematic analysis of truncated promoter variants, we clearly defined the region required for efficient *in vivo* silencing by CgpS (see Fig. S6 in the supplemental material). It is important to note that we almost exclusively relied on *in vivo* approaches, including ChAP-seq analysis and reporter assays, to define the parameters affecting silencing and counter-silencing at the systems level. Although *in vitro* analysis of protein-DNA fragments (often linear DNA) is frequently applied and has provided valuable insights into the binding behavior of XS proteins (20, 47, 49), the conditions do not reflect physiologically relevant situations (DNA topology, protein-protein interaction, and interference); consequently, the results have to be interpreted with caution.

**GntR-dependent counter-silencing is a disruptive mechanism.** While xenogeneic silencing neutralizes the potentially negative effect of invading foreign DNA, counter-silencing allows the integration into the host regulatory network and thereby provides access to horizontally acquired genes. This principle has been almost exclusively studied for H-NS in proteobacteria, and several types of TFs were shown to counteract H-NS silencing *in vivo* (15, 50–53). In the case of Lsr2, the mycobacterial iron-dependent regulator IdeR represents, to the best of our knowledge, the only example of an investigated Lsr2 counter-silencer. IdeR enables the iron-dependent activation of ferritin by alleviating Lsr2 repression at the *bfrB* locus (54).

During bacterial evolution, mutations leading to the formation of TF operator sequences within silenced promoters allow the controlled expression of the previously silenced genes by TF-mediated counter-silencing. In this work, the artificial insertion of the 15-bp short operator sequences of the gluconate-dependent TF GntR within different CgpS target promoters allowed us to study the potential and constraints of counter-silencing of this Lsr2-like XS protein. Binding of GntR to several CgpS target promoters led to transcription initiation of the silenced phage promoters, demonstrating that small changes in the DNA sequence added a further regulatory layer for expression control.

All tested CgpS target promoters showed significant reporter output in the absence of CgpS, confirming that they promote transcription and that CgpS inhibits promoter activity, presumably by hindering open complex formation or by trapping the open complex once it has formed (55). Previous studies already suggested that, without

xenogeneic silencing, open complex formation is typically not the rate-limiting step at AT-rich promoters of horizontally acquired genes, meaning they are constitutively active (33, 56, 57). In the case of the H-NS target promoter *pagC*, an *in vitro* approach demonstrated RNA polymerase binding and open complex formation in the absence of additional factors, confirming that this promoter alone is transcriptionally competent (33).

In general, two different mechanisms of counter-silencing are conceivable. In one scenario (disruptive mechanism), the interference of TF and XS protein leads to a local disruption of the XS nucleoprotein complex, thereby enabling binding of the RNA polymerase to the DNA. Another possibility is that counter-silencing allows for supportive contacts between the RNA polymerase and the TF itself or more distal DNA regions (supportive mechanism). In this study, binding of GntR to the promoter constructs in the absence of the XS CgpS resulted in reduced reporter outputs, although counter-silencing was observed in the wild type. This result strongly speaks for a disruptive rather than a supportive GntR-mediated counter-silencing mechanism.

**GntR binding close to the CgpS nucleation site is a prerequisite for efficient counter-silencing.** By the systematic analysis of promoter variants with varied positions of the GntR operator site, we clearly defined the window where binding of a specific TF led to counter-silencing. Counter-silencing of the Lsr2-like XS CgpS was most efficient at positions close to the position of maximal CgpS binding in a range of approximately 25 bp (Fig. 5 and Fig. S5), demonstrating that the position of GntR binding is critical for counter-silencing.

Previous studies by Will et al. revealed that counter-silencing and classical activation are different mechanisms of gene regulation (33). While TFs acting as activators typically bind to conserved promoter architectures and promote transcription either by changing the DNA conformation or by recruiting the RNA polymerase (58), the principle of counter-silencing allows a higher degree of flexibility in terms of promoter architecture (33). For the PhoPQ regulon of *Salmonella enterica* serovar Typhimurium, it was shown that PhoP activates core promoters featuring a precise operator position overlapping the −35 box. In contrast, horizontally acquired PhoP target genes show rather diverse promoter architectures, and here transcriptional activation is achieved by counter-silencing of H-NS. In these reported examples, the distances between the TSS and the closest PhoP binding site vary by only 34 bp (33, 59). This is in a range similar to that for our results and those obtained in previous studies for the H-NS target promoter $P_{bgl}$, where the insertion of TF operator sites counteracted H-NS silencing in a comparable window (34).

It is intriguing that in the context of xenogeneic silencing binding of a TF at positions close to the TSS leads to promoter activation, where it would cause a block of transcription at classical promoters (44, 60). Indeed, GntR binding in the absence of the XS CgpS resulted in reduced reporter outputs of several synthetic promoter constructs tested in this study (Fig. S1 and S4). However, counter-silencing was observed in the presence of CgpS in the wild type. These results demonstrate the potential of the counter-silencing principle to convert a repressor to an activating, tunable counter-silencer, thereby facilitating the integration of horizontally acquired DNA into host regulatory networks. Overall, these data illustrate how interference of TFs is shaping global regulatory networks and that the regulatory impact of TF binding is strongly affected by competition with other DNA-binding proteins.

## MATERIALS AND METHODS

**Bacterial strains and cultivation conditions.** All bacterial strains and plasmids used in this project are listed in Table S2A to C in the supplemental material. The strain *C. glutamicum* ATCC 13032 (61) was used as the wild-type strain. Detailed information about general growth conditions, microtiter cultivations used to monitor cell growth and fluorescence (62), and cultivations in the microfluidic chip device (46, 63) is available in the supplemental material (Text S1).

**Recombinant DNA work.** All standard molecular methods, such as PCR, DNA restriction, and Gibson assembly, were performed according to previously described standard protocols (64, 65) or according to the manufacturer's instructions. All plasmids were constructed by Gibson assembly. Details on plasmid construction are provided in Table S2C. DNA sequencing and synthesis of oligonucleotides used for

amplification of DNA fragments (inserts for Gibson assembly [Table S2D], biotinylated DNA fragments for surface plasmon resonance [SPR] spectroscopy [Table S2E], and DNA fragments for electrophoretic mobility shift assays [EMSA] [Table S2F]) and sequencing (Table S2G), as well as synthesis of DNA sequences (Table S2H), were performed by Eurofins Genomics (Ebersberg, Germany). Chromosomal DNA of *C. glutamicum* ATCC 13032 was used as the PCR template and was prepared as described previously (66). Detailed information about construction of strain Δphage::$P_{cgpS}$-*cgpS* via two-step homologous recombination (67) and the design of disruptive counter-silencing constructs is available in the supplemental material (Text S1).

**Determination of TSS.** The determination of TSS and data analysis were performed with *C. glutamicum* wild-type cells by Vertis Biotechnology AG (Freising, Germany) using the Cappable-seq method developed by Ettwiller and Schildkraut (68). Prophage induction was triggered by adding mitomycin C. Detailed information about cultivation conditions, RNA preparation, and data analysis can be found in the supplemental material (Text S1). Relevant TSS were assigned to phage and nonphage CgpS target promoters when they were located in the promoter region 500 bp upstream of the start codon and directed in gene orientation (Table S1). Multiple TSS assigned to the same promoter were ranked depending on their enrichment scores.

**Plots of CgpS coverage and GC profiles.** Normalized CgpS coverage values obtained from previous ChAP-seq analysis of Pfeifer and colleagues (4) and GC content of the reference *C. glutamicum* genome BX927147 (69) were plotted to the corresponding genome positions. Both parameters were calculated by a rolling mean with a window size of 50 bp and a step size of 10 bp using R (http://www.R-project.org) (70). The position of maximal CgpS coverage was centered, and the promoter orientation was normalized (start codon of the corresponding gene is located on the right site). Identified TSS positions were added. Ends of graphs are defined by the range of the CgpS binding peaks identified in previous ChAP-seq analysis (4). Plotting was performed either by R (70) or by GraphPad Prism 7.00 (GraphPad Software, La Jolla, CA).

**Analyses of AT-rich stretches in CgpS binding regions.** The *C. glutamicum* genome (BX927147 [69]) was scanned for AT-rich stretches using a custom python script (submitted to GitHub at https://github.com/afilipch/afp/blob/master/genomic/get_at_stretches.py). For further details, see the supplemental material (Text S1).

**Protein purification, SPR spectroscopy, and EMSA.** Information about purification of Strep-tagged CgpS and His-tagged GntR and the performed *in vitro* binding assays (SPR spectroscopy and EMSA) can be found in the supplemental material (Text S1).

**Data availability.** The custom python script used for scanning for AT-rich stretches is available in the GitHub repository (https://github.com/afilipch/afp/blob/master/genomic/get_at_stretches.py). Data from previously reported ChAP-seq analysis (4) are available at the GEO database (https://www.ncbi.nlm.nih.gov/geo) under accession number GSE141132.

## SUPPLEMENTAL MATERIAL

Supplemental material is available online only.

**TEXT S1**, PDF file, 0.2 MB.

**FIG S1**, TIF file, 0.2 MB.

**FIG S2**, TIF file, 0.2 MB.

**FIG S3**, TIF file, 0.1 MB.

**FIG S4**, TIF file, 0.1 MB.

**FIG S5**, TIF file, 0.3 MB.

**FIG S6**, TIF file, 0.2 MB.

**TABLE S1**, XLSX file, 0.03 MB.

**TABLE S2**, DOCX file, 0.1 MB.

## ACKNOWLEDGMENTS

We thank the European Research Council (ERC Starting Grant, grant number 757563), the Helmholtz Association (grant number W2/W3-096), and the Deutsche Forschungsgemeinschaft (SPP 1617 grant number FR2759/2-2) for financial support.

We thank Eugen Pfeifer for excellent discussions, for help with R, and for the plasmid pK19mobsacB-1199_1201-$P_{cgpS}$-*cgpS*. We thank Iska Steffens for her help with the EMSAs and Aël Hardy for critical reading of the manuscript. We are very grateful for the opportunity to use the Bioanalytics core facility of the JGU Biocenter and to Kirsten Jung for using the Bioanalytics core facility of the LMU Munich for SPR analyses.

## REFERENCES

1. Ochman H, Lawrence JG, Groisman EA. 2000. Lateral gene transfer and the nature of bacterial innovation. Nature 405:299–304. https://doi.org/10.1038/35012500.

2. Dorman CJ. 2014. H-NS-like nucleoid-associated proteins, mobile genetic elements and horizontal gene transfer in bacteria. Plasmid 75:1–11. https://doi.org/10.1016/j.plasmid.2014.06.004.

3. Navarre WW. 2016. The impact of gene silencing on horizontal gene transfer and bacterial evolution. Adv Microb Physiol 69:157–186. https://doi.org/10.1016/bs.ampbs.2016.07.004.
4. Pfeifer E, Hünnefeld M, Popa O, Polen T, Kohlheyer D, Baumgart M, Frunzke J. 2016. Silencing of cryptic prophages in *Corynebacterium glutamicum*. Nucleic Acids Res 44:10117–10131. https://doi.org/10.1093/nar/gkw692.
5. Vogan AA, Higgs PG. 2011. The advantages and disadvantages of horizontal gene transfer and the emergence of the first species. Biol Direct 6:1. https://doi.org/10.1186/1745-6150-6-1.
6. Park C, Zhang J. 2012. High expression hampers horizontal gene transfer. Genome Biol Evol 4:523–532. https://doi.org/10.1093/gbe/evs030.
7. Baltrus DA. 2013. Exploring the costs of horizontal gene transfer. Trends Ecol Evol 28:489–495. https://doi.org/10.1016/j.tree.2013.04.002.
8. Lamberte LE, Baniulyte G, Singh SS, Stringer AM, Bonocora RP, Stracy M, Kapanidis AN, Wade JT, Grainger DC. 2017. Horizontally acquired AT-rich genes in *Escherichia coli* cause toxicity by sequestering RNA polymerase. Nat Microbiol 2:16249. https://doi.org/10.1038/nmicrobiol.2016.249.
9. Doron S, Melamed S, Ofir G, Leavitt A, Lopatina A, Keren M, Amitai G, Sorek R, Doron S, Melamed S, Ofir G, Leavitt A, Lopatina A, Keren M, Amitai G, Sorek R. 2018. Systematic discovery of antiphage defense systems in the microbial pangenome. Science 359:eaar4120. https://doi.org/10.1126/science.aar4120.
10. Labrie SJ, Samson JE, Moineau S. 2010. Bacteriophage resistance mechanisms. Nat Rev Microbiol 8:317–327. https://doi.org/10.1038/nrmicro2315.
11. Sorek R, Lawrence CM, Wiedenheft B. 2013. CRISPR-mediated adaptive immune systems in bacteria and archaea. Annu Rev Biochem 82:237–266. https://doi.org/10.1146/annurev-biochem-072911-172315.
12. Roberts RJ. 2005. How restriction enzymes became the workhorses of molecular biology. Proc Natl Acad Sci U S A 102:5905–5908. https://doi.org/10.1073/pnas.0500923102.
13. Navarre WW, McClelland M, Libby SJ, Fang FC. 2007. Silencing of xenogeneic DNA by H-NS-facilitation of lateral gene transfer in bacteria by a defense system that recognizes foreign DNA. Genes Dev 21:1456–1471. https://doi.org/10.1101/gad.1543107.
14. Navarre WW, Porwollik S, Wang Y, McClelland M, Rosen H, Libby SJ, Fang FC. 2006. Selective silencing of foreign DNA with low GC content by the H-NS protein in *Salmonella*. Science 313:236–238. https://doi.org/10.1126/science.1128794.
15. Heroven AK, Nagel G, Tran HJ, Parr S, Dersch P. 2004. RovA is autoregulated and antagonizes H-NS-mediated silencing of invasin and *rovA* expression in *Yersinia pseudotuberculosis*. Mol Microbiol 53:871–888. https://doi.org/10.1111/j.1365-2958.2004.04162.x.
16. Oshima T, Ishikawa S, Kurokawa K, Aiba H, Ogasawara N. 2006. *Escherichia coli* histone-like protein H-NS preferentially binds to horizontally acquired DNA in association with RNA polymerase. DNA Res 13:141–153. https://doi.org/10.1093/dnares/dsl009.
17. Tendeng C, Soutourina OA, Danchin A, Bertin PN. 2003. MvaT proteins in *Pseudomonas spp.*: a novel class of H-NS-like proteins. Microbiology 149:3047–3050. https://doi.org/10.1099/mic.0.C0125-0.
18. Gordon BR, Imperial R, Wang L, Navarre WW, Liu J. 2008. Lsr2 of *Mycobacterium* represents a novel class of H-NS-like proteins. J Bacteriol 190:7052–7059. https://doi.org/10.1128/JB.00733-08.
19. Gordon BR, Li Y, Wang L, Sintsova A, van Bakel H, Tian S, Navarre WW, Xia B, Liu J. 2010. Lsr2 is a nucleoid-associated protein that targets AT-rich sequences and virulence genes in *Mycobacterium tuberculosis*. Proc Natl Acad Sci U S A 107:5154–5159. https://doi.org/10.1073/pnas.0913551107.
20. Duan B, Ding P, Hughes TR, Navarre WW, Liu J, Xia B. 2018. How bacterial xenogeneic silencer rok distinguishes foreign from self DNA in its resident genome. Nucleic Acids Res 46:10514–10529. https://doi.org/10.1093/nar/gky836.
21. Smits WK, Grossman AD. 2010. The transcriptional regulator Rok binds A+T-rich DNA and is involved in repression of a mobile genetic element in *Bacillus subtilis*. PLoS Genet 6:e1001207. https://doi.org/10.1371/journal.pgen.1001207.
22. Gordon BR, Li Y, Cote A, Weirauch MT, Ding P, Hughes TR, Navarre WW, Xia B, Liu J. 2011. Structural basis for recognition of AT-rich DNA by unrelated xenogeneic silencing proteins. Proc Natl Acad Sci U S A 108:10690–10695. https://doi.org/10.1073/pnas.1102544108.
23. Castang S, Dove SL. 2010. High-order oligomerization is required for the function of the H-NS family member MvaT in *Pseudomonas aeruginosa*. Mol Microbiol 78:916–931. https://doi.org/10.1111/j.1365-2958.2010.07378.x.
24. Daubin V, Lerat E, Perrière G. 2003. The source of laterally transferred genes in bacterial genomes. Genome Biol 4:R57. https://doi.org/10.1186/gb-2003-4-9-r57.
25. Hildebrand F, Meyer A, Eyre-Walker A. 2010. Evidence of selection upon genomic GC content in bacteria. PLoS Genet 6:e1001107. https://doi.org/10.1371/journal.pgen.1001107.
26. Zamenhof S, Brawerman G, Chargaff E. 1952. On the desoxypentose nucleic acids from several microorganisms. Biochim Biophys Acta 9:402–405. https://doi.org/10.1016/0006-3002(52)90184-4.
27. Spurio R, Falconi M, Brandi A, Pon CL, Gualerzi CO. 1997. The oligomeric structure of nucleoid protein H-NS is necessary for recognition of intrinsically curved DNA and for DNA bending. EMBO J 16:1795–1805. https://doi.org/10.1093/emboj/16.7.1795.
28. Winardhi RS, Fu W, Castang S, Li Y, Dove SL, Yan J. 2012. Higher order oligomerization is required for H-NS family member MvaT to form gene-silencing nucleoprotein filament. Nucleic Acids Res 40:8942–8952. https://doi.org/10.1093/nar/gks669.
29. Chen JM, Ren H, Shaw JE, Wang YJ, Li M, Leung AS, Tran V, Berbenetz NM, Kocíncová D, Yip CM, Reyrat JM, Liu J. 2008. Lsr2 of *Mycobacterium tuberculosis* is a DNA-bridging protein. Nucleic Acids Res 36:2123–2135. https://doi.org/10.1093/nar/gkm1162.
30. Lim CJ, Lee SY, Kenney LJ, Yan J. 2012. Nucleoprotein filament formation is the structural basis for bacterial protein H-NS gene silencing. Sci Rep 2:509. https://doi.org/10.1038/srep00509.
31. Landick R, Wade JT, Grainger DC. 2015. H-NS and RNA polymerase: a love-hate relationship? Curr Opin Microbiol 24:53–59. https://doi.org/10.1016/j.mib.2015.01.009.
32. Will WR, Navarre WW, Fang FC. 2015. Integrated circuits: how transcriptional silencing and counter-silencing facilitate bacterial evolution. Curr Opin Microbiol 23:8–13. https://doi.org/10.1016/j.mib.2014.10.005.
33. Will WR, Bale DH, Reid PJ, Libby SJ, Fang FC. 2014. Evolutionary expansion of a regulatory network by counter-silencing. Nat Commun 5:5270. https://doi.org/10.1038/ncomms6270.
34. Caramel A, Schnetz K. 1998. Lac and lambda repressors relieve silencing of the *Escherichia coli bgl* promoter. Activation by alteration of a repressing nucleoprotein complex. J Mol Biol 284:875–883. https://doi.org/10.1006/jmbi.1998.2191.
35. Kane KA, Dorman CJ. 2011. Rational design of an artificial genetic switch: co-option of the H-NS-repressed *proU* operon by the VirB virulence master regulator. J Bacteriol 193:5950–5960. https://doi.org/10.1128/JB.05557-11.
36. Colangeli R, Helb D, Vilchèze C, Hazbón MH, Lee C-G, Safi H, Sayers B, Sardone I, Jones MB, Fleischmann RD, Peterson SN, Jacobs WR, Jr, Alland D. 2007. Transcriptional regulation of multi-drug tolerance and antibiotic-induced responses by the histone-like protein Lsr2 in *M. tuberculosis*. PLoS Pathog 3:e87. https://doi.org/10.1371/journal.ppat.0030087.
37. Colangeli R, Haq A, Arcus VL, Summers E, Magliozzo RS, McBride A, Mitra AK, Radjainia M, Khajo A, Jacobs WR, Salgame P, Alland D. 2009. The multifunctional histone-like protein Lsr2 protects mycobacteria against reactive oxygen intermediates. Proc Natl Acad Sci U S A 106:4414–4418. https://doi.org/10.1073/pnas.0810126106.
38. Pfeifer E, Hünnefeld M, Popa O, Frunzke J. 2019. Impact of xenogeneic silencing on phage-host interactions. J Mol Biol 431:4670–4683. https://doi.org/10.1016/j.jmb.2019.02.011.
39. Gehrke EJ, Zhang X, Pimentel-Elardo SM, Johnson AR, Rees CA, Jones SE, Hindra GSS, Turvey S, Boursalie S, Hill JE, Carlson EE, Nodwell JR, Elliot MA. 2019. Silencing cryptic specialized metabolism in Streptomyces by the nucleoid-associated protein Lsr2. Elife 431:e47691. https://doi.org/10.7554/eLife.47691.
40. Pfeifer-Sancar K, Mentz A, Rückert C, Kalinowski J. 2013. Comprehensive analysis of the *Corynebacterium glutamicum* transcriptome using an improved RNAseq technique. BMC Genomics 14:888. https://doi.org/10.1186/1471-2164-14-888.
41. Bailey TL, Boden M, Buske FA, Frith M, Grant CE, Clementi L, Ren J, Li WW, Noble WS. 2009. MEME Suite: tools for motif discovery and searching. Nucleic Acids Res 37:W202–W208. https://doi.org/10.1093/nar/gkp335.
42. Grant CE, Bailey TL, Noble WS. 2011. FIMO: scanning for occurrences of a given motif. Bioinformatics 27:1017–1018. https://doi.org/10.1093/bioinformatics/btr064.
43. Frunzke J, Engels V, Hasenbein S, Gätgens C, Bott M. 2008. Co-ordinated regulation of gluconate catabolism and glucose uptake in *Corynebacterium glutamicum* by two functionally equivalent transcriptional regulators, GntR1 and GntR2. Mol Microbiol 67:305–322. https://doi.org/10.1111/j.1365-2958.2007.06020.x.

44. Rojo F. 1999. Repression of transcription initiation in bacteria. J Bacteriol 181:2987–2991. https://doi.org/10.1128/JB.181.10.2987-2991.1999.
45. Rydenfelt M, Garcia HG, Cox RS, III, Phillips R. 2014. The influence of promoter architectures and regulatory motifs on gene expression in *Escherichia coli*. PLoS One 9:e114347. https://doi.org/10.1371/journal.pone.0114347.
46. Grünberger A, Probst C, Helfrich S, Nanda A, Stute B, Wiechert W, von Lieres E, Nöh K, Frunzke J, Kohlheyer D. 2015. Spatiotemporal microbial single-cell analysis using a high-throughput microfluidics cultivation platform. Cytometry A 87:1101–1115. https://doi.org/10.1002/cyto.a.22779.
47. Ding P, McFarland KA, Jin S, Tong G, Duan B, Yang A, Hughes TR, Liu J, Dove SL, Navarre WW, Xia B. 2015. A novel AT-rich DNA recognition mechanism for bacterial xenogeneic silencer MvaT. PLoS Pathog 11:e1004967. https://doi.org/10.1371/journal.ppat.1004967.
48. Lang B, Blot N, Bouffartigues E, Buckle M, Geertz M, Gualerzi CO, Mavathur R, Muskhelishvili G, Pon CL, Rimsky S, Stella S, Babu MM, Travers A. 2007. High-affinity DNA binding sites for H-NS provide a molecular basis for selective silencing within proteobacterial genomes. Nucleic Acids Res 35:6330–6337. https://doi.org/10.1093/nar/gkm712.
49. Gulvady R, Gao Y, Kenney LJ, Yan J. 2018. A single molecule analysis of H-NS uncouples DNA binding affinity from DNA specificity. Nucleic Acids Res 46:10216–10224. https://doi.org/10.1093/nar/gky826.
50. Dillon SC, Espinosa E, Hokamp K, Ussery DW, Casadesús J, Dorman CJ. 2012. LeuO is a global regulator of gene expression in *Salmonella enterica* serovar Typhimurium. Mol Microbiol 85:1072–1089. https://doi.org/10.1111/j.1365-2958.2012.08162.x.
51. Yu RR, DiRita VJ. 2002. Regulation of gene expression in *Vibrio cholerae* by ToxT involves both antirepression and RNA polymerase stimulation. Mol Microbiol 43:119–134. https://doi.org/10.1046/j.1365-2958.2002.02721.x.
52. Navarre WW, Halsey TA, Walthers D, Frye J, McClelland M, Potter JL, Kenney LJ, Gunn JS, Fang FC, Libby SJ. 2005. Co-regulation of *Salmonella enterica* genes required for virulence and resistance to antimicrobial peptides by SlyA and PhoP/PhoQ. Mol Microbiol 56:492–508. https://doi.org/10.1111/j.1365-2958.2005.04553.x.
53. Shimada T, Bridier A, Briandet R, Ishihama A. 2011. Novel roles of LeuO in transcription regulation of *E. coli* genome: antagonistic interplay with the universal silencer H-NS. Mol Microbiol 82:378–397. https://doi.org/10.1111/j.1365-2958.2011.07818.x.
54. Kurthkoti K, Tare P, Paitchowdhury R, Gowthami VN, Garcia MJ, Colangeli R, Chatterji D, Nagaraja V, Rodriguez GM. 2015. The mycobacterial iron-dependent regulator IdeR induces ferritin (*bfrB*) by alleviating Lsr2 repression. Mol Microbiol 98:864–877. https://doi.org/10.1111/mmi.13166.
55. Shin M, Song M, Rhee JH, Hong Y, Kim YJ, Seok YJ, Ha KS, Jung SH, Choy HE. 2005. DNA looping-mediated repression by histone-like protein H-NS: specific requirement of Esigma70 as a cofactor for looping. Genes Dev 19:2388–2398. https://doi.org/10.1101/gad.1316305.
56. Jordi BJ, Higgins CF. 2000. The downstream regulatory element of the *proU* operon of *Salmonella typhimurium* inhibits open complex formation by RNA polymerase at a distance. J Biol Chem 275:12123–12128. https://doi.org/10.1074/jbc.275.16.12123.
57. Nagarajavel V, Madhusudan S, Dole S, Rahmouni AR, Schnetz K. 2007. Repression by binding of H-NS within the transcription unit. J Biol Chem 282:23622–23630. https://doi.org/10.1074/jbc.M702753200.
58. Lee DJ, Minchin SD, Busby SJ. 2012. Activating transcription in bacteria. Annu Rev Microbiol 66:125–152. https://doi.org/10.1146/annurev-micro-092611-150012.
59. Zwir I, Latifi T, Perez JC, Huang H, Groisman EA. 2012. The promoter architectural landscape of the *Salmonella* PhoP regulon. Mol Microbiol 84:463–485. https://doi.org/10.1111/j.1365-2958.2012.08036.x.
60. Sanchez A, Osborne ML, Friedman LJ, Kondev J, Gelles J. 2011. Mechanism of transcriptional repression at a bacterial promoter by analysis of single molecules. EMBO J 30:3940–3946. https://doi.org/10.1038/emboj.2011.273.
61. Kinoshita S, Udaka S, Shimono M. 1957. Studies on the amino acid fermentation. Part 1. Production of L-glutamic acid by various microorganisms. J Gen Appl Microbiol 3:193–205. https://doi.org/10.2323/jgam.3.193.
62. Kensy F, Zang E, Faulhammer C, Tan RK, Büchs J. 2009. Validation of a high-throughput fermentation system based on online monitoring of biomass and fluorescence in continuously shaken microtiter plates. Microb Cell Fact 8:31. https://doi.org/10.1186/1475-2859-8-31.
63. Grünberger A, Paczia N, Probst C, Schendzielorz G, Eggeling L, Noack S, Wiechert W, Kohlheyer D. 2012. A disposable picolitre bioreactor for cultivation and investigation of industrially relevant bacteria on the single cell level. Lab Chip 12:2060–2068. https://doi.org/10.1039/c2lc40156h.
64. Sambrook J, Russel DW. 2001. Molecular cloning: a laboratory manual, 3rd ed. Cold Spring Harbor Laboratory Press, Cold Spring Harbor, NY.
65. Gibson DG, Young L, Chuang RY, Venter JC, Hutchison CA, III, Smith HO. 2009. Enzymatic assembly of DNA molecules up to several hundred kilobases. Nat Methods 6:343–345. https://doi.org/10.1038/nmeth.1318.
66. Eikmanns BJ, Thum-Schmitz N, Eggeling L, Ludtke KU, Sahm H. 1994. Nucleotide sequence, expression and transcriptional analysis of the *Corynebacterium glutamicum gltA* gene encoding citrate synthase. Microbiology 140:1817–1828. https://doi.org/10.1099/13500872-140-8-1817.
67. Niebisch A, Bott M. 2001. Molecular analysis of the cytochrome $bc_1$-$aa_3$ branch of the *Corynebacterium glutamicum* respiratory chain containing an unusual diheme cytochrome $c_1$. Arch Microbiol 175:282–294. https://doi.org/10.1007/s002030100262.
68. Ettwiller L, Buswell J, Yigit E, Schildkraut I. 2016. A novel enrichment strategy reveals unprecedented number of novel transcription start sites at single base resolution in a model prokaryote and the gut microbiome. BMC Genomics 17:199. https://doi.org/10.1186/s12864-016-2539-z.
69. Kalinowski J, Bathe B, Bartels D, Bischoff N, Bott M, Burkovski A, Dusch N, Eggeling L, Eikmanns BJ, Gaigalat L, Goesmann A, Hartmann M, Huthmacher K, Krämer R, Linke B, McHardy AC, Meyer F, Möckel B, Pfefferle W, Pühler A, Rey DA, Rückert C, Rupp O, Sahm H, Wendisch VF, Wiegräbe I, Tauch A. 2003. The complete *Corynebacterium glutamicum* ATCC 13032 genome sequence and its impact on the production of L-aspartate-derived amino acids and vitamins. J Biotechnol 104:5–25. https://doi.org/10.1016/s0168-1656(03)00154-8.
70. R Development Core Team. 2016. R: a language and environment for statistical computing. R Foundation for Statistical Computing, Vienna, Austria.

## 3.2. Inducible expression systems based on xenogeneic silencing and counter-silencing and the design of a metabolic toggle switch

**Wiechert, J.**, Gätgens, C., Wirtz, A. and Frunzke, J.

*Manuscript submitted*, 2020.

| Contributor Role | Contributor |
|---|---|
| Conceptualization | JW 70 %, JF 30 % |
| Formal analysis | JW 100 % |
| Investigation/Experiments | JW 70 %, GC 20 %, AW 10 % |
| Methodology | JW 65 %, GC 15 %, AW 10 %, JF 10 % |
| Project administration | JW 70 %, JF 30 % |
| Software | - |
| Supervision | JW 60 %, JF 40 % |
| Visualization | JW 100 % |
| Writing – original draft | JW 90 %, JF 10 % |
| Writing – review & editing | JW 50 %, JF 50 % |

Overall contribution JW: 85 %

All data analyses and the visualization of the data was performed by JW. JW performed most of the presented experimental work or was involved in the execution. GC did the qRT-PCR experiment (Fig. 3C), the microtiter growth experiment with L-valine production strains (Fig 6C) as well as the glucose measurements (Fig S3). The cultivation approaches for comparison of productivity of different L-valine production strains was conducted by GC and JW together. The HPLC measurements were done by JW and AW from the group of Dr. Tino Polen from the Forschungszentrum Jülich. The manuscript text was mainly written by JW.

**Inducible expression systems based on xenogeneic silencing and counter-silencing and the design of a metabolic toggle switch**

Johanna Wiechert[a], Cornelia Gätgens[a], Astrid Wirtz[a], and Julia Frunzke[a,*]

[a]Institut für Bio- und Geowissenschaften, IBG-1: Biotechnologie, Forschungszentrum Jülich, Jülich, Germany

* Address correspondence to Prof. Dr. Julia Frunzke, j.frunzke@fz-juelich.de;

ORCID 0000-0001-6209-7950

Key words: synthetic biology, metabolic toggle switch, synthetic promoter library, expression system, L-valine production, xenogeneic silencing, counter-silencing

## Abstract

Inducible expression systems represent key modules in synthetic regulatory circuit designs and metabolic engineering approaches. However, many established systems are often limited in terms of applications due to high background expression levels and inducer toxicity. In bacteria, xenogeneic silencing (XS) proteins are involved in the tight control of horizontally acquired, AT-rich DNA. The action of XS proteins may be opposed by interference with a specific transcription factor, resulting in the phenomenon of counter-silencing, thereby activating gene expression. In this study, we harnessed this principle for the construction of a synthetic promoter library consisting of phage promoters targeted by an Lsr2-like XS protein of *Corynebacterium glutamicum*. Counter-silencing was achieved by inserting the operator sequence of the gluconate-responsive transcription factor GntR within silenced promoter regions. The GntR-dependent promoter library is comprised of 28 activated and 16 repressed regulatory elements featuring effector-dependent tunability. For selected candidates, background expression levels were confirmed to be significantly reduced in comparison to established heterologous expression systems. Finally, a GntR-dependent genetic toggle switch was implemented in a *C. glutamicum* L-valine production strain allowing the dynamic redirection of carbon flux between biomass and product formation.

.

## Introduction

Inducible expression systems allow the rational and precise control of transcription and are the most frequently used mechanisms for controlling gene expression in synthetic biology and metabolic engineering approaches (Liu et al., 2016; Patek et al., 2013). They usually form the first layer in synthetic regulatory circuits allowing the response to extra- and intracellular stimuli and are applied for the accurate coordination of metabolic fluxes in various microbial production strains (Liu et al., 2016; Xia et al., 2019). In many bacterial model strains, for instance in the industrial platform strain *Corynebacterium glutamicum*, the widely used expression systems $P_{tac}$ (Patek et al., 2013), $P_{araBAD}$ (Ben-Samoun et al., 1999) and $P_{tet}$ (Lausberg et al., 2012; Radmacher et al., 2005) are key parts used for circuit design. They are well established but limited in terms of applications due to considerably high background expression levels, heterogeneous inducer uptake, inducer toxicity or high inducer costs (Baritugo et al., 2018; Patek et al., 2013; Yim et al., 2013; Zhang et al., 2012b). Especially approaches where gene products are toxic to the recipient cell or disturb the central carbon flux are in demand for very stringent control of gene expression (Baritugo et al., 2018). Besides the set of heterologous expression systems, the repertoire of homologous inducible promoter systems is comparatively small for *C. glutamicum* (Binder et al., 2012; Hentschel et al., 2013; Letek et al., 2006; Mustafi et al., 2012; Okibe et al., 2010; Plassmeier et al., 2013) and only a few promoter libraries were constructed containing either constitutive promoters (Rytter et al., 2014; Shang et al., 2018; Yim et al., 2013) or synthetic, Isopropyl-β-D-1-thiogalactopyranoside- (IPTG-) inducible regulatory elements (Rytter et al., 2014).

In a recent project, we designed synthetic promoter constructs for *C. glutamicum,* which were regulated by the mechanisms of xenogeneic silencing and counter-silencing. Xenogeneic silencing is based on specialized nucleoid-associated proteins, so-called xenogeneic silencers (XS), which preferentially bind to horizontally acquired AT-rich DNA (Navarre, 2016; Pfeifer et al., 2019; Will et al., 2015). Known XS proteins are grouped into four classes including H-NS-like XS protein from proteobacteria (Navarre et al., 2006; Oshima et al., 2006), Lsr2-like proteins present in *Actinomycetes* (Gordon et al., 2008), MvaT/U-like XS of gammaproteobacteria of the order *Pseudomonodales* (Tendeng et al., 2003), and Rok found in different *Bacillus* strains (Smits and Grossman, 2010). The major function of the prophage encoded Lsr2-like XS protein CgpS from *C. glutamicum* is the silencing of cryptic prophage elements to maintain their lysogenic state (Pfeifer et al., 2016). CgpS binds to its target promoters and oligomerization of this XS protein leads to the formation of a nucleoprotein complex tightly inhibiting transcription (Pfeifer et al., 2016) (silencing, Figure 1). In our recent study, we inserted the operator site of the regulator of gluconate catabolism GntR at different positions within various CgpS target promoters serving as platforms for the construction of synthetic counter-silencer promoters (Wiechert et al., 2020). Binding of the transcription factor (TF) GntR to its operator

sequence in the absence of gluconate leads to repression of its native target promoter $P_{gntK}$ (Frunzke et al., 2008). In contrast, binding of GntR to the synthetic counter-silencer promoter was shown to interfere with the nucleoprotein complex allowing the RNA polymerase to bind and to initiate transcription (Wiechert et al., 2020) (counter-silencing, Figure 1).

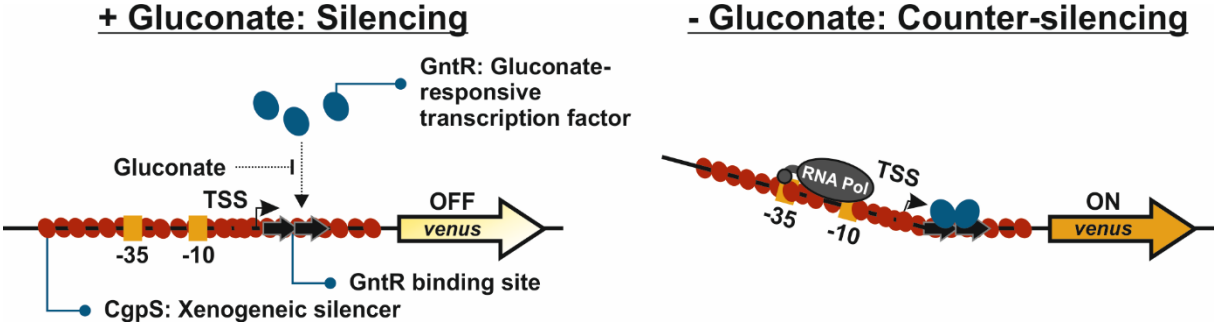


**Figure 1: Schematic overview of the GntR-dependent mechanism of counter-silencing.** Synthetic counter-silencer constructs are based on phage promoters targeted by the xenogeneic silencer CgpS (red ovals). The 15 bp short operator sequence (black arrows) of the regulator of gluconate catabolism GntR (blue ovals) (Frunzke et al., 2008) was inserted within the silenced promoter regions. In the absence of the effector molecule gluconate, binding of GntR to its operator sequence will interfere with the silencer-DNA complex leading to transcription initiation. Adapted from (Wiechert et al., 2020).

Appropriate inducible expression systems are key modules for the design of synthetic regulatory circuits such as toggle switches and are frequently applied in metabolic engineering strategies aiming at improving the performance of bacterial production strains (Xia et al., 2019). Several natural and non-natural biotechnological products such as amino acids, organic acids and alcohols are derived from metabolites from the central carbon metabolism such as the glycolysis and the tricarboxylic acid (TCA) cycle, thereby competing with pathways essential for bacterial growth and physiology (Doong et al., 2018; Gupta et al., 2017; Soma et al., 2014; Soma et al., 2017; Tsuruno et al., 2015). To achieve a redirection of carbon flux towards the molecule of interest, recent rationally engineered production strains were often based on permanent knockouts or knockdowns of genes concerning the central carbon metabolism (Becker et al., 2011; Blombach et al., 2008; Blombach et al., 2007; Hüser et al., 2005; Krause et al., 2010; Litsanov et al., 2012; Peters-Wendisch et al., 2005). This may, however, have detrimental effects on cellular fitness resulting in metabolic imbalances as well as in impaired growth rates and final cell densities, thereby reducing the overall productivity of a fermentation process (Brockman and Prather, 2015b). As an alternative strategy for these static engineering approaches, recent synthetic biology studies aimed at the dynamic redirection of carbon flux between cell growth and product biosynthesis by using metabolic toggle switches or other synthetic genetic circuits for the control of metabolic flux (Brockman and Prather, 2015a; Doong et al., 2018; Farmer and Liao, 2000; Gupta et al., 2017; Lo et al., 2016; Soma et al., 2014; Soma et al., 2017; Tsuruno et al., 2015; Zhang et al., 2012a). For instance, Soma and colleagues constructed a metabolic toggle switch for isopropanol production in *Escherichia coli*. This synthetic genetic circuit allows switching between growth and

production mode by controlling the conditional knockout of the citrate synthase GltA and the simultaneous upregulation of a synthetic isopropanol production pathway, both competing for acetyl-CoA (Soma et al., 2014; Soma et al., 2017). Using a comparable circuit architecture, Tsuruno and colleagues constructed a metabolic toggle switch for the redirection of the central carbon flux from glycerol towards 3-hydroypropionic acid (Tsuruno et al., 2015).

In this work, we systematically tested and compared a broad set of synthetic promoters based on the principle of xenogeneic silencing and counter-silencing. The resulting promoter library comprised 44 synthetic promoters regulated by GntR in a gluconate-dependent manner. Comparison to established expression systems revealed very low background expression and good tunability of the resulting constructs. Finally, a GntR-based genetic toggle switch was implemented in *C. glutamicum* for the dynamic switch between cell growth and L-valine production. By controlling the activity of the pyruvate dehydrogenase complex (PDHC), the redirection of carbon flux towards L-valine biosynthesis was regulated.

## Results and Discussion

### A synthetic promoter library based on the principles of xenogeneic silencing and counter-silencing

Xenogeneic silencing and counter-silencing represent efficient mechanisms for the tight control of gene expression (Wiechert et al., 2020). Following a synthetic counter-silencing approach, we recently demonstrated that binding of the TF GntR within promoters silenced by the XS protein CgpS allows their effector-responsive reactivation (Wiechert et al., 2020). However, depending on the architecture of the phage promoter and the position of the inserted GntR binding site, counter-silencing promoters strongly vary in dynamic range as well as minimal and maximal promoter activities (Wiechert et al., 2020). Here, we systematically tested and compared a broad set of gluconate-dependent, inducible promoters, which are based on the counter-silencing principle. Figure 2 provides an overview of synthetic promoter variants activated by counter-silencing (Figure 2B) or repressed (Figure 2C) by GntR binding (p-values < 0.05). Promoter activity was measured by means of the fluorescence output (production of the Venus reporter protein) over time (Wiechert et al., 2020). Constructs activated by GntR-mediated counter-silencing showed a 100-fold range in maximal reporter output (-gluconate; 0.009 to 0.89 a.u. under the applied conditions) with small increment sizes and a large range of non-induced background levels (+gluconate; ranging from 0.005 to 0.43 a.u. under the applied conditions). Fold-change ratios of the individual promoters (-gluconate/+gluconate) ranged from 1.2-fold to 5-fold. However, not all synthetic promoter variants were activated by GntR binding. Depending on the core promoter part and the position of the binding, GntR binding led to the repression of gene expression in some cases. These constructs showed a 70-fold range in induced expression strength (+gluconate). Remarkably, several synthetic promoter variants appeared to have very low background expression levels. Lowest background expression levels among constructs repressed by GntR binding were observed for $P_{cg1977}$ 0, while the minimum background activity of activated counter-silencer constructs was detected for $P_{priP}$ +5. In *C. glutamicum*, standard systems used for inducible gene expression are heterologous expression systems like the IPTG inducible promoters $P_{lac}$, $P_{tac}$ and $P_{trc}$ (Patek et al., 2013), the arabinose-dependent promoter $P_{araBAD}$ (Ben-Samoun et al., 1999), the anhydrotetracycline inducible promoter $P_{tet}$ (Lausberg et al., 2012; Radmacher et al., 2005) and the heat induced $P_RP_L$ promoter of bacteriophage λ (Tsuchiya and Morinaga, 1988). Remarkably, the set of native inducible promoter systems is comparatively small. Described were promoters induced by gluconate namely $P_{git1}$ (Okibe et al., 2010), $P_{gntK}$ (Hentschel et al., 2013; Letek et al., 2006) and $P_{gntP}$ (Letek et al., 2006), the $P_{malE}$ promoter induced by maltose (Okibe et al., 2010), the propionate inducible $P_{prpD2}$ promoter (Plassmeier et al., 2013) as well as the amino acid responsive biosensors Lrp-$P_{brnFE}$ (Mustafi et al., 2012) and LysG-$P_{lysE}$ (Binder et al., 2012). So far, only a few promoter libraries have been constructed

containing either constitutive promoters (Rytter et al., 2014; Shang et al., 2018; Yim et al., 2013) or synthetic, IPTG-inducible regulatory elements (Rytter et al., 2014).

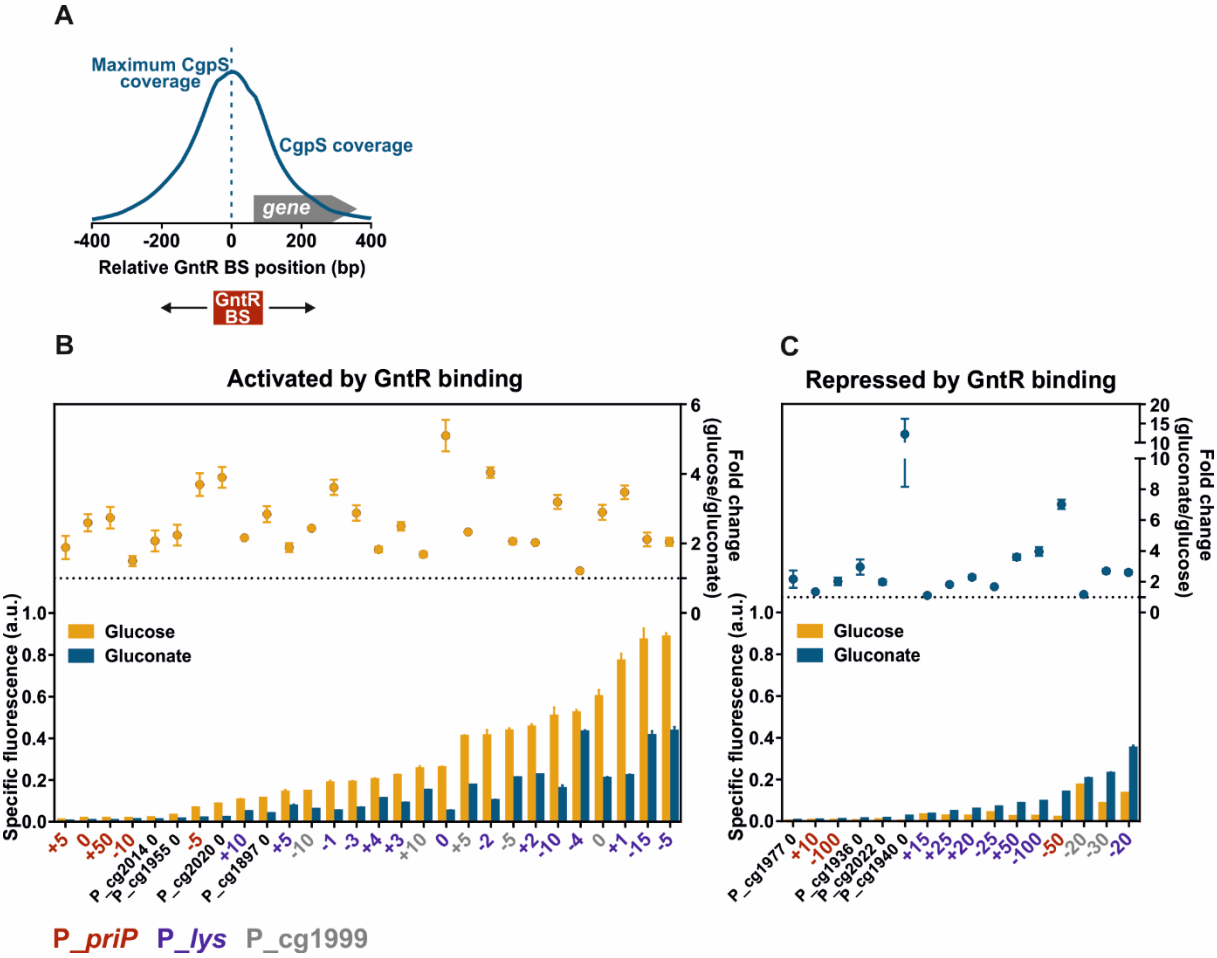


**Figure 2: A synthetic GntR-dependent promoter library based on different CgpS target promoters with inserted GntR binding sites.** The library consists of different recently described counter-silencer promoters (Wiechert et al., 2020) as well as additional promoter variants based on the phage promoter $P_{priP}$ following the same design approach. **A)** Definition of the binding site position. Schematic overview of a representative phage promoter which is bound by CgpS. The positions of the GntR binding site (BS) were referred to the nucleotide position associated with maximal CgpS binding (Pfeifer et al., 2016). The position directly upstream of this nucleotide was defined as position 0, negative numbers describe upstream and positive numbers downstream positions. **B/C)** Shown are reporter outputs driven by the promoters in the presence (gluconate) and absence (glucose) of the effector molecule after five hours of cultivation and the corresponding fold-change ratios. Promoters are grouped into two sets depending on their response to gluconate availability: activation by GntR binding (counter-silencing) **(B)** and repression by GntR binding **(C)** (p-values <0.05). Constructs based on the phage promoter $P_{priP}$, $P_{lys}$, or $P_{cg1999}$ are color-coded and names are reduced to the position of the GntR binding site. Cells harbouring the plasmid-based synthetic promoter constructs were grown in CGXII medium supplemented with either 111/100 mM glucose or 100 mM gluconate. Bars represent the means and error bars the standard deviation of at least three biological replicates. Names indicate the platform promoter and the position of the GntR binding site positions. Specific fluorescence values were background corrected by subtracting values of strains harbouring the control plasmid pJC1-*venus*-term (no promoter in front of *venus*) (Baumgart et al., 2013).

The here presented set of promoters being either activated or repressed by GntR binding provided a gluconate-dependent promoter library covering a broad range of promoter activities which may be highly useful for synthetic biology or metabolic engineering approaches demanding for tightly controlled and inducible regulation of gene expression. In favor for biotechnological applications, the

effector molecule gluconate is a non-toxic, degradable and cost-efficient effector molecule compared to the frequently used inducer IPTG.

## Counter-silencing-based promoters permit tight control of gene expression

To validate the performance of counter-silencing constructs as expression systems, the synthetic promoters $P_{priP}$_CS_0 and $P_{lys}$_CS_0 were exemplarily compared with the native GntR target promoter $P_{gntK}$ and the well-established expression systems $P_{tac}$ and $P_{tet}$ on protein (Venus) and transcript level (*venus* mRNA). Therefore, all promoters were fused to the reporter gene *venus* via a consistent linker containing a ribosomal binding site to avoid differences in translation efficiency and were integrated into the plasmid pJC1. Since the genes encoding for the TFs LacI and TetR are not present in the *C. glutamicum* genome, the *lacI* and *tetR* genes were additionally inserted into the respective plasmids (Figure 3A). Analysis of the reporter levels under inducing and non-inducing conditions revealed a wide range of expression levels for the different constructs (Figure 3B). The lowest background level was observed for the $P_{priP}$-based counter-silencer (6% of $P_{tet}$) which also showed the lowest induced reporter output. The $P_{lys}$ counter-silencer and the native GntR target promoter $P_{gntK}$ showed similar, but inverted response to gluconate availability. Both showed at least 5-fold lower background levels when compared to $P_{tet}$ emphasizing their potential for application demanding stringent control of gene expression (Figure 3B). Similar ranges were observed on transcript levels using quantitative real-time PCR (qRT-PCR). $P_{lys}$_CS_0 and $P_{gntK}$ showed only 44 and 27% of the background level of $P_{tet}$, respectively, and background expression of $P_{priP}$_CS_0 was even reduced to 15% (Figure 3C), confirming that synthetic counter-silencer promoters represent suitable tools for tightly controlled gene expression.

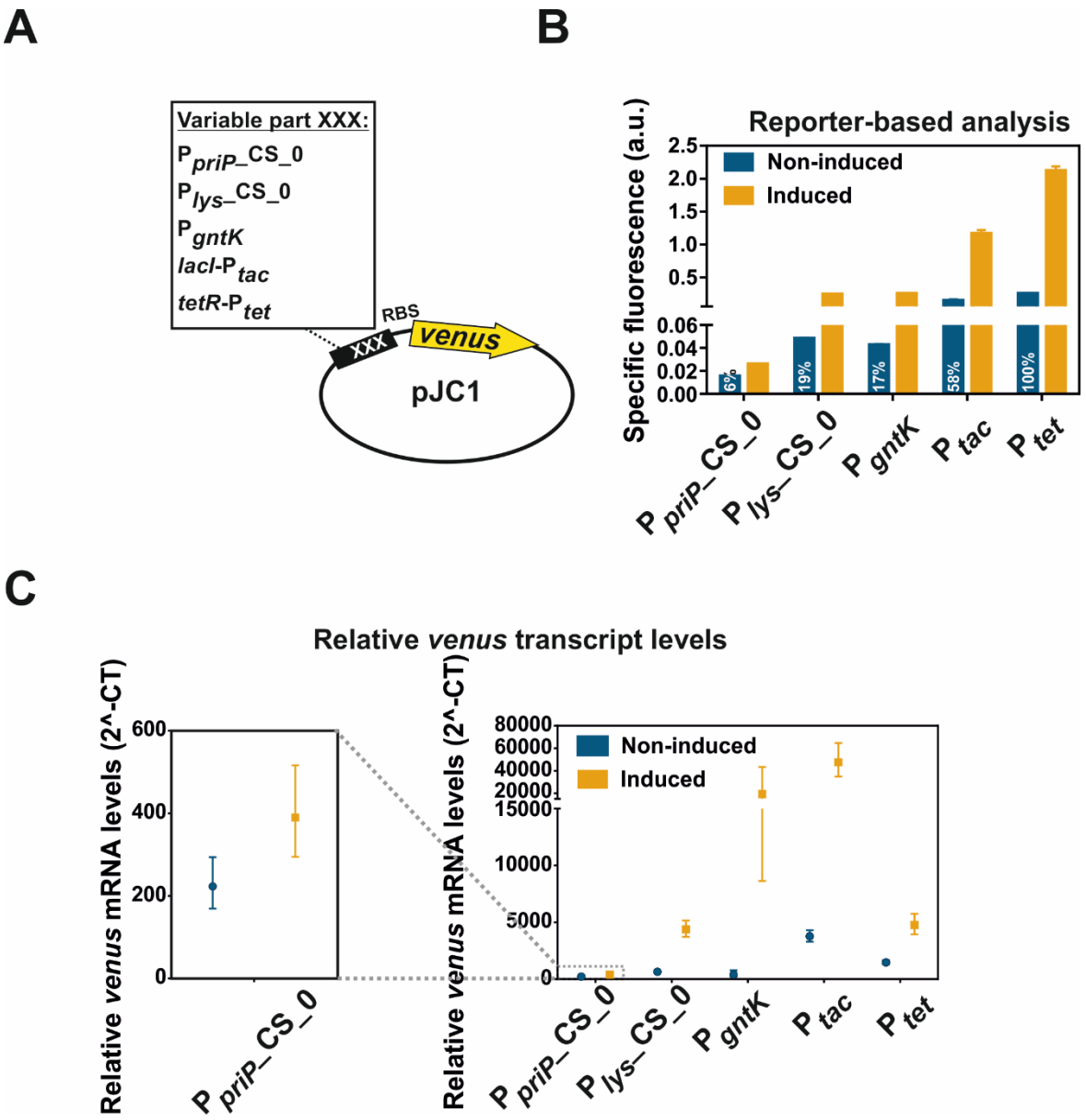


**Figure 3: Comparison of counter-silencing constructs with established expression systems. A)** For the comparison of the counter-silencer constructs $P_{lys}$_CS_0 and $P_{priP}$_CS_0 (Wiechert et al., 2020) as well as the native GntR target promoter $P_{gntK}$ with the established expression systems $P_{tac}$ and $P_{tet}$, all of the different promoters were cloned into the plasmid pJC1 and fused to the reporter gene *venus* via a consistent linker containing a ribosomal binding site (RBS; AGGAG (Pfeifer-Sancar et al., 2013)). *C. glutamicum* wild type cells harbouring the plasmid-based constructs were cultivated in a microtiter cultivation system under inducing and non-inducing conditions depending on the particular promoter construct: $P_{priP}$_CS_0 and $P_{lys}$_CS_0: +: 100 mM glucose, -: 100 mM gluconate; $P_{gntK}$: +: 100 mM gluconate, -: 100 mM glucose; $P_{tac}$: +: 100 µM IPTG, -: 0 µM IPTG; $P_{tet}$: +: 235 nM ATc, -:.0 nM ATc **B)** Reporter outputs of the native GntR target promoter $P_{gntK}$ as well as $P_{priP}$- and $P_{lys}$-based counter-silencer constructs ($P_{priP}$_CS_0; $P_{lys}$_CS_0) in comparison to the established expression systems $P_{tac}$ and $P_{tet}$ after five hours of cultivation. All strains were pre-cultivated in CGXII containing 100 mM gluconate. Bars show the mean and error bars the standard deviation of specific fluorescence of biological triplicates. Indicated numbers represent the percentage of the background expression level of $P_{tet}$. **C)** Promoter-derived relative *venus* transcript levels measured by quantitative real-time PCR after five hours of cultivation under non-inducing and inducing conditions. Symbols represent the means and error bars the range of relative *venus* mRNA levels measured in biological and technical duplicates. All strains were pre-cultivated under non-inducing conditions.

### Tunability of native and synthetic GntR target promoters

Tunability of promoters, for example by varying the amount of effector molecule, is an important feature for their applicability as bacterial expression systems in synthetic and biotechnological applications.

In this study, the impact of varying gluconate concentrations on temporal dynamics and dynamic ranges of promoter activities of the native GntR target promoter $P_{gntK}$ and the counter-silencer promoter $P_{lys}$_CS_0 were characterized. Both promoters inversely react to GntR binding and, therefore, to gluconate availability (Wiechert et al., 2020) (Figure 4). GntR binding within the synthetic counter-silencer promoter $P_{lys}$_CS_0 leads to promoter activation due to efficient interference between GntR and the CgpS-DNA complex (Wiechert et al., 2020). In contrast, binding of GntR to the native target promoter $P_{gntK}$ leads to promoter repression (Frunzke et al., 2008) (Figure 4A).

Highest $P_{lys}$_CS_0-derived reporter outputs were reached in the absence of gluconate (0 mM), meaning that the default state in the absence of the effector molecule of this construct is ON. In contrast, maximal $P_{gntK}$ promoter activity was observed in the presence of highest gluconate concentrations (100 mM), demonstrating the inverted response of both systems (Figure 4B). The default state in the absence of gluconate of $P_{gntK}$ promoter activity is OFF and the signal remained stable in this state after cells had entered the stationary phase (Figure 4B). In contrast, in the presence of 100 mM gluconate, $P_{lys}$_CS_0 promoter activities stayed low during the first 11 hours of cultivations, but reporter outputs strongly increased shortly after cells had entered the stationary phase (Figure S1). At this time point, gluconate was probably fully consumed allowing GntR to bind to the DNA and to interfere with the silencer-DNA complex. Small amounts of 1 mM supplemented gluconate also led to reduced reporter outputs in the beginning of the cultivation, however, the fluorescence signal already increased after two hours of exponential growth phase. Increasing amounts of supplemented gluconate (10 and 50 mM) gradually shifted the time point of induction, demonstrating the potential of counter-silencer promoters as expression systems with temporal tunability (Figure 4B). In contrast, a positive correlation between gluconate concentrations and reporter outputs was observed for $P_{gntK}$ (Figure 4B) demonstrating the opportunity of fine-tuning maximal promoter activity. Comparably to the tunability of maximal $P_{gntK}$ activity by varying the gluconate concentration, the previously designed $P_{tet}$-based expression system pCLTON1 showed an ATc-dependent gradual increase of reporter outputs (Lausberg et al., 2012), while a T7 expression system differentially reacts to increasing amounts of the effector molecule IPTG (Kortmann et al., 2015).

Upon transport into the cell, gluconate is phosphorylated by the gluconate-specific kinase GntK to 6-phosphogluconate which is further metabolized in the pentose phosphate pathway (Frunzke et al., 2008). To reduce degradation rates of the effector molecule gluconate, we deleted the *gntK* gene

encoding for the gluconate kinase GntK. Analysis of activities of the counter-silencer promoter $P_{lys}$_CS_0 in a *C. glutamicum* Δ*gntK* deletion strain revealed the gradual temporal shift of the time point of reporter output increase. However, the time periods of low promoter activity were significantly extended and already 10 mM gluconate led to an almost complete repression of $P_{lys}$_CS_0 promoter activity (Figure 4C, D). On the other hand, constitutively high effector concentrations (Δ*gntK*) led to more than 2.5-fold higher $P_{gntK}$ reporter outputs in comparison to the wild type (Figure 4C, D). The assumed increased and more stable intracellular gluconate levels were only reduced by dilution effects during cell growth comparable to the use of non-degradable structural sugar analogues like IPTG. However, the higher levels of gluconate can affect cell growth of Δ*gntK* (Figure S1), therefore, fine-tuning of effector concentrations must be considered for potential applications of this strain.

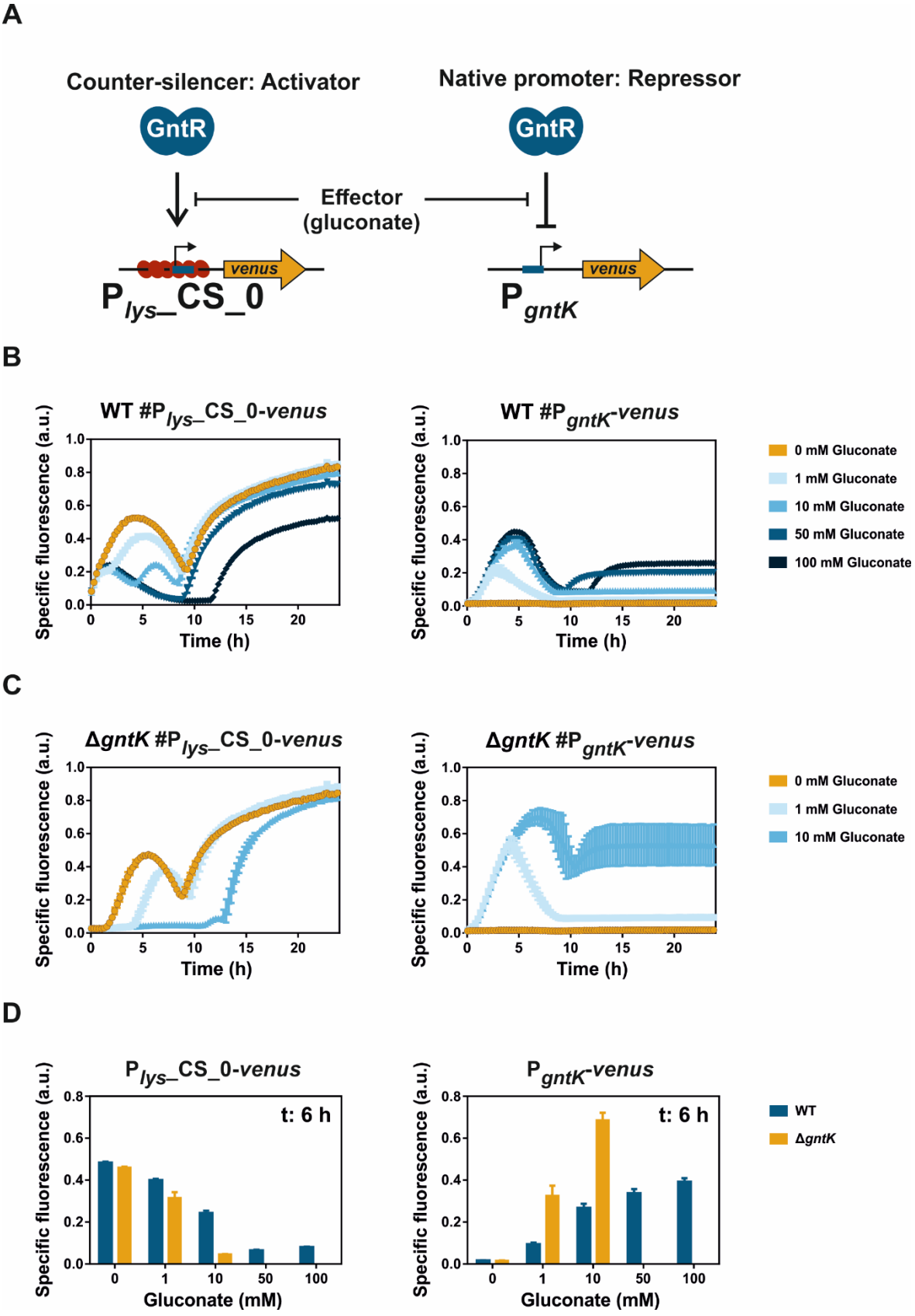


**Figure 4: Tunability of the counter-silencer construct $P_{lys}$_CS_0 and the native GntR target promoter $P_{gntK}$. A)** Shown are schematic overviews of both promoter constructs. **B/C)** Reporter outputs (specific Venus fluorescence) of *C. glutamicum* wild type (WT) **(B)** or *C. glutamicum* strain Δ*gntK* **(C)** harbouring the plasmid-based constructs pJC1-$P_{lys}$_CS_0-*venus* or pJC1-$P_{gntK}$-*venus*. Graphs show the mean and error bars the standard deviation of specific Venus fluorescence of biological triplicates over time. Increasing gluconate concentrations are indicated as shades of blue. **D)** Bar plots show the reporter outputs (specific Venus fluorescence, from B and C) after six hours of cultivation. Cells were cultivated in a microtiter cultivation

system in CGXII medium supplemented with glucose (100 mM in analysis of pJC1-$P_{gntK}$-*venus* and 111 mM for characterization of pJC1-$P_{lys}$_CS_0-*venus*) and either no or varying amounts of gluconate as effector. Backscatter and fluorescence were measured at 15 min intervals. Corresponding backscatter values are given in Figure S1.

## A GntR-based genetic toggle switch

Based on their similar, but inverted response to gluconate availability, the native GntR target promoter $P_{gntK}$ and the synthetic $P_{lys}$ counter-silencing construct ($P_{lys}$_CS_0) were recently combined in a gluconate-dependent, GntR-controlled bistable genetic toggle switch (Wiechert et al., 2020). Switching between different expression states was monitored by fusing the counter-silencer promoter $P_{lys}$_CS_0 to the reporter gene *venus* and the native GntR target promoter $P_{gntK}$ to the reporter gene *e2-crimson* (Figure 5A). Previous analysis of the toggle state and its switching dynamics had confirmed its principal functionality. The addition of gluconate led to a switch in reporter outputs from Venus to E2-Crimson, while the removement of gluconate had the inverted effect (Wiechert et al., 2020). In this study, we characterized the reversibility and robustness of the GntR-dependent toggle system in long-term experiments. Therefore, we cultivated *C. glutamicum* wild type cells harbouring the plasmid-based toggle design in a microfluidic cultivation system starting with continuous supply of CGXII minimal medium containing 100 mM glucose as carbon source. The cells had been in a stable Venus-dominant state until the cultivation medium was switched to medium containing 100 mM gluconate after the first 3.5 hours of cultivation. Gluconate interfered with binding of GntR to its operator site leading to $P_{gntK}$ activation and restoring of silencing of $P_{lys}$_CS_0, visualized by the following switch of the toggle from the Venus- to the E2-Crimson-state within the next eight hours of cultivation. In the following, a stable expression profile was observed demonstrating the robustness of the toggle design. During cultivations, single cells occurred which stayed in one of the both toggle states. However, these cells had also stopped to divide hinting that they were in a dormant state. Three consecutive medium switches revealed the dynamic reversibility of the toggle switch (Figure 5B).

Previously, Gardner and colleagues designed a bistable synthetic toggle switch inspired by the genetic switch of bacteriophage λ governing the lysis-lysogenic decision (Gardner et al., 2000). This network consists of two repressors, namely Cro and CI, and their corresponding promoters $P_R$ and $P_{RM}$, each being repressed by the gene product of the other (Khalil and Collins, 2010). Comparably, in the modular synthetic toggle switch variants constructed by Gardner and colleagues, the authors imitated this circuit design by combining the IPTG-dependent LacI-$P_{trc}$ expression system with the temperature-sensitive λ repressor ($CI_{ts}$) and its corresponding promoter $P_L$slcon or the anhydrotetracycline (ATc) inducible TetR-$P_L$tetO-1 system (Gardner et al., 2000). This design principle was successfully applied as metabolic toggle switch for improving product formation in engineered *E. coli* strains (Soma et al., 2014; Soma et al., 2017; Tsuruno et al., 2015). However, especially inappropriate TF synthesis and

degradation rates and insufficient repressor strengths were discussed as major challenges for toggle stability and functionality (Gardner et al., 2000). In contrast to this circuit architecture, the here presented toggle is controlled by only one effector molecule, namely gluconate, and one specific TF, namely GntR. This design is simple but also very robust and allows the use of native TF levels, thereby circumventing challenges like TF synthesis and degradation rates. Furthermore, due to the circuit architecture, both sides of the toggle are independent of each other allowing tuning of one side of the toggle without affecting the other.

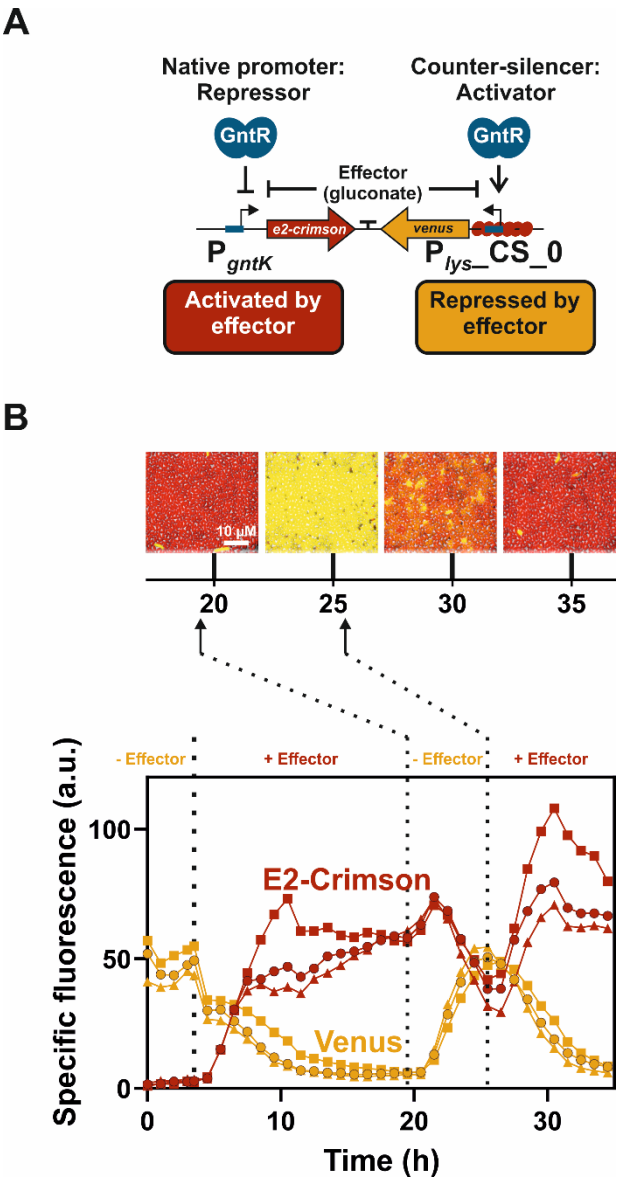


**Figure 5: Reversibility of the GntR-dependent toggle switch. A)** Schematic overview of the GntR-dependent toggle switch (adapted from (Wiechert et al., 2020)). **B)** Reversible switch between both reporter outputs. *C. glutamicum* wild type cells harbouring the plasmid-based toggle were cultivated in a microfluidic cultivation system (Grünberger et al., 2015) with continuous supply of CGXII medium supplemented with either 100 mM glucose or 100 mM gluconate and analyzed by time-lapse microscopy at 15 min intervals. Cells were pre-cultivated in shaking flasks in the absence of the effector molecule gluconate (100 mM glucose). After the first 3.5 h (left dotted vertical line) of cultivation in the microfluidic chip in the absence of gluconate, the medium supply was switched to CGXII supplemented with 100 mM gluconate. Further switches of effector supply were performed after 19.5 and 25.5 h (dotted vertical lines). The graphs show the background corrected specific

fluorescence (Venus and E2-Crimson) of three independent microcolonies (circles, squares, triangles) over time and images display one representative colony (triangle) after 20, 25, 30 and 35 h of cultivation.

### Implementation of a metabolic toggle switch for dynamic control of L-valine production

In a next step, the GntR-dependent toggle switch was implemented for the dynamic control of growth and L-valine biosynthesis in *C. glutamicum*. L-valine, an essential amino acid for human and animals, is used for a variety of application ranging from supplementation in human and animal nutrition, as precursor for herbicides, antibiotics and anti-viral drugs and as compound in cosmetic industries (Oldiges et al., 2014). L-valine is formed from two molecule of the precursor pyruvate in a pathway comprising four reaction steps catalyzed by acetohydroxyacid synthase (AHAS, *ilvBN*), acetohydroxyacid isomeroreductase (AHAIR, *ilvC*), dihydroxyacid dehydratase (DHAD, *ilvD*) and transaminase B (TA, *ilvE*) (Figure 6A). The theoretical yield for L-valine production from glucose is one mol L-valine per mol glucose (Oldiges et al., 2014). Several, previously established L-valine production strains were constructed by engineering the activity of the PDHC, which catalyzes the competing conversion of pyruvate to acetyl-CoA (Figure 6A). Engineering strategies ranged from the deletion of the *aceE* gene encoding the E1 subunit of the enzyme complex, which leads to a permanent PDHC inactivity, to a reduction of *aceE* expression by promoter exchanges (Blombach et al., 2008; Blombach et al., 2007; Buchholz et al., 2013; Ma et al., 2018; Schreiner et al., 2005). Growth of cells with inactive PDHC is decoupled from L-valine production and depends on costly carbon sources like acetate, which enables only low biomass yields (Blombach et al., 2007; Schreiner et al., 2005). After acetate depletion, glucose is consumed and converted to L-valine (Blombach et al., 2007). The dynamic control of precursor supply and of flux through biosynthetic routes, for example by applying synthetic regulatory circuits like the presented GntR-dependent toggle, can represent an alternate strategy to the static permanent knockout approaches. For instance, this design may allow to overcome the growth dependency on acetate.

For the construction of the toggle-based L-valine production strain, the native *aceE* promoter was replaced by the gluconate-dependent promoter $P_{gntK}$. $P_{gntK}$ is repressed in the absence of gluconate leading to PDHC downregulation (Figure 6B). Growth analysis of the $P_{gntK}$-*aceE* strain in comparison to the previously designed Δ*aceE* deletion strain revealed that both strains did not grow in medium containing glucose as sole carbon source for 40 hours of cultivation (Figure 6C). Both strains grew in medium containing glucose and acetate but showed relatively low final backscatter values (Figure 6C). In contrast, the $P_{gntK}$-*aceE* strain reached 3.4-fold higher backscatter values in medium containing 222 mM glucose and 51 mM gluconate in comparison to the acetate-glucose approach (molarity of carbon: 254 mM acetate > 51 mM gluconate, factor 1.7) (Figure 6C). The gluconate-induced *aceE* expression allowed the co-utilization of glucose, as shown by the significantly reduced backscatter values when

cells were cultivated in medium containing only 51 mM gluconate (Figure 6C). Remarkably, no differences in cell growth were observed between *C. glutamicum* $P_{gntK}$-*aceE* and wild type cells in minimal medium containing 100 mM gluconate (Figure S2). The costs for gluconate are in a comparable range as those for glucose, while acetate represents a more costly carbon source (https://www.sigmaaldrich.com, Table S1) highlighting the economic potential of the dynamic gluconate controlled PDHC activity.

Previously applied successful engineering strategies targeting PDHC activity were based on *aceE* promoter replacements leading to reduced or growth phase-dependent *aceE* expression and acetate-independent cell growth (Buchholz et al., 2013; Ma et al., 2018). These approaches were either based on weaker, but constitutive mutated promoter variants of *dapA* (Buchholz et al., 2013) or on a growth-regulated promoter of an industrial used L-leucine strain ($P_{CP\_2836}$; *C. glutamicum* CP) (Ma et al., 2018). However, in contrast to an effector-responsive expression system like the gluconate-dependent promoter $P_{gntK}$ (Figure 4), both regulatory circuits are independent of inducers and cannot be influenced by extracellular supplementation of effector molecules. Thus, fine-tuning of strain performance is constrained, for instance regarding the time point of switching or maximal promoter activities.

In the absence of gluconate, when the PDHC is inactive in the toggle strain, pyruvate is available for L-valine production. Therefore, the counter-silencer $P_{lys}$_CS_0, as counterpart of the toggle, was used to control the overexpression of the L-valine biosynthesis genes *ilvBNCE* (combined in a synthetic operon) (Figure 6B). The plasmid-based construct was analyzed in the dynamic $P_{gntK}$-*aceE* strain and in the static Δ*aceE* deletion strain in comparison to the same strains harbouring the empty plasmid pJC1 (pJC1-*venus*-term) or the previously designed plasmid pJC4-$P_{ilvB}$-*ilvBNC*-$P_{ilvE}$-*ilvE* (pJC4-*ilvBNCE*) (Radmacher et al., 2002). pJC4-$P_{ilvB}$-*ilvBNC*-$P_{ilvE}$-*ilvE* containing L-valine biosynthesis genes under control of their native promoters served as reference for strain performance. For comparison of L-valine productivity, all strains were cultivated in CGXII minimal medium containing 222 mM glucose and 254 mM acetate. This cultivation condition fully erased the benefit of dynamic *aceE* and *ilvBNCE* expression (*aceE*: OFF state; *ilvBNCE*: ON state); however, it allows comparison of strain performance independent of cell densities. Analysis of the culture supernatant revealed that after 46 hours of cultivation glucose was fully consumed by the production strains, while L-valine titers reached maximal values (Figure S3).

Both platform strains $P_{gntK}$-*aceE* and Δ*aceE* produced comparable amounts of L-valine during cultivations in the absence of gluconate indicating that the PDHC was inactive in the toggle strain and that this redirected carbon flux towards L-valine (Figure 6D, Table 1).

The toggle strain $P_{gntK}$-*aceE* #pJC1-$P_{lys}$_CS_0-*ilvBNC*-RBS-*ilvE* produced 1.9-fold higher amounts of L-valine than cells harbouring the empty plasmid pJC1 (Figure 6D, Table 1), confirming the importance of increased levels of biosynthesis enzymes. However, in comparison to the previously characterized plasmid pJC4-$P_{ilvB}$-*ilvBNC*-$P_{ilvE}$-*ilvE* (pJC4-*ilvBNCE*) (Radmacher et al., 2002), L-valine titers were reduced by about 50% in strains Δ*aceE* and $P_{gntK}$-*aceE*. In contrast, pyruvate-derived by-product formation (L-alanine) was 4-5-fold increased (Figure 6D, Table 1). This shift in amino acid concentrations hinted towards limitations in the conversion of pyruvate to L-valine, apparently caused by lower promoter activity of the counter-silencer ($P_{lys}$_CS_0) compared to the native promoters $P_{ilvB}$ and/or $P_{ilvE}$ and the resulting lower enzyme levels. AHAS (*ilvBN*) is the key enzyme of the L-valine biosynthesis pathway and catalyzed the first reaction step. AHAS is feedback inhibited by branched chain amino acids like L-valine (Eggeling et al., 1987; Elišáková et al., 2005) and its biosynthesis intermediate α-ketoisovalerate (Krause et al., 2010). In previous AHAS engineering approaches, a genomically encoded, feedback resistant enzyme variant led to increased L-valine production (Elišáková et al., 2005), suggesting that this reaction step can be a bottleneck for efficient substrate product conversion. Consistently, several engineering approaches succeeded in increasing L-valine titers by increasing the gene dosage of L-valine biosynthesis genes by plasmid-based expression (Blombach et al., 2007; Elišáková et al., 2005; Radmacher et al., 2002; Sahm and Eggeling, 1999).

In conclusion, the production performance of the here presented toggle strain was not optimal in comparison to previously established L-valine production strains, probably due to lower *ilvBNCE* transcription levels. However, the GntR-dependent promoter library contains much stronger counter-silencer promoters (Figure 2) which might represent promising candidates for further toggle strain optimizations.

In the absence of gluconate, both platform strains ($P_{gntK}$-*aceE* and Δ*aceE*) produced comparable amounts of L-valine indicating that the PDHC was inactive in the toggle strain redirecting carbon flux towards L-valine (Figure 6D, Table 1). However, higher cell densities of the *C. glutamicum* $P_{gntK}$-*aceE* strain observed during co-utilization of 222 mM glucose and 51 mM gluconate (Figure 6C) showed on the one hand the potential to overcome growth dependency on costly and inefficient carbon sources like acetate and, on the other hand, the potential to improve substrate product conversion by accelerating biomass formation. Further in-depth analyses of this effect are indispensable for final evaluation of the dynamically controlled $P_{gntK}$-*aceE* strain.

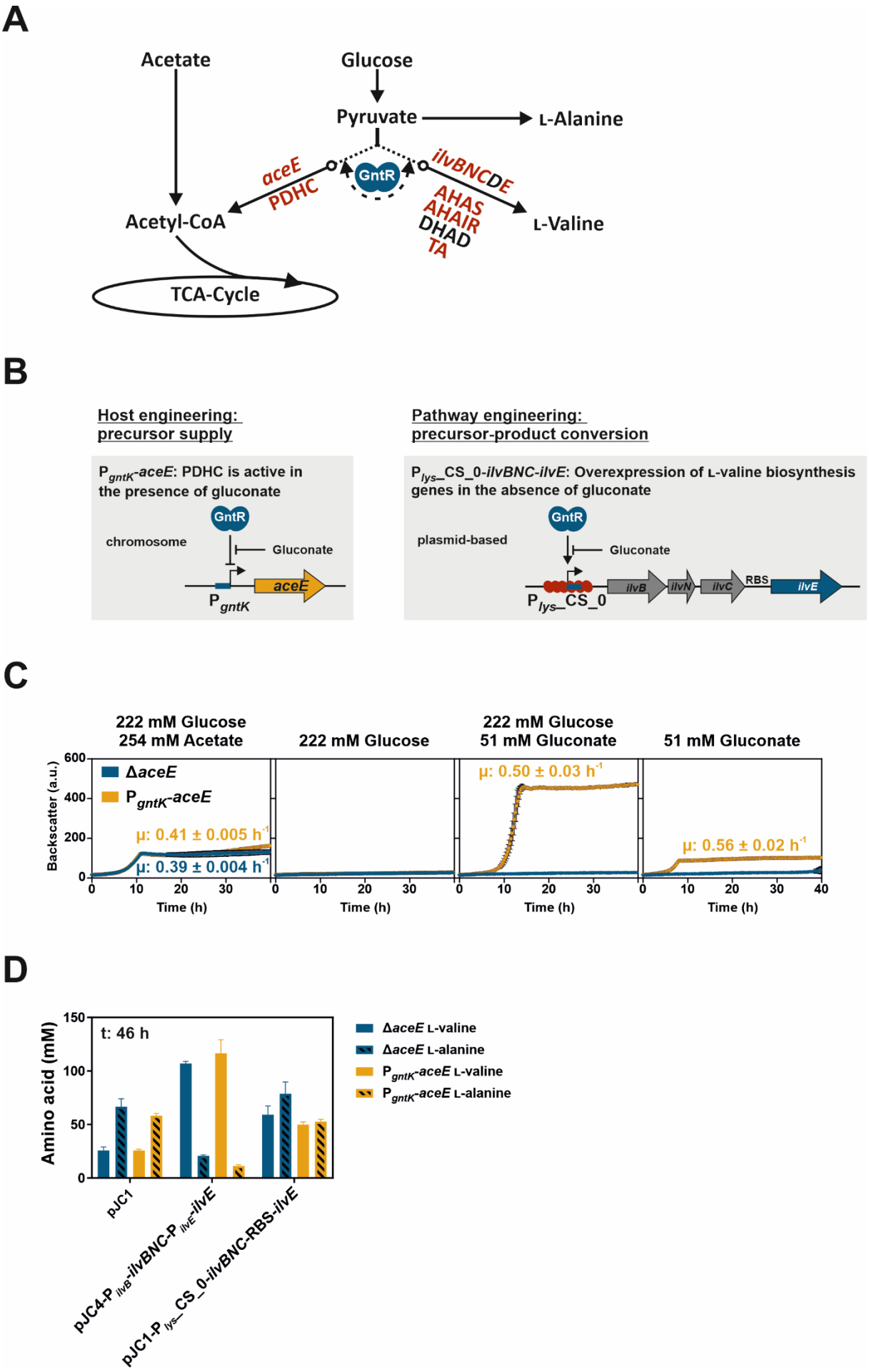
A
Acetate
Glucose
Pyruvate
L-Alanine
aceE
PDHC
GntR
ilvBNCDE
AHAS
AHAIR
DHAD
TA
Acetyl-CoA
L-Valine
TCA-Cycle
B
Host engineering:
precursor supply
Pathway engineering:
precursor-product conversion
PgntK-aceE: PDHC is active in the presence of gluconate
chromosome
GntR
Gluconate
aceE
PgntK
Plys_CS_0-ilvBNC-ilvE: Overexpression of L-valine biosynthesis genes in the absence of gluconate
plasmid-based
GntR
Gluconate
ilvB
ilvN
ilvC
RBS
ilvE
Plys_CS_0
C
222 mM Glucose
254 mM Acetate
222 mM Glucose
222 mM Glucose
51 mM Gluconate
51 mM Gluconate
Backscatter (a.u.)
ΔaceE
PgntK-aceE
μ: 0.41 ± 0.005 h-1
μ: 0.39 ± 0.004 h-1
μ: 0.50 ± 0.03 h-1
μ: 0.56 ± 0.02 h-1
Time (h)
D
Amino acid (mM)
t: 46 h
ΔaceE L-valine
ΔaceE L-alanine
PgntK-aceE L-valine
PgntK-aceE L-alanine
pJC1
pJC4-PilvB-ilvBNC-PilvE-ilvE
pJC1-Plys_CS_0-ilvBNC-RBS-ilvE

**Figure 6: Application of the GntR-dependent toggle for the dynamic switch between growth and L-valine production. A)** Schematic representation of relevant parts of the central carbon metabolism and the L-valine biosynthesis pathway of *C. glutamicum*. The GntR-dependent toggle controlled the redirection of the carbon flux allowing the conversion of pyruvate to either L-valine or acetyl-CoA entering the tricarboxylic acid cycle (TCA-Cycle). *aceE* encodes for the E1 subunit of the pyruvate dehydrogenase complex (PDHC), which converts pyruvate to acetyl-CoA. L-valine is formed from pyruvate in a four-step reaction pathway catalyzed by acetohydroxyacid synthase (AHAS, *ilvBN*), acetohydroxyacid isomeroreductase (AHAIR, *ilvC*), dihydroxyacid dehydratase (DHAD, *ilvD*), and transaminase B (TA, *ilvE*). Dynamically controlled genes and their products are highlighted in red. **B)** Schematic overview of the genetic background of the dynamic L-valine production strain. The native promoter of the *aceE* gene was replaced by the GntR target promoter $P_{gntK}$ allowing control of PDHC activity. The L-valine biosynthesis genes were combined in a synthetic operon by fusing *ilvE* via a linker containing an RBS sequence to the end of the operon *ilvBNC*. Its expression was controlled by the synthetic GntR counter-silencer promoter $P_{lys}$_CS_0. **C)** Growth of the strain with dynamically controlled *aceE* expression ($P_{gntK}$-*aceE*) in comparison to the previously established Δ*aceE* strain (Blombach et al., 2007; Schreiner et al., 2005). Both strains had been pre-cultivated in CGXII containing 222 mM glucose and 254 mM acetate before they were cultivated in a microtiter cultivation system in medium with either 222 mM glucose and 254 mM acetate, 222 mM glucose, 222 mM glucose and 51 mM gluconate or 51 mM gluconate. Calculated growth rates (μ) are given (colour-coded) when significant growth had been observed. **D)** L-valine titers of the *aceE* toggle strain ($P_{gntK}$-*aceE*) and the Δ*aceE* L-valine production strain harbouring either the empty control plasmid pJC1 (pJC1-*venus*-term (Baumgart et al., 2013)), plasmid-based L-valine biosynthesis genes controlled by the counter-silencer (pJC1-$P_{lys}$_CS_0-*ilvBNC*-RBS-*ilvE*) or the natively regulated variant pJC4-$P_{ilvB}$-*ilvBNC*-$P_{ilvE}$-*ilvE* (pJC4-*ilvBNCE*; (Radmacher et al., 2002)). All strains were cultivated in CGXII supplemented with 222 mM glucose and 254 mM acetate. Bar plots represent the L-valine and L-alanine titers of biological triplicates and error bars the corresponding standard deviations after 46 h of cultivation. L-valine and L-alanine titers, glucose concentrations and cell densities ($OD_{600}$) are shown in Figure S3. Further details are given in Table 1.

**Table 1: Product (L-valine) and by-product (L-alanine) formation of strains $P_{gntK}$-*aceE* and Δ*aceE*.** Corresponding bar plots are shown in Figure 6D. Given are the amino acid concentrations, L-valine titers, cell dry weight- (CDW-) specific L-valine titers and L-valine yields after 46 h of cultivation. Means and standard deviations of biological triplicates are listed.

| Plasmid | Strain | $OD_{600}$ | L-valine (mM) | L-alanine (mM) | L-valine titer (g/l) | Specific titer (g L-valine/ g CDW) | Yield (g L-valine/ g glucose) |
|---|---|---|---|---|---|---|---|
| **pJC1** | Δ*aceE* | 45.9 ± 1.0 | 25.9 ± 2.6 | 66.7 ± 6.0 | 3.0 ± 0.31 | 0.26 ± 0.02 | 0.087 ± 0.007 |
| | $P_{gntK}$-*aceE* | 48.7 ± 1.5 | 25.8 ± 0.9 | 58.3 ± 1.8 | 3.0 ± 0.11 | 0.25 ± 0.02 | 0.076 ± 0.003 |
| **pJC4-$P_{ilvB}$-*ilvBNC*-$P_{ilvE}$-*ilvE*** | Δ*aceE* | 41.1 ± 0.8 | 106.9 ± 1.7 | 20.8 ± 0.8 | 12.5 ± 0.2 | 1.22 ± 0.01 | 0.313 ± 0.005 |
| | $P_{gntK}$-*aceE* | 44.3 ± 1.1 | 116.5 ± 10.4 | 11.3 ± 1.0 | 13.7 ± 1.22 | 1.23 ± 0.1 | 0.341 ± 0.03 |
| **pJC1-$P_{lys}$_CS_0-*ilvBNC*-RBS-*ilvE*** | Δ*aceE* | 43.3 ± 0.4 | 59.2 ± 6.7 | 78.8 ± 9.0 | 6.9 ± 0.78 | 0.64 ± 0.07 | 0.175 ± 0.022 |
| | $P_{gntK}$-*aceE* | 46.6 ± 0.1 | 50.0 ± 2.0 | 52.6 ± 1.8 | 5.85 ± 0.24 | 0.5 ± 0.02 | 0.146 ± 0.006 |

## Conclusion

Tightly controlled, inducible promoter systems are key modules in biotechnological and synthetic biological applications and the most frequently used principle for controlling gene expression (Liu et al., 2016; Patek et al., 2013). In this study, we demonstrated the potential of synthetic counter-silencer promoters as expression system allowing a more stringent control of gene expression in comparison to well-established systems such as $P_{tac}$ and $P_{tet}$. These promoters were tightly repressed by CgpS-mediated xenogeneic silencing and significantly induced by GntR-dependent counter-silencing. Synthetic promoter variants were combined in a GntR-dependent bilateral promoter library comprising in total 44 regulatory elements which were repressed (16 promoters) or activated (28 promoters) in the presence of the non-toxic and cheap effector molecule gluconate. These sets of regulatory elements provided a wide range of promoter activities, which could fulfil the requirements of various applications.

The effect of varying effector concentrations on the dynamics and timing of promoter activities was analyzed in detail for exemplary chosen synthetic GntR target promoters revealing that counter-silencer constructs are expression systems with temporal tunability.

Furthermore, we performed a comprehensive characterization and application of a GntR-dependent toggle switch allowing opposed expression of two sets of target genes. This toggle is controlled by only one TF (GntR) and one effector molecule (gluconate) and combines two promoters – a native target promoter and a synthetic counter-silencer promoter – both inversely responsive to gluconate dependent GntR binding (Wiechert et al., 2020). Finally, the GntR-dependent toggle was successfully applied as metabolic toggle switch for the dynamic redirection of carbon flux between the growth-related formation of acetyl-CoA and L-valine biosynthesis, both competing for the precursor molecule pyruvate.

In conclusion, our results demonstrated the high potential of promoters being controlled by xenogeneic silencing counter-silencing for synthetic circuit designs and as tightly controlled gene expression systems.

## Material and Methods

### Bacterial strains and cultivation conditions

All bacterial strains and plasmids used in this project are listed in Table S2, S3 and S4. The strain *C. glutamicum* ATCC 13032 (Kinoshita et al., 1957) served as wild type strain. For cultivations of *C. glutamicum* strains, brain heart infusion (BHI, Difco Laboratories, Detroit, MI, USA) complex medium was inoculated with a single colony from a fresh agar plate and incubated for 8 to 16 hours. For cultivation of Δ*aceE* deletion strains as well as cells with dynamically controlled *aceE* expression ($P_{gntK}$-*aceE*), 85 mM potassium acetate was supplemented to the BHI medium. All cultivation steps were performed at 30°C, 900 rpm and 75% humidity in 96 deep-well plates (VWR, Radnor, PA) in a Microtron incubator shaker (Infors, Bottmingen, Switzerland). For reporter-based assays and analysis of relative *venus* transcript levels driven by the different expression systems, BHI pre-cultures were used to inoculate a second overnight pre-culture in CGXII minimal medium (Keilhauer et al., 1993) supplemented with 25 µg/ml kanamycin and 100 mM gluconate or 100 mM glucose. For growth analysis of Δ*aceE*- and $P_{gntK}$-*aceE*-based strains, the second overnight preculture was performed in CGXII minimal medium containing 222 mM glucose and 254 mM acetate. Subsequently, the pre-culture was used to inoculate the main culture at a start $OD_{600}$ of one. For reporter-based assays, the main cultures were grown in CGXII medium with 25 µg/ml kanamycin and 100 mM gluconate, 100/111 mM glucose without or with varying supplemented amounts of gluconate (0, 1, 10, 50, 100 mM), 100 mM glucose with either 100 µM IPTG (induction of $P_{tac}$) or 235 nM ATc (induction of $P_{tet}$). Growth analysis of the Δ*aceE* deletion strains as well as cells with dynamically controlled *aceE* expression ($P_{gntK}$-*aceE*) was performed in CGXII minimal medium supplemented with either 222 mM glucose and 254 mM acetate, 222 mM glucose, 222 mM glucose and 51 mM gluconate or 51 mM gluconate. *E. coli* DH5α were used for plasmid amplification and cells were cultivated in Lysogeny Broth (LB) medium or on LB agar plates at 37°C. If needed, 50 µg/ml kanamycin was added.

### Microtiter cultivation to monitor cell growth and fluorescence

Analysis of cell growth and reporter-based assays were performed in microliter scale in the BioLector® microcultivation system (m2p-labs, Aachen, Germany) (Kensy et al., 2009). Main cultures with a volume of 750 µl (see Bacterial strains and cultivation conditions) were incubated in 48-well FlowerPlates® (m2p-labs, Aachen, Germany) at 30°C and 1200 rpm. If needed, Venus fluorescence was measured with an excitation wavelength of 508 nm and emission wavelength of 532 nm (signal gain factor 60). Biomass production was measured as backscattered light intensity of sent light with a wavelength of 620 nm (signal gain factor 20). All samples were measured at 15 min intervals. Arbitrary units (a.u.) of specific fluorescence were calculated by dividing the Venus signal by the backscatter

signal per time point (Kensy et al., 2009). Growth rates were determined for the exponential growth phase based on the backscatter signal.

**Microtiter cultivation of L-valine production strains**

For comparison of the productivity of the L-valine production strains Δ*aceE* and $P_{gntK}$-*aceE* harbouring different plasmids, per strain, three single colonies from a fresh agar plate were used to inoculate 4 ml BHI supplemented with 85 mM potassium acetate and 25 µg/ml kanamycin. After 10 hours of cultivation at 30 °C and 160 rpm, 2 ml of the first preculture were transferred into 25 ml CGXII minimal medium supplemented with 222 mM glucose, 154 mM potassium acetate and 25 µg/ml kanamycin. Cultivation of the second preculture was performed at 30 °C and 120 rpm for 13 hours. Subsequently, cells were washed with 20 ml 0.9% NaCl solution and used to inoculate 25 ml CGXII containing 222 mM glucose, 154 mM potassium acetate and 25 µg/ml kanamycin. Cultivation was performed in 96 deep-well plates (VWR, Radnor, PA). Therefore, 15 * 1.5 ml aliquots were transferred into the plates and incubated at 30 °C, 900 rpm and 75% humidity in a Microtron incubator shaker (Infors, Bottmingen, Switzerland). Per sample time point and clone, the 1.5 ml culture volume of one well was transferred into a 2 ml reaction tube. Separation of cells and supernatant was performed by centrifugation for 5 min at 5000 rpm and 4 °C. The supernatant was transferred into a fresh 1.5 ml tube and stored at -20 °C before it was used for quantification of L-valine, L-alanine and glucose concentrations.

**Cultivation in microfluidic chip devices**

For the characterization of reversibility and dynamics of the fluorescence-based GntR-dependent toggle (pJC1-$P_{lys}$_CS_0-*venus*-T-$P_{gntK}$-*e2-crimson*) (Wiechert et al., 2020), *C. glutamicum* wild type cells harbouring the plasmid-based construct were cultivated in an in-house developed microfluidic platform (Grünberger et al., 2012; Grünberger et al., 2015). The experimental setup and chip design was performed as previously described (Grünberger et al., 2013). Venus and E2-Crimson fluorescence as well as phase contrast were imaged at 15 min intervals by fully motorized inverted Nikon Eclipse Ti microscope (Nikon GmbH, Düsseldorf, Germany) as described before (Grünberger et al., 2012; Grünberger et al., 2015; Helfrich et al., 2015). The exposure times for phase contrast was 100 ms, for Venus 200 ms and for E2-Crimson 300 ms. In the microfluidic chip system, cells were cultivated in CGXII medium supplemented with 25 µg/ml kanamycin and either 100 mM gluconate or 100 mM glucose. A high-precision syringe pump system (neMESYS, Cetoni GmbH, Korbussen, Germany) and disposable syringes (Omnifix-F Tuberculin, 1 ml; B. Braun Melsungen AG, Melsungen, Germany) were used to achieve continuous medium supply (flow rate of 200 nl/min) and waste removal during the cultivation. The switches of carbon source supply between gluconate and glucose were performed by changing the syringes and the connecting tubing to ensure an immediate medium switch. The temperature was

set to 30°C using an incubator system (PeCon GmbH, Erbach, Germany). Data analysis on colony level was performed using the image-processing package Fiji (Schindelin et al., 2012) which is based on ImageJ (Rueden et al., 2017). Measured fluorescence data were background normalized and plotted with GraphPad prism 7.00 (GraphPad Software, La Jolla. CA. USA).

**Recombinant DNA work**

All standard molecular methods such as DNA restriction, PCR and Gibson assembly were performed according to manufacturer instructions or following previously described standard protocols (Gibson et al., 2009; Sambrook and Russel, 2001). Details on plasmid construction by Gibson assembly are provided in Table S4. DNA sequencing and synthesis of oligonucleotides used for amplification of DNA fragments for plasmid construction (Table S5) and sequencing (Table S6 and S7) were performed by Eurofins Genomics (Ebersberg, Germany). Chromosomal DNA of *C. glutamicum* ATCC 13032 used as PCR template was prepared as described previously (Eikmanns et al., 1994). $P_{priP}$-based counter-silencer promoters were constructed as previously described (Wiechert et al., 2020).

**Construction of strains Δ*gntK* and $P_{gntK}$-*aceE***

For the deletion of the gene *gntK* encoding the gluconate kinase GntK, *C. glutamicum* ATCC 13032 wild type cells (Kinoshita et al., 1957) were transformed with the pK19mobsacB-Δ*gntK* deletion plasmid (Table S4). The plasmid pK19-*mobsacB*-Δ$P_{aceE}$-*aceE* was used to delete the *aceE* gene and its promoter before the plasmid pK19mobsacB-$P_{gntK}$-*aceE* was used for the re-integration of the *aceE* gene under control of the GntR target promoter $P_{gntK}$ within its native locus. Subsequently, two step homologous recombination and selection was performed as described previously (Niebisch and Bott, 2001). Successful integration was verified by sequencing, all primers are listed in Table S7.

**Quantitative Real-time PCR (qRT-PCR)**

For the comparison of promoter strength of $P_{gntK}$, $P_{lys}$_CS_0 and $P_{priP}$_CS_0 with the established promoter systems $P_{tet}$ and $P_{tac}$ on transcript levels, promoter sequences were cloned into the plasmid pJC1 and fused to the reporter gene *venus* via a consistent linker containing the ribosomal binding site (AGGAG (Pfeifer-Sancar et al., 2013)). Since LacI and TetR are natively not encoded in the chromosome of *C. glutamicum,* the corresponding genes were inserted into the respective plasmids. Duplicates of single clones of *C. glutamicum* wild type cells harbouring the plasmid-based constructs or the control plasmid pJC1-*venus*-term (no appropriate promoter in front of *venus* (Baumgart et al., 2013)) were analyzed. The first BHI pre-culture (see Bacterial strains and cultivation conditions) was used to inoculate the second pre-culture in CGXII medium with either 100 mM gluconate or glucose as carbon source (non-inducing conditions). Cells from the second overnight pre-culture were used to inoculate

1.6 ml of the main culture starting with $OD_{600}$ of one. All cultivation was performed in 96 deep-well plates (VWR, Radnor, PA). Cells harbouring different constructs were cultivated under non-inducing and inducing conditions depending on the particular promoter construct: $P_{priP}$_CS_0 and $P_{lys}$_CS_0: +: 100 mM glucose, -: 100 mM gluconate; $P_{gntK}$: +: 100 mM gluconate, -: 100 mM glucose; $P_{tac}$: +: 100 µM IPTG, -: 0 µM IPTG; $P_{tet}$: +: 235 nM ATc, -: 0 nM ATc. After five hours of incubation, cells were cooled down on ice and harvested by centrifugation (4 °C, 10 min, 11,325g). Cell pellets were snap-frozen in liquid nitrogen and stored at -80 °C until use.

Total RNA was isolated using the Monarch® Total RNA Miniprep Kit (New England Bio Labs, Ipswitch, MA, USA) following the manufacturer protocol. qRT-PCR was performed with 5 ng total RNA and primers listed in Table S8 using the Luna® Universal One-Step RT-qPCR Kit (New England Biolabs, Ipswitch, USA). Measurements of the relative *venus* expression levels were done in biological and technical duplicates with a qTower 2.2 system (Analytik Jena, Jena, Germany). The chromosomal encoded *ddh* gene served as reference gene. The software qPCR-soft 3.1 (Analytik Jena, Jena, Germany) was used for obtaining the corresponding $C_T$-values. Means of relative *venus* expression levels and the corresponding range were calculated based on the 2^(-$C_T$) method of Livak and Schmittgen (Livak and Schmittgen, 2001) using the following equations:

$$\Delta\mathrm{Ct} = \text{mean CT } (venus) - \text{mean CT } (ddh)$$

$$\text{SD } \Delta\mathrm{Ct} = \sqrt{(\text{SD CT } (venus))^2 + (\text{SD CT } (ddh))^2}$$

$$\text{Relative } venus \text{ expression levels} = 2^{-\Delta\mathrm{CT}}$$

Plots in Figure 3C are showing the means of relative *venus* expression levels and error bars their range. Maximum and minimum of the range was calculated by the following equations:

$$\text{Maximum of range for relative } venus \text{ expression levels} = 2^{-(\Delta\mathrm{CT}+\text{SD } \Delta\mathrm{CT})}$$

$$\text{Minimum of range for relative } venus \text{ expression levels} = 2^{-(\Delta\mathrm{CT}-\text{SD } \Delta\mathrm{CT})}$$

**Quantification of amino acid concentrations**

The amino acids L-valine and L-alanine were quantified as ortho-phthaldialdehyde derivatives by using ultra-high performance liquid chromatography (uHPLC) or high performance liquid chromatography (HPLC) with an automatic pre-column derivatization. Derivatives were separated by reverse-phase chromatography using an Agilent 1290 Infinity LC ChemStation or an Agilent 1260 Infinity II LC system (Agilent, Santa Clara, USA) equipped with a fluorescence detector. A gradient of sodium borate buffer (10 mM $Na_2HPO_4$, 10 mM $Na_2B_4O_7$, pH 8.2) and methanol was applied as eluent for the Zorbax Eclipse AAA 3.5 micron 4.6 x 7.5 mm column (Agilent, Santa Clara, USA). Prior to analysis, samples were centrifuged for 5 min at 16,000 x g and were either measured directly or as dilutions of 1:100, 1:400 or 1:1000 in $ddH_2O$.

**Determination of the glucose concentration in the culture supernatant**

Glucose concentrations in the supernatant were measured with the D-Glucose UV-Test Kit (R-Biopharm, Darmstadt, Germany) according to the manufacturer's instructions (absorption was measured at 340 nm) with the modification that measurements were performed with only half of the indicated reaction volume. Glucose concentrations were calculated as described in the manufacturer manual.

## Acknowledgement

We thank the European Research Council (ERC Starting Grant, grant number 757563) and the Helmholtz Association (grant number W2/W3-096) for financial support.

## References

Baritugo, K. A., Kim, H. T., David, Y., Choi, J. I., Hong, S. H., Jeong, K. J., Choi, J. H., Joo, J. C. and Park, S. J. (2018). Metabolic engineering of *Corynebacterium glutamicum* for fermentative production of chemicals in biorefinery. *Appl. Microbiol. Biotechnol. 102*, 3915-3937, doi: *10.1007/s00253-018-8896-6.*

Baumgart, M., Unthan, S., Rückert, C., Sivalingam, J., Grünberger, A., Kalinowski, J., Bott, M., Noack, S. and Frunzke, J. (2013). Construction of a prophage-free variant of *Corynebacterium glutamicum* ATCC 13032 for use as a platform strain for basic research and industrial biotechnology. *Appl. Environ. Microbiol. 79*, 6006-6015, doi: *10.1128/aem.01634-13.*

Becker, J., Zelder, O., Hafner, S., Schroder, H. and Wittmann, C. (2011). From zero to hero--design-based systems metabolic engineering of *Corynebacterium glutamicum* for L-lysine production. *Metab. Eng. 13*, 159-168, doi: *10.1016/j.ymben.2011.01.003.*

Ben-Samoun, K., Leblon, G. and Reyes, O. (1999). Positively regulated expression of the *Escherichia coli araBAD* promoter in *Corynebacterium glutamicum*. *FEMS Microbiol. Lett. 174*, 125-130, doi: *10.1111/j.1574-6968.1999.tb13558.x.*

Binder, S., Schendzielorz, G., Stäbler, N., Krumbach, K., Hoffmann, K., Bott, M. and Eggeling, L. (2012). A high-throughput approach to identify genomic variants of bacterial metabolite producers at the single-cell level. *Genome Biology. 13*, R40, doi: *10.1186/gb-2012-13-5-r40.*

Blombach, B., Schreiner, M. E., Bartek, T., Oldiges, M. and Eikmanns, B. J. (2008). *Corynebacterium glutamicum* tailored for high-yield L-valine production. *Appl. Microbiol. Biotechnol. 79*, 471-479, doi: *10.1007/s00253-008-1444-z.*

Blombach, B., Schreiner, M. E., Holatko, J., Bartek, T., Oldiges, M. and Eikmanns, B. J. (2007). L-valine production with pyruvate dehydrogenase complex-deficient *Corynebacterium glutamicum*. *Appl. Environ. Microbiol. 73*, 2079-2084, doi: *10.1128/AEM.02826-06.*

Brockman, I. M. and Prather, K. L. J. (2015a). Dynamic knockdown of *E. coli* central metabolism for redirecting fluxes of primary metabolites. *Metab. Eng. 28*, 104-113, doi: *10.1016/j.ymben.2014.12.005.*

Brockman, I. M. and Prather, K. L. J. (2015b). Dynamic metabolic engineering: New strategies for developing responsive cell factories. *Biotechnol. J. 10*, 1360-1369, doi: *10.1002/biot.201400422.*

Buchholz, J., Schwentner, A., Brunnenkan, B., Gabris, C., Grimm, S., Gerstmeir, R., Takors, R., Eikmanns, B. J. and Blombach, B. (2013). Platform engineering of *Corynebacterium glutamicum* with

reduced pyruvate dehydrogenase complex activity for improved production of L-lysine, L-valine, and 2-ketoisovalerate. *Appl. Environ. Microbiol. 79*, 5566-5575, doi: *10.1128/aem.01741-13.*

Doong, S. J., Gupta, A. and Prather, K. L. J. (2018). Layered dynamic regulation for improving metabolic pathway productivity in *Escherichia coli*. *Proc. Natl. Acad. Sci. U. S. A. 115*, 2964-2969, doi: *10.1073/pnas.1716920115.*

Eggeling, I., Cordes, C., Eggeling, L. and Sahm, H. (1987). Regulation of acetohydroxy acid synthase in *Corynebacterium glutamicum* during fermentation of α-ketobutyrate to l-isoleucine. *Appl. Microbiol. Biotechnol. 25*, 346-351, doi: *10.1007/BF00252545.*

Eikmanns, B. J., Thum-Schmitz, N., Eggeling, L., Ludtke, K. U. and Sahm, H. (1994). Nucleotide sequence, expression and transcriptional analysis of the *Corynebacterium glutamicum gltA* gene encoding citrate synthase. *Microbiology. 140 ( Pt 8)*, 1817-1828, doi: *10.1099/13500872-140-8-1817.*

Elišáková, V., Pátek, M., Holátko, J., Nešvera, J., Leyval, D., Goergen, J.-L. and Delaunay, S. (2005). Feedback-resistant acetohydroxy acid synthase increases valine production in *Corynebacterium glutamicum*. *Appl. Environ. Microbiol. 71*, 207-213, doi: *10.1128/AEM.71.1.207-213.2005.*

Farmer, W. R. and Liao, J. C. (2000). Improving lycopene production in *Escherichia coli* by engineering metabolic control. *Nat. Biotechnol. 18*, 533-537, doi: *10.1038/75398.*

Frunzke, J., Engels, V., Hasenbein, S., Gatgens, C. and Bott, M. (2008). Co-ordinated regulation of gluconate catabolism and glucose uptake in *Corynebacterium glutamicum* by two functionally equivalent transcriptional regulators, GntR1 and GntR2. *Mol. Microbiol. 67*, 305-322, doi: *10.1111/j.1365-2958.2007.06020.x.*

Gardner, T. S., Cantor, C. R. and Collins, J. J. (2000). Construction of a genetic toggle switch in *Escherichia coli*. *Nature. 403*, 339-342, doi: *10.1038/35002131.*

Gibson, D. G., Young, L., Chuang, R. Y., Venter, J. C., Hutchison, C. A., 3rd and Smith, H. O. (2009). Enzymatic assembly of DNA molecules up to several hundred kilobases. *Nat. Methods. 6*, 343-345, doi: *10.1038/nmeth.1318.*

Gordon, B. R., Imperial, R., Wang, L., Navarre, W. W. and Liu, J. (2008). Lsr2 of *Mycobacterium* represents a novel class of H-NS-like proteins. *J. Bacteriol. 190*, 7052-7059, doi: *10.1128/JB.00733-08.*

Grünberger, A., Paczia, N., Probst, C., Schendzielorz, G., Eggeling, L., Noack, S., Wiechert, W. and Kohlheyer, D. (2012). A disposable picolitre bioreactor for cultivation and investigation of industrially relevant bacteria on the single cell level. *Lab Chip. 12*, 2060-2068, doi: *10.1039/c2lc40156h.*

Grünberger, A., Probst, C., Helfrich, S., Nanda, A., Stute, B., Wiechert, W., von Lieres, E., Nöh, K., Frunzke, J. and Kohlheyer, D. (2015). Spatiotemporal microbial single-cell analysis using a high-throughput microfluidics cultivation platform. *Cytometry A. 87*, 1101-1115, doi: *10.1002/cyto.a.22779.*

Grünberger, A., Probst, C., Heyer, A., Wiechert, W., Frunzke, J. and Kohlheyer, D. (2013). Microfluidic picoliter bioreactor for microbial single-cell analysis: fabrication, system setup, and operation. *J. Vis. Exp.*, e50560, doi: *10.3791/50560.*

Gupta, A., Reizman, I. M., Reisch, C. R. and Prather, K. L. (2017). Dynamic regulation of metabolic flux in engineered bacteria using a pathway-independent quorum-sensing circuit. *Nat. Biotechnol. 35*, 273-279, doi: *10.1038/nbt.3796.*

Helfrich, S., Pfeifer, E., Krämer, C., Sachs, C. C., Wiechert, W., Kohlheyer, D., Nöh, K. and Frunzke, J. (2015). Live cell imaging of SOS and prophage dynamics in isogenic bacterial populations. *Mol. Microbiol. 98*, 636-650, doi: *10.1111/mmi.13147.*

Hentschel, E., Will, C., Mustafi, N., Burkovski, A., Rehm, N. and Frunzke, J. (2013). Destabilized eYFP variants for dynamic gene expression studies in *Corynebacterium glutamicum*. *Microb. Biotechnol. 6*, 196-201, doi: *10.1111/j.1751-7915.2012.00360.x.*

Hüser, A. T., Chassagnole, C., Lindley, N. D., Merkamm, M., Guyonvarch, A., Elišáková, V., Pátek, M., Kalinowski, J., Brune, I., Pühler, A. and Tauch, A. (2005). Rational design of a *Corynebacterium*

*glutamicum* pantothenate production strain and its characterization by metabolic flux analysis and gnome-wide transcriptional profiling. *Appl. Environ. Microbiol. 71*, 3255-3268, doi: *10.1128/AEM.71.6.3255-3268.2005*

Keilhauer, C., Eggeling, L. and Sahm, H. (1993). Isoleucine synthesis in *Corynebacterium glutamicum*: molecular analysis of the *ilvB-ilvN-ilvC* operon. *J. Bacteriol. 175*, 5595-5603,

Kensy, F., Zang, E., Faulhammer, C., Tan, R. K. and Büchs, J. (2009). Validation of a high-throughput fermentation system based on online monitoring of biomass and fluorescence in continuously shaken microtiter plates. *Microb. Cell Fact. 8*, 31, doi: *10.1186/1475-2859-8-31.*

Khalil, A. S. and Collins, J. J. (2010). Synthetic biology: applications come of age. *Nat. Rev. Genet. 11*, 367-379, doi: *10.1038/nrg2775.*

Kinoshita, S., Udaka, S. and Shimono, M. (1957). Studies on the amino acid fermentation. Part 1. Production of L-glutamic acid by various microorganisms. *J. Gen. Appl. Microbiol. 3*, 193-205, doi: *10.2323/jgam.3.193.*

Kortmann, M., Kuhl, V., Klaffl, S. and Bott, M. (2015). A chromosomally encoded T7 RNA polymerase-dependent gene expression system for *Corynebacterium glutamicum*: construction and comparative evaluation at the single-cell level. *Microb. Biotechnol. 8*, 253-265, doi: *10.1111/1751-7915.12236.*

Krause, F. S., Blombach, B. and Eikmanns, B. J. (2010). Metabolic engineering of *Corynebacterium glutamicum* for 2-ketoisovalerate production. *Appl. Environ. Microbiol. 76*, 8053-8061, doi: *10.1128/AEM.01710-10.*

Lausberg, F., Chattopadhyay, A. R., Heyer, A., Eggeling, L. and Freudl, R. (2012). A tetracycline inducible expression vector for *Corynebacterium glutamicum* allowing tightly regulable gene expression. *Plasmid. 68*, 142-147, doi: *10.1016/j.plasmid.2012.05.001.*

Letek, M., Valbuena, N., Ramos, A., Ordonez, E., Gil, J. A. and Mateos, L. M. (2006). Characterization and use of catabolite-repressed promoters from gluconate genes in *Corynebacterium glutamicum*. *J. Bacteriol. 188*, 409-423, doi: *10.1128/jb.188.2.409-423.2006.*

Litsanov, B., Kabus, A., Brocker, M. and Bott, M. (2012). Efficient aerobic succinate production from glucose in minimal medium with *Corynebacterium glutamicum*. *Microb. Biotechnol. 5*, 116-128, doi: *10.1111/j.1751-7915.2011.00310.x.*

Liu, X., Yang, Y., Zhang, W., Sun, Y., Peng, F., Jeffrey, L., Harvey, L., McNeil, B. and Bai, Z. (2016). Expression of recombinant protein using *Corynebacterium glutamicum*: progress, challenges and applications. *Crit. Rev. Biotechnol. 36*, 652-664, doi: *10.3109/07388551.2015.1004519.*

Livak, K. J. and Schmittgen, T. D. (2001). Analysis of relative gene expression data using real-time quantitative PCR and the 2(-Delta Delta C(T)) Method. *Methods. 25*, 402-408, doi: *10.1006/meth.2001.1262.*

Lo, T. M., Chng, S. H., Teo, W. S., Cho, H. S. and Chang, M. W. (2016). A two-layer gene circuit for decoupling cell growth from metabolite production. *Cell Syst. 3*, 133-143, doi: *10.1016/j.cels.2016.07.012.*

Ma, Y., Cui, Y., Du, L., Liu, X., Xie, X. and Chen, N. (2018). Identification and application of a growth-regulated promoter for improving L-valine production in *Corynebacterium glutamicum*. *Microb. Cell Fact. 17*, 185, doi: *10.1186/s12934-018-1031-7.*

Mustafi, N., Grünberger, A., Kohlheyer, D., Bott, M. and Frunzke, J. (2012). The development and application of a single-cell biosensor for the detection of L-methionine and branched-chain amino acids. *Metab. Eng. 14*, 449-457, doi: *10.1016/j.ymben.2012.02.002.*

Navarre, W. W. (2016). The impact of gene silencing on horizontal gene transfer and bacterial evolution. *Adv. Microb. Physiol. 69*, 157-186, doi: *10.1016/bs.ampbs.2016.07.004.*

Navarre, W. W., Porwollik, S., Wang, Y., McClelland, M., Rosen, H., Libby, S. J. and Fang, F. C. (2006). Selective silencing of foreign DNA with low GC content by the H-NS protein in *Salmonella*. *Science. 313*, 236-238, doi: *10.1126/science.1128794.*

Niebisch, A. and Bott, M. (2001). Molecular analysis of the cytochrome $bc_1$-$aa_3$ branch of the *Corynebacterium glutamicum* respiratory chain containing an unusual diheme cytochrome $c_1$. *Arch. Microbiol. 175*, 282-294,

Okibe, N., Suzuki, N., Inui, M. and Yukawa, H. (2010). Isolation, evaluation and use of two strong, carbon source-inducible promoters from *Corynebacterium glutamicum*. *Lett. Appl. Microbiol. 50*, 173-180, doi: *10.1111/j.1472-765X.2009.02776.x.*

Oldiges, M., Eikmanns, B. J. and Blombach, B. (2014). Application of metabolic engineering for the biotechnological production of L-valine. *Appl. Microbiol. Biotechnol. 98*, 5859-5870, doi: *10.1007/s00253-014-5782-8.*

Oshima, T., Ishikawa, S., Kurokawa, K., Aiba, H. and Ogasawara, N. (2006). *Escherichia coli* histone-like protein H-NS preferentially binds to horizontally acquired DNA in association with RNA polymerase. *DNA Res. 13*, 141-153, doi: *10.1093/dnares/dsl009.*

Patek, M., Holatko, J., Busche, T., Kalinowski, J. and Nesvera, J. (2013). *Corynebacterium glutamicum* promoters: a practical approach. *Microb. Biotechnol. 6*, 103-117, doi: *10.1111/1751-7915.12019.*

Peters-Wendisch, P., Stolz, M., Etterich, H., Kennerknecht, N., Sahm, H. and Eggeling, L. (2005). Metabolic engineering of *Corynebacterium glutamicum* for L-Serine production. *Appl. Environ. Microbiol. 71*, 7139-7144, doi: *10.1128/AEM.71.11.7139-7144.2005.*

Pfeifer-Sancar, K., Mentz, A., Rückert, C. and Kalinowski, J. (2013). Comprehensive analysis of the *Corynebacterium glutamicum* transcriptome using an improved RNAseq technique. *BMC genomics. 14*, 888-888, doi: *10.1186/1471-2164-14-888.*

Pfeifer, E., Hünnefeld, M., Popa, O. and Frunzke, J. (2019). Impact of xenogeneic silencing on phage-host interactions. *J Mol Biol. 431*, 4670-4683, doi: *10.1016/j.jmb.2019.02.011.*

Pfeifer, E., Hünnefeld, M., Popa, O., Polen, T., Kohlheyer, D., Baumgart, M. and Frunzke, J. (2016). Silencing of cryptic prophages in *Corynebacterium glutamicum*. *Nucleic Acids Res. 44*, 10117-10131, doi: *10.1093/nar/gkw692.*

Plassmeier, J. K., Busche, T., Molck, S., Persicke, M., Puhler, A., Ruckert, C. and Kalinowski, J. (2013). A propionate-inducible expression system based on the *Corynebacterium glutamicum prpD2* promoter and PrpR activator and its application for the redirection of amino acid biosynthesis pathways. *J. Biotechnol. 163*, 225-232, doi: *10.1016/j.jbiotec.2012.08.009.*

Radmacher, E., Stansen, K. C., Besra, G. S., Alderwick, L. J., Maughan, W. N., Hollweg, G., Sahm, H., Wendisch, V. F. and Eggeling, L. (2005). Ethambutol, a cell wall inhibitor of *Mycobacterium tuberculosis*, elicits L-glutamate efflux of *Corynebacterium glutamicum*. *Microbiology. 151*, 1359-1368, doi: *10.1099/mic.0.27804-0.*

Radmacher, E., Vaitsikova, A., Burger, U., Krumbach, K., Sahm, H. and Eggeling, L. (2002). Linking central metabolism with increased pathway flux: L-valine accumulation by *Corynebacterium glutamicum*. *Appl. Environ. Microbiol. 68*, 2246-2250, doi: *10.1128/aem.68.5.2246-2250.2002.*

Rueden, C. T., Schindelin, J., Hiner, M. C., DeZonia, B. E., Walter, A. E., Arena, E. T. and Eliceiri, K. W. (2017). ImageJ2: ImageJ for the next generation of scientific image data. *BMC Bioinformatics. 18*, 529, doi: *10.1186/s12859-017-1934-z.*

Rytter, J. V., Helmark, S., Chen, J., Lezyk, M. J., Solem, C. and Jensen, P. R. (2014). Synthetic promoter libraries for *Corynebacterium glutamicum*. *Appl. Microbiol. Biotechnol. 98*, 2617-2623, doi: *10.1007/s00253-013-5481-x.*

Sahm, H. and Eggeling, L. (1999). D-Pantothenate synthesis in *Corynebacterium glutamicum* and use of *panBC* and genes encoding L-valine synthesis for D-pantothenate overproduction. *Appl. Environ. Microbiol. 65*, 1973-1979,

Sambrook, J. and Russel, W. D., 2001. Molecular Cloning: A Laboratory Manual (3rd edition). Cold Spring Harbor Laboratory Press, Cold Spring Harbor, NY.

Schindelin, J., Arganda-Carreras, I., Frise, E., Kaynig, V., Longair, M., Pietzsch, T., Preibisch, S., Rueden, C., Saalfeld, S., Schmid, B., Tinevez, J. Y., White, D. J., Hartenstein, V., Eliceiri, K., Tomancak, P. and Cardona, A. (2012). Fiji: an open-source platform for biological-image analysis. *Nat. Methods. 9*, 676-682, doi: *10.1038/nmeth.2019.*

Schreiner, M. E., Fiur, D., Holatko, J., Patek, M. and Eikmanns, B. J. (2005). E1 enzyme of the pyruvate dehydrogenase complex in *Corynebacterium glutamicum*: molecular analysis of the gene and phylogenetic aspects. *J. Bacteriol. 187*, 6005-6018, doi: *10.1128/JB.187.17.6005-6018.2005.*

Shang, X., Chai, X., Lu, X., Li, Y., Zhang, Y., Wang, G., Zhang, C., Liu, S., Zhang, Y., Ma, J. and Wen, T. (2018). Native promoters of *Corynebacterium glutamicum* and its application in L-lysine production. *Biotechnol. Lett. 40*, 383-391, doi: *10.1007/s10529-017-2479-y.*

Smits, W. K. and Grossman, A. D. (2010). The transcriptional regulator Rok binds A+T-rich DNA and is involved in repression of a mobile genetic element in *Bacillus subtilis*. *PLoS Genet. 6*, e1001207, doi: *10.1371/journal.pgen.1001207.*

Soma, Y., Tsuruno, K., Wada, M., Yokota, A. and Hanai, T. (2014). Metabolic flux redirection from a central metabolic pathway toward a synthetic pathway using a metabolic toggle switch. *Metab. Eng. 23*, 175-184, doi: *10.1016/j.ymben.2014.02.008.*

Soma, Y., Yamaji, T., Matsuda, F. and Hanai, T. (2017). Synthetic metabolic bypass for a metabolic toggle switch enhances acetyl-CoA supply for isopropanol production by *Escherichia coli*. *J. Biosci. Bioeng. 123*, 625-633, doi: *10.1016/j.jbiosc.2016.12.009.*

Tendeng, C., Soutourina, O. A., Danchin, A. and Bertin, P. N. (2003). MvaT proteins in *Pseudomonas spp.*: a novel class of H-NS-like proteins. *Microbiology. 149*, 3047-3050, doi: *10.1099/mic.0.C0125-0.*

Tsuchiya, M. and Morinaga, Y. (1988). Genetic control systems of *Escherichia coli* can confer inducible expression of cloned genes in coryneform bacteria. *Bio/Technology. 6*, 428-430, doi: *10.1038/nbt0488-428.*

Tsuruno, K., Honjo, H. and Hanai, T. (2015). Enhancement of 3-hydroxypropionic acid production from glycerol by using a metabolic toggle switch. *Microb. Cell Fact. 14*, 155, doi: *10.1186/s12934-015-0342-1.*

Wiechert, J., Filipchyk, A., Hünnefeld, M., Gätgens, C., Brehm, J., Heermann, R. and Frunzke, J. (2020). Deciphering the rules underlying xenogeneic silencing and counter-silencing of Lsr2-like proteins using CgpS of *Corynebacterium glutamicum* as a model. *mbio. 11*, e02273-02219, doi: *10.1128/mBio.02273-19*

Will, W. R., Navarre, W. W. and Fang, F. C. (2015). Integrated circuits: how transcriptional silencing and counter-silencing facilitate bacterial evolution. *Curr Opin Microbiol. 23*, 8-13, doi: *10.1016/j.mib.2014.10.005.*

Xia, P. F., Ling, H., Foo, J. L. and Chang, M. W. (2019). Synthetic genetic circuits for programmable biological functionalities. *Biotechnol. Adv. 37*, 107393, doi: *10.1016/j.biotechadv.2019.04.015.*

Yim, S. S., An, S. J., Kang, M., Lee, J. and Jeong, K. J. (2013). Isolation of fully synthetic promoters for high-level gene expression in *Corynebacterium glutamicum*. *Biotechnol. Bioeng. 110*, 2959-2969, doi: *10.1002/bit.24954.*

Zhang, F., Carothers, J. M. and Keasling, J. D. (2012a). Design of a dynamic sensor-regulator system for production of chemicals and fuels derived from fatty acids. *Nat. Biotechnol. 30*, 354-359, doi: *10.1038/nbt.2149.*

Zhang, Y., Shang, X., Lai, S., Zhang, G., Liang, Y. and Wen, T. (2012b). Development and application of an arabinose-inducible expression system by facilitating inducer uptake in *Corynebacterium glutamicum*. *Appl. Environ. Microbiol. 78*, 5831-5838, doi: *10.1128/aem.01147-12.*

## 3.3. Impact of $CO_2$/$HCO_3^-$ availability on anaplerotic flux in pyruvate dehydrogenase complex-deficient *Corynebacterium glutamicum* strains.

Krüger, A.*, **Wiechert, J.***, Gätgens, C., Polen, T., Mahr, R. and Frunzke, J.

* *These authors contributed equally to this work.*

Published in *Journal of Bacteriology*, 2019.

| **Contributor Role** | **Contributor** |
|---|---|
| Conceptualization | AK 20 %, JW 30 %, RM 20 %, JF 30 % |
| Formal Analysis | AK 75 %, RM 20 %, TP 5 % |
| Investigation/Experiments | AK 80 %, CG 10 %, RM 10 % |
| Methodology | AK 25 %, JW 25 %, GC 10 %, RM 15 %, JF 25 % |
| Project Administration | JW 70 %, JF 30 % |
| Software | TP 100 % |
| Supervision | JW 70 %, JF 30 % |
| Visualization | AK 100 % |
| Writing – Original Draft Preparation | AK 10 %, JW 10 %, JF 80 % |
| Writing – Reviewing & Editing | AK 20 %, JW 10 %, JF 70 % |

Overall contribution JW: 30 %

JW was involved in planning of most of the experimental work. Experiments were mainly conducted by AK during her Master thesis time which was supervised by JW.

AMERICAN SOCIETY FOR MICROBIOLOGY | Journal of Bacteriology®

RESEARCH ARTICLE

# Impact of $CO_2/HCO_3^-$ Availability on Anaplerotic Flux in Pyruvate Dehydrogenase Complex-Deficient *Corynebacterium glutamicum* Strains

**Aileen Krüger,[a] Johanna Wiechert,[a] Cornelia Gätgens,[a] Tino Polen,[a] Regina Mahr,[b] Julia Frunzke[a]**

[a]Institut für Bio- und Geowissenschaften, IBG-1: Biotechnology, Forschungszentrum Jülich, Jülich, Germany
[b]SenseUp GmbH, Forschungszentrum Jülich, Jülich, Germany

**ABSTRACT** The pyruvate dehydrogenase complex (PDHC) catalyzes the oxidative decarboxylation of pyruvate, yielding acetyl coenzyme A (acetyl-CoA) and $CO_2$. The PDHC-deficient *Corynebacterium glutamicum* Δ*aceE* strain therefore lacks an important decarboxylation step in its central metabolism. Additional inactivation of *pyc*, encoding pyruvate carboxylase, resulted in a >15-h lag phase in the presence of glucose, while no growth defect was observed on gluconeogenetic substrates, such as acetate. Growth was successfully restored by deletion of *ptsG*, encoding the glucose-specific permease of the phosphotransferase system (PTS), thereby linking the observed phenotype to the increased sensitivity of the Δ*aceE* Δ*pyc* strain to glucose catabolism. In this work, the Δ*aceE* Δ*pyc* strain was used to systematically study the impact of perturbations of the intracellular $CO_2/HCO_3^-$ pool on growth and anaplerotic flux. Remarkably, all measures leading to enhanced $CO_2/HCO_3^-$ levels, such as external addition of $HCO_3^-$, increasing the pH, or rerouting metabolic flux via the pentose phosphate pathway, at least partially eliminated the lag phase of the Δ*aceE* Δ*pyc* strain on glucose medium. In accordance with these results, inactivation of the urease enzyme, lowering the intracellular $CO_2/HCO_3^-$ pool, led to an even longer lag phase, accompanied by the excretion of L-valine and L-alanine. Transcriptome analysis, as well as an adaptive laboratory evolution experiment with the Δ*aceE* Δ*pyc* strain, revealed the reduction of glucose uptake as a key adaptive measure to enhance growth on glucose-acetate mixtures. Taken together, our results highlight the significant impact of the intracellular $CO_2/HCO_3^-$ pool on metabolic flux distribution, which becomes especially evident in engineered strains exhibiting low endogenous $CO_2$ production rates, as exemplified by PDHC-deficient strains.

**IMPORTANCE** $CO_2$ is a ubiquitous product of cellular metabolism and an essential substrate for carboxylation reactions. The pyruvate dehydrogenase complex (PDHC) catalyzes a central metabolic reaction contributing to the intracellular $CO_2/HCO_3^-$ pool in many organisms. In this study, we used a PDHC-deficient strain of *Corynebacterium glutamicum*, which additionally lacked pyruvate carboxylase (Δ*aceE* Δ*pyc*). This strain featured a >15-h lag phase during growth on glucose-acetate mixtures. We used this strain to systematically assess the impact of alterations in the intracellular $CO_2/HCO_3^-$ pool on growth in glucose-acetate medium. Remarkably, all measures enhancing $CO_2/HCO_3^-$ levels successfully restored growth. These results emphasize the strong impact of the intracellular $CO_2/HCO_3^-$ pool on metabolic flux, especially in strains exhibiting low endogenous $CO_2$ production rates.

**KEYWORDS** *Corynebacterium glutamicum*, L-valine, anaplerosis, carbon dioxide, pyruvate carboxylase, pyruvate dehydrogenase complex

**Citation** Krüger A, Wiechert J, Gätgens C, Polen T, Mahr R, Frunzke J. 2019. Impact of $CO_2/HCO_3^-$ availability on anaplerotic flux in pyruvate dehydrogenase complex-deficient *Corynebacterium glutamicum* strains. J Bacteriol 201:e00387-19. https://doi.org/10.1128/JB.00387-19.

**Editor** Anke Becker, Philipps-Universität Marburg



Address correspondence to Regina Mahr, r.mahr@senseup.de, or Julia Frunzke, j.frunzke@fz-juelich.de.

A.K. and J.W. contributed equally to this work.

**Received** 6 June 2019
**Accepted** 19 July 2019
**Accepted manuscript posted online** 29 July 2019
**Published** 20 September 2019

$CO_2$ is an inevitable product and, at the same time, an essential substrate of microbial metabolism. In water, $CO_2$ is in equilibrium with bicarbonate ($HCO_3^-$) and $CO_3^{2-}$, and this equilibrium is influenced by the pH of the medium (1). As products of decarboxylating reactions and substrates for carboxylation, $CO_2$ and $HCO_3^-$ are involved in various metabolic processes. Consequently, the intracellular $CO_2/HCO_3^-$ pool has a significant impact on metabolic fluxes, such as anaplerosis, especially in the early phase of cultivation, when the cell density is low (2).

During aerobic growth, the pyruvate dehydrogenase complex (PDHC), which is conserved in various microbial species, catalyzes an important reaction contributing to the intracellular $CO_2/HCO_3^-$ pool (3, 4). The PDHC is a multienzyme complex belonging to the family of 2-oxo acid dehydrogenase complexes, which also include the $\alpha$-ketoglutarate dehydrogenase complex and the branched-chain 2-keto acid dehydrogenase (3, 5). In particular, the PDHC catalyzes the oxidative decarboxylation of pyruvate to acetyl coenzyme A (acetyl-CoA) and $CO_2$.

The Gram-positive actinobacterium *Corynebacterium glutamicum* represents an important platform strain used in industrial biotechnology for the production of amino acids, proteins, and various other value-added products (6–10). In this organism, the PDHC represents a central target for engineering the metabolic pathways of pyruvate-derived products, including L-valine, isobutanol, ketoisovalerate, and L-lysine. To this end, various studies have focused on the reduction or complete abolishment of PDHC activity in order to improve precursor availability (4, 11–13). Due to the deficiency of PDHC activity, however, cells are not able to grow on glucose as a single carbon source, a difficulty that can be circumvented by the addition of acetyl-CoA refueling substrates, such as acetate. In the presence of both carbon sources—glucose and acetate—PDHC-deficient strains initially form biomass from acetate and subsequently convert glucose into products (e.g., L-valine or L-alanine) in the stationary phase (12). In contrast to *Escherichia coli* or *Bacillus subtilis*, *C. glutamicum* does not normally show the typical diauxic growth behavior but prefers cometabolization of many carbon sources (10, 14). Coutilization of glucose and acetate has been studied in detail, showing that while the consumption rates of both carbon sources decrease, total carbon consumption is comparable to that with growth on either carbon source alone, which is regulated by SugR activity (15). Further examples of sugars or organic acids with which glucose is cometabolized include fructose (16), lactate (17), pyruvate (14), and gluconate (18). It has been shown that upon growth on a mixture of glucose and acetate, the glyoxylate shunt is active and is required to fuel the oxaloacetate pool in wild-type (WT) *C. glutamicum* (15). Here it should be noted that the glyoxylate shunt is active in the presence of acetate but is repressed by glucose (19).

For growth on glycolytic carbon sources, organisms depend on tricarboxylic acid (TCA) cycle-replenishing reactions constituting the anaplerotic node (or phosphoenolpyruvate [PEP]-pyruvate-oxaloacetate node), comprising different carboxylating and decarboxylating reactions (20). Consequently, flux via these reactions is influenced by the intracellular $CO_2/HCO_3^-$ pool. In contrast to most other organisms, *C. glutamicum* possesses both anaplerotic carboxylases, namely, the PEP carboxylase (PEPCx) (EC 4.1.1.31) encoded by the *ppc* gene (21, 22) and the pyruvate carboxylase (PCx) (EC 6.4.1.1) encoded by *pyc* (20, 23). These two $C_3$-carboxylating enzymes catalyze bicarbonate-dependent reactions yielding oxaloacetate from PEP or pyruvate, respectively. It has been shown that in *C. glutamicum*, these two enzymes can replace each other to a certain extent, depending on the intracellular concentrations of the respective effectors for each enzyme. However, under standard conditions during growth on glucose, the biotin-containing PCx contributes 90% of the main anaplerotic activity, in contrast to PEPCx (23). Remarkably, the Michaelis-Menten constants of both carboxylases are about 30-fold higher than those in *Escherichia coli* PEPCx (24). Apparently, a low $CO_2/HCO_3^-$ pool may thus limit anaplerotic flux, which is of special relevance in early phases, when the biomass concentration is low but high aeration may strip dissolved $CO_2$ from the medium.

Several studies have revealed the inhibitory effect of low partial $CO_2$ pressure ($pCO_2$)

on microbial growth (2, 25, 26). In the case of *C. glutamicum*, low $pCO_2$ led to a significant drop in the growth rate in turbidostatic continuous cultures (27) as well as in batch cultures (28). It was further demonstrated that the reduced flux through anaplerotic reactions under low $CO_2/HCO_3^-$ levels led to increased production of the pyruvate-derived amino acids L-alanine and L-valine (28).

While several previous studies have focused on the impact of $CO_2$ by altering the partial $CO_2$ pressure in the process, we applied targeted genetic perturbations to systematically assess the impact of the intracellular $CO_2/HCO_3^-$ pool on the anaplerotic flux and growth of *C. glutamicum*. In this study, we focused on PDHC-deficient strains exhibiting a reduced intracellular $CO_2/HCO_3^-$ pool during growth on glucose-acetate mixtures. The effect of low $CO_2/HCO_3^-$ levels became even more evident upon the additional deletion of the *pyc* gene, encoding the dominant anaplerotic enzyme, leading to a drastically elongated lag phase for a *C. glutamicum* Δ*aceE* Δ*pyc* strain during growth on glucose-acetate mixtures. This effect could be attributed to reduced tolerance of glucose by these strains and was successfully complemented by the deletion of *ptsG*, encoding the glucose-specific permease of the phosphotransferase system (PTS). Remarkably, growth was successfully restored by increasing the intracellular $CO_2/HCO_3^-$ pool by the addition of bicarbonate, by increasing the pH, by rerouting metabolic flux over the pentose phosphate pathway (PPP), or by refueling the oxaloacetate pool by the addition of TCA cycle intermediates to the growth medium. Finally, adaptive laboratory evolution (ALE) of the *C. glutamicum* Δ*aceE* Δ*pyc* strain on minimal medium containing glucose and acetate revealed the abolishment of glucose uptake as a key adaptive strategy to allow for growth on acetate.

## RESULTS

**A lowered intracellular $CO_2/HCO_3^-$ pool impacts the growth of PDHC-deficient strains.** The pyruvate dehydrogenase complex (PDHC) contributes to a key metabolic reaction in the central metabolism by catalyzing the oxidative decarboxylation of pyruvate to acetyl-CoA (Fig. 1), thereby producing 1 molecule of $CO_2$ and 1 molecule of NADH per molecule of pyruvate. Previous studies have already revealed that PDHC-deficient strains feature ~2-fold-decreased excretion of $CO_2$ during exponential growth (29). It is therefore reasonable to assume that a reduction in the intracellular $CO_2/HCO_3^-$ pool has an impact on metabolic flux distribution in PDHC-deficient strains. A simple growth comparison of wild-type *C. glutamicum* and a strain lacking the *aceE* gene (and thus PDHC deficient) revealed a slightly increased lag phase for the Δ*aceE* strain, which became especially evident when cells were grown in microtiter plates, while the maximal growth rate appeared to be unaffected ($0.40 \pm 0.01$ $h^{-1}$ for the Δ*aceE* strain and $0.41 \pm 0.01$ $h^{-1}$ for the WT) (Fig. 2A). Remarkably, this lag phase was completely eliminated by the addition of 100 mM $HCO_3^-$, suggesting that the effect is attributable to the lowered intracellular $CO_2/HCO_3^-$ pool of this mutant (Fig. 2B).

In *C. glutamicum*, the pyruvate carboxylase (PCx) encoded by *pyc* is the dominating $HCO_3^-$-dependent anaplerotic enzyme required for refueling the TCA cycle via oxaloacetate during growth on glycolytic carbon sources (23). In the next experiment, we deleted *pyc* in the Δ*aceE* background in order to examine the influence of different $CO_2/HCO_3^-$ levels on bicarbonate-dependent anaplerosis. Remarkably, the additional deletion of the *pyc* gene resulted in an elongated lag phase of about 20 h and a reduced growth rate for the Δ*aceE* Δ*pyc* strain (maximum growth rate [$\mu_{max}$], $0.27 \pm 0.02$ $h^{-1}$, in contrast to $0.40 \pm 0.01$ $h^{-1}$ for the Δ*aceE* strain) during cultivation in CGXII minimal medium containing glucose and acetate (Fig. 2A). An extended lag phase was also observed for the Δ*pyc* single mutant, but the lag phase was significantly less prominent than that for the PDHC-deficient Δ*aceE* Δ*pyc* variant (Fig. 2C). The growth defects of both strains were successfully complemented by reintroducing the *pyc* gene on plasmid pJC1 under the control of its own promoter (Fig. 2C). Remarkably, this extended lag phase was observed only in the presence of glucose, not during cultivation on minimal medium containing acetate as the sole carbon source (Fig. 2A).

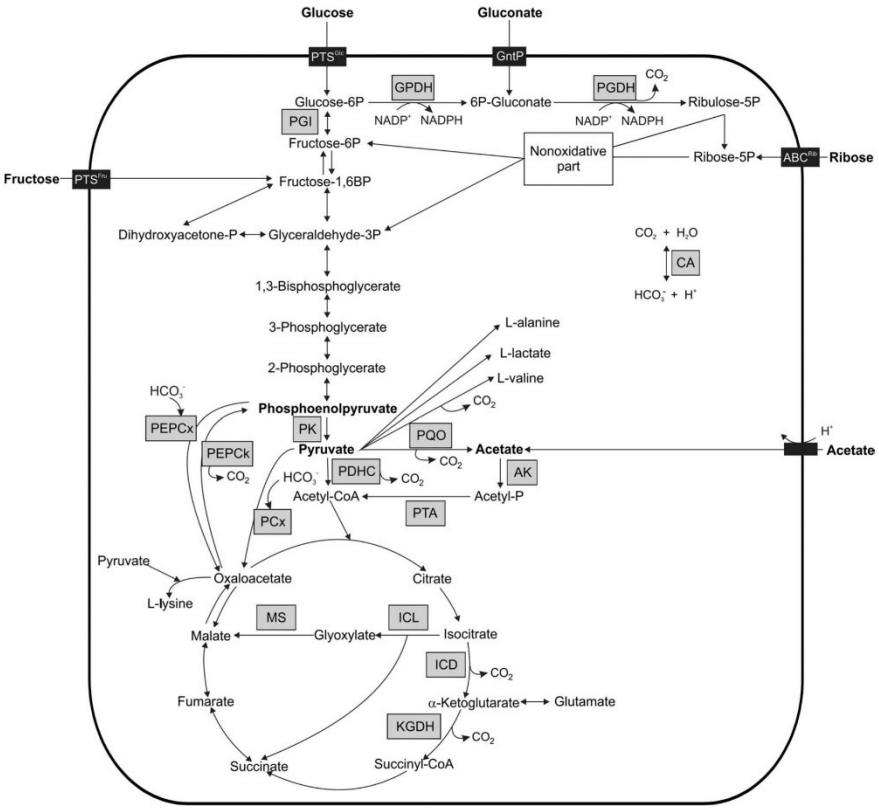


**FIG 1** Schematic overview of the central carbon metabolism of *C. glutamicum*. The main aspects of glycolysis, gluconeogenesis, the pentose phosphate pathway, the TCA cycle, and anaplerosis are shown. Shaded boxes represent relevant enzymes. Carboxylation as well as decarboxylation steps are given. $ABC^{Rib}$, ATP-binding cassette transporter for ribose; AK, acetate kinase; CA, carbonic anhydrase; GntP, gluconate permease; GPDH, glucose-6P dehydrogenase; ICD, isocitrate dehydrogenase; ICL, isocitrate lyase; KGDH, α-ketoglutarate dehydrogenase complex; MS, malate synthase; PCx, pyruvate carboxylase; PDHC, pyruvate dehydrogenase complex; PEPCk, PEP carboxykinase; PEPCx, PEP carboxylase; PGDH, 6-phosphogluconate dehydrogenase; PGI, phosphoglucose isomerase; PK, pyruvate kinase; PQO, pyruvate:quinone oxidoreductase; PTA, phosphotransacetylase; $PTS^{Glc}$, permease of phosphotransferase system for glucose; $PTS^{Fru}$, permease of phosphotransferase system for fructose.

**Glucose uptake results in strongly retarded growth in strains lacking pyruvate carboxylase.** In order to determine whether glucose uptake caused the retarded growth, the Δ*aceE* Δ*pyc* strain was cultivated in the presence of 154 mM acetate and increasing amounts of glucose (100 to 250 mM). In line with our hypothesis, the lag phase showed a stepwise increase as larger amounts of glucose were added to the medium (Fig. 3A). Accordingly, the Δ*aceE* Δ*pyc* strain also showed significantly elongated lag phases on the PTS sugars fructose and sucrose (see Fig. S1 in the supplemental material). In contrast, the glucose concentration did not significantly affect the growth of the Δ*aceE* strain (Fig. 3A), in which the major anaplerotic enzyme PCx still replenishes the oxaloacetate pool.

To link the observed growth phenotype to the uptake of glucose, we deleted the *ptsG* gene, encoding the glucose-specific permease of the PTS, in the Δ*aceE* and Δ*aceE* Δ*pyc* strain backgrounds. The growth and glucose consumption rates of the resulting strains were analyzed during growth on glucose and acetate. Remarkably, deletion of *ptsG* fully restored the growth of the Δ*aceE* Δ*pyc* strain (growth rates were 0.27 ± 0.02

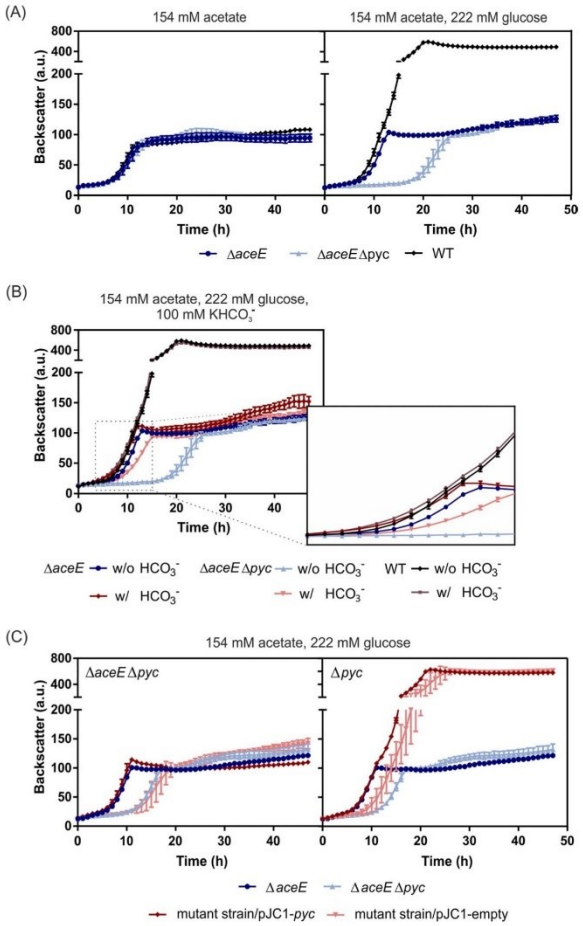


**FIG 2** Impact of glucose on *aceE* and *pyc* mutant strains. The growth curves shown are based on the backscatter measurements (expressed in arbitrary units [a.u.]) in a microtiter cultivation system inoculated at an $OD_{600}$ of 1. Data represent the averages for three biological replicates; error bars, standard deviations. (A) The *C. glutamicum* Δ*aceE* and Δ*aceE* Δ*pyc* strains, as well as the wild type, were inoculated in CGXII medium containing 154 mM acetate (left) or 154 mM acetate plus 222 mM glucose (right). (B) The Δ*aceE* and Δ*aceE* Δ*pyc* strains, as well as WT cells, were cultivated in CGXII medium containing 154 mM acetate and 222 mM glucose, either with (w/) or without (w/o) 100 mM $KHCO_3^-$. The box zooms in on the time interval between 4 h and 15 h. (C) The Δ*aceE* Δ*pyc* (left) and Δ*pyc* (right) strains were transformed with the pJC1-*pyc* plasmid for complementation of the *pyc* deletion or with the pJC1-empty vector as a control. Cultures were inoculated in CGXII medium containing 154 mM acetate, 222 mM glucose, and 25 μg/ml kanamycin.

$h^{-1}$ for the Δ*aceE* Δ*pyc* parental strain and 0.39 ± 0.02 $h^{-1}$ for the Δ*aceE* Δ*pyc* Δ*ptsG* strain) but resulted in reduced final backscatter values, comparable to those with growth on acetate alone (Fig. 3B). Strains lacking the *ptsG* gene consumed only minor amounts of glucose, while the Δ*aceE* and Δ*aceE* Δ*pyc* strains consumed glucose after entering the stationary phase (see Fig. S2 in the supplemental material). The glucose uptake rate of the Δ*aceE* Δ*pyc* strain, 10.87 ± 4.95 nmol $min^{-1}$ $g^{-1}$, was significantly lower than that of the Δ*aceE* strain, 16.81 ± 3.01 nmol $min^{-1}$ $g^{-1}$ (Table 1). In contrast, deletion of *ptsG* did not restore growth on either the PTS substrate fructose (see Fig.

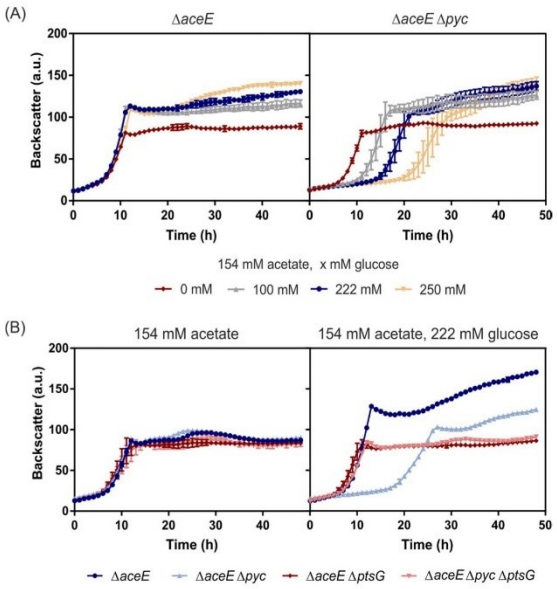


**FIG 3** Influence of glucose consumption on the growth of *C. glutamicum* Δ*aceE* and *C. glutamicum* Δ*aceE* Δ*pyc*. The growth curves shown are based on the backscatter measurements in a microtiter cultivation system, inoculated at an $OD_{600}$ of 1. (A) The Δ*aceE* (left) and Δ*aceE* Δ*pyc* (right) strains were inoculated to an $OD_{600}$ of 1 in CGXII medium containing 154 mM acetate and either no glucose or 100 mM, 222 mM, or 250 mM glucose. (B) Deletion of the *ptsG* gene in the Δ*aceE* and Δ*aceE* Δ*pyc* strains restored growth on glucose-acetate mixtures relative to that for the Δ*aceE* and Δ*aceE* Δ*pyc* parental strains. Data represent the averages for three biological replicates; error bars, standard deviations.

S3), which is imported mainly by the permease encoded by *ptsF* (30, 31), or the non-PTS sugar ribose (see Fig. S4). Taken together, these findings clearly link the observed growth defect of the Δ*aceE* Δ*pyc* strain on glucose-acetate mixtures to the uptake of residual amounts of glucose.

**Increased $HCO_3^-$ availability improves anaplerotic flux in *pyc* mutants.** Next, we used different strategies to alter the intracellular $CO_2/HCO_3^-$ pool. This was achieved by (i) supplementing the medium with $HCO_3^-$, (ii) mutating the endogenous urease gene producing $CO_2$ from urea in the early growth phase, (iii) increasing the pH of the growth medium, or (iv) rerouting metabolic flux via the pentose phosphate pathway (Fig. 4).

As with the Δ*aceE* parental strain, the addition of 100 mM $HCO_3^-$ eliminated the lag phase for PDHC-deficient strains lacking the *pyc* gene (Fig. 2B) during microtiter plate cultivation on glucose-acetate mixtures. Restoration of growth was not possible in a

**TABLE 1** Glucose consumption rates of PDHC-deficient *C. glutamicum* strains in the exponential-growth phase[a]

| Mutation(s) | Glucose consumption rate (nmol $min^{-1}$ $g^{-1}$)[b] |
|---|---|
| Δ*aceE* | 16.81 ± 3.01 |
| Δ*aceE* Δ*pyc* | 10.87 ± 4.95 |
| Δ*aceE* Δ*ptsG* | 7.24 ± 3.97 |
| Δ*aceE* Δ*pyc* Δ*ptsG* | 7.32 ± 1.88 |

[a]For an overview of glucose consumption over the entire time course of the experiment, including the stationary phase, see Fig. S2 in the supplemental material.
[b]Values are means ± standard deviations for three independent biological replicates.

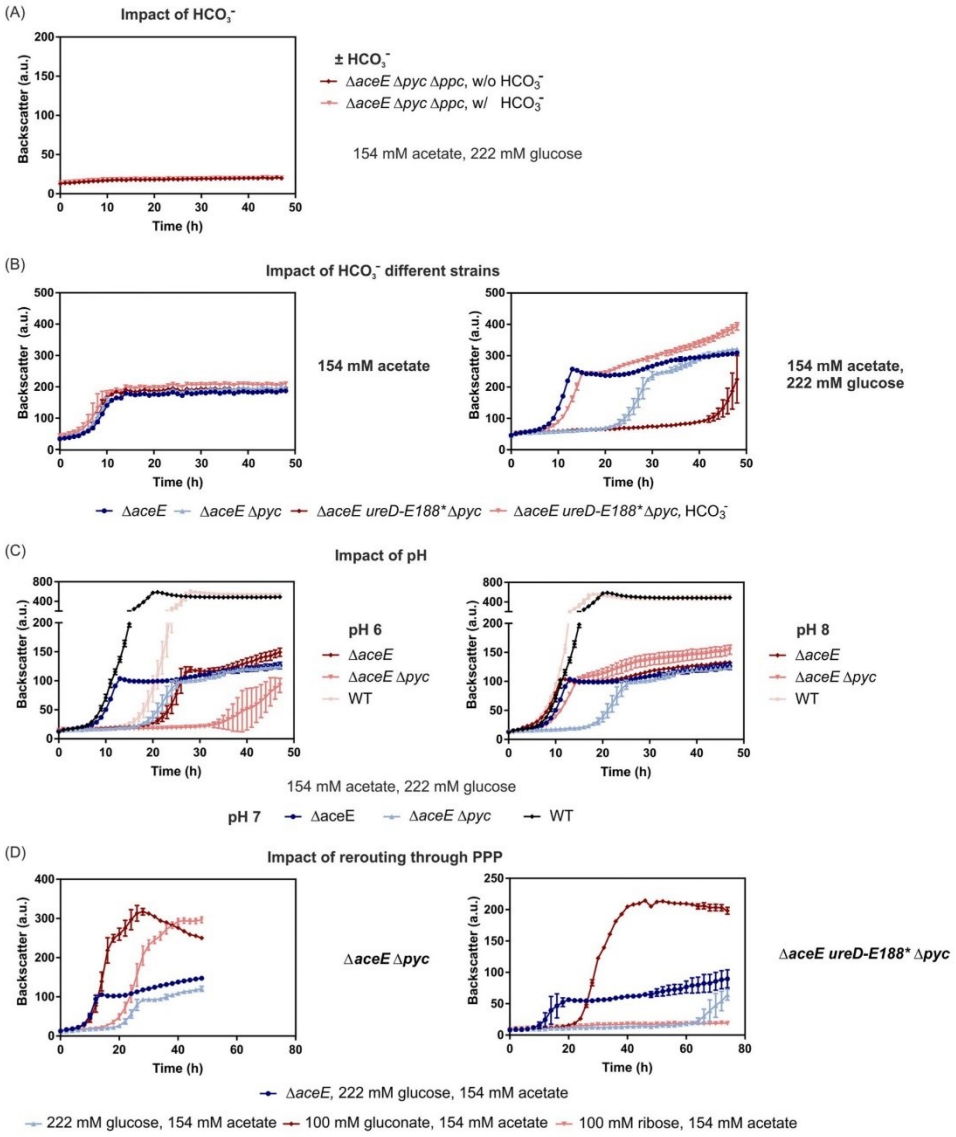


**FIG 4** Increased availability of $HCO_3^-$ improved anaplerotic flux via PEPCx in *pyc*-deficient *C. glutamicum* strains. The growth curves shown are based on the backscatter measurements in a microtiter cultivation system, inoculated at an $OD_{600}$ of 1. Symbols represent the backscatter means for biological triplicates ($n = 3$). (A) The Δ*aceE* Δ*pyc* Δ*ppc* strain was inoculated in CGXII medium containing 154 mM acetate and 222 mM glucose (w/o $HCO_3^-$), and if indicated, 100 mM $KHCO_3^-$ was added (w/ $HCO_3^-$). (B) The Δ*aceE*, Δ*aceE* Δ*pyc*, and Δ*aceE ureD*-E188* Δ*pyc* strains were cultivated in CGXII medium containing 154 mM acetate (left) or 154 mM acetate and 222 mM glucose (right) with or without the addition of $KHCO_3^-$. (C) The Δ*aceE* and Δ*aceE* Δ*pyc* strains, as well as the WT, were cultivated in CGXII medium containing 154 mM acetate and 222 mM glucose adjusted to a pH of 6 (left) or 8 (right), and growth was compared to that with cultivation at pH 7. (D) The Δ*aceE* strain and the Δ*aceE* Δ*pyc* (left) or Δ*aceE ureD*-E188* Δ*pyc* (right) strain were inoculated in different growth media containing 154 mM acetate and either 222 mM glucose, 100 mM gluconate, or 100 mM ribose.

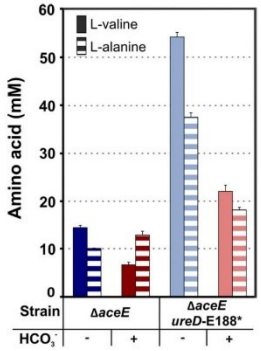


**FIG 5** The intracellular $CO_2$-$HCO_3^-$ pool significantly affects L-valine production. The influence of carbonate on the L-alanine and L-valine production of *C. glutamicum* Δ*aceE* and *C. glutamicum* Δ*aceE ureD*-E188* was investigated. Shown are L-valine and L-alanine titers in the supernatant after 28 h of cultivation in the microtiter cultivation system. Data represent average values from three independent biological replicates using uHPLC.

strain lacking both anaplerotic enzymes PCx and PEPCx, indicating that the positive effect of $HCO_3^-$ on the Δ*aceE* Δ*pyc* strain depends on the increased flux over PEPCx (Fig. 4A; see also Fig. S5 in the supplemental material). In contrast to the finding for PCx-deficient strains, no negative impact of glucose on the growth of the Δ*aceE* Δ*ppc* strain was observed (see Fig. S6), confirming again the superior role of PCx in *C. glutamicum* (23, 32). Interestingly, we also observed a significant impact of the culture volume on the growth of the Δ*aceE* Δ*pyc* strain. Since efficient liquid-air mixing continuously removes $CO_2$ from the culture medium, the lag phase of the Δ*aceE* Δ*pyc* strain was much more prominent during microtiter plate cultivation (~17 h) than in cultures in shake flasks (a ~7-h lag phase in 100-ml cultures and a ~13-h lag phage in 50 ml) (see Fig. S7).

The urease enzyme, catalyzing the degradation of urea to ammonium and carbon dioxide, represents a further important contributor to the intracellular $CO_2$/$HCO_3^-$ pool, especially in the early exponential phase, when cell densities and decarboxylation reaction rates are low. In a previous study, the *ureD*-E188* mutation was found to abolish urease activity in *C. glutamicum* and to enhance L-valine production by PDHC-deficient strains (33). In this study, we introduced the *ureD*-E188* mutation into the Δ*aceE* Δ*pyc* background so as to examine the influence of an even lower $CO_2$/$HCO_3^-$ level on anaplerosis in this strain background. The additional inactivation of the urease enzyme resulted in a significantly elongated lag phase of about 46 h, which could also be complemented by the addition of $HCO_3^-$ (Fig. 4B), demonstrating the importance of the $CO_2$/$HCO_3^-$ pool during the initial growth phase. Furthermore, we assessed the impact of urease mutation on the production of L-valine and L-alanine by the Δ*aceE* and Δ*aceE ureD*-E188* strains and the effect of complementation via $HCO_3^-$ addition. Within 28 h of cultivation, the Δ*aceE* strain produced 15 mM L-valine and 10 mM L-alanine as by-products, while the Δ*aceE ureD*-E188* strain accumulated 54 mM L-valine and 38 mM L-alanine (Fig. 5). The addition of $HCO_3^-$, however, significantly reduced L-valine production, by 54% for the Δ*aceE* strain and 59% for the Δ*aceE ureD*-E188* strain. The concentration of the by-product L-alanine increased by 22% for the Δ*aceE* strain and decreased by 51% for the Δ*aceE ureD*-E188* strain (Fig. 5). The examples of L-valine and L-alanine production illustrate the important role of the intracellular $CO_2$/$HCO_3^-$ levels on metabolic flux in PDHC-deficient strains.

Another approach to influencing the extracellular $HCO_3^-$ availability was to change the pH conditions (2). According to the Bjerrum plot, $CO_2$ is predominant under acidic conditions, while $CO_3^{2-}$ is the dominant form under alkaline conditions. At a pH of

about 8, $HCO_3^-$ is the prevalent form. Since $HCO_3^-$ is the substrate of the anaplerotic enzymes PCx and PEPCx, the pH in the cultivation medium was adjusted to 8 using KOH, leading to an equilibrium shift toward higher $HCO_3^-$ availability. As a negative control, the pH was adjusted to 6 using HCl. While the growth of both strains tested was retarded at pH 6, it was significantly enhanced at pH 8 (Fig. 4C). Thus, elevation of the culture pH improved the growth of PDHC-deficient strains, likely by increasing anaplerotic flux.

The PPP includes another decarboxylation reaction in the central carbon metabolism, the reaction catalyzed by 6-phosphogluconate dehydrogenase (6PGDH), that contributes to the intracellular $CO_2/HCO_3^-$ pool. Remarkably, the lag phases of the Δ*aceE* Δ*pyc* and Δ*aceE ureD*-E188* Δ*pyc* strains were mostly complemented during growth on acetate and gluconate—the latter entering the PPP via gluconate-6-phosphate (Fig. 4D). Growth on ribose, which enters the PPP via ribulose-5-phosphate and thereby bypasses the decarboxylation catalyzed by 6PGDH, showed a significantly elongated lag phase in *pyc*-deficient strains (Fig. 4D). In a further experiment, metabolic/glycolytic flux was rerouted through the PPP by deleting *pgi*, encoding glucose-6-phosphate isomerase. However, deletion of *pgi* resulted in a severe growth defect in the Δ*aceE* background. In this context, the growth of the Δ*aceE* Δ*pyc* strain featured only minor, nonsignificant improvement (see Fig. S8 in the supplemental material).

Taken together, our findings highlight the important impact of the intracellular $CO_2/HCO_3^-$ pool on metabolic flux in the central carbon metabolism. This is especially evident in the Δ*aceE* Δ*pyc* strain, which lacks a central decarboxylation reaction and the key carboxylase PCx in *C. glutamicum*.

**Refueling the TCA cycle improves the growth of *pyc* mutants.** Glucose catabolism requires sufficient anaplerotic flux to replenish TCA cycle intermediates, providing precursors for various anabolic pathways. Therefore, we tested whether the addition of TCA cycle intermediates would complement the negative impact of glucose on the growth of the Δ*aceE* Δ*pyc* strain. Remarkably, all TCA cycle intermediates tested (succinate, malate, citrate, and the glutamate-containing dipeptide Glu-Ala) reduced the extended lag phase of the Δ*aceE* Δ*pyc* strain during growth on glucose-acetate mixtures (Fig. 6A). The value of Δ*t* was defined to give the percentage change of lag phase time compared to the first doubling time of the Δ*aceE* and Δ*aceE* Δ*pyc* strains on glucose-acetate mixtures (100%). The dipeptide Glu-Ala and succinate reduced the elongated lag phase to high extents, by 90% (Δ*t* = 10%) and 85% (Δ*t* = 15%), respectively, while the effects of citrate and malate were weaker (Δ*t*, 40% and 38%, respectively) (Table 2).

Based on previous studies, it was known that the glyoxylate shunt might be switched off during growth on glucose-acetate mixtures, due to the inhibitory effect of glucose (34). In this study, overexpression of the *aceA* and *aceB* genes, encoding the glyoxylate shunt enzymes isocitrate lyase and malate synthase, resulted in a significantly shorter lag phase for the Δ*aceE* Δ*pyc* strain (Fig. 6B). These genes were overexpressed by use of the pJC1 vector harboring an inducible $P_{tac}$ promoter in front of either of two synthetic operon variants (pJC1-$P_{tac}$-*aceA-aceB* and pJC1-$P_{tac}$-*aceB-aceA*). However, it must be noted that for the Δ*aceE* strain, overexpression of *aceA* and *aceB* led to lag phases slightly longer than those with the empty-vector control (Fig. 6B). Expression from the leaky $P_{tac}$ promoter yielded the best result, while induction with isopropyl-β-D-thiogalactopyranoside (IPTG) resulted in severe growth defects (data not shown).

Unusual intermediate accumulation or depletion can provide valuable information regarding intracellular flux imbalances causing the observed growth defects. Gas chromatography–time of flight (GC-ToF) experiments were performed for analysis of the metabolic states by comparing samples of the Δ*aceE* strain during the early-exponential phase, the Δ*aceE* Δ*pyc* strain at the same time point during the lag phase, and the Δ*aceE* Δ*pyc* strain during the early exponential phase (Fig. S9 in the supplemental material shows the sampling scheme). Additionally, samples of both PDHC-

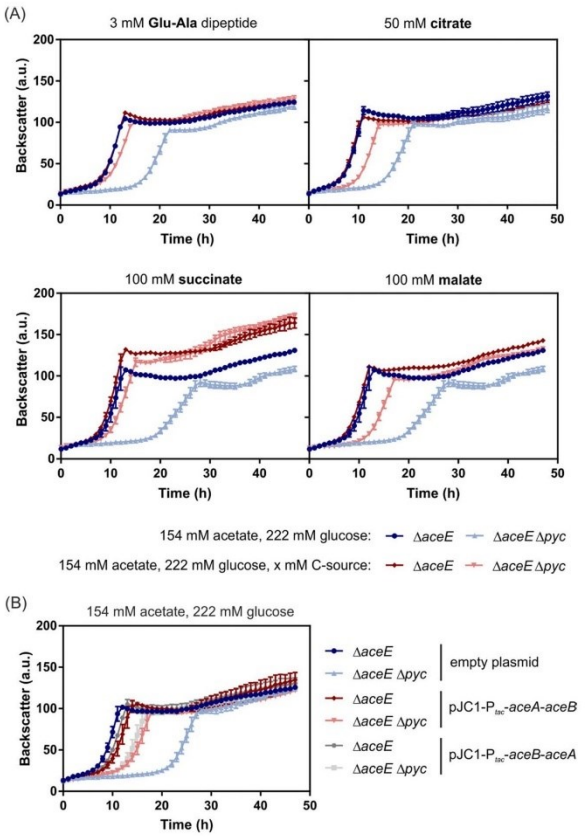


**FIG 6** Refueling the TCA cycle to complement the glucose intolerance of the Δ*aceE* Δ*pyc* strain. The growth curves shown are based on the backscatter measurements in a microtiter cultivation system, while symbols represent the backscatter means for biological triplicates ($n = 3$). The Δ*aceE* and Δ*aceE* Δ*pyc* strains were inoculated to an $OD_{600}$ of 1 into CGXII medium with 154 mM acetate and 222 mM glucose. (A) The TCA cycle-fueling carbon source glutamate (3 mM Glu-Ala dipeptide), citrate (50 mM), succinate (100 mM), or malate (100 mM) was added to the medium in order to analyze the effect on lag phase complementation (shades of red). As a control, growth on 154 mM acetate and 222 mM glucose is shown for the Δ*aceE* (dark blue) and Δ*aceE* Δ*pyc* (light blue) strains in each experiment. (B) The Δ*aceE* and Δ*aceE* Δ*pyc* strains were transformed with the pJC1-$P_{tac}$-*aceA-aceB* or pJC1-$P_{tac}$-*aceB-aceA* plasmid for simultaneous overexpression of the glyoxylate shunt enzymes isocitrate lyase (encoded by *aceA*) and malate synthase (encoded by *aceB*), while the Δ*aceE* Δ*pyc* and Δ*pyc* strains transformed with the empty pJC1 vector served as controls. Cultures were inoculated to an $OD_{600}$ of 1 in CGXII medium containing 154 mM acetate, 222 mM glucose, and 25 μg/ml kanamycin.

deficient strains cultivated with 100 mM $HCO_3^-$ were measured, and WT cells in exponential phase were used as a reference (see Table S1). No significant intermediate accumulation and no occurrence of unusual compounds was observed in the lag-phase sample of the Δ*aceE* Δ*pyc* strain relative to all other samples. Although oxaloacetate cannot be measured by this method, complete depletion of oxaloacetate-derived aspartate was detected in Δ*aceE* Δ*pyc* cells during the lag phase but not during the exponential phase or in $HCO_3^-$-complemented samples. This result supports the hypothesis that oxaloacetate depletion is the key reason for the elongated lag phase.

In order to identify oxaloacetate depletion as a key growth-limiting factor and to decouple this effect from anaplerosis-dependent replenishment, the Δ*pyc*, Δ*pyc* Δ*ppc*,

**TABLE 2** Overview of the lag phases and growth rates of the *C. glutamicum* Δ*aceE* and Δ*aceE* Δ*pyc* strains cultivated with different TCA cycle carbon sources[a]

| Added carbon source (concn [mM]) | *C. glutamicum* Δ*aceE* | | | *C. glutamicum* Δ*aceE* Δ*pyc* | | |
|---|---|---|---|---|---|---|
| | Lag phase[b] | Δ*t* (%)[c] | Growth rate ($h^{-1}$) | Lag phase[b] | Δ*t* (%)[c] | Growth rate ($h^{-1}$) |
| None | – | 0 | 0.41 ± 0.01 | + | 100 | 0.27 ± 0.02 |
| Glu-Ala (3) | – | 0 | 0.35 ± 0.01 | ÷ | 10 | 0.33 ± 0.01 |
| Citrate (50) | – | 0 | 0.39 ± 0.01 | ÷ | 40 | 0.35 ± 0.01 |
| Succinate (100) | – | –8 | 0.36 ± 0.01 | ÷ | 15 | 0.34 ± 0.02 |
| Malate (100) | – | –8 | 0.35 ± 0.01 | ÷ | 38 | 0.35 ± 0.02 |

[a]The strains were cultivated in CGXII medium containing 154 mM acetate and 222 mM glucose with or without a TCA cycle carbon source.
[b]+, lag phase greater than or equal to the lag phase observed for the strain on 154 mM acetate with 222 mM glucose; ÷, shorter lag phase; –, no lag phase.
[c]The difference between the first doubling time of the Δ*aceE* strain and that of the Δ*aceE* Δ*pyc* strain was defined as 100%.

and Δ*aceE* Δ*pyc* Δ*ppc* strains were tested in the presence of different TCA cycle intermediates. Here, mutants lacking both anaplerotic reactions (PCx and PEPCx)—the Δ*pyc* Δ*ppc* and Δ*aceE* Δ*pyc* Δ*ppc* strains—were not able to grow on glucose-acetate mixtures at all (Fig. 4A; also Fig. S5 in the supplemental material). Again, all TCA cycle intermediates were able to complement the glucose sensitivity of these *pyc*-deficient strains, and the growth of the Δ*pyc* Δ*ppc* and Δ*aceE* Δ*pyc* Δ*ppc* strains was effectively restored (Table 3). Nevertheless, slight differences were observed, which might also be caused by differences in the uptake of these carbon sources.

**Adaptation of *C. glutamicum* Δ*aceE* Δ*pyc* to growth on glucose and acetate.** In a previous study, Kotte et al. reported on an elongated lag phase of *E. coli* as a result of glucose-gluconeogenetic substrate shifts (35). This phenomenon was ascribed to the formation of a small subpopulation that is able to start growing after carbon source switches (35). Usually, the growth of a small subpopulation is obscured by typical bulk measurements but can be visualized by single-cell approaches, such as flow cytometry (FC). To this end, the membranes of Δ*aceE* and Δ*aceE* Δ*pyc* cells were stained using the nontoxic green fluorescent dye PKH67 prior to inoculation. During cellular growth, the amount of fluorescent dye is diluted by membrane synthesis, leading to a decrease in the level of single-cell PKH67 fluorescence (35). Stained Δ*aceE* and Δ*aceE* Δ*pyc* cells were cultivated in minimal medium containing glucose and acetate (Fig. 7A). As a nonproliferating control, Δ*aceE* Δ*pyc* cells were incubated in glucose as the sole carbon source. Using flow cytometry, membrane staining was analyzed during cultivation at the single-cell level (Fig. 7B). While the mean of the fluorescence of the whole Δ*aceE* population decreased from $2.7 \times 10^4$ arbitrary units (AU) to $7.5 \times 10^2$ AU, the mean of the fluorescence of the Δ*aceE* Δ*pyc* population incubated in glucose medium alone shifted from $3.1 \times 10^4$ AU to $1.3 \times 10^3$ AU, resulting from a minor dilution/bleaching of fluorescence intensity during incubation. Remarkably, both the Δ*aceE* and Δ*aceE* Δ*pyc* strains featured rather heterogeneous adaptation behavior on glucose-acetate mixtures, which was apparently delayed in the Δ*aceE* Δ*pyc* strain, reflecting the elongated

**TABLE 3** Overview of the lag phases and growth rates of the *C. glutamicum* Δ*pyc*, Δ*pyc* Δ*ppc*, and Δ*aceE* Δ*pyc* Δ*ppc* strains cultivated with different TCA cycle carbon sources[a]

| Added carbon source (concn [mM]) | Result for the *C. glutamicum* strain with the following mutation(s): | | | | | |
|---|---|---|---|---|---|---|
| | Δ*pyc* | | Δ*pyc* Δ*ppc* | | Δ*aceE* Δ*pyc* Δ*ppc* | |
| | $\Delta t_{lag}$ (h)[b] | Growth rate ($h^{-1}$)[c] | $\Delta t_{lag}$ (h) | Growth rate ($h^{-1}$) | $\Delta t_{lag}$ (h) | Growth rate ($h^{-1}$) |
| None | 6 h | 0.17 ± 0.02 | No growth | | No growth | |
| Glu-Ala (3) | ND | ND | 8 | 0.21 ± 0.01 | 30 | 0.14 ± 0.01 |
| Citrate (50) | 3 | 0.19 ± 0.01 | 5 | 0.26 ± 0.01 | 8 | 0.20 ± 0.03 |
| Succinate (100) | 2 | 0.2 ± 0.02 | 3 | 0.16 ± 0.03 | 5 | 0.12 ± 0.03 |
| Malate (100) | 3 | 0.21 ± 0.01 | 17 | 0.18 ± 0.01 | 18 | 0.24 ± 0.01 |

[a]Strains were cultivated in CGXII medium containing 154 mM acetate and 222 mM glucose with or without a TCA cycle carbon source.
[b]Difference in lag phase duration between the Δ*aceE* strain growing on a glucose-acetate mixture and the strain of interest growing on the respective carbon source(s). ND, not determined.
[c]For comparison, the growth rate in a glucose-acetate mixture was 0.41 $h^{-1}$ for the Δ*aceE* strain and 0.28 $h^{-1}$ for the Δ*aceE* Δ*pyc* strain in this experiment.

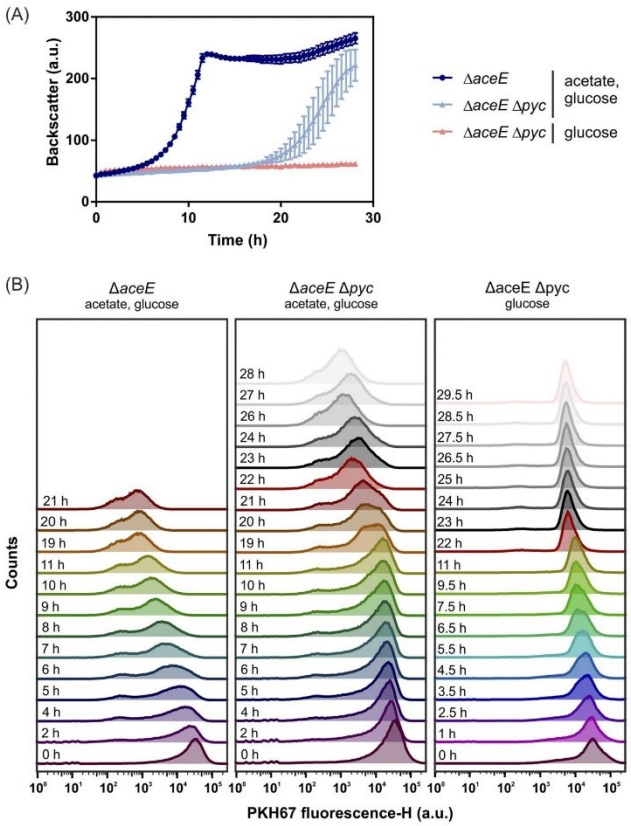


**FIG 7** Heterogeneous adaptation of *C. glutamicum* Δ*aceE* and *C. glutamicum* Δ*aceE* Δ*pyc* during growth on glucose and acetate. To identify a potential growing subpopulation, the fluorescent dye PKH67 was used to stain the membranes of Δ*aceE* and Δ*aceE* Δ*pyc* cells prior to cultivation. The cells were cultivated in a microtiter cultivation system in the presence of 154 mM acetate and 222 mM glucose. As a nongrowing control, the Δ*aceE* Δ*pyc* strain was additionally incubated in CGXII medium containing solely 222 mM glucose. (A) Cell growth was monitored online using a microtiter cultivation system. (B) Staining intensities were measured on the single-cell level during cultivation using flow cytometry (with three biological replicates). Shown are the frequencies of PKH67 staining intensities of one representative culture of each sample over the time course of cultivation. H, height; Counts, cell count.

lag phase. Already in the early phase of cultivation, the populations split into two subpopulations of low and high PKH67 fluorescence, indicating that only a few cells started to proliferate, while a fraction of the population was not able to grow under the same conditions (36–38).

To study the adaptation of the Δ*aceE* Δ*pyc* strain, comparative transcriptome analyses were performed using DNA microarrays. To this end, Δ*aceE* and Δ*aceE* Δ*pyc* cells were harvested at comparable optical densities (ODs) during early exponential phase (see Fig. S9 in the supplemental material). Both strains were cultivated in CGXII medium with 154 mM acetate and 222 mM glucose. Under the conditions chosen, a total of 354 genes showed significantly altered mRNA levels. While 121 genes were at least 1.7-fold upregulated ($P < 0.05$), 233 genes were 0.7-fold downregulated ($P < 0.05$) in the Δ*aceE* Δ*pyc* strain (see Table S2). An overview of expression changes of selected genes is shown in Table 4. Among the various changes in the levels of gene expression,

**TABLE 4** Comparative transcriptome analysis of *C. glutamicum* Δ*aceE* Δ*pyc* and *C. glutamicum* Δ*aceE* during growth on glucose and acetate[a]

| Function and gene locus | Gene name | Annotation | mRNA ratio | *P* |
|---|---|---|---|---|
| PTS component | | | | |
| cg1537 | *ptsG* | Glucose-specific enzyme IIBC component of PTS | 0.59 | 0.02 |
| cg2117 | *ptsI* | PEP:sugar phosphotransferase system enzyme I | 0.67 | 0.01 |
| cg2121 | *ptsH* | Phosphocarrier protein HPr of PTS | 1.16 | *0.11* |
| *myo*-Inositol transport | | | | |
| cg0223 | *iolT1* | *myo*-Inositol transporter | **1.97** | 0.04 |
| cg3387 | *iolT2* | *myo*-Inositol transporter | 1.41 | *0.19* |
| Transcriptional regulation of *ptsG* | | | | |
| cg2783 | *gntR1* | Transcriptional regulator, GntR family | 0.76 | 0.05 |
| cg1935 | *gntR2* | Transcriptional regulator, GntR family | 0.97 | *0.46* |
| cg2115 | *sugR* | DeoR-type transcriptional regulator of *ptsG*, *ptsS*, and *ptsF* | 0.79 | 0.03 |
| Acetate metabolism | | | | |
| cg3047 | *ackA* | Acetate/propionate kinase | **1.99** | 0.01 |
| cg3048 | *pta* | Phosphate acetyltransferase | 1.34 | 0.04 |
| cg2560 | *aceA* | Isocitrate lyase | **1.70** | *0.12* |
| cg2559 | *aceB* | Malate synthase | **1.88** | 0.02 |
| Anaplerosis | | | | |
| cg1787 | *ppc* | Phosphoenolpyruvate carboxylase | 0.91 | *0.32* |
| cg3169 | *pck* | Phosphoenolpyruvate carboxykinase (GTP) | 0.72 | 0.03 |
| cg1458 | *odx* | Oxaloacetate decarboxylase | 1.07 | *0.32* |
| cg3335 | *malE* | Malic enzyme | 0.48 | *0.26* |
| Other functions in the central carbon metabolism | | | | |
| cg0973 | *pgi* | Glucose-6-phosphate isomerase | 0.44 | 0.03 |
| cg2291 | *pyk* | Pyruvate kinase | 0.59 | 0.01 |
| cg2891 | *pqo* | Pyruvate:quinone oxidoreductase | 0.47 | 0.02 |

[a]The expression of selected genes encoding central metabolic enzymes or regulators is given as the ratio of the mRNA level in the Δ*aceE* Δ*pyc* strain to that in the Δ*aceE* strain. mRNA ratios of ≤0.70 are underlined, and mRNA ratios of ≥1.70 are shown in boldface. *P* values of >0.05 (from three biological replicates) are italicized. For the complete data set, see Table S4 in the supplemental material.

we observed 0.59-fold and 0.67-fold downregulation of the PTS components *ptsG* and *ptsI*, respectively, in the Δ*aceE* Δ*pyc* strain, in line with the decreased glucose uptake rates of this strain (Table 1). In contrast, *iolT1*, encoding the *myo*-inositol transporter, which is responsible, *inter alia*, for PTS-independent glucose uptake, was upregulated (39, 40). This is in line with the fact that the *ptsG*-deficient strains still consumed minor amounts of glucose. Interestingly, genes involved in acetate metabolism, including *aceA* and *aceB*, constituting the glyoxylate shunt, displayed increased mRNA levels in the Δ*aceE* Δ*pyc* strain. This may also represent an important adaptive mechanism, since the glyoxylate shunt needs to be active in the Δ*aceE* Δ*pyc* strain to compensate for the loss of TCA cycle intermediates during coconsumption of acetate and glucose, as demonstrated by the effect of *aceA-aceB* overexpression in this study (Fig. 6B). While the mRNA levels of genes encoding anaplerotic enzymes did not show significant changes, the glycolytic genes *pgi* and *pyk* featured ~2-fold-reduced levels in the Δ*aceE* Δ*pyc* mutant. This might well reflect an adaptive mechanism, since downregulation of *pyk* would reduce flux from PEP to pyruvate, and reduced expression of *pgi* would probably lead to increased flux through the PPP, contributing an additional decarboxylation step.

**Less is more: ALE of the Δ*aceE* Δ*pyc* strain reveals rapid inactivation of glucose uptake.** In order to identify key mutations abolishing the lag phase of the Δ*aceE* Δ*pyc* strain, an adaptive laboratory evolution (ALE) experiment was performed. In this ALE experiment, *C. glutamicum* Δ*aceE* Δ*pyc* was grown in CGXII minimal medium containing 154 mM acetate and 222 mM glucose in 16 repetitive-batch cultures overall. Remarkably, after 8 inoculations, a significantly shortened lag phase was already observed; after 10 inoculations, the Δ*aceE* Δ*pyc* strain featured a lag phase similar to that of the

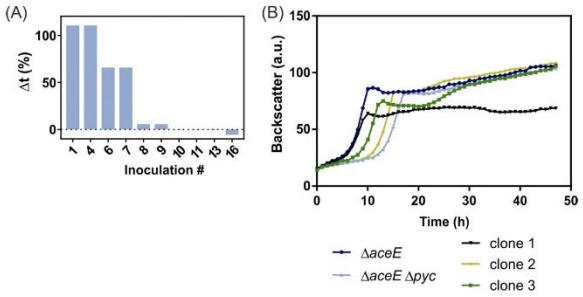


**FIG 8** Adaptive laboratory evolution of *C. glutamicum* Δ*aceE* Δ*pyc*. Growth was analyzed for single inoculation steps obtained from the adaptive laboratory evolution (ALE) approach, which was performed with the Δ*aceE* Δ*pyc* strain in the presence of glucose and acetate. Growth curves are shown based on the backscatter measurements in a microtiter cultivation system. Symbols represent the backscatter means. (A) For growth analysis on the population level, glycerol stocks prepared during the ALE experiment were used for the inoculation of a first preculture in BHI medium supplemented with 51 mM acetate. The second preculture, in CGXII medium containing 154 mM acetate, was then used for inoculation of the main culture in CGXII medium containing 154 mM acetate and 222 mM glucose (starting $OD_{600}$, 1). Shown is the development of the relative lag phase duration after repetitive inoculations of the Δ*aceE* Δ*pyc* strain in media containing glucose and acetate. The difference in the first doubling time between the Δ*aceE* and Δ*aceE* Δ*pyc* strains was set to 100%. For each inoculation, the difference in the lag phase from that for the Δ*aceE* strain was calculated and is given as a percentage. (B) Single clones were isolated from batches 7 (clone 1), 8 (clone 2), and 10 (green) and were cultivated as described above. The Δ*aceE* and Δ*aceE* Δ*pyc* strains served as controls. These single clones were further analyzed by genome sequencing (Table 5).

Δ*aceE* strain (Fig. 8A). In contrast, serial cultivation transfers in CGXII medium containing solely acetate did not lead to improved growth in a glucose-acetate medium, indicating that glucose exerted evolutionary selection pressure (see Fig. S10 in the supplemental material). Genome resequencing of the three selected glucose-acetate clones for which data are presented in Fig. 8B revealed mutations in the *ptsI* gene, encoding the EI enzyme of the PTS, in two independently evolved clones (Table 5). This is in agreement with the reduced biomass formation of both clones, in which glucose uptake was apparently abolished to optimize growth on acetate. The third clone showed only slightly accelerated growth, but biomass formation was not impaired. Here, sequencing revealed a mutation in the *rpsC* gene, encoding the ribosomal S3 protein.

In summary, it was indeed possible to eliminate the observed lag phase of the Δ*aceE* Δ*pyc* strain ascribed to glucose sensitivity by an adaptive laboratory evolution approach. Especially, the mutations identified in the *ptsI* gene are in agreement with other experiments emphasizing the high selective pressure exerted by glucose on PCx-deficient strains when the intracellular $HCO_3^-$ levels are limiting.

## DISCUSSION

During growth on glucose, the pyruvate dehydrogenase complex catalyzes a central metabolic reaction contributing to the intracellular $CO_2/HCO_3^-$ pool. In this study, we systematically perturbed the intracellular $CO_2/HCO_3^-$ pool of PDHC-deficient *C. glutamicum* strains in order to monitor the impact on growth and anaplerotic flux. Even the PDHC-deficient strain *C. glutamicum* Δ*aceE* features a slightly elongated lag phase on glucose-acetate mixtures relative to that of the wild type, while no difference in growth is observed when strains are growing on gluconeogenetic substrates, such as acetate.

**TABLE 5** Key mutations identified in an adaptive laboratory evolution experiment with *C. glutamicum* Δ*aceE* Δ*pyc*

| Clone no. | Batch no. | Gene locus | Gene name | Annotation | Mutation |
|---|---|---|---|---|---|
| 1 | 7 | cg2117 | *ptsI* | EI enzyme, general component of PTS (EC 2.7.3.9) | Exchange, R132H |
| 2 | 8 | cg0601 | *rpsC* | 30S ribosomal protein S3 | Exchange, R225H |
| 3 | 10 | cg2117 | *ptsI* | EI enzyme, general component of PTS (EC 2.7.3.9) | Exchange, G15S |

This is remarkable, since this strain catabolizes only a minor fraction of the glucose provided in the exponential-growth phase but turns to the production of L-valine and L-alanine from glucose in the stationary phase (11, 12). The growth defect of *C. glutamicum* Δ*aceE* was, however, successfully complemented by the addition of $HCO_3^-$, which had no significant effect on the growth of wild-type cells, thus hinting at problems caused by impaired anaplerotic flux in this strain background. By comparing the $CO_2$ production rates of the *C. glutamicum* Δ*aceE* strain and the wild type, Bartek et al. were able to show in a previous study that the Δ*aceE* strain excretes only around 0.83 mmol of $CO_2$ $g^{-1}$ $h^{-1}$, while the wild type excretes ca. 1.65 mmol of $CO_2$ $g^{-1}$ $h^{-1}$ (29). The lower $CO_2$ production rates of the PDHC-deficient strain already indicate a significant impact on the intracellular $CO_2/HCO_3^-$ pool affecting metabolic flux distribution, especially at low cell densities, when $CO_2/HCO_3^-$ is limiting.

The anaplerotic node comprises the essential link between glycolysis/gluconeogenesis and the TCA cycle (20). In contrast to most other organisms, *C. glutamicum* possesses both anaplerotic carboxylases, PEPCx (encoded by *ppc*) and PCx (encoded by *pyc*), catalyzing the anaplerotic bicarbonate-dependent reactions to yield oxaloacetate from PEP or pyruvate, respectively. It was shown that in *C. glutamicum*, these two enzymes can replace each other to a certain extent, depending on the intracellular concentrations of the respective effectors for each enzyme. However, during growth on glucose, the biotin-containing PCx contributes 90% to the main anaplerotic activity, in contrast to PEPCx (23, 32). In our study, deletion of the *pyc* gene resulted in a severely elongated lag phase (>15 h) of the Δ*aceE* Δ*pyc* strain when glucose was present in the medium. Retarded growth of Δ*pyc* strains has been observed previously, and in line with our data, other studies also reported a severe growth defect of a Δ*pyc* strain under low $CO_2/HCO_3^-$ levels (23, 28). This effect appeared to be even more severe when the cells were grown in microtiter plates under $CO_2$-stripping conditions (low culture volume, high air mixing) than when they were grown in higher culture volumes (see Fig. S7 in the supplemental material). The PDHC-deficient mutant strain *C. glutamicum* Δ*aceE* Δ*pyc* was found to react very sensitively to small changes in intracellular bicarbonate availability and was therefore used as a test platform with which to assess systematically the impact of perturbations affecting the intracellular $CO_2/HCO_3^-$ pool. While addition of $HCO_3^-$, an increase in the pH, and higher culture volumes rescued the strain, mutation of the urease accessory protein (*ureD*-E188*), which lowers the intracellular $CO_2/HCO_3^-$ pool, resulted in an even more severe phenotype. It was not possible to restore growth if the second anaplerotic gene, *ppc*, was deleted as well, confirming that the measures mentioned above fostered the flux over the remaining anaplerotic reaction catalyzed by PEPCx.

The mutation in *ureD* was revealed by a previous biosensor-driven evolution approach selecting for mutations enhancing L-valine production in *C. glutamicum* (33). In that study, inactivation of the urease enzyme by the *ureD*-E188* mutation reduced the anaplerotic flux via PCx, resulting in increased precursor availability of pyruvate-derived products, such as L-valine and L-alanine (33). In the present study, we confirmed this finding by complementation with $HCO_3^-$, counteracting the effect of the *ureD*-E188* mutation. In another study, by Blombach et al., lower $CO_2/HCO_3^-$ levels also triggered enhanced production of L-valine and L-alanine by *C. glutamicum* during shake flask cultivation (28). However, a positive impact of anaplerotic reactions has been confirmed for other products, for example, oxaloacetate-derived products, such as L-lysine. In those studies, attempts to overexpress *pyc* or the introduction of deregulated variants significantly improved L-lysine production (41, 42). However, in spite of great efforts and success in the development of L-lysine production strains, the impact of altered $CO_2/HCO_3^-$ levels has not been systematically assessed so far.

Residual glucose consumption by PDHC-deficient *C. glutamicum* strains has already been reported in previous studies (11, 12, 29). The results of this work, however, emphasize that mutants lacking the major anaplerotic route via PCx (Δ*pyc* mutants) are under strong evolutionary pressure in the presence of glucose. Although the strains would be able to grow on the acetate supplied in the growth medium, increasing levels

of glucose resulted in a severely elongated lag phase (as long as >40 h with 250 mM) for *C. glutamicum* Δ*aceE* Δ*pyc*. Besides the above-mentioned efforts to increase the $CO_2/HCO_3^-$ pool, the deletion of the *ptsG* gene itself effectively restored growth on glucose but not on other PTS substrates and not on ribose. These results indicate that growth retardation is not the result of PtsG-dependent regulation as known for *E. coli* (43, 44).

Furthermore, among the three key mutations identified in the ALE experiment, two single nucleotide polymorphisms (SNPs) obtained from independent cell lines were located within the *ptsI* gene, encoding the EI component of the PTS. These findings clearly highlight the problems of residual glucose consumption in strains featuring impaired anaplerotic flux. One reason for the observed growth phenotype might be stress resulting from the intracellular accumulation of sugar phosphates. In *Escherichia coli*, sugar phosphate stress can be caused by the accumulation of any sugar phosphates due to a block in glycolysis (45), e.g., by mutations in *pgi* or *pfkA* (46), or due to excessive glucose uptake caused, e.g., by overexpression of *uhpT*, encoding a sugar phosphate permease (47). The resulting metabolic imbalance causes growth inhibition. For example, in *C. glutamicum*, accumulation of several sugar phosphates, such as fructose-1,6-bisphosphate or PEP, inhibits the key enzyme of the glyoxylate shunt, isocitrate lyase, already at low concentrations (34). To counteract this stress, *E. coli* triggers SgrR, which, in turn, activates SgrS by an unknown signal. The transcription factor SgrS then prevents further uptake of glucose by downregulation of *ptsG* (45, 48, 49). This is in line with the finding of our study showing a slight downregulation of *ptsG* upon resumed growth of the Δ*aceE* Δ*pyc* strain (Table 4). This reduction of glucose uptake via the PTS, which converts PEP to pyruvate during glucose transport, also contributes to increased PEP availability for the remaining anaplerotic reaction catalyzed by PEPCx. Further, this is in line with an upregulation of *iolT1*, which ensures minor usage of glucose without PEP depletion (39, 40). In this context, the downregulation of the *pyk* gene in the Δ*aceE* Δ*pyc* strain can also be interpreted as a potential adaptation to increase the PEP pool, fostering anaplerotic flux. All these strategies counteracting PEP depletion underline the fact that under these conditions, the anaplerotic enzyme PEPCx is not able to deliver appropriate amounts of oxaloacetate in the Δ*aceE* Δ*pyc* strain.

During growth on gluconeogenetic carbon sources—such as acetate—the transcriptional repressor SugR represses the expression of the PTS genes in *C. glutamicum*, including the glucose-specific *ptsG* gene but also *ptsF*, *ptsS*, and general components, such as *ptsI* and *ptsH* (50–52). Derepression appears to be triggered by the accumulation of fructose-6-phosphate (F6P), which is generated from glucose-6-phosphate entering glycolysis. Consequently, F6P accumulation leads to an increase in glucose consumption rates, resulting in parallel catabolization of glucose and acetate (15). The fact that the PDHC-deficient strains are also subject to regulation by SugR has been demonstrated by studies showing that the Δ*aceE* Δ*sugR* strain leads to glucose consumption rates as much as 4-fold higher (53).

In aerobic glucose-based bioprocesses, the endogenous production of $CO_2$ is typically sufficiently high to promote microbial growth even at low cell densities. However, it is well known that the anaerobic growth of some bacteria, such as *E. coli*, requires an external supply of $CO_2/HCO_3^-$ to avoid long lag phases (25, 54, 55). The critical impact of $CO_2/HCO_3^-$ levels may become especially evident under conditions where the endogenous $CO_2$ production rate becomes limiting. This was nicely demonstrated by a recent study of Bracher et al., who showed that long lag phases of engineered, but nonevolved, *Saccharomyces cerevisiae* strains during xylose fermentation could be avoided by sparging the bioreactor cultures with $CO_2$-$N_2$ mixtures (56). Alternatively, the addition of L-aspartate, whose transamination provides oxaloacetate, which refuels the TCA cycle, completely abolished the long adaptation phase of the respective yeast strains. In line with these findings, a recent $^{13}C$ flux analysis with *E. coli* revealed that considerable turnover of lipids via β-oxidation appears to be required for growth on xylose to enhance the intracellular $CO_2/HCO_3^-$ pool to a growth-promoting level that

enables anaplerotic flux (57). These findings are in good agreement with our demonstration in this study that the elongated lag phase of the *C. glutamicum* Δ*aceE* Δ*pyc* strain can be eliminated by various measures, either by increasing the intracellular $CO_2/HCO_3^-$ level or by refueling the TCA cycle with various intermediates, such as citrate, malate, or succinate.

Overall, oxaloacetate depletion appeared to represent a key issue causing the delayed growth of the Δ*aceE* Δ*pyc* strain. Our data revealed that this is caused by impaired anaplerotic flux on glucose due to low intracellular $CO_2/HCO_3^-$ levels as well as reduced activities of glyoxylate cycle enzymes. As known from several organisms, the activity of glyoxylate shunt enzymes is tightly repressed during growth on glucose. In *C. glutamicum*, the transcription of *aceA* (encoding isocitrate lyase) and *aceB* (encoding malate synthase) is repressed by RamB in the presence of glucose (58) and is activated by RamA in the presence of acetate (59). The PDHC-deficient strains in this study were grown on glucose-acetate mixtures. In an earlier study by Wendisch et al., it was emphasized that the anaplerotic function is entirely achieved by the glyoxylate cycle enzymes when wild-type *C. glutamicum* is grown on glucose plus acetate (15). They further revealed that this function can be partly complemented by PEPCx or PCx (15). However, the possibility remains that the glyoxylate cycle enzymes, especially isocitrate lyase, are repressed in the PDHC-deficient mutants due to accumulation of, e.g., sugar phosphates caused by the PDHC and/or *pyc* inactivation. Reinscheid et al. (1994) claimed that the sugar phosphates 3-phosphoglycerate, 6-phosphogluconate, and fructose 1,6-bisphosphate cause inhibition of the isocitrate lyase in *C. glutamicum* (34). Although transcriptional regulation of the glyoxylate shunt is different, isocitrate lyases of *E. coli* are also repressed by glucose catabolites (60–62). Consequently, a repressed glyoxylate shunt due to glucose catabolite accumulation probably also accounts for oxaloacetate depletion in PDHC-deficient strains; this is especially problematic for the Δ*aceE* Δ*pyc* strain, which cannot complement this depletion by anaplerotic pathways due to lower intracellular $CO_2/HCO_3^-$ levels.

Taken together, these results emphasize the important impact of the intracellular $CO_2/HCO_3^-$ pool on metabolic flux distribution, which is especially relevant in engineered strains exhibiting lower endogenous $CO_2$ production rates, as exemplified by PDHC-deficient strains in this study, but also by the performance of pentose-fermenting yeast and *E. coli* strains (56, 57). Consequently, the lack of an important by-product, such as $CO_2$ released by the PDHC, may have a significant impact on cellular metabolism and growth, especially on glycolytic substrates demanding high flux via anaplerotic reactions.

## MATERIALS AND METHODS

**Bacterial strains and growth conditions.** All bacterial strains and plasmids used in this study are listed in Tables 6 and 7, respectively. Mutant strains are based on the wild-type *Corynebacterium glutamicum* strain ATCC 13032 (63).

Standard cultivation of *C. glutamicum* Δ*aceE* cells and derivatives was performed on brain heart infusion (BHI; Difco; BD, Heidelberg, Germany) agar plates containing 51 mM potassium acetate (referred to here as acetate) (ChemSolute; Th. Geyer, Stuttgart, Germany) at 30°C for 2 days. One single colony was picked and was incubated for 8 to 10 h at 30°C in either 4.5 ml or 1 ml BHI containing 154 mM acetate in reaction tubes or deep-well plates (VWR International, PA, USA), respectively. First precultures were used to inoculate second precultures in CGXII minimal medium (64) supplemented with 154 mM acetate either as 10-ml cultures in shake flasks or in 1-ml volumes in deep-well plates. After overnight growth, a main culture was inoculated at an optical density at 600 nm ($OD_{600}$) of 1 in CGXII medium containing 154 mM acetate and either 222 mM D-(+)-glucose monohydrate (Riedel-de Haën, Seelze, Germany) (referred to here as glucose) or any other carbon source as stated, e.g., D-(−)-fructose (Sigma-Aldrich, Taufkirchen, Germany) (referred to as fructose), D-(+)-sucrose (Roth, Karlsruhe, Germany) (referred to as sucrose), D-gluconic acid sodium salt (Sigma-Aldrich, Taufkirchen, Germany) (referred to as gluconate), D-(−)-ribose (Sigma-Aldrich, Taufkirchen, Germany) (referred to as ribose), citric acid monohydrate (Merck Millipore, Darmstadt, Germany) (referred to as citrate), H-Glu-Ala-OH (Bachem AG, Bubendorf, Switzerland) (referred to as Glu-Ala), succinic acid (Sigma-Aldrich, Taufkirchen, Germany) (referred to as succinate), or L-malic acid (Merck Millipore, Darmstadt, Germany) (referred to as malate). To increase the extracellular availability of bicarbonate, 100 mM potassium $HCO_3^-$ (Merck Millipore, Darmstadt, Germany) was added to the basic CGXII solution. The pH was adjusted to 7, and subsequently, the medium was passed through a sterile filter before inoculation. In order to analyze the effects of different pH levels, either HCl (to lower the pH) or KOH (to increase the pH) was added to the CGXII basis, which was sterile

**TABLE 6** Bacterial strains used in this study

| Strain | Characteristics | Source or reference |
|---|---|---|
| *C. glutamicum* | | |
| ATCC 13032 | Wild type, biotin auxotroph | S. Kinoshita et al. (77) |
| Δ*aceE* strain | ATCC 13032 derivative with deletion of *aceE* | M. E. Schreiner et al. (5) |
| Δ*aceE* Δ*pyc* strain | ATCC 13032 derivative with deletions of *aceE* and *pyc* | This work |
| Δ*aceE* Δ*ptsG* strain | ATCC 13032 derivative with deletions of *aceE* and *ptsG* | This work |
| Δ*aceE* Δ*pyc* Δ*ptsG* strain | ATCC 13032 derivative with deletions of *aceE*, *pyc*, and *ptsG* | This work |
| Δ*aceE* Δ*pgi* strain | ATCC 13032 derivative with deletions of *aceE* and *pgi* | This work |
| Δ*aceE* Δ*pyc* Δ*pgi* strain | ATCC 13032 derivative with deletions of *aceE*, *pyc*, and *pgi* | This work |
| Δ*aceE* Δ*ppc* strain | ATCC 13032 derivative with deletions of *aceE* and *ppc* | This work |
| Δ*aceE* Δ*pyc* Δppc strain | ATCC 13032 derivative with deletions of *aceE*, *pyc*, and *ppc* | This work |
| Δ*aceE ureD*-E188* strain | ATCC 13032 derivative with deletion of *aceE* and with *ureD*-E188* (Glu188 replaced by the stop codon) | R. Mahr et al. (33) |
| Δ*aceE ureD*-E188* Δ*pyc* strain | ATCC 13032 derivative with deletions of *aceE* and *pyc* and with *ureD*-E188* (Glu188 replaced by the stop codon) | This work |
| Δ*pyc* strain | ATCC 13032 derivative with deletion of *pyc* | P. G. Peters-Wendisch et al. (23) |
| Δ*pyc* Δ*ppc* strain | ATCC 13032 derivative with deletions of *aceE* and *ppc* | A. Schwentner et al. (78) |
| *E. coli* DH5α | $F^-$ ϕ80*lacZ*ΔM15 Δ(*lacZYA-argF*)*U169 recA1 endA1 hsdR17*($r_K^-$ $m_K^+$) *phoA supE44 thi-1 gyrA96 relA1* $\lambda^-$; for general cloning purposes | Invitrogen |

filtered afterwards. For cultivations in the presence of TCA cycle-filling/refueling substrates, 50 mM citric acid monohydrate (citrate), 3 mM H-Glu-Ala-OH dipeptide (Glu-Ala), 100 mM succinic acid (succinate), or 100 mM L-malic acid (malate) was used. In experiments where gluconate or ribose was used as the carbon source, 100 mM D-gluconic acid sodium salt or 100 mM D-ribose was added, respectively. Biomass formation was monitored during cultivation in shake flasks by measuring the $OD_{600}$ or by measuring backscatter values during microtiter plate cultivation. Where necessary, the medium was also supplemented with 25 μg/ml kanamycin.

*Escherichia coli* DH5α was used for cloning and plasmid isolation. Cells were directly inoculated from a glycerol stock or from a lysogeny broth (LB) agar plate and were grown in shake flasks in LB medium at 37°C. If necessary for selection, the medium was also supplemented with 50 μg/ml kanamycin.

**TABLE 7** Plasmids used in this study

| Plasmid | Characteristics | Source or reference |
|---|---|---|
| pK19*mobsacB* | Contains negative (*sacB*) and positive (Kan$^r$) selection markers for genomic integration and deletion | A. Schäfer et al. (70) |
| pK19*mobsacB*-Δ*pyc* | Kan$^r$; derivative of pK19*mobsacB* for partial *pyc* gene deletion, containing only the first 499 bp and last 493 bp of *pyc*, with the deletion of 2,429 bp in the middle | P. G. Peters-Wendisch et al. (23) |
| pK19*mobsacB*-Δ*ptsG* | Kan$^r$; derivative of pK19*mobsacB* for partial *ptsG* gene deletion, containing only the last 491 bp of *ptsG*, with the deletion of the first 1,561 bp | This work |
| pK19*mobsacB*-Δ*pgi* | Kan$^r$; derivative of pK19*mobsacB* for *pgi* gene deletion, containing only the last 537 bp of *pgi*, with the deletion of the first 1,086 bp | This work |
| pK19*mobsacB*-Δ*ppc* | Kan$^r$; derivative of pK19*mobsacB* for partial *ppc* gene deletion, containing only the first 391 bp and last 447 bp of *ppc*, with the deletion of 1,922 bp in the middle | J. Buchholz et al. (13) |
| pK19*mobsacB-ureD*-E188* | Kan$^r$; derivative of pK19*mobsacB* for *ureD* gene truncation by replacing Glu188 in *ureD* with the stop codon | R. Mahr et al. (33) |
| pJC1 | Kan$^r$ $oriV_{Ec}$ $oriV_{Cg}$; *E. coli-C. glutamicum* shuttle vector | J. Cremer et al. (79) |
| pJC1-*venus*-term-BS | Kan$^r$; derivative of pJC1, containing the terminator sequence of *Bacillus subtilis* behind *venus* | M. Baumgart et al. (74) |
| pJC1-*pyc* | Kan$^r$; derivative of pJC1-*venus*-term-BS, containing *pyc* under the control of its native promoter $P_{pyc}$ | This work |
| pJC1-$P_{tac}$-*aceA-aceB* | Kan$^r$; derivative of pJC1-*venus*-term-BS, containing *lacI* and *aceA* followed by a linking sequence (5′-ACTAGAAATAATTTTGTTTAA CTTTAAGAAGGAGATATACAT-3′) and *aceB* under the control of the inducible promoter $P_{tac}$ | This work |
| pJC1-$P_{tac}$-*aceB-aceA* | Kan$^r$; derivative of pJC1-*venus*-term-BS, containing *lacI* and *aceB* followed by a linking sequence (5′-ACTAGAAATAATTTTGTTTAA CTTTAAGAAGGAGATATACAT-3′) and *aceA* under the control of the inducible promoter $P_{tac}$ | This work |

**Microtiter plate cultivation.** Online monitoring of growth and/or pH was performed in 48-well microtiter FlowerPlates (m2p-labs GmbH, Baesweiler, Germany) sealed with sterile breathable rayon film (VWR International, PA) in a BioLector microtiter cultivation system (m2p-labs GmbH, Baesweiler, Germany) (65). The cultivation conditions were adjusted as described previously (66), and biomass formation was recorded every 15 min as the backscattered light intensity (light wavelength, 620 nm; signal gain factor of 20) for 24 to 72 h at 30°C and 1,200 rpm. pH measurements were performed with 48-well microtiter FlowerPlates equipped with pH optodes. The data obtained were evaluated using BioLection (m2p-labs, Baesweiler, Germany) and GraphPad Prism 7 (GraphPad Software, Inc., San Diego, CA) software.

**ALE.** Adaptive laboratory evolution (ALE) of *C. glutamicum* Δ*aceE* and *C. glutamicum* Δ*aceE* Δ*pyc* was performed in deep-well plates (VWR International, PA) in a main culture of 1 ml CGXII medium containing either 154 mM acetate and 222 mM glucose or solely 154 mM acetate (as a control without selection pressure) adjusted to an $OD_{600}$ of 1. Cells were cultivated for 2 to 3 days before the next generation was inoculated, starting at an $OD_{600}$ of 1, and cultivated again for 2 to 3 days. After each generation step, glycerol stocks of cultures were prepared (20% glycerol) and were stored at −80°C, allowing growth analysis and DNA sequencing of cultures from individual inoculations. In total, 16 serial transfers were analyzed.

**Cloning techniques and recombinant DNA work.** Standard molecular biology methods were performed according to J. Sambrook and D. W. Russell (67). *C. glutamicum* ATCC 13032 chromosomal DNA was used as the template for PCR amplification of DNA fragments and was prepared as described previously (68). DNA fragment and plasmid sequencing, as well as synthesis of oligonucleotides, was performed by Eurofins Genomics (Ebersberg, Germany).

For the construction of plasmids (see Table S3 in the supplemental material), DNA fragments were amplified using the respective oligonucleotides (see Table S4) and were enzymatically assembled into a vector backbone according to reference 69.

To achieve genomic deletion of *pyc*, *ptsG*, *ppc*, and *pgi*, two-step homologous recombination using the pK19*mobsacB* system (70) was implemented. The suicide plasmids (compare Table 7 with Table S2 in the supplemental material) were isolated from *E. coli* cells using the QIAprep spin miniprep kit (Qiagen, Hilden, Germany). Electrocompetent *C. glutamicum* Δ*aceE* and *C. glutamicum* Δ*aceE* Δ*pyc* cells were transformed with these plasmids by electroporation (71). The first and second recombination events were performed and verified as described in previous studies (72). The deletion of *pyc*, *ptsG*, *ppc*, and *pgi* was reviewed by amplification and sequencing using primers shown in Table S1.

**Measurement of glucose concentrations.** To measure the glucose concentration of the culture medium at different time points, cultivation was performed in 50 ml in shaking flasks. During cultivation, 0.5-ml samples were taken every 3 h and were centrifuged (16,000 × *g*). The supernatant was collected and was stored at −20°C until use.

The actual glucose concentration was measured using a D-glucose UV test kit (R-Biopharm, Darmstadt, Germany), and calculations were done, according to the manufacturer's instructions. Absorption was measured at 340 nm.

Further calculations of the glucose uptake rates could be done based on the glucose concentrations and $OD_{600}$ values obtained. According to reference 18, the following equation was used to determine the glucose concentration in nanomoles per gram (dry weight) per hour:

$$\left(\frac{S}{M}\right)\cdot\mu\left[\left(\frac{\text{nmol}\cdot\text{liter}^{-1}\cdot\text{OD}_{600}^{-1}}{\text{gDW}\cdot\text{liter}^{-1}\cdot\text{OD}_{600}^{-1}}\right)\cdot\text{h}^{-1}\right]=\left[\frac{\text{nmol}}{\text{gDW}\cdot\text{h}}\right]$$

where *S* represents the slope of the glucose concentration versus the $OD_{600}$ (expressed as nanomoles per liter per $OD_{600}$ unit), *M* is the correlation between the dry weight and the $OD_{600}$ (expressed in grams [dry weight] per liter per $OD_{600}$ unit), and $\mu$ is the growth rate per hour. According to A. Kabus et al. (73), an $OD_{600}$ of 1 corresponds to 0.25 g (dry weight) $liter^{-1}$, so this value was used as *M* throughout these calculations.

**Quantification of amino acid production.** Using ultrahigh-performance liquid chromatography (uHPLC), amino acids were quantified as *ortho*-phthaldialdehyde derivatives by automatic precolumn derivatization. Derivatives were separated by reverse-phase chromatography on an Agilent (Santa Clara, CA) 1290 Infinity LC ChemStation equipped with a fluorescence detector. As the eluent for the Zorbax Eclipse amino acid analysis (AAA) column (particle size, 3.5 $\mu$m; inside diameter, 4.6 mm; length, 75 mm; Agilent, Santa Clara, CA), a gradient of Na-borate buffer (10 mM $Na_2HPO_4$, 10 mM $Na_2B_4O_7$ [pH 8.2]; adapted to operator's guide) and methanol was applied. Prior to analysis, samples were centrifuged for 10 min at 16,000 × *g* and 4°C and were diluted 1:100.

**Monitoring of cellular proliferation by cell staining.** For the staining of proliferating cells, the PKH67 green fluorescent cell linker kit for general cell membrane labeling (Sigma-Aldrich, Munich, Germany) was used, and the protocol was adapted according to the work of O. Kotte et al. (35). From an exponentially growing preculture in CGXII minimal medium containing 222 mM glucose and 154 mM acetate, $1.5 \times 10^9$ cells were harvested by centrifugation for 4 min at 4,000 × *g* and 4°C. Then the cells were washed again in 5 ml ice-cold CGXII basic solution, without $MgSO_4$, $CaCl_2$, biotin, trace elements, or protocatechuic acid. For staining, the cell pellet was resuspended in 500 $\mu$l dilution buffer C (Sigma-Aldrich, Munich, Germany) at room temperature, and a freshly prepared mixture of 10 $\mu$l PKH67 dye (Sigma-Aldrich, Munich, Germany) and 500 $\mu$l dilution buffer C was added. Subsequently, cells were incubated for 3 min at room temperature, and afterwards, 4 ml ice-cold filtered CGXII basic solution containing 1% (wt/vol) bovine serum albumin, 1 mM $MgSO_4$, and 0.1 mM $CaCl_2$ was added. Then the cells were centrifuged for 4 min at 4,000 × *g* and 4°C, and the cell pellet was washed twice. Finally, the cells

were resuspended in CGXII minimal medium containing 222 mM glucose and 154 mM acetate and were cultivated in a microtiter cultivation system.

**Flow cytometry.** Flow cytometric (FC) analyses were conducted on a FACSAria II flow cytometer (Becton, Dickinson, San Jose, CA) equipped with a blue solid-state laser (excitation, 488 nm). Forward-scatter characteristics (FSC) and side-scatter characteristics (SSC) were recorded as small-angle and orthogonal scatters of the 488-nm laser, respectively. PKH67 fluorescence was detected using a 502-nm long-pass and 530/30-nm band-pass filter set. FACSDiva software, version 6.0, was used to monitor the measurements. During analyses, thresholding on FSC was applied to remove background noise. For FC analyses, PKH67-stained culture samples were diluted to an $OD_{600}$ of 0.05 in FACSFlow sheath fluid buffer (BD, Heidelberg, Germany). FlowJo (version 10.0.8) analysis software was used to visualize and evaluate the data (Tree Star, Ashland, OR).

**DNA microarrays.** For analysis of the transcriptome, *C. glutamicum* Δ*aceE* and *C. glutamicum* Δ*aceE* Δ*pyc* were cultivated in triplicate as described above in 50 ml CGXII medium containing 154 mM acetate and 222 mM glucose in shake flasks. After reaching exponential phase at an $OD_{600}$ of ca. 12 to 15, the cell suspension was harvested by centrifugation (4,256 × *g*, 10 min, 4°C). The resulting pellet was directly frozen in liquid nitrogen and was stored at −80°C. RNA preparation and cDNA synthesis, as well as microchip hybridization, scanning, and evaluation, were performed as described in previous studies (74).

**GC-ToF MS analysis.** For analysis of the metabolome, samples of *C. glutamicum* Δ*aceE* in the exponential phase, as well as samples of *C. glutamicum* Δ*aceE* Δ*pyc* in the stationary and exponential phases, were taken, and cells were disrupted using hot methanol. Further sample preparation, derivatization, mass spectrometry (MS) operation, and peak identification were accomplished according to the method of N. Paczia et al. (75) in an Agilent (Santa Clara, CA) 6890N gas chromatograph coupled to a Waters (Milford, MA) Micromass GCT Premier high-resolution ToF MS. Known metabolites were identified using the in-house database JuPoD, the commercial database NIST17 (National Institute of Standards and Technology, USA), and the GMD database (Max Planck Institute of Molecular Plant Physiology, Golm, Germany) (76).

**Whole-genome sequencing.** In order to sequence the whole genome of *C. glutamicum* Δ*aceE* Δ*pyc* mutants from the ALE experiment using next-generation sequencing (NGS), genomic DNA was prepared using the NucleoSpin microbial DNA kit (Macherey-Nagel, Düren, Germany) according to the manufacturer's instructions. Subsequently, the concentrations of the purified genomic DNA were measured using a Qubit 2.0 fluorometer (Invitrogen, Carlsbad, CA) according to the manufacturer's instructions. Overall, 4 $\mu$g purified genomic DNA was employed for the preparation for genome sequencing using a TruSeq DNA library prep kit and a MiSeq reagent kit, version 1 (Illumina, San Diego, CA, USA), according to the manufacturer's instructions. The sequencing run was performed in a MiSeq system (Illumina, San Diego, CA). Data analysis and base calling were performed with the Illumina instrument software. The resulting FASTQ output files were examined using CLC Genomics Workbench 9 (Qiagen, Aarhus, Denmark).

**Accession number(s).** The microarray data determined in this study are available at NCBI's Gene Expression Omnibus under accession number GSE134218.

## SUPPLEMENTAL MATERIAL

Supplemental material for this article may be found at https://doi.org/10.1128/JB.00387-19.

**SUPPLEMENTAL FILE 1**, PDF file, 1.4 MB.

## ACKNOWLEDGMENTS

We thank Jochem Gätgens for performing GC-ToF analyses, and we thank Bastian Blombach and Stephan Noack for fruitful discussions.

We acknowledge financial support by the Helmholtz Association (grant W2/W3-096).

## REFERENCES

1. Bailey JE, Ollis DF. 1986. Biochemical engineering fundamentals. McGraw-Hill, New York, NY.
2. Blombach B, Takors R. 2015. $CO_2$—intrinsic product, essential substrate, and regulatory trigger of microbial and mammalian production processes. Front Bioeng Biotechnol 3:108. https://doi.org/10.3389/fbioe.2015.00108.
3. de Kok A, Hengeveld AF, Martin A, Westphal AH. 1998. The pyruvate dehydrogenase multi-enzyme complex from Gram-negative bacteria. Biochim Biophys 1385:353–366. https://doi.org/10.1016/S0167-4838(98)00079-X.
4. Eikmanns BJ, Blombach B. 2014. The pyruvate dehydrogenase complex of *Corynebacterium glutamicum*: an attractive target for metabolic engineering. J Biotechnol 192(Pt B):339–345. https://doi.org/10.1016/j.jbiotec.2013.12.019.
5. Schreiner ME, Fiur D, Holátko J, Pátek M, Eikmanns BJ. 2005. E1 enzyme of the pyruvate dehydrogenase complex in *Corynebacterium glutamicum*: molecular analysis of the gene and phylogenetic aspects. J Bacteriol 187:6005–6018. https://doi.org/10.1128/JB.187.17.6005-6018.2005.
6. Becker J, Rohles CM, Wittmann C. 2018. Metabolically engineered *Corynebacterium glutamicum* for bio-based production of chemicals, fuels, materials, and healthcare products. Metab Eng 50:122–141. https://doi.org/10.1016/j.ymben.2018.07.008.
7. Kogure T, Inui M. 2018. Recent advances in metabolic engineering of *Corynebacterium glutamicum* for bioproduction of value-added aromatic chemicals and natural products. Appl Microbiol Biotechnol 102:8685–8705. https://doi.org/10.1007/s00253-018-9289-6.
8. Wang X, Zhang H, Quinn PJ. 2018. Production of L-valine from metabolically engineered *Corynebacterium glutamicum*. Appl Microbiol Biotechnol 102:4319–4330. https://doi.org/10.1007/s00253-018-8952-2.
9. Wendisch VF, Mindt M, Pérez-García F. 2018. Biotechnological production of mono- and diamines using bacteria: recent progress, applications, and perspectives. Appl Microbiol Biotechnol 102:3583–3594. https://doi.org/10.1007/s00253-018-8890-z.

10. Eggeling L, Bott M. 2005. Handbook of *Corynebacterium glutamicum*. Academic Press, Boca Raton, FL.
11. Blombach B, Schreiner ME, Bartek T, Oldiges M, Eikmanns BJ. 2008. *Corynebacterium glutamicum* tailored for high-yield L-valine production. Appl Microbiol Biotechnol 79:471–479. https://doi.org/10.1007/s00253-008-1444-z.
12. Blombach B, Schreiner ME, Holatko J, Bartek T, Oldiges M, Eikmanns BJ. 2007. L-Valine production with pyruvate dehydrogenase complex-deficient *Corynebacterium glutamicum*. Appl Environ Microbiol 73:2079–2084. https://doi.org/10.1128/AEM.02826-06.
13. Buchholz J, Schwentner A, Brunnenkan B, Gabris C, Grimm S, Gerstmeir R, Takors R, Eikmanns BJ, Blombach B. 2013. Platform engineering of *Corynebacterium glutamicum* with reduced pyruvate dehydrogenase complex activity for improved production of L-lysine, L-valine, and 2-ketoisovalerate. Appl Environ Microbiol 79:5566–5575. https://doi.org/10.1128/AEM.01741-13.
14. Cocaign M, Monnet C, Lindley ND. 1993. Batch kinetics of *Corynebacterium glutamicum* during growth on various carbon substrates: use of substrate mixtures to localise metabolic bottlenecks. Appl Microbiol Biotechnol 40:526–530. https://doi.org/10.1007/BF00175743.
15. Wendisch VF, de Graaf AA, Sahm H, Eikmanns BJ. 2000. Quantitative determination of metabolic fluxes during coutilization of two carbon sources: comparative analyses with *Corynebacterium glutamicum* during growth on acetate and/or glucose. J Bacteriol 182:3088–3096. https://doi.org/10.1128/JB.182.11.3088-3096.2000.
16. Dominguez H, Cocaign-Bousquet M, Lindley ND. 1997. Simultaneous consumption of glucose and fructose from sugar mixtures during batch growth of *Corynebacterium glutamicum*. Appl Microbiol Biotechnol 47:600–603. https://doi.org/10.1007/s002530050980.
17. Stansen C, Uy D, Delaunay S, Eggeling L, Goergen J-L, Wendisch VF. 2005. Characterization of a *Corynebacterium glutamicum* lactate utilization operon induced during temperature-triggered glutamate production. Appl Environ Microbiol 71:5920–5928. https://doi.org/10.1128/AEM.71.10.5920-5928.2005.
18. Frunzke J, Engels V, Hasenbein S, Gätgens C, Bott M. 2008. Co-ordinated regulation of gluconate catabolism and glucose uptake in *Corynebacterium glutamicum* by two functionally equivalent transcriptional regulators, GntR1 and GntR2. Mol Microbiol 67:305–322. https://doi.org/10.1111/j.1365-2958.2007.06020.x.
19. Wendisch VF, Spies M, Reinscheid DJ, Schnicke S, Sahm H, Eikmanns BJ. 1997. Regulation of acetate metabolism in *Corynebacterium glutamicum*: transcriptional control of the isocitrate lyase and malate synthase genes. Arch Microbiol 168:262–269. https://doi.org/10.1007/s002030050497.
20. Sauer U, Eikmanns BJ. 2005. The PEP-pyruvate-oxaloacetate node as the switch point for carbon flux distribution in bacteria. FEMS Microbiol Rev 29:765–794. https://doi.org/10.1016/j.femsre.2004.11.002.
21. Eikmanns BJ, Follettie MT, Griot MU, Sinskey AJ. 1989. The phosphoenolpyruvate carboxylase gene of *Corynebacterium glutamicum*: molecular cloning, nucleotide sequence, and expression. Mol Gen Genet 218:330–339. https://doi.org/10.1007/BF00331286.
22. O'Regan M, Thierbach G, Bachmann B, Villeval D, Lepage P, Viret JF, Lemoine Y. 1989. Cloning and nucleotide sequence of the phosphoenolpyruvate carboxylase-coding gene of *Corynebacterium glutamicum* ATCC13032. Gene 77:237–251. https://doi.org/10.1016/0378-1119(89)90072-3.
23. Peters-Wendisch PG, Kreutzer C, Kalinowski J, Patek M, Sahm H, Eikmanns BJ. 1998. Pyruvate carboxylase from *Corynebacterium glutamicum*: characterization, expression and inactivation of the *pyc* gene. Microbiology 144:915–927. https://doi.org/10.1099/00221287-144-4-915.
24. Kai Y, Matsumura H, Inoue T, Terada K, Nagara Y, Yoshinaga T, Kihara A, Tsumura K, Izui K. 1999. Three-dimensional structure of phosphoenolpyruvate carboxylase: a proposed mechanism for allosteric inhibition. Proc Natl Acad Sci U S A 96:823–828. https://doi.org/10.1073/pnas.96.3.823.
25. Repaske R, Repaske AC, Mayer RD. 1974. Carbon dioxide control of lag period and growth of *Streptococcus sanguis*. J Bacteriol 117:652–659.
26. Talley RS, Baugh CL. 1975. Effects of bicarbonate on growth of *Neisseria gonorrhoeae*: replacement of gaseous $CO_2$ atmosphere. Appl Microbiol 29:469–471.
27. Bäumchen C, Knoll A, Husemann B, Seletzky J, Maier B, Dietrich C, Amoabediny G, Buchs J. 2007. Effect of elevated dissolved carbon dioxide concentrations on growth of *Corynebacterium glutamicum* on D-glucose and L-lactate. J Biotechnol 128:868–874. https://doi.org/10.1016/j.jbiotec.2007.01.001.
28. Blombach B, Buchholz J, Busche T, Kalinowski J, Takors R. 2013. Impact of different $CO_2/HCO_3^-$ levels on metabolism and regulation in *Corynebacterium glutamicum*. J Biotechnol 168:331–340. https://doi.org/10.1016/j.jbiotec.2013.10.005.
29. Bartek T, Blombach B, Lang S, Eikmanns BJ, Wiechert W, Oldiges M, Noh K, Noack S. 2011. Comparative $^{13}C$ metabolic flux analysis of pyruvate dehydrogenase complex-deficient, L-valine-producing *Corynebacterium glutamicum*. Appl Environ Microbiol 77:6644–6652. https://doi.org/10.1128/AEM.00575-11.
30. Dominguez H, Lindley ND. 1996. Complete sucrose metabolism requires fructose phosphotransferase activity in *Corynebacterium glutamicum* to ensure phosphorylation of liberated fructose. Appl Environ Microbiol 62:3878–3880.
31. Moon MW, Kim HJ, Oh TK, Shin CS, Lee JS, Kim SJ, Lee JK. 2005. Analyses of enzyme II gene mutants for sugar transport and heterologous expression of fructokinase gene in *Corynebacterium glutamicum* ATCC 13032. FEMS Microbiol Lett 244:259–266. https://doi.org/10.1016/j.femsle.2005.01.053.
32. Peters-Wendisch PG, Eikmanns BJ, Thierbach G, Bachmann B, Sahm H. 1993. Phosphoenolpyruvate carboxylase in *Corynebacterium glutamicum* is dispensable for growth and lysine production. FEMS Microbiol Lett 112:269–274. https://doi.org/10.1111/j.1574-6968.1993.tb06461.x.
33. Mahr R, Gätgens C, Gätgens J, Polen T, Kalinowski J, Frunzke J. 2015. Biosensor-driven adaptive laboratory evolution of L-valine production in *Corynebacterium glutamicum*. Metab Eng 32:184–194. https://doi.org/10.1016/j.ymben.2015.09.017.
34. Reinscheid DJ, Eikmanns BJ, Sahm H. 1994. Characterization of the isocitrate lyase gene from *Corynebacterium glutamicum* and biochemical analysis of the enzyme. J Bacteriol 176:3474–3483. https://doi.org/10.1128/jb.176.12.3474-3483.1994.
35. Kotte O, Volkmer B, Radzikowski JL, Heinemann M. 2014. Phenotypic bistability in *Escherichia coli*'s central carbon metabolism. Mol Syst Biol 10:736. https://doi.org/10.15252/msb.20135022.
36. Takhaveev V, Heinemann M. 2018. Metabolic heterogeneity in clonal microbial populations. Curr Opin Microbiol 45:30–38. https://doi.org/10.1016/j.mib.2018.02.004.
37. Heinemann M, Zenobi R. 2011. Single cell metabolomics. Curr Opin Biotechnol 22:26–31. https://doi.org/10.1016/j.copbio.2010.09.008.
38. Davis KM, Isberg RR. 2016. Defining heterogeneity within bacterial populations via single cell approaches. Bioessays 38:782–790. https://doi.org/10.1002/bies.201500121.
39. Ikeda M, Mizuno Y, Awane SI, Hayashi M, Mitsuhashi S, Takeno S. 2011. Identification and application of a different glucose uptake system that functions as an alternative to the phosphotransferase system in *Corynebacterium glutamicum*. Appl Microbiol Biotechnol 90:1443–1451. https://doi.org/10.1007/s00253-011-3210-x.
40. Lindner SN, Seibold GM, Henrich A, Krämer R, Wendisch VF. 2011. Phosphotransferase system-independent glucose utilization in *Corynebacterium glutamicum* by inositol permeases and glucokinases. Appl Environ Microbiol 77:3571–3581. https://doi.org/10.1128/AEM.02713-10.
41. Peters-Wendisch PG, Schiel B, Wendisch VF, Katsoulidis E, Mockel B, Sahm H, Eikmanns BJ. 2001. Pyruvate carboxylase is a major bottleneck for glutamate and lysine production by *Corynebacterium glutamicum*. J Mol Microbiol Biotechnol 3:295–300.
42. Kortmann M, Mack C, Baumgart M, Bott M. 2019. Pyruvate carboxylase variants enabling improved lysine production from glucose identified by biosensor-based high-throughput fluorescence-activated cell sorting screening. ACS Synth Biol 8:274–281. https://doi.org/10.1021/acssynbio.8b00510.
43. Chatterjee R, Millard CS, Champion K, Clark DP, Donnelly MI. 2001. Mutation of the *ptsG* gene results in increased production of succinate in fermentation of glucose by *Escherichia coli*. Appl Environ Microbiol 67:148–154. https://doi.org/10.1128/AEM.67.1.148-154.2001.
44. Wang Q, Wu C, Chen T, Chen X, Zhao X. 2006. Expression of galactose permease and pyruvate carboxylase in *Escherichia coli ptsG* mutant increases the growth rate and succinate yield under anaerobic conditions. Biotechnol Lett 28:89–93. https://doi.org/10.1007/s10529-005-4952-2.
45. Vanderpool CK, Gottesman S. 2007. The novel transcription factor SgrR coordinates the response to glucose-phosphate stress. J Bacteriol 189:2238–2248. https://doi.org/10.1128/JB.01689-06.
46. Morita T, El-Kazzaz W, Tanaka Y, Inada T, Aiba H. 2003. Accumulation of glucose 6-phosphate or fructose 6-phosphate is responsible for destabilization of glucose transporter mRNA in *Escherichia coli*. J Biol Chem 278:15608–15614. https://doi.org/10.1074/jbc.M300177200.

47. Kadner RJ, Murphy GP, Stephens CM. 1992. Two mechanisms for growth inhibition by elevated transport of sugar phosphates in *Escherichia coli*. J Gen Microbiol 138:2007–2014. https://doi.org/10.1099/00221287-138-10-2007.
48. Kessler JR, Cobe BL, Richards GR. 2017. Stringent response regulators contribute to recovery from glucose phosphate stress in *Escherichia coli*. Appl Environ Microbiol 83:e01636-17. https://doi.org/10.1128/aem.01636-17.
49. Vanderpool CK, Gottesman S. 2004. Involvement of a novel transcriptional activator and small RNA in post-transcriptional regulation of the glucose phosphoenolpyruvate phosphotransferase system. Mol Microbiol 54:1076–1089. https://doi.org/10.1111/j.1365-2958.2004.04348.x.
50. Engels V, Wendisch VF. 2007. The DeoR-type regulator SugR represses expression of *ptsG* in *Corynebacterium glutamicum*. J Bacteriol 189:2955–2966. https://doi.org/10.1128/JB.01596-06.
51. Gaigalat L, Schlüter JP, Hartmann M, Mormann S, Tauch A, Pühler A, Kalinowski J. 2007. The DeoR-type transcriptional regulator SugR acts as a repressor for genes encoding the phosphoenolpyruvate:sugar phosphotransferase system (PTS) in *Corynebacterium glutamicum*. BMC Mol Biol 8:104. https://doi.org/10.1186/1471-2199-8-104.
52. Tanaka Y, Teramoto H, Inui M, Yukawa H. 2008. Regulation of expression of general components of the phosphoenolpyruvate:carbohydrate phosphotransferase system (PTS) by the global regulator SugR in *Corynebacterium glutamicum*. Appl Microbiol Biotechnol 78:309–318. https://doi.org/10.1007/s00253-007-1313-1.
53. Blombach B, Arndt A, Auchter M, Eikmanns BJ. 2009. L-Valine production during growth of pyruvate dehydrogenase complex-deficient *Corynebacterium glutamicum* in the presence of ethanol or by inactivation of the transcriptional regulator SugR. Appl Environ Microbiol 75:1197–1200. https://doi.org/10.1128/AEM.02351-08.
54. Repaske R, Clayton MA. 1978. Control of *Escherichia coli* growth by $CO_2$. J Bacteriol 135:1162–1164.
55. Valley G, Rettger LF. 1927. The influence of carbon dioxide on bacteria. J Bacteriol 14:101–137.
56. Bracher JM, Martinez-Rodriguez OA, Dekker WJC, Verhoeven MD, van Maris AJA, Pronk JT. 2019. Reassessment of requirements for anaerobic xylose fermentation by engineered, non-evolved *Saccharomyces cerevisiae* strains. FEMS Yeast Res 19. https://doi.org/10.1093/femsyr/foy104.
57. Gonzalez JE, Long CP, Antoniewicz MR. 2017. Comprehensive analysis of glucose and xylose metabolism in *Escherichia coli* under aerobic and anaerobic conditions by $^{13}C$ metabolic flux analysis. Metab Eng 39:9–18. https://doi.org/10.1016/j.ymben.2016.11.003.
58. Gerstmeir R, Cramer A, Dangel P, Schaffer S, Eikmanns BJ. 2004. RamB, a novel transcriptional regulator of genes involved in acetate metabolism of *Corynebacterium glutamicum*. J Bacteriol 186:2798–2809. https://doi.org/10.1128/JB.186.9.2798-2809.2004.
59. Cramer A, Gerstmeir R, Schaffer S, Bott M, Eikmanns BJ. 2006. Identification of RamA, a novel LuxR-type transcriptional regulator of genes involved in acetate metabolism of *Corynebacterium glutamicum*. J Bacteriol 188:2554–2567. https://doi.org/10.1128/JB.188.7.2554-2567.2006.
60. Kornberg HL. 1966. The role and control of the glyoxylate cycle in *Escherichia coli*. Biochem J 99:1–11. https://doi.org/10.1042/bj0990001.
61. MacKintosh C, Nimmo HG. 1988. Purification and regulatory properties of isocitrate lyase from *Escherichia coli* ML308. Biochem J 250:25–31. https://doi.org/10.1042/bj2500025.
62. Robertson EF, Reeves HC. 1986. Purification and characterization of isocitrate lyase from *Escherichia coli*. Curr Microbiol 14:347–350. https://doi.org/10.1007/BF01568702.
63. Kalinowski J, Bathe B, Bartels D, Bischoff N, Bott M, Burkovski A, Dusch N, Eggeling L, Eikmanns BJ, Gaigalat L, Goesmann A, Hartmann M, Huthmacher K, Krämer R, Linke B, McHardy AC, Meyer F, Möckel B, Pfefferle W, Pühler A, Rey DA, Rückert C, Rupp O, Sahm H, Wendisch VF, Wiegräbe I, Tauch A. 2003. The complete *Corynebacterium glutamicum* ATCC 13032 genome sequence and its impact on the production of L-aspartate-derived amino acids and vitamins. J Biotechnol 104:5–25. https://doi.org/10.1016/S0168-1656(03)00154-8.
64. Keilhauer C, Eggeling L, Sahm H. 1993. Isoleucine synthesis in *Corynebacterium glutamicum*: molecular analysis of the *ilvB-ilvN-ilvC* operon. J Bacteriol 175:5595–5603. https://doi.org/10.1128/jb.175.17.5595-5603.1993.
65. Kensy F, Zang E, Faulhammer C, Tan RK, Büchs J. 2009. Validation of a high-throughput fermentation system based on online monitoring of biomass and fluorescence in continuously shaken microtiter plates. Microb Cell Fact 8:31. https://doi.org/10.1186/1475-2859-8-31.
66. Mustafi N, Grünberger A, Kohlheyer D, Bott M, Frunzke J. 2012. The development and application of a single-cell biosensor for the detection of L-methionine and branched-chain amino acids. Metab Eng 14:449–457. https://doi.org/10.1016/j.ymben.2012.02.002.
67. Sambrook J, Russell DW. 2001. Molecular cloning: a laboratory manual, 3rd ed. Cold Spring Harbor Laboratory Press, Cold Spring Harbor, NY.
68. Eikmanns BJ, Thum-Schmitz N, Eggeling L, Ludtke K-U, Sahm H. 1994. Nucleotide sequence, expression and transcriptional analysis of the *Corynebacterium glutamicum gltA* gene encoding citrate synthase. Microbiology 140:1817–1828. https://doi.org/10.1099/13500872-140-8-1817.
69. Gibson DG, Young L, Chuang RY, Venter JC, Hutchison CA, Smith HO. 2009. Enzymatic assembly of DNA molecules up to several hundred kilobases. Nat Methods 6:343–345. https://doi.org/10.1038/nmeth.1318.
70. Schäfer A, Tauch A, Jäger W, Kalinowski J, Thierbach G, Pühler A. 1994. Small mobilizable multi-purpose cloning vectors derived from the *Escherichia coli* plasmids pK18 and pK19: selection of defined deletions in the chromosome of *Corynebacterium glutamicum*. Gene 145:69–73. https://doi.org/10.1016/0378-1119(94)90324-7.
71. van der Rest ME, Lange C, Molenaar D. 1999. A heat shock following electroporation induces highly efficient transformation of *Corynebacterium glutamicum* with xenogeneic plasmid DNA. Appl Microbiol Biotechnol 52:541–545. https://doi.org/10.1007/s002530051557.
72. Niebisch A, Bott M. 2001. Molecular analysis of the cytochrome $bc_1$-$aa_3$ branch of the *Corynebacterium glutamicum* respiratory chain containing an unusual diheme cytochrome $c_1$. Arch Microbiol 175:282–294. https://doi.org/10.1007/s002030100262.
73. Kabus A, Georgi T, Wendisch VF, Bott M. 2007. Expression of the *Escherichia coli pntAB* genes encoding a membrane-bound transhydrogenase in *Corynebacterium glutamicum* improves L-lysine formation. Appl Microbiol Biotechnol 75:47–53. https://doi.org/10.1007/s00253-006-0804-9.
74. Baumgart M, Luder K, Grover S, Gätgens C, Besra GS, Frunzke J. 2013. IpsA, a novel LacI-type regulator, is required for inositol-derived lipid formation in *Corynebacteria* and *Mycobacteria*. BMC Biol 11:122. https://doi.org/10.1186/1741-7007-11-122.
75. Paczia N, Nilgen A, Lehmann T, Gätgens J, Wiechert W, Noack S. 2012. Extensive exometabolome analysis reveals extended overflow metabolism in various microorganisms. Microb Cell Fact 11:122. https://doi.org/10.1186/1475-2859-11-122.
76. Hummel J, Strehmel N, Selbig J, Walther D, Kopka J. 2010. Decision tree supported substructure prediction of metabolites from GC-MS profiles. Metabolomics 6:322–333. https://doi.org/10.1007/s11306-010-0198-7.
77. Kinoshita S, Udaka S, Shimono M. 2004. Studies on the amino acid fermentation. Part 1. Production of L-glutamic acid by various microorganisms. J Gen Appl Microbiol 50:331–343.
78. Schwentner A, Feith A, Münch E, Busche T, Rückert C, Kalinowski J, Takors R, Blombach B. 2018. Metabolic engineering to guide evolution: creating a novel mode for L-valine production with *Corynebacterium glutamicum*. Metab Eng 47:31–41. https://doi.org/10.1016/j.ymben.2018.02.015.
79. Cremer J, Eggeling L, Sahm H. 1990. Cloning the *dapA dapB* cluster of the lysine-secreting bacterium *Corynebacterium glutamicum*. Mol Gen Genet 220:478–480. https://doi.org/10.1007/BF00391757.

# 4. Appendix

## 4.1. Evolutionary engineering of *Corynebacterium glutamicum*

Stella, R., **Wiechert, J.**, Noack, S. and Frunzke, J.

Published in *Biotechnology Journal*, 2019.

| Contributor Role | Contributor |
|---|---|
| Conceptualization | RS 35 %, JW 10 %, SN 10 %, JF 45 % |
| Formal Analysis | - |
| Investigation/Experiments | - |
| Methodology | - |
| Project Administration | RS 50 %, JW 5 %, JF 45 % |
| Software | - |
| Supervision | RS 50 %, JF 50 % |
| Visualization | RS 100 % |
| Writing – Original Draft Preparation | RS 60 %, JW 10 %, SN 10 %, JF 20 % |
| Writing – Reviewing & Editing | RS 45 %, JW 5 %, SN 5 %, JF 45 % |

Overall contribution JW: 15 %

The main contribution of JW to this review was the writing of the chapter “Metabolic Engineering to Guide Evolution”.

REVIEW

Biotechnology Journal
www.biotechnology-journal.com

# Evolutionary engineering of *Corynebacterium glutamicum*

*Roberto G. Stella, Johanna Wiechert, Stephan Noack, and Julia Frunzke**

**A unique feature of biotechnology is that we can harness the power of evolution to improve process performance. Rational engineering of microbial strains has led to the establishment of a variety of successful bioprocesses, but it is hampered by the overwhelming complexity of biological systems. Evolutionary engineering represents a straightforward approach for fitness-linked phenotypes (e.g., growth or stress tolerance) and is successfully applied to select for strains with improved properties for particular industrial applications. In recent years, synthetic evolution strategies have enabled selection for increased small molecule production by linking metabolic productivity to growth as a selectable trait. This review summarizes the evolutionary engineering strategies performed with the industrial platform organism *Corynebacterium glutamicum*. An increasing number of recent studies highlight the potential of adaptive laboratory evolution (ALE) to improve growth or stress resistance, implement the utilization of alternative carbon sources, or improve small molecule production. Advances in next-generation sequencing and automation technologies will foster the application of ALE strategies to streamline microbial strains for bioproduction and enhance our understanding of biological systems.**

## 1. Introduction

The Gram-positive actinomycete *Corynebacterium glutamicum* has a long-standing history in microbial biotechnology, following its isolation in 1957 by Kinoshita et al.[1] due to its potential to secrete large amounts of L-glutamate.[2] In the last few decades, *C. glutamicum* has been engineered for the production of a variety of value-added products, including amino acids, organic acids, polymer precursors, aromatic chemicals, and proteins. These achievements are mainly the result of classical metabolic engineering and have been summarized in a number of recent reviews.[3–6]

R. G. Stella, J. Wiechert, Dr. S. Noack, Prof. J. Frunzke
Institute of Bio- and Geosciences, IBG-1: Biotechnology,
Forschungszentrum Jülich
Wilhelm-Johnen-Straße
52428, Jülich, Germany
E-mail: j.frunzke@fz-juelich.de



**DOI: 10.1002/biot.201800444**

Systems biology and metabolic engineering take a rational approach at strain development and are aided by the high level of information available for *C. glutamicum*, including a comprehensive overview on the transcriptomic map and detailed information on metabolic pathways and their regulation.[5,7,8] Strain construction is accelerated by an ever-increasing amount of synthetic biology tools, such as CRISPR/Cpf1[9] and CRISPRi,[10] which has been covered by several reviews.[5,11,12] Transcription factor-based biosensors, which enable the visualization of cellular productivity at the single-cell level, have proven to be a powerful tool for the high-throughput screening of strain or enzyme libraries and for single-cell analysis of producer strains.[13–16]

While rational approaches are indispensable for the development of industrial platform strains in general, their application is often hampered by the overwhelming complexity of biological systems. Even for well-established model systems, like *C. glutamicum* or *Escherichia coli*, we are still not able to quantitatively predict responses to environmental changes or genetic perturbations. However, nature itself provides us with the most powerful approach for the optimization of biological systems: evolution. Evolutionary engineering, also known as adaptive laboratory evolution (ALE), has a long-standing history in the development of microbial production strains and has been heavily applied to improve growth rates, stress, or product tolerance.[17,18] ALE requires microbial growth, which is usually facilitated by repetitive batch cultivations or continuous cultivations, which can be simple (e.g., shake flasks) or more advanced (e.g., pH auxostats).[17,19] When combined with next-generation sequencing and comprehensive omics analysis, ALE strategies can be used to not only obtain better production strains, but also to identify non-intuitive targets for strain engineering, and ultimately to gain a comprehensive understanding of biological pathway regulation. Furthermore, advances in automation of laboratory workflows and microbial phenotyping are fostering a tremendous increase in throughput and efficiency.

This review gives an overview of evolutionary engineering of *C. glutamicum*, including approaches to improve growth on glucose or alternative carbon sources, stress tolerance, or small molecule production by growth coupling strategies and biosensor-guided evolution (**Figure 1**, examples summarized in **Table 1**). We conclude by highlighting the potential of a smart combination of synthetic biology and workflow automation for next-generation evolutionary engineering approaches.

ADVANCED SCIENCE NEWS
www.advancedsciencenews.com

Biotechnology Journal
www.biotechnology-journal.com

## 2. Accelerating Growth on Glucose

The time needed for biomass production represents a key factor in the economic success of biotechnological processes. While ALE approaches have been intensively explored to accelerate the growth of *E. coli*,[37,38] so far, only two recent studies have reported on the evolution of *C. glutamicum* towards higher growth rates on glucose minimal medium (Table 1).[20,21] Interestingly, these studies revealed similar key targets for enhancing metabolic flux and increasing substrate uptake rates for both species, indicating that microorganisms follow similar principles to adapt to fast growth.

Among the key targets for improving growth on glucose, mutations in the *pyk* gene, encoding the pyruvate kinase (PK), were recently described. Reintroduction of the identified single-nucleotide polymorphism (SNPs) into the parental strain caused a significant decrease in PK activity (T12A, and A20V).[20] Furthermore, a mutation of alanine 271 to threonine (A271T) was enriched in one cell line. Intriguingly, a PK enzyme carrying this mutation was previously described as being desensitized toward the allosteric activator fructose 1,6-bisphosphate (FBP), resulting in reduced PK activity upon accumulation of the glycolytic intermediate FBP.[39] Mutations in the *pyk* gene were also identified in the prominent *E. coli* long-term evolution experiment that lasted for more than 25 years,[40] and in a recent study by LaCroix et al.[41] where cells were evolved towards fast growth on glucose. It is interesting to note that fast proliferating eukaryotic cells, like embryonic stem cells and cancer cells, also harbor a less active PKM2 isoform of the PK enzyme.[42,43] From these findings, we can conclude that lowering the PK activity appears to be a conserved strategy of fast-growing cells that need to exploit large amounts of glucose for anabolic pathways.

**Robert Stella** is a Ph.D. student in the group of Prof. Julia Frunzke at Forschungszentrum Jülich, Germany. He received his Master of Science degree in Life Science and Technology from the Delft University of Technology, The Netherlands in 2017. After a research internship at Synthetic Genomics Inc., San Diego, USA in 2017, he started his PhD studies in 2018. His research interests comprise transcription factor-based biosensors, synthetic evolution strategies, lab automation methods, and the intersection of those fields.

**Julia Frunzke** studied Biology at the University of Marburg. From 2004 to 2007 she did her doctoral studies at Forschungszentrum Jülich and obtained her Ph.D. in 2007 from Heinrich Heine University in Düsseldorf, Germany. Subsequently, she was a postdoctoral fellow at the Institute for Microbiology, ETH Zurich, Switzerland. In 2009 she started her own lab at the Institute of Bio- and Geosciences, IBG-1, at Forschungszentrum Jülich where she held her own Helmholtz Young Investigators Group (2011 to 2016) and was Assistant Professor at the HHU. Since 2017 she holds a position as an Associate Professor in Microbiology at HHU.

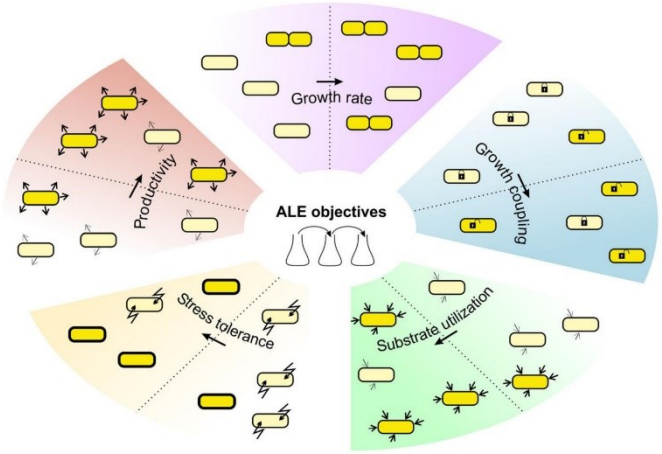


**Figure 1.** Overview of different objectives in *C. glutamicum* ALE studies. ALE has successfully been applied to increase the growth rate,[20,21] substrate utilization,[22] stress tolerance,[23,24] and small molecule production.[25] Growth coupling strategies have been used to increase precursor supply and small molecule production.[26]

 

ADVANCED SCIENCE NEWS
www.advancedsciencenews.com

Biotechnology Journal
www.biotechnology-journal.com

**Table 1.** Overview of ALE studies with *C. glutamicum*.

| ALE target | Experimental setup | ALE duration | Phenotype of evolved strain | Sequencing/ transcriptomics | Proven causal mutations | References |
|---|---|---|---|---|---|---|
| Growth | | | | | | |
| Accelerating growth on glucose minimal media | Repetitive batch in minimal media containing glucose as sole carbon source | Approximately 630 generations | 26% higher growth rate ($0.67 \pm 0.01\ h^{-1}$) | WGS of two independently evolved cell lines, 70 mutations | Mutational hotspots in *pyk*, *fruK*, and *corA* | [20] |
| Accelerating growth on glucose minimal media | Repetitive batch in minimal media containing glucose as sole carbon source | 7 months, approximately 1500 generations | 42% higher growth rate ($0.64 \pm 0.01\ h^{-1}$) | WGS after different ALE times, seven mutations and one genomic deletion (CGP3 element) | *gntR1*-E70K and *ramA*-A52V | [21] |
| Stress tolerance | | | | | | |
| Increased growth at high temperatures | Repetitive batch in rich media, a gradual increase in process temperature | 65 days | Better performance at suboptimal temperatures, increased $T_{max}$ (41.5 °C) | WGS of three evolved isolates, deletion of two genomic regions, 295 total point mutations | *glmU*-E295K and *otsA*-R328H | [27] |
| Increased tolerance to inhibitors in corn stover hydrolysate | Repetitive batch in minimal media with corn stover hydrolysate | 128 days | Higher degradation rate of several inhibitors, higher growth rate on media containing corn stover hydrolysate | WGS of evolved and parental culture, seven mutations; transcriptome comparison between evolved and parental strain | Not determined | [23] |
| Increased tolerance to methanol | Repetitive batch in minimal media containing methanol | 50 generations | Improved growth rate on minimal media with 500–2000 mM methanol | WGS of single isolate, 29 mutations found; transcriptome analysis using DNA microarrays | *metY*-A165T and *cat*-Q342* | [24] |
| Increased tolerance to $H_2O_2$ | Chemostat with a dilution rate of $0.15\ h^{-1}$, growth on minimal media containing glucose, gradual increase of $H_2O_2$ concentration to 10 mM | 1900 h (approximately 411 generations) | Better performance in media containing 10 mM $H_2O_2$ | No sequencing performed; transcriptome analysis using RNAseq | Not determined | [28] |
| Substrate expansion | | | | | | |
| Improved growth on cellobiose | Repetitive batch in minimal media containing cellobiose | 25 days | Improved growth on cellobiose | WGS of two differently evolved strains, ten shared mutations identified; transcriptome analysis using DNA microarrays | Not determined | [29] |
| Improved growth on D-xylose | Automated repetitive batch in minimal media containing D-xylose | 13 days (35 generations) | Twofold increase in growth rate on D-xylose ($0.26 \pm 0.02\ h^{-1}$) | WGS of multiple evolved strains | Upregulation of *iolT1* | [22,30] |
| Co-utilization of xylose and methanol | Repetitive batch in minimal media with xylose and methanol | 206 days (approximately 27 generations) | 20-fold increase in growth rate ($0.03\ h^{-1}$) | WGS of three evolved isolates, six missense mutations; $^{13}C$ flux analysis | Not determined | [31] |
| Metabolic engineering to guide evolution | | | | | | |
| Evolution of a PEP and | Repetitive batch in media containing | 13, 15 or 33 days | | | *icd*-A94D, *icd*-R453C, | [26] |

(*Continued*)

 

ADVANCED SCIENCE NEWS
www.advancedsciencenews.com

Biotechnology Journal
www.biotechnology-journal.com

**Table 1.** (*Continued*)

| ALE target | Experimental setup | ALE duration | Phenotype of evolved strain | Sequencing/ transcriptomics | Proven causal mutations | References |
|---|---|---|---|---|---|---|
| pyruvate carboxylase-deficient strain towards growth on glucose | yeast extract and glucose | | Improved growth rate to 59% of WT ($0.23 \pm 0.01\ h^{-1}$) | WGS of three independently evolved mutants | and *icd*-G407S | |
| Increasing small molecule production | | | | | | |
| Increased fatty acid production | Sequential selection for suppressor mutants on agar plates containing Tween40 or cerulenin | Multiple days | Increased fatty acid production ($322.23 \pm 15.09\ mg\ L^{-1}$) | WGS of best-producing isolate, a total of four mutations | *fasR*-S20D, $fasA^{UP}$-C63G, *fasA*-A2623V and *accD3*-A433T | [32,33] |
| Increased putrescine production | Repetitive batch in rich media containing putrescine, after random mutagenesis | 11 days | Increased putrescine titer ($111.42 \pm 2.56$ mM) | WGS of best-producing isolate, 78 SNPs | Not determined | [34] |
| Increased L-ornithine production | Repetitive batch in media containing glucose and L-ornithine | 70 days | 20% higher L-ornithine titer ($13.6 \pm 0.5\ g\ L^{-1}$) | Not performed | Not determined | [35] |
| Biosensor-guided evolution | | | | | | |
| Increased L-valine production | Repetitive batch in minimal media containing glucose and acetate, selection via biosensor mediated FACS | 6 days | Higher growth rate ($0.41 \pm 0.02\ h^{-1}$) and 63% increased L-valine titer (57 mM) | WGS of evolved culture and two isolates | *glxR*-T93S, *prpD*-T201I, *rpsP*-D30D, and *ureD*-E188* | [25] |
| Plasmid-based protein production | Repetitive batch in minimal media containing glucose, selection via biosensor mediated FACS | 8 days | Higher plasmid copy number | Sequencing of plasmid backbone | Several inactivating mutations in *parB* | [36] |

Further key targets identified by Pfeifer et al.[20] were mutations in *fruK*, which encodes for 1-phosphofructokinase (Pfk1). In a previous study, deletion of the *fruK* gene was actually reported to enhance glucose uptake of *C. glutamicum*.[44] The authors speculated that this was the result of an accumulation of F1P relieving *ptsG* repression via the SugR regulator. However, further analyses are required to understand the impact of Pfk1 on the sugar phosphate pool and its impact on regulatory networks in these strains.

The *corA* gene, coding for a putative $Mg^{2+}/Co^{2+}$ transport protein,[45] represented an unexpected mutational hotspot in the *C. glutamicum* long-term evolution and was also identified, but not discussed, in the *E. coli* experiment of LaCroix et al.[20,41] $Mg^{2+}$ limitation was previously described to increase glucose consumption rates and metabolic flux of *E. coli* in the stationary phase. Here, the authors assumed that reduced $Mg^{2+}$ levels might cause a block in pyruvate dehydrogenase (PDH) activity, leading to an accumulation of upstream intermediates like 2-phosphoenolpyruvate (PEP), which stimulate glucose uptake.[46] However, the availability of magnesium ions is known to affect a variety of different enzymes and to have an impact on the stability of polyphosphates.[45] For example, the biologically active form of ATP is a complex with $Mg^{2+}$. Based on these findings, we can conclude that mutation of *corA* linked to magnesium limitation appears to be a prime target to enhance glucose uptake, but the underlying mechanism is not fully understood and requires further theoretical and experimental attention.

In another recent ALE experiment, *C. glutamicum* cultures were evolved for about 1500 generations in defined media with glucose.[21] The evolved cell line was found to lack large parts of the CGP3 element. Deletion of the prophage CGP3 was also revealed as a competitive fitness advantage in the other *C. glutamicum* ALE study, where a competitive growth experiment showed that a prophage-free strain (MB001) outcompetes the wild type.[20] Besides the lack of the prophage element, the authors found mutations in the *gntR1* gene, encoding a repressor of

 

ADVANCED SCIENCE NEWS
www.advancedsciencenews.com

Biotechnology Journal
www.biotechnology-journal.com

gluconate catabolism and an activator of *ptsG*,[47] and in *ramA*, encoding a LuxR-type regulator, which inherits a global role in the coordination of the central metabolism.[48] Re-introduction into the wild-type background revealed that both mutations significantly increased the growth rate and glucose consumption rate (Table 1).[21] Metabolomic flux and transcriptome analysis showed an increased flux through the pentose phosphate pathway but did not indicate significant rewiring of the central metabolic network, which is in agreement with similar studies on *E. coli*.[49]

## 3. Improving Performance under Industrial Conditions

Evolutionary engineering provides an efficient means to improve the performance of microbial strains under harsh industrial conditions and/or to realize the utilization of second and third generation feedstock.[50,51] Recent studies have employed ALE strategies for both aspects, and while the division is not always clear (e.g., in the case of methanol tolerance and utilization), they will be discussed separately in this section (Table 1).

### 3.1. Improving Stress Tolerance

In an economically optimized bioprocess, microorganisms should be able to grow on low-purity feedstock (lower substrate costs) and at favorable process conditions (e.g., at a higher temperature, to reduce cooling costs). An improved heat tolerance was reported for *C. glutamicum* after a repetitive batch ALE (rbALE) of 65 days, in which the temperature was gradually increased from 38 °C to 41.5 °C.[27] Sequencing of three evolved isolates revealed a surprisingly high amount of 295 point mutations and two genomic deletions in total. This was caused by an acquired mutator phenotype, which resulted in a mutation rate 40- to 80-fold higher than that of the parental strain. A genetic basis for this phenotype was not found. However, the combined reengineering of the mutations *glmU* (E295K) and *otsA*(R328H) resulted in an improved heat tolerance and increased the maximum specific growth rate at 40.7 °C from $0.27 \pm 0.02\ h^{-1}$ to $0.33 \pm 0.03\ h^{-1}$.

Two different studies applied rbALE to increase tolerance for inhibitors present in corn stover hydrolysate[23] and for methanol, which is an impurity found in certain glycerol waste streams.[24] A fixed amount of inhibitor was added, and cells were selected for growth. The corn stover evolved strain showed a higher degradation rate of the inhibitors furfural, HMF, vanillin, syringaldehyde, 4-hydroxybenzaldehyde, and acetic acid.[23] When grown on corn stover hydrolysate, the evolved strain also showed a 68% higher glutamic acid titer and 35% higher yield than the parental strain. The increased glucose consumption rate probably resulted from a higher *ptsI* expression, which codes for a component of the phosphotransferase system (PTS). In the methanol study, tolerance was increased by using media with 50 mM methanol.[24] The evolved strain showed a higher growth rate under methanol concentrations between 500 mM and 2000 mM. Sequencing identified 29 mutations and combined engineering of two of them, *metY* (A165T) and *cat*(Q342*), increased the methanol tolerance of the parental strain to that of the evolved strain. Interestingly, both the reverse engineered strain and the evolved strain lost the ability to grow on ethanol. This showed that, in contrast to an observed beneficial cross-tolerance for isobutanol after ALE for increased temperatures,[27] a single-target ALE approach is typically associated with significant negative trade-off effects.

### 3.2. Increasing Feedstock Flexibility

The utilization of alternative, non-native carbon sources is key to the implementation of non-glucose based second or third generation processes in modern biotechnology, which provides a strong incentive to engineer industrial strains that utilize most of the components present in these substrate feeds. Attractive targets to realize a flexible feedstock concept are, for example, carbon sources derived from complex polymers (e.g., starch, cellulose, or xylan), di- and monosaccharides (e.g., arabinose or xylose), and C1 compounds, such as methanol.[50,51] If a microbe has no native capacity to consume the particular substrate of interest, targeted engineering can provide an initial, nonoptimal strain, which can subsequently be improved by ALE. This combinatorial strategy was applied in three recent publications that describe improved growth on xylose, cellobiose, and methanol (Table 1).[22,29,31]

Two different rbALE approaches were described for the co-utilization of xylose and methanol[31] or xylose and cellobiose.[29] In the xylose and methanol study, targeted engineering was first applied to obtain a strain that required both xylose and ribose for growth. After the first ALE, this strain showed an increased maximum specific growth rate, from $0.03\ h^{-1}$ to $0.15\ h^{-1}$. Then, the evolved strain was rationally engineered for the co-utilization of xylose and methanol and submitted to another round of ALE. After 206 days, the evolved strain was able to grow, but the reported growth rate of $0.03\ h^{-1}$ is still far away from industrial applications. Interestingly, the authors describe the *metY*(G1256A) mutation; another mutation in the same gene (*metY*(A165T)) was also found in the methanol tolerance study.[24] An elegant approach to realize methanol-essential growth was recently reported for *E. coli*.[52] The assimilation of methanol and gluconate was stoichiometrically coupled in a strain that had the ribulose monophosphate cycle. This study highlights the potential of metabolic rerouting for the successful implementation of synthetic methylotrophy in established industrial platform organisms.

In the xylose and cellobiose study, targeted engineering was first applied to obtain two different strains that could grow on cellobiose as the sole carbon source.[29] ALE was performed until growth and cellobiose consumption did not improve anymore. Sequencing analysis revealed a high number of mutations (36 and 300), which could not be explained. After the ALE for cellobiose, a xylose consumption pathway was introduced and co-utilization of xylose and cellobiose was shown.

An improved growth rate on only D-xylose was shown by Radek et al.,[22] using a rationally engineered strain that was subsequently evolved by high-throughput rbALE for 35 generations in only 13 days. A best performer showed more than a doubling of the maximum specific growth rate, compared to the

 

ADVANCED SCIENCE NEWS
www.advancedsciencenews.com

Biotechnology Journal
www.biotechnology-journal.com

parental strain ($0.26 \pm 0.02\,h^{-1}$ and $0.10 \pm 0.02\,h^{-1}$, respectively). Sequencing analysis revealed putative loss-of-function mutations in the transcriptional regulator IolR, involved in myo-inositol uptake and degradation, and cg3388, which encodes a putative transcriptional regulator. In a subsequent study, the functional loss of IolR was shown to result in an upregulation of the gene *iolT1* (encoding the myo-inositol/proton symporter IolT1), and additional reengineering could prove the importance of IolT1 for xylose uptake.[30] Interestingly, the identified mutations are different from those identified by the xylose–methanol ALE study.[31] Altogether, these examples once more highlight the importance of subsequent reengineering of key mutations to expand our knowledge of biological systems.

## 4. Metabolic Engineering to Guide Evolution

Combining evolutionary engineering with rationally engineered system perturbations is a promising approach for the identification of metabolic traits that can be beneficial for target molecule production.[53] Gene knockouts are frequently used to not only investigate the metabolic and regulatory function of gene products,[54,55] but also for predefining the cell's metabolic network with regard to precursor supply for biotechnological applications (**Figure 2**).[56] Growth defects that result from system perturbations by introduction of gene knockouts provide a guided selection pressure toward fitness recovery. This can lead to alternative reoptimized metabolic states, for example by harnessing the underground metabolism by building on promiscuous enzyme activity of the particular species.[54,57]

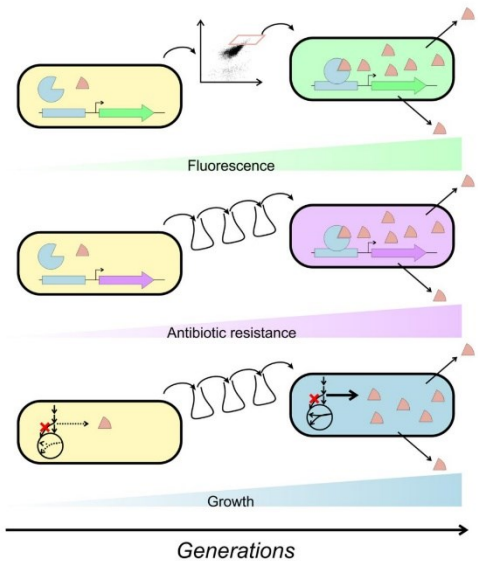


**Figure 2.** Overview of different synthetic evolution approaches to select for increased small molecule production. Synthetic regulatory circuits can be constructed to couple intracellular product concentration to a selectable output, for example to fluorescent protein synthesis,[25] which can be selected for by FACS, or to synthesis of an antibiotic or auxotrophic marker.[58] Metabolic engineering to guide evolution can be applied to increase small molecule production by selecting for growth rate.[26]

Schwentner et al.[26] used the inactivation of anaplerotic reactions to evolve an alternative producer platform for the amino acid L-valine. This effort was motivated by the fact that metabolic engineering of *C. glutamicum* for L-valine production is typically based on complete inactivation or downregulation of the pyruvate dehydrogenase complex (PDHC).[59,60] Schwentner et al. evolutionary engineered an alternative route for increased pyruvate supply by inactivating the genes encoding the PEP and pyruvate carboxylase (*ppc* and *pyc*). The resulting strain was unable to grow on glucose as the sole carbon source since the replenishment of the oxaloacetate pool was impaired.[61] Whole genome sequencing of the evolved strains revealed *icd*, encoding isocitrate dehydrogenase (ICD), as a consistent mutation target in all evolved strains. Re-engineering of the identified key mutations in *icd* revealed an upregulation of the glyoxylate shunt[62] as an alternative route to replenish the oxaloacetate pool in the Δ*pyc* Δ*ppc* background.[26] However, further studies are necessary to identify the molecular mechanisms underlying the activation of the glyoxylate shunt as a secondary effect of reduced ICD activity. In accordance with assumptions of Baumgart et al.,[63] the authors postulated that the reduced ICD activity and the resulting accumulation of isocitrate promote activation of the glyoxylate shunt.[26] Based on a 1.9-fold increased intracellular L-valine level and a predicted increased flux through the PDHC, Schwentner et al. suggested that the re-engineered strains represent promising candidates for L-valine producers. Indeed, plasmid-based overexpression of L-valine biosynthesis genes (pJC4*ilvBNCE*) led to a fourfold-enhanced L-valine product yield in comparison to the wild type.[26]

The study of Schwentner and co-workers demonstrated the potential of guided evolution strategies to improve glucose conversion to value-added compounds like L-valine. In contrast, the previously discussed guided evolution approaches of Lee et al.[29] and Tuyishime et al.[31] resulted in strains showing efficient co-utilization of the alternative substrates xylose and methanol or xylose and cellobiose, demonstrating the broad application spectrum of guided evolution strategies (Table 1).

McCloskey and colleagues intensively studied growth recovery of different *E. coli* knockout strains during ALE at the systems level. The combination of ALE and multiomics technologies provided deep insights into the versatile pathways allowing rebalancing of the metabolite and redox state.[54,55] Furthermore, growth coupling approaches with *E. coli* used the strong evolutionary driving force towards redox homeostasis for increasing fermentative production of lactic acid,[56] 1-butanol,[64] and linear higher alcohols[65] by inactivating competing NADH oxidizing enzymes. These examples highlight that not only the experimental conditions but also the genetic strain background need to be streamlined for the particular aim of the ALE.

 

ADVANCED SCIENCE NEWS
www.advancedsciencenews.com

Biotechnology Journal
www.biotechnology-journal.com

## 5. The Benefit of Automation

A number of different ALE approaches are already established that can roughly be classified according to the cultivation conditions (i.e., chemostat vs repetitive batch culture), experimental throughput (i.e., lab-scale vs microscale bioreactor systems), and degree of automation (i.e., manual vs autonomous operation). See Dragosits et al.[17] and Gresham et al.[66] for a detailed discussion of the advantages and disadvantages of the chemostat and repetitive batch approach.

In recent years, the rbALE approach has become more popular due to its lower costs for operation, simpler experimental implementation, and easier expandability. In short, individual cultivation batches are sequentially inoculated until a termination point (e.g., no further improvement in fitness criterion) is reached. Adaptation and diversification of cells during rbALE depends on the applied selection pressure, which can greatly vary between conditions of feast (i.e., exponential growth) and famine (i.e., stationary phase).

In many cases, selection focuses on higher maximum growth rates, which are best supported by keeping the cells under balanced growth conditions throughout the whole rbALE experiment. The time window of exponential growth depends on the inoculation density, the lag-phase and the specific growth rate, and should become smaller with increasing number of beneficial mutations leading to faster cell population growth and earlier consumption of the usually fixed nutrient resources. Therefore, the application of conventional shaking flasks and offline OD measurements for monitoring biomass growth does not interface with appropriate standardization.

To overcome this limitation, several microbioreactor systems are available that are based on shaken microtiter plates (MTPs), e.g., "GrowthProfiler" (EnzyScreen), "Bioscreen C" (Oy Growth Curves) or "BioLector" (m2p-labs), which employ (quasi)-continuous biomass measurement via integrated image analysis, optical density, or backscatter (see Hemmerich et al.[67] for an comprehensive overview). In addition, MTPs enable a higher throughput to perform replicate ALE experiments under identical conditions[22,68] and thus provide access to important quantities for analyzing the evolutionary process, e.g., in terms of beneficial mutation rates and the occurrence of fixed or converged mutations.[69] It is noteworthy that the typical 1 mL working volume of standard MTPs is also sufficient to carry out further in-depth characterizations of evolved strains using available spectrophotometric assays[70] and quantitative omics technologies.[71]

However, when applied as stand-alone devices for rbALE, the above systems still require the manual passaging of cells from one MTP-well to another. Consequently, there is a high demand for automation to optimally balance available resources (i.e., personnel, material, and time) with the expected outcomes (i.e., strains with improved properties, new knowledge on cellular metabolism, and targets for rational strain design).

As a first step in this direction, a recently established a workflow was reported, which enables the performance of rbALE experiments in an automated manner.[22] By building on an existing microbial phenotyping platform (i.e., Mini Pilot Plant integrating a BioLector system with liquid handling robotics[72]), the workflow covers essential steps for autonomous rbALE, including preparation of different media compositions, their cool temporary storage and the repeated inoculation of individual MTP-cavities in the BioLector. The latter is supported by various online measurements (i.e., backscatter, $pO^2$, pH, and fluorescence) and ensures an instantaneous recording of metabolic adaptation events during ALE experimentation (**Figure 3**.2). Moreover, the setup not only enables dynamic adjustments of passage sizes for keeping genetic diversity, but (if required) also provides access to the full spectrum of applicable selection pressures.

## 6. Evolutionary Engineering of Small Molecule Production

Redirecting cellular metabolism toward the production of small molecules is challenging, because metabolic pathways have been evolved for tight control and our understanding of their regulation is incomplete.[73] For ALE approaches, the difficulty lies in applying a pressure that selects for production of the compound of interest. While traditional approaches select for

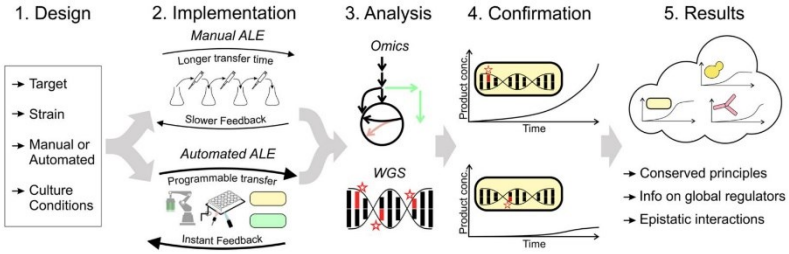


**Figure 3.** Outlook on future ALE strategies. Future ALE studies could implement multiple selection pressures, to optimize industrial performance of microbial strains. Automated approaches allow for simultaneous cultivation of multiple cultures, programmable transfer-time points and instant feedback, especially in combination with biosensors. ALE should be followed by whole genome sequencing analysis and confirmation of causal mutations via re-engineering approaches. Finally, online databases can be used to gather ALE results for different microbial organisms to ultimately increase our knowledge on biological systems.

 

ADVANCED SCIENCE NEWS
www.advancedsciencenews.com

Biotechnology Journal
www.biotechnology-journal.com

suppressor mutants, the development of transcription factor-based biosensors enabled a direct coupling of product formation to an easily selectable output, which resulted in the first reports of "synthetic evolution."[16,74–76] For *C. glutamicum*, ALE for increased small molecule production has been shown for fatty acids, L-ornithine, putrescine, plasmid-based proteins, and L-valine (Table 1).

### 6.1. Selection for Suppressor Mutants

Early efforts on the improvement of small molecule production focused on the application of random mutagenesis (UV- or chemical mutagenesis) and on selection schemes based on the resistance to antimetabolites or product analogs inhibiting growth. Key enzymes of biosynthetic pathways (e.g., amino acid biosynthesis) are typically feedback-inhibited by the particular end-product of the pathway. Application of product analogous antimetabolites enabled the efficient isolation of mutations causing feedback-resistance of key enzymes.[2]

Two groups have recently published work on improving small molecule production by selecting suppressor mutants. Takeno et al.[32] used two different chemicals, Tween40 and cerulenin, to select for mutants with a higher fatty acid production, using multiple selection steps on agar plates. Jiang et al.[35] applied rbALE in media containing the desired product, L-ornithine, to select for mutants resistant to product inhibition. In both studies, the final product titer could be improved with the evolved strain, from $3.21 \pm 0.06\ mg\ L^{-1}$ to $279.95 \pm 8.50\ mg\ L^{-1}$ for fatty acids,[32] and from $10.2 \pm 0.2\ g\ L^{-1}$ to $13.6 \pm 0.5\ g\ L^{-1}$ for L-ornithine.[35] While Jiang et al. did not perform whole genome sequencing, Takeno et al. reported three mutations in the genes responsible for fatty acid synthesis. Takeno et al.[33] repeated the selection step on cerulenin plates and identified one additional mutation. Re-engineering of this mutation in the previously evolved strain resulted in a 1.2-fold higher oleic acid titer. This shows how iterative selection of a parental strain can be used to find different mutations that have an additive effect on productivity. The L-ornithine evolved strain was further engineered for putrescine production.[34] Random mutagenesis in combination with rbALE in media containing putrescine resulted in a strain showing a twofold higher final putrescine titer (111.42 ± 2.56 mM). Sequencing analysis revealed 78 SNPs; further analysis suggested that a decrease in the activity of the α-ketoglutarate decarboxylase OdhA and an increase in the major facilitator superfamily permease CgmA, a putative putrescine permease, contributed to a higher putrescine production.

### 6.2. Biosensor-Guided Evolution

Biosensors can greatly increase the throughput and selectivity for ALE, and thereby accelerate strain development (Figure 2). Initially, two studies reported on transcription factor-based biosensors that were designed to induce *eyfp* expression in response to higher intracellular amino acid concentrations in *C. glutamicum*. The pSenLys biosensor detects amino acids with a basic side chain[13] and the Lrp biosensor detects L-methionine and branched chain amino acids.[14] Both studies showed that random mutagenesis coupled to FACS could be used to select for cells with higher productivity, illustrating the use of biosensors to screen for producers strains. However, applying random mutagenesis results in many mutations. Binder et al.[13] reported 268 SNPs and a similar study reported 83 SNPs.[77] This high number of mutations complicates the identification of causal ones.

In a recent study, Mahr et al.[25] described a biosensor-guided ALE approach based on the native mutagenesis rate, by applying multiple rounds of selection using the Lrp biosensor (Table 1). The L-valine producer strain *C. glutamiucm* Δ*ace*, which produces valine in the stationary phase, was used as the parental strain. Five iterative evolution steps were performed and, in each step, the top 10% fluorescent cells were transferred by FACS. After only five iterations, a single isolate showed a twofold increase in L-valine production compared to the parental strain. Only seven mutations were identified after whole genome sequencing. This is in large contrast to the higher number of mutations found when random mutagenesis is applied. The identified *ureD*(E188*) mutation resulted in a truncated version of the urease accessory protein and was shown to increase the final L-valine titer (44.2 mM for evolved strain) by more than 100%.[25] A low amount of mutations was also the result of a simple biosensor ALE experiment, in which iterative FACS selection was done with a strain containing a plasmid-based *egfp*. Only one mutation was identified, a loss of function of *parB*, which resulted in tenfold higher plasmid copy numbers.[36] Further examples for biosensor-guided evolution approaches in *E. coli* are the coupling of mutation rate to small molecule production[76] and the selection of improved producers via an antibiotic-based positive and negative selection strategy.[58]

The mutations identified by ALE can be further investigated by targeted mutagenesis followed by biosensor mediated screening, which was shown for the *argB* gene using pSenLys[78] and for the RBS sequence in *tktA* using the ShiR-based shikimate sensor.[79] An interesting method was described by Binder et al.,[80] who designed a rapid recombineering and screening approach, based on the RectT recombinase from prophage Rac and the pSenLys sensor, which was applied to screen for mutations in *murE* with an impact on L-lysine production.[80] Furthermore, studies in *E. coli* have demonstrated the use of multiplexed genome engineering in combination with barcoding to increase mutation rates and enable tracking of mutations.[81,82] Altogether, these approaches demonstrate the potential of transcription factor-based biosensors for the design of synthetic evolution schemes to enable the improvement of microbial small molecule production.

## 7. Conclusions

In engineering disciplines, the possibility of process improvement via evolution is a feature unique to biotechnology. But what do we learn from the comparison of different ALE endeavors? Evolution of living organisms is shaped by the particular environmental conditions (like media composition, gas supply, etc.), the genetic background, and by the mode of cultivation (batch, chemostat, solid media), including passage time and culture volume. For example, LaCroix et al.[41]

 

achieved a significant increase of growth rates in a shorter time compared to the Lenski experiment, because batch cultures where propagated during the exponential phase rather than inoculated from stationary phase cultures. These examples demonstrate that an ALE setup must be efficiently tailored to the particular scientific aim. However, most studies only focus on one aspect of industrial performance (e.g., productivity or stress tolerance). A more integrative approach could combine several improvement targets into one experiment. Especially, the development of biosensors could aid in this field, as they allow for coupling of producers to a selectable output under industrial conditions. This could even be extended with high-throughput technologies enabling the design of novel ALE strategies (Figure 3).

Several recent examples highlight the fact that ALE or untargeted selection strategies should be complemented by sequencing, and possibly by transcriptome analyses and re-engineering to obtain novel information on enzyme properties or pathway regulation. Especially in the absence of a random mutagenesis step, the amount of mutations is most of the times low enough to allow for reverse engineering and an in-depth characterization of specific mutations. This is in contrast to classical genome breeding approaches where a high number of induced mutations (e.g., via UV radiation) may result in the accumulation on non-beneficial side mutations having a negative impact on genome stability. Often, different mutations found in different studies can result in an additive effect, but it can be hard to keep track of all described mutations. Recent database efforts such as the AleDB could aid in improving our understanding of metabolic regulations.[69] A more systemic analysis of ALE experiments combined with sophisticated data management will accelerate the identification of causative key mutations and epistatic interactions resulting in improved strain properties.

## Acknowledgements

The authors acknowledge funding from the Helmholtz Association (grant W2/W3-096). Further funding was obtained from Bioeconomy Science Center (BioSC, Grant. No. 325-40000213) as part of the Focus FUND project "HyImPAct—Hybrid processes for important precursor and active pharmaceutical ingredients."

## Conflict of Interest

The authors declare no conflict of interest.

## Keywords

adaptive laboratory evolution (ALE), biosensors, *Corynebacterium glutamicum*, evolutionary engineering, laboratory automation

Received: November 29, 2018
Revised: January 23, 2019
Published online: June 7, 2019

[1] S. Kinoshita, S. Udaka, M. Shimono, *J. Gen. Appl. Microbiol.* **1957**, *3*, 193.
[2] L. Eggeling, M. Bott, *Handbook of Corynebacterium glutamicum*, CRC press, Boca Raton, FL **2005**.
[3] J. Becker, C. Wittmann, *Curr. Opin. Biotechnol.* **2012**, *23*, 718.
[4] V. F. Wendisch, J. M. P. Jorge, F. Pérez-García, E. Sgobba, *World J. Microbiol. Biotechnol.* **2016**, *32*, 105.
[5] J. Becker, C. M. Rohles, C. Wittmann, *Metab. Eng.* **2018**, *50*, 122.
[6] K-.A. G. Baritugo, H. T. Kim, Y. C. David, J. H. Choi, J. Choi, T. W. Kim, C. Park, S. H. Hong, J-.G. Na, K. J. Jeong, J. C. Joo, S. J. Park, *Biofuels, Bioprod. Biorefin.* **2018**, *12*, 899.
[7] K. Pfeifer-Sancar, A. Mentz, C. Rückert, J. Kalinowski, *BMC Genomics* **2013**, *14*, 888.
[8] J. Kalinowski, B. Bathe, D. Bartels, N. Bischoff, M. Bott, A. Burkovski, N. Dusch, L. Eggeling, B. J. Eikmanns, L. Gaigalat, A. Goesmann, M. Hartmann, K. Huthmacher, R. Krämer, B. Linke, A. C. McHardy, F. Meyer, B. Möckel, W. Pfefferle, A. Pühler, D. A. Rey, C. Rückert, O. Rupp, H. Sahm, V. F. Wendisch, I. Wiegräbe, A. Tauch, *J. Biotechnol.* **2003**, *104*, 5.
[9] Y. Jiang, F. Qian, J. Yang, Y. Liu, F. Dong, C. Xu, B. Sun, B. Chen, X. Xu, Y. Li, R. Wang, S. Yang, *Nat. Commun.* **2017**, *8*, 15179.
[10] S. Cleto, J. V. Jensen, V. F. Wendisch, T. K. Lu, *ACS Synth. Biol.* **2016**, *5*, 375.
[11] K-. A. Baritugo, H. T. Kim, Y. David, J. Choi, S. H. Hong, K. J. Jeong, J. H. Choi, J. C. Joo, S. J. Park, *Appl. Microbiol. Biotechnol.* **2018**, *102*, 3915.
[12] V. F. Wendisch, *Curr. Opin. Biotechnol.* **2014**, *30*, 51.
[13] S. Binder, G. Schendzielorz, N. Stäbler, K. Krumbach, K. Hoffmann, M. Bott, L. Eggeling, *Genome Biol.* **2012**, *13*, R40.
[14] N. Mustafi, A. Grünberger, D. Kohlheyer, M. Bott, J. Frunzke, *Metab. Eng.* **2012**, *14*, 449.
[15] N. Mustafi, A. Grünberger, R. Mahr, S. Helfrich, K. Nöh, B. Blombach, D. Kohlheyer, J. Frunzke, *PLoS One* **2014**, *9*, e85731.
[16] R. Mahr, J. Frunzke, *Appl. Microbiol. Biotechnol.* **2016**, *100*, 79.
[17] M. Dragosits, D. Mattanovich, *Microb. Cell Fact.* **2013**, *12*, 64.
[18] V. A. Portnoy, D. Bezdan, K. Zengler, *Curr. Opin. Biotechnol.* **2011**, *22*, 590.
[19] R. Mans, J-. M. G. Daran, J. T. Pronk, *Curr. Opin. Biotechnol.* **2018**, *50*, 47.
[20] E. Pfeifer, C. Gätgens, T. Polen, J. Frunzke, *Sci. Rep.* **2017**, *7*, 16780.
[21] Z. Wang, J. Liu, L. Chen, A. P. Zeng, C. Solem, P. R. Jensen, *Metab. Eng.* **2018**, *48*, 1.
[22] A. Radek, N. Tenhaef, M. F. Müller, C. Brüsseler, W. Wiechert, J. Marienhagen, T. Polen, S. Noack, *Bioresour. Technol.* **2017**, *245*, 1377.
[23] X. Wang, I. Khushk, Y. Xiao, Q. Gao, J. Bao, *Appl. Microbiol. Biotechnol.* **2018**, *102*, 377.
[24] L. Leßmeier, V. F. Wendisch, *BMC Microbiol.* **2015**, *15*, 216.
[25] R. Mahr, C. Gätgens, J. Gätgens, T. Polen, J. Kalinowski, J. Frunzke, *Metab. Eng.* **2015**, *32*, 184.
[26] A. Schwentner, A. Feith, E. Münch, T. Busche, C. Rückert, J. Kalinowski, R. Takors, B. Blombach, *Metab. Eng.* **2018**, *47*, 31.
[27] S. Oide, W. Gunji, Y. Moteki, S. Yamamoto, M. Suda, T. Jojima, H. Yukawa, M. Inui, *Appl. Environ. Microbiol.* **2015**, *81*, 2284.
[28] J.-Y. Lee, J. Seo, E.-S. Kim, H.-S. Lee, P. Kim, *Biotechnol. Lett.* **2013**, *35*, 709.
[29] J. Lee, J. N. Saddler, Y. Um, H. M. Woo, *Microb. Cell Fact.* **2016**, *15*, 20.
[30] C. Brüsseler, A. Radek, N. Tenhaef, K. Krumbach, S. Noack, J. Marienhagen, *Bioresour. Technol.* **2018**, *249*, 953.
[31] P. Tuyishime, Y. Wang, L. Fan, Q. Zhang, Q. Li, P. Zheng, J. Sun, Y. Ma, *Metab. Eng.* **2018**, *49*, 220.
[32] S. Takeno, M. Takasaki, A. Urabayashi, A. Mimura, T. Muramatsu, S. Mitsuhashi, M. Ikeda, *Appl. Environ. Microbiol.* **2013**, *79*, 6775.
[33] S. Takeno, N. Murata, M. Kura, M. Takasaki, M. Hayashi, M. Ikeda, *Appl. Microbiol. Biotechnol.* **2018**, *102*, 10603.
[34] Z. Li, Y. P. Shen, X. L. Jiang, L. S. Feng, J. Z. Liu, *J. Ind. Microbiol. Biotechnol.* **2018**, *45*, 123.
[35] L. Y. Jiang, S. G. Chen, Y. Y. Zhang, J. Z. Liu, *BMC Biotechnol.* **2013**, *13*, 47.

 

[36] J. W. Choi, S. S. Yim, K. J. Jeong, *Appl. Microbiol. Biotechnol.* **2018**, *102*, 873.
[37] J. E. Barrick, R. E. Lenski, *Nat. Rev. Genet.* **2013**, *14*, 827.
[38] R. E. Lenski, *ISME J.* **2017**, *11*, 2181.
[39] G. Valentini, L. Chiarelli, R. Fortin, M. L. Speranza, A. Galizzi, A. Mattevi, *J. Biol. Chem.* **2000**, *275*, 18145.
[40] R. Woods, D. Schneider, C. L. Winkworth, M. A. Riley, R. E. Lenski, *Proc. Natl. Acad. Sci.* **2006**, *103*, 9107.
[41] R. A. LaCroix, T. E. Sandberg, E. J. O'brien, J. Utrilla, A. Ebrahim, G. I. Guzman, R. Szubin, B. O. Palsson, A. M. Feist, *Appl. Environ. Microbiol.* **2015**, *81*, 17.
[42] G. Dong, Q. Mao, W. Xia, Y. Xu, J. Wang, L. Xu, F. Jiang, *Oncol. Lett.* **2016**, *11*, 1980.
[43] M. A. Iqbal, V. Gupta, P. Gopinath, S. Mazurek, R. N. K. Bamezai, *FEBS Lett.* **2014**, *588*, 2685.
[44] Z. Wang, S. H. J. Chan, S. Sudarsan, L. M. Blank, P. R. Jensen, C. Solem, *Metab. Eng.* **2016**, *38*, 344.
[45] E. a Groisman, K. Hollands, M. A. Kriner, E. J. Lee, S. Y. Park, M. H. Pontes, *Annu. Rev. Genet.* **2014**, *47*, 625.
[46] V. Chubukov, U. Sauer, *Appl. Environ. Microbiol.* **2014**, *80*, 2901.
[47] J. Frunzke, V. Engels, S. Hasenbein, C. Gätgens, M. Bott, *Mol. Microbiol* **2008**, *67*, 305.
[48] A. Shah, B. Blombach, R. Gauttam, B. J. Eikmanns, *Appl. Microbiol. Biotechnol.* **2018**, *102*, 5901.
[49] C. P. Long, J. E. Gonzalez, A. M. Feist, B. O. Palsson, M. R. Antoniewicz, *Metab. Eng.* **2017**, *44*, 100.
[50] N. Buschke, R. Schäfer, J. Becker, C. Wittmann, *Bioresour. Technol.* **2013**, *135*, 544.
[51] V. F. Wendisch, L. F. Brito, M. Gil Lopez, G. Hennig, J. Pfeifenschneider, E. Sgobba, K. H. Veldmann, *J. Biotechnol.* **2016**, *234*, 139.
[52] F. Meyer, P. Keller, J. Hartl, O. G. Gröninger, P. Kiefer, J. A. Vorholt, *Nat. Commun.* **2018**, *9*, 1508.
[53] K. Tokuyama, Y. Toya, T. Horinouchi, C. Furusawa, F. Matsuda, H. Shimizu, *Biotechnol. Bioeng.* **2018**, *115*, 1542.
[54] D. McCloskey, S. Xu, T. E. Sandberg, E. Brunk, Y. Hefner, R. Szubin, A. M. Feist, B. O. Palsson, *Appl. Environ. Microbiol.* **2018**, *84*, e00823.
[55] D. McCloskey, S. Xu, T. E. Sandberg, E. Brunk, Y. Hefner, R. Szubin, A. M. Feist, B. O. Palsson, *Nat. Commun.* **2018**, *9*, 3796.
[56] S. S. Fong, A. P. Burgard, C. D. Herring, E. M. Knight, F. R. Blattner, C. D. Maranas, B. O. Palsson, *Biotechnol. Bioeng.* **2005**, *91*, 643.
[57] J. Rosenberg, F. M. Commichau, *Trends Biotechnol.* **2018**, *37*(*1*), 29.
[58] S. Raman, J. K. Rogers, N. D. Taylor, G. M. Church, *Proc. Natl. Acad. Sci. U. S. A.* **2014**, *111*, 17803.
[59] M. Oldiges, B. J. Eikmanns, B. Blombach, *Appl. Microbiol. Biotechnol.* **2014**, *98*, 5859.
[60] B. J. Eikmanns, B. Blombach, *J. Biotechnol.* **2014**, *192*, 339.
[61] P. G. Peters-wendisch, C. Kreutzer, J. Kalinowski, M. Patek, H. Sahm, B. J. Eikmanns, *Microbiology* **1998**, *144*, 915.
[62] V. F. Wendisch, M. Spies, D. J. Reinscheid, S. Schnicke, H. Sahm, B. J. Eikmanns, *Arch. Microbiol.* **1997**, *168*, 262.
[63] M. Baumgart, N. Mustafi, A. Krug, M. Bott, *J. Bacteriol.* **2011**, *193*, 6864.
[64] C. R. Shen, E. I. Lan, Y. Dekishima, A. Baez, K. M. Cho, J. C. Liao, *Appl. Environ. Microbiol.* **2011**, *77*, 2905.
[65] H. B. Machado, Y. Dekishima, H. Luo, E. I. Lan, J. C. Liao, *Metab. Eng.* **2012**, *14*, 504.
[66] D. Gresham, J. Hong, *FEMS Microbiol. Rev.* **2015**, *39*, 2.
[67] J. Hemmerich, S. Noack, W. Wiechert, M. Oldiges, *Biotechnol. J.* **2018**, *13*, 1700141.
[68] M. Baumgart, S. Unthan, R. Kloß, A. Radek, T. Polen, N. Tenhaef, M. F. Müller, A. Küberl, D. Siebert, N. Brühl, K. Marin, S. Hans, R. Krämer, M. Bott, J. Kalinowski, W. Wiechert, G. Seibold, J. Frunzke, C. Rückert, V. F. Wendisch, S. Noack, *ACS Synth. Biol.* **2018**, *7*, 132.
[69] P. V. Phaneuf, D. Gosting, B. O. Palsson, A. M. Feist, *Nucleic Acids Res* **2018**, gky983.
[70] J. Hemmerich, N. Tenhaef, C. Steffens, J. Kappelmann, M. Weiske, S. J. Reich, W. Wiechert, M. Oldiges, S. Noack, *Biotechnol. J* **2018**, 1800428.
[71] S. Noack, R. Voges, J. Gätgens, W. Wiechert, *J. Biotechnol.* **2017**, *258*, 13.
[72] S. Unthan, A. Radek, W. Wiechert, M. Oldiges, S. Noack, *Microb. Cell Fact.* **2015**, *14*, 32.
[73] J. Nielsen, J. D. Keasling, *Cell* **2016**, *164*, 1185.
[74] T. C. Williams, I. S. Pretorius, I. T. Paulsen, *Trends Biotechnol.* **2016**, *34*, 371.
[75] J. L. Lin, J. M. Wagner, H. S. Alper, *Biotechnol. Adv.* **2017**, *35*, 950.
[76] H. H. Chou, J. D. Keasling, *Nat. Commun.* **2013**, *4*, 2595.
[77] X. Zhang, X. Zhang, G. Xu, X. Zhang, J. Shi, Z. Xu, *Appl. Microbiol. Biotechnol.* **2018**, *102*, 5939.
[78] G. Schendzielorz, M. Dippong, A. Grünberger, D. Kohlheyer, A. Yoshida, S. Binder, C. Nishiyama, M. Nishiyama, M. Bott, L. Eggeling, *ACS Synth. Biol.* **2014**, *3*, 21.
[79] C. Liu, B. Zhang, Y. M. Liu, K. Q. Yang, S. J. Liu, *ACS Synth. Biol.* **2018**, *7*, 591.
[80] S. Binder, S. Siedler, J. Marienhagen, M. Bott, L. Eggeling, *Nucleic Acids Res.* **2013**, *41*, 6360.
[81] A. D. Garst, M. C. Bassalo, G. Pines, S. A. Lynch, A. L. Halweg-Edwards, R. Liu, L. Liang, Z. Wang, R. Zeitoun, W. G. Alexander, R. T. Gill, *Nat. Biotechnol.* **2017**, *35*, 48.
[82] J. R. Warner, P. J. Reeder, A. Karimpour-Fard, L. B. A. Woodruff, R. T. Gill, *Nat. Biotechnol.* **2010**, *28*, 856.

 

## 4.2. Lichtblicke in der mikrobiellen Stammentwicklung

**Wiechert, J.** and Frunzke, J.

Published in *Nachrichten aus der Chemie*, 2018.

| Contributor Role | Contributor |
|---|---|
| Conceptualization | JW 30 %, JF 70 % |
| Formal Analysis | - |
| Investigation/Experiments | - |
| Methodology | - |
| Project Administration | JW 20 %, JF 80 % |
| Software | - |
| Supervision | JF 100 % |
| Visualization | JW 100 % |
| Writing – Original Draft Preparation | JW 70 %, JF 30 % |
| Writing – Reviewing & Editing | JW 40 %, JW 60 % |

Overall contribution JW: 50 %

Figures were prepared by JW. The writing of the original draft was mainly done by JW. JW took part in the revision and editing process.

# Lichtblicke in der mikrobiellen Stammentwicklung

**Johanna Wiechert, Julia Frunzke**

*Biosensoren der Zelle nutzen die natürliche Sensorik eines Organismus, um etwa eine Metabolitenkonzentration in ein optisches Signal umzuwandeln. Als vielseitig verwendbares Werkzeug helfen sie, bakterielle Stämme für die biotechnische Produktion zu entwickeln und zu optimieren.*

◆ Seit Jahrtausenden nutzt der Mensch das enorme metabolische Potenzial von Mikroorganismen, um Brot, Käse oder Wein herzustellen. Seit dem 20. Jahrhundert werden mit Metabolic Engineering gezielt mikrobielle Stämme erzeugt, mit denen sich unter anderem Proteine, Aminosäuren, organische Säuren und Vorstufen von Polymeren produzieren lassen.[1)] Einfache, nachwachsende Substrate in mikrobiellen Prozessen sind eine kostengünstige Alternative zu erdölbasierten und energieintensiven chemischen Prozessschritten. Über fünf Millionen Tonnen Aminosäuren produziert die Industrie jährlich mit dem Bodenbakterium *Corynebacterium glutamicum* (*C. glutamicum*).[2)]

Mikroorganismen sind typischerweise nicht von Natur aus dafür ausgestattet, bestimmte Substanzen in großen Mengen herzustellen. Produktionsstämme zu entwickeln und die biotechnischen Prozesse zu optimieren, ist oft das zentrale Problem. Viele der heute verwendeten Produktionsstämme stammen aus klassischer Zufallsmutagenese und anschließenden chromatographischen und massenspektrometrischen Selektionsverfahren.[3)] Die Mutationsrate etwa durch UV-Licht zu steigern ermöglicht eine hoch diverse Stammbibliothek. Jedoch ist eine effiziente Hochdurchsatzanalyse von Stammbibliotheken nur begrenzt möglich, da sie dauert und teuer ist.[3)] Eine Lösung für dieses Problem sind genetisch kodierte Biosensoren, die eine intrazelluläre Metabolitenkonzentration in ein optisches, leicht messbares Signal übersetzen.

## Biosensoren als biotechnisches Werkzeug

◆ Mikroorganismen nutzen ein umfangreiches Repertoire an Mechanismen, das auf Proteinen oder kleinen RNA basiert, um intra- und extrazelluläre Signale wahrzunehmen und darauf zu reagieren.

Abhängig von physiologischen Parametern wie der intrazellulären Konzentration bestimmter Stoffwechselprodukte kontrollieren die Transkriptionsfaktoren die Genexpression über die Bindung an den entsprechenden Promotor des Zielgens. Vereint man diese Zielpromotoren mit einem Aktuatorgen, lässt sich dieses effektorabhängig exprimieren (Abbildung 1A, S. 590).

Ist der Aktuator ein Fluoreszenzgen, wird die intrazelluläre Metabolitenkonzentration in ein Fluoreszenzsignal übersetzt. Mit solchen Biosensoren lassen sich biotechnisch relevante Metaboliten mit optischen Methoden auf Einzelzellebene sichtbar machen. Beispiele für Biosensoren, die in der Vergangenheit in *C. glutamicum* etabliert wurden, sind der Lrp-[4)] und der LysG-Biosensor.[5)]

Der Lrp-Biosensor basiert auf dem Transkriptionsfaktor Lrp (leucine-responsive protein) und macht die intrazellulären L-Methionin-, L-Valin-, L-Leucin- und L-Isoleucin-Konzentrationen sichtbar (Abbildung 1B, S. 590).[4)] Eine erhöhte intrazelluläre Konzentration dieser Aminosäuren führt dazu, dass Lrp an seinen Zielpromoter (*brnFE*) bindet. Außerdem wird dadurch die Expression eines spezifischen Exportsystems aktiviert.[6)] Durch die Fusion des Zielpromoters mit dem Reportergen *eyfp* (enhanced yellow fluorescent protein) wird die intrazelluläre Konzentration der Effektoraminosäuren in ein Fluoreszenzsignal übersetzt.[4)] ➜

**QUERGELESEN**

- Biosensoren weisen Aminosäuren, Dicarbonsäuren oder Alkohole nach.
- Genetisch kodierte Biosensoren übersetzen intrazelluläre Metabolitenkonzentrationen in ein optisch messbares Signal, etwa Fluoreszenz. Das macht Metabolite in Hochdurchsatzscreenings erfassbar.
- Mit solchen Sensoren lassen sich Mikroorganismen so manipulieren, dass sie große Mengen einer bestimmten Substanz produzieren.

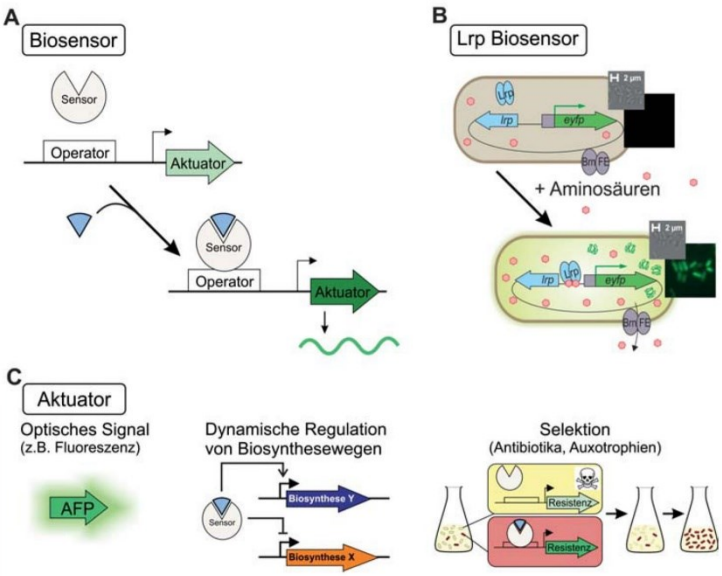


*Abb. 1. A) Aufbau eines Transkriptionsfaktor(TF)-basierten Biosensors. Abhängig vom Effektor (blaues Dreieck) bindet der TF an den Zielpromotor und beeinflusst so die Transkription des Aktuatorgens. B) Aufbau und Funktion des Lrp-Biosensors.[4] C) Es sind verschiedene Ausgangssignale des Biosensors wählbar.[1,4]*

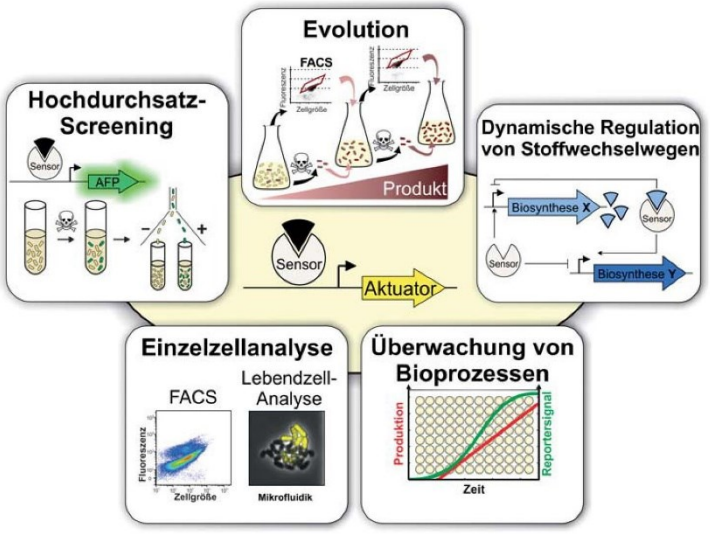


*Abb. 2. Anwendungen genetisch kodierter Biosensoren in der Biotechnologie. Biosensoren, die die intrazelluläre Konzentration eines spezifischen Metaboliten in ein optisches Signal wie Fluoreszenz übersetzen, dienen der nichtinvasiven Überwachung von Bioprozessen und für die zeitlich aufgelöste Visualisierung der Produktion auf Einzelzellebene. In Hochdurchsatzscreenings oder bei adaptiver Evolution ermöglichen Biosensoren, Klone mit erhöhter Produktivität aus großen Stammbibliotheken oder Populationen auszuwählen und anzureichern.[1]*

Der Aufbau des LysG-Biosensors basiert auf einem ähnlichen Prinzip, ebenso wie etliche andere Beispiele aus den letzten Jahren.[5]

Mit Biosensoren lassen sich nicht nur Aminosäuren detektieren. So gibt es Biosensoren, die Dicarbonsäuren (Succinat) und Alkohole (Butanol) nachweisen.[7]

Die Art des Signals eines Biosensors lässt sich je nach Anwendung wählen. Sie produzieren nicht nur effektorabhängig Autofluoreszenzproteine (AFP), sondern die Biosensoren lassen sich auch in zellinterne oder -externe regulatorische Schaltkreise integrieren, um einzelne Biosynthesewege dynamisch zu regulieren (Abbildung 1C). Die Expression der Biosynthesegene ist dabei beispielsweise von der Verfügbarkeit einer bestimmten metabolischen Vorstufe abhängig. Alternativ lässt sich durch die effektorabhängige Expression von Selektionsmarkern wie Antibiotikaresistenzen[7] das Überleben der Zellen an ihre Produktivität koppeln: Nur Zellen mit den gewünschten Eigenschaften vermehren sich (Abbildung 1C).

### Anwendung von Biosensoren

◆ Biosensoren lassen sich vielseitig anwenden (Abbildung 2).[1] Sie ermöglichen etwa, Bioprozesse im Bioreaktor mit hoher Zeitauflösung zu überwachen. Mit dem Lrp-Biosensor ließ sich für einen *C.-glutamicum*-L-Valin-Produzenten (*ΔaceE*) eine zeitliche Entkopplung von Wachstum und L-Valin-Produktion nachweisen.[4] Dass Mikroorganismen gleichen Genotyps variable Phänotypen bilden können, ist eine universelle Überlebensstrategie, kann jedoch die Ausbeute in biotechnischen Produktionen reduzieren.[8] Wie die Analyse des L-Valin-Produzenten *C. glutamicum ΔaceE* im mikrofluidischen Kultivierungssystem kombiniert mit dem Lrp-Biosensor zeigt, entstehen während der L-Valin-Produktion unproduktive Subpopulationen.[9]

Neben Mikroskopie eignet sich Durchflusszytometrie, um Fluoreszenz auf Einzelzellebene zu messen. Die intrazelluläre Produktkonzentration sichtbar zu machen, ist die Voraussetzung, um Zellen unterschiedlicher Produktivität fluoreszenzaktiviert zu sortieren (fluoreszenzaktivierte Sortierung, FACS).

Biosensorgestützte FACS-Hochdurchsatzscreenings von Mutantenbibliotheken, die durch Zufallsmutagenese erstellt wurden, sind Methode der Wahl, um Klone mit gesteigerter Produktivität zu isolieren.[4,5] Auf Basis der Lrp- und LysG-Biosensoren ließen sich in ähnlichen Ansätzen mit FACS-Screening aus chemisch mutagenisierten *C.-glutamicum*-Wildtypzellen Klone isolieren, die etwa zehnmal mehr Aminosäure produzieren als die Ursprungszelle.[4,5]

## Biosensorbasierte Evolution

◆ Die vielen Mutationen, die durch Zufallsmutagenese entstehen, erschweren es, produktionsrelevante Mutationen zu identifizieren. Hier hilft der Blick auf natürliche Systeme und Organismen.

Auch natürliche Mutageneseraten von $10^{-10}$ bis $10^{-9}$ Mutationen pro Basenpaar und Replikation führen bereits zu genetischer Diversität (Abbildung 3, S. 592).[10] Diese ist zusammen mit der Selektion vorteilhafter Mutationen die Triebfeder der Evolution. Im natürlichen Lebensraum des Mikroorganismus etablieren sich vor allem fitnessrelevante Mutationen.

Dass sich evolutive Ansätze für die Stammoptimierung anwenden lassen, hat sich bereits an einer verbesserten Anpassung an Stressbedingungen gezeigt. Die Toleranz von *C. glutamicum* gegenüber Isobutanol und Hitze steigerte sich durch wiederholtes Einwirken des Stressstimulus.[11] Dabei besteht ein direkter Zusammenhang zwischen der Fitness des Organismus und der zu optimierenden Stammeigenschaft, sodass während der experimentellen Evolution vorteilhafte Mutationen entstanden. Typischerweise treten bei solch evolutionsbasierten Ansätzen nur wenige Mutationen auf – ein Vorteil verglichen mit der Zufallsmutagenese.

Bei biotechnisch relevanten Metaboliten funktioniert dieses evolutionsbasierte Vorgehen jedoch nur eingeschränkt. Denn oft sinkt mit gesteigerter Produktion die Fitness der Zellen. Das lässt sich durch Biosensoren ändern und liefert damit die Basis, um mit biosensorgestützten Evolutionsansätzen mikrobielle Produktionsstämme zu verbessern. In einer aktuellen Studie geschah dies durch die Kombination von FACS-Hochdurchsatz-Screenings und dem optischen Signal des Lrp-Biosensors. Durch wiederholte FACS-Screenings ließ sich ein künstlicher Selektionsdruck auf die Produktivität des L-Valin-Produzenten *C. glutamicum ΔaceE* ausüben.[12] Innerhalb weniger Tage steigerten abwechselnde Sortierung und Rekultivierung sowohl das Wachstum als auch den Produkttiter um bis zu 100 Prozent (Abbildung 3A, S. 592). Die anschließende Genomanalyse isolierter Klone zeigt nur sieben Mutationen. Die Analyse dieser Mutationen zeigt eine gesteigerte Produkt- (L-Valin) und eine reduzierte Nebenproduktbildung (L-Alanin) sowie eine positive Wirkung auf das Zellwachstum (Abbildungen 3B und C).[12] ➜

**Johanna Wiechert**, Jahrgang 1989, studierte von 2010 bis 2016 Biologie an den Universitäten Osnabrück und Düsseldorf. Seit 2016 promoviert sie am Forschungszentrum Jülich in der synthetischen Biologie.

**Julia Frunzke**, Jahrgang 1980, studierte Biologie an der Universität Marburg und promovierte im Jahr 2007 am Institut für Biotechnologie des Forschungszentrums Jülich. Nach einem Postdoktorat an der ETH Zürich war sie von 2009 bis 2013 Gruppenleiterin am Institut für Bio- und Geowissenschaften des Forschungszentrums Jülich. Ab 2013 war sie zunächst Juniorprofessorin an der Universität Düsseldorf, seit 2017 ist sie dort W2-Professorin.

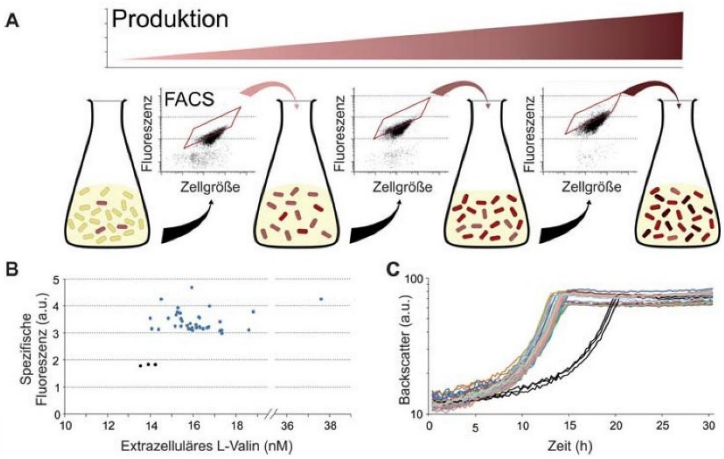


*Abb. 3. Biosensorbasierte Evolution des L-Valin-Produzenten* C. glutamicum ΔaceE. *A) Evolutionsansatz: Natürliche Mutagenese führt zu genetischer Variabilität. Das Signal des Lrp-Biosensors dient als künstlicher Selektionsdruck. Durch wiederholte Sortierungen und Rekultivierungen reichern sich Zellen mit hohem Sensorsignal an. B) Klone des evolvierten (blau) ΔaceE-Sensorstamms haben ein stärkeres Lrp-Sensorsignal und produzieren mehr L-Valin als nicht evolvierte Klone (schwarz). Zudem bilden sie schneller mehr Biomasse (C).*[12]

## Neue Biosensoren entwickeln

◆ Biotechnische Produktionsstämme basieren in den meisten Fällen auf gut untersuchten Transkriptionsfaktoren. Damit entsteht gewissermaßen ein neuer Flaschenhals bei der zeit- und kosteneffizienten Entwicklung neuer Schaltkreise und Sensoren.

Promotorbibliotheken, Transkriptom- und Proteomdaten können das Repertoire nützlicher Transkriptionsfaktoren zwar erweitern, jedoch sind Sensitivität, dynamischer Bereich oder Effektorspezifität natürlicher Systeme nicht immer optimal für die jeweilige Anwendung. Hier bietet die synthetische Biologie durch Kombinieren orthogonaler Bausteine Lösungsansätze, um Schaltkreise oder Sensoren mit den gewünschten Eigenschaften zu entwerfen. Dennoch wissen wir nach wie vor zu wenig über biologische Systeme, um uns auf rationales Design zu beschränken. Sowohl um neue Biosensoren zu entwickeln als auch um neue produktionsrelevante Mutationen zu identifizieren, sehen wir Potenzial in der Kombination von synthetischer Biologie und mikrobieller Evolution.

Literatur und Anmerkungen

1) *R. Mahr, J. Frunzke,* Appl. Microbiol. Biotechnol. *2016,* 100, *79–90.*
2) *V. F. Wendisch,* Curr. Opin. Biotechnol. *2014,* 30, *51–58.*
3) *M. Schallmey, J. Frunzke, L. Eggeling, J. Marienhagen,* Curr. Opin. Biotechnol. *2014,* 26, *148–154.*
4) *N. Mustafi, A. Grunberger, D. Kohlheyer, M. Bott, J. Frunzke,* Metab. Eng. *2012,* 14, *449–457.*
5) *S. Binder, G. Schendzielorz, N. Stabler, K. Krumbach, K. Hoffmann, M. Bott, L. Eggeling,* Genome Biol. *2012,* 13, *R40.*
6) *C. Lange, N. Mustafi, J. Frunzke, N. Kennerknecht, M. Wessel, M. Bott, V. F. Wendisch,* J. Biotechnol. *2012,* 158, *231–241.*
7) *J. A. Dietrich, D. L. Shis, A. Alikhani, J. D. Keasling,* ACS Synth. Biol. *2013,* 2, *47–58.*
8) *S. Muller, H. Harms, T. Bley,* Curr. Opin. Biotechnol. *2010,* 21, *100–113.*
9) *N. Mustafi, A. Grunberger, R. Mahr, S. Helfrich, K. Noh, B. Blombach, D. Kohlheyer, J. Frunzke,* PLoS One *2014,* 9, *e85731.*
10) *J. E. Barrick, R. E. Lenski,* Nat. Rev. Genet. *2013,* 14, *827–839.*
11) *S. Oide, W. Gunji, Y. Moteki, S. Yamamoto, M. Suda, T. Jojima, H. Yukawa, M. Inui,* Appl. Environ. Microbiol. *2015,* 81, *2284–2298.*
12) *R. Mahr, C. Gatgens, J. Gatgens, T. Polen, J. Kalinowski, J. Frunzke,* Metab. Eng. *2015,* 32, *184–194.*

*Genetisch codierte Biosensoren für die Entwicklung mikrobieller Produktionsstämme im Hochdurchsatz nutzt das Unternehmen SenseUp in Jülich: www.senseup.de*

## 4.3. Supplemental material to "Deciphering the rules underlying xenogeneic silencing and counter-silencing of Lsr2-like proteins using CgpS of *Corynebacterium glutamicum* as a model"



**Supplemental Material to:**

Deciphering the rules underlying xenogeneic silencing and counter-silencing of Lsr2-like proteins using CgpS of *Corynebacterium glutamicum* as a model

Johanna Wiechert[a], Andrei Filipchyk[a], Max Hünnefeld[a], Cornelia Gätgens[a], Jannis Brehm[b], Ralf Heermann[b], and Julia Frunzke[a#]

[a]Institut für Bio- und Geowissenschaften, IBG-1: Biotechnologie, Forschungszentrum Jülich, Jülich, Germany

[b]Institut für Molekulare Physiologie, Mikrobiologie und Weinforschung, Johannes-Gutenberg-Universität Mainz, Mainz, Germany

**Content:**

**SUPPLEMENTAL MATERIAL**

**Text S1: Supplementary information on methods used in this study**

## Growth conditions, monitoring of cell growth and fluorescence during microtiter cultivation and cultivation in the microfluidic chip device

### Growth conditions

For all cultivations of *C. glutamicum* strains, brain heart infusion (BHI, Difco Laboratories, Detroit, MI, USA) complex medium was inoculated with a single colony from a fresh agar plate and incubated for 8 to 16 hours. All cultivation steps were performed at 30°C. For reporter-based assays, BHI pre-cultures were used to inoculate a second overnight pre-culture in CGXII minimal medium (1) supplemented with 25 µg/ml kanamycin and 100/111 mM glucose or 100 mM gluconate. Subsequently, the pre-culture was used to inoculate the main culture at a start $OD_{600}$ of 1. Main cultures were cultivated in CGXII medium with 25 µg/ml kanamycin and 100/111 mM glucose, 100 mM gluconate or 100 mM fructose. *E. coli* DH5α and BL21 (DE3) were used for plasmid amplification and *cgpS* overexpression, respectively. Strains were cultivated in Lysogeny Broth (LB) media or on LB agar plates at 37°C. If needed, 50 µg/ml kanamycin was added. *Vibrio natriegens* Vmax™ (Synthetic Genomics, San Diego, CA, USA) was used for GntR (Cg2783) protein production and cells were cultivated in BHIN complex medium (BHI + 15 g/l NaCl) supplemented with 50 µg/ml carbenicillin at 30°C.

### Microtiter cultivation to monitor cell growth and fluorescence

Reporter-based analysis in microliter scale was performed in the BioLector® microcultivation system (m2p-labs, Aachen, Germany) (2). Therefore, 750 µl of the main culture (see Growth conditions) were cultivated in 48-well FlowerPlates (m2p-labs, Aachen, Germany) at 30°C and 1200 rpm. Biomass production was measured as backscattered light intensity of sent light with a wavelength of 620 nm (signal gain factor 20). Venus fluorescence was measured with an excitation wavelength of 508 nm and emission wavelength of 532 nm (signal gain factor 60). Samples were measured at 15 min intervals. Arbitrary units (a.u.) of specific fluorescence were calculated by dividing the Venus signal by the backscatter signal per time point (2). Obtained specific fluorescence values were background corrected by subtracting values of strains harboring the control plasmid pJC1-*venus*-term (no promoter in front of *venus*) (3) which were cultivated under comparable conditions. Shown fold changes were calculated based on the ratio of induced versus non-induced reporter outputs and correspond to reporter inducibility.

**Cultivation in microfluidic chip device**

The temporal dynamics of the genetic toggle switch were analyzed on single-cell level by cultivating *C. glutamicum* wild type cells harboring the plasmid-based construct in an in-house developed microfluidic platform (4, 5). The chip design and the experimental setup was performed as described before (6). Phase contrast as well as Venus and E2-Crimson fluorescence were imaged at 20 min intervals by fully motorized inverted Nikon Eclipse Ti microscope (Nikon GmbH, Düsseldorf, Germany) as described previously (4, 5, 7). The exposure times for phase contrast was 100 ms, for Venus 200 ms and for E2-crimson 300 ms. Cells were cultivated in the microfluidic chip system in CGXII medium supplemented

with 25 µg/ml kanamycin and either 100 mM gluconate or 111 mM glucose. Continuous medium supply with a flow rate of 200 nl/min and waste removal was achieved by a high-precision syringe pump system (neMESYS, Cetoni GmbH, Korbussen, Germany) using disposable syringes (Omnifix-F Tuberculin, 1 ml; B. Braun Melsungen AG, Melsungen, Germany). After 17 hours of cultivation, the carbon source supply was switched from gluconate to glucose or vice versa by changing the syringes and the connecting tubing to ensure an immediate medium change. The temperature was set to 30°C during the complete cultivation using an incubator system (PeCon GmbH, Erbach, Germany). Data analysis was performed using the image-processing package Fiji (8) which is based on ImageJ (9) on colony level. Obtained fluorescence data were background normalized and plotted with GraphPad prism 7.00 (GraphPad Software, La Jolla. CA. USA).

**Construction of strain ΔphageP$_{cgpS}$-*cgpS* and design of disruptive counter-silencing constructs**

**Construction of strain ΔphageP$_{cgpS}$-*cgpS***

Re-integration of *cgpS* in the prophage-free strain Δphage (MB001) (3) with its native promoter was performed with the pK19mobsacB-1199_1201-P$_{cgpS}$-*cgpS* integration plasmid. This plasmid contains the *cgpS* gene fused to its native promoter, which was flanked by 500 bp upstream and downstream regions of the integration site (intergenic region of cg1199-cg1201). Two step homologous recombination and selection was performed as described previously (10). Successful integration was verified by sequencing using the oligonucleotides cg1199_1201_seq_fw and cg1199_1201_seq_rv (Table S2G).

68

69 **Design of disruptive counter-silencing constructs**

70 Reporter studies were performed based on plasmid pJC1 (approximately 30 copies per
71 cell) (11, 12). All counter-silencing constructs were based on the same design scheme.
72 First, the native promoter region was amplified from *C. glutamicum* genomic DNA, fused
73 to the gene *venus* via a consistent linker, which contains a ribosomal binding site, and
74 inserted into the pJC1 plasmid using Gibson assembly (13). To ensure that all regulatory
75 promoter elements are present, forward primers were designed so that the 5´-sequence
76 end coincided with the upstream end of the CgpS binding peak (14). Reverse primers
77 were chosen so that the promoter constructs contain the first 30 bp of the coding
78 sequence. The resulting plasmids serve as template for the counter-silencer constructs.
79 Overlap PCR was performed for the insertion of the GntR binding site (BS:
80 TATGATAGTACCAAT) (15) at different positions. All constructed plasmids are listed in
81 Table S2C and oligonucleotides are listed in Table S2D.

82

83 **Determination of transcriptional start sites (TSS)**

84 For the determination of the TSS, C. glutamicum wild type cells were cultivated in CGXII
85 supplemented with 111 mM glucose starting at an $OD_{600}$ of 1. After one-hour cultivation
86 at 30°C, the SOS response was induced by adding 600 nM MMC leading to prophage
87 induction (16). 50 ml cultures were harvested on ice after one, three and six hours of
88 cultivation at 30°C, respectively. Pellets after centrifugation (5300 *g*, 4°C, 15 min) were
89 snap-frozen in liquid nitrogen and stored at -80°C until use. Total RNA was prepared using
90 the RNeasy Mini Kit (QIAGEN, Venlo, Netherlands) according to the manufacturer

protocol. Subsequently, all three RNA samples were pooled in approximately equal amounts. The determination of the TSS and data analysis was performed by Vertis Biotechnology AG (Vertis Biotechnology AG, Freising, Germany) using the Cappable-seq method developed by Ettwiller and Schildkraut (17). Obtained reads were mapped against the reference *C. glutamicum* genome BX927147 (18). Relative read score at a certain position and in a certain orientation (+ or - strand) (RRSio = (number of reads at position i in orientation o/total number of mapped reads)*1000000) were calculated by the company for a non-enriched control library (cutoff: 0) and for the enriched Cappable-seq library (cutoff: 5). The enrichment score (enrichment score = log2 (RRSio TSS / RRSio control) was calculated based on the RRSio of both libraries (cutoff: 3). Five bp of upstream and downstream region were used for clustering of TSS. Relevant TSS located in the promoter region (500 bp upstream of the start codon) and directed in gene orientation were assigned to relevant phage genes. Multiple TSS mapped to the same promoter were ranked depending on their enrichment scores (Table S1).

**Analyses of AT-rich stretches in CgpS binding regions**

Scanning of the *C. glutamicum* genome (BX927147 (18)) for AT-rich stretches was performed using a custom python script (submitted to GitHub: https://github.com/afilipch/afp/blob/master/genomic/get_at_stretches.py). AT-rich stretches were determined as the longest possible sequences with at least 70% adenosine/thymidine (AT)-content and a number of guanosines (G) and cytidines (C) below a particular threshold. The scan was performed multiple times with incrementing the limit for maximal allowed G/C interruptions inside AT-rich sequences. The results of

these multiple scans were then pulled together without further collapsing, meaning that the discovered AT-rich sequences with different G/C numbers may overlap each other. AT-rich regions were then grouped based on their lengths and G/C numbers (or number of AT steps). The grouping was done in a way to fulfil two requirements: the groups should be roughly equal and cover the whole dynamic range of the selected parameters. Subsequently, the fraction of AT-rich stretches overlapping (full overlap) with CgpS binding peaks were identified for each group (sequences were previously deposited in the GEO database (ncbi.nlm.nih.gov/geo) under accession number GSE80674).

**Protein purification, surface plasmon resonance (SPR) spectroscopy and electrophoretic mobility shift assay (EMSA)**

**Protein purification**

C-terminal Strep-tagged CgpS (Cg1966) was heterologously overproduced in *E. coli* BL21 (DE3) (19) harboring the plasmid pAN6-*cgpS*-Strep (14). Cell cultivation and protein purification was performed as described before by Pfeifer and colleagues (14) except for an increased amount of 15 mM d-desthiobiotin in the elution buffer. Purified Strep-tagged CgpS was used for surface plasmon resonance measurements.

GntR (Cg2783) with a 21 amino acids long N-terminal decahistidine tag (MGHHHHHHHHHHSSGHIEGRH) was heterologously overproduced in *Vibrio natriegens* Vmax™ (Synthetic Genomics, San Diego, CA, USA) harboring the plasmid pET16b-*gntR1* (15). Cells were grown in BHIN complex medium (BHI + 15 g/l NaCl) supplemented with 50 µg/ml carbenicillin and incubated at 30°C. Protein production was induced by the addition of 1 mM Isopropyl-β-D-1-thiogalactopyranoside (IPTG) at an $OD_{600}$ of 0.3. After

four hours of subsequent cultivation, cells were harvested by centrifugation (5300 *g*, 4°C, 15 min). The pellet was resuspended in TNI20 buffer (20 mM Tris/HCl pH 7.9, 300 mM NaCl and 20 mM imidazole) and cells were disrupted by three passages through a French pressure cell (SLM Aminco, Spectronic Instruments, Rochester, NY, USA) at 172 mPa. To remove cell debris, cell lysate was centrifuged at 5300 *g*, 4°C for 15 min and subsequently ultracentrifuged for one hour (229000 *g*, 4°C). His-tagged GntR protein from the supernatant was purified with gravity-flow chromatography using Ni-NTA agarose columns (QIAGEN, Venlo, Netherlands). Columns were washed with TNI20 buffer followed by protein elution with TNI200 buffer (20 mM Tris/HCl pH 7.9, 300 mM NaCl and 200 mM imidazole). Protein fractions were pooled and buffer was exchanged against TG buffer (30 mM Tris/HCl pH 7.5, 10% (v/v) glycerol) using a PD-10 Desalting Column (GE Healthcare, Chicago, IL, USA). Subsequently, GntR was snap-frozen in liquid nitrogen and stored at -80°C before it was used for EMSAs.

**Surface plasmon resonance (SPR) spectroscopy**

Binding of Strep-tagged CgpS to native or synthetic target promoters was analyzed by SPR analysis in a Biacore T200 and a Biacore 3000 device (GE Healthcare, Freiburg, Germany) using carboxy-methyl dextran sensor chips pre-coated with streptavidin (XanTec SAD500L (XanTec Bioanalytics GmbH, Düsseldorf, Germany) and Sensor Chip SA (GE Healthcare, Freiburg, Germany). As first step, DNA-fragments covering the respective promoters or the promoter region of the gene cg3336 (negative control) were amplified by using biotinylated primer *via* two-step PCR as described in Table S2E. All experiments were carried out at a constant temperature of 25°C in HBS-EP+ buffer (10

mM HEPES pH 7.4, 150 mM NaCl, 3 mM EDTA, 0.05% (v/v) detergent P20). Before immobilization of the DNA fragments, the chips were equilibrated by three injections of 1 M NaCl/50 mM NaOH using a flow rate of 10 µl/min. Then, 10 nM of the respective double-stranded biotinylated DNA fragment was injected at a flow rate of 10 µl/min for a total contact time of 420 s. The chips were then washed by injecting 1 M NaCl/50 mM NaOH/50% (v/v) isopropanol. Approximately 300-550 RU (response units) of the relevant DNA fragment was bound per flow cell. Binding analysis of CgpS with the five DNA fragments $P_{cg3336}$, $P_{cg1999}$, $P_{cg1999}$_A-T/G-C, the native phage promoter $P_{lys}$ or the corresponding counter-silencer construct $P_{lys}$_CS_0 were performed at a flow rate of 30 µl/min in HBS-EP+ buffer at 25°C. Various concentrations of CgpS (1 nM–5000 nM) dissolved in HBS-EP+ buffer, were passed over the flow cells for 180 s, and the complexes formed were allowed to dissociate for 420 s before the next cycle started. After each cycle, the surface was regenerated by injection of 2.5 M NaCl for 30 s, followed by 0.5% (w/v) SDS for 60 s, at a flow rate of 30 µl/min. All experiments were performed at 25°C. Sensorgrams were recorded using Biacore T200 Control Software 2.0 or Biacore 3000 Control Software 4.1.2, respectively, and analyzed with Biacore T200 Evaluation Software 2.0, BIAevaluation software 4.1.1 or TraceDrawer software 1.5 (Ridgeview Instruments, Uppsala, Schweden). The surface of flow cell 1 was not coated and used to obtain blank sensorgrams for subtraction of the bulk refractive index background. The referenced sensorgrams were normalized to a baseline of 0. Peaks in the sensorgrams at the beginning and the end of the injection are due to the run-time difference between the flow cells for each chip.

**Electrophoretic mobility shift assay (EMSA)**

Binding of GntR to the native $P_{lys}$ promoter and the corresponding counter-silencer construct $P_{lys}$_CS_0 was analyzed by electrophoretic mobility shift assays (EMSAs). Primers and templates used for the PCR amplification of DNA fragments are listed in Table S2F. The PCR products were purified from an agarose gel with the PCR clean-up and gel extraction kit of Macherey Nagel (Düren, Germany). 14 nM DNA fragments covering the promoter regions ($P_{lys}$: 518 bp; $P_{lys}$_CS_0: 533 bp) were incubated for 15 min at room temperature with varying amounts (0, 28, 70, 140, 180 or 210 nM) of N-terminal tagged GntR (decahistidine tag) (15) in binding buffer (200 mM Tris/HCl pH 7.5, 200 mM KCl, 25 mM MgCl2, 25% (v/v) glycerol, 0.5 mM EDTA). If indicated, 100 mM gluconate or glucose was added to the binding buffer. All samples were loaded onto a native 10% polyacrylamide gel (loading dye: 0.01% (w/v) xylene cyanol dye, 0.01% (w/v) bromophenol blue dye, 20% (v/v) glycerol, 1xTBE (89 mM Tris base, 89 mM boric acid, 2 mM $Na_2$-EDTA)) and electrophoresis was performed at 170 V and room temperature with 1x TBE buffer. Gels were stained with SybrGreen I following the manufacturer instructions (Sigma-Aldrich, St. Louis, MO, USA).

200 **REFERENCES**


201 1. Keilhauer C, Eggeling L, Sahm H. 1993. Isoleucine synthesis in *Corynebacterium*
202 *glutamicum*: molecular analysis of the *ilvB-ilvN-ilvC* operon. J Bacteriol 175:5595-
203 5603.
204 2. Kensy F, Zang E, Faulhammer C, Tan RK, Büchs J. 2009. Validation of a high-
205 throughput fermentation system based on online monitoring of biomass and
206 fluorescence in continuously shaken microtiter plates. Microb Cell Fact 8:31.
207 3. Baumgart M, Unthan S, Rückert C, Sivalingam J, Grünberger A, Kalinowski J,
208 Bott M, Noack S, Frunzke J. 2013. Construction of a prophage-free variant of
209 *Corynebacterium glutamicum* ATCC 13032 for use as a platform strain for basic
210 research and industrial biotechnology. Appl Environ Microbiol 79:6006-6015.
211 4. Grünberger A, Paczia N, Probst C, Schendzielorz G, Eggeling L, Noack S,
212 Wiechert W, Kohlheyer D. 2012. A disposable picolitre bioreactor for cultivation
213 and investigation of industrially relevant bacteria on the single cell level. Lab Chip
214 12:2060-2068.
215 5. Grünberger A, Probst C, Helfrich S, Nanda A, Stute B, Wiechert W, von Lieres E,
216 Nöh K, Frunzke J, Kohlheyer D. 2015. Spatiotemporal microbial single-cell
217 analysis using a high-throughput microfluidics cultivation platform. Cytometry A
218 87:1101-1115.
219 6. Grünberger A, Probst C, Heyer A, Wiechert W, Frunzke J, Kohlheyer D. 2013.
220 Microfluidic picoliter bioreactor for microbial single-cell analysis: fabrication,
221 system setup, and operation. J Vis Exp doi:10.3791/50560:e50560.

7. Helfrich S, Pfeifer E, Krämer C, Sachs CC, Wiechert W, Kohlheyer D, Nöh K, Frunzke J. 2015. Live cell imaging of SOS and prophage dynamics in isogenic bacterial populations. Mol Microbiol 98:636-650.

8. Schindelin J, Arganda-Carreras I, Frise E, Kaynig V, Longair M, Pietzsch T, Preibisch S, Rueden C, Saalfeld S, Schmid B, Tinevez JY, White DJ, Hartenstein V, Eliceiri K, Tomancak P, Cardona A. 2012. Fiji: an open-source platform for biological-image analysis. Nat methods 9:676-682.

9. Rueden CT, Schindelin J, Hiner MC, DeZonia BE, Walter AE, Arena ET, Eliceiri KW. 2017. ImageJ2: ImageJ for the next generation of scientific image data. BMC Bioinformatics 18:529.

10. Niebisch A, Bott M. 2001. Molecular analysis of the cytochrome $bc_1$-$aa_3$ branch of the *Corynebacterium glutamicum* respiratory chain containing an unusual diheme cytochrome $c_1$. Arch Microbiol 175:282-294.

11. Cremer J, Eggeling L, Sahm H. 1990. Cloning the *dapA dapB* cluster of the lysine-secreting bacterium *Corynebacterium glutamicum*. Mol Gen Genet 220:478-480.

12. Eggeling L, Bott M. 2008. The genus *Corynebacterium*, p 355-375. *In* Goldman E, Green LH (ed), Practical Handbook of Microbiology, 2nd ed. CRC Press, Boca Raton, FL, USA.

13. Gibson DG, Young L, Chuang RY, Venter JC, Hutchison CA, 3rd, Smith HO. 2009. Enzymatic assembly of DNA molecules up to several hundred kilobases. Nat Methods 6:343-345.

14. Pfeifer E, Hünnefeld M, Popa O, Polen T, Kohlheyer D, Baumgart M, Frunzke J. 2016. Silencing of cryptic prophages in *Corynebacterium glutamicum*. Nucleic Acids Res 44:10117-10131.

15. Frunzke J, Engels V, Hasenbein S, Gätgens C, Bott M. 2008. Co-ordinated regulation of gluconate catabolism and glucose uptake in *Corynebacterium glutamicum* by two functionally equivalent transcriptional regulators, GntR1 and GntR2. Mol Microbiol 67:305-322.

16. Nanda AM, Heyer A, Krämer C, Grünberger A, Kohlheyer D, Frunzke J. 2014. Analysis of SOS-induced spontaneous prophage induction in *Corynebacterium glutamicum* at the single-cell level. J Bacteriol 196:180-188.

17. Ettwiller L, Buswell J, Yigit E, Schildkraut I. 2016. A novel enrichment strategy reveals unprecedented number of novel transcription start sites at single base resolution in a model prokaryote and the gut microbiome. BMC Genomics 17:199.

18. Kalinowski J, Bathe B, Bartels D, Bischoff N, Bott M, Burkovski A, Dusch N, Eggeling L, Eikmanns BJ, Gaigalat L, Goesmann A, Hartmann M, Huthmacher K, Krämer R, Linke B, McHardy AC, Meyer F, Möckel B, Pfefferle W, Pühler A, Rey DA, Rückert C, Rupp O, Sahm H, Wendisch VF, Wiegräbe I, Tauch A. 2003. The complete *Corynebacterium glutamicum* ATCC 13032 genome sequence and its impact on the production of L-aspartate-derived amino acids and vitamins. J Biotechnol 104:5-25.

19. Studier FW, Moffatt BA. 1986. Use of bacteriophage T7 RNA polymerase to direct selective high-level expression of cloned genes. J Mol Biol 189:113-130.

## Table S1: TSS analysis of relevant phage and non-phage-related CgpS target promoters after prophage induction with mitomycin C.

**Table S1: TSS analysis of relevant phage CgpS target promoters after prophage induction with mitomycin C.** TSS positions of phage-related CgpS targets located maximal 500 bp upstream of the start codon and orientated in the appropriate direction are listed. TSS identified in previous studies of Pfeifer-Sancar and colleagues (K. Pfeifer-Sancar, A. Mentz, C. Rückert, and J. Kalinowski, BMC Genomics 14:888, 2013, doi: 10.1186/1471-2164-14-888) (accession number of the sequencing run: ERR356819 (https://trace.ncbi.nlm.nih.gov/Traces/sra/?run=ERR356819)) are given in column TSS ERR356819. TSS determination after mitomycin C induction was performed by Vertis Biotechnology AG (Freising, Germany) using the Cappable-seq method developed by Ettwiller and Schildkraut (L Ettwiller, J Buswell, E Yigit , and I Schildkraut, BMC Genomics 17:199, 2016, doi:10.1186/s12864-016-2539-z). Additionally, positions of maximal CgpS coverage and ranges of CgpS binding peaks (E. Pfeifer, M. Hünnefeld, O. Popa, T. Polen, D. Kohlheyer, M. Baumgart, and J. Frunzke, Nucleic Acids Res 44:10117-10131, 2016, doi: 10.1093/nar/gkw692; GEO database (ncbi.nlm.nih.gov/geo), accession number GSE141132) are listed. Promoters were grouped into three different classes based on the CgpS coverage peak width (Class 0: < 500 bp (grey); class 1: 500 bp - 850 bp (orange); class 2: > 850 bp (blue). Distance TSS-Position maximal CgpS coverage peak*: TSS located upstream of maximal CgpS binding peak: negative value; downstream: positive values.

| Locus | Class | Gene start | Gene end | Strand | CgpS peak start | CgpS peak end | Peak width (bp) | Position maximal CgpS peak | TSS ERR356819 | TSS CAPPABLE_SEQ | Relative read score CAPPABLE_SEQ (RRS) | Enrich-ment score CAPPABLE_SEQ | Distance TSS-Position maximal CgpS coverage peak* | Distance TSS-ATG |
|---|---|---|---|---|---|---|---|---|---|---|---|---|---|---|
| **cg1891** | Class 2 | 1781586 | 1781023 | - | 1781272 | 1782247 | 975 | 1781685 | / | | | | | |
| | | | | | | | | | | 1781664 | 516 | 4.84 | 21 | 78 |
| **cg1895** | Class 2 | 1786945 | 1784363 | - | 1786615 | 1787489 | 874 | 1787044 | / | | | | | |
| | | | | | | | | | | 1787045 | 559 | 4.54 | -1 | 100 |
| | | | | | | | | | | 1787064 | 86 | 4.1 | -20 | 119 |
| **cg1896** | Class 0 | 1788316 | 1787201 | - | 1788157 | 1788501 | 344 | 1788341 | / | | | | | |
| | | | | | | | | | | / | | | | |
| **cg1897** | Class 1 | 1790301 | 1788376 | - | 1789987 | 1790769 | 782 | 1790389 | 1790360 | | | | | |
| | | | | | | | | | | 1790326 | 139 | 3.31 | 63 | 25 |
| | | | | | | | | | | 1790360 | 1188 | 3.15 | 29 | 59 |
| | | | | | | | | | | 1790779 | 82 | 3.19 | -390 | 478 |
| **cg1905** | Class 0 | 1795186 | 1796295 | + | 1794804 | 1795079 | 275 | 1794937 | 1794978 | | | | | |
| | | | | | | | | | | 1794881 | 155 | 4.11 | -56 | 305 |
| | | | | | | | | | | 1795037 | 317 | 4.06 | 100 | 149 |
| | | | | | | | | | | 1795152 | 67 | 6.06 | 215 | 34 |
| **cg1910** | Class 0 | 1799441 | 1799319 | - | 1799243 | 1799650 | 407 | 1799454 | 1799699 | | | | | |
| | | | | | | | | | | 1799486 | 211 | 4.4 | -32 | 45 |
| | | | | | | | | | | 1799564 | 264 | 3.58 | -110 | 123 |
| | | | | | | | | | | 1799699 | 7460 | 3.58 | -245 | 258 |
| **cg1911** | Class 1 | 1800229 | 1799492 | - | 1799994 | 1800619 | 625 | 1800361 | 1800279 | | | | | |

| | | | | | | | | | | | | | | | |
|---|---|---|---|---|---|---|---|---|---|---|---|---|---|---|---|
| | | | | | | | | | | 1800279 | 4586 | 4.08 | 82 | 50 |
| | | | | | | | | | | 1800374 | 358 | 5.68 | -13 | 145 |
| | | | | | | | | | | 1800383 | 242 | 4.6 | -22 | 154 |
| | | | | | | | | | | 1800405 | 83 | 4.05 | -44 | 176 |
| | | | | | | | | | | 1800583 | 125 | 6.96 | -222 | 354 |
| **cg1917** | Class 2 | 1804049 | 1803624 | - | 1803794 | 1804670 | 876 | 1804202 | 1804078 | | | | | |
| | | | | | | | | | | 1804049 | 246 | 6.36 | 153 | 0 |
| | | | | | | | | | | 1804061 | 217 | 4.95 | 141 | 12 |
| | | | | | | | | | | 1804078 | 10441 | 4.31 | 124 | 29 |
| | | | | | | | | | | 1804110 | 279 | 3.08 | 92 | 61 |
| | | | | | | | | | | 1804153 | 136 | 4.28 | 49 | 104 |
| **cg1936** | Class 2 | 1816359 | 1817126 | + | 1815683 | 1816747 | 1064 | 1816143 | / | | | | | |
| | | | | | | | | | | 1816311 | 1126 | 7.33 | 168 | 48 |
| **cg1938** | Class 1 | 1817923 | 1818111 | + | 1817286 | 1818040 | 754 | 1817726 | / | | | | | |
| | | | | | | | | | | / | | | | |
| **cg1940** | Class 2 | 1818604 | 1819278 | + | 1818041 | 1818913 | 872 | 1818495 | / | | | | | |
| | | | | | | | | | | 1818523 | 1047 | 5.78 | 28 | 81 |
| | | | | | | | | | | 1818536 | 1066 | 6.74 | 41 | 68 |
| | | | | | | | | | | 1818543 | 232 | 4.4 | 48 | 61 |
| **cg1955** | Class 1 | 1832237 | 1833538 | + | 1831721 | 1832564 | 843 | 1832185 | / | | | | | |
| | | | | | | | | | | 1832083 | 71 | 3.15 | -102 | 154 |
| **cg1957** | Class 1 | 1836400 | 1835618 | - | 1836032 | 1836584 | 552 | 1836450 | 1836678 | | | | | |
| | | | | | | | | | | 1836417 | 80 | 4.73 | 33 | 17 |
| | | | | | | | | | | 1836440 | 61 | 3.61 | 10 | 40 |
| | | | | | | | | | | 1836678 | 290005 | 3.95 | -228 | 278 |
| | | | | | | | | | | 1836690 | 136 | 5.09 | -240 | 290 |
| | | | | | | | | | | 1836701 | 56 | 5.8 | -251 | 301 |
| | | | | | | | | | | 1836716 | 121 | 4.11 | -266 | 316 |
| | | | | | | | | | | 1836755 | 71 | 6.14 | -305 | 355 |
| | | | | | | | | | | 1836807 | 542 | 5.18 | -357 | 407 |
| **cg1959 (*priP*)** | Class 1 | 1838024 | 1839799 | + | 1837413 | 1838254 | 841 | 1837816 | / | | | | | |
| | | | | | | | | | | 1837828 | 82 | 3.77 | 12 | 196 |

| | | | | | | | | | | | | | | |
|---|---|---|---|---|---|---|---|---|---|---|---|---|---|---|
| **cg1966** | Class 2 | 1848158 | 1847802 | - | 1847834 | 1849164 | 1330 | 1848409 | 1848331 | | | | | |
| | | | | | | | | | | 1848174 | 67 | 5.07 | 235 | 16 |
| | | | | | | | | | | 1848193 | 13207 | 5.89 | 216 | 35 |
| | | | | | | | | | | 1848331 | 12126 | 5.3 | 78 | 173 |
| | | | | | | | | | | 1848341 | 361 | 4.1 | 68 | 183 |
| | | | | | | | | | | 1848460 | 55 | 5.77 | -51 | 302 |
| | | | | | | | | | | 1848517 | 127 | 3.99 | -108 | 359 |
| **cg1974 (*lys*)** | Class 1 | 1852521 | 1851943 | - | 1852165 | 1852965 | 800 | 1852575 | 1852602 | | | | | |
| | | | | | | | | | | 1852556 | 116 | 4.54 | 19 | 35 |
| | | | | | | | | | | 1852569 | 479 | 4.51 | 6 | 48 |
| | | | | | | | | | | 1852602 | 13356 | 5.53 | -27 | 81 |
| **cg1977** | Class 2 | 1855754 | 1856329 | + | 1855101 | 1856067 | 966 | 1855602 | / | | | | | |
| | | | | | | | | | | 1855404 | 1826 | 5.05 | -198 | 350 |
| | | | | | | | | | | 1855658 | 921 | 5.94 | 56 | 96 |
| | | | | | | | | | | 1855697 | 551 | 3.46 | 95 | 57 |
| **cg1995** | Class 2 | 1879358 | 1872849 | - | 1879004 | 1879871 | 867 | 1879430 | / | | | | | |
| | | | | | | | | | | 1879426 | 19097 | 4.53 | 4 | 68 |
| | | | | | | | | | | 1879438 | 161 | 6.33 | -8 | 80 |
| **cg1999** | Class 1 | 1885462 | 1883939 | - | 1885101 | 1885910 | 809 | 1885499 | 1885490 | | | | | |
| | | | | | | | | | | 1885472 | 74 | 6.2 | 27 | 10 |
| | | | | | | | | | | 1885490 | 2966 | 5.14 | 9 | 28 |
| | | | | | | | | | | 1885530 | 1091 | 5.23 | -31 | 68 |
| | | | | | | | | | | 1885601 | 109 | 5.18 | -102 | 139 |
| | | | | | | | | | | 1885955 | 685 | 6.1 | -456 | 493 |
| **cg2000** | Class 1 | 1886360 | 1885689 | - | 1886103 | 1886740 | 637 | 1886415 | 1886388 | | | | | |
| | | | | | | | | | | 1886679 | 194 | 3.69 | -264 | 319 |
| **cg2002** | Class 0 | 1888877 | 1889065 | + | 1888491 | 1888872 | 381 | 1888671 | / | | | | | |
| | | | | | | | | | | 1888568 | 78 | 6.28 | -103 | 309 |
| **cg2004** | Class 2 | 1890917 | 1889700 | - | 1890532 | 1891390 | 858 | 1890960 | 1890948 | | | | | |
| | | | | | | | | | | 1890925 | 773 | 5.2 | 35 | 8 |
| | | | | | | | | | | 1890945 | 6451 | 4.54 | 15 | 28 |
| | | | | | | | | | | 1890967 | 705 | 4.25 | -7 | 50 |
| **cg2006** | Class 1 | 1894509 | 1893301 | - | 1894115 | 1894885 | 770 | 1894543 | 1894509 | | | | | |
| | | | | | | | | | | 1894509 | 945 | 4.46 | 34 | 0 |

| | | | | | | | | | | | | | | |
|---|---|---|---|---|---|---|---|---|---|---|---|---|---|---|
| | | | | | | | | | 1894632 | 93 | 6.53 | -89 | 123 |
| | | | | | | | | | 1894705 | 60 | 5.9 | -162 | 196 |
| | | | | | | | | | 1894864 | 202 | 6.66 | -321 | 355 |
| **cg2008** | Class 1 | 1898703 | 1896208 | - | 1898376 | 1899221 | 845 | 1898780 | 1898761 | | | | | |
| | | | | | | | | | / | | | | | |
| **cg2011** | Class 1 | 1902388 | 1901273 | - | 1902030 | 1902751 | 721 | 1902443 | / | | | | | |
| | | | | | | | | | 1902413 | 61 | 3.93 | 30 | 25 |
| | | | | | | | | | 1902437 | 242 | 5.92 | 6 | 49 |
| **cg2014** | Class 2 | 1904355 | 1903474 | - | 1904017 | 1904900 | 883 | 1904446 | 1904428 | | | | | |
| | | | | | | | | | 1904355 | 110 | 6.77 | 91 | 0 |
| | | | | | | | | | 1904428 | 28397 | 7.2 | 18 | 73 |
| **cg2018** | Class 1 | 1910132 | 1909434 | - | 1909773 | 1910579 | 806 | 1910175 | / | | | | | |
| | | | | | | | | | 1910180 | 5139 | 5.51 | -5 | 48 |
| | | | | | | | | | 1910430 | 83 | 6.37 | -255 | 298 |
| | | | | | | | | | 1910597 | 67 | 6.06 | -422 | 465 |
| **cg2020** | Class 1 | 1911980 | 1910970 | - | 1911615 | 1912370 | 755 | 1912012 | / | | | | | |
| | | | | | | | | | / | | | | | |
| **cg2022** | Class 1 | 1915265 | 1913802 | - | 1914947 | 1915574 | 627 | 1915292 | / | | | | | |
| | | | | | | | | | 1915290 | 223 | 4.48 | 2 | 25 |
| | | | | | | | | | 1915305 | 68 | 3.28 | -13 | 40 |
| | | | | | | | | | 1915315 | 2282 | 4.25 | -23 | 50 |
| **cg2023** | Class 1 | 1915801 | 1915442 | - | 1915575 | 1916307 | 732 | 1915888 | / | | | | | |
| | | | | | | | | | 1915810 | 94 | 4.97 | 78 | 9 |
| | | | | | | | | | 1915853 | 313 | 3.77 | 35 | 52 |
| | | | | | | | | | 1916048 | 117 | 5.28 | -160 | 247 |
| **cg2032** | Class 1 | 1927482 | 1923016 | - | 1927172 | 1927972 | 800 | 1927582 | 1927569 | | | | | |
| | | | | | | | | | 1927569 | 4681 | 4.99 | 13 | 87 |
| | | | | | | | | | 1927831 | 126 | 3.17 | -249 | 349 |
| | | | | | | | | | 1927946 | 248 | 6.37 | -364 | 464 |
| **cg2043** | Class 0 | 1937384 | 1936440 | - | 1937475 | 1937714 | 239 | 1937547 | 1937565 | | | | | |
| | | | | | | | | | 1937397 | 846 | 4.87 | 150 | 13 |
| | | | | | | | | | 1937460 | 143 | 6.16 | 87 | 76 |
| | | | | | | | | | 1937547 | 647 | 5.53 | 0 | 163 |
| | | | | | | | | | 1937565 | 6447 | 4.78 | -18 | 181 |

| | | | | | | | | | | | | | | |
|---|---|---|---|---|---|---|---|---|---|---|---|---|---|---|
| | | | | | | | | | 1937583 | 822 | 5.98 | -36 | 199 |
| | | | | | | | | | 1937601 | 997 | 6.26 | -54 | 217 |
| | | | | | | | | | 1937619 | 299 | 5.9 | -72 | 235 |
| | | | | | | | | | 1937681 | 191 | 6.58 | -134 | 297 |
| **cg2062** | Class 1 | 1952922 | 1950490 | - | 1952591 | 1953318 | 727 | 1952975 | / | | | | |
| | | | | | | | | | 1952954 | 10405 | 5.41 | 21 | 32 |
| | | | | | | | | | 1952986 | 159 | 5.31 | -11 | 64 |
| | | | | | | | | | 1952995 | 297 | 5.04 | -20 | 73 |
| **cg2064** | Class 2 | 1956294 | 1954015 | - | 1955922 | 1956864 | 942 | 1956319 | / | | | | |
| | | | | | | | | | 1956318 | 6396 | 6.4 | 1 | 24 |
| **cg2065** | Class 1 | 1959750 | 1957672 | - | 1959401 | 1960230 | 829 | 1959770 | / | | | | |
| | | | | | | | | | 1959792 | 1287 | 6.01 | -22 | 42 |
| | | | | | | | | | 1959810 | 327 | 6.35 | -40 | 60 |

**Table S1: TSS analysis of non-phage-related CgpS target promoters after induction with mitomycin C.** TSS positions located maximal 500 bp upstream of the start codon and orientated in the appropriate direction are listed. TSS identified in previous studies of Pfeifer-Sancar and colleagues (K. Pfeifer-Sancar, A. Mentz, C. Rückert, and J. Kalinowski, BMC Genomics 14:888, 2013, doi: 10.1186/1471-2164-14-888) (accession number of the sequencing run: ERR356819 (https://trace.ncbi.nlm.nih.gov/Traces/sra/?run=ERR356819)) are given in column TSS ERR356819. TSS determination after mitomycin C induction was performed by Vertis Biotechnology AG (Freising, Germany) using the Cappable-seq method developed by Ettwiller and Schildkraut (L Ettwiller, J Buswell, E Yigit , and I Schildkraut, BMC Genomics 17:199, 2016, doi:10.1186/s12864-016-2539-z). Additionally, positions of maximal CgpS coverage and ranges of CgpS binding peaks (E. Pfeifer, M. Hünnefeld, O. Popa, T. Polen, D. Kohlheyer, M. Baumgart, and J. Frunzke, Nucleic Acids Res 44:10117-10131, 2016, doi: 10.1093/nar/gkw692) are listed. Distance TSS-Position maximal CgpS coverage peak*: TSS located upstream of maximal CgpS binding peak: negative value; downstream: positive values.

| Locus | Gene start | Gene end | Strand | CgpS peak start | CgpS peak end | Peak width (bp) | Position maximal CgpS peak | TSS ERR356819 | TSS CAPPABLE_SEQ | Relative read score CAPPABLE_SEQ (RRS) | Enrich-ment score CAPPABLE_SEQ | Distance TSS-Position maximal CgpS coverage peak* | Distance TSS-ATG |
|---|---|---|---|---|---|---|---|---|---|---|---|---|---|
| **cg0002** | 1920 | 1594 | - | 1863 | 2163 | 301 | 2007 | / | | | | | |
| | | | | | | | | | / | | | | |
| **cg0160** | 136566 | 136120 | - | 136573 | 136691 | 119 | 136649 | 136543 | | | | 106 | -23 |
| | | | | | | | | | / | | | | |
| **cg0432** | 380843 | 379848 | - | 380625 | 381100 | 476 | 380893 | 380902 | | | | -9 | 59 |
| | | | | | | | | | 380902 | 600 | 3.84 | -9 | 59 |
| | | | | | | | | | 380975 | 476 | 3.99 | -82 | 132 |
| | | | | | | | | | 381009 | 157 | 4.97 | -116 | 166 |
| | | | | | | | | | 381209 | 85 | 5.41 | -316 | 366 |
| **cg0435** | 381949 | 383112 | + | 381669 | 381862 | 194 | 381726 | 381491 | | | | -235 | 458 |
| | | | | | | | | 381726 | | | | 0 | 223 |
| | | | | | | | | 381861 | | | | 135 | 88 |
| | | | | | | | | | 381491 | 1816 | 3.93 | -235 | 458 |
| | | | | | | | | | 381726 | 55 | 4.19 | 0 | 223 |
| | | | | | | | | | 381861 | 103 | 4.69 | 135 | 88 |
| **cg0442** | 389249 | 390172 | + | 389104 | 389315 | 212 | 389207 | 389249 | | | | | 0 |
| | | | | | | | | | 389249 | 1534 | 5.45 | 42 | 0 |
| **cg0723** | 640893 | 639775 | - | 640718 | 641333 | 616 | 641032 | 641007 | | | | 25 | 114 |
| | | | | | | | | | 641007 | 107 | 6.73 | 25 | 114 |
| **cg0726** | 642340 | 641690 | - | 642039 | 642708 | 670 | 642376 | / | | | | | |
| | | | | | | | | | 642358 | 90 | 4.9 | 18 | 18 |
| | | | | | | | | | 642386 | 1285 | 6.63 | -10 | 46 |

| | | | | | | | | | | | | | |
|---|---|---|---|---|---|---|---|---|---|---|---|---|---|
| **cg1028** | 960467 | 959310 | - | 960435 | 960830 | 396 | 960616 | / | | | | | |
| | | | | | | | | | 960571 | 343 | 4.61 | 45 | 104 |
| | | | | | | | | | 960580 | 262 | 3.79 | 36 | 113 |
| | | | | | | | | | 960615 | 282 | 7.14 | | 148 |
| **cg1347** | 1258070 | 1256202 | - | 1258077 | 1258437 | 361 | 1258267 | / | | | | | |
| | | | | | | | | | / | | | | |
| **cg1444** | 1346402 | 1346890 | + | 1346292 | 1346511 | 220 | 1346400 | 1346402 | | | | 2 | 0 |
| | | | | | | | | | 1346230 | 485 | 5.6 | -170 | 172 |
| **cg1517** | 1409328 | 1409023 | - | 1409317 | 1409598 | 282 | 1409451 | 1409389 | | | | | 61 |
| | | | | | | | | | 1409389 | 59 | 4.88 | 62 | 61 |
| **cg1609** | 1499791 | 1498259 | - | 1499717 | 1499969 | 253 | 1499819 | / | | | | | |
| | | | | | | | | | 1499936 | 1102 | 4.86 | -117 | 145 |
| **cg2462** | 2349440 | 2349952 | + | 2349310 | 2349518 | 209 | 2349453 | 2349571 | | | | 118 | -131 |
| | | | | | | | | | 2349160 | 62 | 4.37 | -293 | 280 |
| | | | | | | | | | 2349208 | 240 | 4.21 | -245 | 232 |
| **cg2722** | 2594635 | 2595282 | + | 2594491 | 2594660 | 170 | 2594601 | 2594635 | | | | 34 | 0 |
| | | | | | | | | | 2594285 | 3274 | 4.22 | -316 | 350 |
| | | | | | | | | | 2594474 | 318 | 4.85 | -127 | 161 |
| **cg2783** | 2647165 | 2647917 | + | 2646731 | 2647420 | 690 | 2647059 | 2647114 | | | | | 51 |
| | | | | | | | | | 2647114 | 2028 | 3.42 | 55 | 51 |
| **cg2896** | 2757790 | 2755646 | - | 2757694 | 2757991 | 298 | 2757862 | 2757823 | | | | 39 | 33 |
| | | | | | | | | | / | | | | |
| **cg2903** | 2763214 | 2762783 | - | 2763310 | 2763542 | 233 | 2763408 | 2763250 | | | | 158 | 36 |
| | | | | | | | | 2763255 | | | | 153 | 41 |
| | | | | | | | | 2763263 | | | | 145 | 49 |
| | | | | | | | | 2763371 | | | | 37 | 157 |
| | | | | | | | | | 2763371 | 194 | 5.6 | 37 | 157 |
| **cg3057** | 2919709 | 2918942 | - | 2919541 | 2920009 | 469 | 2919730 | 2919739 | | | | -9 | 30 |
| | | | | | | | | | 2919739 | 411 | 3.88 | -9 | 30 |
| | | | | | | | | | 2919928 | 94 | 5.56 | -198 | 219 |
| **cg3342** | 3190514 | 3190191 | - | 3190595 | 3190818 | 224 | 3190716 | / | | | | | |
| | | | | | | | | | 3190624 | 944 | 5.13 | 92 | 110 |

**SUPPLEMENTAL MATERIAL**

**SUPPLEMENTARY INFORMATION: TABLE S2**

**TABLE S2: Strains, plasmids, oligonucleotides and DNA sequences**

**Table S2A: Strains used in this study.**

| Strain | Relevant characteristics | Reference |
|---|---|---|
| ***E. coli*** | | |
| DH5α | F⁻ Φ80*lacZ*ΔM15 Δ(*lacZYA-argF*) U169 *recA1 endA1 hsdR17*($r_K^-$, $m_K^+$) *phoA supE44 thi-1 gyrA96 relA1* $\lambda^-$, strain used for cloning procedures | Invitrogen |
| BL21(DE3) | F⁻ *ompT hsdS*$_B$($r_B^-$ $m_B^-$) *gal dcm* BL21(DE3), strain used for protein production | (1) |
| ***Vibrio natrigens*** | | |
| *Vibrio natriegens* Vmax™ | | Synthetic Genomics, San Diego, CA, USA |
| ***C. glutamicum*** | | |
| ATCC 13032 | Biotin-auxotrophic wild type | (2) |
| Δ*gntR1/2* | Derivate of ATCC 13032 with in-frame deletions of genes *gntR1* (cg2783) and *gntR2* (cg1935) | (3) |
| Δphage (MB001) | Derivate of ATCC 13032 with deletion of prophages CGP1 (cg1507-cg1524), CGP2 (cg1746-cg1752), and CGP3 (cg1890-cg2071) | (4) |
| Δphage::$P_{cgpS}$-*cgpS* | Derivate of Δphage (MB001) with deletion of prophages CGP1 (cg1507-cg1524), CGP2 (cg1746-cg1752), and CGP3 (cg1890-cg2071) and re-integrated cgpS together with its native promoter in the | This work |

| | | |
|---|---|---|
| | intergenic region of cg1199-cg1201 | |

**Table S2B: Plasmids from other studies used in this study.**

| Plasmid | Relevant characteristics | Source or reference |
|---|---|---|
| pJC1 | *Kan*$^R$, *Amp*$^R$; *oriV*$_{C.g.}$ , *oriV*$_{E.c.}$ (*C. glutamicum*/*E. coli* shuttle vector) | (5) |
| pJC1-*venus*-term | *Kan*$^R$, pJC1 derivative carrying the *venus* coding sequence followed by a terminator sequence of *Bacillus subtilis* | (4) |
| pJC1-P$_{lysin}$-*e2-crimson* | *Kan*$^R$; pJC1 derivative containing a 250 bp promoter region of the *lys* gene (cg1974) and the first 30 bp of the coding sequence fused to *e2-crimson* gene via a linker containing a stop codon and a RBS | (6) |
| pK19-*mobsacB* | *Kan*$^R$; plasmid for allelic exchange in *C. glutamicum*; (*oriT*, *oriVE.c.*, *sacB*, *lacZ*$\alpha$) | (7) |
| pAN6 | *Kan*$^R$; *C. glutamicum*/*E. coli* shuttle vector for gene expression under control of the P$_{tac}$ promoter; (P$_{tac}$, *lacIq*, pBL1 *oriVC.g.*, pUC18 *oriVE.c.*) | (3) |
| pAN6-*cgpS*-Strep | *Kan*$^R$; pAN6 derivative containing the *cgpS* gene fused C-terminal without stop codon to a sequence encoding a Strep-tag | (8) |
| pET16b | *Amp*$^R$; vector for overexpression of genes in *E. coli*, adding a C-terminal hexahistidine affinity tag to the | Novagen |

| | | |
|---|---|---|
| | synthesized protein (pBR322 *oriVE.c.*, $P_{T7}$, *lacI* ) | |
| pET16b-*gntR1* | *Amp*$^R$; pET16b derivative for overproduction of GntR1 with an N-terminal decahistidine tag. | (3) |

**Table S2C: Plasmids constructed in this work.** Oligonucleotide pairs, which were used for PCR, are given as numbers (Table S2D). DNA templates are indicated in brackets behind the oligonucleotides. The used backbones including the restriction enzymes used for linearization are listed behind (*). Information about region of CgpS bound area and positions of maximal CgpS binding coverage were based on previous studies from Pfeifer and colleagues (8).

| Plasmid | Construction | Relevant characteristics |
|---|---|---|
| **Phage promoter-based constructs** | | |
| pJC1-$P_{cg1897}$-*venus* | Gibson assembly: 459/460 (*C. glutamicum* genome) and 115/116 (pJC1-*venus*-term) into pJC1-*venus*-term *BamHI *BcuI | *Kan*$^R$; pJC1-*venus*-term derivative carrying the CgpS bound area of the promoter of cg1897 (468 bp) and the first 30 bp of the coding sequence fused to the reporter gene *venus* via a linker containing a stop codon and an artificial RBS. |
| pJC1-$P_{cg1897}$::GntR_BS_pos0-*venus* | Gibson assembly: 459/394 (pJC1-$P_{cg1897}$-*venus*) and 393/116 (pJC1-$P_{cg1897}$-*venus*) into pJC1-*venus*-term *BamHI *BcuI | *Kan*$^R$; pJC1-$P_{cg1897}$-*venus* derivative with an inserted GntR BS directly upstream of the position of maximal CgpS binding. |
| pJC1-$P_{cg1936}$-*venus* | Gibson assembly: 449/450 (*C. glutamicum* genome) and 115/116 (pJC1-*venus*-term) into | *Kan*$^R$; pJC1-*venus*-term derivative carrying the CgpS bound area of the promoter of cg1936 (676 |

| | | |
|---|---|---|
| | pJC1-*venus*-term *BamHI *BcuI | bp) and the first 30 bp of the coding sequence fused to the reporter gene *venus* via a linker containing a stop codon and an artificial RBS. |
| pJC1-$P_{cg1936}$::GntR_BS_pos0-*venus* | Gibson assembly: 449/452 (pJC1-$P_{cg1936}$-*venus*) and 451/116 (pJC1-$P_{cg1936}$-*venus*) into pJC1-*venus*-term *BamHI *BcuI | $Kan^R$; pJC1-$P_{cg1936}$-*venus* derivative with an inserted GntR BS directly upstream of the position of maximal CgpS binding. |
| pJC1-$P_{cg1940}$-*venus* | Gibson assembly: 444/445 (*C. glutamicum* genome) and 115/116 (pJC1-*venus*-term) into pJC1-*venus*-term *BamHI *BcuI | $Kan^R$; pJC1-*venus*-term derivative carrying the CgpS bound area of the promoter of cg1940 (563 bp) and the first 30 bp of the coding sequence fused to the reporter gene *venus* via a linker containing a stop codon and an artificial RBS. |
| pJC1-$P_{cg1940}$::GntR_BS_pos0-*venus* | Gibson assembly: 444/447 (pJC1-$P_{cg1940}$-*venus*) and 446/116 (pJC1-$P_{cg1940}$-*venus*) into pJC1-*venus*-term *BamHI *BcuI | $Kan^R$; pJC1-$P_{cg1940}$-*venus* derivative with an inserted GntR BS directly upstream of the position of maximal CgpS binding. |
| pJC1-$P_{cg1955}$-*venus* | Gibson assembly: 387/388 (*C. glutamicum* genome) and 115/116 (pJC1-*venus*-term) into pJC1-*venus*-term *BamHI *BcuI | $Kan^R$; pJC1-*venus*-term derivative carrying the CgpS bound area of the promoter of cg1955 (516 bp) and the first 30 bp of the coding sequence fused to the reporter gene *venus* via a linker containing a stop codon and an artificial RBS. |
| pJC1-$P_{cg1955}$::GntR_BS_pos0-*venus* | Gibson assembly: 387/390 (pJC1-$P_{cg1955}$-*venus*) and 389/116 (pJC1-$P_{cg1955}$-*venus*) into pJC1-*venus*-term *BamHI *BcuI | $Kan^R$; pJC1-$P_{cg1955}$-*venus* derivative with an inserted GntR BS directly upstream of the position of maximal CgpS binding. |
| pJC1-$P_{priP}$-*venus* | Gibson assembly: 200/201 (*C. glutamicum* genome) and 115/116 | $Kan^R$; pJC1-*venus*-term derivative carrying the CgpS bound area of the |

| | | |
|---|---|---|
| | (pJC1-*venus*-term) into pJC1-*venus*-term *BamHI *BcuI | promoter of $P_{priP}$ (611 bp) and the first 30 bp of the coding sequence fused to the reporter gene *venus* via a linker containing a stop codon and an artificial RBS. |
| pJC1-$P_{priP}$::GntR_BS_pos0-*venus* | Gibson assembly: 200/191 (pJC1-$P_{priP}$-*venus*) and 190/116 (pJC1-$P_{priP}$-*venus*) into pJC1-*venus*-term *BamHI *BcuI | $Kan^R$; pJC1-$P_{priP}$-*venus* derivative with an inserted GntR BS directly upstream of the position of maximal CgpS binding. |
| pJC1-$P_{lys}$-*venus* | Gibson assembly: 117/114 (*C. glutamicum* genome) and 115/116 (pJC1-*venus*-term) into pJC1-*venus*-term *BamHI *BcuI | $Kan^R$; pJC1-*venus*-term derivative carrying the CgpS bound area of the promoter of the *lys* gene (cg1974) (444 bp) and the first 30 bp of the coding sequence fused to the reporter gene *venus* via a linker containing a stop codon and an artificial RBS. |
| pJC1-$P_{lys}$::GntR_BS_pos-100-*venus* | Gibson assembly: 117/119 (pJC1-$P_{lys}$-*venus*) and 118/116 (pJC1-$P_{lys}$-*venus*) into pJC1-*venus*-term *BamHI *BcuI | $Kan^R$; pJC1-$P_{lys}$-*venus* derivative with an inserted GntR BS 100 bp upstream of the position of maximal CgpS binding. |
| pJC1-$P_{lys}$::GntR_BS_pos-50-*venus* | Gibson assembly: 117/114 (pEK-A2-$P_{lys}$::GntR_BS-50 bp upstream) and 115/116 (pJC1-*venus*-term) into pJC1-*venus*-term *BamHI *BcuI | $Kan^R$; pJC1-$P_{lys}$-*venus* derivative with an inserted GntR BS 50 bp upstream of the position of maximal CgpS binding. |
| pJC1-$P_{lys}$::GntR_BS_pos-25-*venus* | Gibson assembly: 117/178 (pJC1-$P_{lys}$-*venus*) and 177/116 (pJC1-$P_{lys}$-*venus*) into pJC1-*venus*-term *BamHI *BcuI | $Kan^R$; pJC1-$P_{lys}$-*venus* derivative with an inserted GntR BS 25 bp upstream of the position of maximal CgpS binding. |
| pJC1-$P_{lys}$::GntR_BS_pos-20-*venus* | Gibson assembly: 117/168 (pJC1-$P_{lys}$-*venus*) and 167/116 (pJC1-$P_{lys}$-*venus*) into | $Kan^R$; pJC1-$P_{lys}$-*venus* derivative with an inserted GntR BS 20 bp upstream of the position |

| | | |
|---|---|---|
| | pJC1-*venus*-term *BamHI *BcuI | of maximal CgpS binding. |
| pJC1-$P_{lys}$::GntR_BS_pos-15-*venus* | Gibson assembly: 117/176 (pJC1-$P_{lys}$-*venus*) and 175/116 (pJC1-$P_{lys}$-*venus*) into pJC1-*venus*-term *BamHI *BcuI | $Kan^R$; pJC1-$P_{lys}$-*venus* derivative with an inserted GntR BS 15 bp upstream of the position of maximal CgpS binding. |
| pJC1-$P_{lys}$::GntR_BS_pos-10-*venus* | Gibson assembly: 117/174 (pJC1-$P_{lys}$-*venus*) and 173/116 (pJC1-$P_{lys}$-*venus*) into pJC1-*venus*-term *BamHI *BcuI | $Kan^R$; pJC1-$P_{lys}$-*venus* derivative with an inserted GntR BS 10 bp upstream of the position of maximal CgpS binding. |
| pJC1-$P_{lys}$::GntR_BS_pos-5-*venus* | Gibson assembly: 117/172 (pJC1-$P_{lys}$-*venus*) and 171/116 (pJC1-$P_{lys}$-*venus*) into pJC1-*venus*-term *BamHI *BcuI | $Kan^R$; pJC1-$P_{lys}$-*venus* derivative with an inserted GntR BS 5 bp upstream of the position of maximal CgpS binding. |
| pJC1-$P_{lys}$::GntR_BS_pos-4-*venus* | Gibson assembly: 117/244 (pJC1-$P_{lys}$-*venus*) and 243/116 (pJC1-$P_{lys}$-*venus*) into pJC1-*venus*-term *BamHI *BcuI | $Kan^R$; pJC1-$P_{lys}$-*venus* derivative with an inserted GntR BS 4 bp upstream of the position of maximal CgpS binding. |
| pJC1-$P_{lys}$::GntR_BS_pos-3-*venus* | Gibson assembly: 117/246 (pJC1-$P_{lys}$-*venus*) and 245/116 (pJC1-$P_{lys}$-*venus*) into pJC1-*venus*-term *BamHI *BcuI | $Kan^R$; pJC1-$P_{lys}$-*venus* derivative with an inserted GntR BS 3 bp upstream of the position of maximal CgpS binding. |
| pJC1-$P_{lys}$::GntR_BS_pos-2-*venus* | Gibson assembly: 117/248 (pJC1-$P_{lys}$-*venus*) and 247/116 (pJC1-$P_{lys}$-*venus*) into pJC1-*venus*-term *BamHI *BcuI | $Kan^R$; pJC1-$P_{lys}$-*venus* derivative with an inserted GntR BS 2 bp upstream of the position of maximal CgpS binding. |
| pJC1-$P_{lys}$::GntR_BS_pos-1-*venus* | Gibson assembly: 117/250 (pJC1-$P_{lys}$-*venus*) and 249/116 (pJC1-$P_{lys}$-*venus*) into pJC1-*venus*-term *BamHI *BcuI | $Kan^R$; pJC1-$P_{lys}$-*venus* derivative with an inserted GntR BS 1 bp upstream of the position of maximal CgpS binding. |
| pJC1-$P_{lys}$_CS_0-*venus* | Gibson assembly: 117/125 (pJC1-$P_{lys}$-*venus*) and 124/116 | $Kan^R$; pJC1-$P_{lys}$-*venus* derivative with an inserted GntR BS |

| | | |
|---|---|---|
| | (pJC1-$P_{lys}$-*venus*) into pJC1-*venus*-term *BamHI *BcuI | directly upstream of the position of maximal CgpS binding. |
| pJC1-$P_{lys}$::GntR_BS_pos+1-*venus* | Gibson assembly: 117/212 (pJC1-$P_{lys}$-*venus*) and 211/116 (pJC1-$P_{lys}$-*venus*) into pJC1-*venus*-term *BamHI *BcuI | $Kan^R$; pJC1-$P_{lys}$-*venus* derivative with an inserted GntR BS 1 bp downstream of the position of maximal CgpS binding. |
| pJC1-$P_{lys}$::GntR_BS_pos+2-*venus* | Gibson assembly: 117/252 (pJC1-$P_{lys}$-*venus*) and 251/116 (pJC1-$P_{lys}$-*venus*) into pJC1-*venus*-term *BamHI *BcuI | $Kan^R$; pJC1-$P_{lys}$-*venus* derivative with an inserted GntR BS 2 bp downstream of the position of maximal CgpS binding. |
| pJC1-$P_{lys}$::GntR_BS_pos+3-*venus* | Gibson assembly: 117/254 (pJC1-$P_{lys}$-*venus*) and 253/116 (pJC1-$P_{lys}$-*venus*) into pJC1-*venus*-term *BamHI *BcuI | $Kan^R$; pJC1-$P_{lys}$-*venus* derivative with an inserted GntR BS 3 bp downstream of the position of maximal CgpS binding. |
| pJC1-$P_{lys}$::GntR_BS_pos+4-*venus* | Gibson assembly: 117/256 (pJC1-$P_{lys}$-*venus*) and 255/116 (pJC1-$P_{lys}$-*venus*) into pJC1-*venus*-term *BamHI *BcuI | $Kan^R$; pJC1-$P_{lys}$-*venus* derivative with an inserted GntR BS 4 bp downstream of the position of maximal CgpS binding. |
| pJC1-$P_{lys}$::GntR_BS_pos+5-*venus* | Gibson assembly: 117/180 (pJC1-$P_{lys}$-*venus*) and 179/116 (pJC1-$P_{lys}$-*venus*) into pJC1-*venus*-term *BamHI *BcuI | $Kan^R$; pJC1-$P_{lys}$-*venus* derivative with an inserted GntR BS 5 bp downstream of the position of maximal CgpS binding. |
| pJC1-$P_{lys}$::GntR_BS_pos+10-*venus* | Gibson assembly: 117/182 (pJC1-$P_{lys}$-*venus*) and 181/116 (pJC1-$P_{lys}$-*venus*) into pJC1-*venus*-term *BamHI *BcuI | $Kan^R$; pJC1-$P_{lys}$-*venus* derivative with an inserted GntR BS 10 bp downstream of the position of maximal CgpS binding. |
| pJC1-$P_{lys}$::GntR_BS_pos+15-*venus* | Gibson assembly: 117/184 (pJC1-$P_{lys}$-*venus*) and 183/116 (pJC1-$P_{lys}$-*venus*) into pJC1-*venus*-term *BamHI *BcuI | $Kan^R$; pJC1-$P_{lys}$-*venus* derivative with an inserted GntR BS 15 bp downstream of the position of maximal CgpS binding. |
| pJC1-$P_{lys}$::GntR_BS_pos+20-*venus* | Gibson assembly: 117/186 (pJC1-$P_{lys}$- | $Kan^R$; pJC1-$P_{lys}$-*venus* derivative with an |

| | | |
|---|---|---|
| | *venus*) and 185/116 (pJC1-$P_{lys}$-*venus*) into pJC1-*venus*-term *BamHI *BcuI | inserted GntR BS 20 bp downstream of the position of maximal CgpS binding. |
| pJC1-$P_{lys}$::GntR_BS_pos+25-*venus* | Gibson assembly: 117/121 (pJC1-$P_{lys}$-*venus*) and 120/116 (pJC1-$P_{lys}$-*venus*) into pJC1-*venus*-term *BamHI *BcuI | *Kan*$^R$; pJC1-$P_{lys}$-*venus* derivative with an inserted GntR BS 25 bp downstream of the position of maximal CgpS binding. |
| pJC1-$P_{lys}$::GntR_BS_pos+50-*venus* | Gibson assembly: 117/188 (pJC1-$P_{lys}$-*venus*) and 187/116 (pJC1-$P_{lys}$-*venus*) into pJC1-*venus*-term *BamHI *BcuI | *Kan*$^R$; pJC1-$P_{lys}$-*venus* derivative with an inserted GntR BS 50 bp downstream of the position of maximal CgpS binding. |
| pJC1-$P_{lys}$::control_sequence_1_pos0-*venus* | Gibson assembly: 117/380 (pJC1-$P_{lys}$-*venus*) and 379/116 (pJC1-$P_{lys}$-*venus*) into pJC1-*venus*-term *BamHI *BcuI | *Kan*$^R$; pJC1-P*lys*-*venus* derivative with an inserted control sequence 1 (CATTAATGATAATGC) directly upstream of the position of maximal CgpS binding. |
| pJC1-$P_{lys}$::control_sequence_2_pos0-*venus* | Gibson assembly: 117/382 (pJC1-$P_{lys}$-*venus*) and 381/116 (pJC1-$P_{lys}$-*venus*) into pJC1-*venus*-term *BamHI *BcuI | *Kan*$^R$; pJC1-$P_{lys}$-*venus* derivative with an inserted control sequence 2 (TATGATAGTAGCAAT) directly upstream of the position of maximal CgpS binding. |
| pJC1-$P_{lys}$(5´Δ300bp)-*venus* | Gibson assembly: 385/116 (pJC1-$P_{lys}$-*venus*) into pJC1-*venus*-term *BamHI *BcuI | *Kan*$^R$; pJC1-$P_{lys}$-*venus* derivative with a 300 bp truncation of the 5´-promoter region. |
| pJC1-$P_{lys}$(5´Δ350bp)-*venus* | Gibson assembly: 386/116 (pJC1-$P_{lys}$-*venus*) into pJC1-*venus*-term *BamHI *BcuI | *Kan*$^R$; pJC1-P*lys*-*venus* derivative with a 350 bp truncation of the 5´-promoter region. |
| pJC1-$P_{lys}$(5´Δ300bp)_CS_0-*venus* | Gibson assembly: 385/116 (pJC1-$P_{lys}$_CS_0-*venus*) into pJC1-*venus*-term *BamHI *BcuI | *Kan*$^R$; pJC1-$P_{lys}$_CS_0-*venus* derivative with a 300 bp truncation of the 5´-promoter region. |
| pJC1-$P_{lys}$(5´Δ350bp)_CS_0-*venus* | Gibson assembly: 386/116 (pJC1- | *Kan*$^R$; pJC1-$P_{lys}$_CS_0-*venus* derivative with a |

| | | |
|---|---|---|
| | $P_{lys}$_CS_0-*venus*) into pJC1-*venus*-term *BamHI *BcuI | 350 bp truncation of the 5´-promoter region. |
| pJC1-$P_{cg1977}$-*venus* | Gibson assembly: 435/436 (*C. glutamicum* genome) and 115/116 (pJC1-*venus*-term) into pJC1-*venus*-term *BamHI *BcuI | *Kan*$^R$; pJC1-*venus*-term derivative carrying the CgpS bound area of the promoter of cg1977 (653 bp) and the first 30 bp of the coding sequence fused to the reporter gene *venus* via a linker containing a stop codon and an artificial RBS. |
| pJC1-$P_{cg1977}$::GntR_BS_pos0-*venus* | Gibson assembly: 435/438 (pJC1-$P_{cg1977}$-*venus*) and 437/116 (pJC1-$P_{cg1977}$-*venus*) into pJC1-*venus*-term *BamHI *BcuI | *Kan*$^R$; pJC1-$P_{cg1977}$-*venus* derivative with an inserted GntR BS directly upstream of the position of maximal CgpS binding. |
| pJC1-$P_{cg1999}$-*venus* | Gibson assembly: 395/396 (*C. glutamicum* genome) and 115/116 (pJC1-*venus*-term) into pJC1-*venus*-term *BamHI *BcuI | *Kan*$^R$; pJC1-*venus*-term derivative carrying the CgpS bound area of the promoter of cg1999 (448 bp) and the first 30 bp of the coding sequence fused to the reporter gene *venus* via a linker containing a stop codon and an artificial RBS. |
| pJC1-$P_{cg1999}$::GntR_BS_pos-30-*venus* | Gibson assembly: 395/575 (pJC1-$P_{cg1999}$-*venus*) and 574/116 (pJC1-$P_{cg1999}$-*venus*) into pJC1-*venus*-term *BamHI *BcuI | *Kan*$^R$; pJC1-$P_{cg1999}$-*venus* derivative with an inserted GntR BS 30 bp upstream of the position of maximal CgpS binding. |
| pJC1-$P_{cg1999}$::GntR_BS_pos-20-*venus* | Gibson assembly: 395/577 (pJC1-$P_{cg1999}$-*venus*) and 576/116 (pJC1-$P_{cg1999}$-*venus*) into pJC1-*venus*-term *BamHI *BcuI | *Kan*$^R$; pJC1-$P_{cg1999}$-*venus* derivative with an inserted GntR BS 20 bp upstream of the position of maximal CgpS binding. |
| pJC1-$P_{cg1999}$::GntR_BS_pos-10-*venus* | Gibson assembly: 395/579 (pJC1-$P_{cg1999}$-*venus*) and 578/116 (pJC1-$P_{cg1999}$-*venus*) into pJC1-*venus*-term *BamHI *BcuI | *Kan*$^R$; pJC1-$P_{cg1999}$-*venus* derivative with an inserted GntR BS 10 bp upstream of the position of maximal CgpS binding. |

| | | |
|---|---|---|
| pJC1-$P_{cg1999}$::GntR_BS_pos-5-*venus* | Gibson assembly: 395/573 (pJC1-$P_{cg1999}$-*venus*) and 572/116 (pJC1-$P_{cg1999}$-*venus*) into pJC1-*venus*-term *BamHI *BcuI | *Kan*$^R$; pJC1-$P_{cg1999}$-*venus* derivative with an inserted GntR BS 5 bp upstream of the position of maximal CgpS binding. |
| pJC1-$P_{cg1999}$::GntR_BS_pos0-*venus* | Gibson assembly: 395/398 (pJC1-$P_{cg1999}$-*venus*) and 397/116 (pJC1-$P_{cg1999}$-*venus*) into pJC1-*venus*-term *BamHI *BcuI | *Kan*$^R$; pJC1-$P_{cg1999}$-*venus* derivative with an inserted GntR BS directly upstream of the position of maximal CgpS binding. |
| pJC1-$P_{cg1999}$::GntR_BS_pos+5-*venus* | Gibson assembly: 395/571 (pJC1-$P_{cg1999}$-*venus*) and 570/116 (pJC1-$P_{cg1999}$-*venus*) into pJC1-*venus*-term *BamHI *BcuI | *Kan*$^R$; pJC1-$P_{cg1999}$-*venus* derivative with an inserted GntR BS 5 bp downstream of the position of maximal CgpS binding. |
| pJC1-$P_{cg1999}$::GntR_BS_pos+10-*venus* | Gibson assembly: 395/581 (pJC1-$P_{cg1999}$-*venus*) and 580/116 (pJC1-$P_{cg1999}$-*venus*) into pJC1-*venus*-term *BamHI *BcuI | *Kan*$^R$; pJC1-$P_{cg1999}$-*venus* derivative with an inserted GntR BS 10 bp downstream of the position of maximal CgpS binding. |
| pJC1-$P_{cg2014}$-*venus* | Gibson assembly: 439/440 (*C. glutamicum* genome) and 115/116 (pJC1-*venus*-term) into pJC1-*venus*-term *BamHI *BcuI | *Kan*$^R$; pJC1-*venus*-term derivative carrying the CgpS bound area of the promoter of cg2014 (545 bp) and the first 30 bp of the coding sequence fused to the reporter gene *venus* via a linker containing a stop codon and an artificial RBS. |
| pJC1-$P_{cg2014}$::GntR_BS_pos0-*venus* | Gibson assembly: 439/442 (pJC1-$P_{cg2014}$-*venus*) and 441/116 (pJC1-$P_{cg2014}$-*venus*) into pJC1-*venus*-term *BamHI *BcuI | *Kan*$^R$; pJC1-$P_{cg2014}$-*venus* derivative with an inserted GntR BS directly upstream of the position of maximal CgpS binding. |
| pJC1-$P_{cg2020}$-*venus* | Gibson assembly: 408/409 (*C. glutamicum* genome) and 115/116 (pJC1-*venus*-term) into pJC1-*venus*-term *BamHI *BcuI | *Kan*$^R$; pJC1-*venus*-term derivative carrying the CgpS bound area of the promoter of cg2020 (390 bp) and the first 30 bp of the coding sequence fused to the reporter |

| | | |
|---|---|---|
| | | gene *venus* via a linker containing a stop codon and an artificial RBS. |
| pJC1-$P_{cg2020}$::GntR_BS_pos0-*venus* | Gibson assembly: 408/411 (pJC1-$P_{cg2020}$-*venus*) and 410/116 (pJC1-$P_{cg2020}$-*venus*) into pJC1-*venus*-term *BamHI *BcuI | $Kan^R$; pJC1-$P_{cg2020}$-*venus* derivative with an inserted GntR BS directly upstream of the position of maximal CgpS binding. |
| pJC1-$P_{cg2022}$-*venus* | Gibson assembly: 416/417 (*C. glutamicum* genome) and 115/116 (pJC1-*venus*-term) into pJC1-*venus*-term *BamHI *BcuI | $Kan^R$; pJC1-*venus*-term derivative carrying the CgpS bound area of the promoter of cg2022 (309 bp) and the first 30 bp of the coding sequence fused to the reporter gene *venus* via a linker containing a stop codon and an artificial RBS. |
| pJC1-$P_{cg2022}$::GntR_BS_pos0-*venus* | Gibson assembly: 416/419 (pJC1-$P_{cg2022}$-*venus*) and 418/116 (pJC1-$P_{cg2022}$-*venus*) into pJC1-*venus*-term *BamHI *BcuI | $Kan^R$; pJC1-$P_{cg2022}$-*venus* derivative with an inserted GntR BS directly upstream of the position of maximal CgpS binding. |
| pJC1-$P_{cg2032}$-*venus* | Gibson assembly: 412/413 (*C. glutamicum* genome) and 115/116 (pJC1-*venus*-term) into pJC1-*venus*-term *BamHI *BcuI | $Kan^R$; pJC1-*venus*-term derivative carrying the CgpS bound area of the promoter of cg2032 (490 bp) and the first 30 bp of the coding sequence fused to the reporter gene *venus* via a linker containing a stop codon and an artificial RBS. |
| pJC1-$P_{cg2032}$::GntR_BS_pos0-*venus* | Gibson assembly: 412/415 (pJC1-$P_{cg2032}$-*venus*) and 414/116 (pJC1-$P_{cg2032}$-*venus*) into pJC1-*venus*-term *BamHI *BcuI | $Kan^R$; pJC1-$P_{cg2032}$-*venus* derivative with an inserted GntR BS directly upstream of the position of maximal CgpS binding. |
| **Synthetic $P_{cg1999}$ promoter variants** | | |
| pJC1-$P_{cg1999}$_A-T/G-C-*venus* | Gibson assembly: 501/505 (pJC1-$P_{cg1999}$_A-T/G-C) and 115/116 (pJC1-*venus*-term) into | $Kan^R$; pJC1-*venus*-term derivative carrying a synthetic promoter based on a 50 bp region of $P_{cg1999}$ containing |

| | | |
|---|---|---|
| | pJC1-*venus*-term *BamHI *BcuI | core promoter elements (TSS, -10 and -35 box), the identified binding motif and the nucleotide associated with maximal CgpS coverage. GC-profile of $P_{cg1999}$ was maintain in the adjacent flanks but A/T and G/C were swapped. The promoter was fused to the reporter gene *venus* via a linker containing a stop codon and an artificial RBS. The distance between TSS, start of coding region and artificial 30 bp coding region as well as the linker containing the RBS were consistent with the template sequence of $P_{cg1999}$. |
| pJC1-$P_{cg1999}$_rand-*venus* | Gibson assembly: 497/498 (pEX-K168-Synthetic-sequence1) and 115/116 (pJC1-*venus*-term) into pJC1-*venus*-term *BamHI *BcuI | *Kan*$^R$; pJC1-*venus*-term derivative carrying a synthetic promoter based on a 50 bp region of $P_{cg1999}$ containing core promoter elements (TSS, -10 and -35 box), the identified binding motif and the nucleotide associated with maximal CgpS coverage. The adjacent sequences were randomized and fused to the reporter gene *venus* via a linker containing a stop codon and an artificial RBS. The distance between TSS, start of coding region and artificial 30 bp coding region as well as the linker containing the RBS were consistent |

| | | |
|---|---|---|
| | | with the template sequence of $P_{cg1999}$. |
| **Synthetic $P_{lys}$ promoter variants** | | |
| pJC1-$P_{lys}$_A-T/G-C_70bp-*venus* | Gibson assembly: 560/601 (gene strand $P_{lys}$_A-T/G-C) and 115/116 (pJC1-*venus*-term) into pJC1-*venus*-term *BamHI *BcuI | *Kan*$^R$; pJC1-*venus*-term derivative carrying a synthetic promoter based on a 70 bp region of $P_{lys}$ containing core promoter elements (TSS, -10 and -35 box). GC-profile of $P_{lys}$ was maintain in the adjacent flanks but A/T and G/C were swapped. The promoter was fused to the reporter gene *venus* via a linker containing a stop codon and an artificial RBS. The distance between TSS, start of coding region and artificial 30 bp coding region as well as the linker containing the RBS were consistent with the template sequence of $P_{lys}$. |
| pJC1-$P_{lys}$_A-T/G-C_80bp-*venus* | Gibson assembly: 560/618 (pJC1-$P_{lys}$_A-T/G-C_70bp-*venus*) and 617/116 (pJC1-$P_{lys}$_A-T/G-C_70bp-*venus*) into pJC1-*venus*-term *BamHI *BcuI | *Kan*$^R$; pJC1-*venus*-term derivative carrying a synthetic promoter based on a 80 bp region of $P_{lys}$ containing core promoter elements (TSS, -10 and -35 box) and the identified binding motif. GC-profile of $P_{lys}$ was maintain in the adjacent flanks but A/T and G/C were swapped. The promoter was fused to the reporter gene *venus* via a linker containing a stop codon and an artificial RBS. The distance between TSS, start of coding region |

| | | |
|---|---|---|
| | | and artificial 30 bp coding region as well as the linker containing the RBS were consistent with the template sequence of $P_{lys}$. |
| pJC1-$P_{lys}$_A-T/G-C_70bp-*venus* | Gibson assembly: 560/601 (gene strand $P_{lys}$_A-T/G-C) and 115/116 (pJC1-*venus*-term) into pJC1-*venus*-term *BamHI *BcuI | *Kan*$^R$; pJC1-*venus*-term derivative carrying a synthetic promoter based on a 100 bp region of $P_{lys}$ containing core promoter elements (TSS, -10 and -35 box), the identified binding motif and the nucleotide associated with maximal CgpS coverage (8). GC-profile of $P_{lys}$ was maintain in the adjacent flanks but A/T and G/C were swapped. The promoter was fused to the reporter gene *venus* via a linker containing a stop codon and an artificial RBS. The distance between TSS, start of coding region and artificial 30 bp coding region as well as the linker containing the RBS were consistent with the template sequence of $P_{lys}$. |
| **Further reporter constructs** | | |
| pJC1-$P_{gntK}$-*venus* | Gibson assembly: 203/204 (*C. glutamicum* genome) and 115/116 (pJC1-*venus*-term) into pJC1-*venus*-term *BamHI *BcuI | *Kan*$^R$; pJC1-*venus*-term derivative carrying the $P_{gntK}$ promoter (307 bp) ($P_{cg2732}$) and the first 30 bp of the coding sequence fused to the reporter gene *venus* via a linker containing a stop codon and an artificial RBS. |
| pJC1-$P_{gntK}$-*e2-crimson* | Gibson assembly: 203/204 (*C. glutamicum* | *Kan*$^R$; pJC1-*venus*-term derivative carrying the |

| | | |
|---|---|---|
| | genome) and 259/260 (pJC1-$P_{lysin}$-*e2-crimson*) into pJC1-*venus*-term *BamHI *BcuI | $P_{gntK}$ promoter (307 bp) ($P_{cg2732}$) and the first 30 bp of the coding sequence fused to the reporter gene *e2-crimson* via a linker containing a stop codon and an artificial RBS. |
| **GntR-dependent toggle** | | |
| pJC1-$P_{lys}$_CS_0-*venus*-T-$P_{gntK}$-*e2-crimson* | Gibson assembly: 117/263 (pJC1-$P_{lys}$_CS_0-*venus*) and 261/262 (pJC1-$P_{gntK}$-*e2-crimson*) into pJC1-*venus*-term *BamHI *BcuI | *Kan*$^R$; pJC1-*venus*-term derivative carrying the construct $P_{lys}$_CS_0-*venus* and the oppositely oriented $P_{gntK}$-*e2-crimson* construct. |
| **Templates used for preparation of DNA fragments for surface plasmon resonance analysis** | | |
| pJC1-$P_{cg3336}$ | Gibson assembly: 516/517 (*C. glutamicum* genome) into pJC1-*venus*-term *BamHI *BcuI | *Kan*$^R$; pJC1-*venus*-term derivative carrying a 1238 bp region covering the promoter region of cg3336 |
| pJC1-$P_{cg1999}$ | Gibson assembly: 520/521 (*C. glutamicum* genome) into pJC1-*venus*-term *BamHI *BcuI | *Kan*$^R$; pJC1-*venus*-term derivative carrying a 1363 bp region covering the promoter region of c1999 |
| pJC1-$P_{cg1999}$_A-T/G-C | Gibson assembly: 501/503 (pEX-K168-Cg1999-AT-GCSwitch) and 502/504 (pEX-K168-Cg1999-AT-GCSwitch) into pJC1-*venus*-term *BamHI *BcuI | *Kan*$^R$; pJC1-*venus*-term derivative carrying the sequence $P_{cg1999}$_A-T/G-C encoded in pEX-K168-Cg1999-AT-GCSwitch (Table S2H) with nucleotide exchanges to ATG at positions 331-333 |
| pJC1-$P_{lys}$_CS_0 | Gibson assembly: 117/125 (*C. glutamicum* genome) and 124/404 (*C. glutamicum* genome) into pJC1-*venus*-term *BamHI *BcuI | *Kan*$^R$; pJC1-*venus*-term derivative carrying the CgpS bound area of the promoter of *lys* (cg1974) (444 bp) with an inserted GntR BS directly upstream of the position of maximal CgpS binding and the first 179 bp of the *lys* gene. |

| ***cgpS* integration plasmid** | | |
|---|---|---|
| pK19*mobsacB*-1199_1201-$P_{cgpS}$-*cgpS* | Gibson assembly: E227/E228 (*C. glutamicum* genome), E245/E115 (*C. glutamicum* genome) and E229/E230 (*C. glutamicum* genome) into pK19*mobsacB* *HindIII *EcoRI | *Kan*$^R$; pK19-*mobsacB* derivative for the re-integration of *cgpS* and its native promoter (500+351bp) into the intergenic region of cg1199-cg1201 (500 bp upstream and downstream flanking region). |

18

19

20 **Table S2D: Oligonucleotides used in this study for plasmid constructions.**

| **Oligonucleotide number** | **Sequence (5´→3´)** |
|---|---|
| 114 | TGATATCTCCTTCTTAAAGTTCAATTTTTCGGCATTGCG CCTTTAATCGC |
| 115 | TGAACTTTAAGAAGGAGATATCATATGGTGAGCAAGGG CGAGGAG |
| 116 | AAAACGACGGCCAGTACTAGTTACTTGTACAGCTCGTC CATGCC |
| 117 | AGCGACGCCGCAGGGGGATCCGCTCAAGGAAGAGTT CTTCATTGGTC |
| 118 | GCCTTTATGATAGTACCAATTCGAGAACTGGGTGTAGT GATTTCTG |
| 119 | GTTCTCGAATTGGTACTATCATAAAGGCTTTTTCTCTCA TGACCTACCC |
| 120 | GGGAACATTATGATAGTACCAATTAAACGGGTAAAGGT AAAGGACAAACG |
| 121 | CCCGTTTAATTGGTACTATCATAATGTTCCCTGGATACT ACAAATTAAAC |
| 124 | GATACTAGAGTTATGATAGTACCAATTTAATTTGTAGTA TCCAGGGAAC |
| 125 | AAATTAAATTGGTACTATCATAACTCTAGTATCTTATTAA TTTCTGTTAC |
| 167 | CAGATATGATAGTACCAATAATTAATAAGATACTAGAGT TTAATTTGTAG |
| 168 | CTTATTAATTATTGGTACTATCATATCTGTTACTATTAAC ATATAGGTTT |
| 171 | GATACTTATGATAGTACCAATAGAGTTTAATTTGTAGTA TCCAGGGAAC |

16

| | |
|---|---|
| 172 | CTCTATTGGTACTATCATAAGTATCTTATTAATTTCTGTTACTATTAAC |
| 173 | GTATGATAGTACCAATATACTAGAGTTTAATTTGTAGTATCCAGGG |
| 174 | GTATATTGGTACTATCATACTTATTAATTTCTGTTACTATTAACATATAG |
| 175 | ATTATATGATAGTACCAATATAAGATACTAGAGTTTAATTTGTAGTATCC |
| 176 | CTTATATTGGTACTATCATATAATTTCTGTTACTATTAACATATAGG |
| 177 | TATATGATAGTACCAATACAGAAATTAATAAGATACTAGAGTTTAATTTG |
| 178 | ATTTCTGTATTGGTACTATCATATACTATTAACATATAGGTTTTTTAAAG |
| 179 | GTTTAATTATGATAGTACCAATTTGTAGTATCCAGGGAACATTAAACGG |
| 180 | AAATTGGTACTATCATAATTAAACTCTAGTATCTTATTAATTTCTGTTAC |
| 181 | GTATATGATAGTACCAATGTATCCAGGGAACATTAAACGGGTAAAG |
| 182 | TACATTGGTACTATCATATACAAATTAAACTCTAGTATCTTATTAATTTC |
| 183 | GTATCTATGATAGTACCAATCAGGGAACATTAAACGGGTAAAGGTAAAG |
| 184 | CCCTGATTGGTACTATCATAGATACTACAAATTAAACTCTAGTATC |
| 185 | CCAGGGTATGATAGTACCAATAACATTAAACGGGTAAAGGTAAAGGAC |
| 186 | GTTATTGGTACTATCATACCCTGGATACTACAAATTAAACTCTAGTATC |
| 187 | GGTAAAGGACAAATATGATAGTACCAATCGAACATGGCGATTAAAGGCGC |
| 188 | GTTCGATTGGTACTATCATATTTGTCCTTTACCTTTACCCGTTTAATG |
| 190 | CTTATGATAGTACCAATAAGCTTGTTTAAATTGAAACTTCGTTATATTC |
| 191 | CTTATTGGTACTATCATAAGTAATAAAGAAACTCAACGGTTTATTAAGAC |
| 200 | AGCGACGCCGCAGGGGGATCCTGATGTAACGCTTATATTATTTTAAG |
| 201 | TGATATCTCCTTCTTAAAGTTCATGGGTCGTGGCTGTCTGTGGTGTC |
| 203 | AGCGACGCCGCAGGGGGATCCGTATCAATGGAATCCGGGACGC |
| 204 | TGATATCTCCTTCTTAAAGTTCAGACAATATGTAAGCCTTCGGCTGC |

| | |
|---|---|
| 211 | GATACTAGAGTTTATGATAGTACCAATTAATTTGTAGTA TCCAGGGAAC |
| 212 | AATTAATTGGTACTATCATAAACTCTAGTATCTTATTAAT TTCTGTTAC |
| 243 | GATACTATATGATAGTACCAATGAGTTTAATTTGTAGTA TCCAGGG |
| 244 | CTCATTGGTACTATCATATAGTATCTTATTAATTTCTGTT ACTATTAAC |
| 245 | GATACTAGTATGATAGTACCAATAGTTTAATTTGTAGTA TCCAGGGAAC |
| 246 | CTATTGGTACTATCATACTAGTATCTTATTAATTTCTGTT AC |
| 247 | GATACTAGATATGATAGTACCAATGTTTAATTTGTAGTA TCCAGGGAAC |
| 248 | CATTGGTACTATCATATCTAGTATCTTATTAATTTCTGTT AC |
| 249 | GTATGATAGTACCAATTTTAATTTGTAGTATCCAGGGAA CATTAAAC |
| 250 | AATTAAAATTGGTACTATCATACTCTAGTATCTTATTAAT TTCTGTTAC |
| 251 | GAGTTTTATGATAGTACCAATAATTTGTAGTATCCAGGG AACATTAAAC |
| 252 | AATTATTGGTACTATCATAAAACTCTAGTATCTTATTAAT TTCTGTTAC |
| 253 | GAGTTTATATGATAGTACCAATATTTGTAGTATCCAGGG AACATTAAAC |
| 254 | CTACAAATATTGGTACTATCATATAAACTCTAGTATCTT ATTAATTTCTG |
| 255 | GAGTTTAATATGATAGTACCAATTTTGTAGTATCCAGGG AACATTAAACG |
| 256 | CTACAAAATTGGTACTATCATATTAAACTCTAGTATCTT ATTAATTTCTG |
| 259 | TGAACTTTAAGAAGGAGATATCATATGGATAGCACTGA GAACGTCATC |
| 260 | AAAACGACGGCCAGTACTAGCTACTGGAACAGGTGGT GG |
| 261 | GAAAGGCTCAGTCGAAAGACTGGGCCTTTCGTTTTATC TACTGGAACAGGTGGTGG |
| 262 | AAAACGACGGCCAGTACTAGGTATCAATGGAATCCGG GACGC |
| 263 | GTCTTTCGACTGAGCCTTTCGTTTTATTTTACTTGTACA GCTCGTCCATG |
| 379 | GATACTAGAGTCATTAATGATAATGCTTAATTTGTAGTA TCCAGGGAAC |
| 380 | AAATTAAGCATTATCATTAATGACTCTAGTATCTTATTAA TTTCTGTTAC |

| | |
|---|---|
| 381 | GATACTAGAGTTATGATAGTAGCAATTTAATTTGTAGTA TCCAGGGAAC |
| 382 | AAATTAAATTGCTACTATCATAACTCTAGTATCTTATTAA TTTCTGTTAC |
| 385 | AGCGACGCCGCAGGGGGATCCGTGTAGTGATTTCTGT TGCAGGTTTATG |
| 386 | AGCGACGCCGCAGGGGGATCCATATGTTAATAGTAAC AGAAATTAATAAG |
| 387 | AGCGACGCCGCAGGGGGATCCCACTCTCGCAACACTC GCTC |
| 388 | TGATATCTCCTTCTTAAAGTTCAGATCTTGTGCGGTCTA GATAATGCG |
| 389 | TATGATAGTACCAATAATAACTAGTATTTTTAATGACTTA C |
| 390 | CTAGTTATTATTGGTACTATCATATATTTACTAAATATAG AAGTTAATTG |
| 393 | CACAATTATGATAGTACCAATTATTTCATACATGTGTTA TGTTAATTAC |
| 394 | ATTGGTACTATCATAATTGTGAATACTAAAGTTAATAGT TTC |
| 395 | AGCGACGCCGCAGGGGGATCCATTATGTGCGTATCGC TGCTGCTC |
| 396 | TGATATCTCCTTCTTAAAGTTCATCTGCGCTCGCCAGC AAGTG |
| 397 | GTTAGTTATGATAGTACCAATATATTAATTACTTGATTTA ATTGAAGGGG |
| 398 | ATTGGTACTATCATAACTAACTTAATTGAGTTTATTTTTA CGG |
| 404 | AAAACGACGGCCAGTACTAGGTCACGACCTGATTTTTT ACCTCG |
| 408 | AGCGACGCCGCAGGGGGATCCCGATGTATGTCAGCAA TGAGGTTG |
| 409 | TGATATCTCCTTCTTAAAGTTCAGTCATCCGACCCGCC ATTATTC |
| 410 | GAAACTTTATGATAGTACCAATCAATAACTTAGTAACTT TAAAAGGGG |
| 411 | GATTGGTACTATCATAAAGTTTCTAGAATATAAGTTATT ACACAAAAACG |
| 412 | AGCGACGCCGCAGGGGGATCCATTTGGAATCTTGGTA CTTTGGTGGC |
| 413 | TGATATCTCCTTCTTAAAGTTCAAGGTTGCGGTTCTAAA ACTGTCG |
| 414 | CAATTTTAATGTGTATGATAGTACCAATTTAAAGTTTCT ATATTCCATTCTAAAATAAC |
| 415 | AATTGGTACTATCATACACATTAAAATTGAATATTAAAT GTTGTTTAAAG |

| | |
|---|---|
| 416 | AGCGACGCCGCAGGGGGATCCGCAGATTCAGTGGTTCACCAC |
| 417 | TGATATCTCCTTCTTAAAGTTCAGCTTTTCTCTGCACAGTATTTGTCAT |
| 418 | TAAGTTATGATAGTACCAATTTGTCATTAAAGAAATGGGGTAGAGCTATG |
| 419 | CAAATTGGTACTATCATAACTTATTTTAACTATTTAAAGACTAATTAAATTTAAC |
| 435 | AGCGACGCCGCAGGGGGATCCTTTCCTGCCTTGACATGCGAGAAC |
| 436 | TGATATCTCCTTCTTAAAGTTCAGACTGTGGAGATGATGCGGAATTTC |
| 437 | TAAAATATCGTATGATAGTACCAATGAGTTTATTTATGTGATTTGACCGG |
| 438 | CATTGGTACTATCATACGATATTTTAATCAGATAAATAATTACTAATAAC |
| 439 | AGCGACGCCGCAGGGGGATCCATCCCGTACAGGTATTTTGCGTAGTG |
| 440 | TGATATCTCCTTCTTAAAGTTCAATCTTTATCCTTGCTTCGAAAATTAGC |
| 441 | CAAGTATGATAGTACCAATGTGATTATGCTTCACATTAATACTTAATAAG |
| 442 | CATAATCACATTGGTACTATCATACTTGTCAAACAAATGCAATACTTTTC |
| 444 | AGCGACGCCGCAGGGGGATCCCATATACCCAAGCACTTGGCGATC |
| 445 | TGATATCTCCTTCTTAAAGTTCAAGTTGATGTGGCTGACGTGGTG |
| 446 | CGCGTTTATGATAGTACCAATTCTCTATTTTAATTAATATAATTAATGTAGTTTATTAAC |
| 447 | ATTAAAATAGAGAATTGGTACTATCATAAACGCGATAGGCGTGTATGTGG |
| 449 | AGCGACGCCGCAGGGGGATCCTGCTGCACGAATGCGTAACCTC |
| 450 | TGATATCTCCTTCTTAAAGTTCAGCCGAATATTCGGCGAGTTTTTAG |
| 451 | GAAAAGTCACTTATGATAGTACCAATTAAGCGCACGCTAAAAGCGAATTG |
| 452 | GCGCTTAATTGGTACTATCATAAGTGACTTTTCAATTGTGCTGTAATTG |
| 459 | AGCGACGCCGCAGGGGGATCCTGGAGTCGCGGGTGCTCAAC |
| 460 | TGATATCTCCTTCTTAAAGTTCATACCTCTCGACCCTGTTTATTAAAAG |
| 497 | AGCGACGCCGCAGGGGGATCCGCGCCTCTACGAGACATTGG |

20

| | |
|---|---|
| 498 | GATATCTCCTTCTTAAAGTTCAATAAGGCGAAATACATT TAATAGCAATC |
| 501 | AGCGACGCCGCAGGGGGATCCTATCAGGACGGCTCC TATATCGG |
| 502 | GATTTATAACTTCCCCAAATATCAATGTGCGTTTGTGAA CGACCGCTC |
| 503 | GCGGTCGTTCACAAACGCACATTGATATTTGGGGAAGT TATAAATCAAG |
| 504 | AAAACGACGGCCAGTACTAGTGCACGGGCTAGACGAC CTAG |
| 505 | TGATATCTCCTTCTTAAAGTTCAAGACGCGAGCGGTCG TTCAC |
| 516 | AGCGACGCCGCAGGGGGATCCGCCTCCTCATCGATTT CCGC |
| 517 | AAAACGACGGCCAGTACTAGCCGTAGCAGCGCTTGTC TCG |
| 520 | AGCGACGCCGCAGGGGGATCCGACCACTACCTCAAG GGCGG |
| 521 | AAAACGACGGCCAGTACTAGCAGTTGCAGACGTGTAC GACAC |
| 560 | AGCGACGCCGCAGGGGGATC |
| 570 | GTATATTTATGATAGTACCAATAATTACTTGATTTAATTG AAGGGGTTTA |
| 571 | TTATTGGTACTATCATAAATATACTAACTTAATTGAGTTT ATTTTTACGG |
| 572 | AGTATGATAGTACCAATTTAGTATATTAATTACTTGATTT AATTGAAGGG |
| 573 | TACTAAATTGGTACTATCATACTTAATTGAGTTTATTTTT ACGGTTTAAT |
| 574 | AAATTATATGATAGTACCAATAACCGTAAAAATAAACTC AATTAAGTTAG |
| 575 | TTTTACGGTTATTGGTACTATCATATAATTTACTCTAAG CGAAGACGCCC |
| 576 | TATGATAGTACCAATATAAACTCAATTAAGTTAGTATAT TAATTACTTGATTTAATTG |
| 577 | TGAGTTTATATTGGTACTATCATATTTTACGGTTTAATTT ACTCTAAGCG |
| 578 | AATATGATAGTACCAATTTAAGTTAGTATATTAATTACTT GATTTAATTG |
| 579 | CTTAAATTGGTACTATCATATTGAGTTTATTTTTACGGTT TAATTTACTC |
| 580 | TATTAATTATATGATAGTACCAATCTTGATTTAATTGAAG GGGTTTATAG |
| 581 | TTGGTACTATCATATAATTAATATACTAACTTAATTGAGT TTATTTTTAC |
| 601 | ATGATATCTCCTTCTTAAAGTTCATAAAAAGCCGTAACG |

| | |
|---|---|
| 617 | CAGAAATTAATAAGATACTTCTCAAATTAAACATCATAG GTCCCTTG |
| 618 | TAATTTGAGAAGTATCTTATTAATTTCTGTTACTATTAAC ATATAGGTTT |
| 619 | ACAGAAATTAATAAGATACTAGAGTTTAATTTGTAGTAT CGTCCCTTGTAATTTGCCCATTTCC |
| 620 | AAAACGACGGCCAGTACTAGTTACTTGTACAGCTCGTC CATGCC |
| E115 | TTATTCGAAAGGAATGCCTTCTTTTTCG |
| E227 | GACCATGATTACGCCAAGCTTGAAAATCGGGAGTGGG AAAGAG |
| E228 | GTAGCTACACAGACGACCAGATTCGTGGGCGAAGTGG TTC |
| E229 | AAGGCATTCCTTTCGAATAAGTGAACTCAGAAATGCCA GGATTTG |
| E230 | AAAACGACGGCCAGTGAATTCCAAGACCGTCACCCAA CTAG |
| E245 | CTGGTCGTCTGTGTAGCTAC |

21

22 **Table S2E: Oligonucleotides used for the amplification of DNA probes for surface**
23 **plasmon resonance analysis.** Primers belonging to the same first PCR reaction are
24 alternately shadowed in grey or white. The first PCR product was used as template for the
25 second PCR reaction. The first primer was combined with the primer Biotin-primer (Biotin-
26 GAGGAGTCGTCGATGTGGAGACC), which was 5´-fused to biotin.

| Sample | Oligo-nucleotide number | Sequence (5´→3´) | Template |
|---|---|---|---|
| $P_{cg3336}$ (control) | M259<br>M260 | CGCCCTCACCGGTGG<br>GAGGAGTCGTCGATGTGGA<br>GACCCCAAGATCTTTGGGG<br>AGAGATTTTT | pJC1-$P_{cg3336}$ |
| $P_{cg1999}$ | 710 | ACGTGCCCGATCTGCTGGA TC | pJC1-$P_{cg1999}$ |
| | 709 | GAGGAGTCGTCGATGTGGA<br>GACCATTTGTGGGCGCTTTA<br>ATCGCTAAC | |
| $P_{cg1999}$_A-T/G-C | 507 | TGCACGGGCTAGACGACCT AG | pJC1-$P_{cg1999}$_A-T/G-C |

22

| | | | |
|---|---|---|---|
| | 506 | GAGGAGTCGTCGATGTGGA GACCTAAACACCCGCGAAAT TAGCGATTG | |
| $P_{lys}$ | M263<br>M264 | CTCGACGACGGCCACTG GAGGAGTCGTCGATGTGGA GACCAGTGCCTTCTTTGAGG CTTGA | *C. glutamicum* genome |
| $P_{lys}$_CS_0 | M263<br>M264 | CTCGACGACGGCCACTG GAGGAGTCGTCGATGTGGA GACCAGTGCCTTCTTTGAGG CTTGA | pJC1-$P_{lys}$_CS_0 |

**Table S2F: Oligonucleotides used for electrophoretic mobility shift assays.** Primers and their corresponding templates are alternately shadowed in grey or white.

| Sample | Oligo-nucleotide number | Sequence (5´→3´) | Template |
|---|---|---|---|
| $P_{lys}$ | 117 | AGCGACGCCGCAGGGGGATCCGC TCAAGGAAGAGTTCTTCATTGGTC | pJC1-$P_{lys}$-*venus* |
| | 114 | TGATATCTCCTTCTTAAAGTTCAAT TTTTCGGCATTGCGCCTTTAATCG C | |
| $P_{lys}$_CS_0 | 117 | AGCGACGCCGCAGGGGGATCCGC TCAAGGAAGAGTTCTTCATTGGTC | pJC1-$P_{lys}$_CS_0-*venus* |
| | 114 | TGATATCTCCTTCTTAAAGTTCAAT TTTTCGGCATTGCGCCTTTAATCG C | |

**Table S2G: Oligonucleotides used for sequencing.**

| Oligonucleotide name | Sequence (5´→3´) | Target |
|---|---|---|
| pJC1-MCS-fw | CAGGGACAAGCCACCCGCACA | All pJC1-based plasmids (Table S2C) |
| pJC1-MCS-rv | GGAAGCTAGAGTAAGTAGTTCGC | |
| R274-eYFPK5-seq-rv | GCAGGACCATGTGATCGCGC | pJC1-$P_{lys}$_CS_0-*venus*-T-$P_{gntK}$-*e2-crimson* |
| R216-venus-end-fw | CTCTCGGCATGGACGAGCTGTAC | |
| 492-venus-seq-rv | CTCGAACTTCACCTCGGCGC | |

| | | |
|---|---|---|
| M13-fw | CGCCAGGGTTTTCCCAGTCAC | pK19*mobsacB*-1199_1201-*cgpS* |
| M13-rv | AGCGGATAACAATTTCACACAGGA | |
| cg1199_1201_seq_fw | GTGGAAAAAATTGGGGTTTCCG | Genomically re-integrated $P_{cgpS}$-*cgpS* sequence in the intergenic region of cg1199-cg1201 |
| cg1199_1201_seq_rv | GCTCATTGTCACAGATGGCG | |

33

34

35 **Table S2H: Ordered DNA sequences.** All DNA sequences were synthesized by Eurofins

36 Genomics (Ebersberg, Germany) and provided as plasmids or DNA strands.

| **Ordered Sequences Plasmids** | **Sequence (5´→3´)** |
|---|---|
| pEX-K168-$P_{cg1999}$_A-T/G-C | TATCAGGACGGCTCCTATATCGGTGGGCAGGACAGC<br>TCTCGCGTTGTTGTTCACGAGAACGACCTAAACGACA<br>ACCAATATAAACACCCGCGAAATTAGCGATTGTGAAT<br>TTTGTGAAGAGTTGCGAAGATAGACAGTCGACACATC<br>TACCAGCACCGCCTTAGTAACAGTCGTATCGATATAA<br>AATGTTATACGAGTTAATCAAAGACGCAGACCTTTGC<br>CACGAATACCACTAAGGCCCGCAGAAGCGAATCTCA<br>TTTAAAAACCGTAAAAATAAACTCAATTAAGTTAGTAT<br>ATTAATTACTTGATTTATAACTTCCCCAAATATCATACT<br>GCGTTTGTGAACGACCGCTCGCGTCTTAGCAGTGGT<br>GCCGTCTCGAATTTCGCTACGACCGTGCTCCCCTATT<br>CCACAAAGACGGACCACAGCGTCGCGCCCGCGGTC<br>TCTAGGAGCTGTTGAAGCTAGGTCGTCTAGCCCGTG<br>CA |
| pEX-K168-$P_{cg1999}$_rand | GCGCCTCTACGAGACATTGGATGACCTAGGCTAACT<br>AGGCTTATAGAAGAGGGCACGCACGTACGGTATCGG<br>AGCTTTCATTGCCATTGGTAGGATCAAAACCCGTGAC<br>GAGTTGCTCTCCCATGCTACTATCAGAACTGACAATT<br>TGTAGAGGCCCTGAACGCTTTCAGCCGATTACACAC<br>AAGTGGTGGACTAATATTGGGGAGGCTGCTGCCCAG<br>ATCAATGAGCCTTAGGAGCAGATGATTAATACCGGC<br>GCAATTAAACCGTAAAAATAAACTCAATTAAGTTAGTA<br>TATTAATTACTTGATTTACCTTACCGGATCACGTTAAT<br>GATTGCTATTAAATGTATTTCGCCTTATATCTGCCTCG<br>CTCAAGGTTGCTTAAGCTGGCAACTGTTATTATATGG<br>GTTGCCCGAGCACGGATGGCTCGCTTCAACTCCGCA |

| | |
|---|---|
| | TTGACAGTTTACACACCCGCCGAGACGGGGATTCCG ACT |
| pEK-A2-P*lys*::GntR_BS_pos-50 | GCTCAAGGAAGAGTTCTTCATTGGTCTTTTGTTGCGG GTTGCCGTAGATGATTTCAGGGTGGCTCAAAGTCAG GGAGGTGTAGTCGAATTCGATTGGGTGAAGCCTGTC GCGATTACGGTTTTCGCGCTCGGTACCAGTAATAAAG CTTGCGATGCGGGAGTAATTAACCCGACCTTTGATAA ATACCTGAGTGCCTTCTTTGAGGCTTGATGCCTTGAT CTTTTCGGCGACTGGTGCTGGCTGCACAGGTTGAGG GGTAACTGGGTAGGTCATGAGAGAAAAAGCCTTTCG AGAACTGGGTGTAGTGATTTCTGTTGCAGGTTTATGT AGACGAAACTTATGATAGTACCAATTTAAAAAACCTAT ATGTTAATAGTAACAGAAATTAATAAGATACTAGAGTT TAATTTGTAGTATCCAGGGAACATTAAACGGGTAAAG GTAAAGGACAAACGAACATGGCGATTAAAGGCGCAA TGCCGAAAAAT |
| **Ordered Sequences Gene strands** | |
| P*lys*_A-T/G-C | AGCGACGCCGCAGGGGGATCCCGAGTTCCTTCTCAA GAAGTAACCAGAAAACAACGCCCAACGGCATCTACT AAAGTCCCACCGAGTTTCAGTCCCTCCACATCAGCTT AAGCTAACCCACTTCGGACAGCGCTAATGCCAAAAG CGCGAGCCATGGTCATTATTTCGAACGCTACGCCCT CATTAATTGGGCTGGAAACTATTTATGGACTCACGGA AGAAACTCCGAACTACGGAACTAGAAAAGCCGCTGA CCACGACCGACGTGTCCAACTCCCCATTGACCCATC CAGTACTCTCTTTTTCGGAAAGCTCTTGACCCACAAG TGATTTCTGTTGCAGGTTTATGTAGACGAAACTTTAAA AAACCTATATGTTAATAGTAACAGAAATTATATTCTAT GATCTCAAATTAAACATCATAGGTCCCTTGTAATTTGC CCATTTCCATTTCCTGTTTGCTTGATGCGCTAATTTCC GCGTTACGGCTTTTTATGAACTTTAAGAAGGAGATAT CAT |

**Table S2l: Sequences of the native phage promoters $P_{cg1999}$ and $P_{lys}$ and the corresponding synthetic variants shown in Figure 2.** Highlighted are the core promoter region (blue), the ATG as translational start codon (bold red) and the stop codon introduced after 30 nucleotides (bold yellow). For the native $P_{lys}$ promoter, the 100 bp core promoter region is highlighted.

| Promoter | Sequence (5´→3´) |
|---|---|

| | |
|---|---|
| **$P_{cg1999}$** | |
| $P_{cg1999}$ | ATAGTCCTGCCGAGGATATAGCCACCCGTCCTGTCG<br>AGAGCGCAACAACAAGTGCTCTTGCTGGATTTGCTGT<br>TGGTTATATTTGTGGGCGCTTTAATCGCTAACACTTA<br>AAACACTTCTCAACGCTTCTATCTGTCAGCTGTGTAG<br>ATGGTCGTGGCGGAATCATTGTCAGCATAGCTATATT<br>TTACAATATGCTCAATTAGTTTCTGCGTCTGGAAACG<br>GTGCTTATGGTGATTCCGGGCGTCTTCGCTTAGAGTA<br>AATTAAACCGTAAAAATAAACTCAATTAAGTTAGTATA<br>TTAATTACTTGATTTAATTGAAGGGGTTTATAGT**ATG**A<br>CGCAAACACTTGCTGGCGAGCGCAGA**TGA** |
| $P_{cg1999}$_A-T/G-C | TATCAGGACGGCTCCTATATCGGTGGGCAGGACAGC<br>TCTCGCGTTGTTGTTCACGAGAACGACCTAAACGACA<br>ACCAATATAAACACCCGCGAAATTAGCGATTGTGAAT<br>TTTGTGAAGAGTTGCGAAGATAGACAGTCGACACATC<br>TACCAGCACCGCCTTAGTAACAGTCGTATCGATATAA<br>AATGTTATACGAGTTAATCAAAGACGCAGACCTTTGC<br>CACGAATACCACTAAGGCCCGCAGAAGCGAATCTCA<br>TTTAAAAACCGTAAAAATAAACTCAATTAAGTTAGTAT<br>ATTAATTACTTGATTTATAACTTCCCCAAATATCA**ATG**<br>TGCGTTTGTGAACGACCGCTCGCGTCT**TGA** |
| $P_{cg1999}$_rand | GCGCCTCTACGAGACATTGGATGACCTAGGCTAACT<br>AGGCTTATAGAAGAGGGCACGCACGTACGGTATCGG<br>AGCTTTCATTGCCATTGGTAGGATCAAAACCCGTGAC<br>GAGTTGCTCTCCCATGCTACTATCAGAACTGACAATT<br>TGTAGAGGCCCTGAACGCTTTCAGCCGATTACACAC<br>AAGTGGTGGACTAATATTGGGGAGGCTGCTGCCCAG<br>ATCAATGAGCCTTAGGAGCAGATGATTAATACCGGC<br>GCAATTAAACCGTAAAAATAAACTCAATTAAGTTAGTA<br>TATTAATTACTTGATTTACCTTACCGGATCACGTTA**AT**<br>**G**ATTGCTATTAAATGTATTTCGCCTTAT**TGA** |
| **$P_{lys}$** | |
| $P_{lys}$ | GCTCAAGGAAGAGTTCTTCATTGGTCTTTTGTTGCGG<br>GTTGCCGTAGATGATTTCAGGGTGGCTCAAAGTCAG<br>GGAGGTGTAGTCGAATTCGATTGGGTGAAGCCTGTC<br>GCGATTACGGTTTTCGCGCTCGGTACCAGTAATAAAG<br>CTTGCGATGCGGGAGTAATTAACCCGACCTTTGATAA<br>ATACCTGAGTGCCTTCTTTGAGGCTTGATGCCTTGAT<br>CTTTTCGGCGACTGGTGCTGGCTGCACAGGTTGAGG<br>GGTAACTGGGTAGGTCATGAGAGAAAAAGCCTTTCG<br>AGAACTGGGTGTAGTGATTTCTGTTGCAGGTTTATGT<br>AGACGAAACTTTAAAAAACCTATATGTTAATAGTAACA<br>GAAATTAATAAGATACTAGAGTTTAATTTGTAGTATCC<br>AGGGAACATTAAACGGGTAAAGGTAAAGGACAAACG<br>AAC**ATG**GCGATTAAAGGCGCAATGCCGAAAAAT**TGA** |
| $P_{lys}$_A-T/G-C_70 bp | CGAGTTCCTTCTCAAGAAGTAACCAGAAAACAACGCC<br>CAACGGCATCTACTAAAGTCCCACCGAGTTTCAGTCC |

| | |
|---|---|
| | CTCCACATCAGCTTAAGCTAACCCACTTCGGACAGC<br>GCTAATGCCAAAAGCGCGAGCCATGGTCATTATTTCG<br>AACGCTACGCCCTCATTAATTGGGCTGGAAACTATTT<br>ATGGACTCACGGAAGAAACTCCGAACTACGGAACTA<br>GAAAAGCCGCTGACCACGACCGACGTGTCCAACTCC<br>CCATTGACCCATCCAGTACTCTCTTTTTCGGAAAGCT<br>CTTGACCCACAAGTGATTTCTGTTGCAGGTTTATGTA<br>GACGAAACTTTAAAAAACCTATATGTTAATAGTAACAG<br>AAATTATATTCTATGATCTCAAATTAAACATCATAGGT<br>CCCTTGTAATTTGCCCATTTCCATTTCCTGTTTGCTTG<br>**ATG**CGCTAATTTCCGCGTTACGGCTTTTTA**TGA** |
| $P_{lys}$_A-T/G-C_80 bp | CGAGTTCCTTCTCAAGAAGTAACCAGAAAACAACGCC<br>CAACGGCATCTACTAAAGTCCCACCGAGTTTCAGTCC<br>CTCCACATCAGCTTAAGCTAACCCACTTCGGACAGC<br>GCTAATGCCAAAAGCGCGAGCCATGGTCATTATTTCG<br>AACGCTACGCCCTCATTAATTGGGCTGGAAACTATTT<br>ATGGACTCACGGAAGAAACTCCGAACTACGGAACTA<br>GAAAAGCCGCTGACCACGACCGACGTGTCCAACTCC<br>CCATTGACCCATCCAGTACTCTCTTTTTCGGAAAGCT<br>CTTGACCCACAAGTGATTTCTGTTGCAGGTTTATGTA<br>GACGAAACTTTAAAAAACCTATATGTTAATAGTAACAG<br>AAATTAATAAGATACTTCTCAAATTAAACATCATAGGT<br>CCCTTGTAATTTGCCCATTTCCATTTCCTGTTTGCTTG<br>**ATG**CGCTAATTTCCGCGTTACGGCTTTTTA**TGA** |
| $P_{lys}$_A-T/G-C_100 bp | CGAGTTCCTTCTCAAGAAGTAACCAGAAAACAACGCC<br>CAACGGCATCTACTAAAGTCCCACCGAGTTTCAGTCC<br>CTCCACATCAGCTTAAGCTAACCCACTTCGGACAGC<br>GCTAATGCCAAAAGCGCGAGCCATGGTCATTATTTCG<br>AACGCTACGCCCTCATTAATTGGGCTGGAAACTATTT<br>ATGGACTCACGGAAGAAACTCCGAACTACGGAACTA<br>GAAAAGCCGCTGACCACGACCGACGTGTCCAACTCC<br>CCATTGACCCATCCAGTACTCTCTTTTTCGGAAAGCT<br>CTTGACCCACAAGTGATTTCTGTTGCAGGTTTATGTA<br>GACGAAACTTTAAAAAACCTATATGTTAATAGTAACAG<br>AAATTAATAAGATACTAGAGTTTAATTTGTAGTATCGT<br>CCCTTGTAATTTGCCCATTTCCATTTCCTGTTTGCTTG<br>**ATG**CGCTAATTTCCGCGTTACGGCTTTTTA**TGA** |

47

28

48 **REFERENCES**

49 1. Studier FW, Moffatt BA. 1986. Use of bacteriophage T7 RNA polymerase to direct
50 selective high-level expression of cloned genes. J Mol Biol 189:113-130.
51 2. Kinoshita S, Udaka S, Shimono M. 1957. Studies on the amino acid fermentation.
52 Part 1. Production of L-glutamic acid by various microorganisms. J Gen Appl
53 Microbiol 3:193-205.
54 3. Frunzke J, Engels V, Hasenbein S, Gätgens C, Bott M. 2008. Co-ordinated
55 regulation of gluconate catabolism and glucose uptake in *Corynebacterium*
56 *glutamicum* by two functionally equivalent transcriptional regulators, GntR1 and
57 GntR2. Mol Microbiol 67:305-322.
58 4. Baumgart M, Unthan S, Rückert C, Sivalingam J, Grünberger A, Kalinowski J,
59 Bott M, Noack S, Frunzke J. 2013. Construction of a prophage-free variant of
60 *Corynebacterium glutamicum* ATCC 13032 for use as a platform strain for basic
61 research and industrial biotechnology. Appl Environ Microbiol 79:6006-6015.
62 5. Cremer J, Eggeling L, Sahm H. 1990. Cloning the *dapA dapB* cluster of the
63 lysine-secreting bacterium *Corynebacterium glutamicum*. Mol Gen Genet
64 220:478-480.
65 6. Nanda AM, Heyer A, Krämer C, Grünberger A, Kohlheyer D, Frunzke J. 2014.
66 Analysis of SOS-induced spontaneous prophage induction in *Corynebacterium*
67 *glutamicum* at the single-cell level. J Bacteriol 196:180-188.
68 7. Schäfer A, Tauch A, Jäger W, Kalinowski J, Thierbach G, Pühler A. 1994. Small
69 mobilizable multi-purpose cloning vectors derived from the *Escherichia coli*
70 plasmids pK18 and pK19: selection of defined deletions in the chromosome of
71 *Corynebacterium glutamicum*. Gene 145:69-73.

72 8. Pfeifer E, Hünnefeld M, Popa O, Polen T, Kohlheyer D, Baumgart M, Frunzke J.
73 2016. Silencing of cryptic prophages in *Corynebacterium glutamicum*. Nucleic
74 Acids Res 44:10117-10131.

75

**Supplemental Figures**

References are indicated as numbers. Numbers are given in the reference section of the publication.

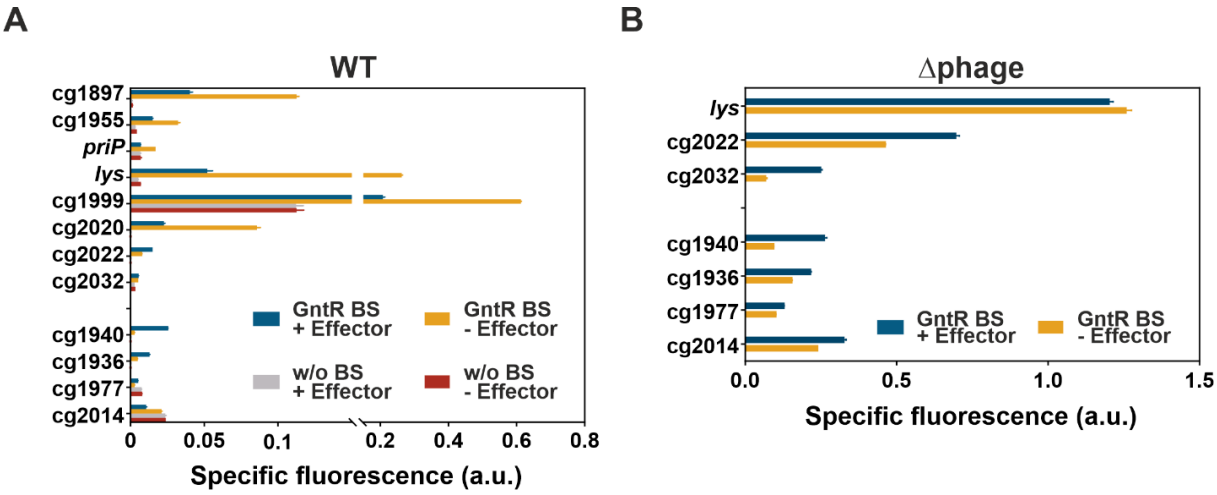


**Figure S1: Counter-silencing of CgpS target promoters. A)** Specific reporter outputs of native phage promoters and corresponding synthetic constructs which were used for the calculation of fold change ratios shown in Figure 3. **B)** To confirm functionality of synthetic promoter variants (GntR BS), which showed only low reporter outputs in the wild type, respective constructs were analyzed in the prophage-free strain Δphage in the absence of the silencer CgpS. All constructs led to significant reporter outputs confirming synthetic promoter functionality (n≥3 biological triplicates).

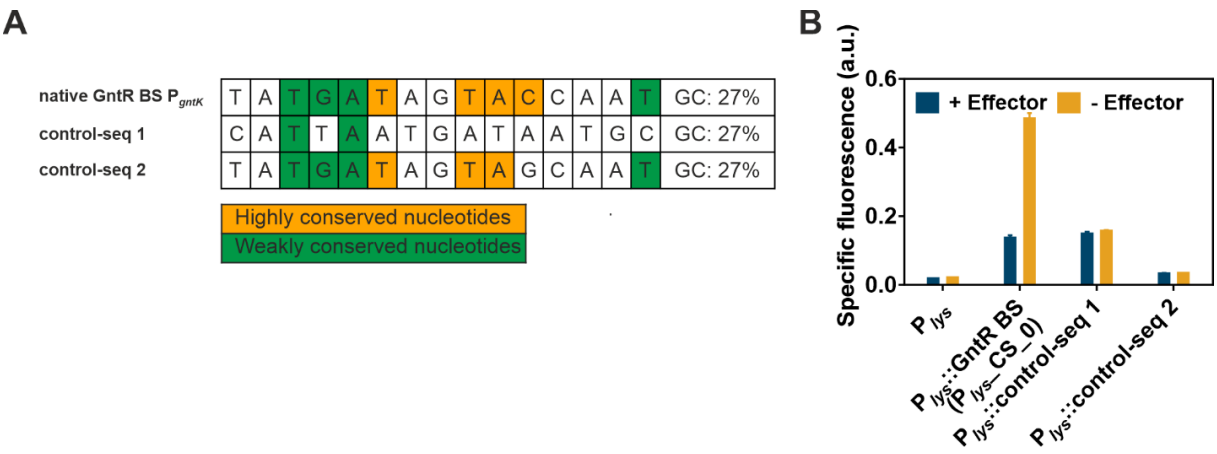


**Figure S2: Effects of inserted sequences independent of GntR binding. A)** The native GntR BS located within the $P_{gntK}$ promoter contains four highly conserved and four weakly conserved nucleotides (43). As controls for sequence insertions, which do not allow for GntR binding, control sequences (control-seq) 1 and 2 were inserted at position 0 within the phage promoter $P_{lys}$. Control-seq 1 contained the same nucleotide composition as the GntR BS but the sequence was randomized. Control-seq 2 was similar to the GntR BS, but one conserved cytosine was replaced with guanine. Based on previous studies, this exchange was expected to abolish GntR binding (43). **B)** Specific reporter outputs of the promoter variants after five hours of cultivation. Promoter constructs (plasmid backbone pJC1) were fused to the reporter gene *venus* and analyzed in *C. glutamicum* wild type. Cells were cultivated in CGXII in the presence (100 mM gluconate) or absence (100 mM glucose) of the effector molecule gluconate in a microtiter cultivation system. The results shown in this graph demonstrate that mutation of the GntR operator site abolished GntR binding in vivo and that the observed counter-silencing effect strictly depends on GntR binding.

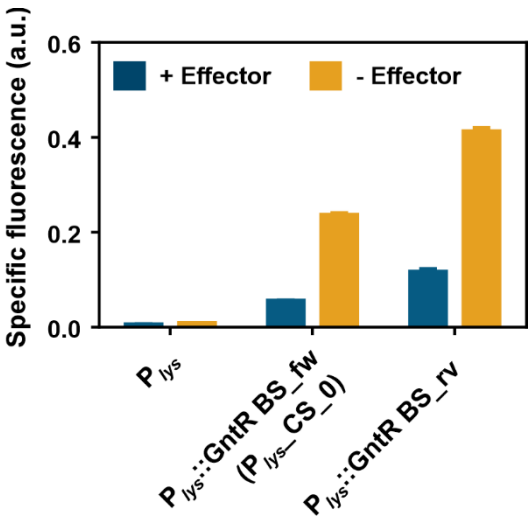


**Figure S3: Effects of directionality of inserted GntR binding site on counter-silencing efficiency.** The 15 bp long GntR BS was inserted either in a forward ($P_{lys}$::GntR BS_fw: $P_{lys}$_CS_0) or in a reverse orientation ($P_{lys}$::GntR BS_rv) in the $P_{lys}$ promoter (position 0) to analyze if the directionality of the GntR BS influence counter-silencing. Promoter constructs (plasmid backbone pJC1) were fused to the reporter gene *venus* and analyzed in *C. glutamicum* wild type. Cells were cultivated in CGXII medium in the presence (100 mM gluconate) or absence (100 mM glucose) of the effector molecule gluconate in a microtiter cultivation system. Presented is the mean of the specific fluorescence after five hours of cultivation (n=3 biological triplicates). These results demonstrated that counter-silencing does not depend on the directionality of GntR operator sites.

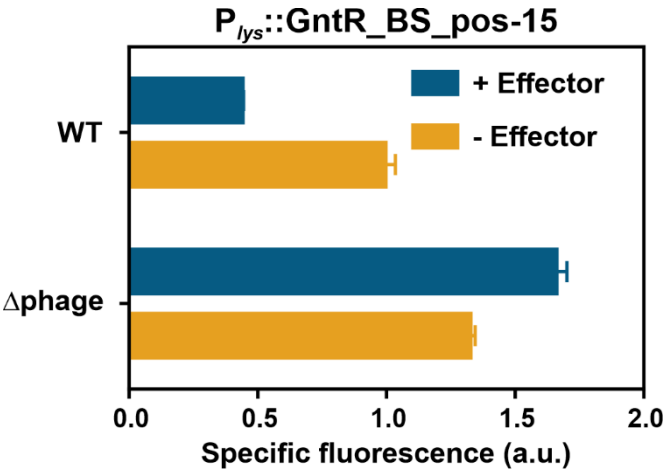


**Figure S4: It's all about context – Impact of GntR binding on the output of the $P_{lys}$ promoter in the presence or absence (Δphage) of CgpS.** Reporter outputs (*venus* expression) driven by a $P_{lys}$ promoter with an inserted GntR operator sequences 15 bp upstream of the maximal CgpS binding peak (11 bp downstream of TSS) in *C. glutamicum* wild type cells and in the absence of CgpS in the strain Δphage. Cells were cultivated in CGXII in the presence (100 mM gluconate) or absence (111 mM glucose) of the effector molecule gluconate in a microtiter cultivation system. Shown are mean values and standard deviation of reporter outputs of biological triplicates after five hours of cultivation.

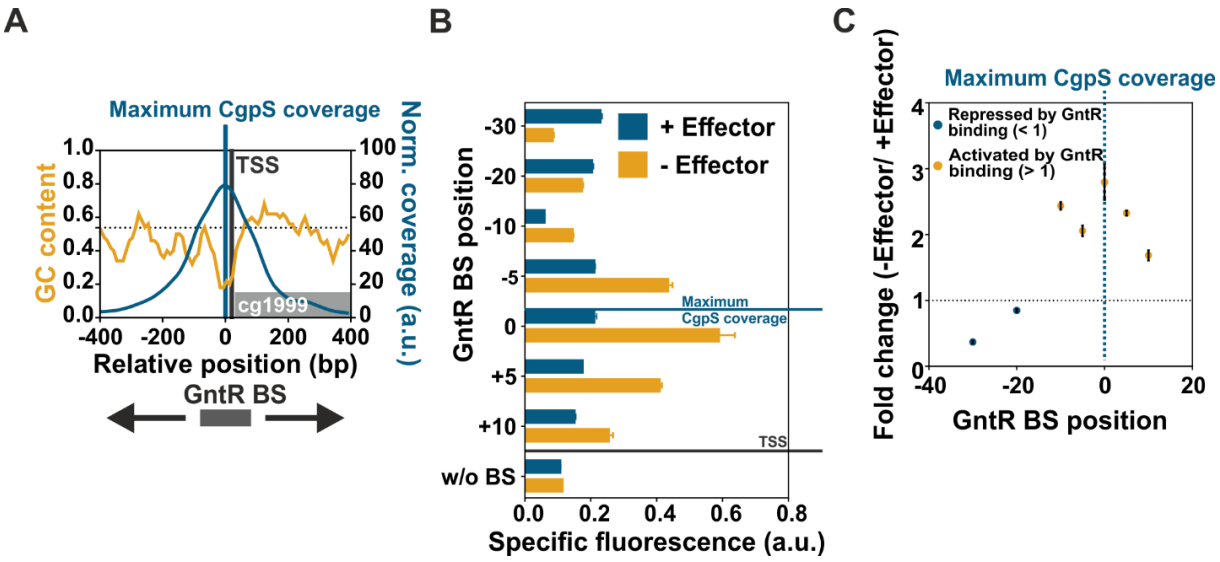


**Figure S5: Impact of GntR binding site (BS) position on inducibility of $P_{cg1999}$-based promoter constructs. A)** Inverse correlation of GC-profile and CgpS binding coverage of the phage promoter $P_{cg1999}$. The highest scored transcriptional start site (TSS) and the position of maximal CgpS binding affinity (4) are shown as vertical lines. BS positions refer to the sequence base associated with maximal CgpS binding peak. The position directly upstream of this nucleotide was defined as position 0. **B)** Impact of inserted GntR BS position on specific reporter outputs in the presence (gluconate) and absence (glucose) of the effector molecule gluconate. Positions of TSS and maximal CgpS coverage are marked by lines. **C)** Impact of GntR binding site position on counter-silencing efficiency of $P_{cg1999}$-based promoter constructs. Ratio of specific reporter outputs, shown in (B), were used for the calculation of their inducibility (fold change). Cells harboring the plasmid-based synthetic promoter constructs were grown in CGXII medium supplemented with either 100 mM glucose or 100 mM gluconate. Bars (B) and dots (C) represent the means and error bars the standard deviation of biological triplicates.

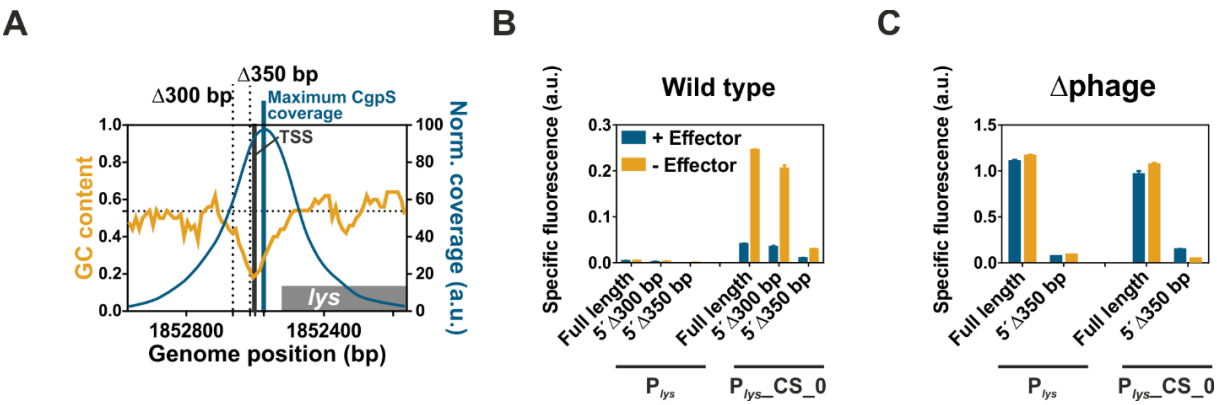


**Figure S6: Definition of the minimal region required for silencing**. **A)** Reporter outputs (*venus* expression) driven by 5´-truncated promoter versions (Δ300 and Δ350 bp truncations) of $P_{lys}$ and $P_{lys}$_CS_0 were analyzed regarding silencing and counter-silencing efficiency. 5´-ends of full-length constructs coincided with the upstream end of the CgpS binding peak ($P_{lys}$: 389 bp, $P_{lys}$_CS_0: 404 bp upstream of the maximal CgpS binding peak). The distance between maximal CgpS binding peak and ATG was in all constructs 85 bp. Full length promoters were compared to variants ending 89 bp (5´ Δ300) or 39 bp (5´ Δ350) upstream of the maximal CgpS binding peak in $P_{lys}$. **B and C)** Specific reporter outputs of the promoter variants after five hours of cultivation. Promoter constructs were fused to the reporter gene *venus* (plasmid backbone pJC1) and analyzed in *C. glutamicum* wild type cells (**B**) and in the prophage-free strain Δphage (Δ*cgpS*) (**C**). Cells were cultivated in CGXII in the presence (100 mM gluconate) or absence (100 mM glucose) of the effector molecule gluconate in a microtiter cultivation system. Shown are mean values and standard deviation of biological triplicates after five hours of cultivation. The results shown in this graph demonstrate that the region >89 bp upstream of the maximal CgpS binding peak of the $P_{lys}$ promoter is neither involved in silencing nor in counter-silencing. Further 50 bp truncation strongly reduced promoter activity of both promoters also in the Δphage strain.

## 4.4. Supplemental material to "Inducible expression systems based on xenogeneic silencing and counter-silencing and the design of a metabolic toggle switch"

## Supporting Information

**Inducible expression systems based on xenogeneic silencing and counter-silencing and the design of a metabolic toggle switch**

Johanna Wiechert[a], Cornelia Gätgens[a], Astrid Wirtz[a], and Julia Frunzke[a#]

[a]Institut für Bio- und Geowissenschaften, IBG-1: Biotechnologie, Forschungszentrum Jülich, Jülich, Germany

# Address correspondence to Prof. Dr. Julia Frunzke, j.frunzke@fz-juelich.de;
ORCID 0000-0001-6209-7950

## Supplemental figures

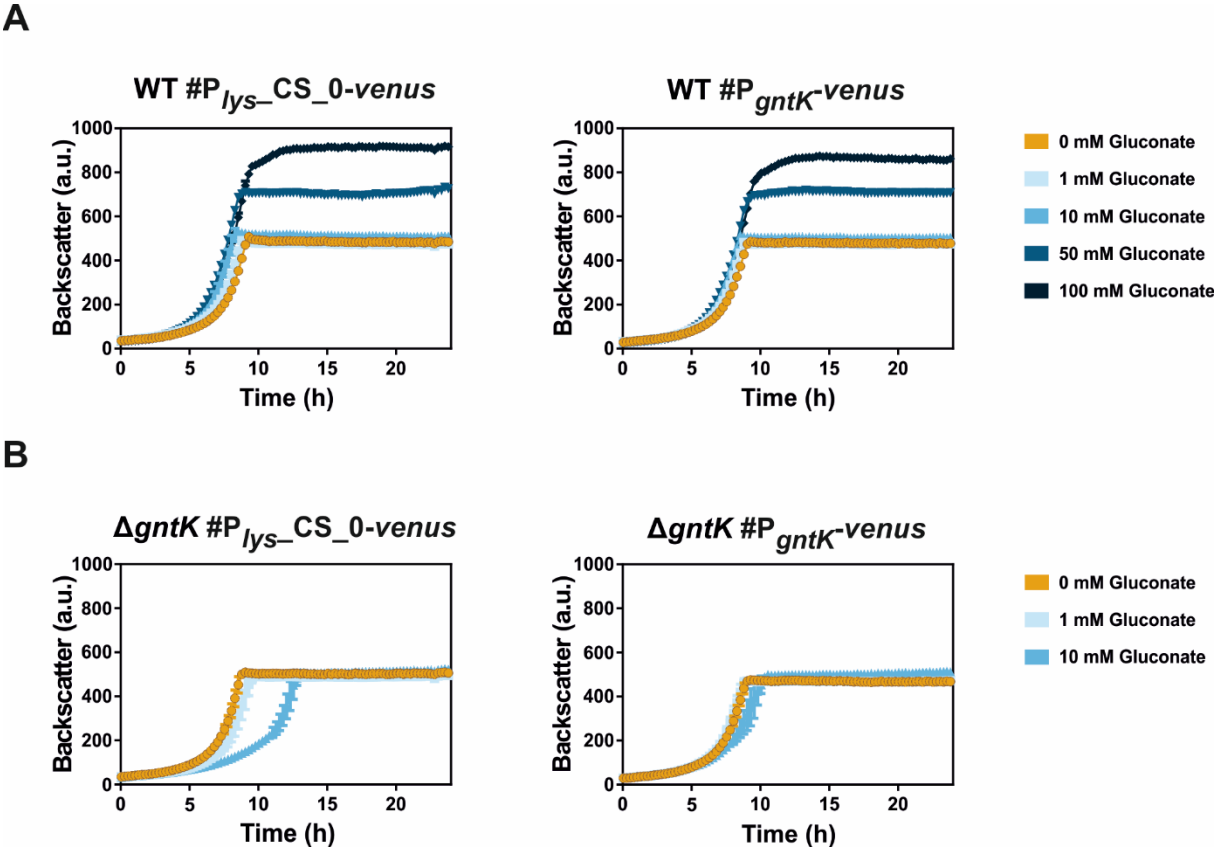


**Figure S1: Growth curves corresponding to the analysis of tunability of the native GntR target promoter $P_{gntK}$ and the synthetic counter-silencer promoter $P_{lys}$_CS_0 shown in Figure 4.** Shown are backscatter values of *C. glutamicum* wild type cells (WT) (A) or *C. glutamicum* cells lacking the gene encoding the gluconate kinase (Δ*gntK*) (B) harbouring the plasmid-based constructs pJC1-$P_{lys}$_CS_0-*venus* or pJC1-$P_{gntK}$-*venus* during cultivation in the presence of different gluconate concentrations. Graphs show the mean and error bars the standard deviation of biological triplicates over time. Cells were cultivated in a microtiter cultivation system in CGXII medium supplemented with constant amounts of glucose (100 mM in analysis of pJC1-$P_{gntK}$-*venus* and 111 mM for characterization of pJC1-$P_{lys}$_CS_0-*venus*) and either no or varying amounts of gluconate as effector. Backscatter was measured at 15 min intervals. The presented data show that varying amounts of gluconate affect the final backscatter values but did not significantly influence growth rates of wild-type cells. In contrast, Δ*gntK* cells displayed reduced growth rates upon addition of gluconate.

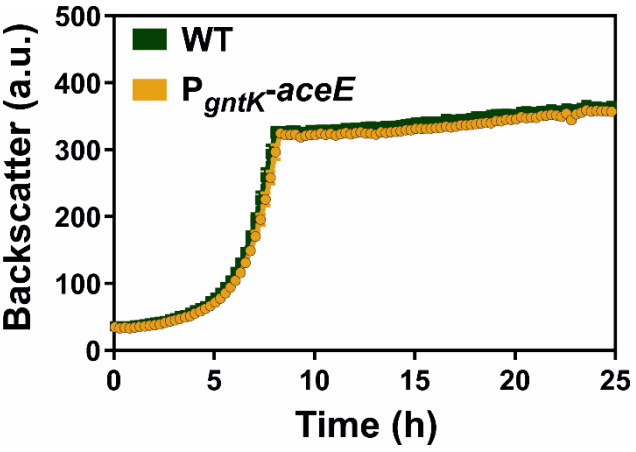


**Figure S2: Growth of the strain with dynamically controlled *aceE* expression ($P_{gntK}$-*aceE*) in comparison to *C. glutamicum* wild type cells, both harbouring the plasmid pJC1-$P_{lys}$_CS_0-*venus*.** Shown are backscatter values of both *C. glutamicum* strains during cultivation in a microtiter cultivation system in CGXII minimal medium with 100 mM gluconate and 25 µg/ml kanamycin. Strains had been pre-cultivated in CGXII containing 100 mM gluconate and 111 mM glucose. Graphs show the mean and error bars the standard deviation of biological triplicates over time. Backscatter was measured at 15 min intervals.

This experiment verified that growth of $P_{gntK}$-*aceE* is not impaired in comparison to wild-type cells in the presence of gluconate (100 mM).

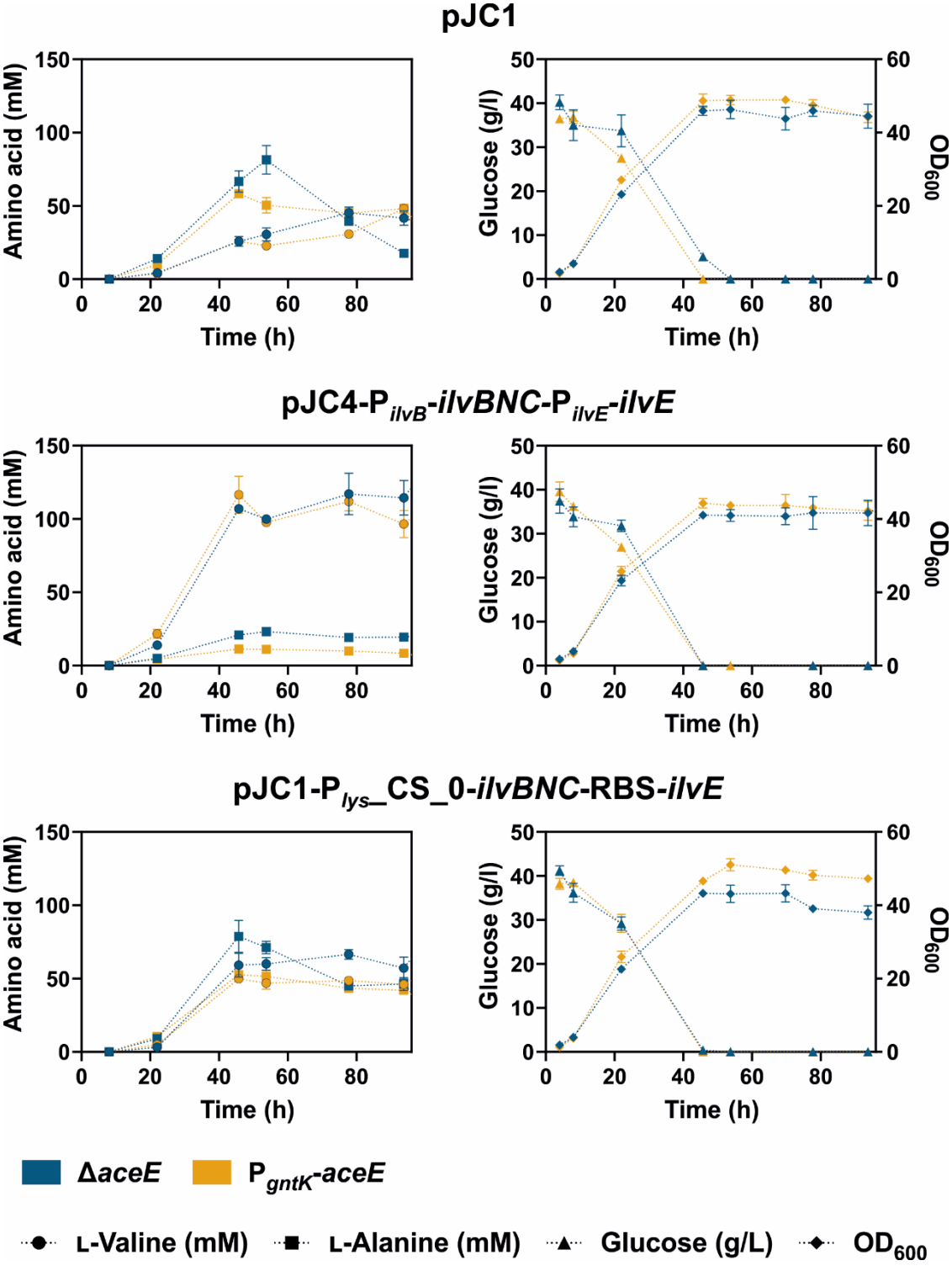


**Figure S3: Growth, glucose consumption, product (L-valine) and by-product (L-alanine) formation during L-valine production.** Cultivation of the strain with dynamically controlled *aceE* expression ($P_{gntK}$-*aceE*) in comparison to the previously established Δ*aceE* strain (Blombach et al., 2007; Schreiner et al., 2005) harbouring either the empty control plasmid pJC1 (pJC1-*venus*-term), plasmid-based L-valine biosynthesis genes controlled by the counter-silencer promoter (pJC1-$P_{lys}$_CS_0-*ilvBNC*-RBS-*ilvE*) or the natively regulated variant pJC4-$P_{ilvB}$-*ilvBNC*-$P_{ilvE}$-*ilvE* (pJC4-*ilvBNCE*) (Radmacher et al., 2002). Cultivation was performed in CGXII supplemented with 25 µg/ml kanamycin, 222 mM glucose and 254 mM acetate. Graphs represent the values of biological triplicates and error bars the corresponding standard deviations after 8, 22, 46, 54, 78 and

94 h of cultivation. Measurements of glucose and L-valine in the supernatant over time revealed that glucose was almost completely consumed after 46 hours of cultivation and L-valine concentrations had mostly reached maximal values.

## Supplemental tables

**Table S1: Overview of prices for glucose, gluconate and acetate provided by Sigma-Aldrich (December 2019, https://www.sigmaaldrich.com).** Considered were powders with minimal purity of 99% and an amount of 1 kg.

| Carbon source (Product ID) | Purity | Amount | Price |
|---|---|---|---|
| D-Gluconic acid sodium salt (G9005) | ≥99% | 1 kg | 49.80 € |
| D-(+)-Glucose (G8270) | ≥99.5% | 1 kg | 48.50 € |
| Potassium acetate (P5708) | ≥99% | 1 kg | 119 € |

**Table S2: Strains used in this study.**

| Strain | Relevant characteristics | Reference or source |
|---|---|---|
| ***E. coli*** | | |
| DH5α | F$^-$ Φ80*lacZ*ΔM15 Δ(*lacZYA-argF*) U169 *recA1 endA1 hsdR17*($r_k^-$, $m_k^+$) *phoA supE44 thi-1 gyrA96 relA1* $\lambda^-$, strain used for cloning procedures | Invitrogen |
| ***C. glutamicum*** | | |
| ATCC 13032 | Biotin-auxotrophic wild type | (Kinoshita et al., 1957) |
| Δ*aceE* | Derivate of ATCC 13032 with in-frame deletions of gene *aceE* (cg2466) | (Schreiner et al., 2005) |
| Δ*gntK* | Derivate of ATCC 13032 with in-frame deletions of gene *gntK* (cg2732) | This work |
| $\Delta P_{aceE}$-*aceE* | Derivate of ATCC 13032 with in-frame deletions of gene *aceE* (cg2466) and its 300 bp upstream promoter region | This work |
| $P_{gntK}$-*aceE* | Derivate of Δ*aceE* with the re-integrated gene *aceE* (cg2466) under control of the promoter $P_{gntK}$. $P_{gntK}$ (303 bp, $P_{cg2732}$). The first 30 bp of the coding sequence of *gntK* were fused to the *aceE* gene via a linker containing a stop codon and an artificial RBS. | This work |

**Table S3: Plasmids from other studies used in this work.**

| Plasmid | Relevant characteristics | Reference |
|---|---|---|
| pJC1 | *Kan*$^R$, *Amp*$^R$; *oriV*$_{C.g.}$, *oriV*$_{E.c.}$; *C. glutamicum*/*E. coli* shuttle vector | (Cremer et al., 1990) |
| pJC1-*venus*-term | *Kan*$^R$, pJC1 derivative carrying the *venus* coding sequence followed by a terminator sequence of *Bacillus subtilis* | (Baumgart et al., 2013) |
| pJC1-P$_{cg1897}$::GntR_BS_pos0-*venus* | *Kan*$^R$; pJC1-*venus*-term derivative carrying the CgpS bound area of the promoter of the gene cg1897 (468 bp) with an inserted GntR BS directly upstream of the position of maximal CgpS binding (Pfeifer et al., 2016) and the first 30 bp of the coding sequence fused to the reporter gene *venus* via a linker containing a stop codon and an artificial RBS. | (Wiechert et al., 2020) |
| pJC1-P$_{cg1936}$::GntR_BS_pos0-*venus* | *Kan*$^R$; pJC1-*venus*-term derivative carrying the CgpS bound area of the promoter of the gene cg1936 (676 bp) with an inserted GntR BS directly upstream of the position of maximal CgpS binding (Pfeifer et al., 2016) and the first 30 bp of the coding sequence fused to the reporter gene *venus* via a linker containing a stop codon and an artificial RBS. | (Wiechert et al., 2020) |
| pJC1-P$_{cg1940}$::GntR_BS_pos0-*venus* | *Kan*$^R$; pJC1-*venus*-term derivative carrying the CgpS bound area of the promoter of the gene cg1940 (563 bp) with an inserted GntR BS directly upstream of the position of maximal CgpS binding (Pfeifer et al., 2016) and the first 30 bp of the coding sequence fused to the reporter gene *venus* via a linker containing a stop codon and an artificial RBS. | (Wiechert et al., 2020) |
| pJC1-P$_{cg1955}$::GntR_BS_pos0-*venus* | *Kan*$^R$; pJC1-*venus*-term derivative carrying the CgpS bound area of the promoter of the gene cg1955 (516 bp) with an inserted GntR BS directly upstream of the position of maximal CgpS binding (Pfeifer et al., 2016) and the first 30 bp of the coding sequence fused to the reporter gene *venus* via a linker containing a stop codon and an artificial RBS. | (Wiechert et al., 2020) |
| pJC1-P$_{cg1977}$::GntR_BS_pos0-*venus* | *Kan*$^R$; pJC1-*venus*-term derivative carrying the CgpS bound area of the promoter of the gene cg1977 (653 bp) with an inserted GntR BS directly upstream of the position of maximal CgpS binding (Pfeifer et al., 2016) and the first 30 bp of the coding sequence fused to the reporter gene *venus* via a linker containing a stop codon and an artificial RBS. | (Wiechert et al., 2020) |

| | | |
|---|---|---|
| pJC1-$P_{cg1999}$::GntR_BS_pos-30-*venus* | *Kan*$^R$; pJC1-*venus*-term derivative carrying the CgpS bound area of the promoter of the gene cg1999 (448 bp) with an inserted GntR BS 30 bp upstream of the position of maximal CgpS binding (Pfeifer et al., 2016) and the first 30 bp of the coding sequence fused to the reporter gene *venus* via a linker containing a stop codon and an artificial RBS. | (Wiechert et al., 2020) |
| pJC1-$P_{cg1999}$::GntR_BS_pos-20-*venus* | *Kan*$^R$; pJC1-*venus*-term derivative carrying the CgpS bound area of the promoter of the gene cg1999 (448 bp) with an inserted GntR BS 20 bp upstream of the position of maximal CgpS binding (Pfeifer et al., 2016) and the first 30 bp of the coding sequence fused to the reporter gene *venus* via a linker containing a stop codon and an artificial RBS. | (Wiechert et al., 2020) |
| pJC1-$P_{cg1999}$::GntR_BS_pos-10-*venus* | *Kan*$^R$; pJC1-*venus*-term derivative carrying the CgpS bound area of the promoter of the gene cg1999 (448 bp) with an inserted GntR BS 10 bp upstream of the position of maximal CgpS binding (Pfeifer et al., 2016) and the first 30 bp of the coding sequence fused to the reporter gene *venus* via a linker containing a stop codon and an artificial RBS. | (Wiechert et al., 2020) |
| pJC1-$P_{cg1999}$::GntR_BS_pos-5-*venus* | *Kan*$^R$; pJC1-*venus*-term derivative carrying the CgpS bound area of the promoter of the gene cg1999 (448 bp) with an inserted GntR BS 5 bp upstream of the position of maximal CgpS binding (Pfeifer et al., 2016) and the first 30 bp of the coding sequence fused to the reporter gene *venus* via a linker containing a stop codon and an artificial RBS. | (Wiechert et al., 2020) |
| pJC1-$P_{cg1999}$::GntR_BS_pos0-*venus* | *Kan*$^R$; pJC1-*venus*-term derivative carrying the CgpS bound area of the promoter of the gene cg1999 (448 bp) with an inserted GntR BS directly upstream of the position of maximal CgpS binding (Pfeifer et al., 2016) and the first 30 bp of the coding sequence fused to the reporter gene *venus* via a linker containing a stop codon and an artificial RBS. | (Wiechert et al., 2020) |
| pJC1-$P_{cg1999}$::GntR_BS_pos+5-*venus* | *Kan*$^R$; pJC1-*venus*-term derivative carrying the CgpS bound area of the promoter of the gene cg1999 (448 bp) with an inserted GntR BS 5 bp downstream of the position of maximal CgpS binding (Pfeifer et al., 2016) and the first 30 bp of the coding sequence fused to the reporter gene *venus* via a linker | (Wiechert et al., 2020) |

| | | |
|---|---|---|
| | containing a stop codon and an artificial RBS. | |
| pJC1-$P_{cg1999}$::GntR_BS_pos+10-*venus* | *Kan*$^R$; pJC1-*venus*-term derivative carrying the CgpS bound area of the promoter of the gene cg1999 (448 bp) with an inserted GntR BS 10 bp downstream of the position of maximal CgpS binding (Pfeifer et al., 2016) and the first 30 bp of the coding sequence fused to the reporter gene *venus* via a linker containing a stop codon and an artificial RBS. | (Wiechert et al., 2020) |
| pJC1-$P_{cg2014}$::GntR_BS_pos0-*venus* | *Kan*$^R$; pJC1-*venus*-term derivative carrying the CgpS bound area of the promoter of the gene cg2014 (545 bp) with an inserted GntR BS directly upstream of the position of maximal CgpS binding (Pfeifer et al., 2016) and the first 30 bp of the coding sequence fused to the reporter gene *venus* via a linker containing a stop codon and an artificial RBS. | (Wiechert et al., 2020) |
| pJC1-$P_{cg2020}$::GntR_BS_pos0-*venus* | *Kan*$^R$; pJC1-*venus*-term derivative carrying the CgpS bound area of the promoter of the gene cg2020 (390 bp) with an inserted GntR BS directly upstream of the position of maximal CgpS binding (Pfeifer et al., 2016) and the first 30 bp of the coding sequence fused to the reporter gene *venus* via a linker containing a stop codon and an artificial RBS. | (Wiechert et al., 2020) |
| pJC1-$P_{cg2022}$::GntR_BS_pos0-*venus* | *Kan*$^R$; pJC1-*venus*-term derivative carrying the CgpS bound area of the promoter of the gene cg2022 (309 bp) with an inserted GntR BS directly upstream of the position of maximal CgpS binding (Pfeifer et al., 2016) and the first 30 bp of the coding sequence fused to the reporter gene *venus* via a linker containing a stop codon and an artificial RBS. | (Wiechert et al., 2020) |
| pJC1-$P_{lys}$::GntR_BS_pos-100-*venus* | *Kan*$^R$; pJC1-*venus*-term derivative carrying the CgpS bound area of the promoter of the *lys* gene (cg1974) (444 bp) with an inserted GntR BS 100 bp upstream of the position of maximal CgpS binding (Pfeifer et al., 2016) and the first 30 bp of the coding sequence fused to the reporter gene *venus* via a linker containing a stop codon and an artificial RBS. | (Wiechert et al., 2020) |
| pJC1-$P_{lys}$::GntR_BS_pos-25-*venus* | *Kan*$^R$; pJC1-*venus*-term derivative carrying the CgpS bound area of the promoter of the *lys* gene (cg1974) (444 bp) with an inserted GntR BS 25 bp upstream of the position of maximal CgpS binding (Pfeifer et al., 2016) and the first 30 bp of the coding sequence | (Wiechert et al., 2020) |

| | | |
|---|---|---|
| | fused to the reporter gene *venus* via a linker containing a stop codon and an artificial RBS. | |
| pJC1-P$_{lys}$::GntR_BS_pos-20-*venus* | *Kan*$^{R}$; pJC1-*venus*-term derivative carrying the CgpS bound area of the promoter of the *lys* gene (cg1974) (444 bp) with an inserted GntR BS 20 bp upstream of the position of maximal CgpS binding (Pfeifer et al., 2016) and the first 30 bp of the coding sequence fused to the reporter gene *venus* via a linker containing a stop codon and an artificial RBS. | (Wiechert et al., 2020) |
| pJC1-P$_{lys}$::GntR_BS_pos-15-*venus* | *Kan*$^{R}$; pJC1-*venus*-term derivative carrying the CgpS bound area of the promoter of the *lys* gene (cg1974) (444 bp) with an inserted GntR BS 15 bp upstream of the position of maximal CgpS binding (Pfeifer et al., 2016) and the first 30 bp of the coding sequence fused to the reporter gene *venus* via a linker containing a stop codon and an artificial RBS. | (Wiechert et al., 2020) |
| pJC1-P$_{lys}$::GntR_BS_pos-10-*venus* | *Kan*$^{R}$; pJC1-*venus*-term derivative carrying the CgpS bound area of the promoter of the *lys* gene (cg1974) (444 bp) with an inserted GntR BS 10 bp upstream of the position of maximal CgpS binding (Pfeifer et al., 2016) and the first 30 bp of the coding sequence fused to the reporter gene *venus* via a linker containing a stop codon and an artificial RBS. | (Wiechert et al., 2020) |
| pJC1-P$_{lys}$::GntR_BS_pos-5-*venus* | *Kan*$^{R}$; pJC1-*venus*-term derivative carrying the CgpS bound area of the promoter of the *lys* gene (cg1974) (444 bp) with an inserted GntR BS 5 bp upstream of the position of maximal CgpS binding (Pfeifer et al., 2016) and the first 30 bp of the coding sequence fused to the reporter gene *venus* via a linker containing a stop codon and an artificial RBS. | (Wiechert et al., 2020) |
| pJC1-P$_{lys}$::GntR_BS_pos-4-*venus* | *Kan*$^{R}$; pJC1-*venus*-term derivative carrying the CgpS bound area of the promoter of the *lys* gene (cg1974) (444 bp) with an inserted GntR BS 4 bp upstream of the position of maximal CgpS binding (Pfeifer et al., 2016) and the first 30 bp of the coding sequence fused to the reporter gene *venus* via a linker containing a stop codon and an artificial RBS. | (Wiechert et al., 2020) |
| pJC1-P$_{lys}$::GntR_BS_pos-3-*venus* | *Kan*$^{R}$; pJC1-*venus*-term derivative carrying the CgpS bound area of the promoter of the *lys* gene (cg1974) (444 bp) with an inserted GntR BS 3 bp upstream of the position of maximal CgpS binding (Pfeifer et al., 2016) | (Wiechert et al., 2020) |

| | | |
|---|---|---|
| | and the first 30 bp of the coding sequence fused to the reporter gene *venus* via a linker containing a stop codon and an artificial RBS. | |
| pJC1-P$_{lys}$::GntR_BS_pos-2-*venus* | *Kan*$^{R}$; pJC1-*venus*-term derivative carrying the CgpS bound area of the promoter of the *lys* gene (cg1974) (444 bp) with an inserted GntR BS 2 bp upstream of the position of maximal CgpS binding (Pfeifer et al., 2016) and the first 30 bp of the coding sequence fused to the reporter gene *venus* via a linker containing a stop codon and an artificial RBS. | (Wiechert et al., 2020) |
| pJC1-P$_{lys}$::GntR_BS_pos-1-*venus* | *Kan*$^{R}$; pJC1-*venus*-term derivative carrying the CgpS bound area of the promoter of the *lys* gene (cg1974) (444 bp) with an inserted GntR BS 1 bp upstream of the position of maximal CgpS binding (Pfeifer et al., 2016) and the first 30 bp of the coding sequence fused to the reporter gene *venus* via a linker containing a stop codon and an artificial RBS. | (Wiechert et al., 2020) |
| pJC1-P$_{lys}$_CS_0-*venus* | *Kan*$^{R}$; pJC1-*venus*-term derivative carrying the CgpS bound area of the promoter of the *lys* gene (cg1974) (444 bp) with an inserted GntR BS directly upstream of the position of maximal CgpS binding (Pfeifer et al., 2016) and the first 30 bp of the coding sequence fused to the reporter gene *venus* via a linker containing a stop codon and an artificial RBS. | (Wiechert et al., 2020) |
| pJC1-P$_{lys}$::GntR_BS_pos+1-*venus* | *Kan*$^{R}$; pJC1-*venus*-term derivative carrying the CgpS bound area of the promoter of the *lys* gene (cg1974) (444 bp) with an inserted GntR BS 1 bp downstream of the position of maximal CgpS binding (Pfeifer et al., 2016) and the first 30 bp of the coding sequence fused to the reporter gene *venus* via a linker containing a stop codon and an artificial RBS. | (Wiechert et al., 2020) |
| pJC1-P$_{lys}$::GntR_BS_pos+2-*venus* | *Kan*$^{R}$; pJC1-*venus*-term derivative carrying the CgpS bound area of the promoter of the *lys* gene (cg1974) (444 bp) with an inserted GntR BS 2 bp downstream of the position of maximal CgpS binding (Pfeifer et al., 2016) and the first 30 bp of the coding sequence fused to the reporter gene *venus* via a linker containing a stop codon and an artificial RBS. | (Wiechert et al., 2020) |
| pJC1-P$_{lys}$::GntR_BS_pos+3-*venus* | *Kan*$^{R}$; pJC1-*venus*-term derivative carrying the CgpS bound area of the promoter of the *lys* gene (cg1974) (444 bp) with an inserted GntR BS 3 bp downstream of the position of | (Wiechert et al., 2020) |

| | | |
|---|---|---|
| | maximal CgpS binding (Pfeifer et al., 2016) and the first 30 bp of the coding sequence fused to the reporter gene *venus* via a linker containing a stop codon and an artificial RBS. | |
| pJC1-P$_{lys}$::GntR_BS_pos+4-*venus* | *Kan*$^{R}$; pJC1-*venus*-term derivative carrying the CgpS bound area of the promoter of the *lys* gene (cg1974) (444 bp) with an inserted GntR BS 4 bp downstream of the position of maximal CgpS binding (Pfeifer et al., 2016) and the first 30 bp of the coding sequence fused to the reporter gene *venus* via a linker containing a stop codon and an artificial RBS. | (Wiechert et al., 2020) |
| pJC1-P$_{lys}$::GntR_BS_pos+5-*venus* | *Kan*$^{R}$; pJC1-*venus*-term derivative carrying the CgpS bound area of the promoter of the *lys* gene (cg1974) (444 bp) with an inserted GntR BS 5 bp downstream of the position of maximal CgpS binding (Pfeifer et al., 2016) and the first 30 bp of the coding sequence fused to the reporter gene *venus* via a linker containing a stop codon and an artificial RBS. | (Wiechert et al., 2020) |
| pJC1-P$_{lys}$::GntR_BS_pos+10-*venus* | *Kan*$^{R}$; pJC1-*venus*-term derivative carrying the CgpS bound area of the promoter of the *lys* gene (cg1974) (444 bp) with an inserted GntR BS 10 bp downstream of the position of maximal CgpS binding (Pfeifer et al., 2016) and the first 30 bp of the coding sequence fused to the reporter gene *venus* via a linker containing a stop codon and an artificial RBS. | (Wiechert et al., 2020) |
| pJC1-P$_{lys}$::GntR_BS_pos+15-*venus* | *Kan*$^{R}$; pJC1-*venus*-term derivative carrying the CgpS bound area of the promoter of the *lys* gene (cg1974) (444 bp) with an inserted GntR BS 15 bp downstream of the position of maximal CgpS binding (Pfeifer et al., 2016) and the first 30 bp of the coding sequence fused to the reporter gene *venus* via a linker containing a stop codon and an artificial RBS. | (Wiechert et al., 2020) |
| pJC1-P$_{lys}$::GntR_BS_pos+20-*venus* | *Kan*$^{R}$; pJC1-*venus*-term derivative carrying the CgpS bound area of the promoter of the *lys* gene (cg1974) (444 bp) with an inserted GntR BS 20 bp downstream of the position of maximal CgpS binding (Pfeifer et al., 2016) and the first 30 bp of the coding sequence fused to the reporter gene *venus* via a linker containing a stop codon and an artificial RBS. | (Wiechert et al., 2020) |
| pJC1-P$_{lys}$::GntR_BS_pos+25-*venus* | *Kan*$^{R}$; pJC1-*venus*-term derivative carrying the CgpS bound area of the promoter of the *lys* gene (cg1974) (444 bp) with an inserted | (Wiechert et al., 2020) |

| | | |
|---|---|---|
| | GntR BS 25 bp downstream of the position of maximal CgpS binding (Pfeifer et al., 2016) and the first 30 bp of the coding sequence fused to the reporter gene *venus* via a linker containing a stop codon and an artificial RBS. | |
| pJC1-$P_{lys}$::GntR_BS_pos+50-*venus* | $Kan^R$; pJC1-*venus*-term derivative carrying the CgpS bound area of the promoter of the *lys* gene (cg1974) (444 bp) with an inserted GntR BS 50 bp downstream of the position of maximal CgpS binding (Pfeifer et al., 2016) and the first 30 bp of the coding sequence fused to the reporter gene *venus* via a linker containing a stop codon and an artificial RBS. | (Wiechert et al., 2020) |
| pJC1-$P_{priP}$_CS_0-*venus* (previously named pJC1-$P_{priP}$::GntR_BS_pos0-*venus*) | $Kan^R$; pJC1-*venus*-term derivative carrying the CgpS bound area of the promoter of $P_{priP}$ (611 bp) with an inserted GntR BS directly upstream of the position of maximal CgpS binding (Pfeifer et al., 2016) and the first 30 bp of the coding sequence fused to the reporter gene *venus* via a linker containing a stop codon and an artificial RBS. | (Wiechert et al., 2020) |
| pJC1-$P_{gntK}$-*venus* | $Kan^R$; pJC1-*venus*-term derivative carrying the $P_{gntK}$ promoter (307 bp) ($P_{cg2732}$) and the first 30 bp of the coding sequence fused to the reporter gene *venus* via a linker containing a stop codon and an artificial RBS. | (Wiechert et al., 2020) |
| pEC-$P_{tetR}$ | $Cm^R$, pGA1 $oriV_{Cg}$, $oriV_{Ec}$, *tetR*, $P_{tet}$; *C. glutamicum*/*E. coli* shuttle vector | (Huber et al., 2017) |
| pEKEx2 | $Kan^R$, pBL1 $oriV_{Cg}$, pUC18 $oriV_{Ec}$, *lacIq*, $P_{tac}$; *C. glutamicum*/*E. coli* shuttle vector | (Eikmanns et al., 1994) |
| pK19-*mobsacB* | $Kan^R$, *oriT*, $oriV_{Ec}$, *sacB*, *lacZ*; plasmid for allelic exchange in *C. glutamicum* | (Schäfer et al., 1994) |
| pJC1-$P_{lys}$_CS_0-*venus*-T-$P_{gntK}$-*e2-crimson* | $Kan^R$; pJC1-*venus*-term derivative carrying the construct $P_{lys}$_CS_0-*venus* and the oppositely oriented $P_{gntK}$-*e2-crimson* construct. | (Wiechert et al., 2020) |
| pJC4-$P_{ilvB}$-*ilvBNC*-$P_{ilvE}$-*ilvE* (previously named pJC4-*ilvBNCE*) | $Kan^R$, $P_{ilvB}$-*ilvBNC*, $P_{ilvE}$-*ilvE* (genes encoding the L-valine biosynthesis enzymes acetohydroxyacid synthase, isomeroreductase and transaminase B under control of their native promoters) | (Radmacher et al., 2002) |

**Table S4: Plasmids constructed in this work.** Oligonucleotide pairs used for PCR are given as numbers (Table S5) with DNA templates indicated in brackets behind. The used backbones including the restriction enzymes used for linearization are listed behind (*). Used primers for sequencing are given as numbers (Table S6).

| Plasmid | Construction | Relevant characteristics | Primer used for sequencing |
|---|---|---|---|
| pJC1-$P_{priP}$::GntR_BS_pos-100-*venus* | Gibson assembly: 200/280 (pJC1-$P_{priP}$- | $Kan^R$; pJC1-$P_{priP}$-*venus* (Wiechert et al., 2020) | R12, R13 |

| | | | |
|---|---|---|---|
| | *venus*) and 279/116 (pJC1-$P_{priP}$-*venus*) into pJC1-*venus*-term *BamHI *BcuI | derivative with an inserted GntR BS 100 bp upstream of the position of maximal CgpS binding (Pfeifer et al., 2016). | |
| pJC1-$P_{priP}$::GntR_BS_pos-50-*venus* | Gibson assembly: 200/278 (pJC1-$P_{priP}$-*venus*) and 277/116 (pJC1-$P_{priP}$-*venus*) into pJC1-*venus*-term *BamHI *BcuI | *Kan*$^R$; pJC1-$P_{priP}$-*venus* (Wiechert et al., 2020) derivative with an inserted GntR BS 50 bp upstream of the position of maximal CgpS binding (Pfeifer et al., 2016). | R12, R13 |
| pJC1-$P_{priP}$::GntR_BS_pos-10-*venus* | Gibson assembly: 200/276 (pJC1-$P_{priP}$-*venus*) and 275/116 (pJC1-$P_{priP}$-*venus*) into pJC1-*venus*-term *BamHI *BcuI | *Kan*$^R$; pJC1-$P_{priP}$-*venus* (Wiechert et al., 2020) derivative with an inserted GntR BS 10 bp upstream of the position of maximal CgpS binding (Pfeifer et al., 2016). | R12, R13 |
| pJC1-$P_{priP}$::GntR_BS_pos-5-*venus* | Gibson assembly: 200/288 (pJC1-$P_{priP}$-*venus*) and 287/116 (pJC1-$P_{priP}$-*venus*) into pJC1-*venus*-term *BamHI *BcuI | *Kan*$^R$; pJC1-$P_{priP}$-*venus* (Wiechert et al., 2020) derivative with an inserted GntR BS 5 bp upstream of the position of maximal CgpS binding (Pfeifer et al., 2016). | R12, R13 |
| pJC1-$P_{priP}$::GntR_BS_pos+5-*venus* | Gibson assembly: 200/290 (pJC1-$P_{priP}$-*venus*) and 289/116 (pJC1-$P_{priP}$-*venus*) into pJC1-*venus*-term *BamHI *BcuI | *Kan*$^R$; pJC1-$P_{priP}$-*venus* (Wiechert et al., 2020) derivative with an inserted GntR BS 5 bp downstream of the position of maximal CgpS binding (Pfeifer et al., 2016). | R12, R13 |
| pJC1-$P_{priP}$::GntR_BS_pos+10-*venus* | Gibson assembly: 200/282 (pJC1-$P_{priP}$-*venus*) and 281/116 (pJC1-$P_{priP}$-*venus*) into pJC1-*venus*-term *BamHI *BcuI | *Kan*$^R$; pJC1-$P_{priP}$-*venus* (Wiechert et al., 2020) derivative with an inserted GntR BS 10 bp downstream of the position of maximal CgpS binding (Pfeifer et al., 2016). | R12, R13 |
| pJC1-$P_{priP}$::GntR_BS_pos+50-*venus* | Gibson assembly: 200/284 (pJC1-$P_{priP}$-*venus*) and 283/116 (pJC1-$P_{priP}$-*venus*) into pJC1-*venus*-term *BamHI *BcuI | *Kan*$^R$; pJC1-$P_{priP}$-*venus* (Wiechert et al., 2020) derivative with an inserted GntR BS 50 bp downstream of the position of maximal | R12, R13 |

| | | | |
|---|---|---|---|
| | | CgpS binding (Pfeifer et al., 2016). | |
| pJC1-*tetR*-$P_{tet}$-*venus* | 547/548 (pEC-$P_{tetR}$) and 115/116 (pJC1-*venus*-term) into pJC1-*venus*-term *BamHI *BcuI | *Kan*$^R$; pJC1-*venus*-term derivative carrying the *tetR* gene and the corresponding $P_{tet}$ promoter fused to the reporter gene *venus* via a linker containing a stop codon and an artificial RBS. | R12, R13, 492 |
| pJC1-*lacI*-$P_{tac}$-*venus* | Gibson assembly: 545/546 (pEKEx2) and 115/116 (pJC1-*venus*-term) into pJC1-*venus*-term *BamHI *BcuI | *Kan*$^R$; pJC1-*venus*-term derivative carrying the *lacI* gene and the corresponding $P_{tac}$ promoter fused to the reporter gene *venus* via a linker containing a stop codon and an artificial RBS. | R12, R13, 293, 399, 492, 546 |
| pJC1-$P_{lys}$_CS_0-*ilvBNC*-RBS-*ilvE* | Gibson assembly: 114/117 (pJC1-$P_{lys}$_CS_0-*venus*), 349/350 (pJC4-*ilvBNCE*) and 351/352 (pJC4-*ilvBNCE*) into pJC1-*venus*-term *BamHI *BcuI | *Kan*$^R$, pJC1-*venus*-term derivative carrying the operon *ilvBNC and* the gene *ilvE* (L-valine biosynthesis genes) which were combined in a synthetic operon controlled by the counter-silencer promoter P_CS_0. | R12, R182, R183, R215, 487, 488, 489, 490 |
| pK19-*mobsacB*-Δ*gntK* | Gibson assembly: 207/208 (*C. glutamicum* genome) and 209/210 (*C. glutamicum* genome) into pK19-*mobsacB* *BamHI *EcoRI | *Kan*$^R$, pK19-*mobsacB* derivative for the chromosomal deletion of the *gntK* gene (cg2732) (530 bp upstream and 524 bp downstream flanking regions). | M19, M20 |
| pK19-*mobsacB*-Δ$P_{aceE}$-*aceE* | Gibson assembly: 62/112 (*C. glutamicum* genome) and 113/65 (*C. glutamicum* genome) into pK19-*mobsacB* *BamHI *EcoRI | *Kan*$^R$, pK19-*mobsacB* derivative for the chromosomal deletion of the *aceE* gene (cg2466) and its 300 bp upstream promoter region (501 bp upstream and 500 bp downstream flanking regions). | M19, M20 |
| pK19-*mobsacB*-$P_{gntK}$-*aceE* | Gibson assembly: 62/63 (*C. glutamicum* genome), 97/92 (*C.* | *Kan*$^R$, pK19-*mobsacB* derivative for the chromosomal integration of the *aceE* | M19, M20, 93, 94, 95, 101, 102 |

| | | |
|---|---|---|
| | *glutamicum* genome), 70/71 (*C. glutamicum* genome) and 64/65 (*C. glutamicum* genome) into pK19-*mobsacB* *BamHI *EcoRI | gene (cg2466) und control of the $P_{gntK}$ promoter (333 bp, $P_{cg2732}$) (501 bp upstream and 500 bp downstream flanking regions). |

**Table S5: Oligonucleotides used for plasmid constructions.**

| Oligonucleotide number | Sequence (5´→3´) |
|---|---|
| 279 | CGCTCGATATGATAGTACCAATTCACGTGCAGCAGCACTCCC |
| 280 | GAATTGGTACTATCATATCGAGCGTTACGAACCATAACTG |
| 277 | GTGCACGTGTATGATAGTACCAATCAACTGTGCGCTAAATGCGTC |
| 278 | CACAGTTGATTGGTACTATCATACACGTGCACACATATGCGCG |
| 275 | GTTTTATGATAGTACCAATCTTTATTACTAAGCTTGTTTAAATTGAAAC |
| 276 | GTAATAAAGATTGGTACTATCATAAAACTCAACGGTTTATTAAGACGC |
| 287 | CTTTATATGATAGTACCAATTTACTAAGCTTGTTTAAATTGAAAC |
| 288 | GTAAATTGGTACTATCATATAAAGAAACTCAACGGTTTATTAAG |
| 289 | CTAAGCTTATGATAGTACCAATTGTTTAAATTGAAACTTCGTTATATTC |
| 290 | CAATTGGTACTATCATAAGCTTAGTAATAAAGAAACTCAACGG |
| 281 | GCTTGTTTTATGATAGTACCAATAAATTGAAACTTCGTTATATTCTG |
| 282 | GTTTCAATTTATTGGTACTATCATAAAACAAGCTTAGTAATAAAGAAAC |
| 283 | GAAAGTAAGTTATGATAGTACCAATAATTAAGTACTTCGGCTCCACG |
| 284 | CTTAATTATTGGTACTATCATAACTTACTTTCTTTAATCAGAATATAAC |
| 285 | CTTTATTACTATATGATAGTACCAATAGCTTGTTTAAATTGAAACTTCG |
| 286 | CAAGCTATTGGTACTATCATATAGTAATAAAGAAACTCAACGG |
| 547 | AGCGACGCCGCAGGGGGATCCTTAAGACCCACTTTCACATTTAAGTTGTTTTTC |
| 548 | ATGATATCTCCTTCTTAAAGTTCAGTGTATCAACAAGCTGGGGATCTTAAGC |
| 115 | TGAACTTTAAGAAGGAGATATCATATGGTGAGCAAGGGCGAGGAG |
| 116 | AAAACGACGGCCAGTACTAGTTACTTGTACAGCTCGTCCATGCC |
| 545 | AGCGACGCCGCAGGGGGATCCTCAAGCCTTCGTCACTGGTCCC |
| 546 | ATGATATCTCCTTCTTAAAGTTCAGGATCCTCTAGAGTCGACCTGC |
| 114 | TGATATCTCCTTCTTAAAGTTCAATTTTTCGGCATTGCGCCTTTAATCGC |
| 117 | AGCGACGCCGCAGGGGGATCCGCTCAAGGAAGAGTTCTTCATTGGTC |
| 349 | TGAACTTTAAGAAGGAGATATCATGTGAATGTGGCAGCTTCTCAAC |
| 350 | ATGTATATCTCCTTCTTAAAGTTAAACAAAATTATTTCTAGTTTAAGCGGTTTCTGCGCG AGC |
| 351 | GTTTAACTTTAAGAAGGAGATATACATGTGTATCTGTCAGGTAGCAGG |
| 352 | AAAACGACGGCCAGTACTAGTTAGCCAACCAGTGGGTAAAGC |
| 207 | CAGGTCGACTCTAGAGGATCATGGTGGCGTCATGCTCGGC |
| 208 | GTCTGTAACCGAGCATCTCTCCTAGACAATATGTAAGCCTTCGGCTG |
| 209 | GAGAGATGCTCGGTTACAGACGCAGAGTGGGTTCGCAACAAATAA |
| 210 | GTTGTAAAACGACGGCCAGTGAATTGCAGGTCGAGTTCTTCCCACAG |
| 62 | CAGGTCGACTCTAGAGGATCTCGATGGACTCGCTGATCAGC |
| 112 | GTCTGTAACCGAGCATCTCTCAAAGAATTATCGGGTAGTTTCCCGC |
| 113 | GAGAGATGCTCGGTTACAGACATCACCTCAAGGGACAGATAAATCC |
| 65 | GTTGTAAAACGACGGCCAGTGAATTCCGTGAGCAATTCAAGCAGGAAC |
| 63 | GGACGAGCTGTACAAGTAAACTAGTAAAGAATTATCGGGTAGTTTCCCGC |

| | |
|---|---|
| 97 | CTAGTTTACTTGTACAGCTCGTCCGAGGATCGTCTCCGCGAAGAG |
| 92 | CATTTCCACACCTCCTGTTGGGTCGACAATATGTAAGCCTTCGGCTGC |
| 70 | GACCCAACAGGAGGTGTGGAAATGGCCGATCAAGCAAAACTTGGTG |
| 71 | GGATTTATCTGTCCCTTGAGGTGATTTATTCCTCAGGAGCGTTTGGATC |
| 64 | GATCCAAACGCTCCTGAGGAATAAATCACCTCAAGGGACAGATAAATCC |

**Table S6: Oligonucleotides used for plasmid sequencing.**

| Oligonucleotide number | Sequence (5´→3´) |
|---|---|
| M19 | CGCCAGGGTTTTCCCAGTCAC |
| M20 | AGCGGATAACAATTTCACACAGGA |
| R12 | CAGGGACAAGCCACCCGCACA |
| R13 | GGAAGCTAGAGTAAGTAGTTCGC |
| R182 | CGATTCCTATGGACCCTGCCACC |
| R183 | GGTGGCAGGCTCCATAGGAATCG |
| R215 | CTGCGTTCTGATTTAATCTGTATCAGG |
| 93 | CTCTGGCAGGTAGCCACCG |
| 94 | CTGCCAGAGCGTCGTGAGAAC |
| 95 | CACACCACGGGGACTGTGG |
| 101 | CTATGGAACCTGAATTCCCAGGC |
| 102 | CTTCAGGTGCCTCACGGTAGG |
| 293 | CGCCGCTTCCACTTTTTCCCG |
| 399 | CACCAAACGTTTCGGCGAGAAGC |
| 487 | GGTCAACGATGAGCTTGAGCTC |
| 488 | CTGCTGGAAACCACCAAGGC |
| 489 | CACTCGGATTGCGCCCATTC |
| 490 | GCCCACATTTGGTGCTGGCC |
| 492 | CTCGAACTTCACCTCGGCGC |
| 546 | ATGATATCTCCTTCTTAAAGTTCAGGATCCTCTAGAGTCGACCTGC |

**Table S7: Oligonucleotides used for sequencing of chromosomal modifications.**

| Strain | Oligonucleotide number | Sequence (5´→3´) |
|---|---|---|
| Δ*gntK* | 313 | GCCCACTGCTCAGCGATTTC |
| | 314 | CGGGGTCGAGTTCTTTGATCC |
| $\Delta P_{aceE}$-*aceE* | 104 | CCAGGGCTCCTTCTTTACCAATG |
| | 105 | CGTTCTTCCCCGGCACTGTG |
| $P_{gntK}$-*aceE* | 93 | CTCTGGCAGGTAGCCACCG |
| | 94 | CTGCCAGAGCGTCGTGAGAAC |
| | 95 | CACACCACGGGGACTGTGG |
| | 101 | CTATGGAACCTGAATTCCCAGGC |
| | 104 | CCAGGGCTCCTTCTTTACCAATG |
| | 105 | CGTTCTTCCCCGGCACTGTG |

**Table S8: Oligonucleotides used for quantitative Real-time PCR (qRT-PCR).**

| Target gene | Oligo-nucleotide number | Sequence (5´→3´) |
|---|---|---|
| ***venus*** | 554 | GCGCACCATCTTCTTCAAGG |
| | 555 | CGGCGGTGATATAGACGTTGTG |
| ***ddh*** | 558 | AGCAGGTATGGAGCAACTTCG |
| | 559 | TGATTACCACCGGCGACAC |

## References


Baumgart, M., Unthan, S., Rückert, C., Sivalingam, J., Grünberger, A., Kalinowski, J., Bott, M., Noack, S. and Frunzke, J. (2013). Construction of a prophage-free variant of *Corynebacterium glutamicum* ATCC 13032 for use as a platform strain for basic research and industrial biotechnology. *Appl. Environ. Microbiol. 79*, 6006-6015, doi: *10.1128/AEM.01634-13.*

Blombach, B., Schreiner, M. E., Holátko, J., Bartek, T., Oldiges, M. and Eikmanns, B. J. (2007). L-valine production with pyruvate dehydrogenase complex-deficient *Corynebacterium glutamicum*. *Appl. Environ. Microbiol. 73*, 2079-2084, doi: *10.1128/AEM.02826-06.*

Cremer, J., Eggeling, L. and Sahm, H. (1990). Cloning the *dapA dapB* cluster of the lysine-secreting bacterium *Corynebacterium glutamicum*. *Mol. Gen. Genet. 220*, 478-480, doi: *10.1007/bf00391757.*

Eikmanns, B. J., Thum-Schmitz, N., Eggeling, L., Ludtke, K. U. and Sahm, H. (1994). Nucleotide sequence, expression and transcriptional analysis of the *Corynebacterium glutamicum gltA* gene encoding citrate synthase. *Microbiology. 140 ( Pt 8)*, 1817-1828, doi: *10.1099/13500872-140-8-1817.*

Huber, I., Palmer, D. J., Ludwig, K. N., Brown, I. R., Warren, M. J. and Frunzke, J. (2017). Construction of recombinant Pdu metabolosome shells for small molecule production in *Corynebacterium glutamicum*. *ACS Synth. Biol. 6*, 2145-2156, doi: *10.1021/acssynbio.7b00167.*

Kinoshita, S., Udaka, S. and Shimono, M. (1957). Studies on the amino acid fermentation. Part 1. Production of L-glutamic acid by various microorganisms. *J. Gen. Appl. Microbiol. 3*, 193-205, doi: *10.2323/jgam.3.193.*

Pfeifer, E., Hünnefeld, M., Popa, O., Polen, T., Kohlheyer, D., Baumgart, M. and Frunzke, J. (2016). Silencing of cryptic prophages in *Corynebacterium glutamicum*. *Nucleic Acids Res. 44*, 10117-10131, doi: *10.1093/nar/gkw692.*

Radmacher, E., Vaitsikova, A., Burger, U., Krumbach, K., Sahm, H. and Eggeling, L. (2002). Linking central metabolism with increased pathway flux: L-valine accumulation by *Corynebacterium glutamicum*. *Appl. Environ. Microbiol. 68*, 2246-2250, doi: *10.1128/aem.68.5.2246-2250.2002.*

Schäfer, A., Tauch, A., Jager, W., Kalinowski, J., Thierbach, G. and Puhler, A. (1994). Small mobilizable multi-purpose cloning vectors derived from the *Escherichia coli* plasmids pK18 and pK19: selection of defined deletions in the chromosome of *Corynebacterium glutamicum*. *Gene. 145*, 69-73,

Schreiner, M. E., Fiur, D., Holátko, J., Pátek, M. and Eikmanns, B. J. (2005). E1 enzyme of the pyruvate dehydrogenase complex in *Corynebacterium glutamicum*: molecular analysis of the gene and phylogenetic aspects. *J. Bacteriol. 187*, 6005-6018, doi: *10.1128/JB.187.17.6005-6018.2005.*

Wiechert, J., Filipchyk, A., Hünnefeld, M., Gätgens, C., Brehm, J., Heermann, R. and Frunzke, J. (2020). Deciphering the rules underlying xenogeneic silencing and counter-silencing of Lsr2-like proteins using CgpS of *Corynebacterium glutamicum* as a model. *mbio. 11*, e02273-02219, doi: *10.1128/mBio.02273-19*

## 4.5. Supplemental material to "Impact of $CO_2/HCO_3^-$ availability on anaplerotic flux in pyruvate dehydrogenase complex-deficient *Corynebacterium glutamicum* strains"

**Supplemental Material to:**
The impact of $CO_2/HCO_3^-$ availability on anaplerotic flux in PDHC-deficient *Corynebacterium glutamicum* strains

Aileen Krüger[a], Johanna Wiechert[a], Cornelia Gätgens[a], Tino Polen[a], Regina Mahr[b#] and Julia Frunzke[a#]

[a] Institut für Bio- und Geowissenschaften, IBG-1: Biotechnology, Forschungszentrum Jülich, 52425 Jülich, Germany

[b] SenseUp GmbH, c/o Campus Forschungszentrum Jülich, 52425 Jülich, Germany

**Content:**

**Table S1: Peak areas for compounds determined via GC-ToF analysis for PDHC-deficient strains.**

| | Area | | | | | |
|---|---|---|---|---|---|---|
| | WT | Δ*aceE* E1* | Δ*aceE* Δ*pyc* E1* | Δ*aceE* Δ*pyc* E2* | Δ*aceE* $HCO_3^-$** | Δ*aceE* Δ*pyc* $HCO_3^-$** |
| Amino acids | | | | | | |
| Alanine | 2503 | 1303 | 845 | 8321 | 3277 | 5299 |
| Aspartate | 998 | 402 | <1 | 383 | 296 | 460 |
| Glutamine | 6603 | 2554 | 1393 | 4430 | 3060 | 4166 |
| Glutamate | 30122 | 9836 | 3249 | 21157 | 17374 | 21093 |
| N-acetyl-Glutamate | 305 | 178 | 116 | 140 | 144 | 216 |
| Glycine | 197 | 110 | - | 168 | 164 | 192 |
| Lysine | 217 | 124 | 112 | 216 | 174 | 257 |
| Proline | 9611 | 4918 | 432 | 8127 | 8609 | 4835 |
| Proline+$CO_2$ | 917 | 625 | 73 | 620 | 737 | 407 |
| Serine | 90 | 52 | <1 | - | 68 | 80 |
| Valine | 177 | 436 | 753 | 1125 | 410 | 285 |
| Glycolysis | | | | | | |
| Glucose | 3819 | 10761 | 7152 | 5901 | 3702 | 3270 |
| Glycerol + Phosphate | 1591 | 804 | 801 | 929 | 1248 | 1262 |
| Glycerol-3-phosphate | 1229 | 751 | 299 | 666 | 928 | 961 |
| 3-phospho-Glycerate | 49 | 78 | 35 | 51 | 117 | 111 |
| Pyruvate | 51 | 85 | - | 278 | 156 | 492 |
| TCA cycle | | | | | | |
| Malate | 218 | 259 | - | 90 | - | 214 |
| Succinate | 1689 | 2135 | 597 | 2848 | 2093 | 5719 |
| Further | | | | | | |
| Lactate | 2436 | 934 | 784 | 915 | 1686 | 401 |
| Trehalose | 31837 | 11813 | 29109 | 7409 | 32045 | 8603 |
| Urea | 233 | 193 | 168 | 144 | 247 | 69 |

Strains were cultivated in 50 ml CGXII containing 154 mM acetate and 222 mM glucose. Compounds were identified based on retention time using in-house database JuPoD.* = E1 corresponds to the first sample extraction where Δ*aceE* reached in the exponential phase, while Δ*aceE* Δ*pyc* was still in lag phase. E2 corresponds to the second sample extraction where Δ*aceE* Δ*pyc* reached the exponential phase. ** = Medium was supplemented with 100 mM $HCO_3^-$.

**Table S2: Analysis of differential gene expression (0.7- and 1.7-fold change) of *C. glutamicum* Δ*aceE* Δ*pyc* and Δ*aceE* growing on CGXII containing 154 mM acetate and 222 mM glucose.** mRNA ratio ≤ 0.70 = downregulation in Δ*aceE* Δ*pyc* (shaded in red), mRNA ratio ≥ 1.7 = upregulation in Δ*aceE* Δ*pyc* (shaded in green), p-values < 0.05.

| Gene | Annotation | mRNA ratio | p-value |
|---|---|---|---|
| cg0791 | *pyc*, pyruvate carboxylase | 0.01 | 0.01 |
| cg1377 | *ssuC*, aliphatic sulfonates transmembrane ABC transporterprotein | 0.04 | 0.02 |
| cg1376 | *ssuD*1, alkanesulfonate monoxygenase | 0.06 | 0.01 |
| cg1379 | *ssuB*, aliphatic sulfonates ATP-binding ABC transporterprotein | 0.08 | 0.00 |
| cg0120 | esterase/lipase/thioesterase family protein | 0.12 | 0.00 |
| cg0111 | hypothetical protein cg0111 | 0.17 | 0.00 |
| cg3219 | *ldhA*, NAD-dependent L-lactate dehydrogenase | 0.18 | 0.02 |
| cg1147 | *ssuI*, FMN-binding protein required for sulfonate and sulfonate ester utilization | 0.19 | 0.00 |
| cg1156 | *ssuD2*, monooxygenase for sulfonate utilization | 0.20 | 0.00 |
| cg2962 | uncharacterized enzyme involved in biosynthesis of extracellular polysaccharides | 0.23 | 0.00 |
| cg1905 | hypothetical protein cg1905 | 0.25 | 0.00 |
| cg2320 | predicted transcriptional regulator | 0.26 | 0.00 |
| cg3226 | putative L-lactate permease | 0.27 | 0.01 |
| cg1484 | putative secreted protein | 0.28 | 0.01 |
| cg3315 | bacterial regulatory protein, MarR family | 0.28 | 0.00 |
| cg0957 | fas-IB, fatty acid synthase | 0.29 | 0.02 |
| cg3118 | *cysI*, sulfite reductase (hemoprotein) | 0.31 | 0.02 |
| cg1907 | putative phosphopantothenoylcysteine synthetase/decarboxylase | 0.31 | 0.01 |
| cg0812 | *dtsR*1, acetyl/propionyl-CoA carboxylase beta chain | 0.31 | 0.01 |
| cg1906 | hypothetical protein cg1906 | 0.32 | 0.00 |
| cg1454 | putative aliphatic sulfonates uptake ABC transporter secreted solute-binding protein | 0.32 | 0.01 |
| cg2958 | *butA*, L-2,3-butanediol dehydrogenase/acetoin reductase | 0.33 | 0.02 |
| cg3179 | *fadD2*, acyl-CoA synthase | 0.35 | 0.00 |

| | | | |
|---|---|---|---|
| cg3117 | hypothetical protein cg3117 | 0.36 | 0.01 |
| cg0683 | permease | 0.36 | 0.00 |
| cg3316 | universal stress protein UspA or related nucleotide-binding protein | 0.37 | 0.00 |
| cg2685 | short chain dehydrogenase | 0.37 | 0.03 |
| cg1380 | *ssuA*, aliphatic sulfonate binding protein | 0.38 | 0.02 |
| cg0277 | *dccT*, dicarboxylate uptake system (succinate, fumarate or L-malate) | 0.40 | 0.04 |
| cg3119 | *cysJ*, probable sulfite reductase (flavoprotein) | 0.41 | 0.00 |
| cg0175 | secreted protein, signal peptide | 0.41 | 0.02 |
| cg3116 | *cysH*, phosphoadenosine-phosphosulfate reductase | 0.42 | 0.01 |
| cg1003 | 5-formyltetrahydrofolate cyclo-ligase | 0.42 | 0.03 |
| cg1268 | *glgA*, glycogen synthase | 0.42 | 0.02 |
| cg3227 | *lldD*, quinone-dependent L-lactate dehydrogenase LldD | 0.43 | 0.01 |
| cg1066 | *urtE*, ABC-type urea uptake system, ATP binding protein | 0.43 | 0.01 |
| cg0241 | hypothetical protein cg0241 | 0.44 | 0.00 |
| cg1399 | permease of the major facilitator superfamily | 0.44 | 0.01 |
| cg0973 | *pgi*, glucose-6-phosphate isomerase | 0.44 | 0.03 |
| cg0240 | membrane protein | 0.45 | 0.00 |
| cg2645 | *clpP1*, ATP-dependent Clp protease proteolytic subunit | 0.45 | 0.01 |
| cg2699 | hypothetical protein cg2699 | 0.45 | 0.03 |
| cg0284 | drug exporter of the RND superfamily | 0.45 | 0.04 |
| cg2891 | *pqo*, pyruvate chinon oxidoreductase | 0.47 | 0.02 |
| cg1744 | *pacL*, cation-transporting ATPase | 0.47 | 0.03 |
| cg2707 | hypothetical protein cg2707 | 0.47 | 0.01 |
| cg2953 | *xylC*, benzaldehyde dehydrogenase | 0.48 | 0.01 |
| cg2456 | Zn-ribbon protein, possibly nucleic acid-binding | 0.48 | 0.02 |
| cg2715 | hypothetical protein cg2715 | 0.48 | 0.01 |
| cg1740 | putative nucleoside-diphosphate-sugar epimerase | 0.48 | 0.00 |
| cg0697 | hypothetical protein cg0697 | 0.49 | 0.02 |
| cg2342 | dehydrogenase | 0.49 | 0.02 |
| cg0514 | hypothetical membrane protein | 0.49 | 0.00 |
| cg3112 | predicted permease | 0.49 | 0.03 |

| | | | |
|---|---|---|---|
| cg3092 | hypothetical protein cg3092 | 0.50 | 0.03 |
| cg0316 | secreted protein | 0.50 | 0.00 |
| cg3223 | NADPH-dependent FMN reductase | 0.50 | 0.01 |
| cg1741 | hypothetical protein cg1741 | 0.50 | 0.01 |
| cg0359 | hypothetical protein cg0359 | 0.51 | 0.03 |
| cg1345 | *narK*, putative nitrate/nitrite transporter | 0.51 | 0.04 |
| cg3218 | pyruvate kinase | 0.52 | 0.01 |
| cg0129 | *putA*, proline dehydrogenase/delta-1-pyrroline-5-carboxylate dehydrogenase | 0.52 | 0.00 |
| cg2910 | transcriptional regulator, LacI family | 0.52 | 0.00 |
| cg2800 | *pgm*, phosphoglucomutase | 0.52 | 0.02 |
| cg1080 | putative multicopper oxidase | 0.52 | 0.00 |
| cg3224 | *LldR*, Repressor of the cg3226-lldD lactate operon | 0.52 | 0.01 |
| cg1081 | ABC-type multidrug transport system, ATPase component | 0.52 | 0.00 |
| cg1742 | hypothetical protein cg1742 | 0.52 | 0.01 |
| cg1619 | putative DNA gyrase inhibitor | 0.53 | 0.01 |
| cg2890 | putative amino acid processing enzyme | 0.53 | 0.01 |
| cg3279 | putative dehydrogenase-fragment | 0.53 | 0.02 |
| cg1045 | hypothetical protein cg1045 | 0.53 | 0.04 |
| cg1246 | hypothetical protein cg1246 | 0.53 | 0.01 |
| cg0892 | hypothetical protein cg0892 | 0.53 | 0.04 |
| cg0387 | *adhE*, putative zinc-type alcohol dehydrogenase transmembrane | 0.53 | 0.03 |
| cg2500 | bacterial regulatory proteins, ArsR family | 0.53 | 0.03 |
| cg2118 | transcriptional regulator of sugar metabolism, DeoR family | 0.53 | 0.01 |
| cg2810 | Na+/H+-dicarboxylate symporter family | 0.54 | 0.02 |
| cg1647 | ABC-type multidrug transport system, permease component | 0.54 | 0.00 |
| cg1002 | putative secreted protein | 0.54 | 0.01 |
| cg1452 | hypothetical protein cg1452 | 0.55 | 0.00 |
| cg3402 | copper chaperone | 0.55 | 0.01 |
| cg3004 | *gabD2*, succinic semialdehyde dehydrogenase | 0.55 | 0.00 |
| cg2305 | *hisD*, histidinol dehydrogenase | 0.55 | 0.05 |
| cg3304 | *dnaB*, replicative DNA helicase | 0.55 | 0.00 |

| | | | |
|---|---|---|---|
| cg1068 | probable oxidoreductase | 0.55 | 0.01 |
| cg1374 | hypothetical protein cg1374 | 0.56 | 0.01 |
| cg3280 | putative secreted protein | 0.56 | 0.02 |
| cg1238 | hypothetical protein cg1238 | 0.56 | 0.02 |
| cg0039 | putative transcriptional regulator | 0.56 | 0.01 |
| cg1111 | *eno*, phosphopyruvate hydratase | 0.57 | 0.03 |
| cg1618 | hypothetical protein cg1618 | 0.57 | 0.01 |
| cg3340 | *dadA*, putative D-amino acid dehydrogenase (deaminating) | 0.57 | 0.02 |
| cg2318 | putative secreted vitamin B12-binding lipoprotein | 0.57 | 0.00 |
| cg0807 | hypothetical protein cg0807 | 0.57 | 0.03 |
| cg2598 | hypothetical protein cg2598 | 0.57 | 0.00 |
| cg3225 | putative serine/threonine-specific protein phosphatase | 0.57 | 0.03 |
| cg2340 | ABC-type amino acid transport system, secreted component | 0.57 | 0.00 |
| cg0513 | hypothetical membrane protein | 0.58 | 0.00 |
| cg0777 | siderophore ABC transporter, ATP-binding protein | 0.58 | 0.02 |
| cg1545 | permease of the major facilitator superfamily | 0.58 | 0.04 |
| cg0755 | *metY*, O-acetylhomoserine sulfhydrylase | 0.58 | 0.01 |
| cg2537 | *brnQ*, branched-chain amino acid uptake carrier | 0.58 | 0.03 |
| cg1525 | *polA*, DNA polymerase I | 0.58 | 0.01 |
| cg0685 | homolog of metal-dependent protease, putative molecular chaperone | 0.58 | 0.01 |
| cg2291 | *pyk*, pyruvate kinase | 0.58 | 0.01 |
| cg2770 | hypothetical protein cg2770 | 0.58 | 0.03 |
| cg3128 | ABC-type transport system, ATPase component | 0.59 | 0.01 |
| cg0780 | membrane protein ribonuclease BN-like family | 0.59 | 0.01 |
| cg0611 | secreted protein | 0.59 | 0.00 |
| cg0176 | permease | 0.59 | 0.02 |
| cg0358 | hydrolase or acyltransferase | 0.59 | 0.01 |
| cg0122 | putative glycerol 3-phosphate dehydrogenase | 0.59 | 0.05 |
| cg2304 | *hisC*, histidinol-phosphate aminotransferase | 0.59 | 0.01 |
| cg1537 | *ptsG*, glucose-specific enzyme II BC component of PTS | 0.59 | 0.02 |
| cg1791 | *gap*, glyceraldehyde-3-phosphate dehydrogenase | 0.59 | 0.02 |

| | | | |
|---|---|---|---|
| cg0976 | *pcrA*, ATP-dependent helicase PCRA | 0.59 | 0.01 |
| cg0260 | *moaC*, molybdenum cofactor biosynthesis protein C | 0.60 | 0.03 |
| cg0464 | *ctpA*, copper-transporting ATPase | 0.60 | 0.02 |
| cg0662 | FAD/FMN-containing dehydrogenase | 0.60 | 0.03 |
| cg2247 | hypothetical protein cg2247 | 0.60 | 0.02 |
| cg1017 | *metS*, methionyl-tRNA synthetase | 0.60 | 0.02 |
| cg1330 | similar to GTP pyrophosphokinase | 0.60 | 0.00 |
| cg2459 | *ptpA*, protein-tyrosine-phosphatase | 0.60 | 0.01 |
| cg0766 | *icd*, isocitrate dehydrogenase | 0.60 | 0.01 |
| cg2877 | *avtA*, aminotransferase, uses alanine, keto-isovalerate and ketobutyrate | 0.61 | 0.01 |
| cg2743 | fas-IA, fatty acid synthase | 0.61 | 0.04 |
| cg2457 | hypothetical protein cg2457 | 0.61 | 0.02 |
| cg1195 | sulfate permease or related transporter (MFS superfamily) | 0.61 | 0.01 |
| cg2556 | uncharacterized iron-regulated membrane protein | 0.61 | 0.00 |
| cg1027 | *dld*, D-lactate dehydrogenase | 0.61 | 0.02 |
| cg0404 | nitroreductase family | 0.61 | 0.00 |
| cg2835 | predicted acetyltransferase | 0.61 | 0.01 |
| cg3399 | permease of the major facilitator superfamily | 0.62 | 0.05 |
| cg2162 | *thyX*, alternative thymidylate synthase | 0.62 | 0.02 |
| cg0896 | hypothetical protein cg0896 | 0.62 | 0.02 |
| cg2104 | *galE*, UDP-glucose 4-epimerase | 0.62 | 0.02 |
| cg0131 | putative oxidoreductase | 0.62 | 0.00 |
| cg3057 | putative secreted protein | 0.62 | 0.00 |
| cg1790 | *pgk*, phosphoglycerate kinase | 0.62 | 0.02 |
| cg2558 | related to aldose 1-epimerase | 0.62 | 0.00 |
| cg2554 | *rbsK2*, probable ribokinase protein | 0.62 | 0.02 |
| cg2536 | *metC*, cystathionine beta-lyase | 0.62 | 0.00 |
| cg0239 | hypothetical protein cg0239 | 0.63 | 0.02 |
| cg2178 | *nusA*, transcription elongation factor NusA | 0.63 | 0.04 |
| cg1908 | hypothetical protein cg1908 | 0.63 | 0.05 |
| cg1603 | hypothetical protein cg1603 | 0.63 | 0.02 |

| | | | |
|---|---|---|---|
| cg1247 | putative secreted protein | 0.63 | 0.00 |
| cg3228 | hypothetical protein cg3228 | 0.63 | 0.04 |
| cg1106 | hypothetical protein cg1106 | 0.63 | 0.03 |
| cg3158 | *nagA*2, beta-N-acetylglucosaminidase precursor | 0.63 | 0.02 |
| cg1691 | *arc*, AAA+ ATPase ARC, pupylation machinery | 0.63 | 0.00 |
| cg0781 | membrane protein | 0.63 | 0.04 |
| cg0934 | hypothetical protein cg0934 | 0.63 | 0.02 |
| cg2867 | *gpx*, glutathione peroxidase | 0.64 | 0.02 |
| cg1683 | superfamily II DNA and RNA helicase | 0.64 | 0.01 |
| cg2605 | predicted acetyltransferase | 0.64 | 0.02 |
| cg1883 | putative secreted protein | 0.64 | 0.05 |
| cg3331 | *ogt*, methylated-DNA--protein-cysteine methyltransferase | 0.64 | 0.00 |
| cg1375 | putative thioredoxin | 0.64 | 0.01 |
| cg2529 | *treS*, trehalose synthase (maltose alpha-D-glucosyltransferase) | 0.64 | 0.00 |
| cg1400 | DNA polymerase III subunit epsilon | 0.64 | 0.00 |
| cg2778 | hypothetical protein cg2778 | 0.64 | 0.01 |
| cg2248 | hypothetical protein cg2248 | 0.64 | 0.01 |
| cg0684 | *papA*, prolyl aminopeptidase A | 0.64 | 0.02 |
| cg2577 | predicted multitransmembrane, metal-binding protein | 0.64 | 0.04 |
| cg2431 | putative transcriptional regulator | 0.64 | 0.01 |
| cg1831 | bacterial regulatory protein, ArsR family | 0.65 | 0.05 |
| cg3332 | putative quinone oxidoreductase | 0.65 | 0.01 |
| cg0712 | secreted protein | 0.65 | 0.00 |
| cg1599 | hypothetical protein cg1599 | 0.65 | 0.00 |
| cg0297 | hypothetical protein cg0297 | 0.65 | 0.03 |
| cg2455 | hypothetical protein cg2455 | 0.65 | 0.01 |
| cg2572 | hypothetical protein cg2572 | 0.65 | 0.01 |
| cg0512 | *hemB*, delta-aminolevulinic acid dehydratase | 0.65 | 0.00 |
| cg0171 | secreted protein | 0.65 | 0.00 |
| cg2521 | *fadD15*, long-chain fatty acid CoA ligase | 0.65 | 0.01 |
| cg0174 | putative transport protein | 0.65 | 0.04 |
| cg1680 | hypothetical protein cg1680 | 0.65 | 0.01 |

| | | | |
|---|---|---|---|
| cg0376 | *dnaX*, putative DNA polymerase III, delta subunit | 0.65 | 0.03 |
| cg2033 | putative secreted protein | 0.66 | 0.02 |
| cg0680 | hypothetical protein cg0680 | 0.66 | 0.04 |
| cg2924 | *cysS*, cysteinyl-tRNA synthetase | 0.66 | 0.01 |
| cg1206 | PEP phosphonomutase or related enzyme | 0.66 | 0.01 |
| cg3236 | *msrA*, peptide methionine sulfoxide reductase | 0.66 | 0.00 |
| cg0481 | *mshA*, glycosyltransferase | 0.66 | 0.01 |
| cg0686 | acetyltransferase, GNAT family | 0.66 | 0.02 |
| cg1035 | TatD related DNase | 0.66 | 0.03 |
| cg3067 | hypothetical protein cg3067 | 0.66 | 0.01 |
| cg0388 | Zn-dependent hydrolase | 0.66 | 0.04 |
| cg2193 | putative lysophospholipase | 0.66 | 0.01 |
| cg1018 | probable ATP-dependent DNA helicase protein | 0.66 | 0.03 |
| cg1423 | putative oxidoreductase (related to aryl-alcohol dehydrogenase) | 0.66 | 0.01 |
| cg1284 | *lipT*, type B carboxylesterase | 0.67 | 0.03 |
| cg2597 | *rne*, probable ribonuclease E (RNase E) protein | 0.67 | 0.05 |
| cg0796 | *prpD*1, 2-methycitrate dehydratase | 0.67 | 0.01 |
| cg2117 | *ptsI*, phosphoenolpyruvate:sugar phosphotransferase system enzymei | 0.67 | 0.01 |
| cg0081 | putative tautomerase | 0.67 | 0.01 |
| cg1630 | *odhI*, essential for glutamine utilization, regulates ODH activity | 0.67 | 0.03 |
| cg2795 | NADPH quinone reductase or related Zn-dependent oxidoreductase | 0.67 | 0.02 |
| cg3253 | *mcbR*, TetR-type transcriptional regulator of sulfur metabolism | 0.67 | 0.03 |
| cg1600 | predicted rRNA methylase | 0.68 | 0.01 |
| cg3069 | hypothetical protein cg3069 | 0.68 | 0.02 |
| cg3068 | *fda*, fructose-bisphosphate aldolase | 0.68 | 0.01 |
| cg0067 | *gabD*3, succinate-semialdehyde dehydrogenase (NADP+) | 0.68 | 0.00 |
| cg0450 | hypothetical protein cg0450 | 0.68 | 0.04 |
| cg2687 | *metB*, cystathionine gamma-synthase | 0.68 | 0.00 |
| cg2323 | *treY*, maltooligosyl trehalose synthase | 0.68 | 0.01 |
| cg3185 | hypothetical protein cg3185 | 0.68 | 0.01 |
| cg1384 | putative NUDIX hydrolase | 0.68 | 0.00 |

| | | | |
|---|---|---|---|
| cg3350 | *nagK*, fumarylpyruvate hydrolase | 0.68 | 0.04 |
| cg0232 | hypothetical secreted protein | 0.69 | 0.00 |
| cg2432 | MUTT/NUDIX family protein | 0.69 | 0.03 |
| cg3034 | *def*, peptide deformylase | 0.69 | 0.02 |
| cg2421 | *sucB*, dihydrolipoamide acetyltransferase | 0.69 | 0.00 |
| cg1401 | *ligA*, DNA ligase | 0.69 | 0.03 |
| cg3423 | *trxC*, thioredoxin | 0.69 | 0.01 |
| cg0128 | secreted protein, signal peptide | 0.69 | 0.03 |
| cg0496 | thiol-disulfide isomerase or thioredoxin | 0.69 | 0.05 |
| cg1048 | haloacid dehalogenase/epoxide hydrolase family | 0.69 | 0.03 |
| cg0015 | *gyrA*, DNA gyrase subunit A | 0.69 | 0.03 |
| cg0854 | *pmmA*, phosphomannomutase | 0.69 | 0.01 |
| cg1318 | DNA repair exonuclease | 0.69 | 0.03 |
| cg0873 | *aroA*, 3-phosphoshikimate 1-carboxyvinyltransferase | 0.69 | 0.01 |
| cg0154 | haloacid dehalogenase-like hydrolase | 0.70 | 0.04 |
| cg2444 | hypothetical protein cg2444 | 0.70 | 0.03 |
| cg0745 | NAD-dependent deacetylase | 0.70 | 0.01 |
| cg2716 | *hyi*, hydroxypyruvate isomerase | 0.70 | 0.02 |
| cg3154 | *udgA*2, UDP-glucose 6-dehydrogenase | 0.70 | 0.01 |
| cg0910 | inositol monophosphatase | 0.70 | 0.03 |
| cg0489 | hypothetical membrane protein | 0.70 | 0.00 |
| cg3168 | SAM-dependent methyltransferase | 0.70 | 0.01 |
| cg3015 | hypothetical protein cg3015 | 1.70 | 0.01 |
| cg1414 | uncharacterized component of ribose/xylose transport systems | 1.70 | 0.00 |
| cg1355 | *prfA*, peptide chain release factor 1 | 1.71 | 0.02 |
| cg2138 | *gluC*, glutamate permease | 1.71 | 0.03 |
| cg1366 | *atpA*, ATP synthase subunit A | 1.71 | 0.05 |
| cg3008 | *porA*, main cell wall channel protein | 1.72 | 0.03 |
| cg2374 | *murE*, UDP-N-acetylmuramoylalanyl-D-glutamate--2,6-diaminopimelate ligase | 1.72 | 0.03 |
| cg1367 | *atpG*, ATP synthase subunit C | 1.72 | 0.02 |
| cg2272 | mutM1, formamidopyrimidine-DNA glycosylase | 1.73 | 0.00 |

| | | | |
|---|---|---|---|
| cg1498 | RecG-like helicase | 1.73 | 0.01 |
| cg0719 | *crtYe*, C50 carotenoid epsilon cyclase | 1.74 | 0.01 |
| cg3266 | *tnp5c*(ISCg5c), transposase | 1.74 | 0.00 |
| cg1706 | *arsC1*, arsenate reductase | 1.74 | 0.02 |
| cg2263 | hypothetical protein cg2263 | 1.75 | 0.00 |
| cg1314 | *putP*, proline transport system | 1.75 | 0.00 |
| cg1349 | membrane protein containing CBS domain | 1.75 | 0.03 |
| cg1122 | putative secreted protein | 1.75 | 0.05 |
| cg1412 | ribose/xylose/arabinose/galactoside ABC-type transport system, permease component | 1.75 | 0.02 |
| cg1123 | *greA*, transcription elongation factor GreA | 1.76 | 0.03 |
| cg0577 | *rpoC*, DNA-directed RNA polymerase beta subunit | 1.78 | 0.03 |
| cg1617 | GTP-binding protein EngA | 1.78 | 0.01 |
| cg2990 | *speE,* spermidine synthase | 1.78 | 0.00 |
| cg2624 | *pcaR*, transcriptional regulator of 4-hydroxybenzoate, protocatechuate, p-cresol pathway | 1.78 | 0.02 |
| cg0690 | *groES*, chaperonin 10 Kd subunit | 1.78 | 0.01 |
| cg2807 | tnp11a(ISCg11a), transposase-fragment | 1.79 | 0.00 |
| cg1041 | *pdxK*, pyridoxal/pyridoxine/pyridoxamine kinase | 1.79 | 0.00 |
| cg2184 | ATPase component of peptide ABC-type transport system, contains duplicated ATPase domains | 1.79 | 0.00 |
| cg3027 | *mrpE*, hypothetical protein cg3027 | 1.80 | 0.02 |
| cg2600 | *tnp1d*(ISCg1d), transposase | 1.80 | 0.00 |
| cg0203 | *iolE*, 2-Keto-myo-inositol dehydratase | 1.80 | 0.00 |
| cg0621 | substrate-specific component SCO2325 of predicted cobalamin ECF transporter | 1.81 | 0.00 |
| cg1218 | *ndnR*, transcriptional repressor of NAD de novo biosynthesis genes | 1.81 | 0.00 |
| cg1586 | *argG*, argininosuccinate synthase | 1.82 | 0.01 |
| cg2269 | predicted permease | 1.82 | 0.00 |
| cg1413 | secreted sugar-binding protein | 1.82 | 0.01 |
| cg0717 | *crtEb*, hypothetical protein cg0717 | 1.82 | 0.00 |
| cg0057 | *pknB*, eukaryotic-type serine/threonine kinase | 1.83 | 0.00 |
| cg1602 | *recN*, DNA repair protein RecN | 1.86 | 0.00 |
| cg2467 | ABC transporter ATP-binding protein | 1.86 | 0.00 |

| | | | |
|---|---|---|---|
| cg2196 | putative secreted or membrane protein | 1.86 | 0.05 |
| cg3385 | *catA3*, catechol 1,2-dioxygenase | 1.86 | 0.00 |
| cg1149 | hypothetical protein cg1149 | 1.87 | 0.04 |
| cg1364 | *atpF*, ATP synthase subunit B | 1.88 | 0.02 |
| cg2559 | *aceB*, malate synthase | 1.88 | 0.02 |
| cg0693 | *groEL*, 60 KDA chaperonin (protein CPN60) (groel protein) C-terminal fragment | 1.88 | 0.04 |
| cg1363 | *atpE*, ATP synthase subunit C | 1.88 | 0.02 |
| cg0691 | *groEL*, 60 KDA chaperonin (protein CPN60) (HSP60)-N-terminal fragment | 1.89 | 0.02 |
| cg1040 | ATPase component of ABC transporters with duplicated ATPase domains | 1.90 | 0.00 |
| cg1902 | putative secreted protein | 1.91 | 0.02 |
| cg0692 | *tnp1c*(ISCg1c), transposase | 1.92 | 0.00 |
| cg1418 | secreted siderophore-binding lipoprotein | 1.92 | 0.00 |
| cg1213 | *tnp1a*(ISCg1a), transposase | 1.93 | 0.04 |
| cg2052 | putative secreted protein | 1.94 | 0.02 |
| cg2676 | ABC-type dipeptide/oligopeptide/nickel transport systems, permease component | 1.94 | 0.01 |
| cg1780 | *devB*, 6-phosphogluconolactonase | 1.94 | 0.01 |
| cg1362 | *atpB*, ATP synthase subunit A | 1.95 | 0.03 |
| cg2265 | *smc*, chromosome segregation ATPase | 1.96 | 0.00 |
| cg0204 | *iolG*, putative oxidoreductase myo-inositol 2-dehydrogena | 1.96 | 0.04 |
| cg3386 | *tcbF*, maleylacetate reductase | 1.96 | 0.01 |
| cg0223 | *iolT1*, myo-Inositol transporter | 1.97 | 0.04 |
| cg1488 | *leuD*, isopropylmalate isomerase small subunit | 1.97 | 0.00 |
| cg1354 | *rho*, transcription termination factor Rho | 1.98 | 0.01 |
| cg1792 | putative transcriptional regulator-WhiA homolog | 1.98 | 0.01 |
| cg2470 | secreted ABC transporter substrate-binding protein | 1.98 | 0.00 |
| cg3047 | *ackA*, acetate/propionate kinase | 1.99 | 0.01 |
| cg1417 | acetyltransferase | 2.00 | 0.00 |
| cg1348 | membrane protein containing CBS domain | 2.01 | 0.03 |
| cg1725 | *mutA*, methylmalonyl-CoA mutase, subunit | 2.01 | 0.01 |
| cg0062 | *ppp*, protein phosphatase | 2.02 | 0.02 |

| | | | |
|---|---|---|---|
| cg1779 | *opcA*, putative subunit of glucose-6-P dehydrogenase | 2.04 | 0.01 |
| cg0323 | conserved hypothetical secreted protein | 2.05 | 0.01 |
| cg3195 | flavin-containing monooxygenase (FMO) | 2.06 | 0.04 |
| cg1812 | *pyrF*, orotidine 5-phosphate decarboxylase | 2.07 | 0.02 |
| cg1344 | *narG*, nitrate reductase 2, alpha subunit | 2.07 | 0.01 |
| cg0417 | *capD*, probable dTDP-glucose 4,6-dehydratase transmembrane protein | 2.08 | 0.00 |
| cg1813 | *carB*, carbamoyl-phosphate synthase large subunit | 2.12 | 0.01 |
| cg3363 | *trpB*, tryptophan synthase subunit beta | 2.14 | 0.00 |
| cg0720 | *crtI2*, phytoene dehydrogenase (desaturase) | 2.15 | 0.01 |
| cg0321 | Na+/H+ antiporter subunit | 2.16 | 0.01 |
| cg0419 | glycosyltransferase | 2.16 | 0.01 |
| cg1365 | *atpH*, ATP synthase subunit D | 2.16 | 0.01 |
| cg0418 | putative aminotransferase | 2.17 | 0.01 |
| cg0325 | hypothetical protein cg0325 | 2.22 | 0.02 |
| cg1215 | *nadC*, quinolinate phosphoribosyltransferase | 2.23 | 0.01 |
| cg3016 | hypothetical protein cg3016 | 2.24 | 0.01 |
| cg3096 | *ald,* alcohol degyhdrogenase | 2.24 | 0.04 |
| cg2939 | ABC-type dipeptide/oligopeptide/nickel transport system, fused permease and ATPase components | 2.29 | 0.02 |
| cg3028 | *mrpF,* hypothetical protein cg3028 | 2.32 | 0.00 |
| cg3029 | *mrpG*, multisubunit Na+/H+ antiporter, g subunit | 2.34 | 0.01 |
| cg3025 | *mrpC*, hypothetical protein cg3025 | 2.34 | 0.01 |
| cg2675 | ATPase component of ABC-type transport system, contains duplicated ATPase domains \| ATPase component of ABC-type transport system, contains duplicated ATPase domains | 2.36 | 0.01 |
| cg1582 | *argB,* acetylglutamate kinase | 2.37 | 0.04 |
| cg2240 | *thiF,* molybdopterin biosynthesis protein MoeB | 2.38 | 0.04 |
| cg3391 | *oxiD*, myo-Inositol dehydrogenase | 2.40 | 0.00 |
| cg0324 | *mnhD*, NADH dehydrogenase subunit N | 2.41 | 0.01 |
| cg2610 | ABC-type dipeptide/oligopeptide/nickel transport system, secreted component | 2.46 | 0.00 |
| cg3017 | hypothetical protein cg3017 | 2.54 | 0.00 |
| cg0837 | hypothetical protein cg0837 | 2.66 | 0.03 |

| | | | |
|---|---|---|---|
| cg0322 | predicted conserved membrane protein | 2.69 | 0.00 |
| cg3026 | *mrpD*, NADH-ubiquinone oxidoreductase/multisubunit Na+/H+ antiporter, D subunit | 2.86 | 0.01 |
| cg3390 | *myo*-Inositol catabolism, sugar phosphate isomerase/epimerase | 2.89 | 0.01 |
| cg3360 | *trpG*, anthranilate synthase component II | 2.97 | 0.01 |
| cg0059 | *pknA*, serine/threonine protein kinase | 3.01 | 0.00 |
| cg0838 | helicase | 3.06 | 0.01 |
| cg3359 | *trpE*, anthranilate synthase component I | 3.08 | 0.00 |
| cg0165 | ABC-2 type transporter | 3.12 | 0.01 |
| cg0061 | *rodA*, putative FTSW/RODA/SPOVE family cell cycle protein | 3.13 | 0.00 |
| cg1724 | *meaB*, accessory protein of methylmalonylCoA mutase | 3.18 | 0.01 |
| cg0018 | hypothetical membrane protein | 3.19 | 0.00 |
| cg0163 | N-acetylglucosaminyltransferase | 3.21 | 0.00 |
| cg1583 | *argD*, acetylornithine aminotransferase | 3.26 | 0.01 |
| cg0060 | *pbpA*, D-alanyl-D-alanine carboxypeptidase | 3.31 | 0.00 |
| cg3362 | *trpCF*, bifunctional indole-3-glycerol phosphate synthase/phosphoribosylanthranilate isomerase | 3.31 | 0.01 |
| cg0162 | membrane spanning protein | 3.33 | 0.00 |
| cg1214 | *nadS*, cysteine desulfurase-like protein involved in Fe-S cluster assembly | 3.44 | 0.00 |
| cg2636 | catA1, catechol 1,2-dioxygenase | 3.50 | 0.01 |
| cg1584 | *argF*, ornithine carbamoyltransferase | 3.81 | 0.01 |
| cg3361 | *trpD*, anthranilate phosphoribosyltransferase | 3.83 | 0.01 |
| cg1585 | *argR*, arginine repressor | 3.96 | 0.00 |
| cg0844 | type II restriction enzyme, methylase subunit | 6.36 | 0.00 |
| cg2430 | hypothetical protein cg2430 | 13.96 | 0.00 |

**Table S3: Overview on plasmids constructed in this study.** In Table 2 in the main text provides a list of all plasmids used in this study.

| Plasmid | Backbone | Restriction-enzymes | Oligonucleotides for insert | Template | Method |
|---|---|---|---|---|---|
| pK19*mobsacB*-Δ*ptsG*-P3 | pK19*mobsacB* (1) | EcoRI, BamHI | A7-ptsG-leftflank-fw<br>A8-ptsG-leftflank-rv<br>A9-ptsG-rightflank-fw<br>A10-ptsG-rightflank-rv | Genomic DNA (*C. glutamicum*) | Gibson assembly |
| pK19*mobsacB*-Δ*pgi* | pK19*mobsacB* (1) | EcoRI, BamHI | A21-pgi-leftflank-fw<br>A22-pgi-leftflank-rv<br>A23-pgi-rightflank-fw<br>A24-pgi-rightflank-rv | Genomic DNA (*C. glutamicum*) | Gibson assembly |
| pJC1-pyc | pJC1-*venus*-term-BS (2) | BamHI, BcuI | A31-pyc-pJC1-fw<br>A32-pyc-pJC1-rv | Genomic DNA (*C. glutamicum*) | Gibson assembly |

59 **Table S4: Oligonucleotides used in this work.**

| Oligonucleotide | Sequence 5'→ 3' | Use |
|---|---|---|
| **Primer for sequencing and strain verification** | | |
| A1-seq-*pyc*-fw | CTGCGCCACGGTTTTGTGAAG | Sequencing *pyc* |
| A2-seq-*pyc*-rv | CAACCACATCTGCACTGCGATC | Sequencing *pyc* |
| A14-seq-*ptsG*-flanks-fw | GGCTCACTGACGTTGACAGTG | Sequencing *ptsG* |
| A15-seq-*ptsG*-flanks-rv | GATATCGCGGGCAACTTGGTC | Sequencing *ptsG* |
| A17-seq-*pgi*-fw | GTGATGGCACCTGCCGATTC | Sequencing *pgi* |
| A18-seq-*pgi*-rv | CGGAATCCACGAAATCGCCG | Sequencing *pgi* |
| 104-*aceE*int-seq-fw | CCAGGGCTCCTTCTTTACCAATG | Sequencing *aceE* |
| 105-*aceE*int-seq-rv | CGTTCTTCCCCGGCACTGTG | Sequencing *aceE* |
| *ppc*del_fw | GGAATAGACTCGCTCGGC | Sequencing *ppc* |
| *ppc*del_rv | GTGAACAGGCTCTCGATGC | Sequencing *ppc* |
| *ureD*_E188*_fw | CGGACTCCCGATAGGGAAGTTTTG | Sequencing *ureD* |
| *ureD*_E188*_rev | CAAAACTTCCCTATCGGGAGTCCG | Sequencing *ureD* |
| 596-*aceA*-Seq-rv | CGAGTTCCTTCTGGAACTTAGCG | Sequencing *aceA* |
| 599-*aceA*-Seq-rv2 | CTTCGGTGCGTGCGATTTCATC | Sequencing *aceA* |
| 597-*aceB*-Seq-fw | CTTCGAAGACTCCGTTGCAGC | Sequencing *aceB* |
| 598-*aceB*-Seq-rv | TTGTTGAGCTCACGGGTGAAG | Sequencing *aceB* |
| 600-*aceB*-Seq-rv2 | GAGCAAGCAGCTCGCGGTTG | Sequencing *aceB* |
| M19-M13-fw | CACTGACCCTTTTGGGACCGC | Sequencing of pK19*mobsacB* |
| M20-M13-rv | AGCGGATAACAATTTCACACAGGA | Sequencing of pK19*mobsacB* |
| R12-pJC1-MCS-fw | CAGGGACAAGCCACCCGCACA | Sequencing of inserts in pJC1 |
| R13-pJC1-MCS-rv | GGAAGCTAGAGTAAGTAGTTCGC | Sequencing of inserts in pJC1 |
| **Construction of plasmid pK19*mobsacB*-Δ*ptsG*-P3 used for deletion of *ptsG*** | | |
| A7-*ptsG*-leftflank-fw | CAGGTCGACTCTAGAGGATCGCTTTTGGCGGGCGC TTCGG | Left flank fw Δ*ptsG* |
| A8-*ptsG*-leftflank-rv | GTCTGTAACCGAGCATCTCTCGTCAAACCTTTCTA AACGTAGGGTCTG | Left flank rv Δ*ptsG* |
| A9-*ptsG*-rightflank-fw | GAGAGATGCTCGGTTACAGACCAGCTAAGCCGAAG CTGGCCG | Right flank fw Δ*ptsG* |
| A10-*ptsG*-rightflank-rv | GTAAAACGACGGCCAGTGAATTGTTACTCGTTCTT GCCGTTGACCTTG | Right flank rv Δ*ptsG* |

**Construction of plasmid pK19*mobsacB*-Δ*pgi* used for deletion of *pgi***

| | | |
|---|---|---|
| A21-*pgi*-leftflank-fw | CAGGTCGACTCTAGAGGATCCAGCACCGACAAACA CGATC | Left flank fw Δ*pgi* |
| A22-*pgi*-leftflank-rv | GTCTGTAACCGAGCATCTCTCGAAAACTCCTTTAT TGTCGTTAAATAAC | Left flank rv Δ*pgi* |
| A23-*pgi*-rightflank-fw | GAGAGATGCTCGGTTACAGACCCTGTTTCCACTGG CACTG | Right flank fw Δ*pgi* |
| A24-*pgi*-rightflank-rv | GTAAAACGACGGCCAGTGAATTGCTACCTATTTGC GCGGTACC | Right flank rv Δ*pgi* |

**Construction of plasmid pJC1-*pyc* used for overexpression of *pyc***

| | | |
|---|---|---|
| A31-*pyc*-pJC1-fw | AGCGACGCCGCAGGGGGATCCGGATTGCTTTGTGC ACTCCTGG | *pyc* fw, including promoter region |
| A32-*pyc*-pJC1-rv | AAAACGACGGCCAGTACTAGCAGAAAGGTTTAGGA AACGACGAC | *pyc* rv |

**Construction of plasmid pJC1-*pyc* used for overexpression of *aceA* and *aceB***

| | | |
|---|---|---|
| 588-*aceA*-fw | CTGAACTTTAAGAAGGAGATATCATATGTCAAACG TTGGAAAGCCACG | Insert 1 *aceA* fw |
| 589-*aceA*-linker-rv | CATATGTATATCTCCTTCTTAAAGTTAAACAAAAT TATTTCTAGTCTAGTTGTGGAACTGGCCTTCTTC | Insert 1 *aceA* rv, including linker |
| 590-*aceB*-linker-fw | GTTTAACTTTAAGAAGGAGATATACATATGACTGA ACAGGAACTGTTGTCTG | Insert 2 *aceB* fw, including linker |
| 591-*aceB*-rv | CTGTAAAACGACGGCCAGTACTAGTTAGTTTTTTG CTTTGAACTCGCGGC | Insert 2 *aceB* rv |

**Construction of plasmid pJC1-*pyc* used for overexpression of *aceB* and *aceA***

| | | |
|---|---|---|
| 584-*aceB*-fw | CTGAACTTTAAGAAGGAGATATCATATGACTGAAC AGGAACTGTTGTCTG | Insert 1 *aceB* fw |
| 585-*aceB*-linker-rv | ATGTATATCTCCTTCTTAAAGTTAAACAAAATTAT TTCTAGTTTAGTTTTTTGCTTTGAACTCGCGG | Insert 1 *aceB* rv, including linker |
| 586-*aceA*-linker-fw | GTTTAACTTTAAGAAGGAGATATACATATGTCAAA CGTTGGAAAGCCACG | Insert 2 *aceA* fw, including linker |
| 587-*aceA*-rv | CTGTAAAACGACGGCCAGTACTAGCTAGTTGTGGA ACTGGCCTTCTTC | Insert 2 *aceA* rv |

Underlined = complementary to backbone, red = linker sequence; fw = forward, rv = reverse

61

62

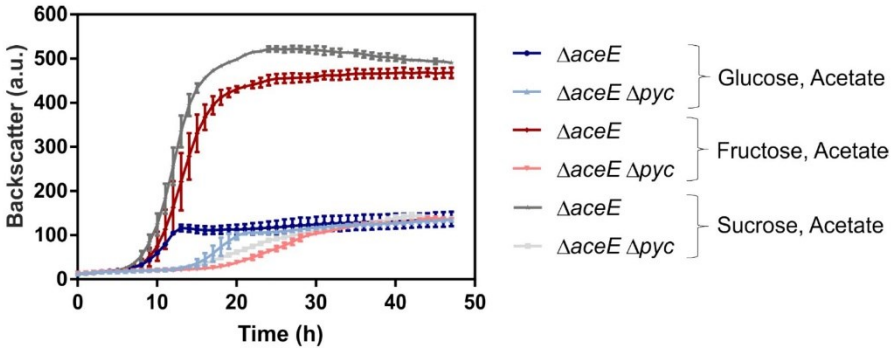


**Figure S1: Effect of different PTS-sugars on growth of *C. glutamicum* ΔaceE and ΔaceE Δpyc.** The strains Δ*aceE* and Δ*aceE* Δ*pyc* were inoculated to an $OD_{600}$ of 1 in CGXII containing 154 Mm acetate and 222 mM of varying PTS sugars: glucose (shades of blue), fructose (shades of red), or sucrose (shades of grey). Growth curves shown are based on the backscatter measurements in a microtiter cultivation system. Symbols represent the backscatter means and error bars their standard deviations of biological triplicates.

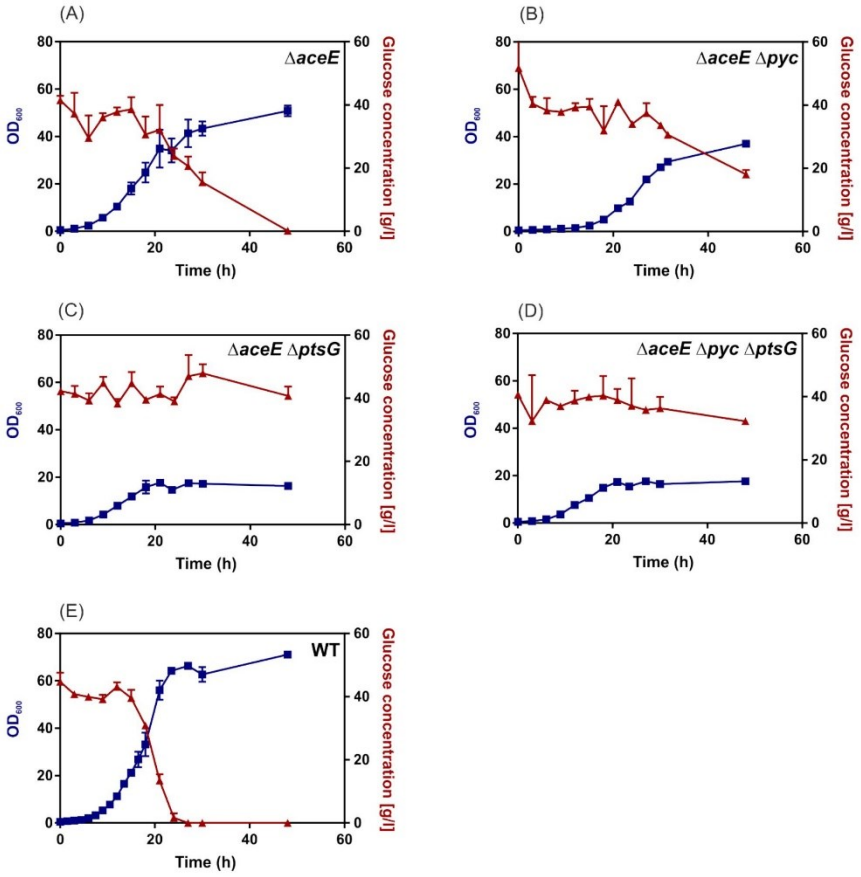


**Figure S2: Growth and glucose consumption of different *C. glutamicum* PDHC-deficient strains.** The PDHC-deficient strains Δ*aceE*, Δ*aceE* Δ*pyc*, Δ*aceE* Δ*ptsG,* Δ*aceE* Δ*pyc* Δ*ptsG* as well as the wild type (WT) as control were inoculated to an $OD_{600}$ of 1 each in 50 ml CGXII containing 154 mM acetate and 222 mM glucose. $OD_{600}$ measurements (blue graphs) and sampling for glucose measurements were performed every 3 h until 33 h and once additionally at 48 h. (A-E) Measurement of glucose concentration was performed with the D-Glucose UV-Test Kit (r-biopharm, Darmstadt, Germany) (red

80 graphs). Symbols represent the $OD_{600}$ means and error bars their standard deviations of
81 biological triplicates.

82

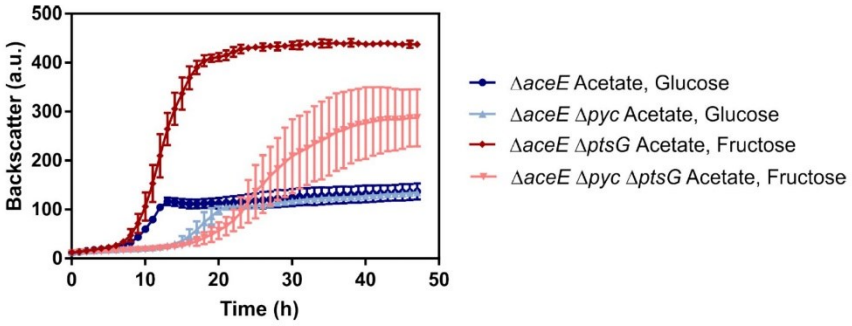


**Figure S3: Effect of PTS-sugar fructose on growth of *ptsG*-deficient *C. glutamicum* Δ*aceE* and Δ*aceE* Δ*pyc*.** Growth curves shown are based on the backscatter measurements in a microtiter cultivation system, inoculated at an $OD_{600}$ of 1. Symbols represent the backscatter means and error bars their standard deviations of biological triplicates.Deletion of the *ptsG* gene was accomplished using the pK19*mobsacB*-system for both strains Δ*aceE* and Δ*aceE* Δ*pyc*. These Δ*ptsG* strains (shades of red) were cultivated in a microtiter cultivation system in CGXII containing 154 mM acetate and 222 mM fructose. Strains Δ*aceE* and Δ*aceE* Δ*pyc* cultivated in 154 mM acetate and 222 mM glucose served as control, and are shown in shades of blue.

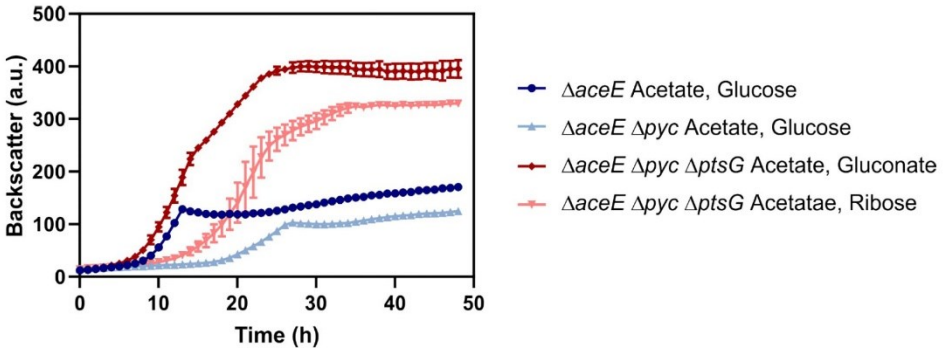


**Figure S4: Effect of gluconate and ribose on growth of *ptsG*-deficient *C. glutamicum* Δ*aceE* Δ*pyc*.** Growth curves shown are based on the backscatter measurements in a microtiter cultivation system, inoculated at an $OD_{600}$ of 1. Symbols represent the backscatter means and error bars their standard deviations of biological triplicates.Deletion of the *ptsG* gene was accomplished using the pK19*mobsacB*-system for both strains Δ*aceE* and Δ*aceE* Δ*pyc*. These Δ*ptsG* strains (shades of red) were cultivated in a microtiter cultivation system in CGXII containing 154 mM acetate and 222 mM gluconate (dark red) or 154 mM acetate and 222 mM ribose (light red). Strains Δ*aceE* and Δ*aceE* Δ*pyc* cultivated in 154 mM acetate and 222 mM glucose served as control, and are shown in shades of blue.

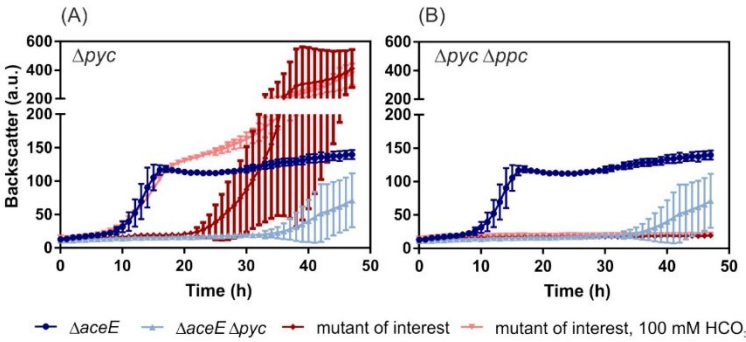


**Figure S5: Addition of $HCO_3^-$ restored growth defects of *pyc*-deficient *C. glutamicum* strains.** The strains (A) Δ*pyc* and (B) Δ*pyc* Δ*ppc* were inoculated to an $OD_{600}$ of 1 in CGXII media containing 154 mM acetate and 222 mM glucose (shown in dark red) or additionally 100 mM $KHCO_3^-$ (shown in light red). Further, Δ*aceE* and Δ*aceE* Δ*pyc* in CGXII media containing 154 mM acetate and 222 mM glucose were cultivated as controls (shown in shades of blue). Growth curves shown are based on the backscatter measurements in a microtiter cultivation system. Symbols represent the backscatter means and error bars their standard deviations of biological triplicates.

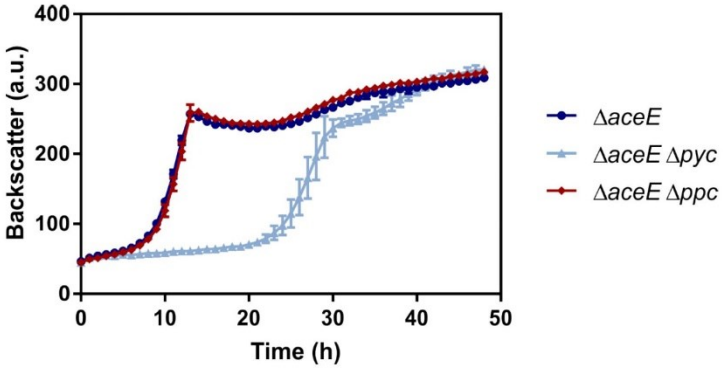


**Figure S6: Growth of the PEPCx-deficient strain Δ*aceE* Δ*ppc*.** The strain Δ*aceE* Δ*ppc* was inoculated to an $OD_{600}$ of 1 in CGXII media containing 154 mM acetate and 222 mM glucose (red). Further, Δ*aceE* and Δ*aceE* Δ*pyc* in CGXII media containing 154 mM acetate and 222 mM glucose were cultivated as controls (shown in shades of blue). Growth curves shown are based on the backscatter measurements in a microtiter cultivation system. Symbols represent the backscatter means and error bars the standard deviations of biological triplicates.

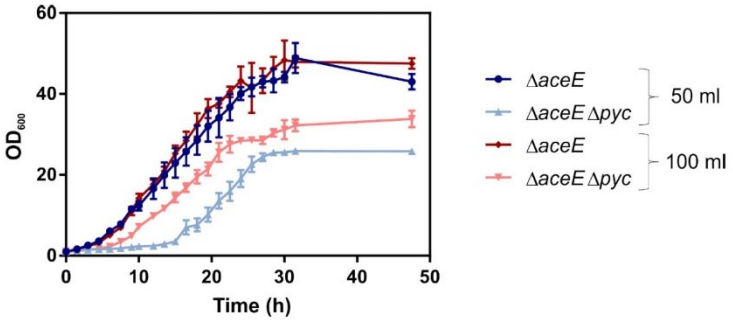


125

126 **Figure S7: Effect of culture volume on the growth of *C. glutamicum* ΔaceE and**
127 **ΔaceE Δpyc.** Main cultures of Δ*aceE* and Δ*aceE* Δ*pyc* were inoculated to an $OD_{600}$ of 1
128 in CGXII containing 154 mM acetate and 222 mM glucose once in 50 ml in a 500 ml
129 shaking flask (shades of blue) and once in 100 ml in a 1 l shaking flask (shades of red).
130 Cultivation was performed in an orbital shaker. Growth curves shown are based on $OD_{600}$
131 measurements which were performed every 90 minutes until 33 h, and an additional
132 measurement after 48 h. Symbols represent the $OD_{600}$ means and error bars their
133 standard deviations of biological triplicates.

134

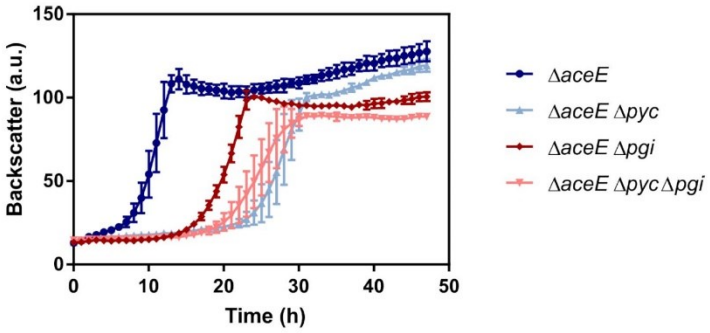


**Figure S8: Deletion of *pgi* in PDHC-deficient strains to reroute flux through the pentose phosphate pathway.** Deletion of the *pgi* gene was accomplished using the pK19*mobsacB* system for both strains Δ*aceE* and Δ*aceE* Δ*pyc*. Generated strains were inoculated in a microtiter cultivation system to an $OD_{600}$ of 1 in CGXII containing 154 mM acetate and 222 mM glucose. Additionally, the parental strains Δ*aceE* and Δ*aceE* Δ*pyc* served as control, and are shown in shades of blue, while Δ*aceE* Δ*pgi* and Δ*aceE* Δ*pyc* Δ*pgi* are shown in shades of red. Growth curves shown are based on the backscatter measurements in a microtiter cultivation system. Symbols represent the backscatter means and error bars their standard deviations of biological triplicates.

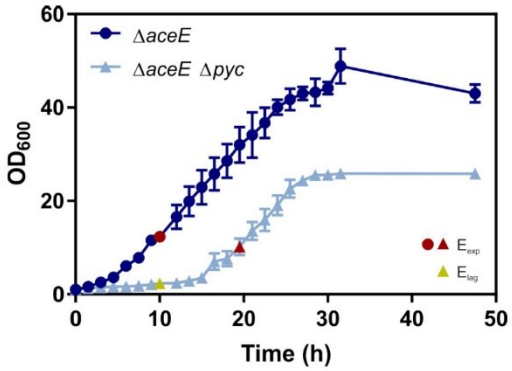


**Figure S9: Growth phase dependent sampling of *C. glutamicum* ΔaceE and ΔaceE Δpyc for DNA microarrays and GC-ToF analysis.** The strains Δ*aceE* and Δ*aceE* Δ*pyc* were cultivated. The main culture was inoculated to an $OD_{600}$ of 1 in 50 ml CGXII containing 154 mM acetate and 222 mM glucose. Cultivation was performed in 500 ml shaking flasks. Growth curves shown are based on $OD_{600}$ measurements which were performed every 90 minutes until 33 h, and an additional measurement after 48 h. Colored data points indicate the time where samples were taken: red = sampling time point during exponential phase ($E_{exp}$) used for DNA microarrays and GC-ToF analysis, yellow = sampling time point during lag phase of Δ*aceE* Δ*pyc* ($E_{lag}$) additionally used for GC-ToF experiments.

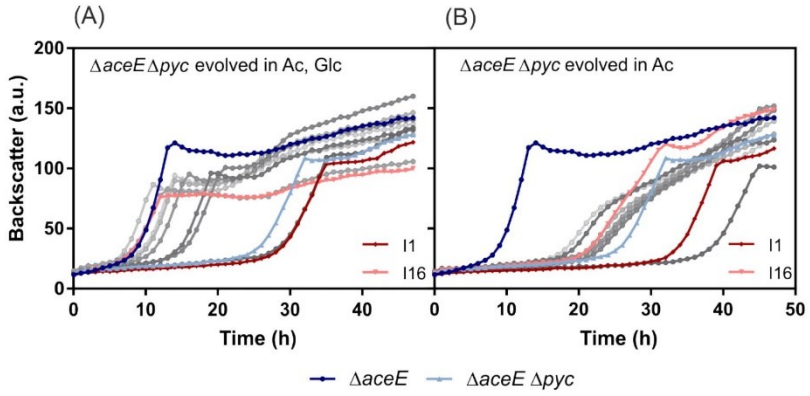


**Figure S10: Adaptive laboratory evolution of *C. glutamicum* ΔaceE Δpyc on acetate.** Growth analysis of single inoculation steps obtained from the adaptive laboratory evolution (ALE) approach which was performed with the strain Δ*aceE* Δ*pyc* (A) with selection pressure in CGXII containing 154 mM acetate and 222 mM glucose and (B) without selection pressure in CGXII containing solely 154 mM acetate. Growth curves are shown based on the backscatter measurements in a microtiter cultivation system. For growth analysis on population level, glycerol stocks which were prepared after batch number 1, 4, 6, 7, 8, 9, 10, 11, 13 and 16 during ALE were directly used for the inoculation of a first pre-culture in BHI supplemented with 51 mM acetate. The second pre-culture in CGXII containing 154 mM acetate was then used for inoculation of the main culture in CGXII containing 154 mM acetate and 222 mM glucose (start $OD_{600}$ of 1). The first and last inoculations are shown in shades of red. The parental strains Δ*aceE* and Δ*aceE* Δ*pyc* (shades of blue) served as controls. Symbols represent the backscatter means. I = Inoculation.

175 **References**

176 1. Schäfer A, Tauch A, Jäger W, Kalinowski J, Thierbach G, Pühler A. 1994. Small
177 mobilizable multi-purpose cloning vectors derived from the *Escherichia coli*
178 plasmids pK18 and pK19: selection of defined deletions in the chromosome of
179 *Corynebacterium glutamicum*. Gene 145:69-73 doi:10.1016/0378-1119(94)90324-
180 7.
181 2. Baumgart M, Luder K, Grover S, Gätgens C, Besra GS, Frunzke J. 2013. IpsA, a
182 novel LacI-type regulator, is required for inositol-derived lipid formation in
183 *Corynebacteria* and *Mycobacteria*. BMC Biol 11 doi:10.1186/1741-7007-11-122.

184

# Acknowledgement

I would like to express my special thanks to Prof. Dr. Julia Frunzke who gave me the opportunity to work on this interesting and exciting topic, for her excellent supervision, for the interest in my project, for the constant support of my work and for the countless inspiring discussions.
Furthermore, I would wish to show my gratitude to Prof. Dr. Matias Zurbriggen for agreeing to be my co-supervisor.
I would like to thank all colleagues involved in the projects; Jannis Brehm and Prof. Dr. Ralf Heermann for the excellent Biacore measurements and Dr. Max Hünnefeld and Dr. Andrei Filipchyk for fruitful discussions and their inputs regarding the CgpS silencing mechanism.
Furthermore, I would like to thank all colleagues from the IBG-1 institute for their help and the nice working atmosphere.
My special thanks go to all former and current group members of AG Frunzke, especially Dr. Eva Davoudi, Dr. Andrei Filipchyk, Dr. Vikas Sharma, Dr. Max Hünnefeld, Aël Hardy, Larissa Kever, Aileen Krüger, Robert Stella, Ulrike Viets, Cornelia Gätgens, Nadine da Silva, Dr. Isabel Huber, Dr. Marc Keppel, Sophia Lorke, Dr. Eugen Pfeifer, Raphael Freiherr von Boeselager, Iska Steffens and Dr. Regina Mahr. Thank you for the nice working atmosphere, for your help, for fruitful discussions and for funny group evenings, lunch breaks and retreats.
I would particularly like to thank Conni for her reliable technical support in the lab, the excellent performance of countless cloning and cultivation experiments and her contribution to my projects. Thanks a lot! Additionally, I would like to thank Astrid Wirtz for her excellent support during numerous HPLC experiments.
A special thanks to my fantastic *proofreading gang*, for their valuable inputs and their time: Eva, Aileen, Aël, Larissa, Robert and Max.
Furthermore, I would like to thank my motivated and hard-working master students Iska and Aileen for their excellent work and their great interest in the projects.

Ich möchte mich ganz besonders an dieser Stelle bei meiner Familie und Freunden bedanken, auf die ich mich immer verlassen kann, die mich stets unterstützt haben und an mich glauben. Danke an meine Eltern, dass sie mir diesen Weg ermöglicht haben.

Elmar danke ich von Herzen für seinen unerschütterlichen Rückhalt, die liebevolle Rundumversorgung während stressiger Zeiten und für seine effektiven Aufmunterungen. Ich danke dir!

# Eidesstattliche Erklärung

Ich versichere an Eides Statt, dass die Dissertation von mir selbständig und ohne unzulässige fremde Hilfe unter Beachtung der „Grundsätze zur Sicherung guter wissenschaftlicher Praxis an der Heinrich-Heine-Universität Düsseldorf“ erstellt worden ist. Die Dissertation wurde in der vorgelegten oder in ähnlicher Form noch bei keiner anderen Institution eingereicht. Ich habe bisher keine erfolglosen Promotionsversuche unternommen.

Johanna Wiechert